Modulators of MHC class I-related protein 1-mediated antigen presentation



Corinna Aileen Kulicke

St Edmund Hall

Trinity Term 2018

Thesis submitted in partial fulfilment of the requirements for the degree of Doctor of Philosophy at the University of Oxford

University of Oxford

MRC Weatherall Institute of Molecular Medicine

Supervisors: Vincenzo Cerundolo, Paul Klenerman, and Mariolina Salio

Modulators of MHC class I-related protein 1-mediated antigen presentation

Corinna Aileen Kulicke, St Edmund Hall, University of Oxford
DPhil thesis submitted in Trinity Term 2018

The monomorphic MHC class I-related protein 1 (MR1) presents bacterial metabolites to mucosal-associated invariant T (MAIT) cells, an innate-like subset of T lymphocytes. The known MAIT-activating MR1 ligands are intermediates of riboflavin synthesis, a pathway specific to certain fungi and bacteria and, thus, intrinsically non-self for humans. Here, a combination of hypothesis-generating and hypothesis-testing approaches was used to identify novel modulators of this non-classical antigen presentation pathway. In particular, a functional genetic screening technique based on insertional mutagenesis of the near-haploid human cell line HAP1 was employed to discover novel players in MR1 antigen presentation and trafficking. The most significant positive regulator of MR1 surface expression identified in this screen was β_2-microglobulin, confirming its indispensable role in the surface translocation of MR1. A number of other putative regulators of MR1 trafficking were taken forward into a CRISPR/Cas9-based validation approach and the ER-localised transporter ATP13A1 was found to affect MR1-mediated antigen presentation by modulating the size of the intracellular pool of MR1. In addition, the role of the soluble N-ethylmaleimide-sensitive factor activating protein receptor (SNARE) Sec22b in MR1-mediated antigen presentation was investigated as knock-down of Sec22b has previously been reported to control MHC class I-mediated cross-presentation. MR1 surface expression was reduced upon Sec22b knock-down and while the SNARE itself did not appear to play a role, RNA sequencing of a Sec22b deficient cell line revealed a number of potential regulators of MR1. Lastly, the capacity of cellular riboflavin

transporters to mediate MR1 ligand import was investigated. Treatment with the riboflavin analogue lumiflavin resulted in decreased MR1 surface expression in various human cell lines by a mechanism that appeared to be independent of the inhibition of riboflavin import. Together, these data contribute to an increasing understanding of MR1-mediated antigen presentation, which is essential for harnessing the therapeutic potential of MAIT cells.

Declaration of authorship

I declare that this thesis represents my own work, except where stated below. It has never been submitted for any other degrees.

Cell sorting was performed by Craig Waugh, Kevin Clark, Paul Sopp, and Sally-Ann Clark, and Margarida Rei in the MRC WIMM Flow Cytometry Facility.

Sanger and Next Generation sequencing was performed by Timothy Rostron, John Frankland, and Margarida Rei at the MRC WIMM Sequencing facility.

Transfection with gene-trap virus, cell sorting, recovery of insertion sites and bioinformatics analysis of the gene trap screen were performed by Erica De Zan (NDM, University of Oxford, UK) and Elmer Stickel (Netherlands Cancer Institute, Amsterdam, The Netherlands).

CRISPR/Cas9 constructs were designed and cloned by Philip Hublitz at the MRC WIMM Genome Engineering Facility.

JAWSII Sec22b KD cells were generated in the lab of Sebastian Amigorena (Institute Curie, Paris, France).

Quality control of the RNA extracted for RNA sequencing was performed by Laura Scifo (RDM, University of Oxford, UK).

Library preparation and sequencing for RNA sequencing was performed by staff of the Oxford Genomics Centre at the Wellcome Centre for Human Genetics (NDM, University of Oxford, UK).

Quantification of SLC52A1, SLC52A2, and SLC52A3 in THP-1 and C1R cells was performed by Claudia Gonzales-Lopez (RDM, University of Oxford, UK).

Acknowledgements

My thanks goes, firstly, to my supervisors Enzo Cerundolo, Paul Klenerman, and Mariolina Salio for giving me the opportunity to do my DPhil in their laboratories and for their invaluable support and guidance at every step of the way. It has been a privilege to work with you.

I am grateful to the Wellcome Trust for funding this work and to Keith Gull, Fiona Powrie, Helen McShane, and Chris Tang for creating a DPhil programme which provides such a strong sense of belonging and an amazing support network including leadership, administration, and students.

The gene-trap screen would not have been possible without our collaborators Sebastian Nijman and Erica De Zan. Thank you for your hard work and dedication and all the encouragement you have offered along the way. Thank you, too, to Paul, Craig, Kevin, and Sally for the many hours spent sorting cells for this project and to Philip Hublitz for his invaluable help with the CRISPR/Cas9 editing work. I would also like to thank Alain Townsend and Holm Uhlig for serving on my thesis committee.

I am extremely grateful to all members of the Cerundolo and Klenerman labs for the time and expertise they have so generously provided and for all the ways in which they have helped me become a better scientist. A special thank you goes to Mao for her day-to-day supervision and to Margarida for our late night chats about science, the universe, and everything. A massive shout-out also to Melissa, Nazish, Claudia, Prathiba, Mike, Lauren, Tianqi, Joachim, Lisette, Abi, and Violaine for making life in the lab (and outside) so much more enjoyable.

On a personal note, I would like to sincerely thank my mentors in the lab and outside of it. Thank you, Mafalda, Nancy, Caroline, and Louise – I could not have done this without you.

A special thank you also goes to my family and friends who have been with me through the ups and downs of the past four years; especially to my mum and dad, Nadja, Finja, Valen, Franzi, and Lara – I am so grateful to have you all in my life.

Last but not least, I would like to thank the girls for their amazing support during the final sprint – whoever invented meal rotas deserves a medal!

To all of you a massive

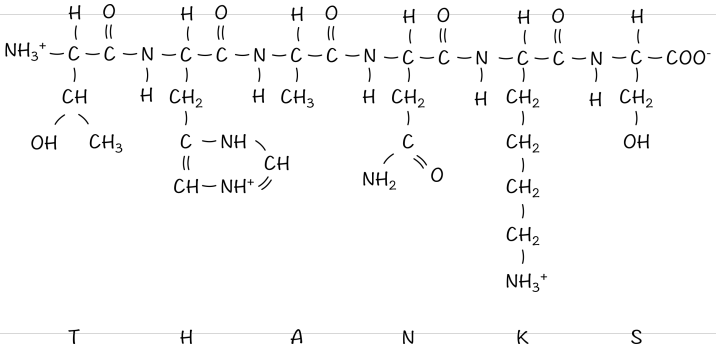


Figure A: THANKS peptide. Essential ingredient of gratitude.

Table of Contents

Abstract 1
Declaration of authorship 3
Acknowledgements 4
List of Abbreviations 9
1 Introduction 13
1.1 The innate immune system 14
1.2 The adaptive immune system 18
1.3 Innate-like lymphocytes 22
1.4 Immune evasion strategies 23
1.5 Basic concepts of antigen presentation 26
1.6 Classical antigen presentation by polymorphic antigen presenting molecules 27
1.6.1 MHC class I-mediated presentation of endogenous proteins 29
1.6.2 MHC class II-mediated presentation of exogenous proteins 31
1.6.3 MHC class I-mediated cross-presentation of exogenous proteins 32
1.7 Non-classical antigen presentation by monomorphic antigen presenting molecules 33
1.7.1 CD1-mediated antigen presentation 34
1.7.2 MR1-mediated antigen presentation 36
1.8 MR1-restricted T cells 46
1.8.1 The innate-like phenotype of MAIT cells 48
1.8.2 Clinical relevance of the MR1-MAIT cell antigen presentation axis 51
1.9 Research questions 55
2 General Materials and Methods 56
2.1 Materials 56
2.1.1 Cells 56
2.1.2 Tissue Culture and Cellular Assay reagents 57
2.1.3 Composition of Tissue Culture Media and Buffers 59
2.1.4 Flow Cytometry, Cell Sorting, and MACS Sorting reagents 61
2.1.5 Enzyme-linked immunosorbent assay (ELISA) reagents 63
2.1.6 Western Blot reagents 63
2.1.7 Molecular Biology reagents 67
2.1.8 Quantitative Real Time (qRT)-PCR reagents 69
2.2 Methods 71
2.2.1 Tissue culture 71
2.2.2 PBMC isolation and MAIT cell sorting 72
2.2.3 Molecular Biology and Cloning 73
2.2.4 Lentiviral particles and Transductions 75
2.2.5 Flow Cytometry 76
2.2.6 Enzyme-linked immunosorbent assay (ELISA) 78
2.2.7 Western Blots 79
2.2.8 Co-immunoprecipitiations 80
2.2.9 qRT-PCRs 81
2.2.10 Data Analysis and Plotting 82
3 A genetic screen to identify novel modulators of MR1 surface expression 83
3.1 Introduction 83
3.2 Chapter specific Materials and Methods 86

3.2.1 Ploidy staining 86
3.2.2 Gene trap mutagenesis 86
3.2.3 Surface staining and sorting 87
3.2.4 Recovery of insertion sites and bioinformatics analysis 88
3.2.5 Design and cloning of CRISPR/Cas9 plasmids 90
3.2.6 Transfection and sorting of gene-edited clones 91
3.3 Generation of HAP1.MR1 clones 93
3.4 Screen results and hit selection 96
3.5 CRISPR-based validation 102
3.6 Discussion 110
4 The role of the ER transporter ATP13A1 in MR1 antigen presentation 119
4.1 Introduction 119
4.2 Chapter specific Materials and Methods 122
4.2.1 Supplementation with exogenous manganese 122
4.2.2 Inhibition of degradation by the proteasome 122
4.2.3 Digestion with Endoglycosidase H 123
4.2.4 Cycloheximide chase assay 123
4.2.5 Culture in manganese-deficient medium 123
4.2.6 Illumina Deep Sequencing 124
4.3 Total MR1 levels in HAP1.MR1 ATP13A1 KO clones 125
4.4 Deconvolution of sgRNAs targeting ATP13A1 in HAP1.MR1 cells 128
4.5 Reconstitution of ATP13A1 expression in HAP1.MR1 ATP13A1 KO clones 137
4.6 The mechanism of the modulatory effect of ATP13A1 on MR1 protein levels 139
4.6.1 Manganese 140
4.6.2 Glycosylation 144
4.6.3 ER stress 145
4.6.4 Protein stability 148
4.7 ATP13A1 in THP-1 cells 151
4.8 Discussion 163
5 The role of the SNARE Sec22b in MR1 antigen presentation 172
5.1 Introduction 172
5.2 Chapter specific Materials and Methods 174
5.2.1 Sec22b KD cells 174
5.2.2 Presentation assays using bacteria 175
5.2.3 Bacterial uptake assays 176
5.2.4 Reconstitution of Sec22b expression 176
5.2.5 RNA sequencing 177
5.3 JAWSII Sec22b KD cells have an MR1 phenotype 180
5.3.1 Surface levels of folded MR1 are reduced in Sec22b KD cells 180
5.3.2 MR1-mediated antigen presentation is affected in Sec22b KD cells 185
5.4 Reconstitution of Sec22b expression does not rescue the MR1 phenotype 189
5.5 Knock-down of Sec22b does not affect MR1 expression in human cell lines 191
5.6 RNA sequencing reveals a number of potential off-target effects of Sec22b KD 195
5.7 Discussion 201
6 The role of cellular riboflavin transporters in MR1 antigen presentation 205

6.1 Introduction 205
6.2 Chapter specific Material and Methods 208
6.2.1 Incubation with lumiflavin 208
6.2.2 Presentation assay with fixed antigen presenting cells 208
6.2.3 Cell culture in deficient media 209
6.2.4 SLC52A2 knock-down and knock-out 209
6.3 Pre-incubation with lumiflavin reduces MR1-mediated antigen presentation 212
6.4 Incubation with lumiflavin reduces MR1 surface expression 217
6.5 Targeting SLC52A2 with shRNAs does not affect MR1 function 225
6.6 Discussion 231
7 Concluding Remarks 239
8 Bibliography 242
9 Supplementary Material 262

List of Abbreviations

5-A-RU	5-amino-ribityl uracil
5-OE-RU	5-(2- oxoethylideneamino)-6-D-ribitylaminouracil
5-OP-RU	5-(2-oxopropylideneamino)-6-D-ribitylaminouracil
6-FP	6-formylpterin
Ac6FP	acetyl-6-formylpterin
ACTB	β-actin
AP2	adaptor protein 2
AP3	adaptor protein 3
APC	antigen presenting cell
APC	allophycocyanin
BCG	Bacillus Calmette–Guérin
BCR	B cell receptor
BFP	blue fluorescent protein
bp	base pair
BSA	bovine serum albumine
BV	Brilliant Violet
cDNA	complementary DNA
CF	cystic fibrosis
CFSE	carboxyfluorescein succinimidyl ester
CI	confidence interval
CLiP	Class II associated Ii peptide
Co-IP	co-immunoprecipitation
cpm	counts per million
CRISPR	clustered regularly interspaced short palindromic repeats
CTL	cytotoxic T lymphocyte
DAMP	damage- (or danger-) associated molecular pattern
DCs	dendritic cells
DMSO	dimethyl sulfoxide
DNA	deoxyribonucleic acid
dNTP	deoxynucleotide
dUTP	deoxyuridine triphosphate (dUTP)
E.coli	*Escherichia coli*
EC	endosomal compartment
EDTA	ethylenediaminetetraacetic acid
ELISA	enzyme-linked immunosorbent assay
EndoH	endoglycosidase H
ER	endoplasmic reticulum
ERAD	ER-associated degradation
ERAP	ER aminopeptidase
EtOH	ethanol
FC	fold change
fcpv	FDR-corrected p-value
FCS	foetal calf serum

FDR	false discovery rate
FITC	fluorescein isothiocyanate
FSC	forward scatter
GAPDH	glyceraldehyde 3-phosphate dehydrogenase
GFP	green fluorescent protein
GM-CSF	granulocyte-macrophage colony-stimulating factor
GTP	guanosine triphosphate
HCMV	human cytolomegavirus
HIU	Human Immunology Unit
HIV	human immunodeficiency virus
HKG	house keeping gene
HLA	human leukocyte antigen
HPRT	hypoxanthine-guanine phosphoribosyltransferase
HTA	Human Tissue Authority
ICS	intracellular staining
IFN	interferon
Ii	invariant chain
IL	interleukin
ILC	innate lymphoid cell
iNKT cell	invariant natural killer T cell
IRAP	insulin-regulated aminopeptidase
KD	knock down
KO	knock out
LAM-PCR	linear amplification-mediated polymerase chain reaction
LAMP1	lysosomal-associated membrane protein 1
LB	Luria Broth
LF	lumiflavin
LTR	long terminal repeat
M. smegmatis	*Mycobacterium smegmatis*
M. tuberculosis	*Mycobacterium tuberculosis*
MAIT cell	mucosal-associated invariant T cell
MG	methyl glyoxal
MHC	major histocompatibility complex
MI	mutational index
MIIC	MHC class II-containing compartment
MR1	MHC class I-related protein I
mRNA	messenger RNA
MTP	microsomal triglyceride transfer protein
MW	molecular weight
NDM	Nuffield Department of Medicine
NK cell	natural killer cell
ns	not significant
o/n	over night
ORF	open reading frame
p	p-value
PAMP	Pathogen-associated molecular pattern

PBS	phosphate-buffered saline
PCR	polymerase chain reaction
PDI	protein disulfide isomerase
PE	phycoerythrin
PFA	paraformaldehyde
PHA	phytohemagglutinin
PI	propidium iodide
PLC	peptide loading complex
PM	plasma membrane
PRR	pattern recognition receptor
PVDF	polyvinylidene difluoride
qRT-PCR	quantitative real time PCR
RAG	recombination-activating gene
RDM	Radcliffe Department of Medicine
RF	riboflavin
RIN	RNA integrity number
RL-6-Me-7-OH	7-hydroxy-6-methyl-8-D-ribityllumazine
RL-6,7-diMe	6,7-dimethyl-8-D-ribityllumazine
RNA	ribonucleic acid
rRL-6-CH2OH	6-hydroxymethyl-8-D-ribityllumazine
RT	room temperature
SCABD	spinocerebellar ataxia with blindness and deafness
scrbl	scramble
SD	standard deviation
SDS	sodium dodecyl sulfate
SDS-PAGE	SDS polyacrylamide gel electrophoresis
sgRNA	single guide RNA
shRNA	small hairpin RNA
SLC	solute carrier
SNARE	soluble N-ethylmaleimide-sensitive factor activating protein receptor
SSC	side scatter
ssDNA	single stranded DNA
Stx18	syntaxin 18
t	time
TAP	transporter associated with antigen processing
TAPBPR	tapasin-related protein
TCR	T cell receptor
T_{FH} cell	T follicular helper cell
T_H cell	T helper cell
TLR	Toll-like receptor
TNF	tumour necrosis factor
TOP	thimet oligopeptidase
TPPII	tripeptidyl peptidase II
UGT1	UDP-glucose:glycoprotein glucosyl-transferase 1
UPR	unfolded protein response

UTR	untranslated region
Vamp4	vesicle-associated membrane protein 4
WIMM	Weatherall Institute of Molecular Medicine
WT	wild type
α	anti
β_2m	β_2-microglobulin

1 Introduction

To protect the body from the potentially fatal effects of infection and cancer, the immune system is equipped with a vast array of detection and effector mechanisms that sense and eliminate infectious agents as well as transformed cells. Through intricately linked interactions of the highly specialised immune cells of the myeloid and lymphoid lineages the control of such immune insults is achieved with an impressive efficiency and effectiveness. Immune cells are generally classified as innate or adaptive reflecting the two arms of the immune system which can be invoked when the anatomical barriers protecting the body are breached by a pathogen and infection is established[1]. In such cases, the innate immune system can be activated by pathogen-associated molecular signatures highly conserved across pathogens[2] or by host-derived molecules signalling the tissue damage caused by infection[3]. Binding of these immunogenic molecules to invariant pattern recognition receptors expressed on innate immune cells activates these cells and initiates an innate immune response[1,2,4]. Activation of innate immunity is rapid and leads to the induction of both broadly-acting anti-microbial effector mechanisms and a general inflammatory state conducive to an ensuing adaptive immune response[1,5–7]. By contrast, the development of an adaptive immune response is slower and more focussed. It is mediated by the activation and clonal expansion of lymphocytes bearing a highly diverse receptor repertoire[1,8–10]. Each receptor is unique to the lymphocyte expressing it and highly

specific to a very limited number of antigens[1,8–12]. In this way, the adaptive immune response can detect and effect effector functions against pathogens which can not be controlled by the innate immune response alone[1]. Importantly, clonal expansion also increases the frequency of pathogen-specific lymphocyte clones in the long term, providing the basis for the formation of immunological memory[13]. Throughout an immune response, the components of the innate and the adaptive immune system are highly dependent on each other for both survival and function. To this end, communication between the different cell types is mediated by physical interactions as well as soluble factors such as cytokines and chemokines[1,14].

1.1 The innate immune system

The first layer of immune defence is comprised of physical and chemical barriers at the surfaces of the body that are exposed to the environment[1]. The skin and the mucosal surfaces of the epithelia lining the respiratory, intestinal, and urogenital tracts not only physically prevent pathogens from entering the body but also contain cells which produce anti-microbial peptides in response to pathogen sensing[15–18]. The mucus produced by goblet cells further enhances this barrier function and plays an important role in the clearance of pathogens from mucosal surfaces[16,19,20].

When pathogens evade or overcome this first barrier they encounter soluble mediators of innate immunity including the complement system and anti-bacterial proteins such as defensins[1,18,21]. The complement system is a specialised set of

proteins which is deposited on microbial surfaces through sequential cleavage of its different components[1,21]. Ultimately, opsonic cleavage products of the complement protein C3 are displayed on the exterior of microorganisms and interact with complement receptors expressed on the surface of many innate immune cells to induce phagocytosis[21–24]. In this way, infectious microorganisms can be marked for phagocytosis even before specific antibodies against the pathogen have been generated[1]. In addition, the C3b fragment catalyses downstream processes culminating in the direct lysis of opsonised bacteria[21,25].

One of the most phagocytic cell types of the immune system, macrophages play an essential role in the removal of infectious agents. These tissue-resident immune cells are mostly derived from circulating monocytes and strategically positioned to sense and engulf invading pathogens[1,5,26]. At steady state, macrophages are pivotal to tissue development and homeostasis, for instance by internalising and recycling apoptotic cells[27], but their immunological functions can be activated by cytokines such as interferon (IFN) γ and through engagement of their pattern recognition receptors (PRRs)[1,4,5,26,27]. These germline-encoded invariant receptors bind conserved pathogen-associated molecular patterns (PAMPs) or danger (or damage)-associated molecular patterns (DAMPs) produced by infected host cells and are the key receptors mediating innate immune responses[1,4,14]. They are expressed on innate immune cells and some non-immune cells and include the members of the toll-like receptor (TLR) family, NOD-like receptors, and cytosolic DNA sensors such as RIG-I and cGAS[4,28].

Classically activated macrophages are characterised by their ability to eliminate internalised pathogens through a variety of anti-microbial mechanisms, most prominently the intracellular degradation of internalised material in acidified phagolysosomes[7,29]. Activation also induces the production and release of complement, pro-inflammatory cytokines and chemokines, and chemical mediators such as nitric oxide from macrophages[5,6]. Some of these released products act on the surrounding endothelial cells to induce local vasodilation and increased vascular permeability at the site of infection[5,6]. This facilitates the extravasation of circulating innate and adaptive immune cells into the affected area and also triggers heat, redness, swelling, and pain, known hallmarks of inflammation[1,4–6].

Another subset of innate immune cells are granulocytes comprising neutrophils, eosinophils, and basophils. The effector functions of these relatively short-lived immune cells are crucially dependent on the release of pre-synthesised proteins from their characteristic cytoplasmic granules into intracellular vacuoles, onto their cell surface, and into the extracellular space[1,30–32]. The contents of these cytoplasmic granules range from proteases and cytotoxins to chemotactic surface receptors and immuno-modulatory cytokines[30,32,33]. While neutrophils are mainly activated in the context of Type I immune responses against bacteria, fungi, and viruses, eosinophils and basophils are implicated in Type II immune responses against parasites and helminths[1,14]. Similarly, mast cells contribute to the immune response against helminths and other pathogens too large to be phagocytosed through degranulation of cytoplasmic granules containing effector molecules

including histamine[1,34]. Their IgE receptor-mediated immune functions are also implicated in allergic responses and in the response to venoms[34].

As opposed to these myeloid cell types, innate lymphoid cells (ILCs) originate from a common lymphoid progenitor shared with the adaptive B and T cells[1]. Like their myeloid counterparts, ILCs sense tissue-derived danger signals and secrete immunomodulatory cytokines and chemokines upon activation[35]. Different subgroups of ILCs are characterised by their transcription factor expression and cytokine profile and their functional plasticity allows for the specific tailoring of the immune response to the pathogen encountered. Type 1 ILCs (ILC1s), for instance, include the cytotoxic natural killer (NK) cells and secrete IFNγ in the context of intestinal inflammation whereas ILC2s produce high amounts of IL-4 and are implicated in Type II allergic responses[35]. Interestingly, increasing evidence that ILCs can display enhanced recall responses upon repeated exposure to a pathogen has recently challenged traditional notions about immunological memory[13].

Dendritic cells (DCs) are specialised antigen presenting cells (APCs) which take up extracellular material in the periphery through constitutive macropinocytosis or receptor-mediated endocytosis, migrate to the draining lymph nodes, and present processed antigen to T cells, thus bridging the innate and the adaptive immune response[1,36]. Licencing of DCs though PRR signalling increases the expression of proteins involved in antigen processing and presentation as well as the expression of co-stimulatory molecules required for T cell priming[36]. Moreover, activated DCs express elevated levels of CCR7 and other chemotactic receptors which render

them more sensitive to chemokines abundant in the lymphatics and induce DC migration from the peripheral tissue to the draining lymph node[1,37,38].

1.2 The adaptive immune system

B cells and T cells are the two major cell types comprising the adaptive immune system[1,39]. Both types of lymphocytes share the expression of highly diverse, somatically rearranged antigen receptors which is the most important property distinguishing them from innate immune cells and confers their extraordinary specificity[8,9,40]. Each lymphocyte expresses a clonal antigen receptor with a unique specificity and this diverse repertoire of specificities enables the immune system to mount an effective response to the immense variety of pathogens it encounters[8,40]. While T cell receptors (TCRs) and B cell receptors (BCRs) are structurally different, both comprise constant regions important for structure and function of the receptor and variable regions essential for antigen specificity[1,8]. For both receptors, the extensive variability in the variable regions is generated through recombination-activating gene (RAG)-mediated somatic recombination of gene segments encoding for the respective receptor subunits[8,9,40,41]. The combination of combinatorial and junctional diversity inherent to this process enables the generation of a repertoire of T cell receptors comprising approximately $2x10^7$ different specificities at any one time[8,40]. Since stochastic recombination of these gene segments also generates auto-reactive antigen receptors, B and T cell development in the bone marrow and the thymus, respectively, is highly controlled and auto-reactive clones are deleted by negative selection prior to release into the periphery[1,8,40].

The structural differences between BCRs and TCRs are also reflected in their function and have important implications for the chemical nature and relative localisation of the antigen they bind. BCRs are membrane-bound forms of immunoglobulins and can be secreted as antibodies upon B cell differentiation[1,40]. Thus, while BCRs and, by extension, antibodies can bind antigen of various chemical nature, they are restricted to soluble and surface antigens directly accessible to the BCR. TCRs, on the other hand, remain surface bound and only bind processed antigen in the context of major histocompatibility (MHC) molecules which enables them to detect internal epitopes revealed only upon extensive antigen processing[1,2,40,42].

Mature naïve T lymphocytes circulate between the blood and the secondary lymphoid organs where they can encounter their cognate antigen presented on an activated DC which has migrated there from the periphery[1,43,44]. Priming of naïve T lymphocytes is highly dependent on the provision of sufficient co-stimulatory signals on the DC and leads to the clonal expansion and differentiation of the activated T cell[1,36,44]. In addition to DCs, the afferent lymph also transports soluble antigen from the interstitial fluid to the secondary lymphoid organ which can activate B cells[43,45]. Upon activation, B cells can differentiate into long-lived plasma cells committed to secreting large quantities of antigen-specific antibody[1,46,47]. Primed T cells, on the other hand, differentiate into effector cells which generally recirculate and migrate into the inflamed tissue where they perform effector functions[1,44]. A subset of both activated B cells and T cells undergoes further epigenetic, transcriptional, and metabolic changes and

differentiates into long-lived memory cells whereas the remaining effector cells undergo apoptosis upon resolution of the infection. These memory T and B cells are poised to perform effector functions more rapidly and intensively upon re-encounter of their cognate antigen to prevent re-infection with the same pathogen[1,13,47–49].

Apart from its TCR each T cell also expresses either CD8 or CD4, co-receptors which differentially interact with MHC class I or MHC class II, respectively, and, thus, determine what class of antigen the T cell will encounter[2,50,51]. Consequently, $CD8^+$ and $CD4^+$ T cells differentiate into different effector subsets[52]. $CD8^+$ T cells which encounter intracellular antigens presented on the MHC class I molecules of infected cells differentiate into cytotoxic T lymphocytes (CTL) expressing potent cytotoxic effector molecules such as perforin and granzymes and are poised to kill infected target cells to limit the spread of infection[1,53,54]. $CD4^+$ T cells, by contrast, will encounter internalised antigen presented on MHC class II molecules and differentiate into different T helper (T_H) cell subsets depending on the combination of cytokines present during their differentiation[14,53,55]. The presence of IL-12 favours T_H1 polarisation, for example, and high concentrations of IL-4 are required for differentiation into T_H2 cells while the signals inducing a T_H17 phenotype include IL-23 and TGF-β[14,55]. Each of these different T helper subsets, in turn, differs in the combination of cytokines it produces and the type of immune response it supports[14,55]. As the cytokine milieu upon T cell differentiation is dependent on the type of innate immune response mounted initially and, thus, reflects the nature of the invading pathogen, the T cell help can be specifically tailored to the pathogen encountered. Moreover, $CD4^+$ T cells can increase the co-

stimulatory capacity of DCs through CD40-CD40 ligand signalling and, in this way, enable DCs to provide the co-stimulation needed for the priming of $CD8^+$ T cells[36,56]. Hence, initiation of the $CD8^+$ T cell response is tightly linked to successful $CD4^+$ T cell activation, particularly in the context of chronic viral infection[57]. Furthermore, activation of both $CD4^+$ and $CD8^+$ T cell is also pivotal in anti-tumour immune responses[58,59].

T follicular helper (T_{FH}) cells represent a specialised subset of T helper cell which remains in the lymph node and provides essential help for B cell differentiation and affinity maturation of the BCR[1,45]. Upon activation, both T_{FH} and B cells migrate to border between the T cell zone and the B cell follicle within the secondary lymphoid organ and a germinal centre is formed[44,45,60]. Here, B cells undergo affinity maturation through repeated cycles of somatic hypermutation in the genes encoding for their BCR and clonal selection through competition for T cell help[45,61]. As B cells internalise antigen through receptor-mediated endocytosis of their BCR, the availability of antigen to present to T_{FH} cells on MHC class II molecules is directly related to the affinity of the BCR to its cognate antigen[61]. This provides a mechanism by which T_{FH} cells can read out the affinity of the hypermutated BCR and select for B cells with a high affinity BCR which will produce high affinity antibodies upon differentiation into plasma cells[45,61].

The antibodies secreted into the plasma by fully differentiated plasma cells have at least three important functions[1,62]. Firstly, the neutralisation of soluble antigen such as viruses and toxins prevents binding to host targets and, thus, interferes with viral replication and pathogen-associated toxicity. Secondly, opsonisation of

larger pathogens targets them for phagocytosis mediated by receptors on phagocytes which recognise the constant Fc portion of antibodies. In addition, Fc receptor engagement can result in antibody-dependent cell-mediated cytotoxicity. Thirdly, the Fc portion of antibodies bound to the surface of pathogenic microorganisms enhances complement deposition and related effector functions[1,21,62]. This enhancement of innate effector functions by the adaptive immune system is just one example of the “two-tiered” structure of many immune responses where the signals provided by innate sensor cells determine which types of effector cells the adaptive immune cells differentiate into. This, in turn, determines which innate effector functions are augmented as a result.[14] Thus, innate and adaptive immune responses are inherently linked and share many of their effector functions.

1.3 Innate-like lymphocytes

The traditional distinction between the innate and the adaptive arms of the immune system has become increasingly blurry in recent years as cell types with overlapping functions are described[63]. Invariant Natural Killer T (iNKT) cells, γδ T cells, and mucosal-associated invariant T (MAIT) cells are examples of cell types that feature phenotypic and functional properties traditionally attributed to adaptive immunity as well as those conventionally associated with innate responses[63–65]. For example, while iNKT and MAIT cells express somatically rearranged TCRs, their α- and β-chain usage is extremely restricted, substantially limiting the diversity of antigen specificity characteristic of adaptive immunity[65]. Other innate-like properties of these specialised T cell subsets include responsiveness to

cytokines such as IL-12 and IL-18 even in the absence of TCR engagement[66,67], the ability to rapidly secrete pro-inflammatory cytokines, and relatively high precursor frequencies as compared to classical naïve T cells, obviating the need for clonal expansion[64,65]. Intriguingly, neither iNKT nor MAIT cells are restricted by classical peptide-presenting MHC molecules but rather by non-classical MHC class I-like molecules presenting non-proteinaceous antigens[65]. This recognition of a pathogen- or danger-associated molecular signature as opposed to highly processed peptide antigen further exemplifies the innate features of these cell types[64].

1.4 Immune evasion strategies

While the immune system is uniquely equipped to detect, contain, and eliminate both infectious and non-infectious threats to health, pathogens as well as transformed cells have evolved numerous strategies to evade the immune response at any of these stages. Mediated by a vast variety of molecular and cellular mechanisms, these evasion strategies can have devastating systemic effects impacting the entire immune system. Despite the diversity of mechanisms and effector molecules, bacterial and viral escape mechanisms are generally based on similar underlying concepts, summarised by Finlay and McFadden as secretion of immunomodulatory molecules or toxins, expression of modulators on the pathogen surface, inhibition of complement, killing of immune cells, inhibition of cytokines and chemokines, modulation of apoptosis and autophagy, antigenic hypervariability, interference with TLR signalling, blockade of antimicrobial

molecules, interference with intrinsic intracellular pathways, hiding from immunosurveillance, and blockade of adaptive immunity [68].

Staphylococcus aureus is a prime example of a pathogen secreting immunomodulatory molecules and toxins as it produces a variety of extracellular cytolytic proteins targeting either immune cells specifically or mammalian cells more generally[7]. LukAB, LukED, HlgAB, HlgCB, and LukSF-PV all represent *Staphylococcus aureus* leukocidins specifically targeting immune cells through interaction with receptors expressed on macrophages, monocytes, and neutrophils[7].

Viruses, bacteria, and cancer have all developed evasion mechanisms to inhibit complement-mediated immunity. Strategies employed by pathogens include the sequestration and display of the soluble human complement inhibitory protein C4BP on bacterial surfaces[69], the induction of host membrane-bound complement regulatory proteins in Human Cytomegalovirus (HCMV)-infected cells[69,70], and the incorporation of those cellular complement regulatory proteins into the virions of HCMV[71]. Similarly, surface expression of the membrane-bound complement inhibitory proteins CD46, CD55, and CD59 is increased in many primary cancers and cancer cell lines and represents just one of the many ways in which cancer cells evade complement-dependent cytotoxicity[72].

A prominent example for the killing of immune cells, the human immunodeficiency virus (HIV) subverts the immune response through its tropism for $CD4^+$ T cells which is mediated by the molecular interaction between the viral gp120 protein

and CD4[73–75]. Specific infection and, consequently, elimination of these cells results in the loss of the T cell help indispensable for an effective adaptive immune response[76].

In a similarly systemic manner, *Mycobacterium tuberculosis* (*M. tuberculosis*) can induce IL-4-driven T_H2 immune responses in the host, thus diverting energy and resources away from a protective T_H1 response[77,78]. Interfering with cytokine signalling in this way provides an important survival advantage for virulent *M. tuberculosis* strains[77].

High mutation rates of both cancers and viruses represent a more cell-intrinsic evasion strategy and prevent immune detection as frequent alterations in antigens render activated effector cells unable to detect and eliminate target cells. In HIV, this elevated rate of mutation is the result of multiple factors including a high replication rate, expression of an error-prone reverse transcriptase, and the ability to hijack the host DNA-mutating APOBEC enzymes tasked to introduce lethal mutations into the viral genome[79,80].

Sensing of a pathogen or cancer cell by the immune system is also commonly prevented by interfering with antigen presentation. Examples of this include pox and herpesviruses expressing K3 and K5 ubiquitin ligases which target MHC class I molecules for proteasomal degradation[81] and downregulation of components of the antigen processing and presentation machinery by tumour cells[82]. *M. tuberculosis* interferes with the presentation of processed antigen by preventing the fusion of phagosomes with lysosomes, thus averting the delivery of lysosomal

proteins including not only degradative enzymes but also MHC class II molecules[83,84].

These examples illustrate just some of the inventive mechanisms that have evolved to escape and subvert the immune system. They emphasise the importance of further refining our understanding of the molecular mechanisms of immunity such as antigen presentation in order to optimally support and harness its protective power.

1.5 Basic concepts of antigen presentation

In order to mount an effective immune response to an infection, the immune system must first detect the presence of the infectious agent. To achieve this, it is equipped with a plethora of recognition systems which specifically interact with the molecular signature associated with infectious agents and trigger host defence mechanisms. The pathogen-derived molecules recognised range from components of the bacterial cell wall detected by pattern recognition receptors of the innate immune system[2,4] to highly processed peptide antigens presented to T cells on polymorphic antigen presenting molecules as part of an adaptive immune response[53,85,86]. In between these two extremes lie the non-classical, monomorphic antigen presenting molecules which present non-peptidic molecular products to T cells. Examples include the presentation of lipid antigens to iNKT cells by the CD1 family of glycoproteins[87–93], MR1-mediated presentation of microbial vitamin metabolites to MAIT cells[94–96], and the recognition of phosphoantigens in the context of Butyrophilin 3A1 by γδ T cells [97–100]. While

peptide presentation by the polymorphic MHC class I and II molecules has been extensively studied over the last four decades[86], how non-peptidic antigens are presented is less well understood. It is clear, however, that each class of antigens requires a specialised presentation mechanism reflecting both the intracellular distribution and the biochemical properties of the antigen (Figure 1.1)

1.6 Classical antigen presentation by polymorphic antigen presenting molecules

As a general concept, MHC class I molecules are thought to sample the cytosolic proteome whereas MHC class II molecules are loaded with peptides derived from either self or internalised exogenous material processed in the endolysosomal compartment[53,85,86]. In addition, the two pathways intersect in the special cases of cross-presentation and autophagy. In the first case MHC class I molecules present exogenous peptides either generated in an endolysosomal compartment and loaded onto recycling MHC class I or processed in the cytosol and loaded onto nascent antigen presenting molecules[85,86,101]. In the second case intracellular proteins are delivered to MHC class II-containing organelles as a result of autophagy and consequently presented in the context of this class of antigen presenting molecules[102–104]. While MHC class I molecules present peptide to $CD8^+$ cytotoxic T cells, peptide antigens presented in the context of MHC class II molecules are recognised by $CD4^+$ T helper cells[50–52]. Both classes of classical MHC-encoded antigen presenting molecules form non-covalently linked heterodimers: MHC class I consist of a heavy chain and a light chain known as β_2-

microglobulin (β_2m) whereas MHC class II molecules are composed of the two structurally similar α and β subunits[105–107].

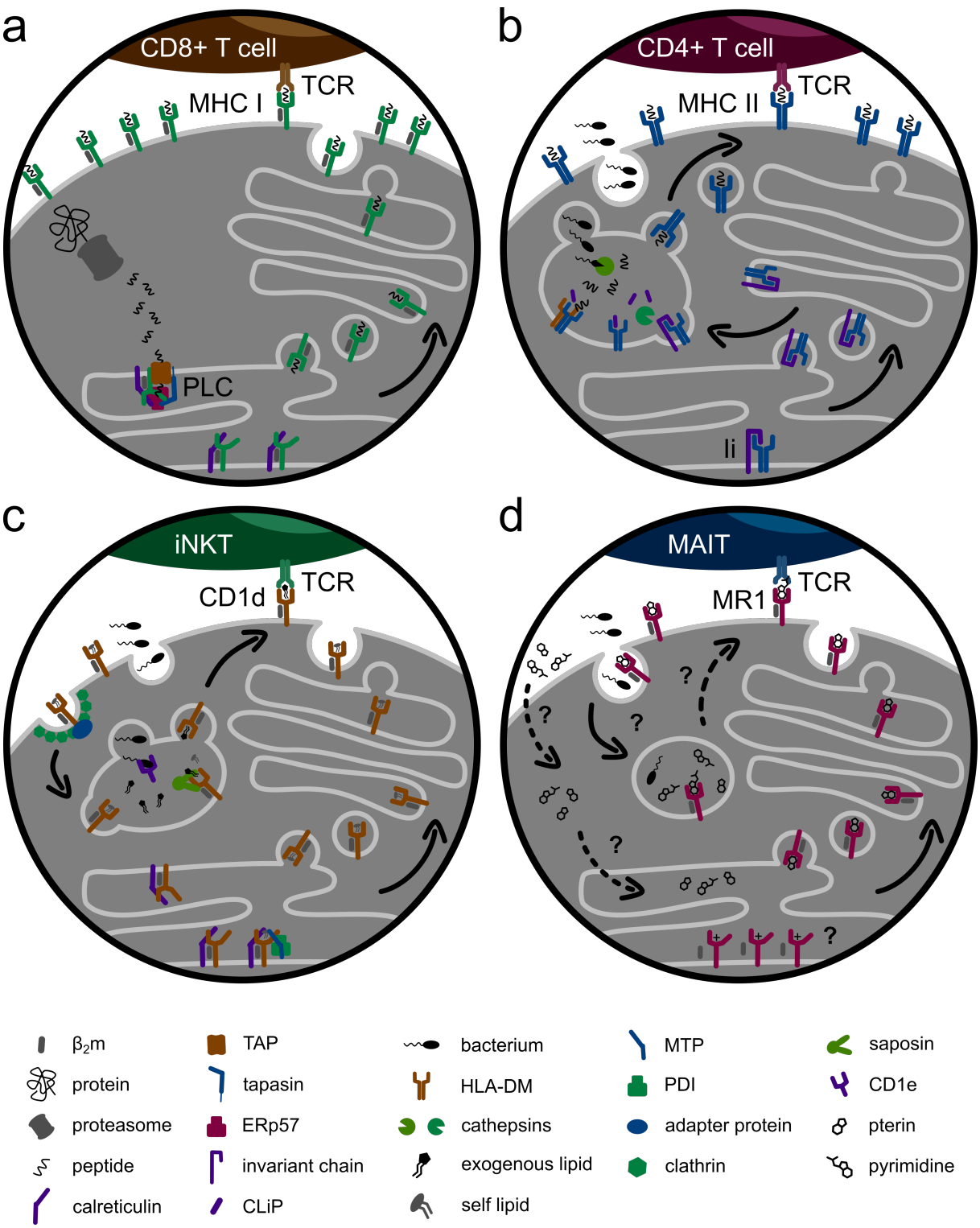


Figure 1.1: The four MHC and MHC I-like antigen presentation pathways Cartoon representations of the basic principles of the four major MHC and MHC I-like antigen presentation pathways. (a) Cytosolic protein is degraded by the proteasome, imported into the ER by TAP and loaded onto MHC class I molecules by the peptide loading complex (PLC). Loaded MHC I molecules leave the ER via the secretory pathway and are presented at the cell surface. (b) MHC class II molecules associate with the invariant chain Ii in the ER and traffic to the MHC class II containing compartment where Ii is degraded by cathepsins leaving only the Class II associated Ii peptide (CLiP). CLiP is exchanged for endosomal peptides by HLA-DM and MHC II:peptide complexes are presented at the cell surface. (c) CD1d associates with calreticulin in the ER and is loaded with self lipids in a process dependent on the microsomal triglyceride transfer protein (MTP) which forms a heterodimer with protein disulfide isomerase (PDI). This allows ER egress and trafficking to the cell surface. Surface CD1d is internalised in clathrin-coated vesicles and sorted by adapter proteins into the endolysosomal compartment where its lipid can be exchanged for internalised microbial lipids with the help of saposins and CD1e before CD1d recycles back to the cell surface. (d) MR1 resides in the ER in a ligand-receptive form. Upon neutralisation of the positive charge of K43, MR1 translocates to the cell surface. Soluble ligand is likely loaded in the ER whereas microbe-associated ligand may be loaded in an endolysosomal compartment and MR1 may recycle to the cell surface. Dashed arrows and question marks denote areas under investigation. TCR = T cell receptor.

Another shared feature of the classical antigen presenting molecules is their high level of polymorphism[108,109]. It is this polymorphism that allows each MHC allele to present a distinct set of peptides[110–112] and, in combination with a broad specificity that is only restricted by a few anchor residues, confers the ability to cover the breadth of peptide antigens needed for effective immunosurveillance[86,105,113–115].

1.6.1 MHC class I-mediated presentation of endogenous proteins

While the detailed mechanisms can differ depending on the HLA allele and source of antigenic protein, the general principles underlying the presentation of endogenous peptide antigen by MHC class I molecules are well established[53,85,86]. Proteins synthesised inside the cell are proteolytically cleaved by the proteasome[116,117], further processed by cytosolic proteases such as thimet oligopeptidase (TOP) and tripeptidyl peptidase II (TPPII)[118–120], and transported into the endoplasmic reticulum (ER) by the transporter associated with antigen processing (TAP)[121–125]. In the lumen of the ER peptides are further trimmed by

ER aminopeptidases (ERAP) 1 and 2 which have different substrate specificities and perform complementary functions in generating peptides of the amino acid length optimally accommodated in the MHC class I binding groove[126–128]. N-terminal trimming of peptides in the absence of MHC class I has been shown *in vitro*[129] but accumulating evidence supports a model in which ERAP1 primarily acts on temporarily exposed N-termini of peptides bound by MHC class I molecules *in vivo*[130–132].

In the ER, partially folded MHC class I molecules are stabilised within the peptide loading complex (PLC). This multi-component chaperone consists of tapasin, ERp57, Calreticulin, and TAP itself and mediates the loading of antigen onto peptide-receptive MHC class I molecules[53,85,86]. After initial peptide binding, MHC class I molecules undergo extensive peptide editing catalysed by tapasin[133–138] and TAP binding protein, related (TAPBPR)[139–141], allowing them to sample a wide range of peptide antigens[142]. Only MHC class I molecules loaded with the right affinity peptide are able to undergo the conformational change needed to pass the ER quality control mechanisms and enter the secretory pathway[143–146]. One of the cellular mechanisms central to MHC class I assembly and this quality control is UDP-glucose:glycoprotein glucosyl-transferase 1 (UGT1)-mediated reglucosylation of N-linked glycans in the MHC class I heavy chain[147,148]. At the cell surface peptide:MHC class I complexes are stable for a limited period of time but rapidly internalised after dissociation of the peptide and the ensuing conformational change[149]. Both the dissociation from β_2-microglobulin (β_2m)[146,150–152] and ubiquitination by cellular ubiquitin ligases[153–155] have been implicated in the regulation of this process. Internalised MHC class I molecules can either be routed

towards the lysosome for degradation or acquire a new ligand in an endosomal compartment and recycle back to the cell surface[53,101,156] (discussed below).

1.6.2 MHC class II-mediated presentation of exogenous proteins

Like MHC class I molecules, MHC class II molecules are synthesised in the ER. However, loading of MHC class II in this organelle is prevented by binding of the invariant chain Ii, which stabilises the MHC class II fold and occupies the peptide binding groove[157–161]. In addition, the cytoplasmic tail of Ii features a sorting motif which effects the trafficking of the Ii – MHC class II complex from the trans-Golgi network directly to an endosomal compartment known as MHC class II compartment (MIIC)[162–166]. There, Ii is degraded by resident cathepsins leaving only the class II associated Ii peptide (CLiP) bound in the MHC class II peptide binding groove intact[53,86,167,168]. Exchange of CLiP for antigenic peptides generated in the highly proteolytic environment of the endosomal compartment is catalysed by the MHC class II-like chaperone HLA-DM[53,85,169–172]. The activity of HLA-DM, in turn, is modulated by another non-classical MHC class II protein named HLA-DO[53,173]. Akin to the role of tapasin in shaping the peptide repertoire presented on MHC class I molecules, DM employs a kinetic proofreading mechanism to determine which peptides are presented on MHC class II[174]. Interestingly, professional antigen presenting cells can adapt the local biochemical microenvironment of their endosomal pathway in a way that favours the preservation of antigenic peptides over the rapid degradation of internalised material depending on maturation state and cell type[53,85,175,176]. Loaded MHC class II molecules are trafficked to the cell surface via secretory vesicles that bud from

MIIC tubules in a process that is dependent on active transport along the cytoskeleton[53,86,177–180]. At the cell surface, the stability, internalisation, and recycling of peptide:MHC class II complexes is tightly controlled by ubiquitination of conserved motifs within the MHC class II cytoplasmic tail[153,181–185].

1.6.3 MHC class I-mediated cross-presentation of exogenous proteins

Cross-presentation of antigens generated in the endolysosomal compartment in the context of MHC class I molecules represents an exception to the spatially separated roles of MHC class I and II. This exception allows MHC class I molecules to sample the pool of endocytic peptides for presentation to $CD8^+$ cytotoxic T cells, an indispensable mechanism for the immune response to pathogens that do not infect antigen presenting cells and to cancer cells[53,86,101]. Two major pathways for antigen generation and loading in cross-presentation have been described and are not mutually exclusive[101]. The vacuolar pathway for cross-presentation involves the processing of internalised proteins by lysosomal proteases and the insulin-regulated aminopeptidase (IRAP) within the phagocytic compartment[186–189]. The lysosomally generated peptides can then replace those bound by recycling MHC class I molecules and the peptide-exchanged complexes are transported back to the cell surface in a mechanism dependent on a conserved sorting motif in the cytoplasmic tail of MHC class I[190]. The cytosolic pathway, on the other hand, involves the translocation of internalised protein into the cytosol for processing by the proteasome and subsequent TAP-dependent transport of the generated peptide into the ER or back into the endosome[191–195]. This pathway is crucially reliant on the delivery of ER-resident proteins to the

phagosome and a critical role for the ER-associated degradation (ERAD) component p97 has been established[195–199]. Even though much progress has been made in elucidating these specialised mechanisms of antigen presentation, the molecular details of both pathways are still under investigation[101]. Recently, the Soluble NSF Attachment Protein Receptor (SNARE) Sec22b was reported to be critical for cross-presentation, in particular for the delivery of ER contents to the phagosome[200–202]. However, this role remains controversial[203,204].

1.7 Non-classical antigen presentation by monomorphic antigen presenting molecules

In addition to the classical, peptide-presenting, polymorphic MHC class I and II molecules, the immune system also comprises an arsenal of monomorphic, non-classical antigen presenting molecules. Most prominently these include the non-classical peptide-presenting molecules HLA-E, HLA-F, and HLA-G as well as MHC class I-related protein 1 (MR1) and the proteins of the CD1 family[105,205]. Like MHC class I and II, the non-classical HLA proteins are encoded in the MHC locus on chromosome 6 and present peptide antigens[105]. They differ from classical MHC class I mainly in their extremely limited polymorphism[206–208], their restricted peptide repertoire[105,209,210], and their function as ligands for activating or inhibitory receptors on innate immune cells[105,211–215]. MR1 and the CD1 proteins, however, are encoded outside of the MHC region in both mice and humans[216,217] and more drastically differ from classical MHC class I. They restrict the non-classical mucosal-associated invariant T (MAIT) and invariant natural killer T (iNKT) cells,

respectively, and their most distinctive feature is the presentation of non-proteinaceous antigen.

1.7.1 CD1-mediated antigen presentation

CD1 proteins have long been known to present lipid antigens[87,89–93] and while there is some overlap in the lipid repertoire presented by each member of the family[87,218], each isoform also associates with a distinct subset of both self and non-self lipid antigens[87,219]. The unique antigen binding cleft topologies of the four CD1 molecules reflect this non-redundancy and form the basis for their lipid specificity[87,220–223]. Unlike the MHC class I antigen processing machinery which extensively modifies the peptide antigen to fit into the peptide binding groove, CD1 molecules employ a variety of molecular strategies to accommodate a broad range of lipid-based ligands[205]. For example, CD1 antigen binding clefts feature networks of hydrophobic tunnels, portals, and notches which allow even long chain alkyl chains to occupy this antigen presenting platform[87,205]. In addition, chaperone-like scaffold lipids and spacer lipids are important modifiers of lipid binding[205,219,224]. In the ER, loading of such endogenous lipids is facilitated by the Microsomal triglyceride transfer protein (MTP)[225,226] and allows CD1 molecules to adopt the conformation required for ER egress. During post-ER lipid exchange, the biochemical properties and size of the scaffold lipids control which regions of the cleft are available for lipid binding and participate in the positioning of the antigenic lipid[205,227]. The nature of the bound ligand in turn impacts the conformation of the T cell receptor (TCR) binding interface[227,228]. In this way, parts of the lipid that do not directly interact with the TCR themselves can modulate TCR binding affinity and,

ultimately, signal strength[229]. One particularly striking example of this is the presentation of small, headless self-lipids in the context of CD1a[230]. Ternary crystal structures of CD1a, β_2m, the self-lipid and the TCR revealed that the lipid itself was concealed inside the antigen binding cleft, thereby allowing the TCR to engage with residues on the outer surface of the antigen presenting molecule itself[230]. These results inspired the concept of a “absence of interference” mode of antigen recognition for auto-reactive CD1a molecules[205].

In addition to antigen cleft architecture, the specific presentation of distinct lipid repertoires on the different CD1 molecules is also mediated by their different subcellular distribution and intracellular trafficking[231–233]. While CD1a mainly localises to the plasma membrane and early endosomes[234–236], CD1b and CD1d sample the lipids present in late endolysosomes [234,235,237], and CD1c is more broadly distributed throughout the endosomal compartment[238]. These distinct intracellular destinations are reached by differential interaction of the tyrosine-containing sorting motifs in the cytoplasmic tails of CD1b, c, and d with the clathrin adapters AP2 and AP3[231,239–241]. In their respective compartments, CD1 proteins are then loaded with lipids taken up through phagocytosis or receptor-mediated endocytosis[242–245]. Importantly, the intracellular trafficking of internalised lipids strongly depends on their biochemical properties[246,247]. Lipid loading in the endolysosomal compartments is critically dependent on the activity of both saposins[248–250] and CD1e, a soluble isoform of CD1 that modulates lipid processing and loading[251–253].

Out of the four known human lipid-presenting molecules CD1d is the most widely studied and best characterised as it is the only isoform with a murine homologue[205,216,254]. However, the recent development of tetramers for CD1a[255], b[256], and c[257] has enabled much progress in elucidating the physiological roles of these molecules and will continue to extend the understanding of this family of non-classical antigen presenting molecules[205].

1.7.2 MR1-mediated antigen presentation

Even though MR1 shares aspects of the molecular and cellular mechanisms of each of the other MHC and MHC-like antigen presentation systems it is also distinctly different from all of them[94,258]. One of the most striking differences consists in the "presentation-on-demand" mechanism employed by MR1 which is distinct from the constitutive cell surface expression and intracellular cycling of the other antigen presenting molecules[53,94]. Like the other MHC and MHC-I like molecules MR1 requires binding of a ligand to complete folding and exit the ER[53,94,231] but unlike the other antigen presenting proteins it mostly remains in the ER at steady state[259,260]. Evidence for this subcellular localisation was obtained by biochemical methods such as endoglycosidase H (EndoH) digestion and immuno-precipitation of surface biotinylated proteins, metabolic labelling of nascent MR1 molecules, and fluorescence microscopy[259–261]. Moreover, MR1 has been found to partially co-localise with $LAMP1^+$ in endolysosomal compartments upon over-expression of a GFP-tagged version of the protein[261,262] and the relative contributions of these two intracellular pools to antigen presentation under physiological expression remain to be determined[258].

Of note, a small population of ligand-receptive MR1 molecules may be transiently expressed at the cell surface even in the absence of ligand[263]. This is supported by the observations that surface MR1 can be loaded with exogenous ligand even if cells have either been fixed[264] or incubated on ice[260] and consistent with a study reporting a minute proportion of unfolded MR1 detectable at the cell surface[265]. Interestingly, an antibody binding an epitope at the F' end of the α2 helix of murine MR1 stabilised the molecule at the cell surface in a conformation capable of stimulating MAIT cells in the absence of agonistic ligand[263]. This is consistent with the requirement for MR1 to adopt a fully folded conformation to activate MAIT cells[265] but raises the question of how these MR1 molecules acquired a conformation allowing them to exit the ER and progress to the cell surface. It is possible that empty MR1 molecules transiently exist at the cell surface after dissociation of non-agonisitic folate-derived ligands ubiquitously present in cell culture medium[95]. Like empty MHC class I molecules[266], empty MR1 molecules have been shown to reach the plasma membrane upon incubation at low temperatures[267], suggesting a shared temperature-dependent quality control mechanism. Strikingly, a mutation in a classical murine MHC class I allele restricting the mobility of the region homologous to that containing the epitope recognised by the MR1-stabilising antibody also enhanced the surface stability of these molecules by increasing their affinity for β_2m and reducing the rate of their internalisation[146]. The affinity of murine MR1 for β_2m in the presence of the stabilising antibody was not tested[263]. Nevertheless, time course experiments showed that the amount of MR1 expressed at the cell surface at any one time was

extremely low[263] consistent with MR1 being predominantly sequestered in the ER in the absence of exogenous ligands.

Even though MR1 itself was discovered over two decades ago[268] its ligand remained elusive until very recently when Kjer-Nielsen *et al.* identified the first classes of MR1 ligands[95]. Refolding experiments of MR1 revealed that its folded conformation was stabilised by pterins produced by photodegradation of folic acid (vitamin B9) in culture medium as well as ribityl lumazine intermediates of riboflavin biosynthesis found in the supernatant of MAIT cell-activating bacteria[95] (Figure 1.2). While the ribityl lumazines induced a potent MAIT cell response, 6-formylpterin stabilised MR1 and induced its translocation to the cell surface without MAIT cell activation[95]. This seminal paper also reported the first crystal structure of the MR1:antigen complex confirming that, like CD1 and MHC class I molecules, MR1 adopts an MHC fold consisting of two semi-parallel α helices atop a β sheet[105] and non-covalently associates with β_2m through interactions with its α3 domain[95]. Unlike MHC class I molecules which feature a solvent-exposed, mostly polar binding groove[107] and CD1 molecules which contain hydrophobic tunnels and portals[87], the MR1 antigen binding cleft is composed of two pockets comprising a highly conserved “aromatic cradle” suited for the accommodation of small molecule metabolites. This aromatic portion of the A’ pocket surrounds the lysine residue K43 which forms a Schiff base with the pterin ligand[95] (Figure 1.2). This unique mode of antigen binding is another distinctive feature of MR1 antigen presentation and sets it apart from the other MHC and MHC-like molecules which non-covalently associate with their ligands.

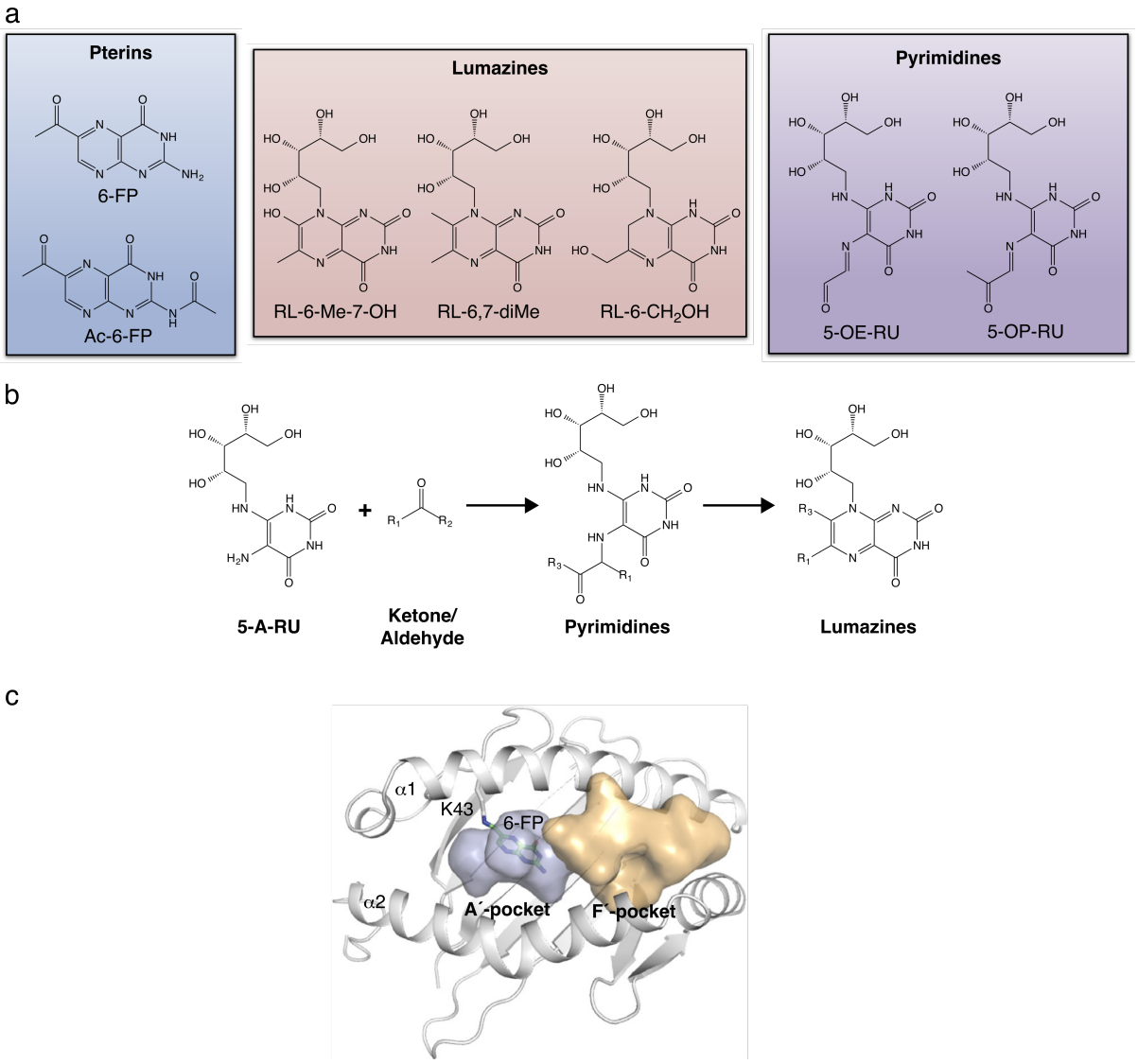


Figure 1.2: MR1-restricted antigens. (a) Chemical structures of published MR1 restricted antigens including the pterins, 6-formyl pterin (6-FP) and acetyl-6- formyl pterin (Ac6FP); the lumazines 7-hydroxy-6-methyl-8-D-ribityllumazine (RL-6-Me-7-OH), 6,7-dimethyl-8-D-ribityllumazine (RL-6,7-diMe) and reduced 6-hydroxymethyl-8-D-ribityllumazine (rRL-6-CH2OH); the pyrimidines 5-(2-oxopropylideneamino)-6-D-ribitylaminouracil (5-OP-RU) and 5-(2-oxoethylideneamino)-6-D-ribitylaminouracil (5-OE-RU). (b) Reaction scheme for the condensation of 5-amino-ribityl uracil (5-A-RU) with small reactive aldehydes or ketones such as glyoxal or methylglyoxal to form pyrimidines and lumazines. (c) Representation of the MR1-6-FP binary crystal structure (PDB ID 4GUP) showing the A0 (blue) and F0 (orange) -pockets, with MR1 shown in white with Lysine 43 and 6-FP shown in stick representation. Figure and caption adapted and reprinted from Current Opinion in Immunology 2015, 34:28–34, Hamish EG McWilliam, Richard W Birkinshaw, Jose A Villadangos, James McCluskey, Jamie Rossjohn, MR1 presentation of vitamin B-based metabolite ligands, pp. 28-34, Copyright (2015), with permission from Elsevier.

Since the publication of these first MR1 ligands work by different groups has revealed many more small molecules capable of stabilising MR1[96,269–272]. Through systematic mutation of the bacterial riboflavin synthesis pathway Corbett *et al*. identified hybrid molecules resulting from the non-enzymatic condensation of the riboflavin precursor 5-amino-6-D-ribitylaminouracil (5-A-RU) with host- or microbe-derived glyoxals as the most potent MAIT cell agonists known to date[96]. The pyrimidine compounds 5-(2-oxopropylideneamino)-6-D-ribitylaminouracil (5-OP-RU) and 5-(2- oxoethylideneamino)-6-D-ribitylaminouracil (5-OE-RU) are formed when 5-A-RU reacts with methylglyoxal or glyoxal, respectively and this reaction yields the carbonyl group that can form the Schiff base with K43[94,96]. The pyrimidine compounds are prone to spontaneous condensation resulting in ring closure and conversion into ribityl lumazines unless they are trapped in their unstable form by binding to MR1[96] (Figure 1.2). A recent *in silico* screen for other MR1 ligands furthermore revealed that drug and drug-like molecules can be presented in the context of MR1[271]. While some of the novel MR1 ligands identified in this screen were capable of activating MAIT cells, others were MAIT cell antagonists[271]. In addition, *Streptococcus pyogenes* which does not express the enzymes needed for riboflavin synthesis has been shown to activate a T cell clone in an MR1-dependent manner, although the identity of this ligand has not yet been reported[273]. Consistent with this, the MR1 ligandome from *Escherichia coli* (*E.coli*) and *Mycobacterium smegmatis* (*M. smegmatis*) was found to comprise molecules that were not derivatives of 5-A-RU based on a comprehensive mass spectrometric analysis[270]. Thus, the complete spectrum of MR1 ligands remains to be determined. Interestingly, all MR1 ligands identified to date bind in the A'

pocket of the molecules whereas the F' pocket has consistently been found empty in crystal structures[269,272].

MR1 surface expression is tightly regulated and dependent on ligand availability[94]. This is exemplified by the extremely low MR1 surface expression of most human cell lines[267,274] despite ubiquitous expression of MR1 mRNA[268,275] at steady state. Moreover, intracellular levels of MR1 protein are higher than cell surface levels in a number of human cell lines[263,276], further supporting this conclusion. Nevertheless detectable levels of endogenous MR1 have been reported at the cell surface of a variety of human cells, most notably intestinal B cells[274] and the airway epithelial cell line BEAS-2B[262,277]. Over-expression of MR1 in cell lines with low endogenous protein levels has also been show to result in increased surface expression even in the absence of exogenous ligand[262,267,274,276]. As widely used tissue culture media such as RPMI-1640 contain folic acid and photodegradation products of this vitamin can stabilise MR1[95] it is generally assumed that this baseline expression is due to MR1 ligands present in the extracellular medium. Yet, when C1R cells over-expressing MR1 were cultured in folate-deficient medium MR1 surface expression was still increased compared to wild-type C1R[260]. A drastic change is observed when purified MR1 ligands are added to tissue culture medium: upon ligand binding MR1 rapidly translocates to the cell surface in a Brefeldin A-sensitive manner[260,262]. The extent to which MR1 surface expression increases in response to bacterial infection depends on both the kind of bacteria and the cell type infected[276,278,279]. This rapid change has recently been shown to be mediated by a molecular switch mechanism involving the neutralisation of the positive charge on the lysine residue K43 at the bottom of the

MR1 antigen binding cleft[94,260]. When this lysine residue is mutated to a neutral alanine (K43A), MR1 is constitutively expressed at the cell surface. However, when it is mutated to be constitutively positively charged (K48R), MR1 is retained in the ER even in the presence of stabilising ligand[260]. Furthermore, MR1 only co-immunoprecipitated with β_2m in the presence of ligand in this study, suggesting that ligand is required for stable association between MR1 and the light chain. These results are consistent with a model in which neutralisation of K43 by Schiff base formation with a ligand induces a conformational change in MR1 which allows it to assemble with β_2m and exit the ER.

How the ligand reaches the ER to flip this molecular switch is not known. Due to the hydrophobic nature of their side chains[95,96,271] it appears unlikely that the metabolites should be able to diffuse through cellular lipid bilayers but an ER transporter comparable to TAP for peptide import has not been identified[94,258,272]. Moreover, the chaperones that stabilise empty MR1 molecules in the ER and facilitate its loading are still to be identified. While MR1 associates with both members of the PLC (TAP, tapasin, ERp57, calnexin, calreticulin)[280] and the invariant chain[281] under some experimental conditions, the expression of all of these has been shown to be dispensable for MR1-mediated antigen presentation[264,278,281,282]. It is still unclear, therefore, how MR1 is protected from the degradation mechanisms of the unfolded protein response such as ER-associated degradation (ERAD) in the absence of ligand[272].

In addition, it has been postulated that not all MR1 ligands are loaded in the ER and may, thus, not require access to this compartment. Harriff *et al*. recently

identified cellular determinants of MR1-mediated antigen presentation of *M.tuberculosis*-derived ligands and found that a set of trafficking molecules differently affected the presentation of soluble ligand and microbe-derived ligand[277]. While knock-down of the ER-localised soluble NSF attachment receptor (SNARE) syntaxin 18 (Stx18), the endosome-associated SNARE vesicle-associated membrane protein 4 (Vamp4), and the small GTPase Rab6 all reduced the MAIT cell response to intact *M. tuberculosis*, only Stx18 also affected the surface translocation of MR1 in response to the soluble ligand 6-formylpterin (6-FP)[262]. Furthermore, the presentation of bacterial supernatant was inhibited by pre-treatment with 6-FP whilst presentation of intact bacteria was not[262]. In line with this, differential effects of inhibition of lysosomal acidification or phagocytosis have been reported for the presentation of soluble as compared to bacteria-associated antigen[276]. Together, these data are consistent with a model of endosomal loading for MR1 in the context of intracellular bacterial infection whereas exogenous, soluble ligand can be loaded in the ER[258].

The existence and identity of endogenous ligands which could mediate trafficking to the endosomal compartment either directly or via the plasma membrane remains to be established. Multiple strands of evidence suggest that such ligands exist: firstly, low levels of MR1 surface expression have been demonstrated on a variety of untransfected human cell lines in the absence of defined ligand[258,267,274,276]. Even C1R cells cultured in folate-deficient medium retained some surface expression of MR1 which was increased upon over-expression of the molecule[260]. In fact, this phenomenon has been used as an argument against the existence of an endogenous ligand reasoning that an endogenous ligand

would have to be produced in limiting quantities in order to be consistent with the prevalence of intracellular localisation over cell surface expression for MR1[94]. These two interpretations could be reconciled by an additional level of regulation which controls the egress of MR1 from the ER such as the existence of ligands that actively retain MR1 in the ER. Secondly, mutation of residues in the MR1 binding groove interfered with MR1 surface expression even in the absence of defined ligand, supporting the notion of an endogenous ligand being required for cell surface translocation under such circumstances[265]. Thirdly, autoreactive MR1-restricted T cells have been identified in healthy individuals[283] and MAIT cells were recently reported to reduce the viability of a colorectal cancer cell line in the absence of bacterial infection[284], lending further credibility to the existence of a non-microbial, host-derived class of MR1 ligands. The existence of such a self ligand(s) would also explain how MAIT cells are selected in the thymus *in utero* before exposure to the microbiome[258,285]. The identity of potential endogenous MR1 ligands is subject to intense investigations.

Furthermore, it remains to be determined whether and how MR1 ligand exchange in the endolysosomal compartment is catalysed and which proteins act as chaperones in this context. Of note, Schiff bases are relatively labile at low pH[286] which may facilitate ligand exchange in the acidic microenvironment of the endolysosomal compartment.

Another open question regards the regulatory mechanisms controlling MR1 trafficking, internalisation and potentially recycling[94]. The MR1 cytoplasmic tail

features neither a tyrosine based motif comparable to that found in CD1 cytoplasmic tails nor a lysine which could be ubiquitinated[268].

Based on the data available to date four potential loading mechanisms for MR1 have been proposed in a recent review which are not mutually exclusive[258]:

1. Soluble, exogenous ligand may encounter ligand-receptive MR1 in the ER which it can enter by an unknown mechanism.
2. Soluble, exogenous ligand may replace an endogenous ligand non-covalently bound to MR1 at the cell surface or an endogenous ligand bound via a Schiff base under the destabilising acidic conditions in the endolysosomal compartment.
3. Phagocytosed intact bacteria may encounter MR1 in an endolysosomal compartment after MR1 has been delivered there and microbe-derived ligand may replace the endogenous ligand that enabled the trafficking.
4. Bacteria infecting the cytoplasm may intersect with MR1 after autophagy and fusion with MR1-containing endolysosomal compartments.

The molecular machinery modulating any of the above pathways remains to be identified and is the subject of on-going efforts in the field (Table 1.1).

Table 1.1: Open questions in MR1-mediated antigen presentation Summary of selected aspects of the four known antigen presentation systems with an emphasis on aspects not resolved for MR1. MHC I = MHC class I, MHC II = MHC class II, PM = plasma membrane, MIIC = MHC class II-containing compartment, EC = endosomal compartment, MTP = Microsomal triglyceride transfer protein, AP = adapter protein.

	MHC I	MHC II	CD1	MR1
ligand	self or non-self peptide	self or non-self peptide	self or non-self lipid	exogenous metabolites
mode of ligand binding	non-covalent via anchor residues	non-covalent via anchor residues	non-covalent in hydrophobic tunnels	Schiff base with K43 or non-covalent
intracellular distribution at steady state	PM	MIIC	CD1a: PM + early EC CD1b: late EC CD1c: throughout EC CD1d: late EC	ER (and late EC)
chaperones stabilising empty conformation (during initial loading or exchange)	PLC, TAPBPR	HLA-DM	MTP, saposins, CD1e	**?**
ligand occupying antigen binding cleft to allow ER egress	self or non-self peptide	invariant chain	scaffold and spacer lipids	**?**
access to ligand	TAP-mediated ER import	direct delivery of MHCII to phagosomes	residency in EC	**?**
determinants of intracellular trafficking	complex stability and ubiquitination	dileucine motif of invariant chain and ubiquitination	tyrosine motif in cytoplasmic tail and AP binding	**?**

1.8 MR1-restricted T cells

MR1[268] and the T cell population now known as mucosal associated invariant T (MAIT) cells[282,287] were discovered separately and the restriction of these T cells by the non-classical MHC I-like molecule was only established in 2003[288]. In a key publication Treiner *et al.* showed that MAIT cells were activated by MR1 over-

expressing antigen presenting cells in a TCR-dependent manner. They further demonstrated that MAIT cells are dependent on both MR1 and the microbiota for their development[288]. Molecularly, this specialised T cell subset is characterized by high expression of the C-type lectin CD161[289,290] and the canonical Vα7.2-Jα33/12/20 TCR α chain[282,287,291] in humans. The use of a single TCR α chain paired with a limited number of TCRβ chains[282,287] forms the basis of its semi-invariant nature and mediates its restriction to MR1[292]. MAIT cells have been described as having effector memory cell features based on their $CD45RO^{+}$ $CD45RA^{-}$ $CD62L^{lo}$ $CD95^{hi}$ $CD122^{int}$ $CD127^{int}$ surface phenotype in adult blood and express chemokine receptors indicative of tissue-homing[282,290]. This is consistent with their enrichment in the intestinal lamina propria, liver, and other peripheral sites[288,290,293].

Since then, tetramer technology has revealed that the T cells restricted by MR1 are more clonally diverse than originally thought and include T cells expressing TCRs that do not contain the Vα7.2 segment[270,273,283,294]. Such non-canonical MR1-reactive T cells were either autoreactive[283,294], folate-reactive[294], or recognised a microbial ligand derived from a bacterium that does not express the enzymes of the riboflavin synthesis pathway[273]. Some $Vα7.2^{-}$ T cell clones also recognised riboflavin-derived ligand in the context of MR1[270,294] though with a TCR docking mode distinct from that of canonical MAIT cells[294]. The full repertoire as well as the physiological role of these clonally diverse MR1-restiricted T cells are the subject of on-going investigations. However, the most abundant T cell subset restricted by MR1 in humans remain MAIT cells.

1.8.1 The innate-like phenotype of MAIT cells

Owing to their restricted TCR repertoire, their relative abundance, and their effector-memory phenotype MAIT cells are counted towards the innate-like lymphocytes[295,296]. Their high numbers and poised phenotype allow them to rapidly carry out effector functions in response to their cognate microbial antigens and place them at the interface between the innate and the adaptive immune system[295,296].

Although initially identified and named after their enrichment in the gut lamina propria[288], MAIT cells are also highly abundant in human peripheral blood[290,291] and other mucosal sites such as the liver[290] and the lung[278,288]. In adult blood they make up 1-8% of circulating T cells[295] which is much higher than the frequency of comparable invariant T cell subsets such as invariant natural killer T (iNKT) cells[296]. In the liver, MAIT cells can constitute more than 40% of T cells[290,297] consistent with the high level of tissue homing markers expressed on their cell surface. In particular, MAIT cells express CCR5, CCR6, CXCR6, and CCR9 but not CCR7 which is associated with homing to lymphoid organs[290]. Interestingly, liver-resident MAIT cells display a more activated phenotype than MAIT cells in the blood based on the surface expression of CD69, CD38, and HLA-DR *ex vivo*[297], suggesting that MAIT cells at different anatomical locations may differ from each other. Consistent with this hypothesis, foetal MAIT cells in the small intestine were capable of producing IL-22 in response to a bacterial stimulus whereas those in the liver or lung were not[285] supporting a role for the local environment in shaping the MAIT cell phenotype. Furthermore, tissue-resident MAIT cells in the intestinal mucosa express elevated levels of both activation markers and inhibitory

receptors[298]. This likely reflects their continuous exposure to commensal bacteria and may represent a mechanism to prevent their uncontrolled activation under these conditions[298].

In humans, MAIT cells are characterised by the expression of a semi-invariant TCR composed of the Vα7.2 segment most commonly joined to the Jα33, Jα12, or Jα20 joining region[282,287,291] and paired with a limited number of Vβ chains, predominantly Vβ2 and Vβ13[282,291,293]. Interestingly, differences in Vβ chain usage have been shown to fine-tune the ligand specificity of the MAIT cell TCR[292,294,299]. For example, Gold *et al.* found that MAIT cells with distinct TCR Vβ clonotypes were activated in response to infection with three different bacteria *ex vivo*, suggesting that different clonotypes were specific for the MR1 ligands derived from *Mycobacterium smegmatis*, *Salmonella typhimurium*, or *Candida albicans*, respectively[299]. This is consistent with accumulating evidence that distinct MAIT TCR Vβ clonotypes expand within an individual over the course of infections with *Vibrio cholerae*[300], *Shigella flexneri*[301], *Salmonella enterica*[302,303], and *Mycobacterium tuberculosis*[304] in experimental human or non-human primate models. A pivotal role for the TCR Vβ chain in MAIT cell-mediated immunity is further supported by the finding that MAIT cells expressing different Vβ clonotypes secreted different cytokine combinations in response to the same pathogen[305]. The role of such differential recognition of microbial ligands during infections is currently being investigated.

In addition to their semi-invariant TCR, MAIT cells express a characteristic set of phenotypic markers at their cell surface. They are characterised by their high

expression of cytokine receptors for interleukin (IL) 7[297], IL-12, and IL-18[264,290] as well as CD26 and the C-type lectin CD161[264,289,290]. Importantly, MAIT cells are $CD45RA^{low}$ $CD45RO^{+}$ $CD62L^{low}$ $CD95^{high}$ $CD122^{mid}$ $CD127^{mid}$ reflecting their effector memory phenotype[282,290]. Their potential to rapidly exert effector functions upon antigen encounter is further underscored by their expression of perforin and granzymes A, B, and K upon activation[290,306]. Upon activation MAIT cells can contribute to the immune response both directly through lysing bacterially infected cells[293,301,306] and indirectly by the secretion of potent immunomodulatory cytokines such as interferon (IFN) γ, tumour necrosis factor (TNF) α, IL-2, IL-17, GM-CSF and MIP1β[95,290,293,297]. Furthermore, they have the capacity to induce the maturation of DCs via the CD40-CD40 ligand axis[307]. As a result, DCs secrete IL-12 which can transactivate NK cells[307]. In this way, MAIT cells shape the ensuing immune response beyond their own repertoire of effector functions.

Together, these features place MAIT cells in a powerful position to contribute to antimicrobial immunity. Indeed, antimicrobial activity is a hallmark of MAIT cells and they have been shown to be activated in response to cells infected with a variety of riboflavin-producing bacteria and fungi including *Candida albicans*, *Escherichia coli*, *Klebsiella pneumoniae*, *Mycobacterium tuberculosis*, *Pseudomonas aeruginosa*, *Saccharomyces cerevisiae*, *Salmonella enterica*, *Staphylococcus aureus*, *Streptococcus pneumoniae*, and *Vibrio cholerae*[264,278,300,308,309] (for a full list see reference [231]).

1.8.2 Clinical relevance of the MR1-MAIT cell antigen presentation axis

In humans the frequency of circulating MAIT cells is reduced in the context of many bacterial[264,278,302,303,310–312] and viral[313–315] infections and in some disease settings this has been shown to correlate with an accumulation of MAIT cells at the site of infection[304,316,317]. In addition, activated MAIT cells become more proliferative and expand in number[302–304]. Thus, both recruitment of circulating MAITs and proliferation of MAIT cells in the affected tissue appear to play a role in MAIT cell-mediated immunity. In mice accumulation of MAIT cells in the lung has been shown after infection with pulmonary pathogens such as *Klebsiella pneumonia* and *Francisella tularensis* and played an important role in the successful clearance of the pathogen[318,319]. Interestingly, administration of purified MR1 ligand only induced a comparable accumulation upon co-administration of TLR ligands, emphasising the importance of co-stimulatory signals for the MAIT cell immune response[320].

Recently MAIT cells have also been shown to be critical in the murine immune response to *Legionella longbeachae*, a causative agent of legionellosis and a significant health burden in the US and Autralasia[321]. Control of this pathogen was dependent on the accumulation of MAIT cells in the lung in both immune-competent and -deficient animals. MAIT cells were particularly potent in the latter case as adoptive transfer of MAIT cells into immunodeficient animals rescued these from lethal infection[321]. The mechanism of protection was dependent on MR1 as well as cytokines secreted by the activated MAIT cells including IFNγ and GM-CSF[321]. This is in line with the *Francisella tularensis* model in animals deficient of MR1, and hence MAIT cells[322]. Upon infection with the pathogen, these mice

exhibited delayed recruitment of conventional T cells due to a lack of GM-CSF at the site of infection[322]. Similarly, MAIT cells were associated with increased recruitment of immune cells in a mouse model of *Helicobacter pylori*-induced gastritis, but here this contributed to increased immunopathology and exacerbation of the disease[323]. Hence, MAIT cell activity can contribute to both protection and pathology.

According to the constraint metrics of the ExAC browser[324] the human MR1 gene is relatively tolerant to variation meaning that loss of its function does not significantly impact viability. However, this is also true for the CD1 genes and even HLA-A, suggesting that the effects of loss of function of this gene in isolation may be more subtle. Indeed, a single nucleotide polymorphism in the MR1 gene has been linked to increased susceptibility to *Mycobacterium tuberculosis*[325]. Moreover, the extremely high level of conservation among MR1 homologues[275] and the similarly highly conserved MAIT TCR[282,288] suggest that this antigen presentation system is likely to have been subject to strong evolutionary pressure.

Interestingly, MAIT cells are much more frequent in human peripheral blood than iNKT cells whereas the opposite is true in mice[282,290,295]. It has been suggested that they compete for the same thymic niche during development[326], providing a mechanistic basis for their inversely correlated frequencies. In light of this apparent co-regulation, it is conceivable that these two invariant T cell subsets could carry out overlapping functions.

Importantly, the *Legionella longbeachae* mouse model mentioned above revealed a more profound impact of the MR1-MAIT axis in immuno-deficient animals[321]. In this study, a significant effect of MR1/MAIT cell deficiency on bacterial growth control was evident sooner after pulmonary infection when $CD4^+$ were depleted compared to animals with a normal $CD4^+$ T cell compartment. Strikingly, adoptive transfer of MAIT cells into $Rag2^{-/-}\gamma C^{-/-}$ mice protected these animals from a lethal dose of the respiratory pathogen[321]. These results are consistent with a more critical role of this antigen presentation system in settings of heightened sensibility to infections. Indeed, a similar trend is observed in humans as MAIT cells have been shown to correlate with severity of pulmonary complications in patients with cystic fibrosis (CF)[310]. Similarly, hospitalised patients with lower MAIT cell frequency have been reported to be more likely to acquire additional infections nosocomially[312]. However, these data are correlative and it is not clear whether additional infections caused a loss of circulating MAIT cells or a lower MAIT cell frequency increased the susceptibility to disease exacerbation. Strikingly, Pincikova *et al.* reported a case study of a CF patient deficient of circulating MAIT cells who was unable to control bacterial infections to an extent beyond that normally seen with CF[327]. Other T cell subsets were unaltered in this patient[327] and while this case is the only one reported to date it lends further support to the notion that MAIT cells contribute to the control of microbial infections, particularly in settings of increased susceptibility.

Apart from infectious diseases MAIT cells have also been investigated in the contexts of cancer[328–331], sterile inflammation[332–334], and autoimmunity[335–337]. Emerging evidence suggests that they can participate in both protection and

pathogenesis in some circumstances and further investigations in these fields are warranted. Furthermore, a role for MAIT cell-mediated immunity in the context of viral infections is increasingly appreciated[338]. While MAIT cells are not activated by virally infected cells directly[264,278] they can be stimulated in a TCR-independent manner by combinations of cytokines such as IL-12 and IL-18[67]. The relevance of this cytokine-driven activation in the context of dengue, hepatitis C, and influenza virus infection was recently established[315,339]. Together, these findings open new avenues of research and constitute opportunities to reveal more therapeutic potential for the MR1-MAIT cell axis[329].

In conclusion, the MR1 antigen presentation pathway is an exceptionally attractive target for therapeutic biologics as the monomorphic nature of the presenting molecule renders it independent of individual variations in HLA expression. Hence, a treatment targeting this pathway could be mass-produced and used in patients across a wide variety of genetic backgrounds. The high frequency of MAIT cells in the blood and mucosal tissue further add to this attraction. Moreover, the presentation of small molecule metabolites as opposed to peptide antigens presents an additional advantage over traditional antigen presentation pathways, particularly in settings where classical peptide-specific T cells are unable to effectively resolve infection such as latent infections. A better understanding of this non-classical antigen presentation pathway is, thus, crucial for harnessing the protective potential of MAIT cells in such therapeutic approaches.

1.9 Research questions

In view of the many open questions with regard to MR1 trafficking and loading the work presented in this thesis set out to identify novel modulators of MR1 intracellular trafficking. Using both hypothesis-generating and targeted approaches the following research questions are addressed:

1. Which proteins modulate MR1 surface expression in the presence of soluble ligand?
2. How do these proteins affect MR1-mediated antigen presentation?
3. Does the SNARE Sec22b play a role in MR1 trafficking?
4. Is there a role for cellular riboflavin importers in MR1 ligand import?

These questions were addressed using a combination of genetic screening, RNASeq, flow cytometry, and cellular and biochemical approaches as described in the following chapters.

2
General Materials and Methods

2.1 Materials

Chemicals were generally purchased from Sigma-Aldrich. Some were from Thermo Scientific or VWR.

2.1.1 Cells

THP-1, C1R, and HEK293T cells were a kind gift from Mariolina Salio (RDM, University of Oxford, UK) and originally purchased from ATCC. JAWSII Sec22b KD and scramble control cells were a kind gift from Sebastian Amigorena (Institut Curie, PSL Research University, France). NY-ESO-reactive T cell clone 4D8 was kindly provided by Ji-Li Chen (RDM, University of Oxford, UK). HAP1 WT 1524 was kindly provided by Sebastian Nijman (NDM, University of Oxford, UK). MAIT cells were sorted from human PBMCs isolated from leukocyte cones obtained from the NHS Blood and Transplant Unit as described below. This work was covered by HTA licence number 12433.

2.1.2 Tissue Culture and Cellular Assay reagents

Components of Media	Catalogue Number	Supplier
RPMI-1640	R8758-500ML 21875-034	Sigma-Aldrich or Gibco
IMDM	21980032	Gibco
DMEM	D5796-500ML	Sigma-Aldrich
Foetal Calf Serum (FCS)	10500-064 F9665	Gibco or Sigma-Aldrich
Human Serum	-	pool of serum from 15 Blood Bank donors
200 mM L-Glutamine	G7513-100ML	Sigma-Aldrich
Penicillin-Streptomycin (10 000 U/ml penicillin + 10 mg/ml streptomycin)	P0781-100ML	Sigma-Aldrich
100x Non-essential amino acids	11140-035	Gibco
100 mM Sodium Pyruvate	11360-039	Gibco
1 M HEPES	15630-056	Gibco
50 mM β-mercaptoethanol	31350-010	Gibco
Human IL-2	-	this lab (produced as previously described[340])
Recombinant Murine GM-CSF	315-03	PeproTech
phytohaemagglutinin (PHA)	R30852801	Thermo Scientific

Tissue Culture Reagents	Catalogue Number	Supplier
1x Phosphate Buffered Saline (PBS)	J61196 BE17-516F K812-500ML	Alfa Aesar or Lonza or VWR
HBSS, with calcium and magnesium	24020091	Life Technologies
Ethylenediaminetetraacetic acid (EDTA) - 0.5 mM	E522-100ML	VWR
0.05% Trypsin+EDTA	25300-054	Gibco
Trypan Blue	15250-061 T10282	Gibco or Life Technologies
RBC Lysis Buffer	1045722	QIAGEN
Lymphoprep	1116508	Alere Technologies
Dimethyl sulfoxide (DMSO)	D2650-100ML	Sigma-Aldrich
Gentamycin	BE02-012E	Lonza
Puromycin	A11138-03	Gibco
Recombinant Human IL-12	130-096-704	Miltenyi Biotec
Recombinant Human IL-18	9124-IL	Bio-Techne (R&D Systems)

Cellular Assay Reagents	Catalogue Number	Supplier
Manganese(II) chloride 0.1 M Solution	48795-1ML-F	Sigma-Aldrich
X-tremeGENE 9 DNA Transfection Reagent	06365779001	Roche
TurboFectin 8.0	TF81001	Origene Technologies
Lipofectamine 2000 Transfection Reagent	11668019	Invitrogen
Opti-MEM I Reduced Serum Medium	31985062	Life Technologies

Acetyl-6-formylpterin (Ac6FP)	11.418	Schirks Laboratories
5-amino-6-D-ribitylaminouracil (5-A-RU)	-	kind gift from Gurdyal Besra (University of Birmingham, UK) synthesised as in[307]
Bacillus Calmette–Guérin (BCG) SSI strain	-	Statens Serum Institute
αMR1 blocking antibody (clone 26.5)	-	HIU lab management (purified from hybridoma supernatant)
IgG2a control antibody	-	HIU lab management (purified from hybridoma supernatant)

Tissue culture plastic was from Corning or Greiner Bio-One.

2.1.3 Composition of Tissue Culture Media and Buffers

Medium/Buffer	**Composition**
supplement mix	2 mM Glutamine 1 mM Sodium Pyruvate 1x Non-essential amino acids 100 U/ml penicillin + 100 µg/ml streptomycin 10 mM HEPES 50 µM β-mercaptoethanol
R10	RPMI-1640 10% FCS supplement mix
I10	IMDM 10% FCS 100 U/ml penicillin + 100 µg/ml streptomycin

D10	DMEM 10% FCS supplement mix
T cell medium	IMDM 10% human serum (FCS for Sec22b experiments) approximately 5000 U/ml IL-2 supplement mix
$RPMI_H$	RPMI-1640 10 mM HEPES
PBSE	PBS 1 mM EDTA
FLOW	PBS 10% FCS
FLOWE	PBS 10% FCS 2 mM EDTA
ELISA Coating Buffer	0.1 M NaHCO3, ph ≈8
ELISA Developing Solution A	10 mM citric acid monohydrate
ELISA Developing Solution B	250 mM Na2HPO4 · 2H2O
Co-IP Lysis Buffer	50 mM Tris pH 7.5 150 mM NaCl 1 mM EDTA 0.5% NP40 (IGEPAL CA-630)
PBST	PBS 0.1% Tween (some Western Blots washed in 0.5%)
Blocking Buffer	PBS 0.1% Tween 5% BSA

2.1.4 Flow Cytometry, Cell Sorting, and MACS Sorting reagents

Flow Cytometry and MACS reagents	**Catalogue Number**	**Supplier**
MACS LS columns	130-042-401	Miltenyi Biotec
CD2 Microbeads, human	130-091-114	Miltenyi Biotec
PE Microbeads	130-048-801	Miltenyi Biotec
live/dead stain (aqua)	L34966 423101	Life Technologies or BioLegend
Propidium Iodide	P4864	Sigma-Aldrich
gammanorm 16.5% (165 mg/ml) normal immunoglobulin (as Fc block)	-	octopharma
Fc Receptor Binding Inhibitor Antibody	14-9161-73	eBioscience
TruStain fcX™ (anti-mouse CD16/32)	101320 101301	BioLegend or BioLegend
Intracellular Staining (ICS) Fixation Buffer	00-8222-49	eBioscience
10x Permeabilisation Buffer	00-8333-56	eBioscience
BD Falcon 35um Cell Strainer in 2x75mm Polystyrene Tube	352235	Corning
OneComp eBeads Compensation Beads	01-1111-42	Life Technologies
Paraformaldehyde (PFA)	RT-15710	Electron Microscopy Sciences

Antibodies	Fluorophore	Cat. No.	Supplier
MR1 (clone 26.5)	APC	361108	BioLegend
IgG2a control	APC	400222	BioLegend
HLA-ABC (clone W6/32)	FITC	311403	BioLegend
HLA-ABC (clone W6/32)	APC-Cy7	311425	BioLegend
HLA-ABC (clone G46-2.6)	FITC	555552	BD Biosciences
CD69	eFluor450	48-0699-42	eBioscience
CD25	APC	555434	BD Biosciences
CD2	PE	12-0029-42	eBioscience
CD3	eFluor780	47-0036-42	eBioscience
CD161	APC	17-1619-42	eBioscience
Vα7.2 TCR	BV605	351720	BioLegend
Vα7.2 TCR	PE	351705	BioLegend
Vβ2 TCR	PE	130-110-095	Miltenyi Biotec
H-2K^{b}	FITC	116505	BioLegend
IgG2a control	FITC	400210	BioLegend
MR1 (clone 26.5)	-	-	HIU lab management (purified from hybridoma supernatant)
IgG2a control	-	-	HIU lab management (purified from hybridoma supernatant)
MR1 (polyclonal)	-	13260-1-AP	Proteintech

Goat αmouse secondary antibody	AlexaFluor488	A-11001	Life Technologies
Goat αrabbit secondary antibody	AlexaFluor647	A-21245	Life Technologies

2.1.5 Enzyme-linked immunosorbent assay (ELISA) reagents

ELISA Reagents	**Catalogue Number**	**Supplier**
96 Well Half-Area Microplate	3690	Corning
IFNy capture antibody	551221	BD Biosciences
IFNy detection antibody	554550	BD Biosciences
avidin-peroxidase (1 mg/ml)	A3151-1MG	Sigma-Aldrich
o-Phenylenediamine dihydrochloride (5 mg/tablet)	P3804-50TAB	Sigma-Aldrich
30% H_2O_2	H1009-100ML	Sigma-Aldrich
10x PBS	J62036	Alfa Aesar
IFNy standard	300-02	PeproTech
H_2SO_4	35276-1L	Fluka

2.1.6 Western Blot reagents

Western Blot Reagents	**Catalogue Number**	**Supplier**
RIPA Buffer	R0278-50ML	Sigma
Protease inhibitor	4693159001	Roche

Pierce BCA Protein Assay Kit	23225	Thermo Scientific
BSA standard (2 mg/ml)	23209	Thermo Scientific
4x Loading Buffer	NP0007	Invitrogen
10x Reducing Agent	NP0009	Invitrogen
Precision Plus Protein Dual Colour Standard	1610374	Bio-Rad
HiMark Pre-Stained Standard	LC5699	Invitrogen
3-8% Tris-Acetate gels	EA0378BOX	Life Technologies
4-12% Bis-Tris gels	WG1402BOX NP0321BOX NP0335BOX NP0336BOX NW04122BOX	Life Technologies or Life Technologies or Life Technologies or Life Technologies or Life Technologies
10% Bis-Tris gels	NW00105BOX NP0302BOX NP0315BOX	Life Technologies or Life Technologies or Life Technologies
20x MES SDS Running Buffer	NP0002	Invitrogen
20x MOPS SDS Running Buffer	NP0001	Invitrogen
Trans-Blot® Turbo™ Mini PVDF Transfer Packs	1704156	Bio-Rad
Trans-Blot® Turbo™ Mini Nitrocellulose Transfer Packs	1704158	Bio-Rad
Trans-Blot® Turbo™ Midi PVDF Transfer Packs	1704157	Bio-Rad
Bovine Serum Albumin (BSA, powder)	A9418-50G BP704-100	Sigma or Fisher Scientific
Tween 20	233360010	Acros Organics

Pierce Protein G Agarose		20398	Thermo Scientific

Antibodies	**host**	**Cat. No.**	**Supplier**
GAPDH	mouse	sc-32233	Santa Cruz
GAPDH	rabbit	5174S	Cell Signaling Technology
ACTB	mouse	sc-47778	Santa Cruz
MR1 (routinely used)	rabbit	13260-1-AP	Proteintech
alternative MR1 (for validation)	mouse	H00003140-M03	Bio-Techne (R&D Systems)
β2-microglobulin (routinely used)	rabbit	ab75853	Abcam
β2-microglobulin (clone BBM.1, also tested)	mouse	-	HIU lab management (purified from hybridoma supernatant)
ATP13A1 (routinely used)	rabbit	16244-1-AP	Proteintech
ATP13A1 (also tested)	goat	PA518860	Thermo Fisher
GANAB	rabbit	NB100-1387	Bio-Techne (R&D Systems)
VAC14	rabbit	15771-1-AP	Proteintech
GRIK2	rabbit	HPA014623	Atlas Antibodies
VPS29	goat	NB100-1387	Bio-Techne (R&D Systems)
REPS1	rabbit	6404S	Cell Signaling Technology
SPPL3	rabbit	NBP1-57070	Bio-Techne (R&D Systems)
ZCCHC11	rabbit	18980-1-AP	Proteintech

RALGAPB	rabbit	TA331831	Origene Technologies
ZCCHC14 (used in blot shown)	rabbit	ab116394	Abcam
ZCCHC14 (also tested)	rabbit	NBP1-71852	Bio-Techne (R&D Systems)
TMEM131	rabbit	NBP1-21369	Bio-Techne (R&D Systems)
CUL-3	mouse	sc-166110	Santa Cruz
RAB10	mouse	sc-101429	Santa Cruz
HERPUD1	rabbit	ab150424	Abcam
MHC I (clone HC10)	mouse	-	HIU lab management (purified from hybridoma supernatant)
Sec22b	mouse	sc-101267	Santa Cruz
SLC52A2 (used in the blot shown)	rabbit	PA5-39700	Thermo Fisher
SLC52A2 (also tested)	rabbit	orb319088	Biorbyt Ltd
IRDye 680RD Goat anti-Mouse IgG (H + L)		P/N 925-68070	LI-COR
IRDye 800CW Goat anti-Rabbit IgG (H + L)		P/N 925-32211	LI-COR
IRDye 800CW Donkey anti-Goat IgG (H + L)		P/N 925-32214	LI-COR
IRDye 680RD Donkey anti-Mouse IgG (H + L)		P/N 925-68072	LI-COR

2.1.7 Molecular Biology reagents

Vectors	Encoded Protein(s)	Source
pCMVR8.91	gag/pol	Mariolina Salio (RDM, University of Oxford, UK; as in Palmowski *et al*.[341])
pMDG	vsv-g	Mariolina Salio (RDM, University of Oxford, UK; as in Palmowski *et al*.[341])
pHR-SIN-IRES-Emerald	empty expression vector backbone	Hemza Ghadbane (RDM, University of Oxford, UK; as in Palmowski *et al*.[341])
pHR-SIN-MR1-IRES-Emerald	hMR1 + GFP	Lauren Howson (RDM, University of Oxford, UK)
pCK001 (pHR-SIN-MR1)	hMR1 without GFP	this thesis
pCK002 (pHR-SIN-mSec22b-IRES-Emerald)	mSec22b + GFP	this thesis
pLV[Exp]-Bsd-{sffv}>hATP13A1 [NM_020410.2]	hATP13A1	VectorBuilder

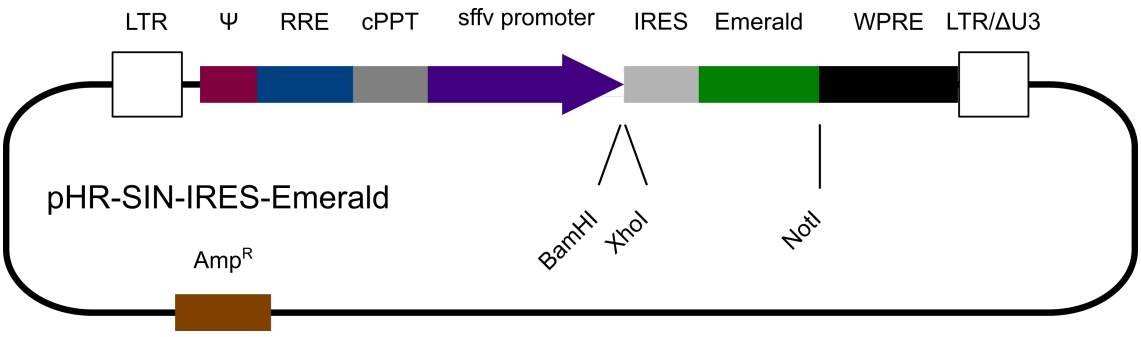


Figure 2.1: Vector map of pHR-SIN-IRES-Emerald. Schematic representation of the pHR-SIN-IRES-Emerald backbone previously generated and originally based on Demaison *et al*.[342]. LTR = long terminal repeat, Ψ = psi packaging sequence, RRE = rev response element, cPPT = central polypurine tract, sffv = spleen focus corming virus, IRES = internal ribosome entry site, WPRE = Woodchuck hepatitis virus posttranscriptional regulatory element, Amp^R = ampicillin resistance gene. Restriction site for the enzymes used in this thesis are indicated. Figure not drawn to scale.

Molecular Biology Reagents	Catalogue Number	Supplier
Dneasy Blood and Tissue Kit	69506	QIAGEN
Proteinase K	AM2546	Ambion
Phusion High-Fidelity DNA Polymerase	M0530S	NEB
dNTP mix (10 mM each)	R0191 N0447L 18427-013	Thermo Fisher or NEB or Invitrogen
DMSO	B0515A	NEB
Agarose	A6877-100G	Sigma Aldrich
10x TBE	T4415-1L	Sigma Aldrich
SYBR Safe	S33102	Invitrogen
Hyper Ladder I	BIO-33053	Bioline
2-Log DNA Ladder (1-100 kb)	N3200S	NEB
Quick-Load Purple 100 bp DNA Ladder	N0551S	NEB
Gel Extraction Kit	28704	QIAGEN
XhoI	R0146	NEB
NotI	R0189	NEB
BamHI	R0136	NEB
T4 DNA Ligase	M0202S	NEB
Luria Broth (LB)	L7658	Sigma Aldrich
LB Broth with agar	L7533	Sigma Aldrich
Ampicillin	A9518	Sigma-Aldrich

QIAprep Spin Miniprep Kit	27104	QIAGEN
QIAfilter Plasmid Midi Kit	12243	QIAGEN
D1000 ScreenTape	5067-5582	Agilent Technologies
D1000 Ladder	5067-5586	Agilent Technologies
D1000 Sample Buffer	5067-5586	Agilent Technologies
Optical Strip Tubes + Caps	401425	Agilent Technologies
Loading Tips for TapeStation	5067-5153	Agilent Technologies
Agincourt Ampure XP beads	A 63881	Beckman Coulter
DH5α bacteria	-	Mariolina Salio (RDM, University of Oxford, UK); originally from Invitrogen
Competent DH5α bacteria ($CaCl_2$ treated)	-	Prathiba Kurupati (RDM, University of Oxford, UK); originally from Invitrogen
Stbl3 bacteria encoding ATP13A1 expression vector	Ecoli(VB180302-1366maw)	VectorBuilder

2.1.8 Quantitative Real Time (qRT)-PCR reagents

qRT-PCR Reagents	**Catalogue Number**	**Supplier**
RNeasy Mini Kit	74104	QIAGEN
RNase-Free DNase Set	79254	QIAGEN
RNAqueous-Micro Total RNA Isolation Kit	AM1931	Ambion
SMARTScribe Reverse Transcriptase	639537	Takara Bio

RETROscript Reverse Transcription Kit	AM1710	Ambion
MicroAmp Fast Optical 96-Well Reaction Plate with Barcode	4346906	Life Technologies
MicroAmp Optical Adhesive Film	4311971	Life Technologies
TaqMan Fast Advanced Master Mix	4444557	Life Technologies

Taqman probes

HPRT	Hs02800695_m1
ACTB	Hs01060665_g1
GAPDH	Hs02758991_g1
MR1 (routinely used)	Hs00155420_m1
MR1 (alternative)	Hs01042278_m1
ATP13A1	Hs00220755_m1
B2M	Hs99999907_m1
IFIT1	Hs01911452_s1
IFNB	Hs02621180_s1
SEC22B	Hs00191681_m1
SLC52A1	Hs00606016_g1
SLC52A2	Hs04194586_s1
SLC52A3	Hs00364295_m1
mHPRT	Mm03024075_m1
mSEC22B	Mm04208139_g1
mMR1	Mm01295591_m1

2.2 Methods

Experiments were generally carried out as described below unless stated otherwise in Chapter specific Materials and Methods or Figure captions.

2.2.1 Tissue culture

Cells were kept at 37° C with 5% CO_2 .THP-1 and C1R cells and their derivatives were cultured in R10, HAP1 cells and their derivatives were cultured in I10, and HEK293T cells were cultured in D10. For JAWSII culture conditions see Chapter 5. Sorted human MAIT cells and T cell clone 4D8 were cultured in T cell medium. T cell clone 4D8 was expanded with irradiated feeder cells. For this, PBMCs from two donors were irradiated by Biomedical Services staff for at least 15 min, combined, and diluted to $5x10^6$/ml before addition of 2 µg/ml PHA. Cells were sub-cultured every 2-4 days depending on confluency. Adherent cells were detached using either PBSE or Trypsin-EDTA. JAWSII cells were harvested with cell scrapers after treatment with Trypsin-EDTA. Cell counts were obtained by manual counting in a Neubauer improved bright line haemocytometer (Paul Marienfeld) after dilution in Trypan Blue. Occasionally, THP-1 cells were counted using a Countess automated cell counter (Life Technologies). Cells were stored in 10% DMSO in FCS in liquid nitrogen storage tanks for long term storage. Cells were generally pelleted at ca. 525 or 425 x g (1 500 rpm in a TX-1000 or TX-400 rotor, respectively) for 5 min in a Heraeaus Megafuge 40R or 16 (both Thermo Scientific) at RT. Cells were tested for mycoplasma contamination as appropriate.

2.2.2 PBMC isolation and MAIT cell sorting

Leukocyte cones were obtained from the NHS Blood and Transplant Unit and diluted in $RPMI_H$ HEPES to a final volume of 120 ml. 30 ml of diluted blood were layered on top of 15 ml Lymphoprep in four 50 ml Falcon tubes each and centrifuged at ca. 850 x g (2 000 rpm in a 6445 rotor in a Multifuge3 S-R) for 30 min at RT with minimal acceleration and deceleration. PBMCs were collected from the intermediate layer into $RPMI_H$ with a Pasteur pipette and pelleted at ca. 525 or 425 x g (1 500 rpm in a TX-1000 or TX-400 rotor, respectively) for 15 min at RT. Cells were resuspended in $RPMI_H$ and pelleted at ca. 230 or 190 x g (1 000 rpm in a TX-1000 or TX-400 rotor, respectively) for 10 min at RT before resuspension in FLOWE Buffer. In parallel to PBMC isolation 1 ml of diluted blood was lysed in RBC Lysis Buffer and surface stained for MAIT cell markers as described below. Samples with suitable MAIT cell numbers were enriched for $CD2^+$ cells by MACS sorting according the manufacturer's protocol. In brief, cells were incubated with CD2 MACS beads on ice, washed in FLOWE Buffer and run over LS columns. Enriched samples were >95% positive for CD2 as determined by flow cytometry. Cells were stored in FLOW Buffer at 4° C o/n before surface staining for CD3, CD161 and the Vα7.2 TCR as described below (without live/dead stain and Fc block). Stained cells were strained into cell strainer cap tubes and $CD3^+$ $Vα7.2^+$ $CD161^{high}$ cells sorted on a FACSAria Fusion or FACSAria III sorter (both BD Biosciences) in the WIMM Flow Cytometry Facility. Sort purity was always >92%. A representative gating strategy can be found in Supplementary Figure 1. On one occasion, cells were additionally stained with Vβ2 TCR antibody and only MAIT cells co-expressing Vα7.2 and Vβ2 were sorted. It is specified in the Figure captions when these cells were used. The $Vβ2^+$ cells

were kindly provided by Mariolina Salio. Once MAIT cells were enriched by staining whole PBMCs with CD161-APC and Vα7.2-PE antibody and MACS sorting with PE microbeads immediately before cell sorting but MAIT cell yields were not as good as with the two-step protocol described above.

2.2.3 Molecular Biology and Cloning

To generate THP-1 and C1R cell lines over-expressing human MR1 without losing a fluorescence channel, the Emerald open reading frame (ORF) was removed from the pHR-SIN-MR1-IRES-Emerald lentiviral expression vector previously generated in this laboratory by Lauren Howson (RDM, University of Oxford, UK). A map of the empty vector backbone can be found in Figure 2.1. To this end, the vector was digested with XhoI and NotI endonucleases and the Emerald coding sequence was replaced with a 21 basepair adapter designed to include a BamHI restriction site to enable screening by PCR. Adapter oligonucleotides were briefly heated to 95° C and annealed on ice before ligating into the gel-purified cut plasmid with T4 ligase. Ligations were transformed into competent DH5α bacteria prepared by Prathiba Kurupati (RDM, University of Oxford, UK) and spread on ampicillin-containing agar plates. Colonies were screened by PCR according to the general PCR conditions specified below and sequences confirmed by Sanger sequencing (HIU Sequencing Facility, University of Oxford, UK). For the murine Sec22b expression vector the murine Sec22b cDNA sequence was cloned into the empty pHR-SIN-IRES-Emerald backbone kindly provided by Hemza Ghadbane (RDM, University of Oxford, UK) using BamHI and XhoI as described in Chapter 5. Vectors were purified using QIAGEN Mini or Midi prep kits according to the

manufacturer's protocol. All oligonucleotide sequences can be found in Supplementary Table 1.

PCR reaction

5x Phusion Buffer	5 µl
Phusion Taq Polymerase	0.25 µl
Forward primer (5 µM)	2.5 µl
Reverse primer (5 µM)	2.5 µl
dNTP mix (10 mM)	0.5 µl
DMSO	0.75 µl
template	x µl
PCR grade water	to 25 µl

PCR cycles

95° or 98° C	1:00 min	x 1
95° or 98° C	0:20 min	
52 - 65°C	0:30 min	x 35
72° C	0:30 – 2:00 min	
72° C	5:00 or 10:00 min	x 1
4° C	∞	

Annealing temperature and extension times were adapted depending on primers and size of the amplicon.

The lentiviral expression vector for human ATP13A1 was purchased from VectorBuilder as a bacterial stock and the identity of the coding sequence verified by Sanger sequencing (HIU Sequencing Facility, University of Oxford, UK). Bacteria were stored in 20% Glycerol in LB at -80° C for long term storage.

For sequencing of CRISPR clones, DNA was extracted using the QIAGEN Blood and Tissue Kit in combination with Ambion Proteinase K. PCR reactions were carried out according to the general protocol outlines above and amplicons were analysed either on 0.8, 1, or 2.0% agarose gel with SYBR Safe or on the Agilent

2200 TapeStation System. Gels were prepared and run in 1x TBE and DNA was extracted with the QIAGEN gel purification kit. Alternatively, PCR reactions were cleaned up with Agincourt Ampure XP beads where applicable. Amplicons and plasmids were sent for Sanger sequencing at the HIU Sequencing Facility and sequences were analysed with SnapGene Viewer (GSL Biotech) and SerialCloner (SerialBasics).

2.2.4 Lentiviral particles and Transductions

For production of lentiviral particles, $3x10^6$ HEK293T cells were seeded into a tissue culture flask and left to adhere o/n. 1.5 µg of packaging vectors encoding gag/pol (pCMVR8.91)[341] and vsv-g (pMDG)[341], respectively, were combined with 2.3 µg of lentiviral expression vector (pHR-SIN-IRES-Emerald backbone[342] with ORF of interest) in endotoxin free water to a final volume of 50 µl. 200 µl Opti-MEM were mixed with 30 µl XtremeGene9, added to the DNA mix drop-wise, and incubated for 15 min at RT. Medium on HEK293T cells was replenished with fresh D10 before addition of the DNA-transfection reagent mix. After 3 days supernatants containing viral particles were centrifuged at ca. 525 or 425 x g (1 500 rpm in a TX-1000 or TX-400 rotor, respectively) for 15 min and used to transduce target cells. Lentiviral particles encoding for shRNAs were purchased directly from Sigma-Aldrich and used for transduction according to the manufacturer's protocol. Sequences of the shRNA target sites can be found in Supplementary Table 1.

50 or 60 000 target cells/well were transduced in <1 ml medium + 1 or 1.5 ml viral particle-containing supernatant in 24-well tissue culture plates. Less volume of viral particle-containing supernatant was used for the Sec22b rescue titration. After 18 – 24 h 500 µl of the supernatant were replaced with 1 ml of fresh medium. MR1 over-expressing cell lines were cell sorted on a Sony SH800 cell sorter based on MR1 surface expression. Cells transduced with lentiviral particles encoding shRNAs were selected with 3 µg/ml puromycin on day 3 after transduction.

2.2.5 Flow Cytometry

Cells were harvested by pipetting and washed in PBS or detached with PBSE, transferred to round-bottom 96-well plates, and pelleted by centrifugation at ca. 525 x g (1 500 rpm in a TX-1000 rotor) for 2-5 min. Cells were resuspended in 10 µl aqua live/dead stain diluted 1:200 in PBS and incubated for 10 min at RT in the dark. After this step all incubations were carried out in the dark.

For surface staining, cells were washed with 200 µl FLOW Buffer and blocked in 5 µl or 10 µl Fc block diluted 1:5 in FLOW Buffer for at least 20 min on ice. If cells were resuspended in 5 µl Fc block antibody mix was added in 5 µl diluted in FLOW Buffer; if cells were in 10 µl Fc block they were split into two wells and 5 µl of primary antibody mix containing either the target antibody or the isotype control antibody. Murine cells were Fc blocked in 20 µl and antibodies were added straight into the Fc block. Samples were not Fc blocked when analysing MAIT cell activation in response to murine JAWSII cell lines and antigen presenting cells were excluded based on FSC vs SSC. Cells were stained on ice for at least 20

min, washed with 200 µl FLOW Buffer, and resuspended in 200 µl fresh FLOW Buffer. When applicable cells were fixed in 2% PFA for at least 20 min at RT before acquisition. For analysis on CyAn or Fortessa analysers cells were transferred to Mini Flow Cytometry tubes. FLOWE Buffer was used throughout the procedure for HAP1 cell lines. On occasion, 10 µl of 10% PI were added to samples just before acquisition instead of staining with aqua live/dead stain.

For intracellular staining, cells were fixed in 100 µl/well of ICS Fixation Buffer for 30 min at RT. Cells were pelleted, the fixative removed, and 200 µl/well of 1x Permeabilisation Buffer added for 10 min at RT. Cells were Fc blocked with the Fc block diluted in 1x Permeabilisation Buffer for at least 20 min on ice. Antibody mixes were added and cells stained for at least 20 min on ice. Cells were washed once in 1x Permeabilisation Buffer and once in FLOW Buffer before resuspension in 200 µl of FLOW Buffer.

Cells stained with unconjugated primary antibody were washed three times in FLOW Buffer or Permeabilisation Buffer depending on the protocol before incubation with 10 µl of secondary antibody diluted in the respective buffer for at least 20 min on ice. Stained cells were washed and prepared for analysis as above.

Single colour controls were either cells or Compensation Beads. One drop of beads was incubated with the same amount of antibody as one well of cells, stained on ice for 15 min, and washed in PBS. Beads were pelleted at ca. 9 500 or

16 000 x g (10 000 or 13 000 rpm in a VWR Microstar 17 tabletop centrifuge) for 2 min and resuspended in PBS.

Cells were analysed on an Attune NxT analyser equipped with four lasers (Life Technologies), a CyAn ADP analyser (Beckman Coulter) or an LSR Fortessa X50 fitted with five lasers (BD Biosciences) in the WIMM Flow Cytometry Facility and data were analysed and displayed using FlowJo v9 or v10 (FlowJo). Y-axes of histograms show modal counts and x-axes are in logarithmic or biexponential scale except for FSC and SSC which are on a linear scale.

2.2.6 Enzyme-linked immunosorbent assay (ELISA)

Half-area 96-well plates were coated with 25 µl/well of capture antibody diluted 1:250 in Coating Buffer at 4° C o/n or for 2 h at 37° C, sealed with self-adhesive film. Plates were washed four to six times in PBST and blocked with FLOW Buffer for at least 20 min at RT. Blocking buffer was removed and 25 µl of culture supernatant added in an appropriate dilution. IFNγ standard was diluted in a 2-fold dilution series in FLOW Buffer from a starting concentration of either 8 or 20 ng/ml. Supernatants were incubated at 37° C for 2-3 h or at 4° C o/n. Plates were washed six times in PBST and 25 µl/well of detection antibody diluted 1:500 in FLOW Buffer was added for 45 min – 1 h at RT. Plates were washed as before and 25 µl/ well of avidin-peroxidase diluted 1:400 in FLOW Buffer was added for 30 min at RT. Plates were washed six times in PBST and once in PBS before addition of 25 µl/well of Developing Solution (2.45 ml Developing Solution A + 2.55 ml Developing Solution B + one 5 mg phenylenediamine tablet and 20 µl 20%

H_2O_2 after the tablet dissolved). 25 µl 2 M H_2SO_4 were added to each well when the standard curve had fully developed and colour intensity was measured at 490 nm in an iMark plate reader (Bio-Rad) and quantified using a 4-parameter standard curve.

2.2.7 Western Blots

To make protein lysates cells were washed in PBS, pelleted, and either resuspended in Co-IP Lysis Buffer supplemented with protease inhibitors, incubated on ice for at least 30 min, and pelleted at ca. 11 500 x g (11 000 rpm in a HEREAEUS Fresco 17 tabletop centrifuge) for 10 min 4° C or resuspended in RIPA buffer supplemented with protease inhibitors, end-over-end rotated at 4° C for at least 30 min, and pelleted at 16 000 x g for 20 min at 4° C. Protein-containing supernatants were collected into fresh tubes and quantified with the Pierce BCA protein assay kit using a two-fold dilution curve of BSA as a standard.

Samples were prepared in 1x Loading Buffer and 1x Reducing Agent to contain equal amounts of protein, boiled at 95° C for at least 5 min, and loaded onto a gel according to their size. Generally, proteins with a molecular weight (MW) below 100 kDa were separated on 4-12% Bis/Tris gels in MES SDS Buffer and proteins with a molecular weight above 100 kDa were separated on 3-8% Tris/Acetate gels in MOPS Buffer. Appropriate MW markers were included. Gels were run at 200V for about 50 min depending on the size of protein, transferred onto a PVDF or nitrocellulose membrane of appropriate size using the TransBlot Turbo Transfer system, and blocked in Blocking Buffer for at least 30 min at RT, shaking. Blocking

Buffer was poured off and membrane cut to size for incubation with different primary antibodies. Membrane fragments were transferred into primary antibody diluted in fresh blocking buffer and incubated at 4° C o/n with agitation.

Membranes were washed five times for at least 5 min or three times for at least 15 min in PBST, incubated with LI-COR® secondary antibodies diluted 1:20 000 in Blocking Buffer for 45 min – 1 h with agitation, washed as before, and dried between tissues before imaging with the Odyssey® Near-Infrared imaging system. Any adjustments to the minimum and maximum points of the display mapping to increase contrast were applied to the entire image shown for each blot. For protein quantification, shapes were drawn around the bands and the median signal intensity controlled for the left/right background was extracted for further analysis.

2.2.8 Co-immunoprecipitiations

The appropriate volume of Protein G agarose resin was washed three times in Co-IP Lysis Buffer and resuspended in Co-IP Lysis Buffer to the original volume. 50 µl of resin were added to each protein lysate for pre-clearing. In parallel, 50 µl of resin per condition were pooled and incubated with equal amounts of αMR1 antibody clone 26.5 or IgG2a isotype control antibody (1.2 mg of antibody per 50 µl of beads). All samples were incubated at 4° C o/n with end-over-end rotation. Antibody-coated beads were split into the appropriate number of tubes and spun at ca. 16 000 x g (13 000 rpm in a HEREAEUS Fresco 17 tabletop centrifuge) for 1 min at 4° C. Supernatants were removed and lysates were added. Samples were incubated at 4° C for at least 4 h with end-over-end rotation and then washed three times in Co-IP Lysis Buffer. Proteins were eluted from the resin by adding a

2x concentrated mixture of Loading Buffer and Reducing Agent and boiling at 95° C for at least 5 min. Proteins were analysed by SDS PAGE as above. For the Sec22b/MR1 Co-immunoprecipitation, cells were lysed in Lysis Buffer containing 20 mM Tris HCl and 1% digitonin instead of NP40.

2.2.9 qRT-PCRs

RNA was extracted from cells using either the QIAGEN RNeasy kit or the Ambion RNAqueous kit according to the manufacturer's instructions including the on-column DNase digestion for the QIAGEN kit and the DNase digestion protocol for the Ambion kit. RNA was quantified by Nanodrop (Thermo Scientific) and equal amounts of RNA were reverse transcribed using one of the kits listed in the Materials section. Only cDNA transcribed with the same kit was directly compared in qRT-PCR reactions. "no RT" and "no RNA" controls were included in all experiments. cDNA was diluted to 10 ng in 4.5 µl/well and added to qRT-PCR plates in duplicates or triplicates. Taqman probes were combined with 2x Fast Taqman Master Mix and 5.5 µl/well added to the cDNA. qRT-PCRs were run on a QuantStudio7 qRT-PCR machine (Life Technologies) and relative expression normalised to the house keeping gene (HKG) and reference sample was calculated according to the formulae shown below.

relative expression normalised to HKG	$= 2^{\Delta C}{}_{T}$	$\Delta C_T = C_T$ (HKG) - C_T (Gene of interest)
relative expression normalised to HKG compared to reference	$= 2^{\Delta\Delta C}{}_{T}$	$\Delta\Delta C_T = \Delta C_T$ (sample) – ΔC_T (reference)

Data are displayed and were statistically analysed as ΔCT or ΔΔCT rather than as fold-change since these parameters are normally distributed and amenable to statistical analysis whereas fold-change values are log normally distributed.

2.2.10 Data Analysis and Plotting

Data were analysed in Excel for Mac 2011 (Microsoft) and plotted using Prism 7 (GraphPad Software). Statistical analysis was performed using Prism 7 (GraphPad Software).

3

A genetic screen to identify novel modulators of MR1 surface expression

3.1 Introduction

While the understanding of the MR1 antigen presentation pathway has grown considerably in recent years there are still many open questions in the field[94,258,272]. It has been reported that most MR1 resides in the ER at steady state and that it only translocates to the cell surface upon ligand binding[95,259,260,262,280]. Two recent reports agree that soluble, extracellular ligands encounter MR1 in an incompletely folded, ligand-receptive state in the ER, but it remains unclear how the antigenic metabolites gain access to, initially, the cytosol and, ultimately, the ER[260,262]. Inside the ER, the molecular machinery facilitating folding and loading of MR1 is still unknown as MR1 physically associates with components of the MHC class peptide loading complex yet does not require it for surface translocation or antigen presentation[280–282]. Furthermore, it has been suggested that intracellular antigens derived from endocytosed bacteria may be retrieved and presented via a pathway distinct from that described for soluble extracellular ligands[258,262,276]. The molecular mechanisms of this alternative loading, including the contribution of recycling through endosomal compartments, are subject to further investigation[94,258,262,272,276].

Here, a previously described functional genetic screen was used to identify novel players in MR1 antigen presentation and trafficking. The technique is based on insertional mutagenesis of the near-haploid human cell line HAP1 and subsequent sorting of the polyclonal mutagenised population[343–345] (Figure 3.1). In particular, a HAP1 clone over-expressing MR1 was transduced with a gene trap virus to inactivate genes in an unbiased manner. Subsequently, the mutagenised population was treated with Acetyl-6-Formylpterin (Ac6FP), an antagonistic MR1 ligand that induces translocation of MR1 to the cell surface[292], and stained for MR1 surface expression. The tails of the distribution were sorted by flow cytometry to enrich for cells in which positive or negative regulators of MR1 were inactivated. Mapping of the viral insertion sites by Illumina deep sequencing allowed identification of genes statistically overrepresented in either of the two sorted populations which constitute putative modulators of MR1 intracellular trafficking or MR1 stability. In this way, both known and novel putative regulators of MR1 trafficking were identified and a subset was taken forward into a CRISPR/Cas9-based validation approach and tested in functional and biochemical assays.

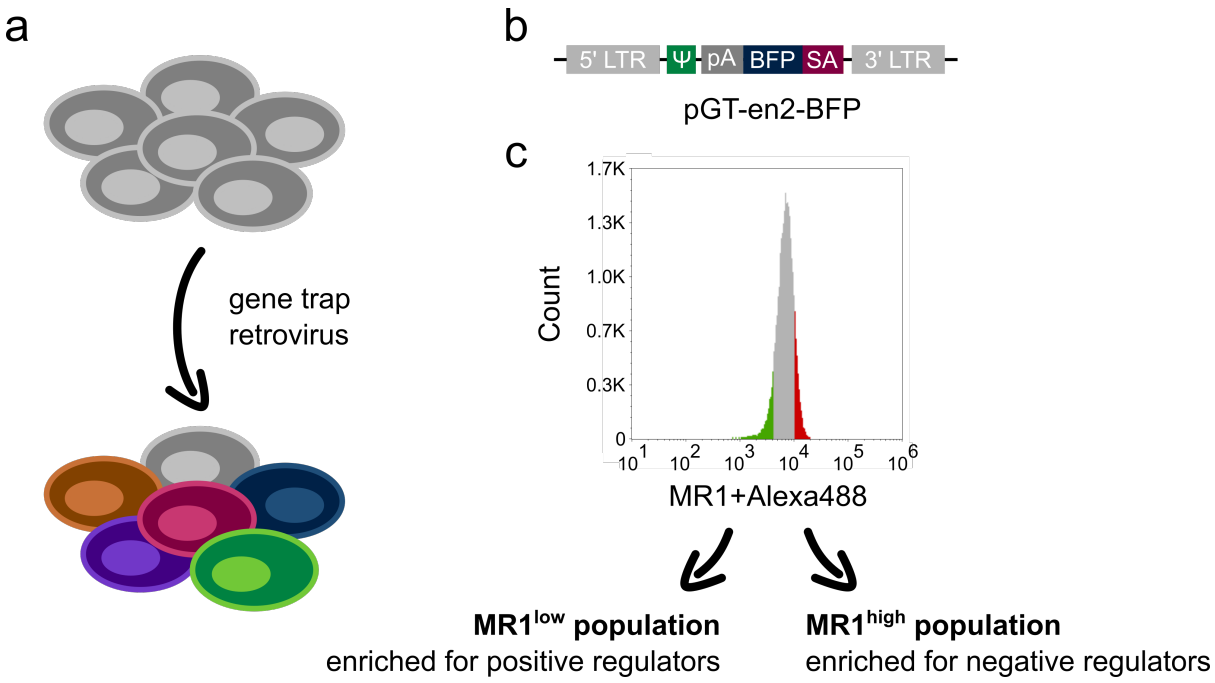


Figure 3.1: Gene trap insertional mutagenesis and sorting strategy. The near-haploid human cell line HAP1 was first transduced to express MR1 (see **Figure 3.2**) and then with a gene trap retrovirus which features a strong adenoviral splice acceptor (a,b). The mutant population was pulsed with 5 μg/ml Ac6FP for 5 hours and the treated cells surface stained for MR1 expression and fixed. $MR1^{high}$ and $MR1^{low}$ populations comprising the top and bottom approximately 1% of the distribution were subsequently sorted by flow cytometry to isolate fractions enriched in null mutants for regulators of MR1 surface expression (c). Figure adapted from Erica De Zan.

3.2 Chapter specific Materials and Methods

Experiments were carried out according to protocols described in General Materials and Methods (Chapter 2) unless stated otherwise in Figure captions or below.

3.2.1 Ploidy staining

Cells were harvested with Trypsin+EDTA (Gibco #25300-054), washed in PBS, and fixed in 70% EtOH (VWR #20821.330) at -20° C for at least 1 h. Fixed cells were pelleted at ca. 850 x g (2 000 rpm in a 6445 rotor in a Multifuge3 S-R) for 10 min and stained in 200 µl of PBS + 0.5 mg/ml RNase A (Invitrogen #12091-021 or VWR #A3832.0050) + 10 µg/ml Propidium Iodide (PI, Sigma-Aldrich #P4864) for 15 min on ice. Cells were washed in PBS and analysed on a flow cytometer with the 561-610/20 or the 561-620/15 channel (depending on the instrument) on linear scale.

3.2.2 Gene trap mutagenesis

Gene trap mutagenesis was carried out as described before[344] with small changes described below. Briefly, HEK293T cells were co-transfected with a gene trap vector encoding for a strong adenoviral splice acceptor as well as blue fluorescent protein (pGT-en2-BFP[344], Figure 3.1) and retroviral packaging plasmids Gag-pol, VSVg, and pAdv[346]. Virus-containing supernatant was harvested and concentrated by ultracentrifugation twice a day for three consecutive days. Concentrates from each day were stored at 4° C o/n and then pooled for transfection. $2x10^7$ cells of HAP1.MR1 clone D9 were seeded in a T175 flask on Day 0 and transduced with concentrated gene-trap retrovirus in the presence of 8 µg/ml of protamine sulphate

(MP Biomedicals #P4380) for three consecutive rounds of transduction on Days 1-3 before expansion and freezing. Gene trap mutagenesis was carried out by Erica De Zan (NDM, University of Oxford, UK).

3.2.3 Surface staining and sorting

Expanded transduced HAP1.MR1 D9 cells were thawed and approximately $3x10^9$ cells were pulsed with 5 µg/ml Ac6FP for 5 h before cell surface staining. Cells were harvested with PBSE, washed in FLOWE, and stained with 10 µg/ml of αMR1 primary antibody (clone 26.5) in FLOWE for 45 min on ice, then washed in FLOWE twice before incubation with 20 µg/ml goat anti-mouse (gαm) secondary antibody coupled to Alexa488 (Life Technologies #A-11001) on ice in the dark. Stained cells were washed twice in PBSE and fixed in ICS Fixation Buffer (eBioscience #00-8222-49) for 30 min at RT, then washed once in PBSE and once in FLOWE, and stored in FLOWE o/n. Fixed cells were washed in 1x Permeabilisation Buffer (eBioscience #00-8333-56, diluted in water) once and then permeabilised for 10 min at RT before resuspension in 0.8 mg/ml RNAseA (Applichem #A3832) solution in 1x Permeabilisation buffer and incubation for 1.5 h at RT in the dark. Subsequently, cells were spun and resuspended in 10 µg/ml PI solution (Thermo Fisher Scientific #P1304MP) in 1x Permeabilisation Buffer for 30 min, then washed in 1x Permeabilisation buffer twice and finally resuspended in FLOWE + 10 µg/ml PI.

Stained cells were sorted on a LE-SH800 sorter (Sony) fitted with a 100 µm chip over four days gating on haploid cells based on PI staining. $MR1^{high}$ and $MR1^{low}$ populations comprising approximately 1% of total, respectively, were sorted

(Figure 3.1, Supplementary Figure 5). In total, $10.3x10^6$ $MR1^{high}$ and $10.2x10^6$ $MR1^{low}$ cells were sorted. Surface staining and sorting was carried out by Erica De Zan (NDM, University of Oxford, UK).

3.2.4 Recovery of insertion sites and bioinformatics analysis

Gene trap insertion sites were recovered using linear amplification-mediated polymerase chain reaction (LAM-PCR) similarly to the protocol described by Blomen *et al.*[343] and Brockmann *et al*.[344]. Briefly, sorted $MR1^{high}$ and $MR1^{low}$ cells were de-crosslinked in buffer AL (QIAGEN, #19075) with Proteinase K o/n and DNA was extracted from the two populations separately using the QIAamp DNA Mini Kit (Qiagen, #51304). LTR-proximal gene regions were amplified from 4x1 µg genomic DNA in four separate reactions per MR1 population using a double-biotinylated primer. Biotinylated single-stranded DNA (ssDNA) was isolated with M-270 streptavidin-coated Dynabeads (LifeTechnologies, #65305). Adapters containing Illumina P5 and P7 adapter sequences were added after the non-biotinylated end of the amplicons was ligated to a ssDNA linker. Libraries were PCR-purified (QIAGEN, #28106) and submitted for deep sequencing on a HiSeq2500 machine (Illumina) generating 50 bp single end reads with the 5' sequencing primer. All primer sequences can be found in Supplementary Table 1.

Recovered sequences were analysed with the pipeline described by Brockmann *et al*.[344]. In short, reads were mapped onto the human reference genome hg19 by running the aligner Bowtie[347] twice, allowing for 0 and 1 bp mismatches to avoid omitting reads that do not map uniquely when tolerating 1 bp mismatch. Reads

were mapped using hg19 protein-coding gene coordinates (Refseq) and intersectBED[348]. A customised BED file was used for both gene mapping and determining the orientation of the integration relative to the gene (sense or antisense). Only sense insertions in non-overlapping gene regions outside the 3' untranslated region (UTR) were considered to have the potential to disrupt gene function and taken into account for further analysis. The number of unique disruptive insertions for a gene in the $MR1^{high}$ or $MR1^{low}$ population was normalised to the total number of insertions in the respective populations and compared to the number of normalised insertions for that gene in the opposite population using a two-sided Fisher's exact test. Significance of enrichment in either of the two tails was determined by applying the Benjamini–Hochberg false discovery rate correction to the calculated p-values. In addition, enrichment in either tail was expressed as the Mutation Index (MI), calculated for each gene as shown below.

$$MI = \frac{\frac{\#\text{ insertions in gene in } MR1^{high}}{(\#\text{ all insertions in } MR1^{high}) - (\#\text{ insertions in gene in } MR1^{high})}}{\frac{\#\text{ insertions in gene in } MR1^{low}}{(\#\text{ all insertions in } MR1I^{low}) - (\#\text{ insertions in gene in } MR1^{low})}}$$

If a gene was sequenced in only one of the populations, one insertion was added in order to enable calculation of the mutational index. Recovery of the insertion sites was carried out by Erica De Zan (NDM, University of Oxford, UK) and Elmer Stickel (Netherlands Cancer Institute, Amsterdam, The Netherlands).

Information on identified hits was collated from the following databases and online tools: PubMed Gene Search, PubMed Protein Search, Genecards[349], UniprotKB[350], Online Mendelian Inheritance in Man (OMIM)[351], Gene Ontology (GO) annotation[352,353], Protein Atlas (www.proteinatlas.org)[354], and ExAC Browser[324].

Functional connectivity within the dataset was explored using the STRING database[355]. For this, 128 selected hits were submitted to the database and unconnected nodes were removed from the resulting network. Evidence for connections based on text mining interactions only (single green lines) was reviewed and connections removed where appropriate. Putative positive regulators and putative negative regulators were coloured in green and red, respectively. Based on literature research, non-significant hits RALA, RALB, and RALBP1 were manually added to the network and coloured in white (see Figure 3.7 and related discussion).

3.2.5 Design and cloning of CRISPR/Cas9 plasmids

For each gene chosen for validation, three one-component CRISPR/Cas9 plasmids with a different single guide RNA (sgRNA) target sequence each were designed based on the Sabatini/Lander CRISPR pooled library[356]. Guides were selected such that they have at least one Guanine (G) at the 5' end or were shortened to a 19-mer starting with a G if necessary. sgRNA sequences were tested for specificity using the UCSC-genome browser BLAT tool (https://genome.ucsc.edu/cgi-bin/hgBlat) and can be found in Supplementary Table 1. Subsequently, oligonucleotides were designed to create overhangs

compatible with a BbsI restriction site and having two or three Guanines at the 5' end of each sgRNA. Oligonucleotides were annealed, phosphorylated with CIP (NEB #M0290L) and cloned into the pX458_Ruby backbone (Addgene #110164). Plasmids were bulk transformed into DH5α bacteria, sequenced, re-transformed individually, and purified following the Qiagen Miniprep spin column protocol (QIAGEN, #27106). CRISPR/Cas9 constructs were designed and cloned by Philip Hublitz in the WIMM Genome Engineering Facility.

3.2.6 Transfection and sorting of gene-edited clones

HAP1.MR1 clone D9 was transfected with CRISPR guides in three consecutive batches. Each time, HAP1.MR1 D9 cells were thawed and after two days, $5x10^5$ cells per target gene were seeded for co-transfection with the three CRISPR/Cas9 plasmids for the respective target gene and left to adhere for about 8 h. A total of 2.4 µg of DNA (800 ng per plasmid) was complexed with 10 µl of TurboFectin 8.0 (OriGene, #TF81001) in 100 µl of Opti-MEM (Life Technologies #31985062) for 15 min at RT and complexes were added to cells in fresh I10 medium. Optimisation of the transfection protocol can be found in Supplementary Figure 6. Cells were harvested for sorting after 2-3 days and stained with live/dead stain aqua (Life Technologies #L34966) and αMR1-APC antibody (BioLegend #361108) on ice in the presence of EDTA. The last batch of cells (Table 3.3) was not stained for MR1 to shorten incubation times and improve viability. A representative gating strategy can be found in Supplementary Figure 7. 120 stained cells per target gene were single-cell sorted into flat-bottom 96-well plates containing single cell medium (IMDM + ⅓ conditioned medium from parent clone D9 + 20% FCS + 50 µg/ml gentamycin (Lonza #BE02-012E)) on a BD FACSAria Fusion or BD

FACSAria III sorter. Clones were picked for expansion approximately two weeks after sorting.

3.3 Generation of HAP1.MR1 clones

Since HAP1 wild-type cells did not express detectable levels of MR1 at either the protein or the mRNA level (Figure 3.2a and Figure 3.4a), HAP1 cells were transduced with lentiviral particles encoding for the human MR1 cDNA sequence (see General Material and Methods; Figure 2.1). The polyclonal HAP1.MR1 population over-expressed functional MR1 as shown by upregulation of surface MR1 in response to Ac6FP and dose-dependent antigen presentation of 5-OP-RU to sorted human MAIT cells (Figure 3.2). Statistical analysis of these results was not possible due to low sample numbers but the same trend was observed in two independent experiments and clones sorted from this polyclonal population further confirmed the expression of functional MR1 (Figure 3.3, Figure 3.4, Chapter 4).

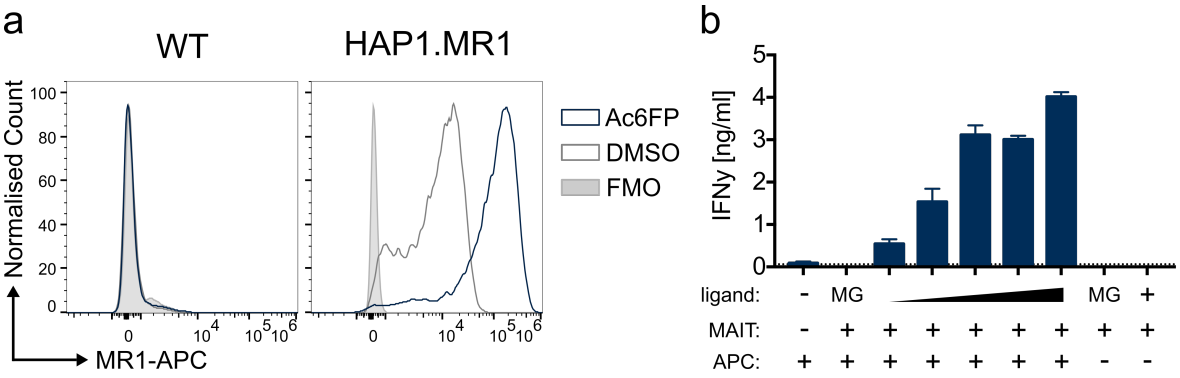


Figure 3.2: Transduced HAP1.MR1 cells over-express functional MR1. HAP1 wild type (WT) cells were transduced with lentiviral particles encoding for human MR1. Bulk-sorted transduced cells were either incubated with 5 µg/ml Ac6FP (blue) or DMSO (grey) over night and surface stained for MR1 (a) or pulsed with 44, 133, 400, 1200, or 3600 nM 5-A-RU in the presence of 5 µM methylglyoxal (MG) for 5 h, washed, and then co-cultured with MAIT cells isolated from human PBMCs for 36 h. Interferon γ (IFNγ) secretion into the supernatant was quantified by ELISA (b). Dashed line in (b) denotes limit of detection. Data in (b) represent technical duplicates with median and range and are representative of two experiments using two different MAIT cell donors for the 44, 400 and 3600 nM concentrations.

To generate an MR1 over-expressing parent clone for the screen, transduced HAP1.MR1 cells were single-cell sorted (for sorting strategy see Supplementary

Figure 2) and cultured in individual wells. The ploidy of the generated clones was analysed (Figure 3.3a) and MR1 surface levels were determined for a number of haploid clones (Figure 3.3b). Since HAP1 cells rapidly divide, a proportion of cells is in G_2-Phase and thus has two sets of chromosomes at any one time. Therefore, two peaks are expected in a ploidy stain, even in the haploid parent clone. All of the tested haploid HAP1.MR1 clones retained responsiveness to Ac6FP and clone D9 was chosen as the parent clone for the screen based on its high expression of MR1 and its staining profile in this and subsequent flow cytometry analyses (Figure 3.3 and data not shown). Although the distribution contained an $MR1^{low}$ shoulder in some pre-tests with cells kept in culture (data not shown), this was not evident in the freshly thawed cells used in the screen itself (Supplementary Figure 5). Ploidy of clone D9 was confirmed again before the screen was performed (data not shown). qRT-PCR confirmed MR1 expression in D9 at the transcript level (difference = 10.99; 95% CI [10.88, 11.09]; $p < 0.0001$) and D9 was able to present 5-OP-RU to sorted human MAIT cells in two independent experiments using MAIT cells from different donors (Figure 3.4).

Since the gene-trap screening technique had so far only been used to analyse total protein levels, the staining protocol had to be adapted for the analysis of a surface protein. Optimisation of the staining method can be found in the Supplementary Material (Supplementary Figure 3). Transfection efficiency in the screen was 48.9% based on BFP expression which underestimates overall transfection efficiency since BFP may not be expressed or might be expressed at low levels if the gene trap virus has integrated in anti-sense orientation or in a lowly expressed locus (Supplementary Figure 4).

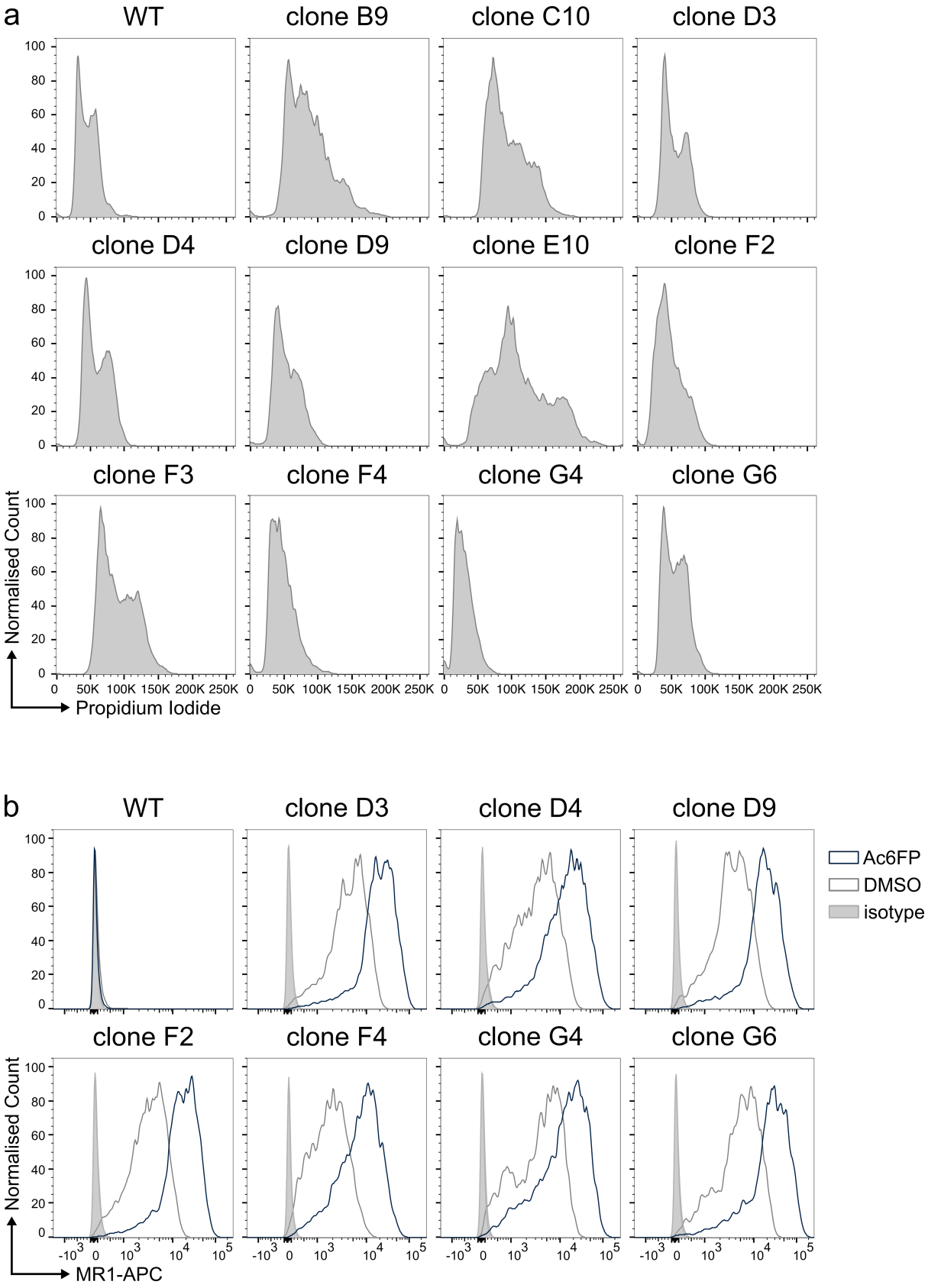


Figure 3.3: Haploid sorted HAP1.MR1 clones retain expression of MR1 and responsiveness to Ac6FP. Transduced HAP1.MR1 single cells were sorted into individual wells by flow cytometry and HAP1.MR1 clones were generated. Clones were tested for ploidy (a) and haploid clones were incubated with 43 µM Acetyl-6-formylpterin (Ac6FP, blue) or DMSO (grey) for 5 h and surface stained for MR1 (b).

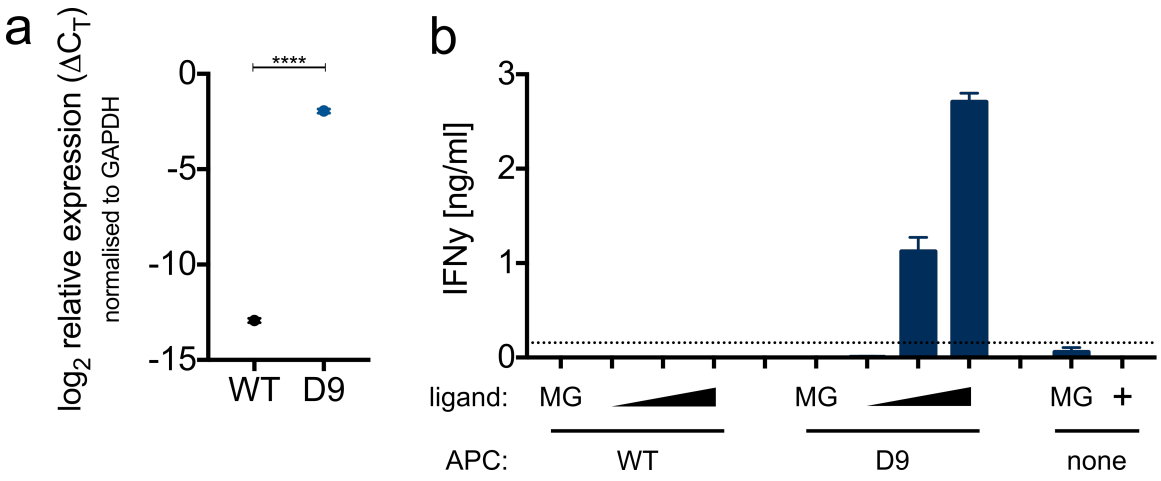


Figure 3.4: HAP1.MR1 clone D9 expresses functional MR1. The HAP1.MR1 clone D9 was tested for MR1 transcript levels (a) and ability to present the MR1 ligand 5-OP-RU to MAIT cells (b). For this, D9 was pulsed with 10, 30, or 100 nM 5-A-RU in the presence of 50 µM methylglyoxal (MG) for 5 h, washed, and then co-cultured with MAIT cells isolated from human PBMCs for 36 h. Interferon γ (IFNγ) secretion into the supernatant was quantified by ELISA. Dashed line in (b) denotes limit of detection. Each symbol in (a) represents technical triplicates with mean and 95% confidence interval. Statistical significance was calculated using an unpaired, two-tailed t-test where * = $p < 0.05$, ** = $p < 0.01$, *** = $p < 0.001$, **** = $p < 0.0001$, ns = not significant. Results in (a) are supported by other experiments including that shown in **Figure 4.3**a. Bars in (b) represent technical duplicates with median and range and are supported by another similar experiment using a different MAIT cell donor and shown in **Figure 6.3**a.

3.4 Screen results and hit selection

In total, >1.75x10^6 unique insertion sites were recovered for each sorted population with approximately 48% being sense insertions (Table 3.1). The 1.74x10^6 unique disruptive insertions across both sorted populations mapped to 16,952 genes, covering about 85% of the currently predicted protein-coding genes in the human genome[357].

Table 3.1: Metadata of the MR1 screen

Cells in MR1^{hi}	Cells in MR1^{low}	Insertions in MR1^{hi}		Insertions in MR1^{low}	
		sense	antisense	sense	antisense
10.3x10^6	10.2x10^6	8.45x10^5	9.27x10^5	8.98x10^5	9.68x10^5

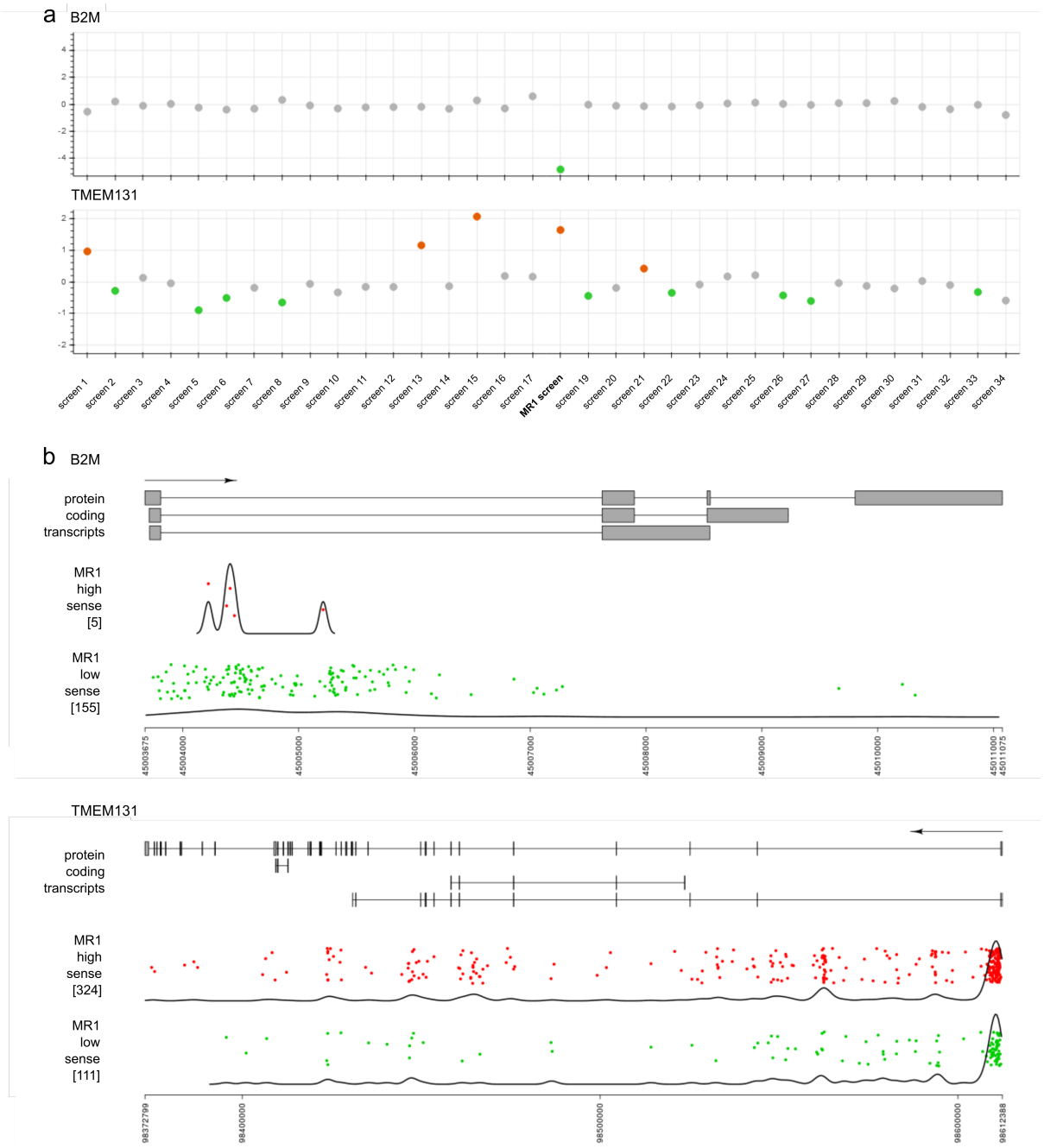


Figure 3.5: Information available for each putative regulator. Each hit can be evaluated based on its uniqueness to the MR1 screen (a) and its Mutation Index, an odds ratio for enrichment in the MR1^{high} tail based on the respective number of sense insertions (b). B2M (top panels) and TMEM131 (bottom panels) are shown as examples for a highly unique positive regulator and a less specific putative negative regulator of MR1 surface expression. Intron/exon structure of alternative protein coding transcripts for each gene is shown. Arrow denotes transcriptional direction. Each dot represents one sense insertion and number of insertions is shown in square brackets. Solid line represents the distribution of insertions across the gene. Genomic location within the chromosome is shown below the graph. Adapted from plots provided by Erica De Zan.

Bioinformatic analysis of the recovered insertion sites revealed both number and position of insertions in each gene and enabled the calculation of the Mutation Index (MI) for each detected gene (Figure 3.5b, Figure 3.6, Supplementary Table 2). This parameter reflects the ratio of the number of sense insertions detected in the $MR1^{high}$ compared to the $MR1^{low}$ population for a given gene and is a measure of enrichment in one or the other tail of the distribution[344] (see Chapter Specific Materials and Methods for details). The MI can also be compared across other screens previously performed in the same laboratory to identify hits unique to the MR1 surface expression screen (Figure 3.5a). Previous screens had mostly focussed on intracellular signalling molecules and comparison of the MI served primarily to exclude unspecific hits which were shared across all screens performed (see also Supplementary Table 2).

Based on these parameters, 200 putative regulators of MR1 surface expression with a false discovery rate (FDR)-corrected p-value (fcpv) < 0.01 were identified, including the MR1 transgene itself and β_2-microglobulin (β_2m), binding of which is a known requirement for MR1 surface translocation[280] (Figure 3.6, Supplementary Table 2). Of these 200 hits, 72 were excluded from further analysis because they were either unspecific hits which frequently come up in this particular kind of screen or because they were genes involved in DNA damage repair, cell cycle control, or transcriptional regulation which is not of interest in this study because MR1 is recombinantly expressed in the system. Applying these filters yielded a total of 84 putative positive regulators and 44 putative negative regulators (Supplementary Table 3 and 4).

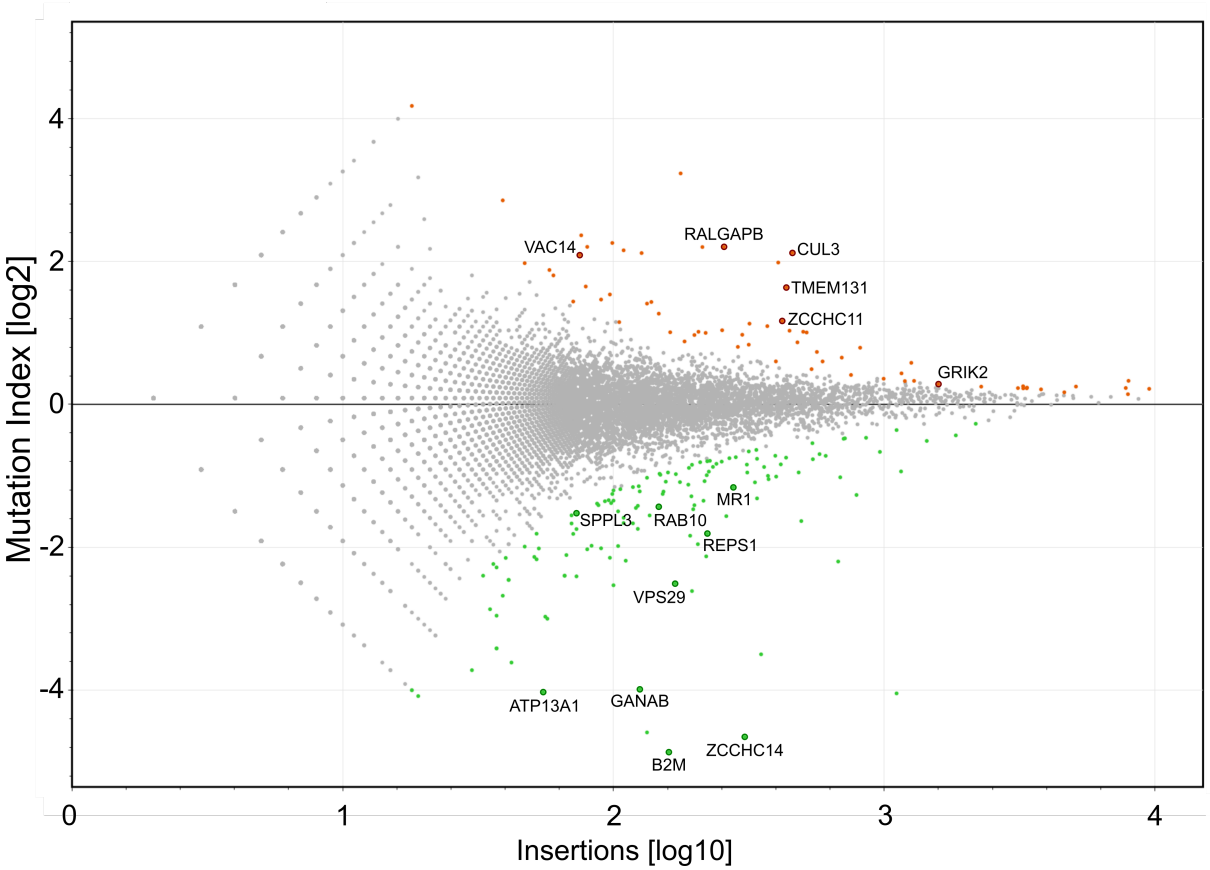


Figure 3.6: A gene-trap screen in HAP1.MR1 clone D9 identifies putative positive and negative regulators of MR1 surface expression. Insertion sites of the gene trap virus were recovered from genomic DNA isolated separately from sorted MR1^{high} and MR1^{low} populations and mapped to a reference genome. For each gene, the odds ratio of it being enriched in the MR1^{high} compared to the MR1^{low} populations was calculated and plotted as the Mutation Index against the total number of sense insertions. Genes significantly (fcpv < 0.01) enriched in the high or low fraction are highlighted in red and green, respectively, and represent putative negative and positive regulators of MR1 surface expression. MR1, its known regulator β_2m (encoded by gene B2M), and the hits selected for validation were manually labelled and their respective data points highlighted. Raw data are available in Supplementary Table 2. Adapted from plot provided by Erica De Zan.

In order to prioritise hits for validation, several parameters including fcpv, MI, number of insertions, uniqueness to the screen, functional annotation, disease association, tolerance to variation, tissue distribution, and subcellular localisation were taken into account (Supplementary Table 3 and 4). As a complimentary approach, a functional protein association network of the full list of 128 significant hits was generated using the STRING database[355] (Figure 3.7). Based on computational predictions, text mining, and information curated in other publicly available databases, this tool generates protein networks which reflect functional

interactions but do not necessarily imply physical interactions between the proteins.

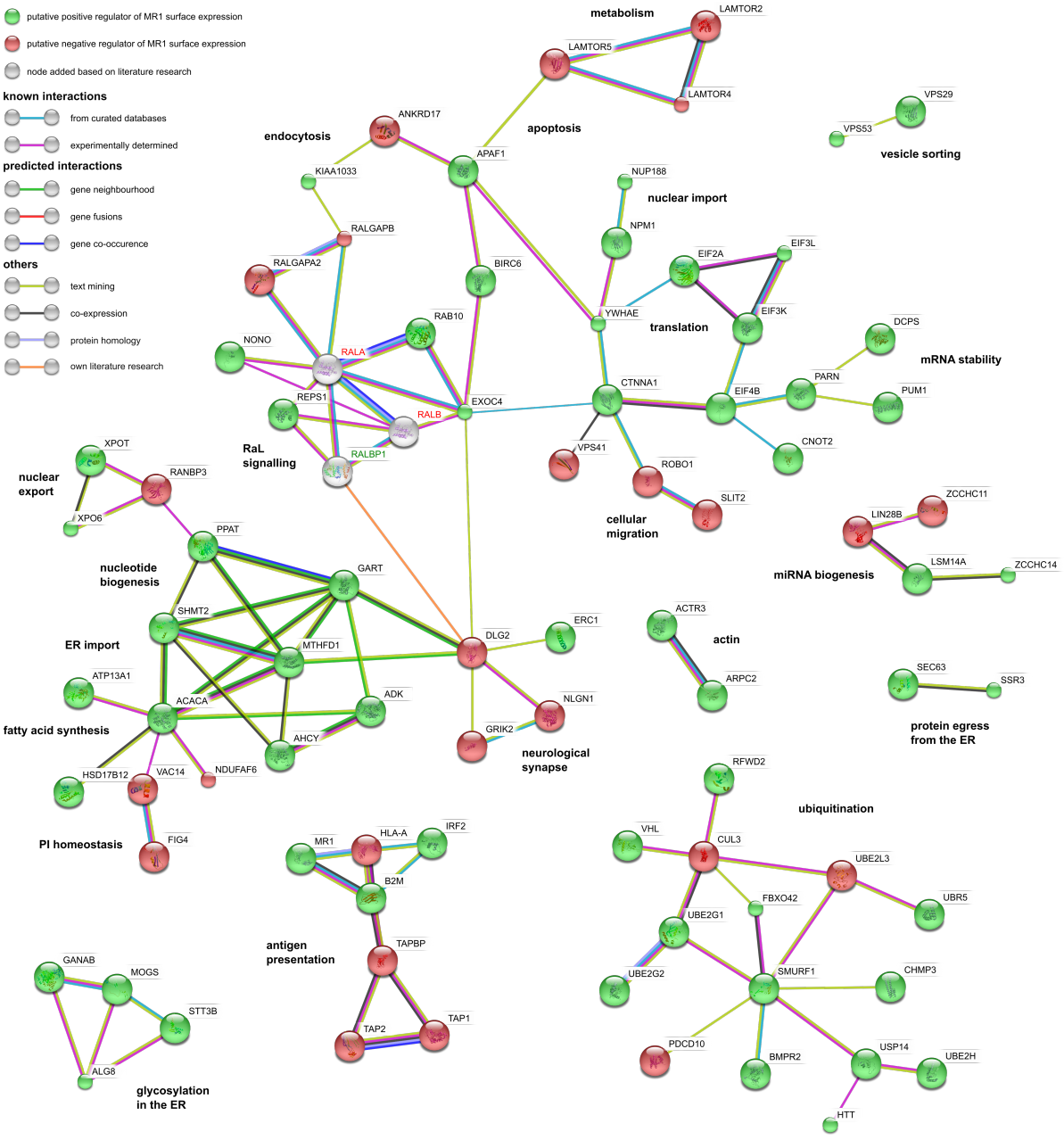


Figure 3.7: Functional protein association analysis reveals functional clusters among screen hits. The list of 128 screen hits was submitted to the STRING database and the resulting network analysed. Unconnected nodes were removed and putative positive (green) and negative (red) regulators colour-coded for clarity. Interactions based on text mining only were reviewed and unsuitable connections removed. Functional clusters were labelled based on functional annotations of connected proteins. Nodes RALA, RALB, and RALBP1 (white) were manually added to the list based on literature research (see text). Larger nodes containing protein structures indicate availability of structural information.

Based on literature research, RALA, RALB, and RALBP1 were added to the network. They were not significant hits with a fcpv < 0.01 cut-off, but are central to the RAL pathway with which a considerable number of significant hits were associated and, thus, enhanced the network. The list of negative regulators comprised two subunits of the RaL GTPase activating protein, RALGAPB (top hit on the fishtail plot, fcpv = 4.01×10^{-24}) and RALGAPA2 (fcpv = 7.34×10^{-3}). At the same time, the RAL binding protein 1 associated Eps domain containing 1 (REPS1) protein was a putative positive regulator. Further research into the RalA pathway revealed that it is implicated in the regulation of the endocytosis of surface receptors on neurons[358,359] and also signals in the context of phagocytosis[360], suggesting that it might play a role in the presentation of bacterial antigens. Of note, this signaling pathway is also involved in many other cellular processes and the top hit RALGAP is, for instance, known to feature in mTOR signalling[361]. Adding the proteins RalA, RalB, and RalBP1 to the network revealed further interactions – for example with NONO, an RNA-binding protein which was also a confirmed hit in an RNAi screen for MHC class II-mediated antigen presentation[362]. Overall, seven of the significant putative regulators are directly functionally associated with the RalA pathway, providing a rationale to include both RALGAPB and REPS1 in the list of hits to validate. In addition, ATP13A1 was taken forward based on its prominent position in the fishtail plot and its predicted function as an ER-localised P_5-ATPase transporter[363]. GANAB, VPS29, ZCCHC14, SPPL3, RAB10, TMEM131, ZCCHC11, CUL3, and VAC14 were chosen for similar reasons (Table 3.2). GRIK2 was a shared hit with the RNASeq experiment described in Chapter 5. B2M was included as a positive control.

Table 3.2: Hits selected for CRISPR/Cas9-based validation Functional annotations are based on Pubmed Gene, GeneCards[349], and UniProtKB[350] entries (Supplementary Table 3 and 4). Copyrightable data from UniProtKB[350] are under the Creative Commons Attribution (CC BY 4.0) License. Putative positive regulators of MR1 surface expression are shown in green, putative negative regulators are shown in red.

Gene	Rationale for validation
REPS1	Ral pathway, fcp-value (top 10)
ATP13A1	position in plot, transporter function, subcellular localisation in ER, low p-value despite relatively few insertions, fcp-value (top 10)
GANAB	position in plot, subcellular localisation in ER, representative of glycoslylation cluster, fcp-value (top 10)
VPS29	position in plot, trafficking function, subcellular localisation in retromer complex, fcp-value (top 10)
ZCCHC14	position in plot, uniqueness, same pathway as ZCCHC11, fcp-value (top 10)
SPPL3	function in immune context and glycosylation, subcellular localisation in ER and Golgi
RAB10	trafficking function, uniqueness, functional connectivity
B2M	control
RALGAPB	position in plot, Ral pathway, fcp-value (top 10)
TMEM131	position in plot, potential role in immune response, fcp-value (top 10)
ZCCHC11	position in plot, fcp-value (top 10), same pathway as ZCCHC14
CUL3	position in plot, fcp-value (top 10), representative of ubiquitin-cluster
VAC14	position in plot, subcellular localisation in endosomal compartment, low p-value despite relatively few insertions
GRIK2	shared with RNASeq (see Chapter 5)

3.5 CRISPR-based validation

For each gene to be validated, three distinct single guide RNAs (sgRNAs) were selected based on the Sabatini/Lander CRISPR pooled library[356] and cloned into a plasmid also coding for the Cas9 nuclease and the red fluorescent protein mRuby2 (see Chapter Specific Materials and Methods). The HAP1.MR1 parent clone D9 was transiently co-transfected with the three plasmids per gene and mRuby2$^+$ cells were single-cell sorted. The number of viable clones varied greatly between target genes and also between batches (Table 3.3). While only 3-5 clones survived when TMEM131, GANAB, or VPS29 were sorted, more than 20 viable clones were generated from cells in which REPS1, CUL3, or RAB10 had been targeted. Overall, survival was much better in batch 3. For most target genes

sporadic surviving clones displayed an altered morphology compared to the parent clone D9 but this was true for all clones in which CUL3 had been targeted (data not shown).

Table 3.3: Statistics of CRISPR/Cas9 KO clones Numbers of viable clones per target genes including numbers successfully screened by Western Blot and KO identified at the protein level. Putative positive regulators of MR1 surface expression are shown in green, putative negative regulators are shown in red. KOs are highlighted in yellow.

	Target gene	Viable clones	Successfully screened	KO
batch 1	B2M	15	11	9
	ZCCHC14	11	10	0
	ATP13A1	13	11	8
	ZCCHC11	11	9	0
	TMEM131	5	4	4
batch 2	GANAB	3	3	0
	VPS29	4	4	0
	VAC14	16	15	0
	GRIK2	12	11	0
batch 3	REPS1	21	17	0
	RALGAPB	15	14	0
	CUL3	25	0	0
	SPPL3	14	14	0
	RAB10	32	0	0

The generated clones were screened for expression of the targeted gene by Western Blot (Figure 3.8). KO clones were obtained for B2M (Figure 3.8a), ATP13A1 (Figure 3.8b), and TMEM131 (Figure 3.8l). Analysis of some of the Western Blots was confounded by the presence of substantial signal from bands not corresponding to the predicted molecular weight of the targeted protein. This was particularly pronounced with the antibodies targeting VAC14, VPS29, REPS1, and RALGAPB (Figure 3.8d,f,g, and j) and constituted a further reason to focus subsequent investigations on those proteins for which a reliable Western Blot

result had been obtained. CUL3 and RAB10 were not detectable in either the parent clone D9 or the edited clones with the antibodies used (data not shown).

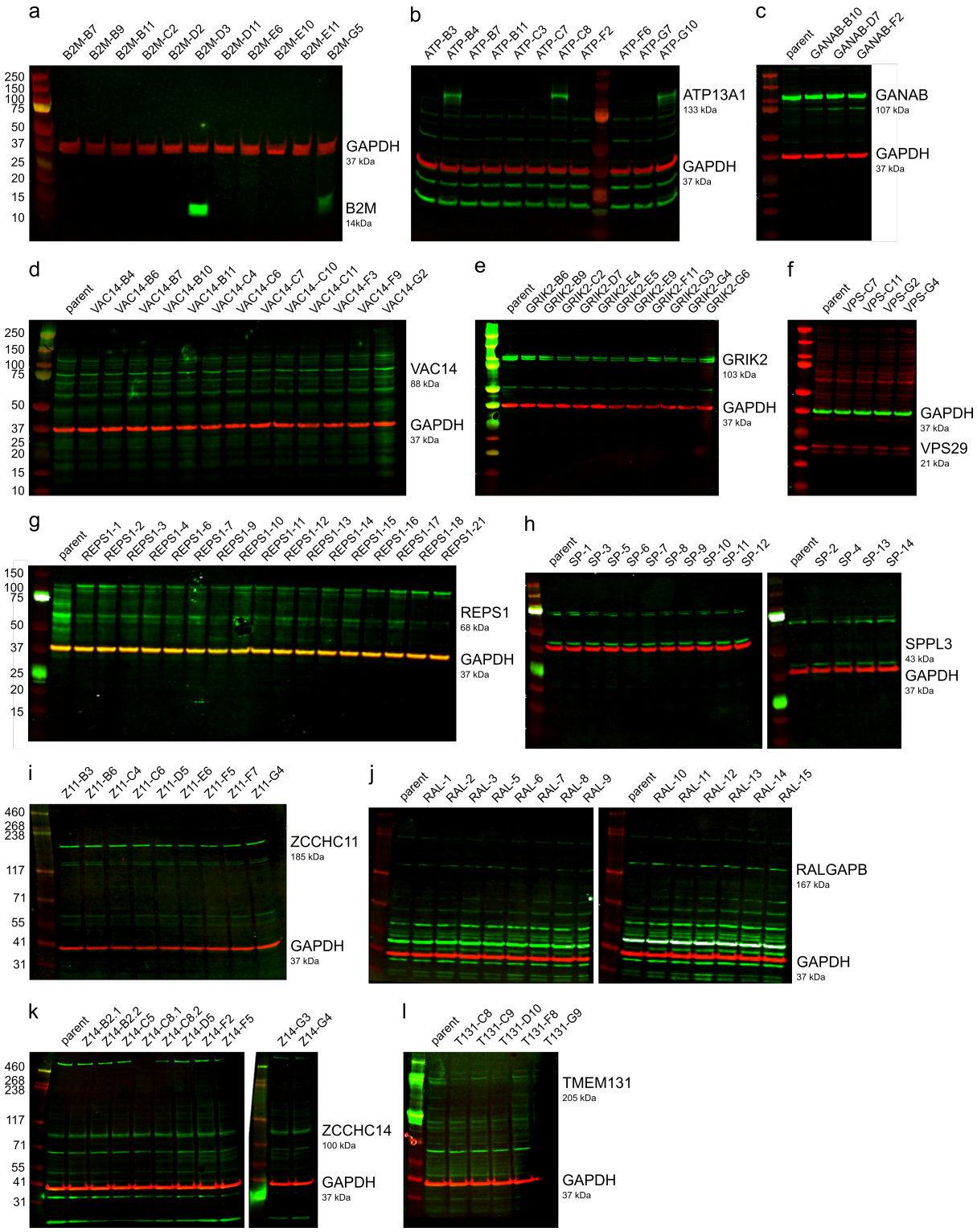


Figure 3.8: CRISPR/Cas9-mediated genome editing yields knock-out clones for validation for some genes. Gene-edited clones for each targeted gene were analysed by Western Blot. Names of the individual clones are shown above the respective lane, parent denotes parent clone D9. Molecular weight markers were either Precision Plus Protein™ Dual Colour Standard (a-h) or HiMark™ Pre-Stained Standard (i-l) and molecular weights of visible marker bands are given in kDa to the left of each row. High molecular weight proteins (i-l) were separated on 3-8% Tris-Acetate gels in MOPS SDS buffer. Some clones for the same target gene had to be analysed on separate gels due to differing protein concentrations (h,j,k). Membranes were incubated with antibodies against GAPDH and gene of interest together and developed with the LI-COR® two-colour system.

A subset of the generated KO-clones was then analysed for MR1 surface expression by flow cytometry and antigen presentation capacity. At baseline, both MHC class I and MR1 surface levels were completely ablated in four B2M KO clones whereas only MR1 surface levels seemed slightly reduced in four ATP13A1 KO clones. Neither MHC class I nor MR1 surface expression appeared consistently affected in TMEM131 KO clones (Figure 3.9, grey histograms). Upon incubation with Ac6FP, B2M KO clones were unable to up-regulate MR1 surface expression, consistent with its known role in MR1 surface translocation[95,260,262,280]. Interestingly, MR1 surface levels increased in response to Ac6FP in ATP13A1 clones but remained lower than those of the parent clone D9. TMEM131 KO clones generally responded to Ac6FP to the same extent as the parent clone even though the duplicates of clones T131-C8 and T131-C9 differed in this respect (Figure 3.9a, blue histograms). Similarly, the duplicates of the HAP1.MR1 D9 parent clone did not show the same distribution, especially in the Ac6FP-treated samples. Based on the lack of MHC class I signal in the ligand-treated sample it appears likely that this particular sample was not stained with enough antibody. This makes it particularly difficult to draw definite conclusions on the effect of ATP13A1 KO and TMEM131 KO on MHC class I surface levels. Furthermore, these results are derived from one experiment only and while the positive control of B2M KO clearly showed the expected clear-cut effect, more experiments are needed to draw substantiated conclusions about the more subtle surface phenotypes seen in the ATP13A1 and TMEM131 KO clones. The experiments shown in Chapter 4 aim to further characterise this phenotype.

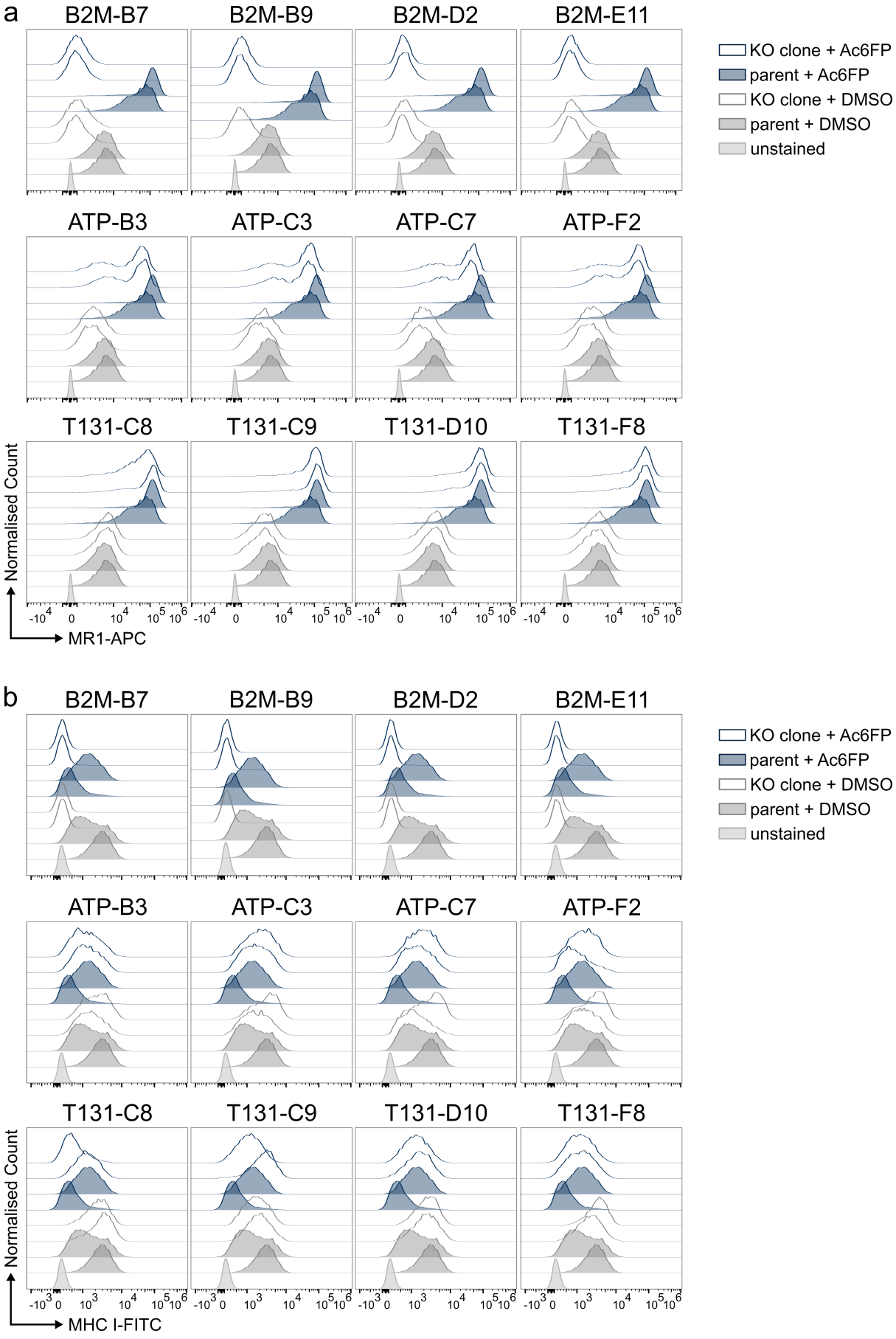

a
B2M-B7
B2M-B9
B2M-D2
B2M-E11
ATP-B3
ATP-C3
ATP-C7
ATP-F2
T131-C8
T131-C9
T131-D10
T131-F8
Normalised Count
MR1-APC
KO clone + Ac6FP
parent + Ac6FP
KO clone + DMSO
parent + DMSO
unstained
b
B2M-B7
B2M-B9
B2M-D2
B2M-E11
ATP-B3
ATP-C3
ATP-C7
ATP-F2
T131-C8
T131-C9
T131-D10
T131-F8
Normalised Count
MHC I-FITC
KO clone + Ac6FP
parent + Ac6FP
KO clone + DMSO
parent + DMSO
unstained

Figure 3.9: MR1 surface expression is reduced in HAP1.MR1 clones deficient for β_2m and ATP13A1. Four HAP.MR1 clones deficient for β_2m (top panels), ATP13A1 (middle panels), or TMEM131 (bottom panels) were pulsed with 1.25 µg/ml Ac6FP (blue) or the equivalent volume of DMSO (grey) for 5 h in duplicates and surface MR1 (a) and MHC class I (b) levels were measured by flow cytometry. Shaded histograms represent the same HAP1.MR1 parent clone D9 sample in each overlay, empty histograms represent the respective KO clone. The live/dead-only stained parent sample is shown as a negative control.

In line with the loss of MR1 surface expression, the ability to present 5-OP-RU to sorted human MAIT cells was lost in HAP1.MR1 B2M KO clones (Figure 3.10). While it was not possible to statistically compare the KO clones to the parent due to different group sizes, the differences in antigen presentation between the B2M, ATP13A1, and TMEM131 KO clones were statistically significant (Kruskal-Wallis test, p = 0.0003). HAP1.MR1 B2M KO clones elicited a significantly lower (p = 0.0059) IFNγ response than TMEM131 KO clones from sorted human MAIT cells (Figure 3.10). The differences between ATP13A1 KO clones and B2M or TMEM131 KO clones did not reach statistical significance with this test. The amount of IFNγ produced by the MAIT cells in response to ATP13A1 KO cells was between 30-50% of that produced in response to the parent clone. Among the KO clones, antigen presentation of MR1 ligand was highest in the four TMEM131 KO clones which elicited 58-100% of the amount of IFNγ produced in response to the parent clone (Figure 3.10). In a second experiment using the same MAIT cell donor and the ATP13A1 KO clones only, a slightly lower reduction compared to the parent clone D9 was observed (data not shown). In the repeat experiment, the magnitude of the IFNγ response elicited by the ATP13A1 KO clones was between 44-81% of that induced by the parent. No such reduction was seen in a third experiment using a different MAIT cell donor but the readings of the ELISA were at or below the limit of detection, making it difficult to interpret that data (data not shown). Like the flow cytometry data, the functional experiment was only carried

out once with all three sets of clones but taking into account that TMEM131 was a putative negative regulator of MR1 and neither the flow cytometry analysis nor the functional data provided any evidence for an increase in MR1 surface expression relative to the parent clone upon loss of TMEM131, further analysis focussed on the role of ATP13A1 in MR1-mediated antigen presentation.

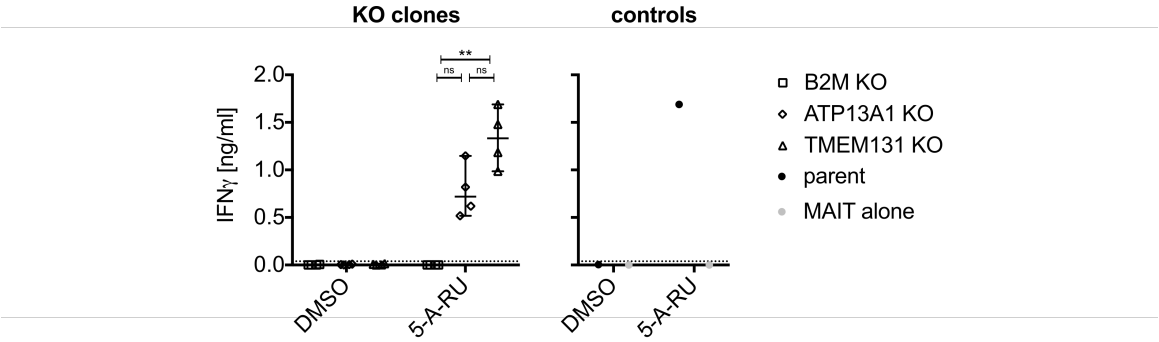


Figure 3.10: Antigen presentation of MR1 ligands is reduced in HAP1.MR1 ATP13A1 KO clones. Four HAP.MR1 clones deficient for β_2m (empty squares), ATP13A1 (empty diamonds), or TMEM131 (empty triangles) were pulsed with 100 ng/ml 5-A-RU and 17 µM MG for 5 h. Ligand was washed off and sorted Vβ2+ MAIT cells were added for 36 h. Interferon γ (IFNγ) secretion into the supernatant was quantified by ELISA. Dashed line denotes limit of detection. Each symbol represents the median of technical duplicates for one clone and median with range is shown. B2M KO, ATP13A1 KO, and TMEM131 KO clones in the presence of ligand were compared statistically and statistical significance was calculated using a Kruskal-Wallis test with Dunn's multiple comparison test. Data for untreated baseline, parent clone D9, and MAIT cell only controls are shown as reference but were not considered in the statistical analysis. * = $p < 0.05$, ** = $p < 0.01$, *** = $p < 0.001$, **** = $p < 0.0001$, ns = not significant.

3.6 Discussion

In this Chapter, an MR1 over-expressing HAP1 clone was generated as a tool to discover novel modulators of MR1 surface expression through an insertional mutagenesis screen. The screen generated a list of 200 putative positive and negative regulators of MR1, some of which were known to affect surface expression of the molecule. Of these hits, approximately two thirds were putative positive regulators whereas only one third were putative negative regulators (Supplementary Table 2). This difference reflects the fact that the screen setup is more powerful in detecting putative positive regulators than negative ones because the screen was carried out in the presence of Ac6FP which results in the translocation of most MR1 molecules to the surface. Therefore, detecting effects of insertions that further increase the amount of MR1 at the cell surface was more difficult.

Considering both sense and antisense insertions, less than $2x10^6$ unique insertions were counted in each of the two sorted populations which comprised approximately $10x10^6$ cells each (Table 3.1). This appears relatively low considering that the screen is designed to introduce one insertion per cell[267] and is approximately half of the number of insertions routinely identified in comparable screens. However, it has to be taken into account that the number of integrations in Table 3.1 a) reflects unique insertions only, meaning that if multiple cells showed the same integration, that particular integration was only counted once and b) comprises only insertions within non-overlapping coding regions, so only a subset of all insertions is reported here. In addition, the use of different fixation and permeabilisation buffers compared to the established screening protocol which

was made necessary by the analysis of cell surface expression only resulted in lower gDNA recovery compared to previous screens. This may also account for the relatively low number of insertions recovered. Of note, gene-trap screens with relatively low numbers of insertions have yielded good results with many validated hits in the past (unpublished observation).

Analysis of the functional connectivity within the list of putative regulators revealed a number of functional clusters. Two big clusters contained proteins related to mRNA stability, translational regulation and ubiquitiniation, cellular processes that can be easily linked to the regulation of protein levels in the cell. However, since these processes are more likely to influence overall protein levels than intracellular trafficking of MR1, only the putative negative regulator CUL3 was chosen for validation as a representative of the ubiquitination cluster due to its low fcpv of $2.92x10^{-41}$. Since the cytoplasmic tail of human MR1 does not contain any lysine residues and lacks known ubiquitination motifs[364] such as those found in the cytoplasmic tail of MHC class II it is unlikely that CUL3 plays a role comparable to that of March-I in MHC class II recycling[365,366] but it may intersect the MR1 trafficking pathway at another point. Alternatively, MR1 could be ubiquitinated at a non-lysine residue as has been reported for some MHC class I molecules[367]. However, the cytoplasmic tail of MR1 does not feature a cysteine either and this particular type of ubiquitination was reported in the context of a viral E3 ubiquitin ligase rather than a cellular one[367].

Similarly, proteins involved in protein egress from and glycosylation in the ER formed two clusters that are directly relatable to the regulation of surface

translocation. N-linked glycosylation in particular has long been known to be tightly linked to protein folding and quality control in the ER[368,369]. Of note, N-linked glycosylation of one of the asparagine residues in the monomorphic antigen presenting molecule CD1d has been shown to be important for the association of the CD1d heavy chain with β_2-microglobulin[370]. Furthermore, efficient peptide loading of classical MHC class I molecules is crucially dependent on their glycan-mediated interaction with calreticulin[147]. The MR1 amino acid sequence contains one consensus sequence for N-linked glycosylation and has been shown to be sensitive to digestion with glycosidases[259,260,280] but a requirement of glycosylation for surface translocation has not been formally demonstrated. Therefore, GANAB was chosen for validation as the glycosylation hit with the lowest p-value (fcpv = 7.54×10^{-23}) and one of the most prominent hits in the fishtail plot (Figure 3.6). GANAB encodes the α subunit of glucosidase II, a key enzyme in glycoprotein processing that trims glycans to generate sugar residues which can be recognised and bound by the ER-resident chaperones calnexin and calreticulin[371–373].

Another notable functional cluster centered around antigen presentation. Apart from β_2m and MR1 itself this cluster featured HLA-A, one of the classical MHC class I genes and three components of the peptide loading complex: TAP1, TAP2, and TAPBP, coding for the two subunits of the transporter associated with antigen processing and the chaperone tapasin[374]. Interestingly, all of these were putative negative regulators of MR1 surface expression, consistent with the hypothesis that MHC class I and MR1 molecules compete for binding of β_2-microglobulin and implying that more MR1 could translocate to the cell surface if folding and loading

of classical MHC class I molecules is disrupted. MR1 has been shown to have a lower affinity for β_2m in mice which further supports this hypothesis[280].

SPPL3, encoding for the Golgi-localised signal peptide peptidase like 3 protein lies between the glycosylation cluster and the antigen presentation cluster as it is reported to be involved in both cellular glycosylation processes and immune regulation[375]. These connections were not present in the functional network generated by STRING, but the gene was chosen for follow-up analysis based on functional annotation and fcpv.

The reasoning behind including REPS1 and RALGAPB in the list of hits to validate is discussed in the results section. Briefly, both are involved in the RALA signaling pathway which links seven of the 200 screen hits and as one of them is a putative positive regulator and one is a putative negative regulator, elucidating their respective roles was particularly intriguing. Another member of the RALA cluster was RAB10, a small GTPase implicated in the regulation of both anterograde intracellular vesicle trafficking and endocytic recycling in models of vesicle sorting and endocytosis[376–379].

Also involved in vesicle sorting is VPS29, a small protein originally described as a structural component of the retromer complex which orchestrates the sorting of cargo proteins in the endosomal network, re-routing endosomal cargo back towards the plasma membrane or into retrograde transport pathways and preventing lysosomal degradation[380]. One of the molecular functions of the retromer complex is recruitment of WASH[381], a regulator of actin polymerization[382]

which also provides a link between the vesicle sorting and actin functional clusters in the STRING network. More recently, VPS29 has also been shown to associate with DSCR3 and C16orf62 to form the retriever complex which promotes cell surface recycling rather than retrograde trafficking in a retromer-independent manner[383]. Whether as part of the retromer or the retriever complex, VPS29 has the potential to crucially impact the fate of surface MR1 molecules – either by acting on MR1 itself or via another cell surface regulator.

Another smaller functional cluster contained hits related to miRNA biogenesis. Since both ZCCHC11 and ZCCHC14 were prominent hits in the fishtail plot and had opposite effects on MR1 surface levels while being implicated in the same cellular process they, too, were chosen for further validation. ZCCHC11 encodes the 3' terminal uridylyl transferase (TUTase) TUT4 which regulates the stability of a subset of miRNAs in a Lin28-mediated suppression mechanism[384]. Much less is known about the molecular function of ZCCHC14. While two GWAS studies have found associations between single nucleotide polymorphisms in the ZCCHC14 gene and addictive tendencies[385,386], functional annotations to date rely on inferences from electronic annotation (UniprotKB entry Q8WYQ9).

TMEM131 encodes for a little studied multi-pass transmembrane protein. It has been reported to be upregulated in T cell precursors upon entry into the thymus in mice[387] and is hypomethylated in subjects with Trisomy 21[388]. It was chosen for validation based on its prominent position in the fishtail plot and its suggested role in the immune response together with its low p-value (fcpv = 4.76×10^{-25}).

A functional cluster around ACACA, the gene encoding Acetyl-CoA carboxylase 1, contained genes involved in various aspects of lipid biology such as fatty acid synthesis and phosphatidylinositol homeostasis. One such hit was VAC14, an activator of the lipid kinase PIKfyve and, thus, indirect regulator of phosphatidylinositol homeostasis in endosomal membranes which is especially important for the correct formation and function of multivescular bodies[389,390]. VAC14 particularly stood out due to its subcellular localisation to endosomal compartments and its position in the fishtail plot (Figure 3.6).

The most interesting hit based on its functional annotation and prominent position in the fishtail plot was ATP13A1, encoding an ER-localised transporter (Figure 3.6). Its homologue in yeast, *spf1*, encodes for a protein that is involved in the transport of Manganese (Mn) from the cytosol into the ER and the human protein has been shown to localise to the ER as well[363]. Knock-down of human ATP13A1 has been reported to phenocopy some of the features of *spf1* KO such as induction of ER-stress and increased activity of cytosolic Mn-dependent enzymes[363]. ATP13A1 is one of only five mammalian P_5-ATPases and differs from its paralogues ATP13A2-5 in its intron/exon structure, supporting the notion that it represents its own sub-class of P_5-ATPases[391]. It has also been suggested that Spf1p, and by extension ATP13A1, may transport a non-metallic substrate[392]. Therefore, it was considered the most promising novel hit identified in the screen, hypothesizing that it may transport MR1 ligands into the ER.

The low number of surviving clones for some targeted genes may be due to various factors. For example, a substantial proportion of HAP1.MR1 cells die in the

process of staining for flow cytometry after staining with the live/dead marker (data not shown). Therefore, a proportion of the sorted live/dead$^-$mRuby2$^+$ cells may already have been dead or dying at the time of sorting. This is why in the last batch cells were not stained for MR1 prior to sorting and sorted plates were moved to 37° C on a rolling basis rather than being stored on ice for the duration of the sort. These measures shortened the amount of time transduced cells were exposed to cold temperatures and EDTA-containing buffer which correlated with overall higher numbers of surviving clones (Table 3.3).

A separate challenge is the lack of KO clones on the protein level even for those target genes that did yield a relatively high number of clones (e.g. VAC14 and RALGAPB). One explanation could be essentiality of the targeted gene, meaning that only clones that have been transfected (i.e. were mRuby2$^+$ at the time of sorting) but have not been efficiently edited or edited in such a way that protein is still produced (e.g. in frame mutations) survive. This possibility could be addressed by screening the generated clones on the genetic rather than the protein level by sequencing. Relatedly, the numbers of sorted cells and, therefore, screened clones may simply be too low to find KO clones for the target genes in question, particularly for those targets with a very low number of clones (GANAB and VPS29). Editing efficiency for the sgRNAs that did yield clones (targeting B2M, ATP13A1, and TMEM131) was extremely high (72 - 100%) but this cannot be expected for all guides. Another round of transfection and sorting for GANAB and VPS29 using the conditions used in batch 3 and sorting more than two plates may yield KO clones for further analysis. Re-analysis of the RAB10 and CUL3 clones with a different antibody may also reveal KO clones among these. Likewise, the

staining protocol and the antibody choice for VAC14, VPS29, REPS1, and RALGAPB should be optimised to reliably interpret protein expression in these clones.

In a preliminary experiment, changes in MR1 surface expression were observed in KO clones for both putative positive regulators that yielded KO clones - β_2m and ATP13A1 - whereas MR1 levels were not increased in clones deficient for the putative negative regulator TMEM131 (Figure 3.9). Surface expression of MHC class I molecules in the same experiment was difficult to compare due to technical reasons but did not appear to be reduced in the ATP13A1 KO clones or increased in the TMEM131 KO clones tested. B2M KO clones did not express any MHC class I at their surface, consistent with the known requirement of its product β_2-microglobulin for MHC class I surface expression[393,394].

Similar trends were observed in a functional assay testing the antigen presentation capacity of the generated KO clones. While B2M KO clones were unable to present synthetic MR1 ligand to sorted human MAIT cells, antigen presentation appered to be reduced in ATP13A1 KO cells although this did not reach statistical significance. The capacity to present MR1 ligand did not appear increased in the four TMEM131 KO clones tested in an initial experiment (Figure 3.10).

Taken together, these results support the hypothesis that MR1 expression in HAP1.MR1 cells is partially dependent on ATP13A1 expression and it remains to be determined whether this is due to an effect on the transcriptional, translational,

or post-translational level. The further characterisation of the MR1 phenotype in HAP1.MR1 ATP13A1 KO cells is the subject of the next chapter of this thesis.

4

The role of the ER transporter ATP13A1 in MR1 antigen presentation

4.1 Introduction

In the previous chapter an insertional mutagenesis screen identified the ER-localised P_5-ATPase ATP13A1 as a modulator of MR1 surface expression in an MR1 over-expressing HAP1 clone. ATP13A1 is the mammalian orthologue of the yeast ATPase Spf1p (also known as Cod1p) and is unique among the five known mammalian P_5-ATPases[391]. It differs from its paralogues ATP13A2-5 in its intron/exon structure and is predicted to have resulted from an earlier gene duplication than the other isoforms. In addition, ATP13A1 features a stretch of 67 amino acids which is not present in the other mammalian isoforms in either human or mouse but in the yeast, *C.elegans*, and *D.melanogaster* orthologues[391,395]. Like all P-type ATPases, ATP13A1 features a central DKTGTLT motif containing the catalytic aspartate[391,395–397] and it also contains conserved nucleotide binding domains[391,395]. Topology predictions have identified at least 10 putative transmembrane domains for mammalian ATP13A1[391]. The yeast homologue Spf1p could not be easily classified based on topology as it had features of both heavy metal-binding and non-heavy metal-binding ATPases[398].

The function and substrate specificity of the P_5-ATPases remained elusive for a long time but recent advances are shedding light on the substrates of at least some of the members of this family of transporters. ATP13A2 is a lysosomal cation pump implicated in the development of a juvenile form of Parkinson's disease[399] whereas ATP13A3 has recently been reported as a putative polyamine transporter[400] and a SNP in ATP13A5 may be associated with atypical presentation of Hailey-Hailey disease[401]. Both ATP13A1 and ATP13A4 localise to the ER and have been reported to be involved in calcium homeostasis[363,392,402]. However, direct calcium transport activity has not been shown for ATP13A1 and ATPase activity of purified Spf1p was not dependent on or enhanced in the presence of calcium *in vitro*[392]. The concentration of manganese in microsomes isolated from *Δspf1* cells has been shown to be decreased compared to that in wild type microsomes, though other divalent cations such as calcium and magnesium were not tested in this experiment[363]. Therefore, the full range of substrates for ATP13A1 remains to be determined and it has been suggested that it may include non-metallic substrates[392].

In the context of MR1 antigen presentation, ATP13A1 is a particular promising target because of its localisation to the ER and its transporter function. Since it is still unclear how soluble MR1 ligands access the ER where they encounter partially folded, ligand-receptive MR1 molecules[260,272] it is tempting to speculate that ATP13A1 may have a role analogous to TAP which transports antigenic peptides into the ER for loading onto MHC class I molecules[125,403–406]. Like TAP, ATP13A1 localises to the ER[392,403] and has ATPase activity[125,392].

Regulated degradation of HMG2p, the yeast isozyme of HMG-CoA reductase, has been shown to be specifically dependent on Spf1p[407], giving a rationale to the hypothesis that ATP13A1 may be involved in regulating MR1 protein stability in the ER and, thus, indirectly MR1 surface expression.

Alternatively, ATP13A1 could indirectly influence MR1 protein folding, loading, or stability in the ER by modulating ion concentrations in this compartment. Divalent cations such as calcium and manganese are important co-factors for many enzymes and disturbing their homeostasis leads to defects in glycoprotein processing[363,392,398,408]. Consistent with this, deficiency for Spf1p and ATP13A1 caused ER stress in yeast and human cells, respectively[363,392,397,408,409]. In yeast, double knock-outs deficient for *spf1* and the unfolded-protein response mediator Hac1p were synthetic lethal[392] and *spf1* was one of the top hits in a screen for proteins involved in protein folding in the ER[409]. Moreover, a more global role for intracellular manganese in the context of an immune response has been demonstrated recently[410].

In this chapter, the effect of ATP13A1 KO on MR1 surface expression is further characterised in both the HAP1.MR1 clone and in THP-1 cells, a monocytic cell line commonly used as an antigen-presenting cell in the MAIT/MR1 field[276,283,297,411–413].

4.2 Chapter specific Materials and Methods

Experiments were carried out according to protocols described in General Materials and Methods (Chapter 2) unless stated otherwise in Figure captions or below.

4.2.1 Supplementation with exogenous manganese

Four wells of $0.5x10^6$ cells per well were plated for each cell line and left to adhere for at least 8 h. Medium was exchanged for medium containing 100 µM $MnCl_2$ (Sigma-Aldrich #48795-1ML-F) at the indicated time points. At t = 0, cells were rinsed with PBS before harvesting in 100 µl of RIPA buffer supplemented with protease inhibitors as in General Material and Methods. For RNA extraction $0.25x10^6$ cells were plated per well, treated as above at indicated time points and harvested directly in buffer RLT (QIAGEN #79216) at t = 0. RNA was extracted and reverse-transcribed as in General Materials and Methods. For flow cytometric analysis, $5x10^4$ cells were plated in duplicate for each time point, treated as above, and harvested with PBSE before staining as in General Materials and Methods.

4.2.2 Inhibition of degradation by the proteasome

$1x10^6$ cells per well were plated for each cell line and left to adhere o/n. Cells were incubated in medium containing either 10 µM MG-132 (Sigma-Aldrich #M7449), 10 µM NMS-873 (Sigma-Aldrich #SML1128), or the equivalent volume of DMSO for four hours. Cells were washed with PBS and harvested in 100 µl of RIPA buffer supplemented with protease inhibitors as in General Materials and Methods.

4.2.3 Digestion with Endoglycosidase H

Equal amounts of protein from RIPA cell lysates were digested with Endoglycosidase H (EndoH, NEB #P0703S) according to manufacturer's instructions. Protein was denatured in supplied Denaturation Buffer for 10 min at 100° C before splitting each sample in two. One half was incubated with the enzyme in the appropriate Glycobuffer and the other half with Glycobuffer only. Loading buffer and reducing agent were added to each reaction and samples were analysed by SDS-PAGE as in General Materials and Methods.

4.2.4 Cycloheximide chase assay

Five wells of $1x10^6$ cells per well were plated for each cell line and left to adhere o/n. Medium was exchanged for medium containing 100 µM Cycloheximide (Sigma-Aldrich #01810-1G) at the indicated time points. At t = -8h, medium on the untreated samples was exchanged for fresh medium for better comparison. At t = 0, cells were rinsed with PBS before harvesting in 150 µl of RIPA buffer supplemented with protease inhibitors as in General Material and Methods. For flow cytometric analysis, $1x10^5$ cells were plated in duplicate for each time point, treated as above, and harvested with PBSE before staining as in General Materials and Methods.

4.2.5 Culture in manganese-deficient medium

THP-1 or THP-1.MR1 cells were cultured in AIM V Serum Free Medium (Gibco #12055091) for at least five days before incubation in AIM V medium supplemented with the indicated concentrations of $MnCl_2$ (Sigma-Aldrich #48795-

1ML-F) for 24 h. Cells were harvested and processed as in General Materials and Methods.

4.2.6 Illumina Deep Sequencing

Regions around the sgRNA target sited were amplified from cDNA using primers that generated overhangs compatible with Illumina adapters (Supplementary Table 1). PCR products were gel-purified (QIAGEN #28704) and bar-coded using the Illumina index adapter series D5 and D7 (Supplementary Table 1, oligonucleotide sequences © 2018 Illumina, Inc. All rights reserved.). Barcoded amplicons were analysed on an Agilent 2200 TapeStation System, cleaned up with Agincourt Ampure XP beads (Beckman Coulter #A 63881), pooled in equimolar ratios, and quantified on a Qubit3 Fluorometer. The library was sequenced paired-end (20 nt + 280 nt) on an Illumina Miseq machine using the Miseq Reagent Nano Kit V2 300-cycle (Illumina #MS-103-1001) by Margarida Rei at the MRC WIMM Sequencing facility. Sequences were analysed using CRISPResso[414].

4.3 Total MR1 levels in HAP1.MR1 ATP13A1 KO clones

To further characterise the MR1 phenotype in the HAP1.MR1 ATP13A1 KO clones described in Chapter 3, total MR1 protein levels of four clones were analysed by Western Blot. Interestingly, ATP13A1 but not B2M or TMEM131 KO clones had much lower MR1 protein levels compared to the parent clone D9. ATP13A1 KO clones expressed as little as 17-33% of parent MR1 protein levels (Figure 4.1). It was not possible to directly compare the KO clones to the HAP1.MR1 parent clone D9 due to differences in group size, but comparisons between the total MR1 protein levels in the B2M, ATP13A1, and TMEM131 KO clones revealed statistically significantly lower MR1 levels in ATP13A1 KO clones compared to B2M (p = 0.0134) but not TMEM131 (p = 0.1873) KO clones. Similar results were obtained when more B2M and ATP13A1 KO clones were compared in the absence of the parent clone D9 in another experiment (data not shown). Total MR1 protein levels were not significantly different between B2M KO clones and TMEM131 KO clones (p = 0.9804). This suggests that the MR1 surface phenotype observed in ATP13A1 KO clones may be due to a reduced level of overall MR1 protein rather than a specific reduction of the MR1 pool at the cell surface.

To test whether the reduced total MR1 protein level was due to less transcription of the MR1 transgene in the ATP13A1 KO clones, MR1 mRNA levels were determined. Albeit subtle in magnitude, there was a statistically significant (difference = -0.3487; 95% CI [-0.6283, -0.06912]; p = 0.0225) reduction in MR1 transcript levels in the ATP13A1 KO clones compared to the B2M KO clones. ATP13A1 KO clones expressed 62-83% of parent MR1 transcript levels whereas B2M KO clones expressed 83-106% (Figure 4.1c). A similarly statistically

significant difference was detected when comparing only B2M and ATP13A1 KO clones in another qRT-PCR whereas a third experiment measuring MR1 transcript levels in ATP13A1 KO clones only found no difference relative to the parent clone D9 although this could not be tested statistically. While the biological significance of these findings remains to be determined, it provided a rationale for investigating potential differences between the co-transfected sgRNAs.

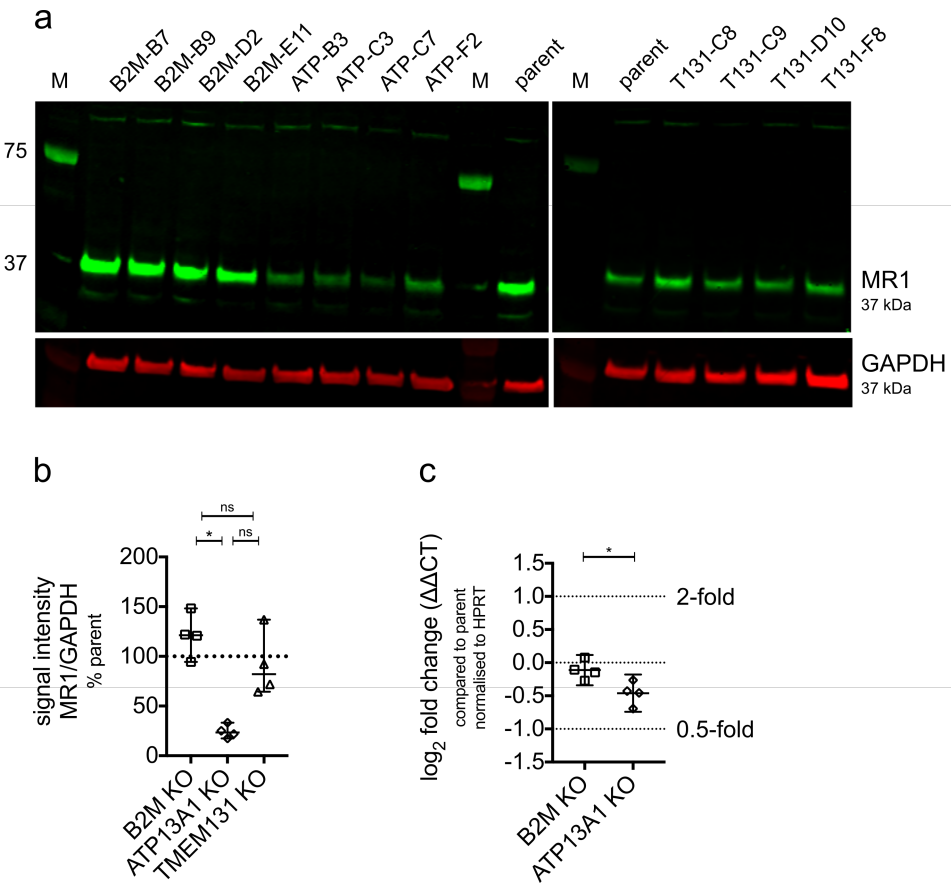


Figure 4.1: Total MR1 protein levels and MR1 transcript levels are reduced in ATP13A1 KO clones co-transfected with multiple sgRNAs. Total MR1 protein levels (a, b) and MR1 transcript levels (c) were measured in four HAP1.MR1 clones deficient for β_2m (B2M), ATP13A1 (ATP), or TMEM131 (T131). Signal intensity of Western Blots was quantified with the Odyssey® Near-Infrared imaging system (b). MR1 and GAPDH were measured simultaneously on the same membranes but are displayed separately due to equal molecular weights. M denotes molecular weight marker and molecular weights of visible marker bands are indicated in kDa to the left of the blots. Parent denotes HAP1.MR1 parent clone D9. Dashed line in (b) indicates parent level. Each symbol in (b) represents one clone and median with range is shown for each group. MR1 transcript levels in (c) were determined by qRT-PCR and are shown normalised to HPRT and relative to the parent clone D9. Each symbol represents the mean of technical duplicates for one clone and mean with 95% confidence interval is shown. Dashed lines indicate $\Delta\Delta C_T$ corresponding to 0, 0.5-fold, and 2-fold difference compared to the D9 parent clone. Statistical significance was calculated using the Kruskal-Wallis test with Dunn's multiple comparison test in (b) and an unpaired, two-tailed t-test in (c). * = $p < 0.05$, ** = $p < 0.01$, *** = $p < 0.001$, **** = $p < 0.0001$, ns = not significant.

4.4 Deconvolution of sgRNAs targeting ATP13A1 in HAP1.MR1 cells

To investigate the possibility that one of the three co-transfected sgRNAs targeting ATP13A1 had off-target effects affecting MR1 transcription in these cells and to further validate the observations made in the co-transfected clones, ATP13A1 KO clones were generated using the three ATP13A1 sgRNAs separately. Viable clones were screened by Western Blot and total MR1 levels were also measured. Loss of ATP13A1 and reduced MR1 protein levels coincided in all screened clones except for clone 3-15 which had lower MR1 levels despite expressing ATP13A1 (Figure 4.2). Since signal intensities for MR1 of ATP13A1-expressing clones were frequently saturated at imaging settings that allowed the detection of MR1 in ATP13A1 KO clones, quantification of signal intensity was not possible for most ATP13A1-expressing clones. Thus, it was not possible to calculate statistical significance as both sample size and standard deviations were unequal between the two groups with less than three ATP13A1-expressing clones reliably quantifiable relative to the parent clone. Therefore, this result requires re-analysis with more data points in each group before statistically supported conclusions can be drawn. Nevertheless, the correlation between ATP13A1 status and MR1 protein level in 31 out of 32 clones is striking. For the KO clones chosen for further analysis (1-7, 2-20, and 3-1), reduced MR1 expression was confirmed multiple times including blotting with a different αMR1 antibody (data not shown).

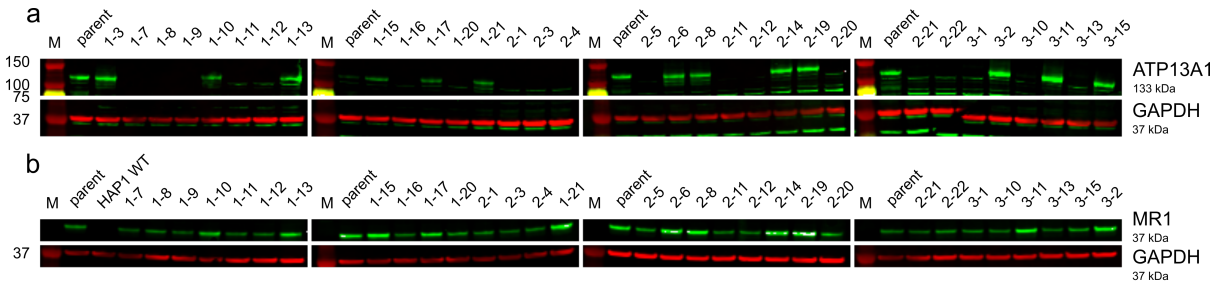


Figure 4.2: Total MR1 levels are reduced in HAP1.MR1 ATP13A1 KO clones generated with three different sgRNAs. HAP1.MR1 clone D9 cells were transiently transfected with three different sgRNAs targeting ATP13A1 (1-3), single cell sorted and cultured as individual clones. Expression of ATP13A1 (a) and MR1 (b) was determined for 12 clones transfected with guide 1, 13 clones transfected with guide 2, and 6 clones transfected with guide 3 by Western Blot. Relevant portions of Western Blots are shown. Loading control GAPDH was imaged on the same blots as the gene of interest but is shown separately in b due to equal molecular weights. Parent denotes HAP1.MR1 parent clone D9. M denotes molecular weight marker and molecular weights of visible marker bands are indicated in kDa to the left of the blots. Results for clones 1-7, 1-17, 2-19, 2-20, 3-1, and 3-15 are also supported by the Western Blot data shown in **Figure 4.7**b.

To test whether MR1 transcript levels were reduced in ATP13A1 KO clones transfected with each of the three sgRNAs, mRNA levels were measured in three clones expressing ATP13A1 and three ATP13A1 KO clones for each guide and compared to parent transcript levels. MR1 transcript levels were variable across clones and statistically significantly reduced in the ATP13A1 KO clones generated with sgRNA2 (difference = -0.9607; 95% CI [-1.605, -0.316]; p = 0.0144) but not sgRNA1 (difference = -0.4373; 95% CI [-1.181, 0.3064]; p = 0.1779) when compared to their ATP13A1-expressing counterparts (Figure 4.3). No statistical comparison could be made for the clones generated with sgRNA3 as clone 3-15 can not be considered ATP13A1-sufficient due to a mutation in a highly conserved locus within the ATP13A1 gene (discussed below, see Figure 4.4) Compared to the HAP1.MR1 parent clone D9, however, MR1 mRNA levels were only lower in one of the 12 ATP13A1 KO clones tested (Figure 4.3). It should be noted, however, that the RNA for the WT and parent samples represents a different passage as keeping the WT and parent clones in culture during the expansion of

the sorted clones would likely have resulted in their becoming polyploid. A later experiment using RNA extracted from cells thawed and cultured for the same amount of time confirmed that KO clones 1-7, 2-20, and 3-1 expressed the same amount of MR1 mRNA as the parent clone D9 (Figure 4.10) but more data are needed to draw a firm conclusion. Importantly, statistical significance is not equivalent to biological significance and MR1 expression in all clones was within 2-fold of the parent expression level except for clone 3-2 which expressed 2.5 times the amount of MR1 transcript expressed in the parent clone. Of note, ploidy of clones 1-3, 1-13, 2-6, 2-14, 3-2, and 3-11 was not determined and their relatively high expression of MR1 may stem from having multiple copies of the MR1 locus. Clone 2-19 was haploid when tested (data not shown) and still expressed about twice as much MR1 mRNA as the parent clone. Based on their MR1 expression level comparable to the parent clone D9, clones 1-7, 2-20, and 3-1 were chosen for further analysis. In addition, clones 1-17 and 2-19 were included as controls as they had been transfected but still expressed the protein and clone 3-15 was further analysed because it showed an MR1 phenotype despite expressing ATP13A1 in the Western Blot (Figure 4.2).

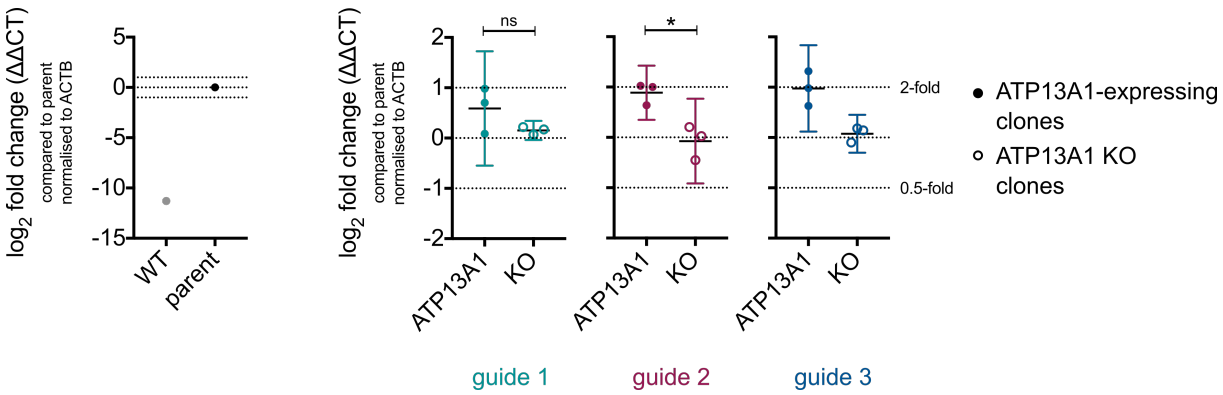


Figure 4.3: MR1 transcript levels are variable across clones transfected with individual sgRNAs. MR1 transcript levels in HAP1.MR1 clones transiently transfected with one of three distinct single guide RNAs targeting ATP13A1 were determined by qRT-PCR and are shown compared to the parent clone D9 and normalised to HPRT. Parent denotes HAP1.MR1 parent clone D9. Colour coding represents the sgRNA used to generate the respective clone. RNA from clones was extracted simultaneously but reverse transcribed in two batches. Each symbol represents the mean of technical duplicates for one clone and mean with 95% confidence interval is shown. Dashed lines indicate $\Delta\Delta C_T$ corresponding to 0, 0.5-fold, and 2-fold difference compared to the D9 parent clone. Statistical significance was calculated using an unpaired, two-tailed t-test comparing the ATP13A1-expressing to the ATP13A1 KO clones for each guide. Data for parent clone D9 and WT controls are shown as reference but were not considered in the statistical analysis.* = $p < 0.05$, ** = $p < 0.01$, *** = $p < 0.001$, **** = $p < 0.0001$, ns = not significant. Similar results were obtained for KO clones 1-7, 2-20, and 3-1 in another experiment although this could not be analysed statistically (see **Figure 4.10**c).

To better understand the nature of the underlying the mutations and confirm that the clones were bona-fide KO for ATP13A1, the regions spanning the respective sgRNA target sites were amplified from genomic DNA from clones 1-7, 1-17, 2-19, 2-20, 3-1, and 3-15 and submitted for Sanger sequencing. Sequence analysis showed that the ATP13A1 locus was edited even in the clones still expressing the protein (Figure 4.4). The ATP13A1 gene in clone 1-17 has a nine bp deletion resulting in the in-frame loss of three amino acids, presumably allowing the production of functional protein. Similarly, gene editing has resulted in a two bp swap in clone 2-19 causing two amino acids to change but leaving the reading frame intact. A six bp deletion in clone 3-15 has equally left the reading frame intact but the resulting amino acid change has altered a highly conserved region within the amino acid sequence[395] potentially resulting in the production of

dysfunctional protein. The importance of this GxPF motif is not only underscored by its conservation across yeast, murine and human ATP13A1 homologues[391,395], but also by the observation that a construct lacking the C-terminal region of the protein including this motif was unable to rescue the spf1 KO phenotype in yeast[398]. It was, therefore, conceivable that alterations in this region resulted in the production of defective protein, which could explain the “KO-like” phenotype of clone 3-15. Due to this observation, clone 3-15 could not be considered an ATP13A1-sufficient clone and statistical analysis could not include this clone in the control group. Clones 1-7 and 3-1 featured frame-shift mutations and clone 2-20 had an 18 bp deletion resulting in the loss of six amino acids. In conjunction with the Western Blot results, these three clones can therefore be considered bona fide KO for ATP13A1. All three regions were amplified in the parent clone D9 as a control and all sequences obtained from this clone aligned with the NCBI Reference Sequence NC_000019.10 (data not shown).

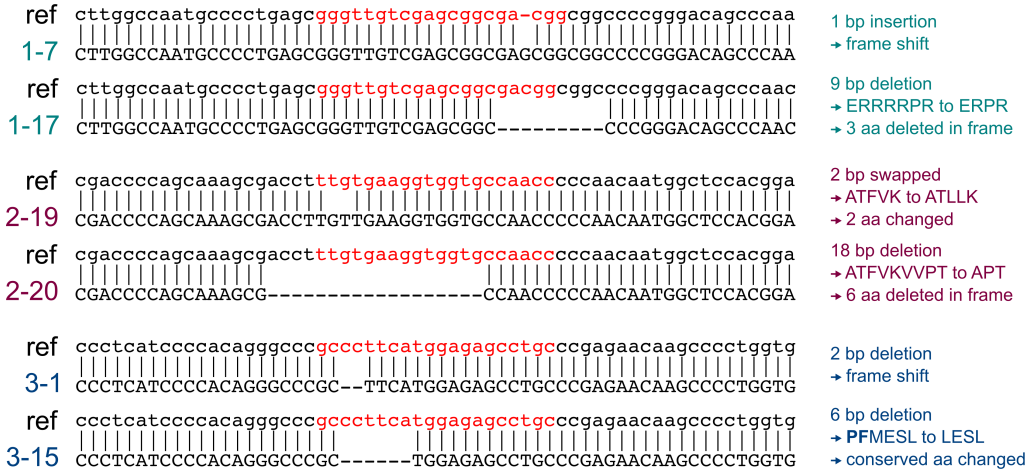


Figure 4.4: HAP1.MR1 ATP13A1 KO clones 1-7, 2-20, and 3-1 are bona fide KO for ATP13A1. Genomic regions around sgRNA target sites were amplified and sequenced in HAP1.MR1 ATP13A1 clones. Names of the clones are given on the left and sequences are shown aligned to the NCBI Reference Sequence NC_000019.10 with sgRNA target sites highlighted in red. Colour coding for clones as in **Figure 4.3**. Consequences of gene editing are summarised to the right of each sequence. bp = base pair; aa = amino acid

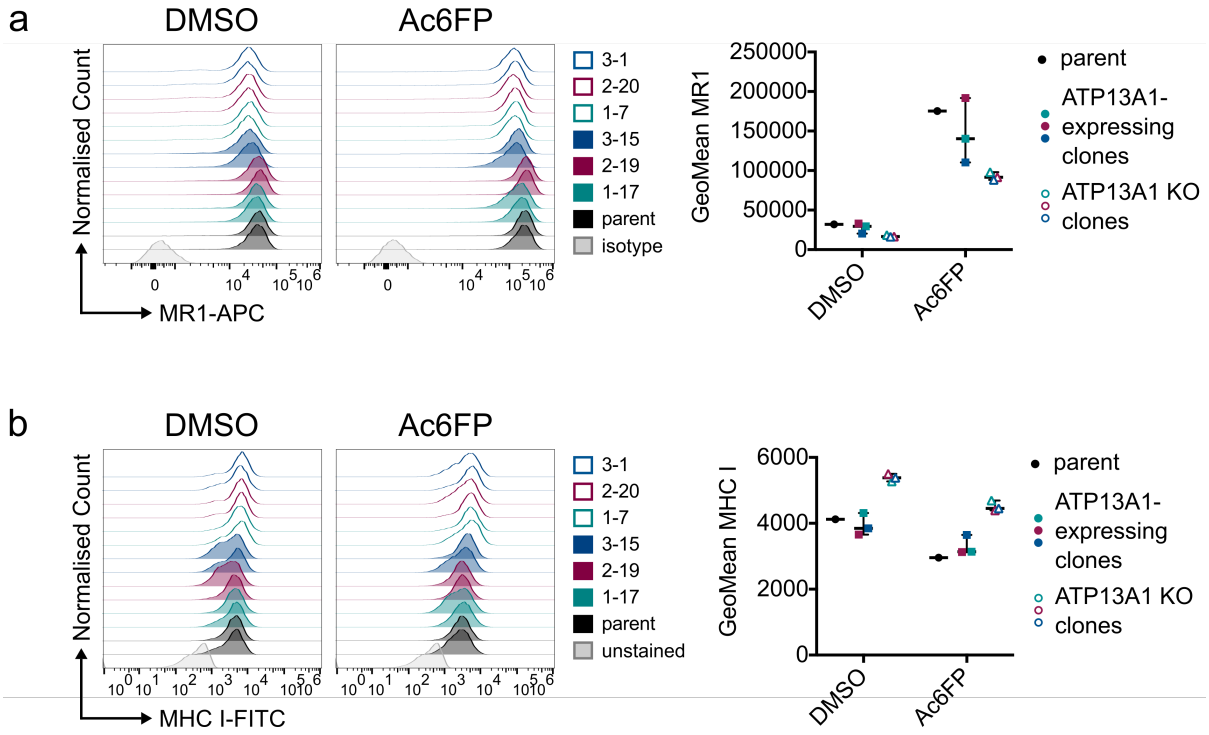


Figure 4.5: MR1 but not MHC-I surface levels are reduced in HAP1.MR1 ATP13A1 KO clones in the presence and absence of stabilising ligand. HAP1.MR1 ATP13A1 clones expressing ATP13A1 (shaded histograms and bars) or not (empty histograms and bars) were pulsed with 5 µg/ml Ac6FP or DMSO solvent control in duplicates and stained for surface expression of MR1 (a) and MHC class I (b). Parent denotes HAP1.MR1 parent clone D9. Colours indicate sgRNA used to generate the respective clone. Cells stained with APC-conjugated isotype control antibody (a) or stained with live/dead stain only (b) are shown as control. Each symbol represents the median of technical duplicates for one clone and median with range is shown.

Next, MR1 and MHC class I surface levels in the selected clones were tested to validate the surface phenotype observed in clones co-transfected with three pooled sgRNAs. Indeed, MR1 surface levels appeared consistently lower in ATP13A1 KO clones compared to both the parent clone D9 and their ATP13A1-expressing counterparts in one complete experiment (Figure 4.5). This difference held in both in the presence and absence of the MR1-stabilising ligand Ac6FP. The only exception was clone 3-15 which had reduced MR1 surface levels despite expressing ATP13A1. This is consistent with the reduced total MR1 expression (Figure 4.2) and the sequencing result (Figure 4.4) of this clone. A similar trend was observed for the parent clone D9, clones 1-7 and 1-17 as well as clones 3-1

and 3-15 in another experiment using 1 and 10 μg/ml Ac6FP although there was some variation between duplicates for clone 1-17 (data not shown). MHC class I surface levels were unaffected by incubation with Ac6FP but mildly elevated in the HAP1.MR1 ATP13A1 KO clones (Figure 4.5). Since clone 3-15 could not be considered as ATP13A1-sufficient based on the sequencing data (Figure 4.4), statistical analysis of the difference between ATP13A1-expressing and ATP13A1 KO clones was not possible. Thus, the results obtained should be considered trends and additional experiments are needed to strengthen the conclusions drawn. Of note, reduced MR1 surface expression compared to the HAP1.MR1 parent clone D9 at baseline was also observed in later experiments (see for example Figure 4.11) but was not directly compared with ATP13A1-expressing clones in those experiments and is, thus, not amenable to the statistical comparison of ATP13A1-sufficient vs ATP13A1 KO clones.

Antigen presentation of the synthetic MR1 ligand 5-A-RU to sorted human MAIT cells was also reduced in the clones deficient for ATP13A1 but not in those expressing the transporter (Figure 4.6), similarly to the clones transfected with all three guides. This effect titrated with the ligand concentration. As observed for MR1 surface staining and Western Blot, clone 3-15 behaved more like a KO clone than one expressing ATP13A1. For the same reason described for the flow cytometry data, statistical analysis of these data was not possible and further evidence is needed to substantiate these conclusions.

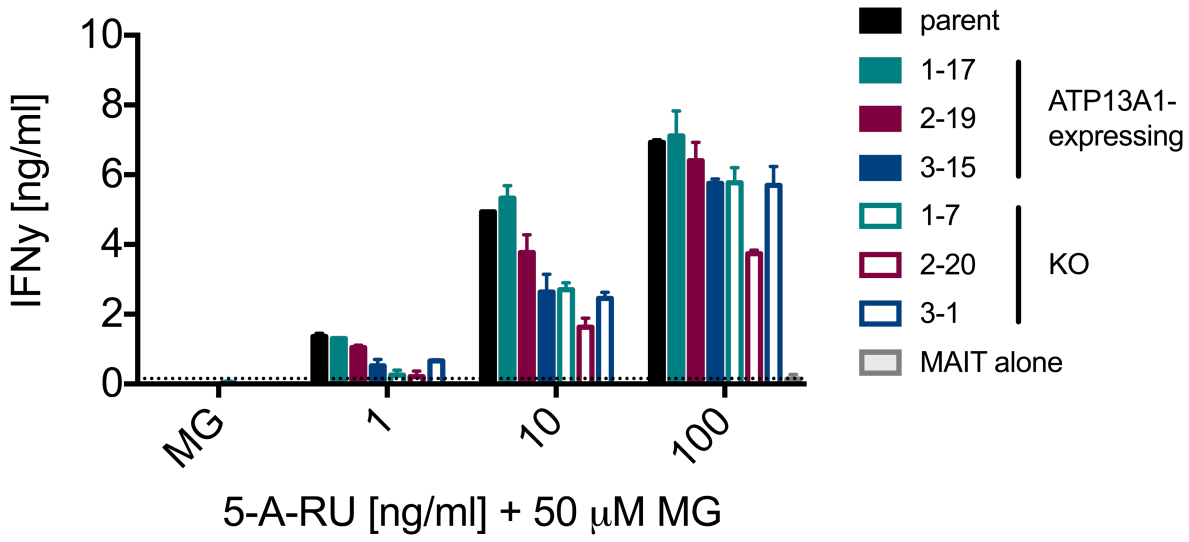


Figure 4.6: Antigen presentation of MR1 ligand appears reduced in HAP1.MR1 ATP13A1 KO clones transfected with three different sgRNAs. Three HAP.MR1 clones expressing ATP13A1 (filled bars) or not (empty bars) were pulsed with 1-100 ng/ml 5-A-RU and 50 μM MG for 5 h. Ligand was washed off and sorted human MAIT cells were added for 36 h. Interferon γ (IFNγ) secretion into the supernatant was quantified by ELISA. Parent denotes HAP1.MR1 parent clone D9, dashed line denotes limit of detection. Colour coding indicates sgRNA used in transfection: teal = guide 1, maroon = guide 2, blue = guide 3. Data represent technical duplicates and are plotted as median with range. The experiment was repeated with similar results using a different MAIT cell donor and 100 ng/ml 5-A-RU only.

To exclude differential expression of the light chain β_2-microglobulin (β_2m) as a limiting factor for MR1 surface expression in the HAP1.MR1 ATP13A1 KO clones, B2M transcript levels and β_2m protein levels were determined. β_2m expression was not lower in ATP13A1 KO clones than in their ATP13A1-expressing counterparts or the parent clone D9, consistent with the observation that surface MR1 expression was upregulated in response to Ac6FP and MHC class I expression was not reduced in these clones (Figure 4.5). MR1 was immuno-blotted for in parallel and results confirmed the MR1 phenotype described in Figure 4.2. Again, ATP13A1 KO clones could not be statistically compared to ATP13A1-sufficient clones but two independent experiments did not give any indication for reduced β_2m expression in the ATP13A1 KO clones generated with

individual sgRNAs. It should be noted, however, that B2M expression appeared slightly variable among the ATP13A1 KO clones generated with the pool of three sgRNAs in one preliminary experiment (data not shown).

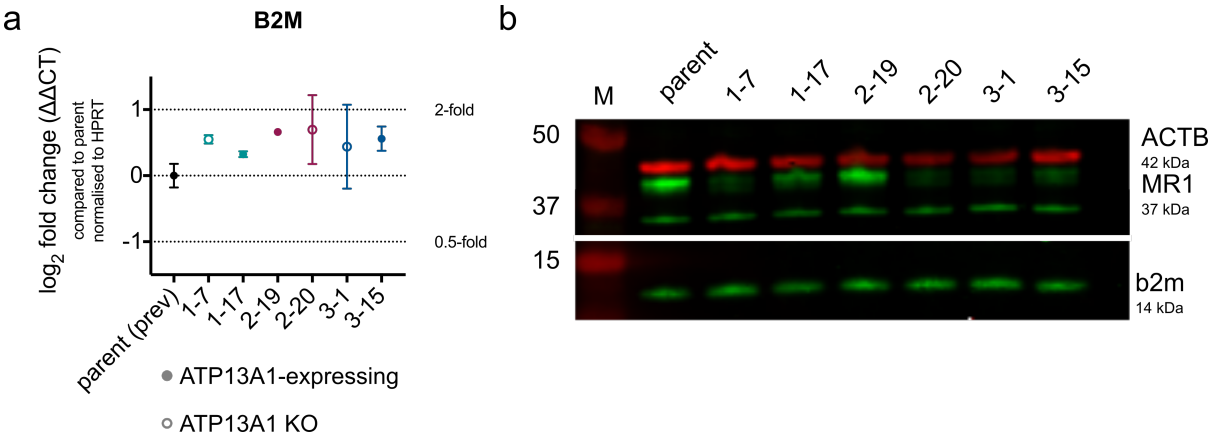


Figure 4.7: Expression of β_2-microglobulin is not a limiting factor in HAP1.MR1 ATP13A1 KO clones. Expression of β_2-microglobulin in HAP1.MR1 clones expressing ATP13A1 or not was measured at the mRNA (a) and protein (b) level. Parent denotes HAP1.MR1 parent clone D9. Each symbol in (a) represents the mean of technical duplicates and is shown with 95% confidence interval. Dashed lines indicate $\Delta\Delta C_T$ corresponding to 0, 0.5-fold, and 2-fold difference compared to the D9 parent clone. Colour coding in (a) indicates sgRNA used in transfection: teal = guide 1, maroon = guide 2, blue = guide 3. M in (b) denotes protein marker and molecular weights of visible marker bands are indicated in kDa to the left of the blots. Loading control ACTB is shown in red and MR1 and β_2m are shown in green. The membrane was cut at the 25 kDa marker band prior to antibody incubation. B2M transcript levels were measured in the same cDNA samples as MR1 shown in **Figure 4.3**. Western Blot is representative of two independent experiments for KO clones 1-7, 2-20, and 3-1.

To further delineate which folding states of MR1 were affected by the ATP13A1 KO, MR1 was immuno-precipitated from HAP1.MR1 ATP13A1 KO clones with the conformation-specific antibody clone 26.5 before immuno-blotting with a pan-conformational polyclonal antibody in one test experiment. As expected based on the literature[260], the majority of the protein remained in the unbound fraction indicating that only a small subset of the MR1 molecules expressed in both the HAP1.MR1 parent clone and the HAP1.MR1 ATP13A1 KO clones was folded in the absence of exogenous ligand (Figure 4.8). These preliminary data also

suggest that both unfolded and folded MR1 levels were reduced in the HAP1.MR1 ATP13A1 KO clones.

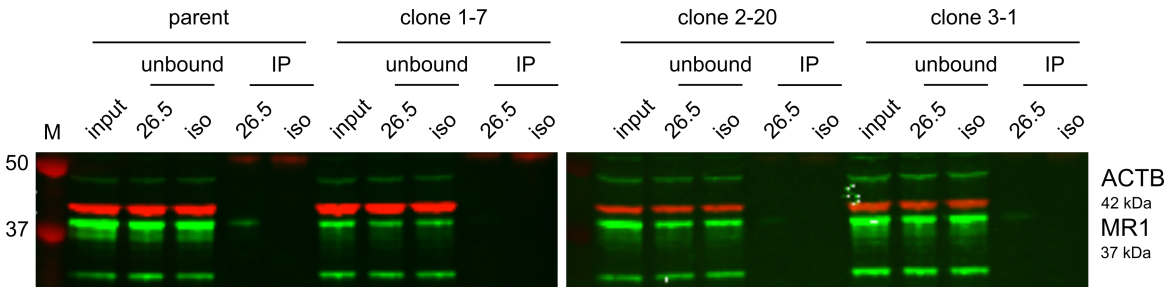


Figure 4.8: Levels of folded and unfolded MR1 are reduced in HAP1.MR1 ATP13A1 KO clones. Equal cell numbers of the indicated HAP1.MR1 ATP13A1 KO clones and the HAP1.MR1 parent clone D9 (parent) were lysed and pre-cleared with Protein G agarose resin before immuno-precipitation with the confirmation-specific αMR1 antibody clone 26.5 (26.5) or murine IgG2a isotype antibody (iso). Immuno-precipitates and unbound fractions were separated by SDS-PAGE along with input samples and immuno-blotted for MR1 (green) and loading control ACTB (red). M denotes protein marker and molecular weights of visible marker bands are indicated in kDa to the left of the blot.

4.5 Reconstitution of ATP13A1 expression in HAP1.MR1 ATP13A1 KO clones

To ascertain whether the observed MR1 phenotype could be attributed to the lack of ATP13A1, the three ATP13A1 KO clones as well as the ATP13A1-expressing clone 3-15 were transduced with lentiviral particles encoding the cDNA for human ATP13A1. ATP13A1 over-expression in the polyclonal, transduced cell population was confirmed by Western Blot and rescued MR1 protein levels above parent levels (Figure 4.9a). This finding corroborates the conclusion that β_2m is not the limiting factor in this system. ATP13A1 over-expression also partially restored the antigen presentation capacity of all three HAP1.MR1 ATP13A1 KO clones (Figure 4.9b). In all cases, more IFNγ was produced in response to the reconstituted cell line even though parent levels were not reached. It should be noted that statistical

comparison of clonal populations with polyclonal cell lines may be subject to inherent limitations because there may be variability within the polyclonal population which is not present in the clonal parent cell line. Here, the median of three pooled cell lines in each group was compared to mitigate the potential effect of this difference in variability. Since Gaussian distribution of the data was not assumed, a two-way ANOVA could not be performed to test for an interaction between ATP13A1 status and ligand concentration. Pairwise statistical comparison of ATP13A1 KO vs reconstituted cells at the highest 5-A-RU concentration did not reveal statistically significant differences with the non-parametric statististical test used. Nevertheless, the trends reported here are consistent across experiments and assays, further strengthening the general conclusion that the MR1 phenotype can be rescued by reconstitution of ATP13A1 expression.

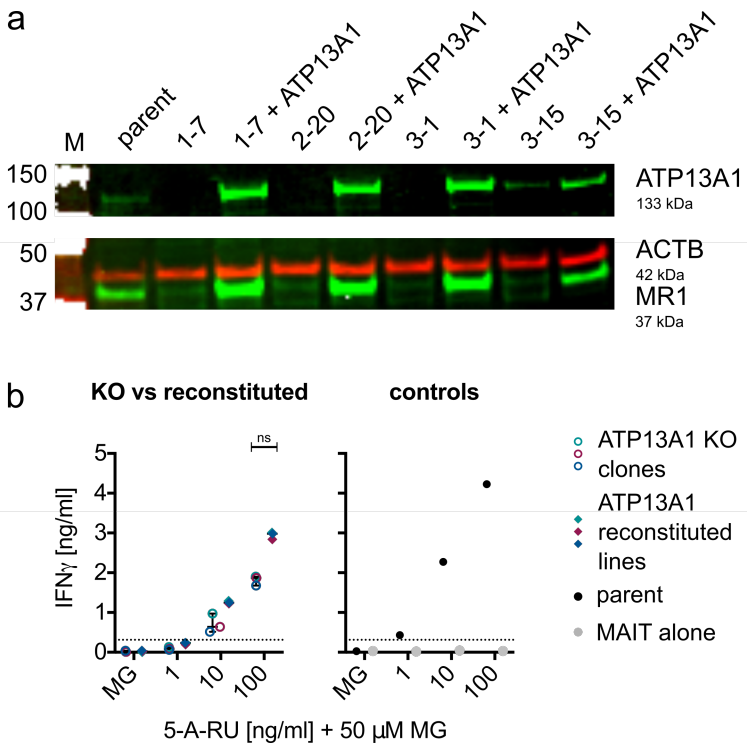


Figure 4.9: Over-expression of ATP13A1 rescues total MR1 levels in HAP1.MR1 ATP13A1 KO clones and partially restores antigen presentation. Four HAP1.MR1 ATP13A1 clones were transduced with lentiviral particles encoding human ATP13A1 and polyclonal transduced populations were analysed for protein expression of ATP13A1 and MR1 (a) as well as antigen presentation capacity (b). The membrane was cut before incubation with separate antibodies for (a) and loading control ACTB is shown in red. M denotes protein marker and molecular weights of visible marker bands are indicated in kDa to the left of the blots. Parent denotes HAP1.MR1 parent clone D9. Dashed line in (b) denotes limit of detection. Colour coding in (b) indicates sgRNA used in transfection: teal = clone 1-7, maroon = clone 2-20, blue = clone 3-1. Each symbol in (b) represents the median of technical duplicates for one clone and median with range is shown for the groups. Data for parent clone D9 and MAIT cell only controls are shown as reference. Statistical significance at 100 ng/ml 5-A-RU was calculated using the Wilcoxon matched-pairs signed rank test where * = $p < 0.05$, ** = $p < 0.01$, *** = $p < 0.001$, **** = $p < 0.0001$, ns = not significant. Data in (b) are representative of two experiments using two different MAIT cell donors.

4.6 The mechanism of the modulatory effect of ATP13A1 on MR1 protein levels

Having established that HAP1.MR1 ATP13A1 KO clones indeed display an MR1 phenotype attributable to ATP13A1 deficiency, the mechanism by which ATP13A1 expression modulates MR1 protein levels was investigated. As discussed in the introduction, ATP13A1 may conceivably influence MR1 protein levels directly or indirectly in a variety of ways including modulation of the intracellular – and

particularly intra-ER – Manganese levels, general ER stress, altered glycosylation, and protein stability as a consequence of altered or defective protein folding. In the following experiments these different hypotheses were addressed.

4.6.1 Manganese

Since an Spf1p-deficient yeast strain was shown to have a reduced Manganese concentration in the ER[363], the effect of manganese concentrations in the medium on MR1 levels was tested. HAP1.MR1 ATP13A1 KO clones were incubated in medium supplemented with exogenous manganese and MR1 levels were followed over time. A preliminary experiment suggested that HAP1.MR1 ATP13A1 KO clones upregulated their MR1 surface expression upon prolonged culture in Mn-supplemented medium (Figure 4.10a). Analysis of three pooled ATP13A1 KO clones revealed a statistically significant (p = 0.0342) increase in MR1 surface levels after 12 h of Mn-supplementation as compared to baseline. MHC class I levels were not consistently affected by addition of manganese in the same experiment. However, this experiment was confounded by extensive cell death at late time points and no definite conclusions could be drawn.

It has recently been reported that incubation with comparable levels of manganese triggered a type I interferon response in THP-1 cells, rendering the cells more sensitive to cytoplasmic DNA and poised for an antiviral immune response[410]. Therefore, it was conceivable that the increased MR1 surface expression could be ascribed to the induction of type I interferons which may, in turn, increase MR1 transcription. Since MR1 was expressed as a transgene from an exogenous

promoter in the HAP1.MR1 clones it was unlikely that normal regulatory mechanisms would apply, but the possibility still had to be formally excluded. Indeed, quantification of the transcripts of two interferon-induced genes as well as MR1 itself gave no evidence for a type I interferon response in the ATP13A1 KO clones under the experimental conditions used (Figure 4.10c). Neither IFIT1 nor MR1 transcript levels were increased in these cells after 24 h in Mn-supplemented medium (Figure 4.10c) and IFNB transcripts could not be reliably detected at either time point (data not shown). Therefore, the observed increase in MR1 surface expression was likely not due to increased transcription of the MR1 transgene. Interestingly, both IFIT1 and MR1 gene expression appeared slightly increased in the HAP1.MR1 parent clone D9 upon culture in Mn-supplemented medium for 24 h. Both the statistical and the biological significance of this upregulation could not be inferred from the single preliminary experiment performed.

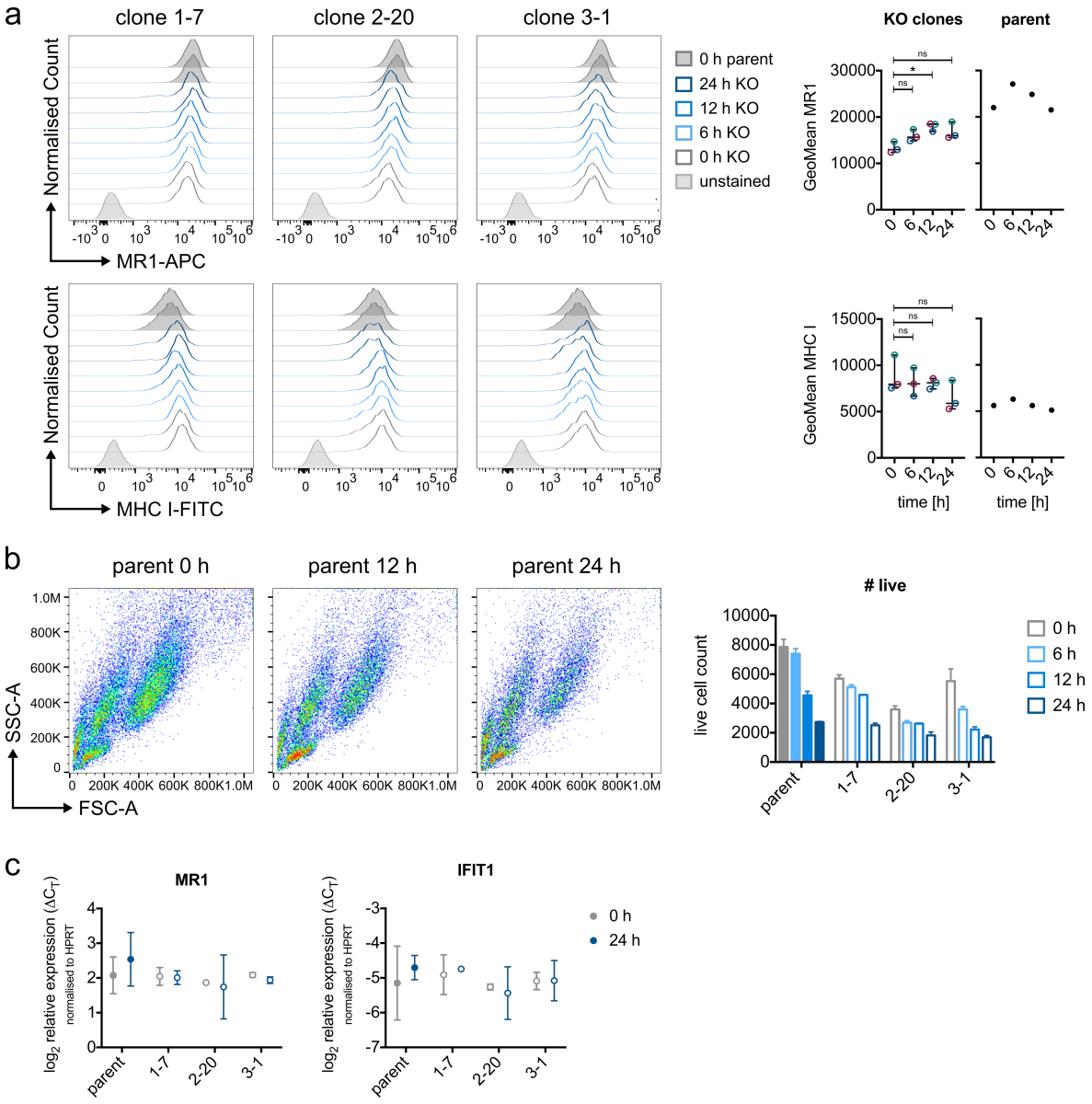


Figure 4.10: Exogenous addition of Mn^{2+} partially restores MR1 surface expression but does not induce a Type I-interferon response in HAP1.MR1 ATP13A1 KO clones. HAP1.MR1 ATP13A1 KO clones 1-7, 2-20, and 3-1 (empty histograms) and parent clone D9 (parent, filled histograms) were cultured in medium supplemented with 100 µM of $MnCl_2$ for 0-24 h and MR1 (top panels) as well as MHC class I (bottom panels) surface levels were analysed by flow cytometry. The unstained parent sample is shown as a negative control and the untreated parent sample is shown for comparison. The geometric mean (GeoMean) is shown to the right of the histograms. Each symbol represents the median of technical duplicates for one clone and colour coding indicates sgRNA used in transfection: teal = clone 1-7, maroon = clone 2-20, blue = clone 3-1. Median with range is shown for each time point. Statistical significance was calculated using the Friedman test with Dunn's multiple comparisons test comparing each time point to t = 0. Data for parent clone D9 are shown as reference but were not considered in the statistical analysis. * = $p < 0.05$, ** = $p < 0.01$, *** = $p < 0.001$, **** = $p < 0.0001$, ns = not significant. Representative forward scatter (FSC-A) versus side scatter (SSC-A) plots and numbers of viable cells for each sample are shown in (b). Bars represent median of technical duplicates with range. The same volume of stained cells was acquired for each sample. Transcript levels of MR1 and IFIT1 were quantified by qRT-PCR (c). Data are shown normalised to HPRT and each symbol represents the mean of technical duplicates with the 95% confidence interval.

Since culture in Mn-supplemented medium for extended period of time led to a substantial reduction in viable cells (Figure 4.10b), shorter time courses were performed for the analysis of total MR1 protein levels upon addition of exogenous manganese. Over a period of six hours, total MR1 protein expression marginally increased in all three HAP1.MR1 ATP13A1 KO clones and reached statistical significance at t = 6 h (p = 0.0342, Figure 4.11a). Of note, MR1 surface levels were not changed in this shorter time span in one preliminary experiment (Figure 4.11b).

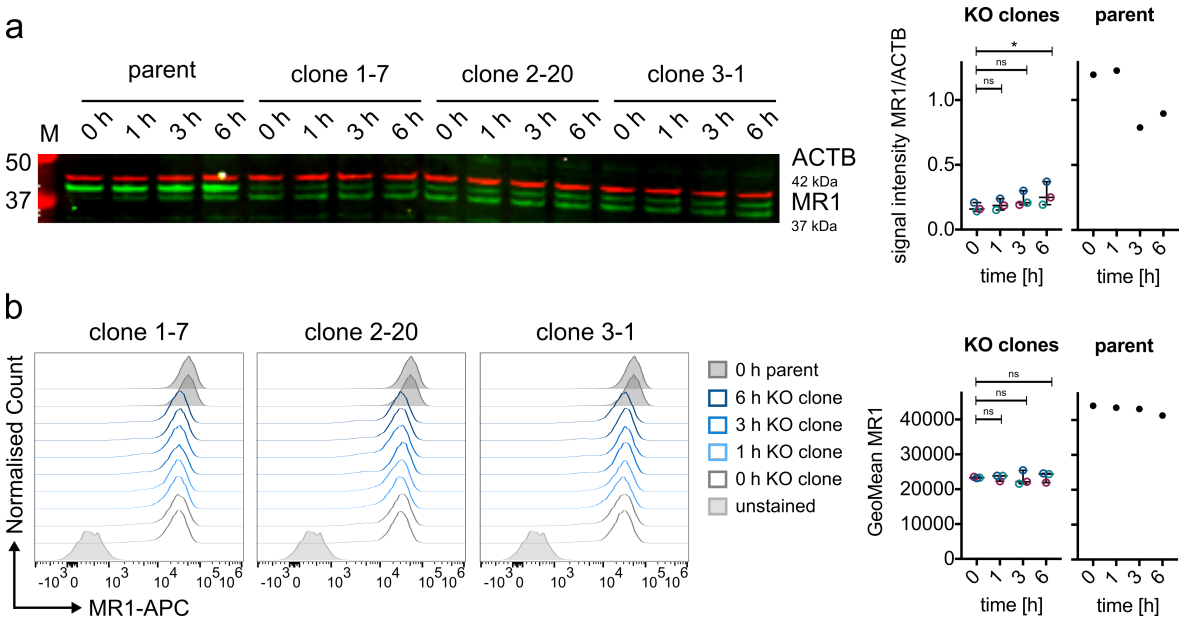


Figure 4.11: Exogenous addition of Mn^{2+} partially restores total MR1 levels in HAP1.MR1 ATP13A1 KO clones. HAP1.MR1 ATP13A1 KO clones 1-7, 2-20, and 3-1 (empty histograms and bars) and parent clone D9 (parent, filled histograms and bars) were cultured in medium supplemented with 100 µM of $MnCl_2$ for 0-6 h and total MR1 protein expression (a) as well as surface levels (b) were analysed. Protein expression was quantified with the Odyssey® Near-Infrared imaging system and MR1 intensity (green) normalised to loading control ACTB (red) is shown to the right of the blot. Parent denotes HAP1.MR1 parent clone D9. M denotes molecular weight marker and molecular weights of visible marker bands are indicated in kDa to the left of the blot. The unstained parent sample is shown as a negative control and the untreated parent sample is shown for comparison in (b). Each symbol in (a) represents one clone. In (b), ich symbol represents the median of technical duplicates for one clone. Colour coding indicates sgRNA used in transfection: teal = clone 1-7, maroon = clone 2-20, blue = clone 3-1. Median with range is shown for each time point. Statistical significance was calculated using the Friedman test with Dunn's multiple comparisons test. Data for parent clone D9 are shown as reference but were not considered in the statistical analysis. * = $p < 0.05$, ** = $p < 0.01$, *** = $p < 0.001$, **** = $p < 0.0001$, ns = not significant. Western Blot results are representative of two independent experiments although the 3 h time point was not included for all clones in the repeat.

4.6.2 Glycosylation

Another phenotype frequently reported for *spf1* KO strains is hypoglycosylation of proteins[363,398,408]. To investigate the glycosylation state of MR1 in the HAP1.MR1 ATP13A1 KO clones, whole cell lysates were digested with Endoglycosidase H (EndoH), a glycosidase which cleaves N-linked high-mannose oligosaccharides from glycoproteins. Since EndoH cannot cleave the highly complex polysaccharide residues generated during post-translational modification in the Golgi apparatus, sensitivity to EndoH digestion can also be used as a proxy of ER-residency[415,416]. At steady state, most cellular MR1 is EndoH-sensitive, reflecting its localisation to the ER[259,260,280]. Accordingly, the cellular MR1 pool in the HAP1.MR1 parent clone D9 was also sensitive to digestion with EndoH (Figure 4.12). This appears to be in contradiction with the flow cytometry data showing MR1 surface expression even at baseline in this clone (Figure 3.4, Figure 3.9, Figure 4.5), indicating that a proportion of the total cellular MR1 should be EndoH resistant. This discrepancy could be explained by taking into account that the HAP1.MR1 cells over-express MR1 and, thus, the intensity of the larger ER-resident MR1 population may be too high to detect the smaller EndoH-resistant fraction with the same detection settings. Additional experiments investigating EndoH resistance of MR1 in the presence of stabilising ligand are necessary to further investigate this phenotype. Interestingly, the much smaller pool of MR1 molecules in the HAP1.MR1 ATP13A1 KO clones was equally sensitive to the endoglycosidase indicating that these molecules are glycosylated normally within the ER (Figure 4.12). Intact core-glycosylation has in fact been demonstrated in *spf1* KO strains as well[408], further supporting the finding that MR1 is not hypoglycosylated in the HAP1.MR1 ATP13A1 KO clones. Of note, in one of the four sets of lysates analysed, a lower

band was detected across all conditions which may correspond to an unglycosylated MR1 species (data not shown). However, the presence of this band could not be confirmed in any of the other blots and it was unclear whether it was specific. Furthermore, it was present in the parent as well as the KO clones, making the observation unlikely to be related to the loss of ATP13A1.

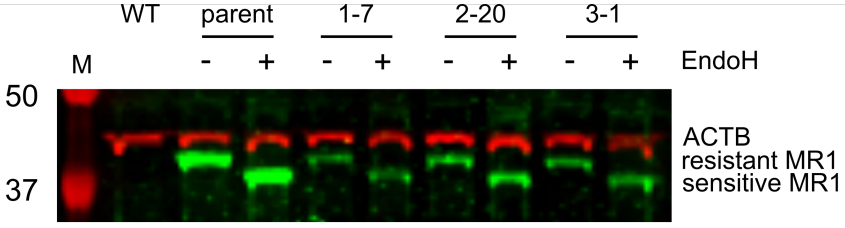


Figure 4.12: ER-resident MR1 is N-glycosylated in HAP1.MR1 ATP13A1 KO clones. Cell lysates of HAP1.MR1 parent clone D9 (parent) and HAP1.MR1 ATP13A1 KO clones 1-7, 2-20, and 3-1 were digested with endoglycosylase H (EndoH, +) or not (-). Digests were separated by SDS-PAGE and immuno-blotted for MR1 (green) and loading control ACTB (red). MR1-deficient mock-treated HAP1 wild type (WT) lysates were included to identify unspecific binding. M denotes protein marker and molecular weights of visible marker bands are indicated in kDa to the left of the blot. Data are representative of four similar independent experiments.

4.6.3 ER stress

Since *spf1* KO in yeast is associated with severe ER stress[363,392,397,408,409], it could be hypothesized that the reduced levels of total MR1 protein in the HAP1.MR1 ATP13A1 KO clones may due to a global effect on protein homeostasis caused by the induction of the unfolded protein response (UPR) in response to a imbalanced ER environment. Since general ER stress may also affect other proteins processed in the ER, protein levels of another glycosylated antigen presenting molecule were determined in the HAP1.MR1 ATP13A1 KO clones. MHC class I protein expression was not affected by the loss of ATP13A1 in the way that MR1 was (Figure 4.13, compare Figure 4.2), confirming that the effect of loss of

ATP13A1 in HAP1.MR1 cells is specific to MR1. MR1 levels were determined in the same lysates and reduced as before (data not shown). Of note, the antibody used to detect MHC class I by Western Blot does not react with HLA-A and HLA-G alleles[417]. Hence, potential allele-specific effects on MHC class I molecules would not be detected in this assay. Since the experiment was carried out twice, the sample size was too small to perform statistical analysis and further repeats of the experiment are needed to draw statistically supported conclusions.

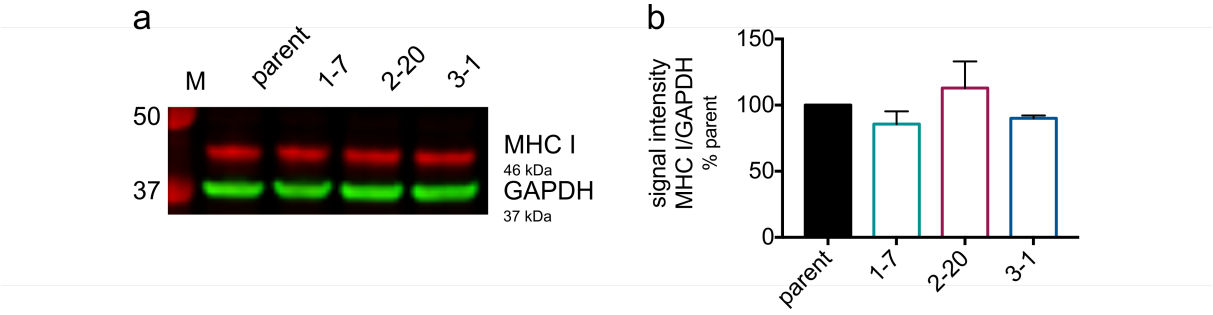


Figure 4.13: MHC class I protein levels are unaffected in HAP1.MR1 ATP13A1 KO clones. Cell lysates from HAP1.MR1 parent clone D9 (parent) and the three independent ATP13A1 KO clones 1-7, 2-20, and 3-1 were separated by SDS-PAGE on two gels in parallel and immuno-blotted for MHC class I (red, HC10 antibody) and the loading control GAPDH (green). Protein expression was quantified with the Odyssey® Near-Infrared imaging system and MHC class I intensity normalised to loading control is shown in (b) as % of parent. Data in (b) are pooled from two experiments and shown as median with range. M denotes molecular weight marker and molecular weights of visible marker bands are indicated in kDa to the left of the blot. Western Blot is representative of two experiments.

To measure ER stress more directly, induction of the ER stress protein HERPUD1 and XBP1 splicing were examined in the HAP1.MR1 ATP13A1 KO clones in a preliminary experiment. HERPUD1 is part of the ER-associated degradation (ERAD) machinery and highly up-regulated in response to ER stress[418–420]. XBP1, on the other hand, is a transcription factor that controls the expression of UPR proteins in response to ER stress and is itself activated by alternative splicing of its mRNA[421,422]. Thus, the shorter splice variant of the XBP1 transcript can be used as a readout for ER stress.

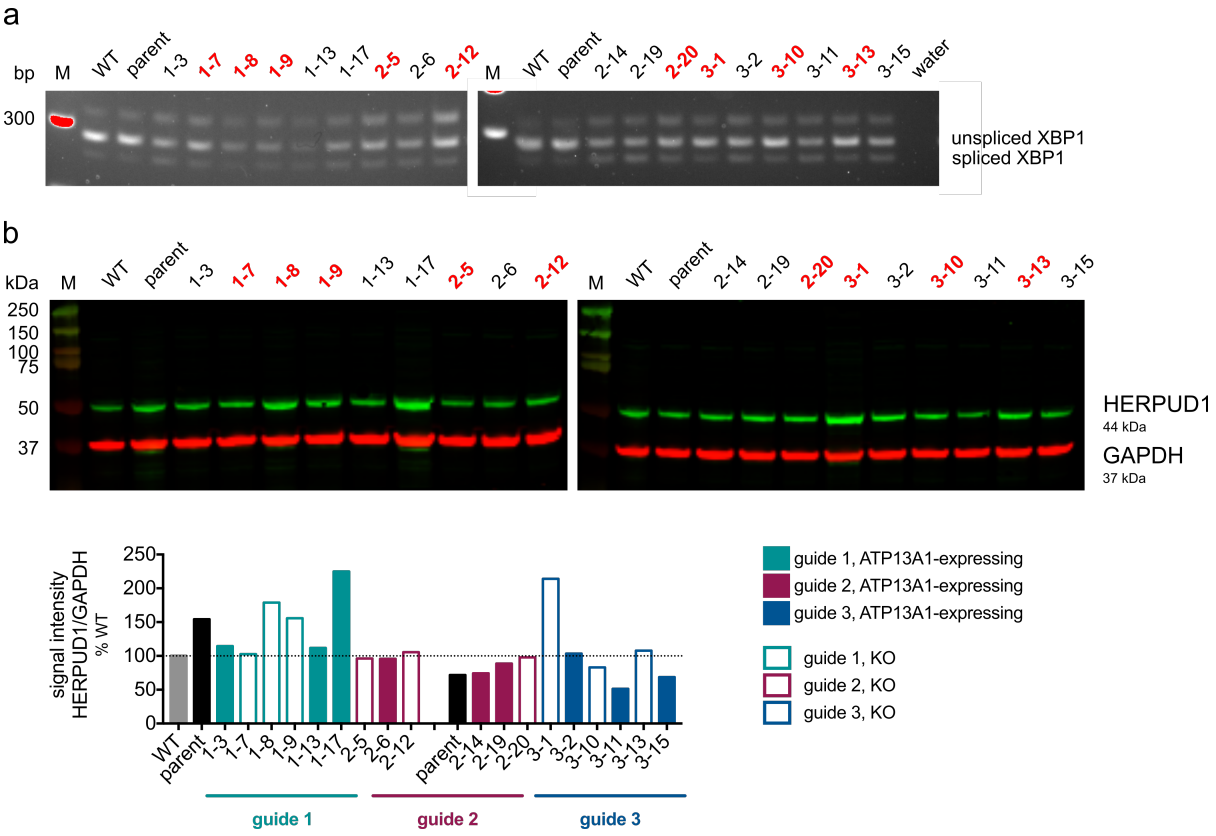


Figure 4.14: ATP13A1 knock out does not cause elevated ER stress in HAP1.MR1 ATP13A1 KO clones. cDNA of indicated HAP1.MR1 clones was amplified with Peter Walter's XBP1 primers and analysed for the splice variant on a 2.5% agarose gel (a). (b) Protein lysates of clones were separated by SDS-PAGE and immuno-blotted for HERPUD1 (green) and loading control GAPDH (red). ATP13A1 KO clones are highlighted in red. Protein expression was quantified with the Odyssey® Near-Infrared imaging system and HERPUD1 intensity normalised to loading control GAPDH is shown below the blot in (b) as % of the WT band on each blot. M denotes molecular weight or fragment size marker and values of visible marker bands are indicated in base pairs (bp) or kDa to the left of the images. Parent denotes HAP1.MR1 parent clone D9. Colour coding in (b) represents the sgRNA used to generate the respective clone. Dashed line indicates 100% for clarity.

Even though the baseline level of spliced XBP1 appeared slightly higher in the transfected clones compared to the untransfected HAP1.MR1 parent clone and the HAP1 WT, this band was present regardless of whether the clones expressed ATP13A1 or not (Figure 4.14a). Of note, there was no evidence of an elevated ER stress level in the HAP1.MR1 parent clone D9 compared to the HAP1 WT, indicating that over-expression of MR1 does not *per se* cause substantial ER stress in this system. Similarly, there was no correlation between ATP13A1 expression and HERPUD1 levels (Figure 4.14b). Although some clones expressed

up to two times more HERPUD1 than the HAP1 WT (1-17 and 3-1), these clones differed in their ATP13A1 status and the observed differences may be attributable to higher overall protein levels in these samples based on the intensity of unspecific background bands (data not shown). Furthermore, interpretation of these data is confounded by the absence of a positive control for ER-stress such as treatment with the inhibitor thapsigargin[423]. Since these results represent very preliminary data, any conclusions must be drawn with caution and await further experiments.

4.6.4 Protein stability

To investigate whether MR1 protein was continuously degraded in the HAP1.MR1 ATP13A1 KO clones, proteasomal degradation was inhibited globally with the reversible peptide aldehyde inhibitor MG-132[424,425]. In parallel, ER-associated degradation (ERAD) of proteins was inhibited at a different step with the irreversible P97 inhibitor NMS-873[426]. P97 mediates the translocation of ubiquitinated target proteins from the ER lumen into the cytosol and, thus, helps channel misfolded proteins towards proteolysis[426,427]. Even though proteasomal degradation was successfully inhibited under the conditions used as shown by the stabilisation of HERPUD1, this inhibition did not lead to an increase in MR1 protein levels in one initial test (Figure 4.15). If these results are confirmed by future experiments it could be concluded that the reduced MR1 protein levels in HAP1.MR1 ATP13A1 KO cells are mediated by a mechanism other than proteasomal degradation.

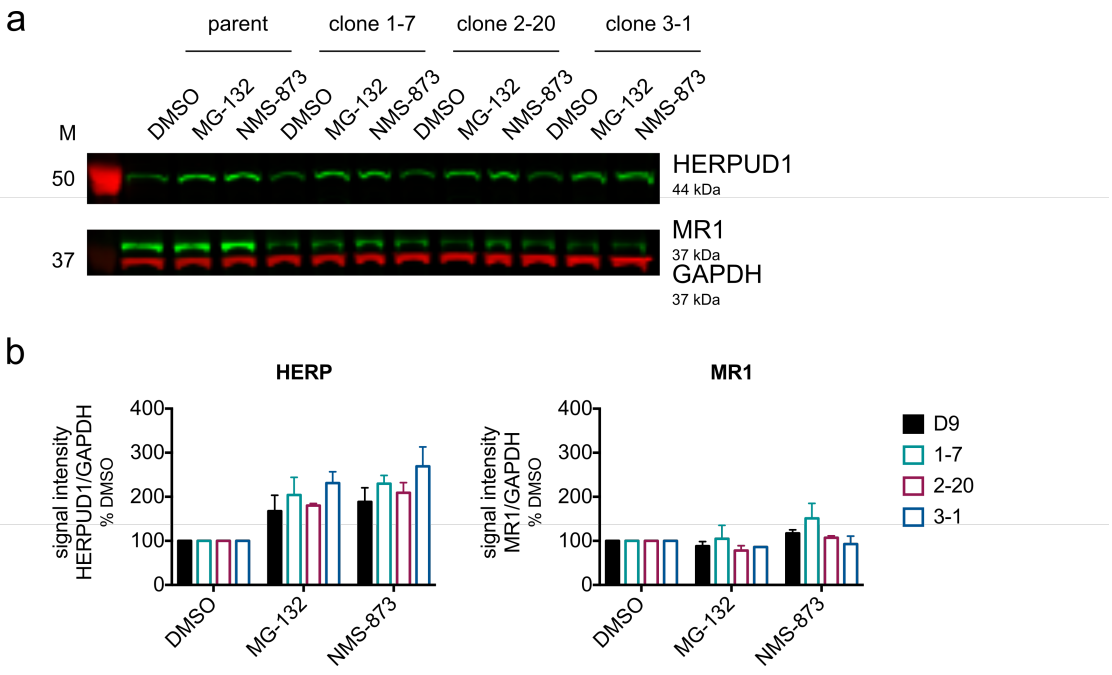


Figure 4.15: Inhibition of proteasomal degradation does not restore MR1 protein levels in HAP1.MR1 ATP13A1 KO clones. (a) Three independent HAP1.MR1 clones and the HAP1.MR1 parent clone D9 (parent) were incubated with MG-132 or NMS-873 for four hours in duplicates. Protein lysates were separated by SDS-PAGE and immuno-blotted for HERPUD1 (green, top panel), MR1 (green, bottom panel), and GAPDH (red, bottom panel) with the duplicates on two separate gels. Western Blot of one of the two duplicate gels is shown in (a). Membranes were cut prior to primary antibody incubation. (b) Protein expression was quantified with the Odyssey® Near-Infrared imaging system and HERPUD1 or MR1 intensity normalised to loading control GAPDH is shown as % of the respective DMSO control. Bars represent median of the duplicates with range. M denotes protein marker and molecular weights of visible marker bands are indicated in kDa to the left of the blot. Colour coding in (b) represents the sgRNA used to generate the respective clone. MG-132 data are representative of two experiments with similar results.

Next, protein translation was inhibited to determine whether the rate of MR1 degradation differed between the HAP1.MR1 parent clone and the HAP1.MR1 ATP13A1 KO clones. When HAP1.MR1 ATP13A1 KO clones were cultured in the presence of cycloheximide, both MR1 surface expression and total protein levels declined over time. Although MR1 surface levels appeared to decline slightly faster in HAP1.MR1 ATP13A1 KO clones, there was no notable difference in the rates of decay of total protein compared to the HAP1.MR1 parent clone D9 (Figure 4.16). Statistical analysis of these preliminary data was not possible due to the different group sizes of the D9 parent clone and the KO clones and a lack of biological repeats at the time of analysis. Therefore, these conclusions should be regarded

as general trends and more definitive answers can only be found upon repetition of the experiment. Based on the available data, the turnover of surface MHC class I molecules also seemed marginally faster in HAP1.MR1 ATP13A1 KO clones than in the HAP1.MR1 parent clone D9 although the variation between duplicates was marked (Figure 4.16a). Since the flow cytometric analysis revealed extensive cell death after 8 h of incubation with cycloheximide (data not shown), only the 0 – 4 h time points were considered for quantitative analysis.

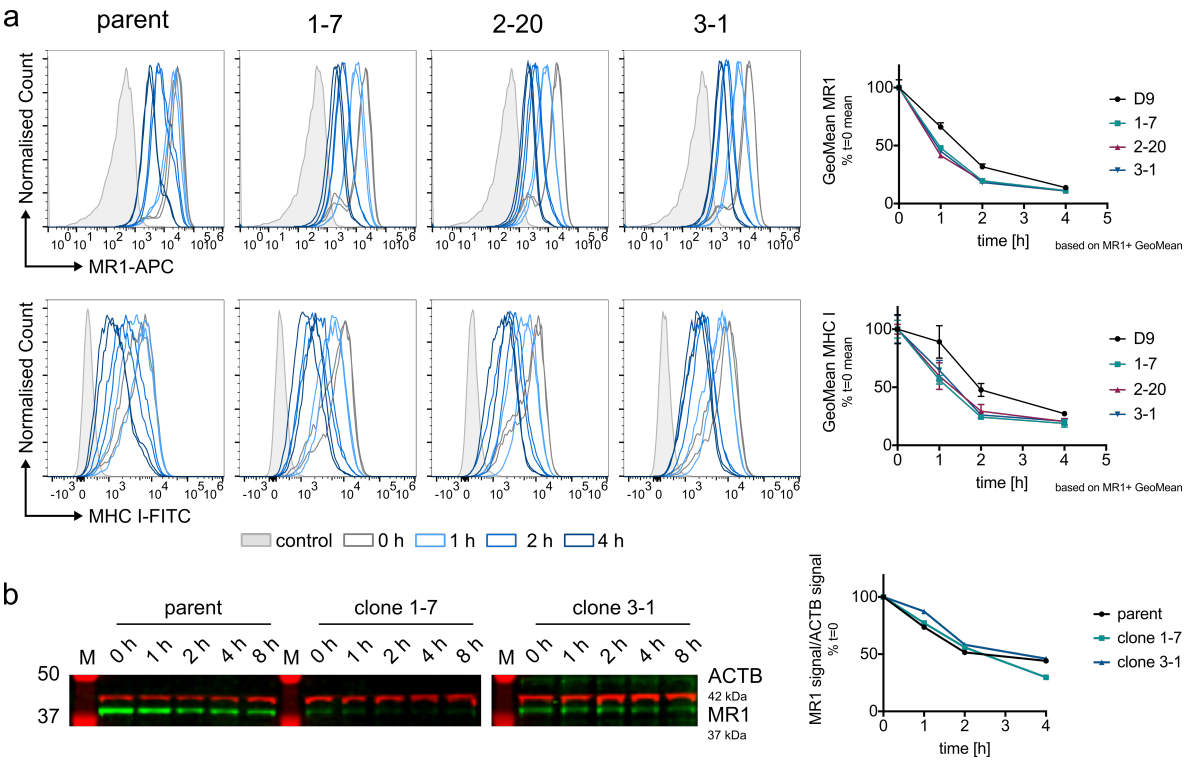


Figure 4.16: Pre-synthesised MR1 is turned over with similar kinetics in HAP1.MR1 ATP13A1 KO clones. HAP1.MR1 ATP13A1 KO clones and HAP1.MR1 parent clone D9 were incubated with cycloheximide for the indicated amount of time and MR1 (top panels) and MHC class I (bottom panels) surface levels (a) and total protein levels (b) were determined by flow cytometry and Western Blot. Cells stained with APC-conjugated isotype control antibody (MR1, top panels) or stained with live/dead stain only (MHC I, bottom panel) are shown as controls in histograms (a). Degradation is plotted as % GeoMean of the median GeoMean of the respective duplicates at t = 0, gating on MR1+ cells to compare only cells expressing MR1 at baseline. Symbols represent median of the technical duplicates with range. Blots shown in (b) were re-imaged with intensities optimised per clone for quantification and protein expression was quantified with the Odyssey® Near-Infrared imaging system. MR1 intensity normalised to loading control ACTB is shown to the right of the blot as % of the respective t = 0 band. M denotes protein marker and molecular weights of visible marker bands are indicated in kDa to the left of the blot. Colour coding represents the sgRNA used to generate the respective clone. Flow cytometry data are representative of two experiments with similar results.

4.7 ATP13A1 in THP-1 cells

To establish whether the ATP13A1-dependent MR1 phenotype observed in HAP1.MR1 ATP13A1 KO clones also held in a different cellular context, the effect of manganese deficiency on MR1 surface levels in THP-1 cells over-expressing MR1 (THP-1.MR1) was investigated. As lack of ATP13A1, loss of the homologue

of which has been shown to cause reduced manganese concentrations in the ER[363], resulted in reduced MR1 surface expression in HAP1.MR1 cells and this could be partially rescued by addition of exogenous manganese (Figure 4.10) it was hypothesised that culturing cells expressing ATP13A1 in medium without manganese might lead to reduced MR1 surface expression. When THP-1.MR1 cells were kept in Mn-supplemented medium for 24 h after culture in serum-free, Mn-depleted medium, MR1 surface expression was slightly increased compared to cells cultured without manganese. However, there was no reduction of MR1 surface levels in cells cultured without manganese compared to those kept in normal medium containing manganese derived from the supplemented foetal calf serum (Figure 4.17a). MHC class I surface expression, by contrast, was highest in cells cultured in regular R10, consistent with a stabilising effect of serum-derived peptides. Since both technical and biological repeats for this experiment were less than three, statistical analysis could not be performed on these data and more experiments are needed to draw statistically supported conclusions.

In a preliminary experiment, total MR1 protein levels were generally lower in clone TM25 compared to clone TM14 and also appeared to be more sensitive to changes in manganese concentration in TM25. Interestingly, total MR1 levels were lowest upon culture in Mn-supplemented medium for both THP-1.MR1 clones (Figure 4.17b). Total MR1 protein levels could not be determined by Western Blot for THP-1 WT cells as endogenous expression levels are below the limit of detection (data not shown).

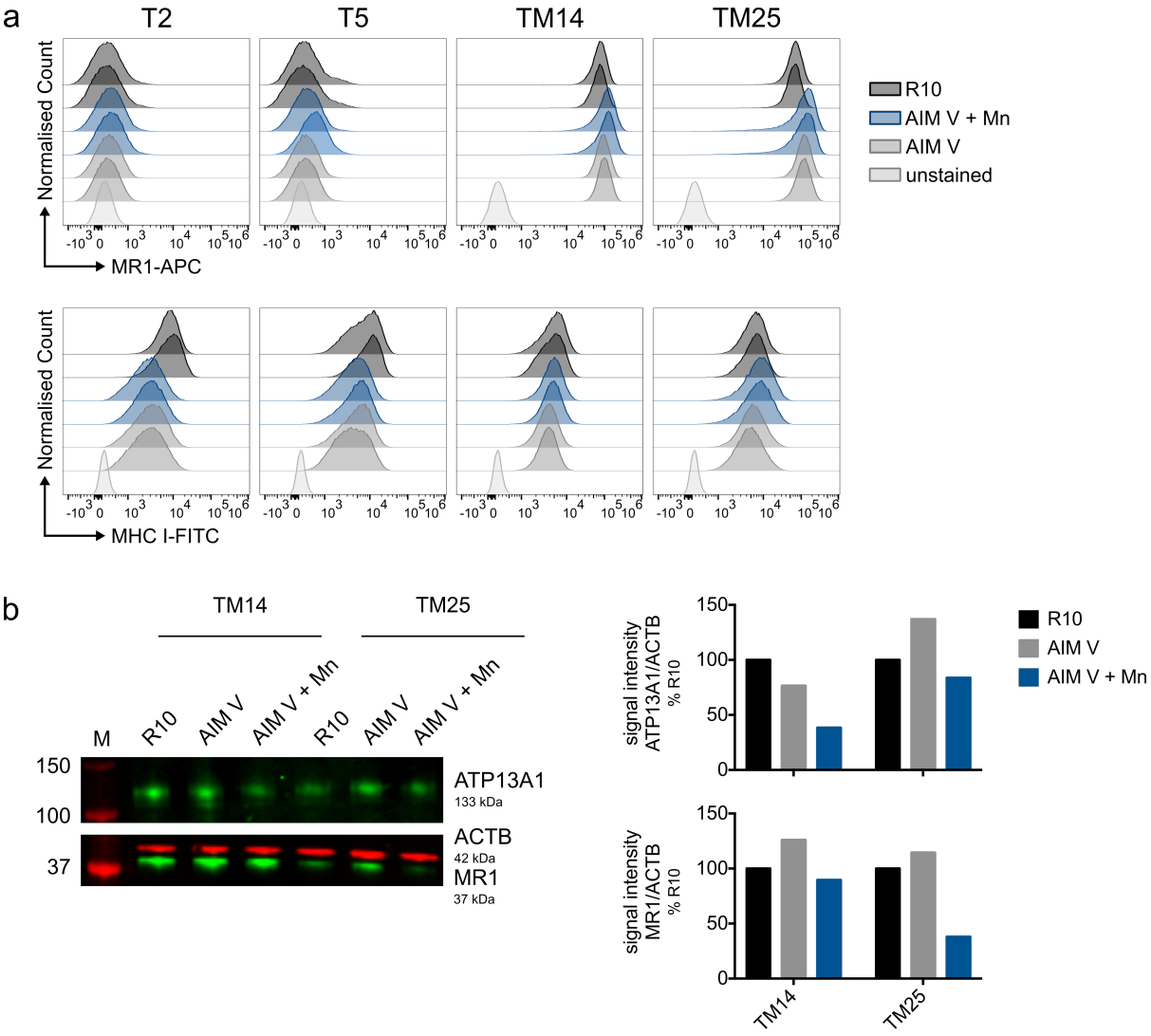


Figure 4.17: MR1 surface levels are not reduced in THP-1 cells upon culture in manganese-free medium. THP-1 WT clones T2 and T5 as well as THP-1 MR1 over-expressing clones TM14 and TM25 were cultured without manganese for six days (AIM V) or not (R10). For the last 24 h cells were either kept in AIM V alone (AIM V, dark grey), AIM V supplemented with 100 µM of $MnCl_2$ (AIM V + Mn, blue), or R10 (black). MR1 and MHC class I surface levels (a) and total MR1 protein expression (b) were determined. A pooled sample stained with live/dead marker only is shown as a negative control in (a) (unstained). M in (b) denotes protein marker and molecular weights of visible marker bands are indicated in kDa to the left of the blots. Loading control ACTB is shown in red and MR1 and ATP13A1 are shown in green. The membrane was cut prior to antibody incubation. Protein expression was quantified with the Odyssey® Near-Infrared imaging system and MR1 intensity (green) normalised to loading control ACTB (red) is shown to the right of the blot. Flow cytometry data are representative of two independent experiments.

Of note, expression of the transporter ATP13A1 itself did not appear to be consistently affected by changes in extracellular manganese concentrations in the same experiment (Figure 4.17b). In clone TM14, ATP13A1 protein expression was highest when cells were kept in R10 whereas the transporter was most highly

expressed upon culture in AIM V in clone TM25. For both clones, ATP13A1 levels were lowest when cells were grown in Mn-supplemented medium. However, these are very preliminary results and more data are needed to draw substantiated conclusions on the effect of Mn-deficiency on the expression levels of MR1 and ATP13A1.

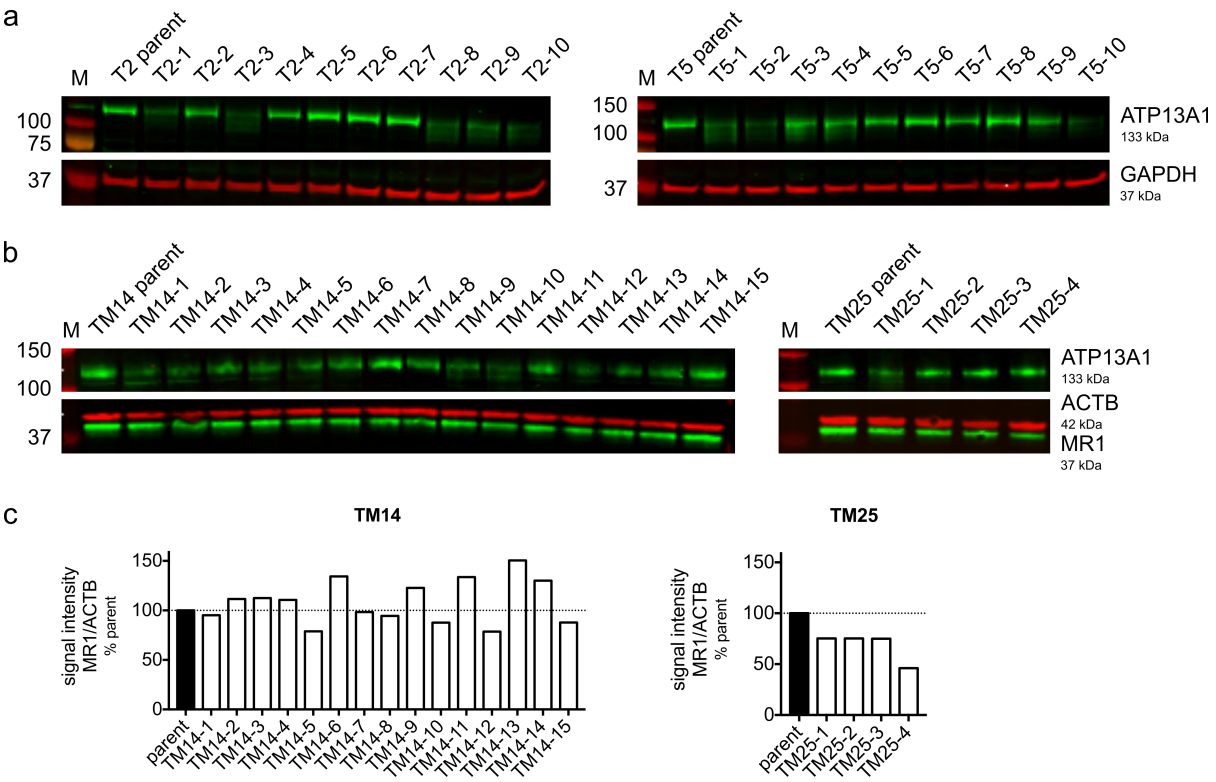


Figure 4.18: CRISPR/Cas9-mediated knock-down of ATP13A1 in THP-1.MR1 cells does not reduce total MR1 protein levels. Two THP-1 WT clones (T2, T5) and two THP-1.MR1 clones (TM14, TM25) were co-transfected with three sgRNAs targeting ATP13A1 and single cell sorted. ATP13A1 expression in viable clones was analysed by Western Blot (a,b). MR1 protein levels in THP-1.MR1 clones were determined by Western Blot (b) and quantified with the Odyssey® Near-Infrared imaging system (c). In a membranes were incubated with αATP13A1 and αGAPDH primary antibody together and relevant portions of the blot are shown. In (b) membranes were cut prior to incubation with αATP13A1 or αMR1 and αACTB primary antibodies. M denotes molecular weight marker and molecular weights of visible marker bands are indicated in kDa to the left of the blots. Dashed line in (c) indicates parent level.

In order to more specifically address the role of ATP13A1 in THP-1 cells, THP-1 clones over-expressing MR1 or not were transiently transfected with the same pool of three sgRNAs targeting ATP13A1 used in the HAP1 clones. To enable direct comparison of the ATP13A1-deficient clones to a single parent clone, THP-1

WT and THP-1.MR1 populations were first sub-cloned before transfection of two individual parent clones each (THP-1 WT: T2 and T5, THP-1.MR1: TM14 and TM25). As with the HAP1.MR1 transfectants, mRuby+ cells were single cell sorted (for sorting strategy see Supplementary Figure 8) and individual clones grown up.

Since THP-1 cells have at least two copies of each chromosome except for chromosome 10[428] complete knock-out of ATP13A1 was not achieved, but substantial knock-down appeared to have occured in a number of clones (Figure 4.18a and b). However, while multiple Western Blot analyses of the lysates were performed to minimise the effect of potential technical sources of variability, variation among independently prepared parental samples was not directly compared. Thus, the variability of ATP13A1 expression levels in the parent clones is not known and the observed variations in ATP13A1 surface expression may be attributable to factors other than mutations in the ATP13A1 gene such as metabolic state, cell cycle, or general clonal variation. Interestingly, total MR1 protein levels were not consistently affected in THP-1.MR1 ATP13A1 KD clones in contrast to the observations made in HAP1.MR1 ATP13A1 KO clones. Even though MR1 expression was slightly reduced in some clones this did not necessarily correlate with ATP13A1 status (Figure 4.18c).

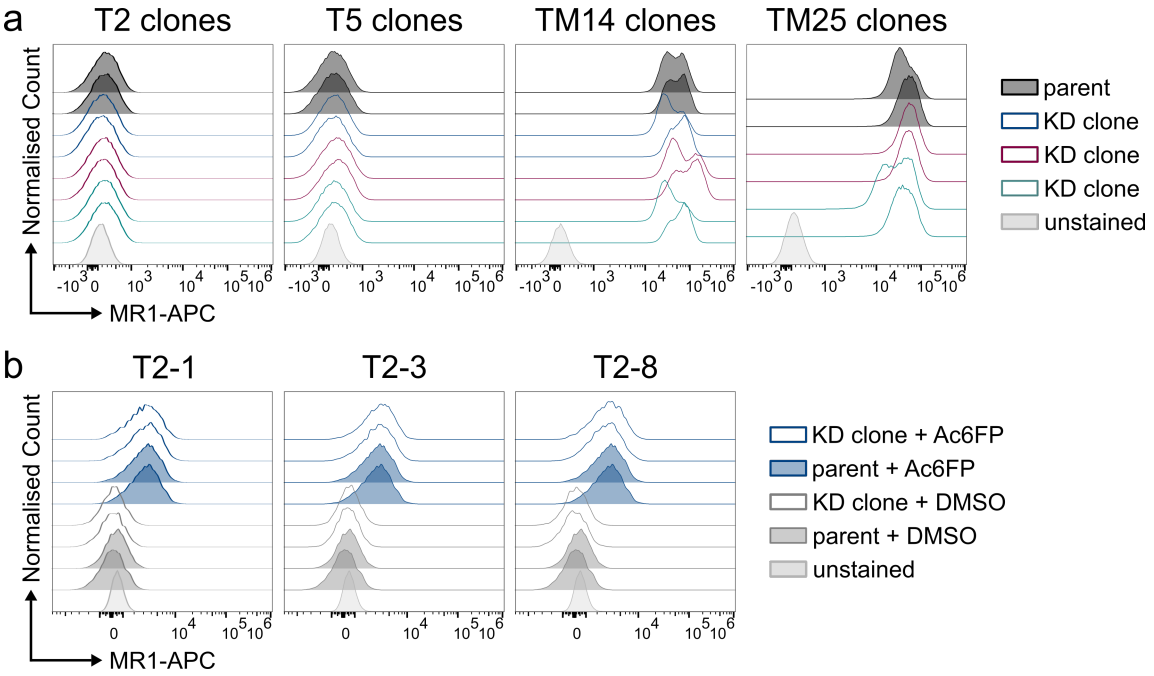


Figure 4.19: CRISPR/Cas9-mediated knock-down of ATP13A1 does not reduce MR1 surface levels in THP1 or THP1.MR1 cells. Three ATP13A1 KD clones per parent clone (empty histograms, coloured) were stained for surface MR1 at baseline in duplicates (a) and compared to their respective parent clone (filled histograms, black). The three T2 clones T2-1, T2-3, and T2-8 and the T2 parent clone (parent) were pulsed with 100 µg/ml Ac6FP (blue) or the equivalent volume of DMSO (grey) for 5 h in duplicates and surface MR1 levels were measured by flow cytometry (b). Shaded histograms represent parent clone T2, empty histograms represent the respective KD clone. The live/dead-only stained respective parent sample is shown as a negative control.

Next, MR1 surface levels were measured by flow cytometry in a subset of clones for each parent clone. Based on the Western Blot results, clones T2-1, T2-3, T2-8, T5-1, T5-2, T5-10, TM14-2, TM14-5, TM14-6, TM25-1, and TM25-4 were chosen for this.

At baseline, none of the examined clones had lower MR1 surface expression than the respective parent clone (Figure 4.19a). Since MR1 surface expression was very close to the limit of detection in the THP-1 WT clones, T2 clones T2-1, T2-3, and T2-8 were incubated with the MR1-stabilising ligand Ac6FP. Ac6FP treatment increased MR1 surface expression in all three THP-1 ATP13A1 KD clones as well as the parent and did not reveal differences in MR1 surface levels attributable to

loss of ATP13A1 (Figure 4.19b). Since this analysis was only carried out once and in technical duplicates, statistical analysis could not be performed. More experiments would be needed to draw statistically supported conclusions but since sequencing revealed that none of the clones obtained had been efficiently edited (see below, Figure 4.22) these were not carried out.

When the same subset of THP1 ATP13A1 KD clones was used in a functional assay to present antigenic MR1 ligand to sorted human MAIT cells, the IFNγ-response was largely unaffected except for the two clones T2-3 and T2-8 (Figure 4.20). In two independent experiments using different MAIT cell donors, these two clones elicited an approximately 2-fold reduction in the IFNγ-response compared to their parent clone T2. However, it should be noted that there is also a considerable difference in the magnitude of the IFNγ-response triggered by the two parent clones T2 and T5 (Figure 4.20, top panels), suggesting that clone-to-clone variation can be substantial in this system. Also, a third functional experiment using one of the MAIT cell donors used before showed a much smaller difference in antigen presentation capacity of T2-3 and T2-8 compared to the parent clone T2 (data not shown).

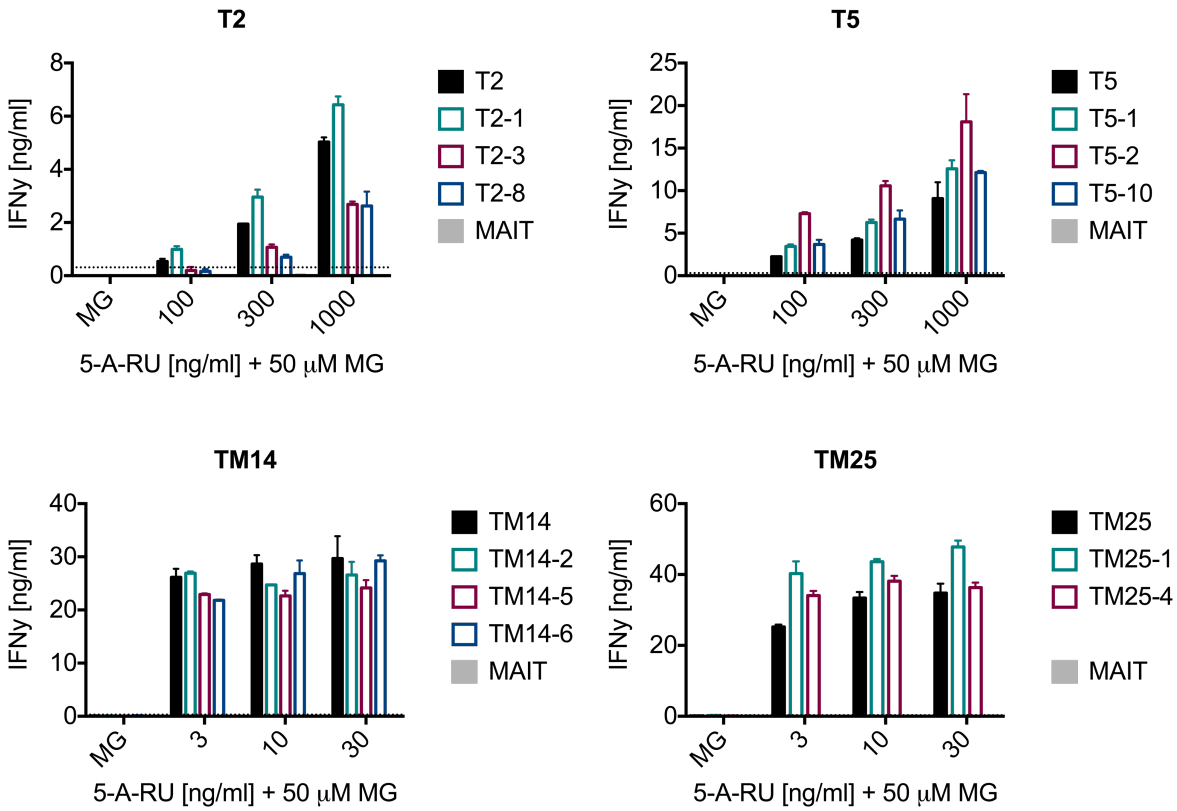


Figure 4.20: CRISPR/Cas9-mediated knock-down of ATP13A1 affects antigen presentation in a subset of THP-1 clones. Two or three THP-1 clones over-expressing MR1 (TM, bottom panels) or not (T, top panels) deficient for ATP13A1 and their respective parent clones were pulsed with the indicated concentrations of 5-A-RU and 50 μM MG for 5 h. Ligand was washed off and sorted human MAIT cells were added for 36 h. Interferon γ (IFNγ) secretion into the supernatant was quantified by ELISA. Dashed lines denote limit of detection. Bars represent median of technical duplicates with range and data are representative of two experiments using two different MAIT cell donors, but not of a third experiment using T2 clones only.

To test whether the ATP13A1 knock-down in these THP-1 clones had an effect on ER stress levels HERPUD1 expression was measured by Western Blot. If, for instance, ER-stress levels differed between T2-1 compared to T2-3 and T2-8, this may provide an explanation for their differential antigen presentation phenotype. To further investigate this particular subset of clones, XBP1-splicing was also investigated in the clones derived from THP-1 parent clone T2. In addition, the growth kinetics of the T2 clones were followed over time to exclude a confounding effect of differential growth rates.

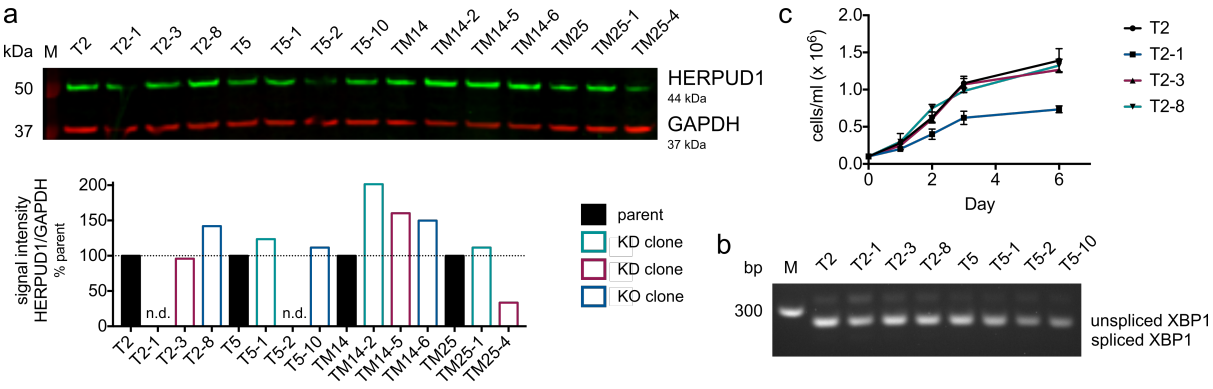


Figure 4.21: CRISPR/Cas9-mediated knock-down of ATP13A1 does not trigger the ER-stress response in THP-1 or THP-1.MR1 clones. Protein lysates of the indicated clones were separated by SDS-PAGE and immuno-blotted for HERPUD1 (green) and the loading control GAPDH (red) in (a). Protein expression was quantified with the Odyssey® Near-Infrared imaging system and HERPUD1 intensity normalised to loading control GAPDH is as % of the respective parent band below the blot in (a). Protein expression was not quantified for clones T2-1 and T5-1 due to scratched lanes (n.d. = no data). Dashed line indicates 100 % for clarity. cDNA of indicated clones was amplified with Peter Walter's XBP1 primers and analysed for the splice variant on a 2.5% agarose gel (b). M denotes molecular weight or fragment size marker and values of visible marker bands are indicated in base pairs (bp) or kDa to the left of the images. Equal cell numbers of clones indicated in (c) were seeded in duplicates and cells counted at the indicated time points. Symbols represent median of the duplicates with range. Growth curve data are representative of two experiments with similar results.

Neither the HERPUD1 Western Blot nor the XBP1-splicing assay provided any evidence for elevated ER-stress levels in the THP-1 ATP13A1 KD clones in a preliminary experiment (Figure 4.21). HERPUD1 expression was slightly elevated in TM14 clones (approximately 150 – 200% of parent levels), but the statistical significance of this observation awaits confirmation in repeat experiments including a positive control for ER stress. Only unspliced XBP1 transcript was detectable in all clones, lending further support to the absence of ER stress in these clones. Importantly, the two T2 ATP13A1 KD clones which had an antigen presentation phenotype (T2-3 and T2-8) grew with the same kinetics as the THP-1 parent clone T2 in two independent experiments. This makes it seem unlikely that the antigen presentation defect was caused by reduced cell growth though statistical analysis of these data was not possible due to a lack of technical and biological repeats. (Figure 4.21c).

Finally, ATP13A1 expression in the THP-1 clones was investigated at the transcriptional level. Neither ATP13A1 nor MR1 transcript levels were reduced in the THP-1 ATP13A1 KD clones in one qRT-PCR (Figure 4.22). In fact, ATP13A1 transcript levels were statistically significantly elevated in two clones compared to the respective parent clone (difference = -0.1759; 95% CI [-0.2613, -0.09055]; p = 0.0009 for T2-1 and difference = -0.2005; 95% CI [-0.2859, -0.1152]; p = 0.0004 for T2-3). However, the magnitude of this effect was extremely small and its biological significance can only be assessed after further experiments have been performed. Thus, the data generated so far indicate that the gene editing procedure has not resulted in reduced ATP13A1 transcript levels. More importantly, next generation deep sequencing of the sgRNA target sites in the clonal cDNA revealed that the cDNA expressed in the T2 clones was not edited (Table 4.1, Figure 4.22). In all clones, the percentage of unedited WT reads aligning to the reference sequence was between 82 and 96% at all three target sites (Table 4.1). The detected alleles that differed from the reference sequence were present at extremely low (< 1%) frequencies and usually single nucleotide substitutions localised away from the predicted cleavage position present in both the THP-1 ATP13A1 KD clones and the THP-1 parent clone T2. This raised the question of why ATP13A1 protein expression was reduced in these clones (Figure 4.18).

Table 4.1: Summary of deep sequencing results cDNA from the indicated THP-1 ATP13A1 KD clones and the THP-1 parent clone T2 was prepared from RNA. Regions around the three co-transfected sgRNA target sites were amplified from the cDNA, sequenced by Illumina deep sequencing, and analysed with CRISPResso[414]. The percentage and absolute number of reads that perfectly aligned to the reference amplicon are shown per clone and target site (sgRNA).

clone	sgRNA target site	% WT sequence at target site	number of WT reads
T2 parent	1	84.78	145052
T2 parent	2	94.06	75042
T2 parent	3	94.9	94975
T2-1	1	82.61	174261
T2-1	2	93.4	72826
T2-1	3	92.98	99057
T2-3	1	85.2	148031
T2-3	2	94.37	57312
T2-3	3	95.15	87927
T2-8	1	87.83	110987
T2-8	2	94.61	65438
T2-8	3	95.47	67209

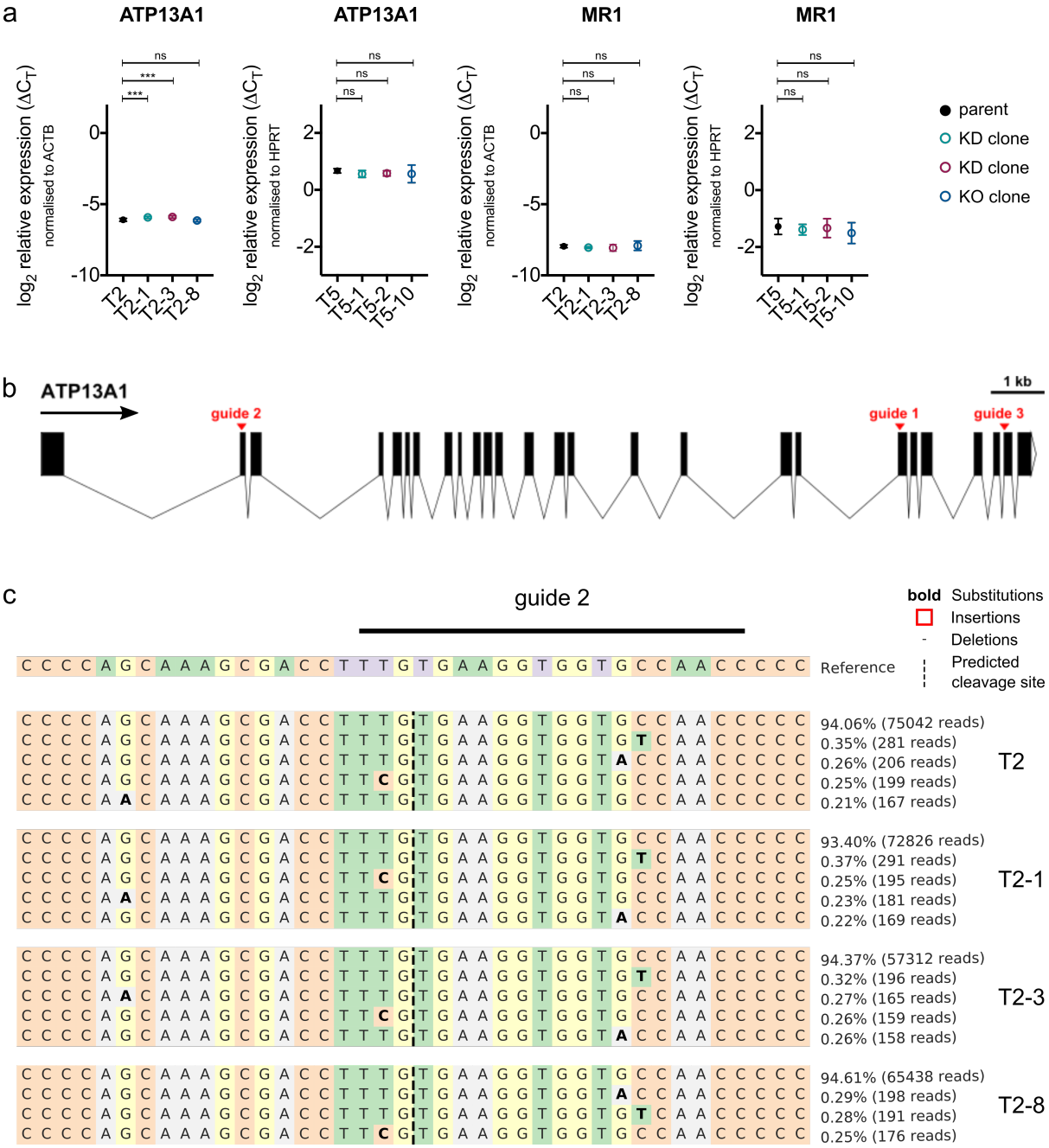


Figure 4.22: THP-1 ATP13A1 KD clones express normal levels of intact ATP13A1 mRNA. cDNA was generated from RNA extracted from the indicated THP-1 ATP13A1 KD clones and analysed for transcript levels of ATP13A1 (a, top panels) and MR1 (a, bottom panels). Each symbol represents the mean of technical triplicates with 95% confidence interval. Statistical significance was calculated using ordinary one-way analysis of variance (ANOVA) with Dunnett's multiple comparisons test comparing each clone to the respecitive parent. where * = $p < 0.05$, ** = $p < 0.01$, *** = $p < 0.001$, **** = $p < 0.0001$, ns = not significant. Regions around the three co-transfected sgRNA target sites were amplified from the cDNA, sequenced by Illumina deep sequencing, and analysed with CRISPResso[414]. The distribution of the identified alleles around sgRNA 2 for each sequenced clone is shown in (c) as an example. Positions of the sgRNA target sequences with respect to the intron/exon structure of the ATP13A1 gene are shown in (b). Arrow denotes direction of transcription. The plot was generated using the Exon-Intron Graphic Maker available at wormweb.org/exonintron based on the NCBI Reference Sequence NC_000019.10.

4.8 Discussion

In this chapter, the MR1 phenotype in HAP1.MR1 ATP13A1 KO clones was further defined and potential molecular mechanisms underlying this effect were explored. It was established that HAP1.MR1 clones deficient for ATP13A1 after transfection with either one of three or a combination of the three sgRNAs targeting the Cas9 nuclease to different loci within the ATP13A1 gene had greatly reduced overall MR1 protein levels. This smaller pool of total cellular MR1 also appears to manifest as reduced surface expression both at baseline and in the presence of the MR1-stabilising ligand Ac6FP as well as an antigen presentation defect although these effects could not be analysed statistically. Recombinant over-expression of ATP13A1 in HAP1.MR1 ATP13A1 KO clones restored MR1 protein levels, lending further support to the conclusion that the observed phenotype was due to loss of the transporter. MR1 transcript levels were statistically significantly reduced in some ATP13A1 KO clones but the biological significance of the < 2-fold reduction remains to be determined. To characterise the mechanism underlying the reduced MR1 protein levels upon loss of ATP13A1, various post-translational mechanisms potentially affecting MR1 folding and protein stability were investigated.

Firstly, the impact of extracellular manganese concentrations on MR1 protein levels was assessed. Supplementation of the medium with manganese led to a statistically significant but modest increase of both MR1 surface expression and total MR1 protein levels in HAP1.MR1 ATP13A1 KO clones. This increase was observed despite the fact that these clones do not express ATP13A1 which has been reported to transport Mn into the ER[363] and should, therefore, not be able to

import exogenously supplied manganese into the ER to alleviate the phenotype. However, it has been shown that vesicle-mediated anterograde Mn flux from the ER to the *cis*-Golgi can bypass the need for the Golgi-localised Mn-transporter Pmr1 in yeast[429] and that the two transporters Spf1p and Pmrp can partially compensate the loss of function of the respective other[408]. This makes it appear feasible that retrograde vesicular transport could also supply manganese from the lumen of the Golgi apparatus to the ER in the HAP1.MR1 ATP13A1 KO cells. In this way, manganese concentrations in the ER could still be increased by supplying exogenous manganese even in the absence of a dedicated ER-localised manganese transporter.

Interestingly, preliminary results suggest that neither MR1 surface levels nor total MR1 protein expression were reduced in THP-1.MR1 cells cultured in manganese-free medium (Figure 4.19), indicating that this metal ion is not required for proper MR1 protein expression as a general principle. One possible explanation for this result is that THP-1 cells may be less sensitive to manganese-deficiency than HAP1 cells, allowing them to over-express MR1 even in the absence of manganese. Alternatively, the MR1 phenotype observed in the HAP1.MR1 ATP13A1 KO clones may not be mediated by the manganese-transporting function of the transporter but may be due to another, manganese-independent functionality.

For example, manganese is not the only metal that has been shown to be impacted by loss of ATP13A1 or its homologue *spf1*. Indeed, Spf1p has also been implicated in the homeostasis of other divalent cations such as calcium and

magnesium, though only magnesium enhanced its ATPase function *in vitro*. Both manganese and calcium had inhibitory rather than activating effects on ATPase function of Spf1p[392,398,407,408,430]. Since the range of metal substrates, or indeed non-ionic substrates, of ATP13A1 remains to be determined and experiments to date have been mostly restricted to the yeast model system it would be extremely beneficial to directly measure the concentrations of potential substrates of the transporter in the ER of wild type and ATP13A1 KO cells. Two complementary approaches towards this aim could provide valuable insights: on the one hand, the concentrations of a variety of metals could be quantified by inductively coupled plasma mass spectrometry (ICP-MS) in microsomes derived from human ATP13A1 KO cells as performed by Cohen *et al*. in yeast[363]. This would allow the comparison of the substrate range of the mammalian transporter and the yeast transporter as well as providing a comprehensive view of which metals are differentially compartmentalised upon loss of ATP13A1. Extending the mass spectrometry analysis to electrospray ionisation tandem mass spectrometry (ESI-MS/MS) would further allow the quantification of organic compounds[431] such as riboflavin or the MR1 ligands Ac6FP or 5-OP-RU in the microsomes of these clones. Comparing the concentrations of these compounds in wild type compared to ATP13A1 KO clones would allow to also test the hypothesis that ATP13A1 may transport the MR1 ligand into the ER. As a complementary approach, the import of specific divalent cations into the ER could be tested using the calcium-sensitive dye Fura2 and its derivatives. While Fura2 fluoresces upon binding of calcium it can also bind manganese which quenches the fluorescent signal. Since Fura2 compartmentalises into the ER in certain cell types, quenching of the ER signal upon addition of exogenous manganese could be used as a read-out for

manganese import into the ER[432–434]. If ATP13A1, like Spf1p, regulates the manganese homeostasis in the ER, less quenching should be observed in ATP13A1 KO clones compared to the wild type. Furthermore, it would be useful to test whether exogenous addition of other divalent cations can increase MR1 protein levels in HAP1.MR1 ATP13A1 KO clones in the same way that manganese did and whether culturing HAP1.MR1 wild type cells in the absence of manganese reduces their MR1 expression levels.

Secondly, the glycosylation state of MR1 in the HAP1.MR1 ATP13A1 KO clones was determined as *spf* KO yeast strains have been frequently reported to have a hypoglycosylation phenotype[363,398,408]. The MR1 protein sequence features one known *N*-linked glycosylation site at Asn 86[280] and most MR1 resides in a pre-Golgi compartment at steady state as reflected by its sensitivity to digestion with endoglucosidase H[259,260,280]. Digestion with Endo H confirmed this to be the case also in the HAP1.MR1 ATP13A1 KO clones, making it seem unlikely that a glycosylation defect is the cause for the reduced MR1 protein levels at baseline. This is consistent with reports that Endo H-sensitive core glycosylation is intact in *spf1* KO yeast strains and only higher order polysaccharide residues could not be processed in these mutants[408]. Therefore, the acquisition of EndoH resistance upon incubation with the MR1-stabilising ligand Ac6FP should be investigated in the ATP13A1 KO clones to determine whether protein glycosylation at later steps of the secretory pathway is impaired.

Thirdly, ER stress and, relatedly, protein turnover were investigated to address the hypothesis that disturbed ion homeostasis in the ER of HAP1.MR1 ATP13A1 KO

cells caused misfolding of MR1 and degradation by ER-associated degradation (ERAD) in a stressed ER environment. The yeast homologue of ATP13A1 has been implicated in multiple screens looking for proteins required for protein folding and/or the unfolded protein response (UPR)[409,435], providing a rationale for this hypothesis. It has also been shown that a double KO of *spf1* and the UPR regulator *hac1* is synthetic lethal in yeast[392] whereas loss of the ERAD components *hrd1* and *ubc7* in an *spf1* KO strain rescued the constitutive degradation of Hmg2p in those mutants[407]. In the latter system, loss of *spf1* led to the specific and continuous degradation of hydroxyl-methylglutaryl-coenzyme A reductase (Hmg2p or HMGR), a well characterised substrate of controlled ERAD in both yeast and mammals[436,437]. Like the low MR1 protein levels, degradation of this enzyme was very specific and a comparable protein was unaffected in the *spf1* mutants[407]. It was, thus, feasible to hypothesise that a similar mechanism may apply to MR1 in the HAP1.MR1 ATP13A1 KO clones, causing the protein to be constitutively degraded. Interestingly, the human homologue of *ubc7* is UBE2G2 which was on the list of putative positive regulators of MR1 generated from the genetic screen described in Chapter 3. Considering that *ubc7* is a negative regulator of Hmg2p in the yeast system described above, this was a first hint that MR1 may not be regulated by the same mechanism in the HAP1.MR1 ATP13A1 KO clones.

Indeed, although they represent preliminary tests and require much more thorough investigation to draw definitive conclusions, the experiments described in sections 4.6.3 and 4.6.4 of this chapter provide no evidence of constitutive degradation of MR1 protein as a result of ER stress in HAP1.MR1 ATP13A1 KO clones. Neither

XBP1 splicing nor HERDUP1 induction were specifically associated with loss of ATP13A1 and the rate of protein degradation after blockade of translation in the ATP13A1 KO clones was comparable to that in the wild type. Moreover, inhibition of the ubiquitin-proteasome system did not stabilise MR1 protein levels in the HAP1.MR1 ATP13A1 KO clones, strengthening the hypothesis that MR1 is not post-translationally degraded in these cells.

Although MR1 transcript levels were reduced in some of the HAP1.MR1 ATP13A1 KO clones when compared to their ATP-sufficient counterparts, the magnitude of this effect was small. Comparison of the KO clones to the HAP1.MR1 parent clone could not be assessed statistically but there was no evidence that MR1 transcript levels were lower in the ATP13A1 KO clones compared to the parent. To reach substantiated clonclusions on the effect of loss of ATP13A1 on MR1 transcript levels more data are needed.

Taken together, the tentative conclusions drawn from the preliminary results presented would be consistent with a model in which MR1 protein levels are reduced in HAP1.MR1 ATP13A1 KO clones because the rate of translation of MR1 is specifically decreased in these cells. To test this hypothesis, the rate of translation of MR1 mRNA should be quantified in the HAP1.MR1 ATP13A1 KO clones and compared to those in the HAP1.MR1 parent clone. One way to achieve this would be a radio-labelled pulse-chase experiment allowing both the quantification of nascent MR1 right after the pulse and the more accurate determination of degradation rates of the protein throughout the chase. This approach has so far been hampered by the lack of an antibody that is not

conformation-specific and still suitable for immuno-precipitation. Over-expression of an HA-tagged MR1 construct in the ATP13A1 KO clones would overcome this problem and provide valuable insights into the regulation of MR1 translation in the absence of the transporter. A more direct approach to quantifying the rate of translation of MR1 in these cells would be ribosomal profiling[438] in the ATP13A1-expressing clones compared to the ATP13A1 KO clones.

The mechanism by which ATP13A1 could specifically regulate the translation of the MR1 transgene in the HAP1.MR1 ATP13A1 KO cells remains elusive at this point. While it seems unlikely that altered ion concentrations within the ER would affect rates of translation which takes place in the cytosol, it has to be taken into account that lack of an ER importer also impacts the ion homeostasis of the cytosol. In fact, it has been shown in yeast that loss of *spf1* enhances the activity of cytosolic manganese-dependent enzymes[363] and induces compensatory mechanisms such as expression of a vacuolar calcium pump[392]. Loss of *spf1* also altered the lipid composition of the ER membrane in yeast[439] which could conceivably influence the efficiency of ribosome binding to the rough ER. However, such a scenario should also impact the translation of other co-translationally translocated proteins such as MHC class I which is unaffected in HAP1.MR1 ATP13A1 cells.

Alternatively, it is also possible that the observed phenotype is related to the locus or the loci where the MR1 transgene integrated in the HAP1.MR1 parent clone D9. In yeast, loss of *spf1* lead to substantial induction of calcium-responsive genes and loss of manganese homeostasis resulted in the upregulation of cell cycle

regulators[440]. To investigate a potential effect of the MR1 integration site(s), ATP13A1 could be knocked out in a different MR1-over-expressing HAP1 clone such as clone F2 (Figure 3.2). As a complementary approach, over-expression of a different glycoprotein in the HAP1.MR1 ATP13A1 KO clones would allow to probe the specificity of the observed phenotype to MR1. This would also address the hypothesis that the phenotype is due to over-expression of a glycoprotein in general rather than MR1 itself.

In addition, it would be informative to determine whether over-expression of ATP13A1 in a wild type background can increase MR1 protein levels. Therefore, the ATP13A1 expression vector should be introduced into the HAP1.MR1 parent clone D9 as well as other HAP1.MR1 clones (Figure 3.2) and other cell lines to gauge the extent to which this phenomenon is generalizable.

The attempts to broaden the investigation of the role of ATP13A1 in MR1-mediated antigen presentation to another cell line presented here are difficult to interpret. Even though ATP13A1 protein levels appeared to be slightly reduced in some THP-1 clones yielded after co-transfection with three CRISPR/Cas9 plasmids encoding for three different sgRNAs targeting ATP13A1, these clones did not consistently share the MR1 phenotype observed in HAP1.MR1 ATP13A1 KO clones and seemed to express the same levels of unedited ATP13A1 transcript as the parent clone. One technical issue in this analysis was the position of the Taqman probe used for the quantification of ATP13A1 transcripts: it annealed just downstream of the target site closest to the 5'-end of the ATP13A1 mRNA (sgRNA 2) and may, thus, give an inaccurate estimate of the amount of

ATP13A1 transcript in these clones. If the two guide RNAs targeting sites further downstream had modified the ATP13A1 coding sequence in the clones in a way that left the 5' portion intact, a proportion of the detected transcripts may be truncated transcripts and the qRT-PCR may not have reflected these changes. In that case, the deep sequencing result would also only reflect the intact full-length transcripts as truncated species would not have yielded a PCR product. It seems unlikely, however, that if the sgRNAs had successfully guided the Cas9 nuclease to the 3' target sites it would only have edited in a way that resulted in truncated transcripts but not in a way that introduced point mutations or shorter indels. Repeating the qRT-PCR with Taqman probes annealing downstream of the other two guide RNA target sites may clarify this question. Furthermore, deep sequencing of the genomic loci rather than the expressed cDNA may prove informative as well.

In conclusion, while the MR1 phenotype in the HAP1.MR1 ATP13A1 KO clones has been confirmed, the mechanism by which this transporter exerts its modulatory function remains to be clarified. Furthermore, it is imperative to determine whether and to what extent the described phenotype replicates in other cellular systems. Therefore, a number of robust ATP13A1 knock-out cell lines should be established to fully elucidate the role of the ER transporter ATP13A1 in MR1 antigen presentation.

5 The role of the SNARE Sec22b in MR1 antigen presentation

5.1 Introduction

Soluble NSF attachment protein receptor (SNARE) proteins are essential mediators of vesicular trafficking. Being specific in both their sub-cellular localisation and their interaction with other SNAREs they provide the specificity needed for the delivery of transport vesicles from one cellular compartment to another and facilitate membrane fusion between the vesicle and the target membrane[441–444]. SNAREs tend to adopt a helical conformation which allows them to form tightly packed cores featuring parallel α-helical bundles and Leucine zipper-like structures. The stiffness of these multimeric complexes allows them to transmit mechanical force onto the opposing membranes and, thus, to overcome the energy barrier associated with membrane fusion[443,445,446].

Since much of the cell biology of MR1 loading and trafficking is still ill defined and vesicular transport is very likely to affect the delivery of either the antigen(s) or MR1 itself to the loading compartment, investigating the role of mediators of vesicular trafficking in MR1-mediated antigen presentation was of great interest. Further incentive came from the finding that the SNARE Sec22b[201,447] was a hit in an shRNA screen looking for modulators of MR1-mediated presentation of *M.*

tuberculosis antigen[262]. In this paper, transduction of the human airway epithelial cell line BEAS-2B with shRNAs targeting Sec22b lead to a reduced IFNγ ELISPOT response of a human MAIT cell clone upon infection with *M. tuberculosis.* The screen was followed by an siRNA validation approach which further confirmed a potential role for Sec22b in MR1-mediated antigen presentation.

Sec22b has previously been suggested to have an immune function as it was shown to mediate the delivery of ER-resident proteins to phagosomes, an important process in the context of antigen cross-presentation[200,201]. Specifically, a murine dendritic cell line stably expressing an shRNA targeting Sec22b was less able to recruit components of the ER-resident MHC class I peptide loading complex to phagosomes and displayed reduced cross-presentation capacity compared to control cells expressing a scrambled control shRNA. Consistent with this, translocation of antigenic peptides to the cytosol was reduced and phagosomal proteolytic activity was enhanced in the Sec22b KD cells[200]. Indeed, Sec22b had been shown to mediate the recruitment of ER-membranes to phagocytic cups before[448] and this Sec22b-dependent recruitment of ER-derived material to phagosomes is hijacked by the intracellular pathogen *Legionella pneumophila* which exploits the cellular process to aid the establishment of its replicative organelle[449,450].

Taken together, these findings provided a rationale to hypothesise that Sec22b may play a role in MR1 trafficking, for example by delivering MR1 directly from the ER to the endo- or phagosomal compartment for loading with antigen derived from phagocytosed bacteria.

5.2 Chapter specific Materials and Methods

Experiments were carried out according to protocols described in General Materials and Methods (Chapter 2) unless stated otherwise in Figure captions or below.

5.2.1 Sec22b KD cells

The murine dendritic cell line JAWSII lentivirally transduced with either Sec22b or scramble control (scrbl) shRNA was a kind gift from Sebastian Amigorena[200]. Cells were cultured in IMDM (Gibco #21980032) supplemented with first 10% and later 20% FCS and supplements as in General Materials and Methods plus 5 ng/ml murine GM-CSF (PeproTech #315-03). Human THP-1 and C1R cell lines were cultured as described in General Materials and Methods. MISSION® shRNA lentiviral particles encoding for shRNAs targeting Sec22b were purchased from Sigma-Aldrich (#SHCLNV-NM_004892; shRNA2: TRCN0000163868, shRNA6: TRCN0000159152, shRNA7: TRCN0000159288, shRNA9: TRCN0000240494, shRNA11: TRCN0000240495, pLKO.1 puro control shRNA: #SHC002V) and a polyclonal population of transduced cells was selected with 3 µg/ml puromycin (Gibco #A11138-03). shRNA target sites with respect to the exon/intron structure of human Sec22b are shown in Figure 5.1. Full sequences are available in Supplementary Table 1.

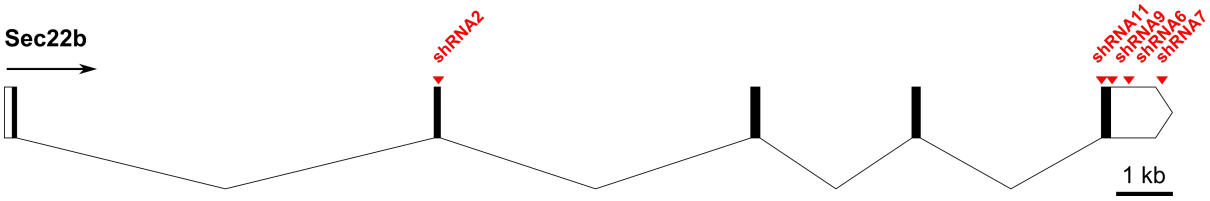


Figure 5.1: Position of shRNA target sites with respect to the exon/intron structure of human Sec22b. Exon are shown as solid bars, 3' and 5' untranslated regions are shown as empty bars. Arrow denotes direction of transcription. Positions of shRNA target sites are indicated by red arrow heads. The plot was generated using the Exon-Intron Graphic Maker available at wormweb.org/exonintron based on the exon/intron boundaries in NCBI Reference Sequence NM_004892.5. Full shRNA sequences are available in Supplementary Table 1.

5.2.2 Presentation assays using bacteria

DH5α *E.coli* were grown in LB broth in parallel with a sterility control at 37° C o/n, shaking. Bacteria were pelleted at ca. 4 000 x g (6 500 rpm in a HEREAEUS Fresco 17 tabletop centrifuge) for 4 min and supernatant was collected and sterile filtered. Bacterial cell pellets were washed 2-3 times in PBS and diluted to an OD_{600} of 0.05, corresponding to approximately $4x10^7$ bacteria/ml (https://www.genomics.agilent.com/biocalculators/calcODBacterial.jsp). 1 ml of the working dilution was UV-inactivated at 254 nm for 10 min and an aliquot was used to inoculate a control culture o/n to confirm inactivation. Bacteria were diluted in PBS or medium to indicated multiplicities of infection (MOI) and pulsed onto 50 000 JAWSII cells/well in medium without antibiotics. Gentamycin (Lonza #BE02-012E) was added to a final concentration of 50 µg/ml after 3 h to kill remaining extracellular bacteria except for the BCG assay. After 1.5 h of gentamycin treatment 10 µg/ml of αMR1 blocking antibody (clone 26.5) or IgG2a isotype control were added for 30 min before addition of 25 000 sorted human MAIT cells. Cells were co-cultured for 36 h at 37° C.

5.2.3 Bacterial uptake assays

Bacteria were grown, washed, diluted to an OD_{600} of 0.5 as above. 2 ml of the working dilution were spun down and bacteria labelled with 5 µM of Carboxyfluorescein succinimidyl ester (CFSE, invitrogen #C34570) for 15 min at 37° C in the dark. Labelled bacteria were washed in PBS 3 times and resuspended in 2 ml. 1 ml was UV-inactivated as above. Bacteria were diluted to the indicated MOIs and added to 50 000 JAWSII cells plated in medium without antibiotics for the indicated amounts of time at the indicated temperatures. At t = 0, samples were stained with live/dead stain aqua before fixation in 2 or 4% paraformaldehyde (Electron Microscopy Sciences #RT-15710) for 30 min at RT before flow cytometric analysis.

5.2.4 Reconstitution of Sec22b expression

The murine Secc2b coding sequence was amplified from cDNA generated from JAWSII cells and cloned into the IRES-GFP lentiviral expression plasmid described in General Materials and Methods (Figure 5.2). Lentiviral particles were generated in HEK293T cells as in General Materials and Methods and JAWSII Sec22b KD cells were transduced with virus-containing supernatant. The first JAWSII rescue cell line (R-1000) was sorted based on GFP expression (Supplementary Figure 9). JAWSII rescue cell lines R-1.9 to R-450 were generated using a serial dilution of the same virus-containing supernatant after freezing and thawing and were not sorted as GFP expression was unimodal (Figure 5.9).

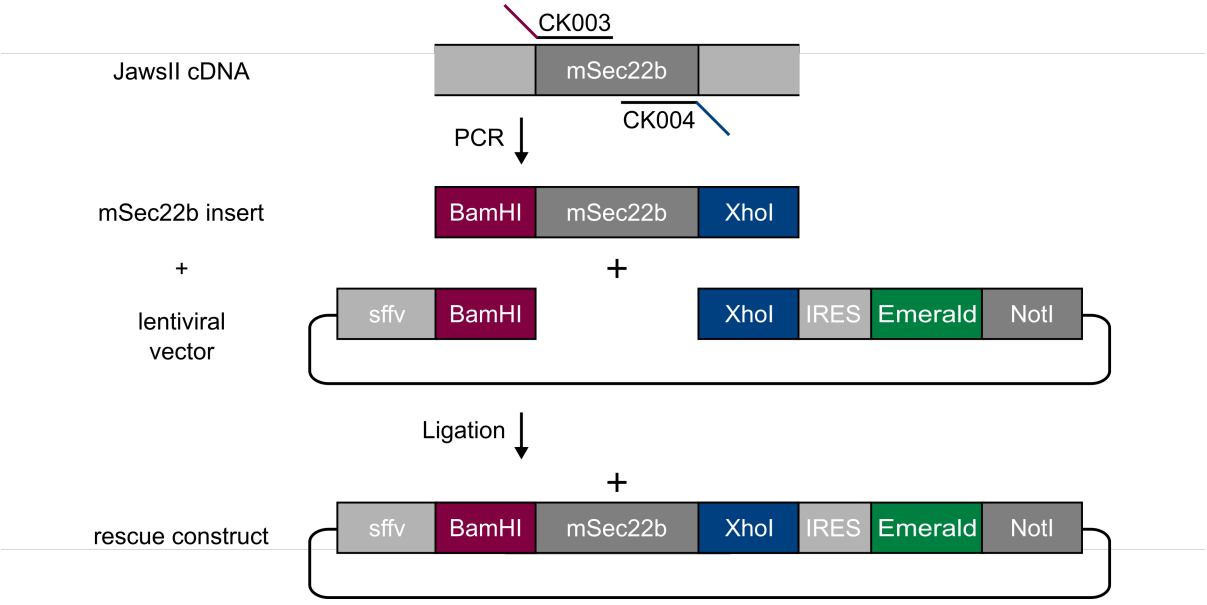


Figure 5.2: Cloning strategy of the murine Sec22b rescue construct. Schematic depiction of the cloning strategy used to generate the mSec22b expression construct pCK002 starting from cDNA made from RNA extracted from JawsII cells. Image not drawn to scale. For primer sequences refer to Supplementary Table 1.

5.2.5 RNA sequencing

RNA was extracted from JAWSII scramble control cells, JAWSII Sec22b KD cells, and JAWSII rescue cell line R-1000 in four biological replicates using either the QIAGEN RNeasy Mini Kit (QIAGEN #74104) or the Ambion RNAqueous™-Micro Total RNA Isolation Kit (Life Technologies #AM1931). Genomic DNA was either digested on the column (QIAGEN system) or in solution in combination with the Ambion DNAse Inactivation Reagent according to the manufacturer's instructions. Extracted RNA was analysed on an Agilent 2100 Bioanalyzer (performed by Laura Scifo) and only samples with an RNA Integrity Number (RIN) >8 were submitted for sequencing. A summary of the submitted samples can be found in Supplementary Table 5. Samples were sent for library preparation and 75 bp paired end next generation sequencing on a HiSeq4000 machine at the

Wellcome Trust Centre for Human Genetics, University of Oxford. There, the samples were enriched for mRNA before reverse transcription. dUTP was incorporated during second strand cDNA synthesis and samples submitted to uridine digestion before amplification. The cDNA was end-paired, A-tailed, and adapter-ligated and the prepared libraries were selected for size and multiplexed before paired end sequencing. Data was provided in fastq file format and analysed under supervision of Nicki Gray and Emmanouela Repapi (Computational Biology Research Group, WIMM, University of Oxford). The quality of the sequencing data was assessed using FastQC (https://www.bioinformatics.babraham.ac.uk/projects/fastqc/) version 0.11.4 and subsequently aggregated with MultiQC[451] (Supplementary Figure 10) before mapping to the mm10 reference genome using the RNAseq aligner STAR[452] version 2.4.2a. The % mapped reads was extracted from the STAR log files. Uniquely mapped reads were filtered based on MAPQ quality score and PCR duplicates were removed using SAMtools[453]. Gene expression was quantified using featureCounts[454] and differential gene expression analysis was carried out in R version 3.1.1 using the edgeR package[455]. A “method” column was included in the DGElist to allow controlling for effects of the different extraction methods. Lowly expressed genes were filtered out, keeping only genes with at least 1 count per million (cpm) for at least four samples and differences in RNA composition were adjusted for using the calcNormFactors function. A design matrix was generated to take the extraction method into account for the general linear model (GLM) and the dispersion was estimated with the glmQLFit

function before testing for differentially expressed genes between two conditions at a time using the QL F-test according to the quasi-likelihood pipeline described in the edgeR User Manual.

5.3 JAWSII Sec22b KD cells have an MR1 phenotype

To test the hypothesis that MR1 loading and trafficking is directly or indirectly dependent on the pre-Golgi SNARE Sec22b, MR1 expression levels and antigen presentation capacity was tested in the murine dendritic cell line JAWSII lentivirally transduced with either Sec22b or scramble control (scrbl) shRNA.

5.3.1 Surface levels of folded MR1 are reduced in Sec22b KD cells

First, Sec22b KD in these cells was confirmed at both the protein and the transcript level (Figure 5.3a and b) to establish the model system. Sec22b transcript levels were significantly lower (difference = -1.509; 95% CI [-1.746, -1.271]; $p < 0.0001$ and difference = -2.957; 95% CI [-3.145, -2.769]; $p < 0.0001$) in Sec22b KD cells in RNA extracted at two different occasions and Sec22b protein expression was reduced in multiple independent Western Blots. Next, MR1 surface levels of these cells were probed by flow cytometry. Interestingly, MR1 surface levels were much lower on JAWSII Sec22b KD cells compared to JAWSII scramble control cells when stained with the conformation-specific αMR1 antibody clone 26.5 which cross-reacts with murine MR1[265] (Figure 5.3c). Despite differences in the mean fluorescence intensity of the isotype control antibody between the two cells lines, when αMR1 GeoMean was normalised to the isotype GeoMean JAWSII scramble control cells still expressed more surface MR1 than JAWSII Sec22b KD cells. JAWSII Sec22b KD cells and scramble control cells had similar FSC vs SSC profiles, suggesting that the increased isotype control signal did not stem from differences in cell size or granularity (Figure 5.3d). To

further investigate the reason for the differential isotype staining, a different isotype control could be tested.

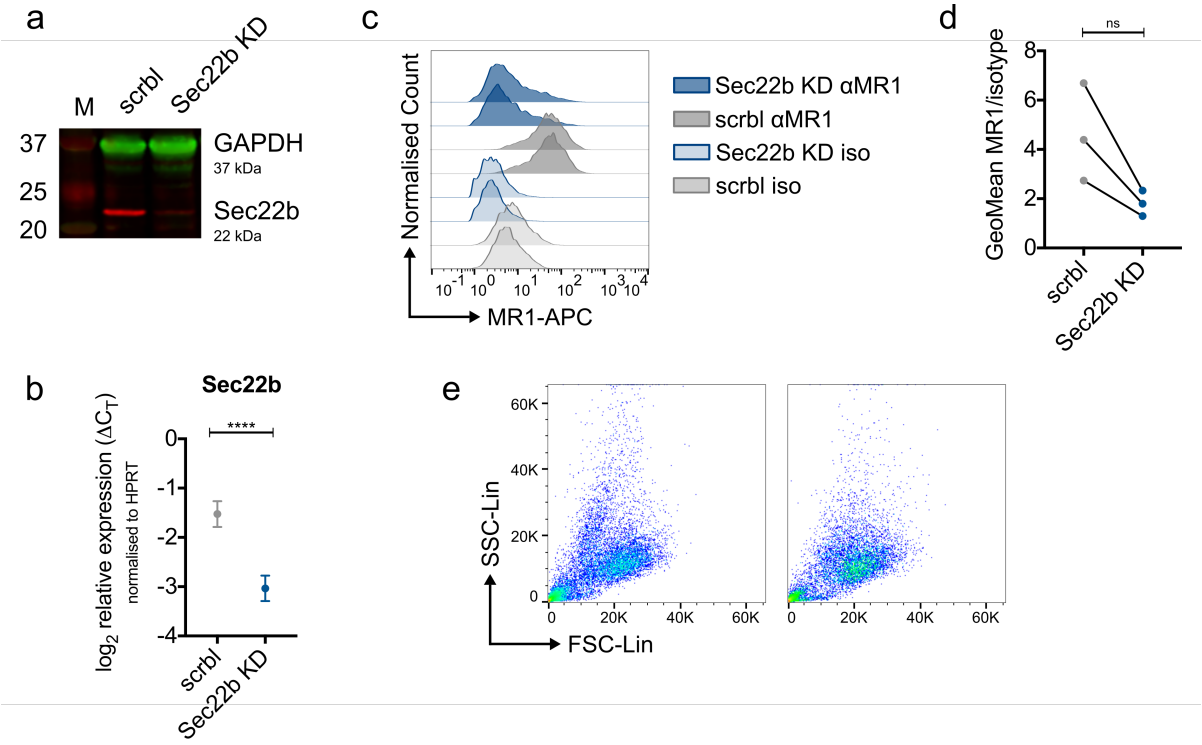


Figure 5.3: Surface levels of folded MR1 are reduced in JAWSII Sec22b KD cells. Sec22b protein (a) and transcript (b) levels were measured in JAWSII cells transduced with scrambled control shRNA (scrbl, grey) or shRNA targeting Sec22b (Sec22b KD, blue). Loading control GAPDH is shown in green in (a). qRT-PCR data in (b) are shown as mean of technical triplicates with 95% confidence interval and are representative of RNA extracted at two different time points and analysed together. (c) MR1 surface levels were measured by flow cytometry, staining with the conformation-specific αMR1 antibody clone 26.5 (αMR1, filled histograms) or murine IgG2a isotype control antibody (iso, tinted histograms). Pooled data from three similar experiments are shown in (d) where each symbol represents one measurement or the median of technical duplicates for one experiment. Forward scatter (FSC) vs side scatter (SSC) plots for representative samples from the experiment shown in (c) are shown in (e). Western Blot data are representative of three experiments including that shown in **Figure 5.9**b. Pooled data in (d) include samples from the experiment shown in **Figure 5.9**c. Statistical significance was calculated using an unpaired t test in (b) and the Wilcoxon matched-pairs signed rank test in (d). * = $p < 0.05$, ** = $p < 0.01$, *** = $p < 0.001$, **** = $p < 0.0001$, ns = not significant.

Although the MR1 surface phenotype in the JAWSII Sec22b KD cells was observed as a general trend in more than 10 different experiments (see for example baseline samples in Figure 5.6), it was not possible to pool all these data for statistical analysis. One reason was a frequently observed bimodal distribution

(see for example Figure 5.6) in some of the samples which invalidated the use of the geometric mean as a means of quantification. Other samples had been treated with DMSO as a solvent control (e.g. Figure 5.6) and could, thus, not be pooled with samples representing the untreated baseline. In total, the samples of three experiments were treated in the same way and amenable to quantification by the geometric mean. These were pooled for statistical analysis and although the same trend was seen in all experiments (Figure 5.3d), the difference between JAWSII Sec22b KD cells and JAWSII scramble control cells did not reach statistical significance as calculated with the Wilcoxon matched-pairs signed rank test (p = 0.25). However, this analysis is confounded by the low statistical power of this test and statistical significance might be achieved with larger sample numbers. Thus, more experiments are required to make statistically supported statements on the effect of Sec22b KD on MR1 surface expression in JAWSII cells. Despite these caveats, the observation of the same trend in multiple experiments using slightly altered protocols and analysis equipment still supported the conclusion that MR1 surface expression was reduced in JAWSII Sec22b KD cells compared to the scramble control cells.

Interestingly, the difference in MR1 surface levels was lost when JAWSII Sec22b KD or scramble control cells were fixed before surface staining with the 26.5 antibody clone in one initial experiment (Figure 5.4a). This suggested the presence of two distinct populations of MR1 molecules on the cell surface of the Sec22b KD cells: those that bind the 26.5 antibody clone at steady state and those that acquire a 26.5-reactive epitope upon fixation. Since the 26.5 antibody clone preferentially binds fully folded MR1[265], it is likely that the difference between these

two populations is their folding state. Consistent with this, preliminary data suggested that a polyclonal antibody that binds all conformational states of MR1 detected equal amounts of MR1 on the cell surface of JawsII scramble and KD cells (Figure 5.4b). Both these observations require further analysis to make conclusive statements about the folding state of the MR1 molecules at the cell surface of JAWSII Sec22b KD cells.

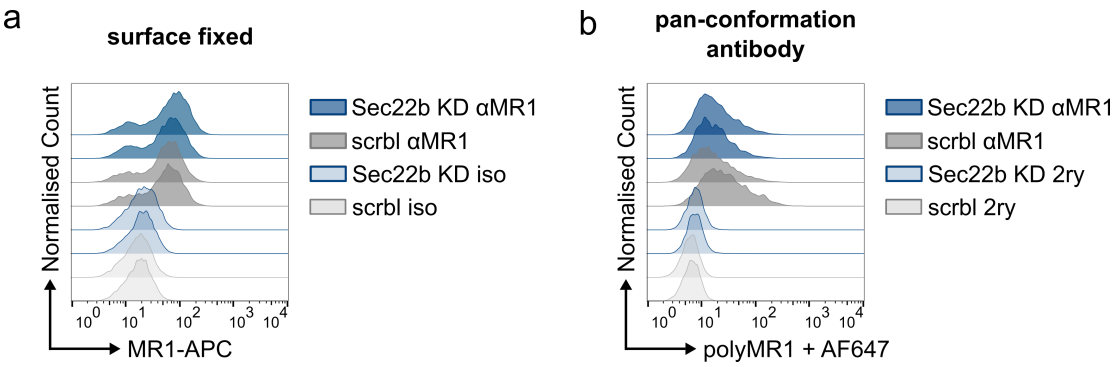


Figure 5.4: Surface levels of unfolded MR1 are unaffected in JAWSII Sec22b KD cells. JAWSII cells transduced with scrambled control shRNA (scrbl, grey) or shRNA targeting Sec22b (Sec22b KD, blue) were either fixed with ICS fixation buffer before surface staining with the APC-conjugated αMR1 antibody clone 26.5 or isotype (a) or surface stained with polyclonal, pan-conformation αMR1 antibody and AlexaFluor647-conjugated secondary antibody (b). Cells stained with secondary antibody only (2ry) are shown as controls in b.

Similarly, when total MR1 protein levels were measured by intracellular staining (ICS) in two experiments, MR1 levels were not lower in JAWSII Sec22b KD than scramble control cells (Figure 5.5a). In one of the two experiments, total intracellular MR1 levels appeared, in fact, slightly elevated in JAWSII Sec22b KD cells as compared to the scramble control cells but this could not be tested statistically (data not shown). Since cells were fixed and permeabilised prior to antibody staining for ICS, this is consistent with the observation that fixation abated the difference in surface expression (Figure 5.3). Of note, MR1 transcript levels in these cells were statistically significantly (difference = 0.8517; 95% CI

[0.6023, 1.101]; p = 0.0007 for extraction 1 and difference = -1.099; 95% CI [-1.391, -0.8069]; p = 0.0005 for extraction 2) different in opposite directions when measured twice but the magnitude of the effect was relatively small in both cases (Figure 5.5b). RNASeq analysis later confirmed that MR1 is not differentially expressed in Sec22b KD compared to scramble control cells (Figure 5.15, Supplementary Table 6). MR1 protein levels were not detectable in either of the two JAWSII cell lines by Western Blot with the polyclonal antibody used (data not shown). Correspondingly, whilst MR1 was readily immuno-precipitated from human MR1 over-expressing THP-1 cells, murine MR1 was not detectable in pull-downs from JAWSII cells (data not shown). Therefore, it was not possible to investigate the direct physical interaction between MR1 and Sec22b in the JAWSII cell lines through co-immunoprecipitation.

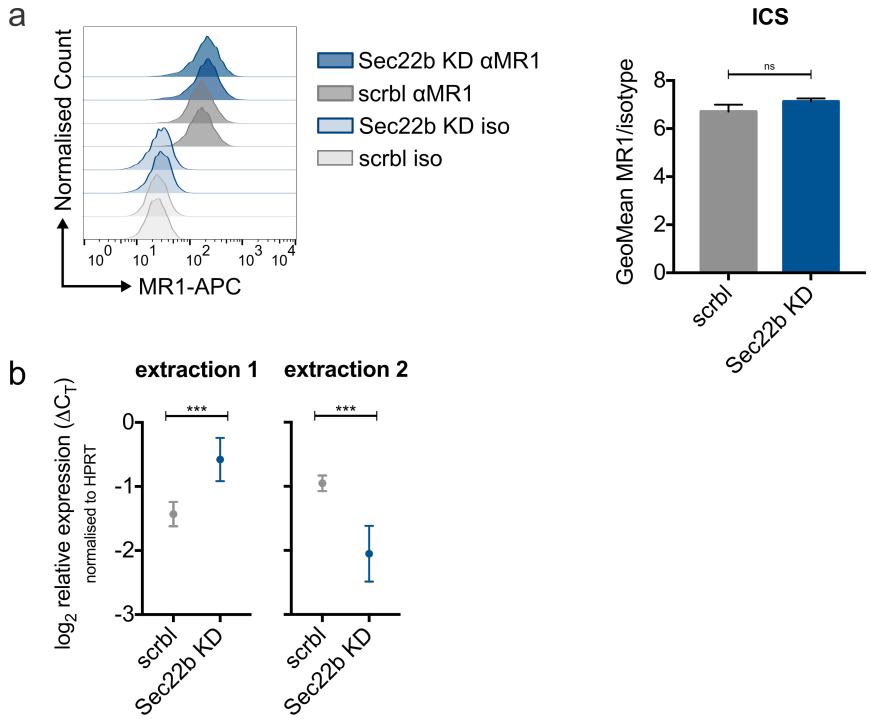


Figure 5.5: Total MR1 protein levels are unaffected in JAWSII Sec22b KD cells. JAWSII cells transduced with scrambled control shRNA (scrbl, grey) or shRNA targeting Sec22b (Sec22b KD, blue) were fixed and permeabilised before staining with the conformation-specific αMR1 antibody clone 26.5 or IgG2a isotype antibody conjugated to APC in quadruplicates. Representative histograms are shown in (a) and GeoMean of MR1 fluorescence intensity relative to the median GeoMean of the isotype control fluorescence intensity is shown as technical quadruplicates with median and range to the right of the histograms. (b) MR1 transcript levels were quantified by qRT-PCR of cDNA generated from RNA extracted at two different time points (extraction 1, extraction 2) and shown as means of technical triplicates with 95% confidence interval. Extraction 1 used the same cDNA samples as the qRT-PCR shown in **Figure 5.3**b. Statistical significance was calculated using the Mann-Whitney test in (a) and an unpaired t test in (b) where * = $p < 0.05$, ** = $p < 0.01$, *** = $p < 0.001$, **** = $p < 0.0001$, ns = not significant.

5.3.2 MR1-mediated antigen presentation is affected in Sec22b KD cells

To further probe the conformation of MR1 in the JAWSII Sec22b KD cells, MR1 surface levels were investigated after pulsing with the MR1-stabilising ligand Ac6FP. Incubation with Ac6FP increased MR1 surface expression in the Sec22b KD cells, though not to the level of the scramble control cells (Figure 5.6). This suggests that a proportion but not all of the MR1 molecules in the Sec22b KD cells are ligand-receptive and can translocate to the cell surface upon loading. MR1 surface levels in JAWSII scramble control cells were less responsive to incubation

with Ac6FP and were only elevated in response to the ligand in one out of three experiments (data not shown). Due to the bimodal distribution of the MR1 surface expression in the Sec22b KD cells in one out of three experiments and the differing ligand concentrations used, these results were not amenable to statistical analysis and should be interpreted as trends rather than definite conclusions. More repeats of the experiment are needed to assess both statistical and biological significance of the difference in MR1 surface levels in the presence of Ac6FP.

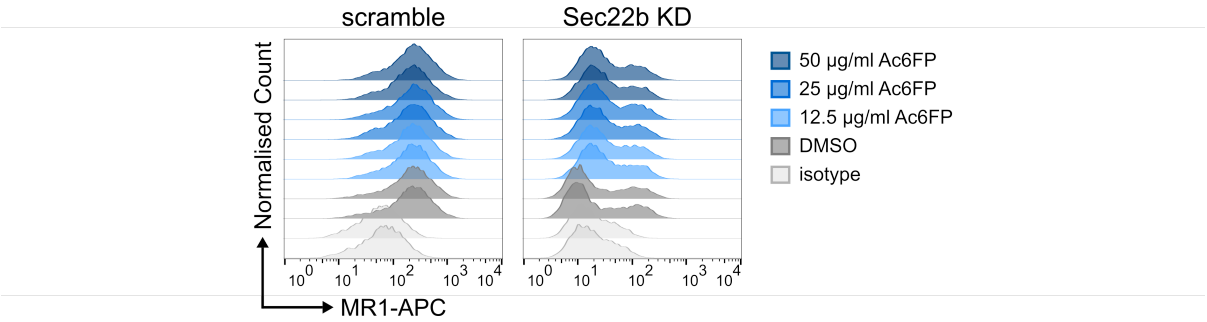


Figure 5.6: MR1 molecules in JAWSII Sec22b KD cells can translocate to the cell surface in the presence of Ac6FP. JAWSII cells transduced with scrambled control shRNA (scramble, left) or shRNA targeting Sec22b (Sec22b KD, right) incubated with Ac6FP at the indicated concentrations for 5 h before staining with the conformation-specific αMR1 antibody clone 26.5 or IgG2a isotype antibody conjugated to APC in duplicates. Data are supported by three similar experiments with similar results, sometimes varying the Ac6FP concentrations.

Next, the functional effect of Sec22b KD with respect to MAIT cell activation was investigated. Since there is almost 90% amino acid sequence homology between human and murine MR1 and uni-directional cross-reactivity between the species[456], sorted human MAIT cells could be used as responders and IFNγ secretion was quantified as a readout. Besides impacting MR1 surface expression, Sec22b KD in JAWSII cells also appeared to reduce antigen presentation by these cells to human MAIT cells in one experiment (Figure 5.7a-c). However, this trend could not be analysed statistically when pooled data for the highest concentrations of stimuli shared across repeat experiments (Figure 5.7d and e) were compared

because two of the three experiments were carried out with the same MAIT cell donor and, thus, the data did not represent independent pairs. Statistical analysis was further confounded by the fact that the highest shared MOI of UV-inactivated bacteria was 10 which did not trigger MAIT cell activation above background levels even in the experiment shown in Figure 5.7a-c. Thus, more data are needed to draw firm conclusions on the effect of Sec22b on MR1-mediated antigen presentation in murine DCs. Interestingly, in the experiment shown, the effect of Sec22b KD appeared most pronounced in the presentation of UV-inactivated bacteria (two out of three experiments) and was more variable when presenting their live counterparts (one out of three experiments, Figure 5.7d and e). This may be due to the limited MR1-dependence and suggests that cytokine-mediated activation of the MAIT cells may play a more dominant role upon infection with live bacteria[67,276]. By contrast, presentation of both bacterial supernatant and UV-inactivated bacteria was almost entirely blocked in the presence an αMR1 blocking antibody. Presentation of ligand-enriched bacterial supernatant was not affected by Sec22b deficiency (Figure 5.7). Uptake of CFSE-labelled live and UV-inactivated bacteria was unaffected by Sec22b knock-down (Figure 5.8) in two independent experiments. In one experiment uptake of UV-inactivated bacteria appeared slightly lower than uptake of live bacteria but there was no difference between Sec22b KD and scramble control cells (data not shown). Although these results were not amenable to statistical analysis due to small sample size, they suggest that the observed phenotype was not due to differential rates of infection. This is consistent with previous reports using the JAWSII Sec22b KD cells[200]. Instead, it would be conceivable that Sec22b was involved in delivering either MR1 or the ligand to the MR1 loading compartment.

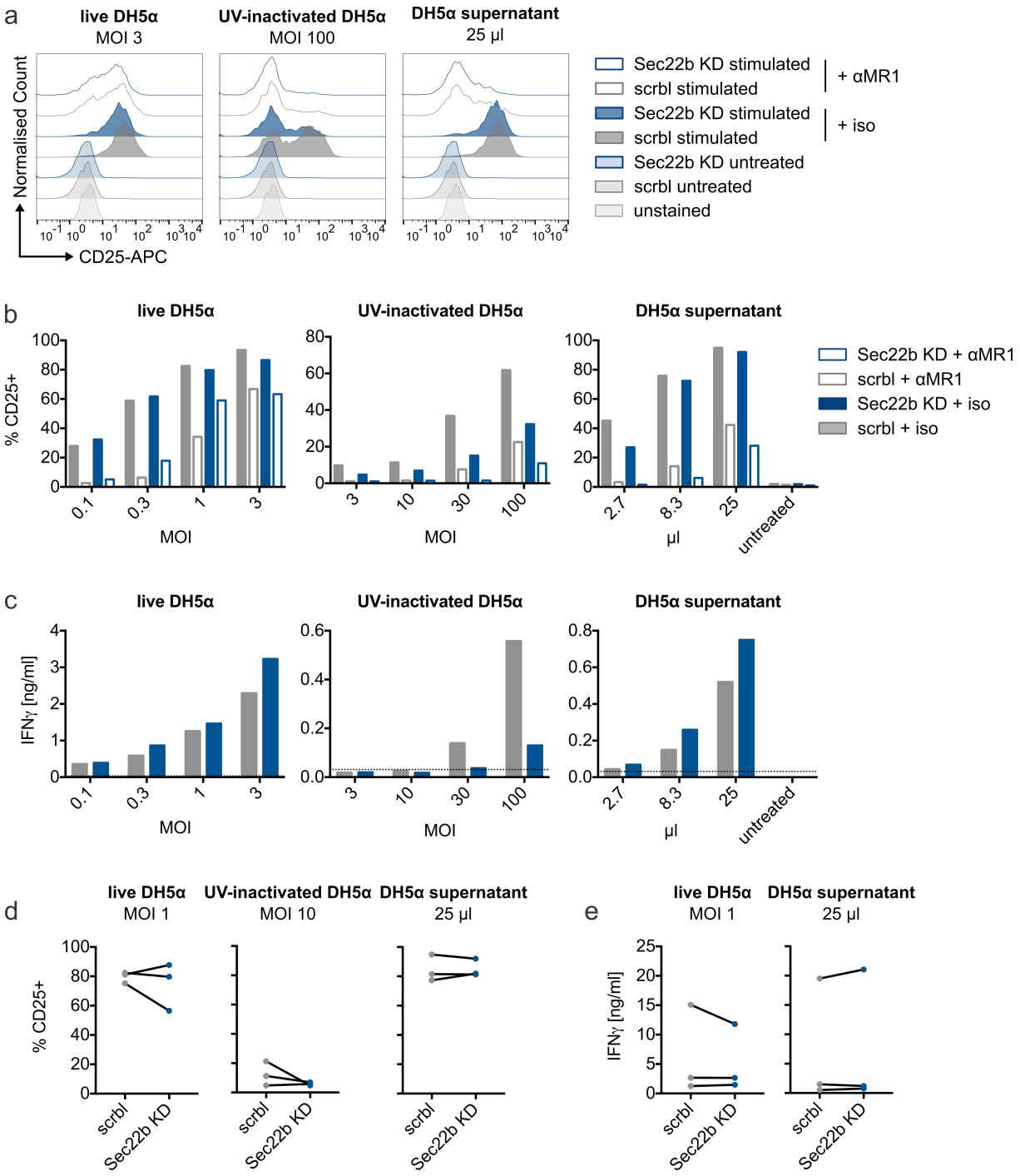


Figure 5.7: Antigen presentation of MR1 ligands is reduced in JAWSII Sec22b KD cells. JAWSII scramble control (grey) or Sec22b KD (blue) cells were pulsed with the indicated stimuli for 5 h before co-culture with sorted human MAIT cells. MAIT cell activation was quantified as % CD25+ cells of CD2+ cells by flow cytometry (a,b) and IFNγ secretion into the supernatant was assessed by ELISA (c). αMR1 blocking antibody clone 26.5 (+ αMR1, empty histograms and bars) or IgG2a isotype control antibody (+ iso, filled histograms and bars) were added 0.5 h before addition of MAIT cells. Histograms for the highest concentration of each stimulus are shown in (a). Data for the highest concentration of each stimulus shared across three repeat experiments using two different MAIT cell donors were pooled in (d) and (e). ELISA data for UV-inactivated bacteria at MOI = 10 were below the limit of detection.

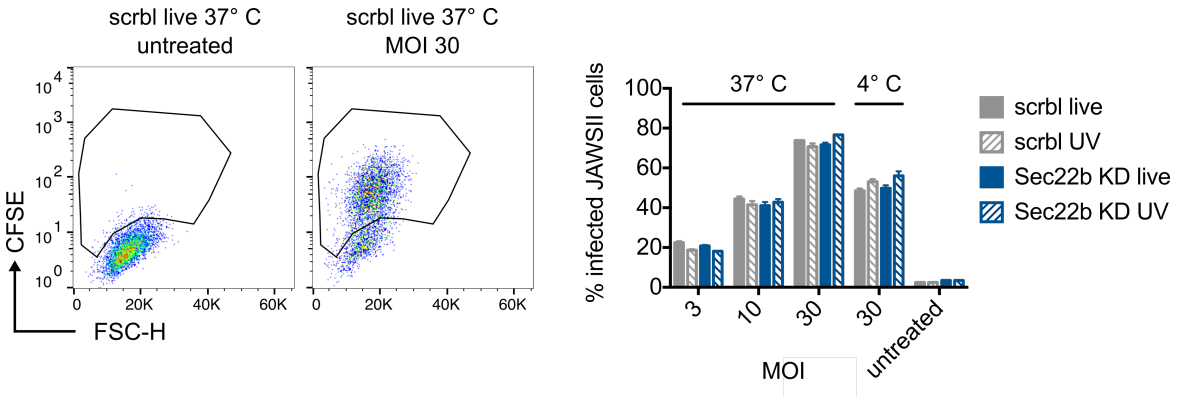


Figure 5.8: Uptake of DH5α bacteria is unaffected in JAWSII Sec22b KD cells. JAWSII Sec22b KD (blue) or scramble control (grey) cells were incubated with CFSE-labelled UV- inactivated (empty bars) or live (solid bars) DH5α bacteria at the indicated MOI for 3 h at the indicated temperatures. Bacterial uptake was assessed by flow cytometry and exemplary dot plots are shown on the left, gated on live cells. Infection was quantified as % CFSE+ cells and medians of technical duplicates are shown with range on the right. Data are representative of two experiments with similar results.

5.4 Reconstitution of Sec22b expression does not rescue the MR1 phenotype

The above results suggested that Sec22b might affect delivery of antigen derived from internalised bacteria to the loading compartment whereas the loading of soluble ligand was not affected. To ascertain whether the observed phenotype could be attributed to the knock-down of Sec22b, a murine Sec22b rescue construct was generated (Figure 5.2) and transduced into the JAWSII Sec22b KD cell line using lentiviral transduction. The original rescued cell line R-1000 over-expressed Sec22b (Figure 5.9b) which bore the risk of disturbing homeostatic function by providing too much of the SNARE. Therefore, a series of cell lines expressing increasing levels of Sec22b was generated by titrating the amount of virus-containing supernatant (Figure 5.9a and b). Remarkably, MR1 surface expression was not restored at any level of Sec22b reconstitution (Figure 5.9c).

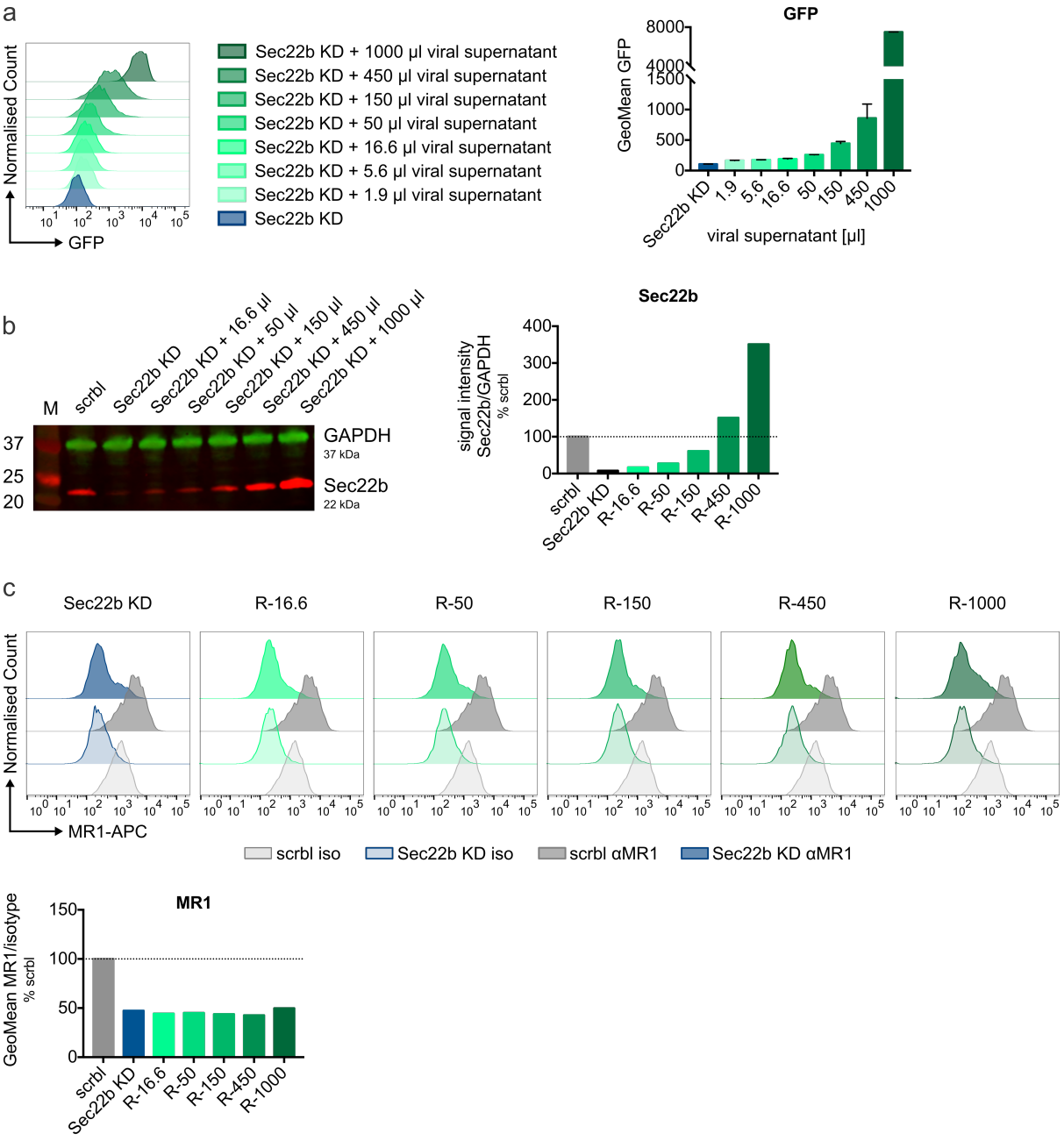


Figure 5.9: Reconstitution of Sec22b expression in JAWSII Sec22b KD cells does not rescue MR1 surface levels. JAWSII Sec22b KD cells were transduced with the indicated amounts of virus-containing supernatant in duplicates and GFP expression was measured by flow cytometry (a). The median geometric mean of the duplicates is shown to the right of the histograms with range. The rescued cell line R-1000 was generated before the titration lines. Sec22b expression in the JAWSII scramble control cell line (scrbl), the Sec22b KD parent cell line and a series of rescue cell lines was determined by Western Blot (b). Protein expression was quantified with the Odyssey® Near-Infrared imaging system and Sec22b intensity (red) normalised to loading control GAPDH (green) is shown to the right of the blot as % of scramble control. M denotes molecular weight marker and molecular weights of visible marker bands are indicated in kDa to the left of the blot. MR1 surface expression in the indicated rescue lines was measured by flow cytometry and GeoMean of MR1 fluorescence intensity relative to the isotype control antibody is shown below the histograms in (c). Dashed lines in (b) and (c) denote 100% for clarity.

While these analyses were not repeated often enough to calculate statistical significance, these initial data did not support the hypothesis that the MR1 phenotype observed in JAWSII Sec22b KD cells was, in fact, due to the reduction in Sec22b.

5.5 Knock-down of Sec22b does not affect MR1 expression in human cell lines

Even though MR1 is highly evolutionary conserved between mice and humans[456], trafficking and processing of immune receptors can differ significantly between the two species as is the case for TLR7, for example[457]. Consistent with a role for Sec22b in human MR1 trafficking, Sec22b knock-down in human bronchial epithelial cells was recently shown to reduce presentation of *M. tuberculosis* ligands to a MAIT cell clone[262], providing a rationale for investigating the role of Sec22b in MR1-mediated antigen presentation in human cells. Therefore, Sec22b was knocked down in human THP-1 and C1R cells using an shRNA approach. Lentiviral particles encoding five different shRNAs targeting human Sec22b were purchased from Sigma-Aldrich (Figure 5.1) and their efficiency in knock-down was assessed by Western Blot (Figure 5.10a and b). Two shRNAs resulted in efficient knock-down of Sec22b at the protein level in THP-1 and C1R cells expressing either endogenous levels of MR1 or over-expressing the protein (Figure 5.10a and b). Subsequently, MR1 surface levels in the cells transduced with these two shRNAs were determined by flow cytometry. MR1 surface levels were not reduced at baseline in the way they were in the JAWSII cells in either THP-1 or C1R cells whether they were over-expressing MR1 or not (Figure 5.10c and d). Of note, a higher isotype staining in the scramble control cells compared to the Sec22b KD

cells as observed in the JAWSII cells was not seen in the human cell lines (data not shown). Next, MR1 surface levels upon pulsing with the MR1-stabilising ligand Acetyl-6-formylpterin (Ac6FP) were tested in THP-1 Sec22b KD cells. Since MR1 surface levels are very low in WT cells, a further reduction may not have been detectable at baseline but could have been expected in the presence of an MR1-stabilising ligand. While incubation with Ac6FP increased MR1 levels at the cell surface, it did so to the same extent regardless of Sec22b knock-down (Figure 5.10e).

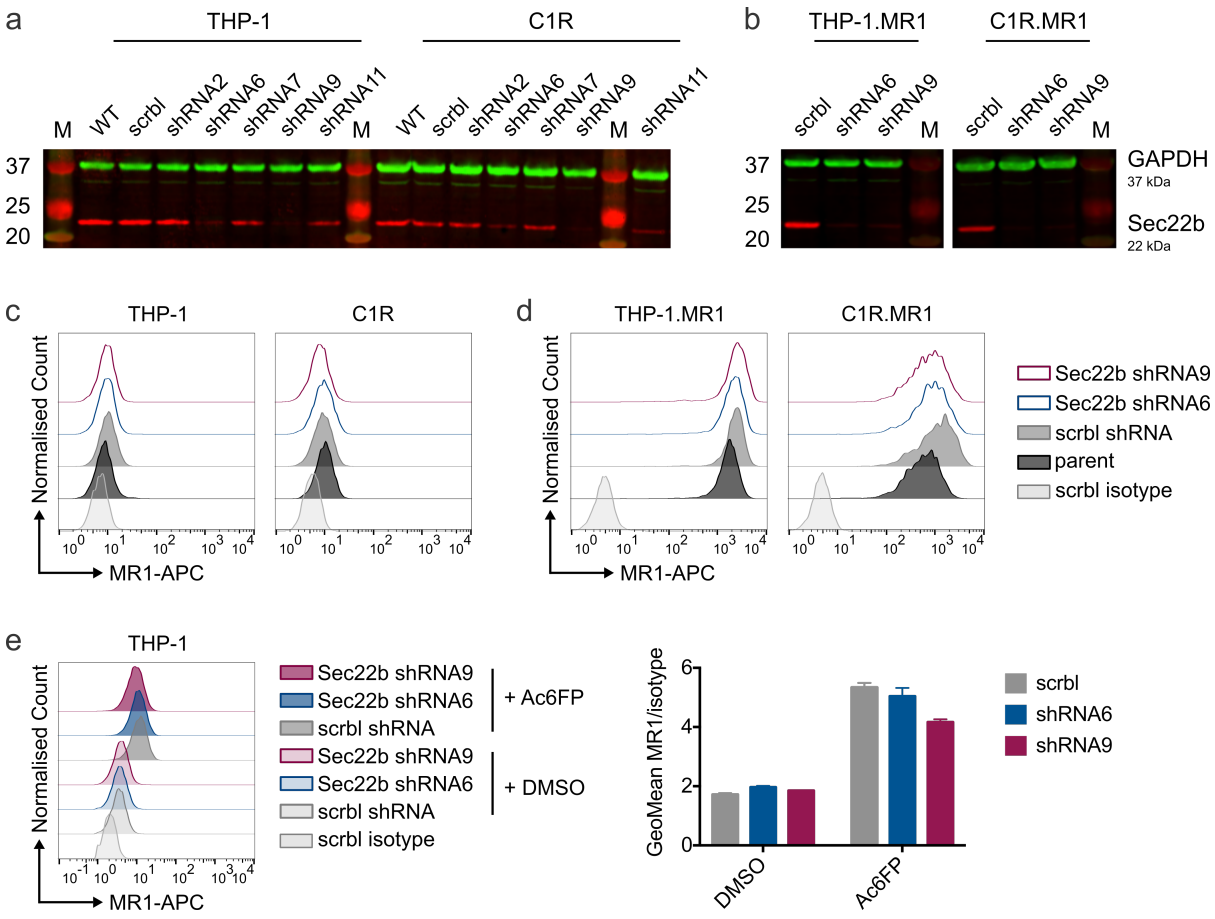


Figure 5.10: Knock-down of Sec22b in human cell lines does not affect MR1 surface levels. THP-1 or C1R cells over-expressing MR1 (THP-1.MR1, C1R.MR1) or nor (THP-1, C1R) were transduced with lentiviral particles coding for scramble control shRNA (scrbl) or the indicated shRNAs targeting Sec22b. Sec22b protein expression (a,b) and MR1 surface in the absence (c,d) or presence (e) of 10 µg/ml of the MR1-stabilising ligand Ac6FP were measured. Parent in (c) and (d) denotes untransduced cell line. Loading control GAPDH is shown in green in (a) and (b). M denotes molecular weight marker and molecular weights of visible marker bands are indicated in kDa to the left of the blot. GeoMean of MR1 fluorescence intensity relative to the isotype control antibody is shown to the right of the histograms in (e) as median of technical duplicates with range.

Thus, human Sec22b KD cells did not seem to recapitulate the MR1 surface phenotype observed in the murine cell line. Similarly, MAIT cell activation in response to live bacteria, UV-inactivated bacteria, synthetic ligand, or the attenuated *M. tuberculosis* vaccine strain BCG presented by human Sec22b KD cells was equal if not higher upon Sec22b knock-down in THP-1 cells (Figure 5.11). The phenotypic analysis of the human Sec22b KD cell lines was not amenable to statistical analysis due to a lack of biological repeats but since there was no indication that Sec22b had an effect on MR1 surface expression in these cellular system no further experiments were performed. To draw more substantiated conclusions on the role of Sec22b in these cell lines more data are needed.

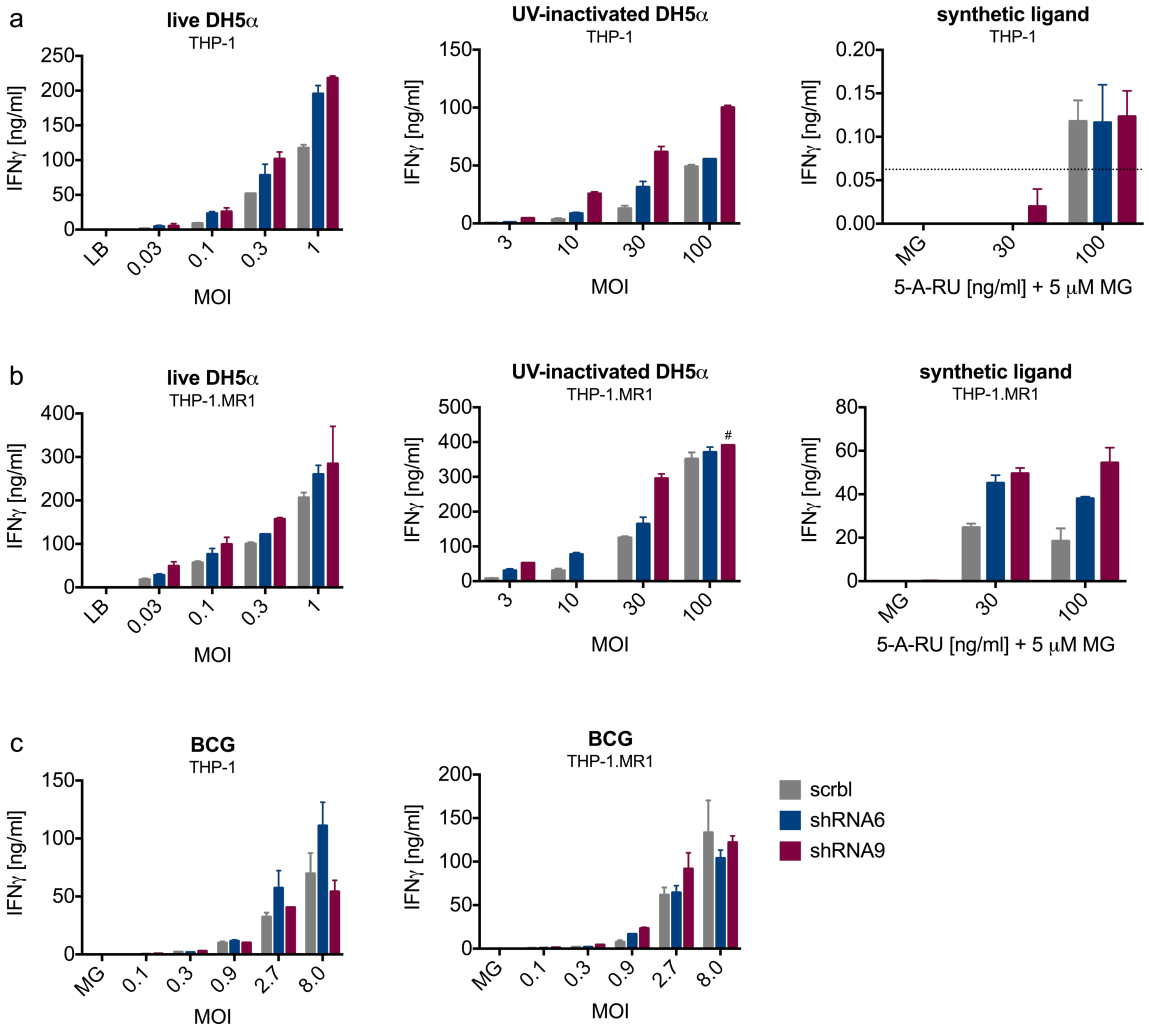


Figure 5.11: Knock-down of Sec22b does not reduce antigen presentation of MR1 ligands in THP-1 cells. THP-1 cells over-expressing MR1 (b) or not (a) and transduced with scramble control shRNA (scrbl, grey) or one of two shRNAs targeting Sec22b (shRNA6 and shRNA9, blue and red) were pulsed with the indicated stimuli for 5 h before co-culture with sorted human MAIT cells after which IFNγ secretion into the supernatant was assessed by ELISA. Bars represent the median of technical duplicates with range. # = no data for one or two of the duplicates.

To investigate whether MR1 and Sec22b might physically interact, MR1 was immuno-precipitated (IP) from THP-1.MR1 whole cell lysates and the precipitate immuno-blotted for Sec22b. While MR1 itself was readily detectable in the IP fraction, Sec22b was not pulled down together with it in a preliminary experiment (Figure 5.12). Further repeats of the experiment including the optimisation of the lysis buffer and Co-IP conditions are needed to make a firm statement on the physical interaction between MR1 and the SNARE.

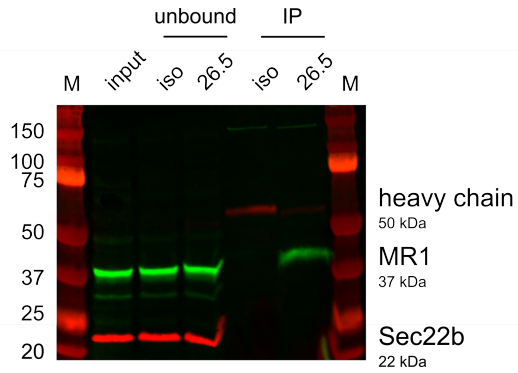


Figure 5.12: MR1 and Sec22b do not co-immunoprecipitate in THP-1.MR1 cells. THP-1.MR1 cells were lysed in lysis buffer containing 1% digitonin and pre-cleared with Protein G agarose resin before immuno-precipitation with the confirmation-specific αMR1 antibody clone 26.5 (26.5) or murine IgG2a isotype antibody (iso). Immuno-precipitates and unbound fractions were separated by SDS-PAGE along with input samples and immuno-blotted for MR1 (green) and Sec22b (red). M denotes protein marker and molecular weights of visible marker bands are indicated in kDa to the left of the blot.

5.6 RNA sequencing reveals a number of potential off-target effects of Sec22b KD

Based on the results reported above, in particular the observation that reconstitution of Sec22b expression failed to rescue the MR1 phenotype in the JAWSII cell line, it was hypothesized that the observed phenotype was due to an off-target effect of the Sec22b shRNA used. Therefore, RNA was extracted from JAWSII Sec22b KD cells, scramble control cells, and reconstituted Sec22b rescue cells and submitted for RNA sequencing to identify other genes which were differentially expressed between the three cell lines. In particular, genes which were down-regulated in both Sec22b KD and Sec22b rescued cells compared to scramble control cells were considered candidates for the off-target gene knocked down by the Sec22b shRNA.

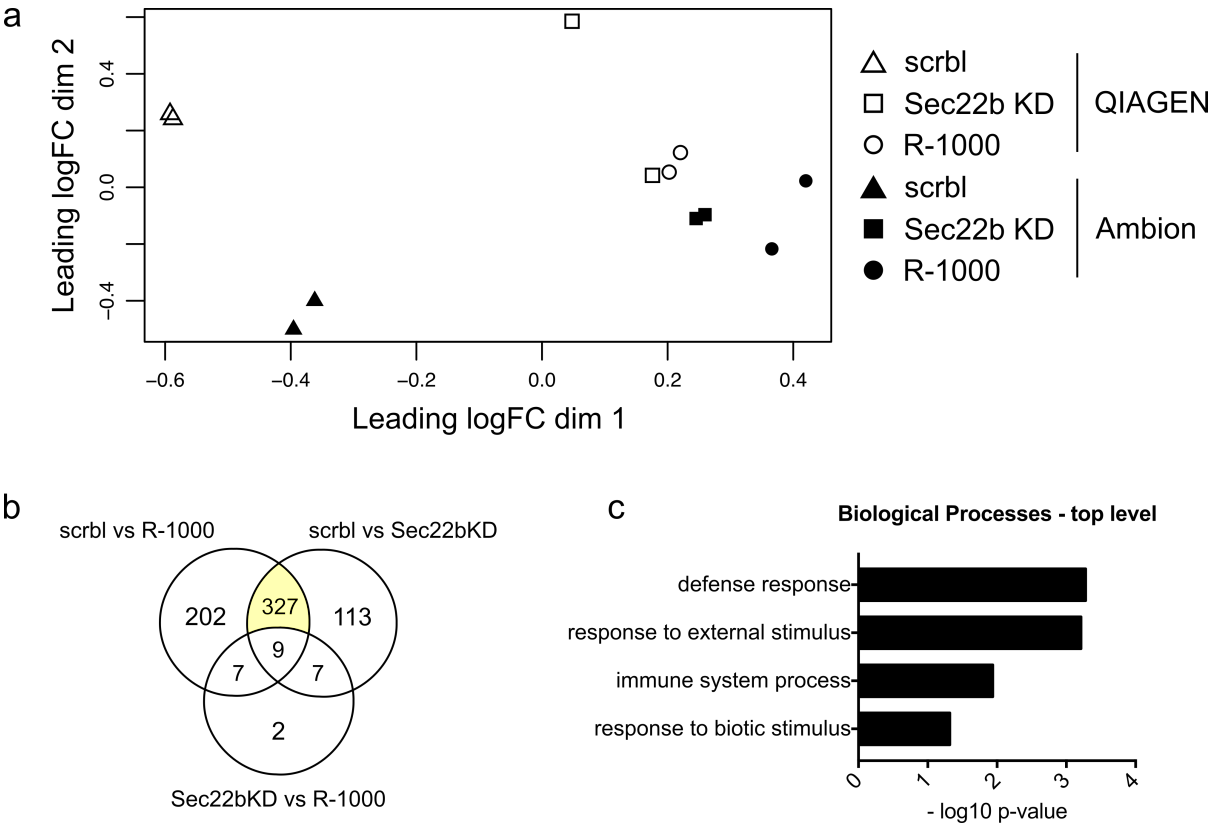


Figure 5.13: RNA sequencing reveals potential off-targets of the Sec22b shRNA in JAWSII Sec22b KD cells. Sample relations within RNASeq data of RNA extracted from JAWSII scramble control cells (scrbl, triangles), Sec22b KD cells (squares), or rescued cell line R-1000 (circles) extracted either with a QIAGEN (empty symbols) or Ambion (filled symbols) in multi-dimensional scaling are plotted in (a). Genes differentially expressed in the different pairwise comparisons and the overlap of these gene lists are shown in (b). Circles are not to scale. The gene set of interest is highlighted in yellow. Highlighted genes in (b) were analysed for GO term[352,353] enrichment using g:Profiler[458] (version r1732_e89_eg36) and top level GO terms significantly ($p < 0.05$) enriched are shown in (c).

Principal component analysis of the RNAseq data set revealed that the method of extraction strongly influences the variation between replicates. While the first dimension discriminates well between samples expressing the Sec22b shRNA (Sec22b KD and R-1000) and those that do not (scrbl), the second dimension clearly separates samples extracted with the QIAGEN Kit from those extracted with the Ambion kit (Figure 5.13a). This result underscores the importance of consistency in RNA extraction protocol across replicates. Because of this observation, the extraction method was taken into account in the general linear model used to calculate differential gene expression. Using the edgeR package in

R genes differentially expressed between the different cell lines were determined and 327 genes with a FDR < 0.01 and a logFC >= |1.5| were found to be differentially expressed between the Sec22b KD cells and the scramble control cells as well as the rescued cell line R-1000 and the scramble control cells but not between the Sec22b KD cells and the R-1000 cells (Figure 5.13b). This subset of genes was analysed for enrichment of gene ontology (GO) terms[352,353] with the online tool g:Profiler[458] and genes related to cellular responses to stimuli including the defence response as well as immune system processes were found to be significantly (p < 0.05) over-represented (Figure 5.13c).

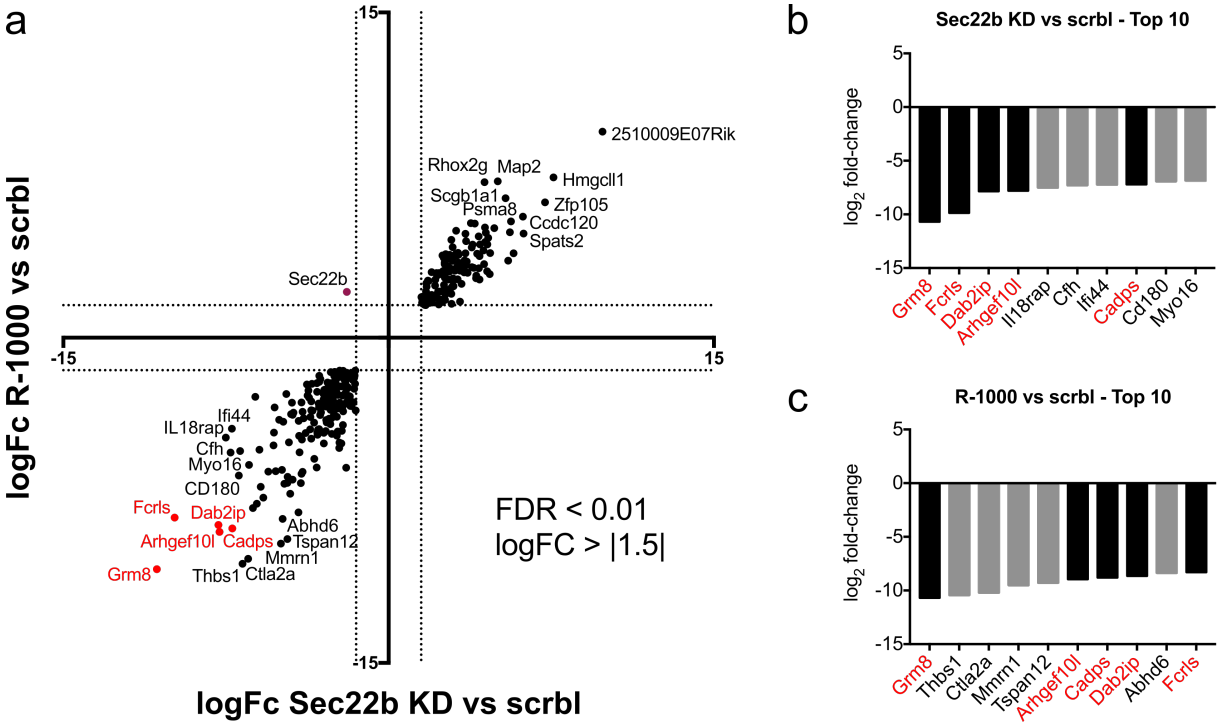


Figure 5.14: The top hits in the gene set of interest include many surface proteins involved in immune function. The logFc of the JAWSII Sec22b KD cell line compared to the scramble control cells is plotted against the logFc of the rescue cell line R-1000 compared to the scramble control cell line for each of the 327 hits identified in **Figure 5.13** and Sec22b in (a). The ten genes with the highest down-regulation relative to the scramble control cell line for the Sec22b KD (b) and R-1000 (c) cells are shown and shared genes highlighted in red. For the full list of differentially expressed genes see **Supplementary Table 6**-9.

Table 5.1: Top 20 differentially expressed genes Names and functional annotation based on Uniprot are shown for the ten genes with the highest down-regulation relative to the scramble control cell line for the Sec22b KD and R-1000 cells each and shared genes highlighted in red. For the full list of differentially expressed genes see **Supplementary Table 9**.

Gene	Encoded protein	Function (Uniprot)
Grm8	Glutamate Metabotropic Receptor 8	G-protein coupled receptor for glutamate (neurotransmitter)
Arhgef10l	Rho guanine nucleotide exchange factor 10-like	guanine nucleotide exchange factor (GEF) for RHOA, RHOB and RHOC
Cadps	Ca2+-dependent secretion activator	involved in exocytosis of vesicles filled with neurotransmitters and neuropeptides
Dab2ip	Disabled Homolog 2-Interacting Protein	scaffold protein implicated in a large spectrum of signaling pathways
Fcrls	Fc receptor-like S	scavenger receptor
Il18rap	Interleukin 18 Receptor Accessory Protein	does not mediate IL18-binding, but involved in IL18-dependent signal transduction
Cfh	Complement factor H	alternative complement pathway
Ifi44	Interferon-induced protein 44	aggregates to form microtubular structures
Cd180	CD antigen 180	may cooperate with MD-1 and TLR4 to mediate the innate immune response to LPS
Myo16	Unconventional myosin-XVI	serves in intracellular movements
Thbs1	Thrombospondin 1	adhesive glycoprotein that mediates cell-to-cell and cell-to-matrix interactions
Ctla2a	Cytotoxic T lymphocyte-associated protein 2 α	secreted protein that inhibits Cathepsin L[459]
Mmrn1	Multimerin 1	storage and stabilization of factor V in platelets
Tspan12	Tetraspanin 12	regulator of cell surface receptor signal transduction
Abhd6	Monoacylglycerol lipase ABHD6	hydrolyzes glycerol monoesters of long-chain fatty acids

Closer inspection of the most down-regulated genes in both the Sec22b KD and R-1000 rescued cells relative to the scramble control cells showed that this subset contained many plasma membrane proteins or those involved in vesicle trafficking, e.g. Cadps and Myo16 (Figure 5.14, Table 5.1). A high proportion of these genes was also involved in immune function or affected by it, such as Fcrls, Cfh, CD180, and Ctla2a, a protein that can be secreted by dendritic cells to induce regulatory T cell polarisation[460,461]. The full list of differentially expressed genes for each comparison can be found in Supplementary Tables 6-8.

Since the expression of a variety of surface receptors and immune mediators was affected in cells expressing the Sec22b shRNA, the murine B2M locus was specifically investigated. Quantification of reads from this gene showed that expression of B2M transcript was much lower in cells transduced with the Sec22b shRNA (Figure 5.15) and B2M was also found to be differentially expressed based on the GLM analysis with an FDR of 0.00045 for scrbl vs Sec22b KD and an FDR of 0.00332 for scrbl vs R-1000 (Supplementary Table 9), providing a potential explanation for the reduced MR1 surface levels. MR1 itself was not differentially regulated in the RNASeq data set (Figure 5.15, Supplementary Table 9). The only hit within the 327 gene subset that was shared between the RNASeq experiment and the screen described in Chapter 3 was GRIK2, encoding for the Glutamate Ionotropic Receptor Kainate Type Subunit 2 (Figure 5.15, Supplementary Table 9). However, this gene had the opposite effect in the two experiments: while it was a putative negative regulator of MR1 surface expression in the gene trap screen, it was also absent from JAWSII Sec22b KD cells which had reduced MR1 surface expression and would, thus, have been inferred to have a positive regulatory role.

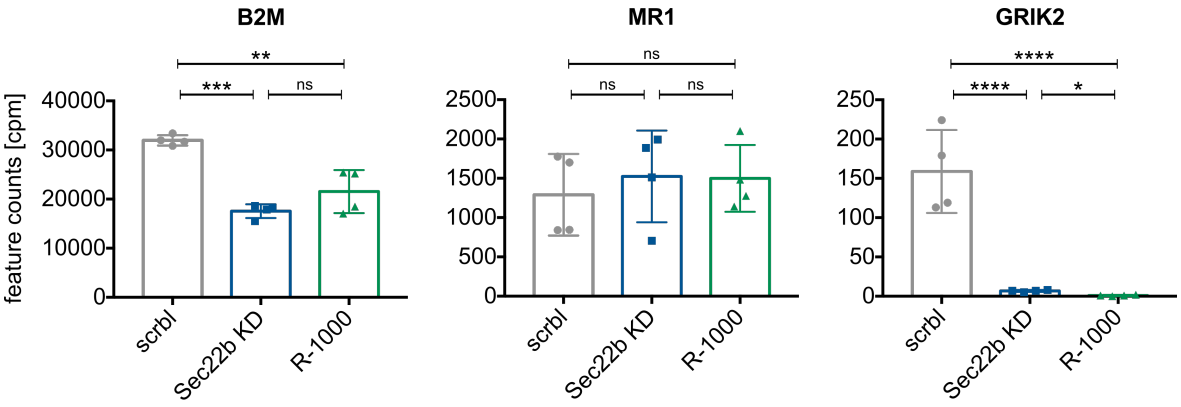


Figure 5.15: B2M and GRIK2 but not MR1 expression is reduced in cells expressing the Sec22b shRNA. Feature counts for the indicated genes were normalised to account for differences in RNA composition and plotted individually for each replicate of the indicated cell line with mean and SD. Statistical significance was calculated using the GLM described in the Chapter specific Materials and Methods. * = FDR < 0.05, ** = FDR < 0.01, *** = FDR < 0.001, **** = FDR < 0.0001, ns = not significant, cpm = counts per million.

5.7 Discussion

While JAWSII Sec22b KD cells displayed a clear reduction in MR1 surface expression accompanied by a more subtle antigen presentation defect, preliminary data indicated that this phenotype could not be rescued upon reconstitution of Sec22b expression. Furthermore, knock-down of Sec22b in human cell lines did not replicate the phenotype observed in the murine dendritic cell line in initial experiments. It was, thus, hypothesised that the apparent Sec22b-dependent phenotype could in fact not be attributed to the loss of Sec22b but, rather, was caused by an off-target effect of the Sec22b shRNA used. The same conclusion was reached in parallel with respect to the cross-presentation defect reported in the same cell line[200,201,203]. When Wu *et al.* attempted to confirm the critical role of Sec22b in cross-presentation *in vivo* they were unable to detect a phenotype in a conditional $CD11c^{Cre}Sec22b^{fl/fl}$ mouse model[203]. Importantly, they were able to confirm the cross-presentation phenotype upon shRNA-mediated knock-down of the SNARE but this effect held true in both Sec22b WT and Sec22b KO cells. Similar to the results reported in this chapter, reconstitution of Sec22b expression in cells transfected with the Sec22b shRNA did not rescue the cross-presentation defect in their system. Like the approach described here, Wu *et al.* performed RNASeq analysis to identify potential off-targets of the Sec22b shRNA and found a number of genes differentially expressed between JAWSII scramble control cells and those expressing an shRNA targeting Sec22b. Although the number of putative off-targets identified in their study was much lower, one of the hits identified – Ccl22[203] – overlapped with the 327 gene list identified here (Supplementary Table 9). If the analysis parameters were set less stringently and genes with a logFC value < 1.5 were included, Wu *et al.*'s significantly

downregulated genes Tbxas1 and P2ry6 could also be found in the RNASeq data set described in Section 5.6 (data not shown). Ccl22 encodes the chemokine CCL22, a ligand for the chemokine receptor CCR4 which is highly expressed on many T cell subsets[462], Tbxas1 codes for an enzyme involved in arachidonic acid metabolism[463,464], and the gene product of P2ry6 is a G-protein coupled extracellular pyrimidine receptor[465], none of which provide an obvious link to a trafficking defect. By contrast, two of the 20 most down-regulated genes of interest identified in this chapter were directly involved in intracellular trafficking: the Ca^{2+}-dependent secretion activator Cadps and the unconventional myosin Myo6. Strikingly, the fold-change of downregulation of these two genes far exceeded that of Sec22b, making it plausible for potential off-target effects to outweigh the effect of Sec22b itself. Therefore, these two genes represent promising candidates for modulators of both cross-presentation and MR1 surface translocation. Their role in both cellular processes remains to be confirmed and further characterised.

It should be noted, however, that the group that made the JAWSII Sec22b KD cells also established a $CD11c^{Cre}Sec22b^{fl/fl}$ mouse model and did observe a cross-presentation defect in DCs from these mice *ex vivo* and *in vivo*[202]. Using littermates rather than WT mice as controls Alloatti *et al.* saw an effect of Sec22b KO in *ex vivo* cross-presentation experiments comparable to those performed by Wu *et al*. as well as a defect in *in vivo* cross-priming and tumour control[202]. Importantly, successful rescue of the observed phenotype by recombinant expression of Sec22b was not reported in either the shRNA *in vitro* system or the mouse model. The discrepancy between the two mouse models has sparked debate in the field and even though there are some potentially significant

differences in the technical approaches of the two studies, these do not suffice to explain the opposite outcomes[204]. Nevertheless, it can be concluded that (a) the role of Sec22b in cross-presentation remains to be further clarified and – of particular relevance for this discussion – (b) that the expression of the Sec22b shRNA modulates the expression of more genes than Sec22b.

In fact, this is not the first time that opposite conclusions have been drawn on the regulatory impact of Sec22b. Whereas Becker *et al.* reported Sec22b to be indispensible for recruitment of ER-membranes to sites of phagocytosis[448], Hatsuzama *et al*. found the SNARE to be a negative regulator of the same process[466]. Again, technical differences in the experimental protocols such as the phagocytosis substrates used may explain the different outcomes, particularly in light of the observation that even the virulence of one and the same bacterium can make a difference to Sec22b involvement[450]. In line with this, Becker et al. showed that Sec22b was only found to be important for the phagocytosis of large (3 µm) particles whereas Hatsuzama *et al*. used zymosan A particles of undefined size[448,466]. Alternatively, differences in the conformation of stably vs transiently over-expressed Sec22b or differences in tags, cell lines, and Stx18 expression levels may account for the contrasting reports[466].

Another explanation for the reduced MR1 surface expression in the JAWSII Sec22b KD cells reported in this chapter may be the reduced expression of B2M in these cells (Figure 5.15) as association with β_2-microglobulin (β_2m) is a known requirement for MR1 surface translocation[259,280]. However, the observation that both MHC class I surface expression levels and direct presentation of soluble

antigenic peptide by MHC class I were unaffected in these cells[200] speaks against this hypothesis as MHC class I surface expression is equally dependent on β_2m[393,394]. Of note, recruitment of MHC class I molecules was found to be independent of Sec22b-mediated delivery of ER-Golgi Intermediate Compartment (ERGIC) material to the phagosome and instead shown to occur from recycling endosomes[201].

Regarding the lack of an effect of Sec22b KD on MR1 surface expression in the human compared to the murine cell lines, it could also be hypothesised that the observed differences are due to the cell type rather than the species. While JAWSII are considered a dendritic cell line, THP-1 cells are monocytic[411] and C1R cells are derived from a B cell line[467]. Thus, the role of Sec22b in antigen presentation may also depend on the immune cell type and be more relevant in the context of professional antigen presenting cells.

While the data presented in this chapter do not formally exclude a role for Sec22b in MR1-mediated antigen presentation they do not support the hypothesis either.

6 The role of cellular riboflavin transporters in MR1 antigen presentation

6.1 Introduction

How soluble MR1 ligands enter the cytosol and, eventually, the MR1 loading compartment remains elusive[94,260,262,272]. While it has not formally been ruled out that the known antigenic ligands cross the plasma membrane by simple diffusion this appears unlikely given the hydrophilic nature of their ribityl moieties[96]. Similarly, the non-stimulatory, folate-derived ligands feature charged functional groups[95,292] making it implausible that they should be able to transit through the lipid bilayer of the plasma membrane or the ER unaided. It has therefore been suggested that soluble extracellular MR1 ligands could either be imported by dedicated transporters or reach the ER via vesicular retrograde transport after endocytosis[94,260]. Since the best characterised antigenic MR1-ligands are intermediates of the riboflavin synthesis pathway[95,96], it was conceivable that these ligands may be imported by the cellular riboflavin transporters.

In humans, riboflavin transport has been most extensively studied in the contexts of dietary uptake, foetal development, and neurodegenerative disorders[468–470]. As humans are unable to synthesise this essential vitamin they are reliant on its acquisition from dietary sources and potentially from the microbiota[468–470]. On a

cellular level, three members of the solute carrier family 52, a dedicated family of transporters encoded by the SLC52A genes, mediate the uptake of riboflavin from the lumen of the gut into the circulation and its subsequent distribution across the body[471–475]. While SLC52A1 and A3 are primarily expressed in the reproductive and intestinal tracts, the A2 isoform is expressed in a variety of tissues, including the spleen, the thymus, and most prominently the brain[472–475]. There, its function appears to be particularly important since mutations in both SLC52A2 and SLC52A3 have been linked to neurological disorders such as Brown-Vialetto-Van Laere syndrome and spinocerebellar ataxia with blindness and deafness (SCABD)[476–481]. Strikingly, many of the symptoms associated with neuropathies caused by mutations in SLC52A2 or SLC52A3 can be alleviated by high-dose oral supplementation of riboflavin[478,479,482–484].

The more widely expressed isoform SLC52A2 was originally predicted to contain 10 transmembrane domains[474] but current analyses annotate 11 putative transmembrane regions (UniProtKB entry #Q9HAB3). Disease-associated mutations have been found in transmembrane domains as well as intra- and extra-cellular loops[474,485] but to date the functional importance of individual protein domains has not been assigned. Riboflavin uptake by this transporter is saturable and independent of extracellular Na^+, Cl^-, and pH[474,475]. At least seven protein-coding transcripts have been reported (Ensembl entry ENSG00000185803, GenBank entry NC_000008.11, Figure 6.1), suggesting that multiple isoforms exist. Consistent with its function SLC52A2 is upregulated at both the transcript and the protein level upon riboflavin deficiency[486].

This chapter reports the experiments performed to test the hypothesis that the cellular riboflavin transporters in general and SLC52A2 in particular are involved in MR1-mediated presentation of soluble, extracellular ligands.

6.2 Chapter specific Material and Methods

Experiments were carried out according to protocols described in General Materials and Methods (Chapter 2) unless stated otherwise in Figure captions or below.

6.2.1 Incubation with lumiflavin

Lumiflavin (Toronto Research Chemicals #L473900) was resuspended in 0.1 M NaOH. 50 000 or 100 000 cells/well were incubated with the indicated concentrations of lumiflavin or the equivalent volume of solvent control (NaOH) for 30 min at 37° C prior to incubation with the indicated concentrations of 5-A-RU+MG or NY-ESO-1 peptide V9 (SLLMWITQV)[487] for 5 h at the same temperature. After pulsing cells were washed and either stained for flow cytometric analysis or co-cultured with 20 000 MAIT cells or the NY-ESO-1 reactive T cell clone 4D8. 4D8 cells and NY-ESO-1 peptide were kindly provided by Ji-Li Chen (RDM, University of Oxford, UK). Neither NaOH nor lumiflavin were toxic to THP-1 cells at the concentrations used (Supplementary Figure 11). Bacteria and bacterial supernatant were prepared as in Chapter 5 and gentamycin added according to the same protocol.

6.2.2 Presentation assay with fixed antigen presenting cells

THP-1.MR1 cells were washed 3 times in HBSS and split into two aliquots. One aliquot was resuspended in 1 ml of 0.05% Glutaraldehyde (Sigma-Aldrich #G3408) in HBSS, the other in 1 ml of HBSS. Cells were fixed at RT for 30 seconds and quenched with 1 ml of sterile filtered 2M Glycine (VWR #101196X) in HBSS for 30-

60 seconds. Both aliquots were washed in HBSS and then twice in full medium before counting and plating 50 000 cells/well. A small aliquot was stained for viability with live/dead stain aqua (invitrogen #L34966) and/or Propidium Iodide (Sigma-Aldrich #P4864). Cells were pre-treated with the indicated concentrations of lumiflavin for 30 min before pulsing with the indicated concentrations of 5-A-RU+MG for 5 h at 37° C. Pulsed cells were washed two times in full medium before co-culture with 20 000 sorted human MAIT cells for 36 h.

6.2.3 Cell culture in deficient media

THP-1.MR1 cells were cultured in RPMI 1640 (Gibco #11875-093), RPMI – folate (Gibco #27016-021), or custom-made RPMI – riboflavin (Gibco #ME16074L1) supplemented with 10% dialysed foetal calf serum (Life Technologies #26400044), 2 mM Glutamine (Sigma-Aldrich #G7513-100ML), 1 mM Sodium Pyruvate (Gibco #11360-039), 1X Non-essential amino acids (Gibco #11140-035), 100 U/ml penicillin + 100 µg/ml streptomycin (Sigma-Aldrich #P0781-100ML), 10 mM HEPES (Gibco #15630-056), and 50 µM β-mercaptoethanol (Gibco #31350-010) for at least 4 days before incubation with lumiflavin and cell surface staining as above.

6.2.4 SLC52A2 knock-down and knock-out

Human THP-1 and C1R cell lines over-expressing MR1 were cultured as described in General Materials and Methods. MISSION® shRNA lentiviral particles encoding for shRNAs targeting SLC52A2 were purchased from Sigma-Aldrich

(#SHCLNV-NM_024531; shRNA3: TRCN0000008274, shRNA4: TRCN0000008272, shRNA5: TRCN0000011421, shRNA7: TRCN0000369172, shRNA9: TRCN0000356989, pLKO.1 puro control shRNA: #SHC002V) and a polyclonal population of transduced cells was selected with 3 µg/ml puromycin (Gibco #A11138-03). For the CRISPR-mediated knock out of SLC52A2, three one-component CRISPR/Cas9 plasmids with a different single guide RNA (sgRNA) target sequence each were designed. Protospacers were identified using the MIT CRISPR Design tool (http://crispr.mit.edu) and their specificity confirmed using the UCSC-genome browser BLAT tool (https://genome.ucsc.edu/cgi-bin/hgBlat). Oligonucleotides were designed to create overhangs compatible with a BbsI restriction site and having at least two Guanines at the 5' end of each sgRNA. Oligonucleotides were annealed, phosphorylated with CIP (NEB #M0290L) and cloned into the pX458 backbone which also encodes GFP (Addgene #48138, kindly provided by Dr. Feng Zhang, Broad Institute of MIT and Harvard, Cambridge, USA). Plasmids were transformed into DH5α bacteria, protospacer sequences verified by sequencing, and purified following the Qiagen Miniprep spin column protocol (QIAGEN, #27106). Efficiency of the guides was confirmed by Surveyor assay[488] in HEK293T cells. HAP1.MR1 clone D9 was transfected and sorted as in Chapter 3 based on GFP expression (Supplementary Figure 14). CRISPR/Cas9 constructs were designed and cloned by Philip Hublitz in the WIMM Genome Engineering Facility. shRNA and sgRNA target sites with respect to the human SLC52A2 coding sequence are shown in Figure 6.1. Full sequences are available in Supplementary Table 1.

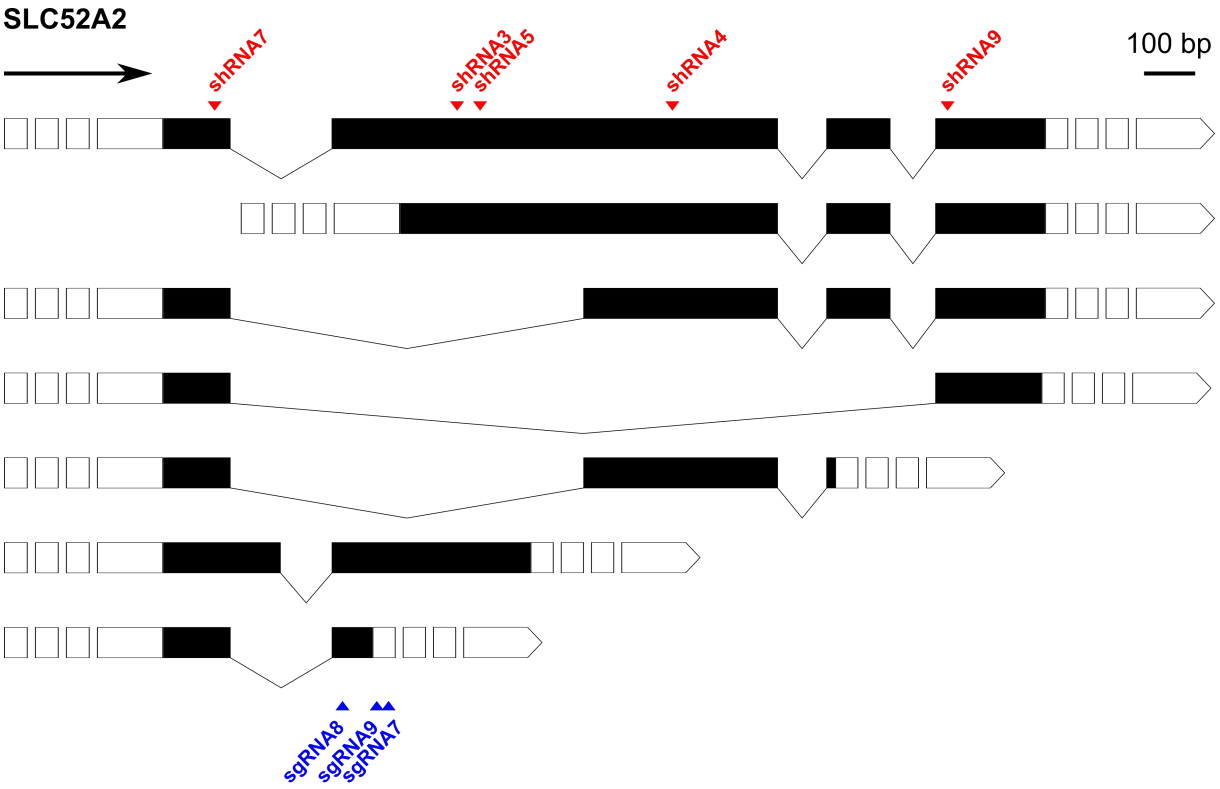


Figure 6.1: Position of shRNA and sgRNA target sites with respect to the exon/intron structure of the coding sequence of human SLC52A2 isoforms. Exons are shown as solid bars, 3' and 5' untranslated regions (UTRs) are shown as dashed empty bars. Since transcript variants vary in length and exon/intron structure of the UTRs, only the consensus coding regions of the reported protein-coding transcript variants are shown. Arrow denotes direction of transcription. Positions of shRNA target sites are indicated by red arrow heads above the graphic. Positions of sgRNA target sites are indicated by blue arrow heads below the graphic. The plot was generated using the Exon-Intron Graphic Maker available at wormweb.org/exonintron based on the exon/intron boundaries in NCBI Reference Sequence NC_000008.11 and the Ensembl transcript list of entry ENSG00000185803. Full shRNA and sgRNA sequences are available in Supplementary Table 1.

6.3 Pre-incubation with lumiflavin reduces MR1-mediated antigen presentation

To investigate the role of the cellular riboflavin transporters in MR1 ligand import, the effect of the riboflavin analogue lumiflavin (LF) on MR1-mediated antigen presentation was tested. Lumiflavin is a structural analogue of riboflavin and has been shown to efficiently inhibit riboflavin uptake by members of the SLC52 transporter family[471,472,475]. Pre-treatment of THP-1 cells over-expressing MR1 (THP-1.MR1) with lumiflavin for 30 min before addition of the riboflavin precursor 5-amino-6-(D-ribitylamino)uracil (5-A-RU) and methylgyoxal (MG) markedly reduced the IFNγ response elicited from sorted human MAIT cells in a concentration dependent manner (Figure 6.2). Pooled data for one particular combination of concentrations from experiments using four different MAIT cell donors all showed the same trend although this did not reach statistical significance when calculated with the Wilcoxon matched-pairs signed rank test. This may be due to the small sample size and, thus, increasing either the number of experiments carried out per donor or the number of donors in order to be able to pool more than five experiments is important to draw statistically supported conclusions. Surface expression of the activation markers CD25 and CD69 was measured in only two experiments and appeared more variably affected by pre-incubation with LF (data not shown). Remarkably, the magnitude of the MAIT cell IFNγ response overall was much lower and the reducing effect of lumiflavin much more pronounced when methylglyoxal was limiting than when it was supplied at 500-fold molar excess to 5-A-RU (Figure 6.2a). This reflects the need for 5-A-RU to undergo condensation with MG to form the potent MAIT-activating MR1 ligand 5-(2-oxopropylideneamino)-6-D-ribitylaminouracil (5-OP-RU)[94,96].

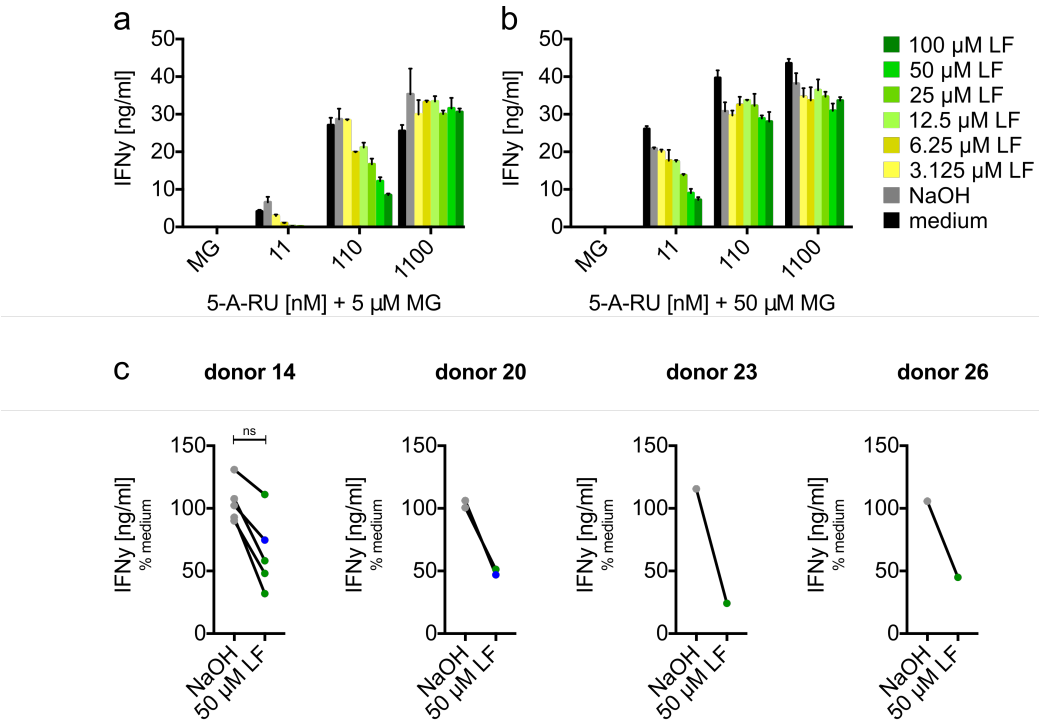


Figure 6.2: Pre-treatment of the antigen presenting cell with lumiflavin reduces the MAIT IFNγ response to exogenous soluble ligand in a dose-dependent manner. THP-1 cells over-expressing MR1 (THP-1.MR1) were pre-treated with the indicated concentrations of lumiflavin (LF, increasing shades of green) or solvent control NaOH for 30 min before pulsing with increasing concentrations of 5-A-RU in the presence of 5 (a) or 50 (b) µM methylglyoxal (MG) for 5 h. Cells were washed in medium before co-culture with human MAIT cells for 36 h. IFNγ concentrations in the supernatant were measured by ELISA and are displayed as median of technical duplicates with range. Data in (c) are pooled from multiple experiments using four different MAIT cell donors including samples from the experiments shown in **Figure 3.2**b, and **Figure 6.4**b. Each symbol represents the median of technical duplicates for one experiment where THP-1.MR1 cells were pulsed with approximately 120 nM 5-A-RU. Data points highlighted in blue are derived form experiments where cells were incubated in I10 rather than R10 because they also included HAP1 samples. Statistical significance was calculated using the Wilcoxon matched-pairs signed rank test where * = $p < 0.05$, ** = $p < 0.01$, *** = $p < 0.001$, **** = $p < 0.0001$, ns = not significant.

To test whether this effect extended to different cell lines the effect of pre-incubation with lumiflavin on MR1-mediated antigen presentation was tested in the MR1 over-expressing HAP1 clone D9 (see Chapter 3) and the MR1 over-expressing human B cell line C1R (C1R.MR1). Indeed, IFNγ production in response to both cell lines was reduced to a similar extent as in the THP-1.MR1 cells when cells were pre-treated with lumiflavin in one initial test each (Figure

6.3). At the highest concentration of lumiflavin (100 µM) and the lowest concentration of 5-A-RU (13 nM) tested, the MAIT cell response was almost completely abolished in C1R.MR1 cells (Figure 6.3b). The maximum amount of IFNγ produced in response to the HAP1.MR1 clone D9 was 10-fold lower than that produced in response to C1R.MR1 cells but was equally abolished at high LF and low ligand concentrations.

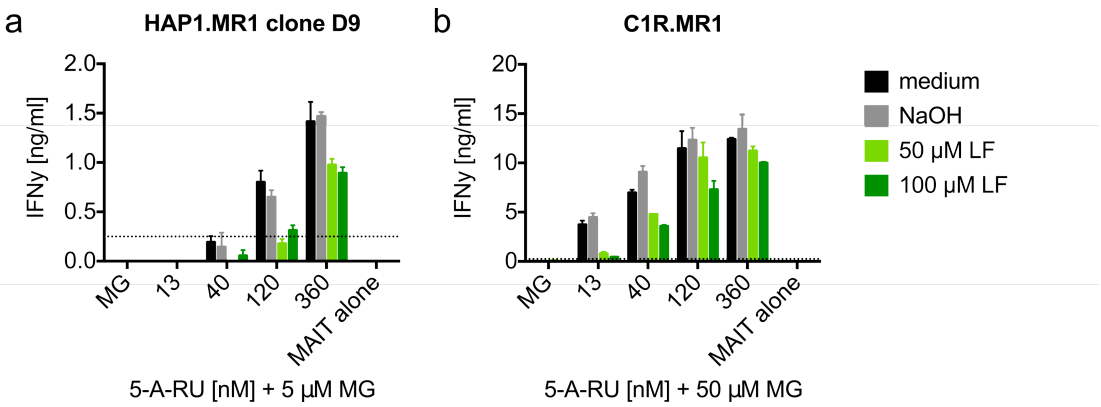


Figure 6.3: Pre-treatment with lumiflavin reduces the MAIT IFNγ response to exogenous soluble ligand in different cell lines. A HAP1 clone over-expressing MR1 (D9, panel a) or C1R.MR1 cells (b) were pre-treated with the indicated concentrations of lumiflavin (LF, increasing shades of green) or solvent control NaOH for 30 min before pulsing with increasing concentrations of 5-A-RU in the presence of 5 (a) or 50 (b) µM methylglyoxal (MG) for 5 h. Cells were washed in medium before co-culture with human MAIT cells for 36 h. IFNγ concentrations in the supernatant were measured by ELISA and are displayed as median of technical duplicates with range. Dashed lines indicate limit of detection.

Next, the effect of lumiflavin on the MAIT cell response to other stimuli was tested to exclude the possibility of a direct effect on MAIT cells and to test whether the observed reduction was specific to MR1-mediated antigen presentation. In a preliminary experiment, neither the presentation of soluble peptide to a cognate T cell clone nor the presentation of bacterial ligands to MAIT cells were impaired when lumiflavin was present during the stimulation (Figure 6.4). However, these results could not be analysed statistically as the experiments were only carried out once and in technical duplicates. To draw substantiated conclusions on the effect

of LF on the activation of peptide-responsive T cells and the MAIT cell response to bacterial antigen more data are needed. Since MAIT cells can also be activated by different combinations of cytokines in a TCR-independent manner[67,315,489] the MAIT cell response to IL-12 and IL-18 in the presence of lumiflavin was also tested. However, the results of two independent experiments did not agree and no definite conclusion could be drawn based on the available data (data not shown).

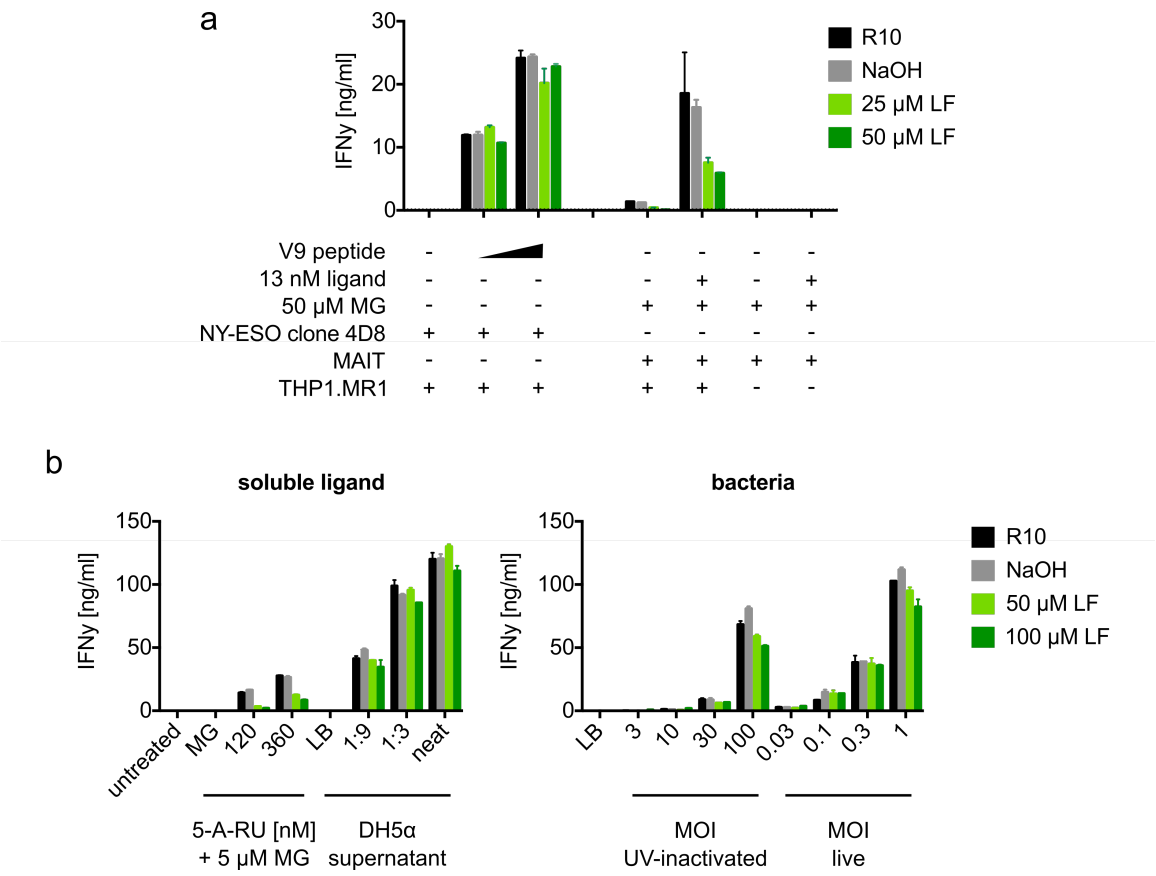


Figure 6.4: Pre-incubation with lumiflavin does not affect the presentation of peptide or bacterial antigen. THP1-MR1 cells were pre-treated with the indicated concentrations of lumiflavin (LF, green) or solvent control NaOH (grey) for 30 min before pulsing with 0.1 or 1 µg/ml of NY-ESO peptide V9 or 13 nM of 5-A-RU + 50 µM of MG (a) or bacterial antigen as indicated (b) for 5 h. Pulsed cells were washed in medium before co-culture with the NY-ESO specific T cell clone 4D8 or sorted human MAIT cells for 36 h. IFNγ concentrations in the supernatant were measured by ELISA and are displayed as median of technical duplicates with range. Dashed lines indicate limit of detection.

In order to test whether active cellular processes were required for lumiflavin to exert its inhibitory function THP-1.MR1 cells were fixed with glutaraldehyde before incubation with lumiflavin and MR1 ligand. Preliminary data suggested that while the IFNγ response to fixed cells was generally 6 to 7-fold smaller than that to unfixed cells, intringuingly, it was further diminished upon pre-incubation with 50 or 100 μM of lumiflavin (Figure 6.5). This would suggest that active cellular import is not required for the effect of lumiflavin and that the analogue could potentially bind to the MR1 antigen binding cleft. However, flow cytometric analysis revealed that less than 20% of the fixed cells stained positive for a live/dead marker after fixation (Supplementary Figure 13a), raising a technical concern in interpreting these experiments. Fixed cells did appear much less metabolically active than unfixed cells based on the colour of the medium after co-culture in both repeat experiments (one shown in Supplementary Figure 13b). In addition, these data were not amenable to statistical analysis due to small sample sizes and, thus, no definitive statements can be made about the requirement of cellular activity for the effect of LF on MR1.

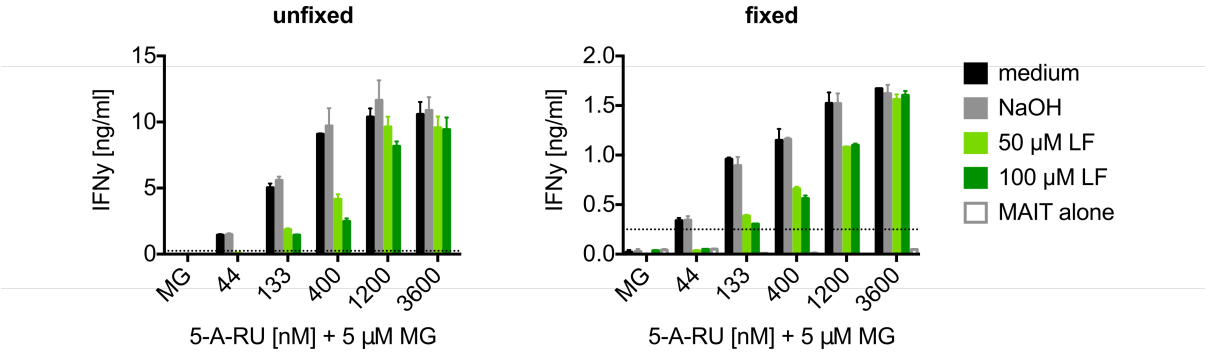


Figure 6.5: The presentation of MR1 ligand by fixed cells is reduced upon pre-incubation with lumiflavin. THP-1.MR1 cells were fixed in 0.05% glutaraldehyde for 30 s, quenched with 2 M glycine, and washed in HBSS before pre-treatment with lumilflavin (LF, green) or solvent control (NaOH, grey) for 30 min and subsequent pulsing with increasing concentrations of 5-A-RU in the presence of 5 µM MG for 5 h. Pulsed cells were washed and co-cultured with sorted human MAIT cells for 36 h. IFNγ concentrations in the supernatant were measured by ELISA and are displayed as median of technical duplicates with range. Dashed lines indicate limit of detection. Data are representative of two experiments with similar results using the same MAIT cell donor.

6.4 Incubation with lumiflavin reduces MR1 surface expression

To pin-point the mechanism by which lumiflavin reduced MR1-mediated antigen presentation, the effect of the analogue on MR1 surface translocation in response to 5-A-RU was investigated by flow cytometry. As in the functional assay, pre-treatment of THP-1.MR1 cells with lumiflavin for 30 min before stimulation with 5-A-RU and MG strikingly diminished MR1 surface translocation in response to ligand (Figure 6.6a), especially at LF concentrations above 50 µM. The effect of 25 and 50 µM LF was more variable with a reduction being evident at the lowest 5-A-RU concentration in one of two later experiments with a smaller titration curve of 5-A-RU and LF (data not shown). However, the αMR1 antiboy used in the experiment that did not show a difference upon LF treatment was coupled to a different fluorophore than the one used routinely and the antibody had not been titrated. Thus, any subtle differences in MR1 surface levels may have been

masked. Usage of a different antibody also meant that the data could not be pooled for statistical analysis and, thus, firm conclusions have to await further results. It should be noted, however, that the general trend of LF reducing MR1 surface expression was confirmed in multiple different experimental settings (see below). Interestingly, MHC class I surface levels were also reduced upon incubation with LF although the variation between technical duplicates was relatively high (Figure 6.6b). When data from multiple experiments were pooled, the effect of LF on MHC class I surface expression did not reach statistical significance, potentially due to a sample size smaller than five. Yet, the same trend could be seen in all three experiments (Figure 6.6c). Lumiflavin was not auto-fluorescent in the channels used except for a signal in the 405-525/50 channel which was used for the live/dead marker (Supplementary Figure 12). Since only cells negative for fluorescence in this channel were gated on, this auto-fluorescence did not affect the downstream analysis.

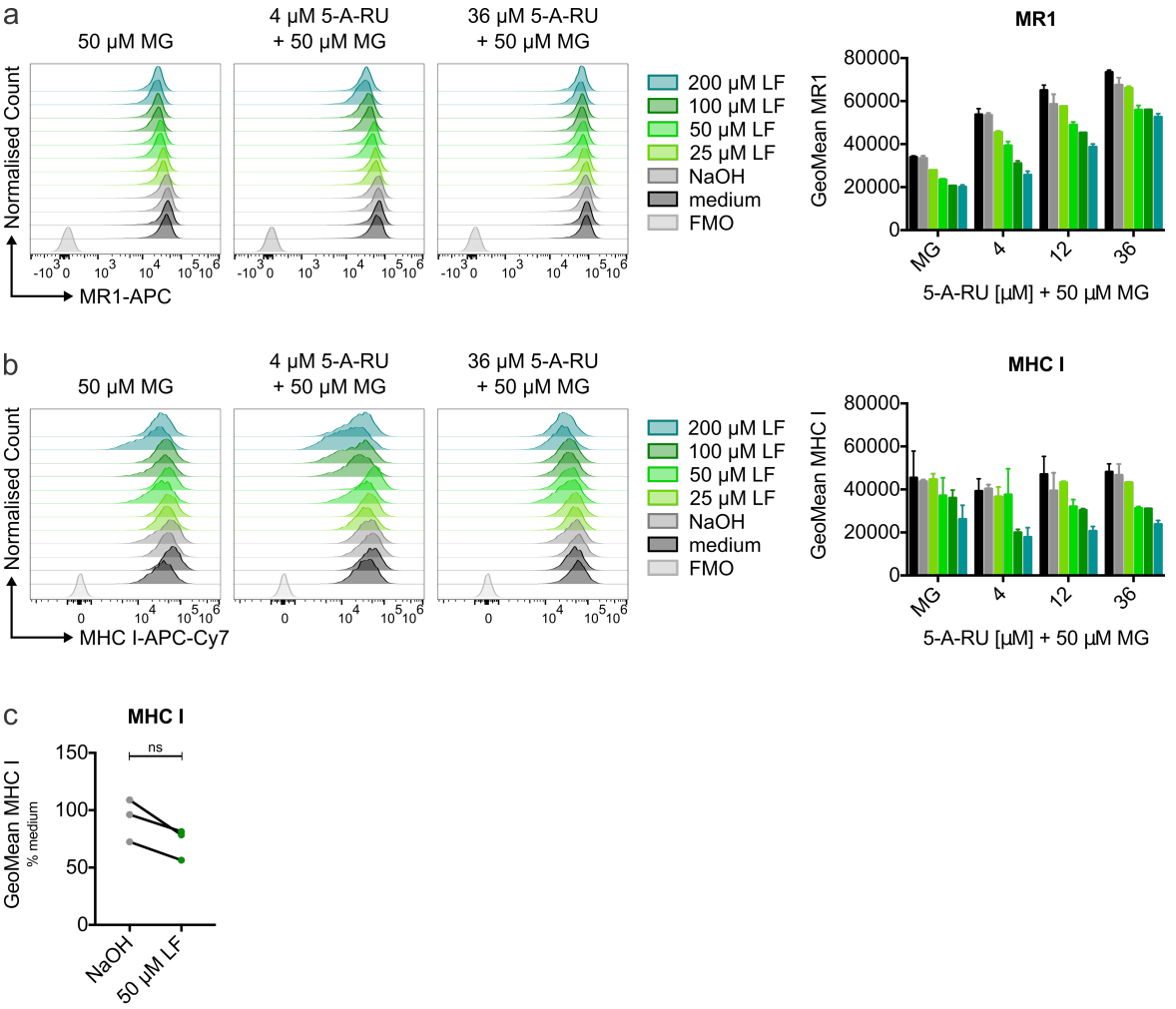


Figure 6.6: Lumiflavin reduces surface translocation of MR1 in response to riboflavin-related ligand. THP-1.MR1 cells were pre-pulsed with 25 – 200 µM lumiflavin (increasing shades of green, LF) for 30 min before incubation with increasing concentrations of 5-A-RU in the presence of LF for 5h in duplicates. MR1 (a) and MHC class I (b) surface levels were measured by flow cytometry. The median geometric means (GeoMean) of the duplicates is shown to the right of the histograms with range. Fluorescence minus one controls are shown in histograms (FMO, light grey). Data are representative of two experiments with similar results. Each symbol in (c) represents the median of technical duplicates of one experiment in which cells were treated with 50 µM of LF for 5 h at baseline (treated with MG only). Statistical significance was calculated using Wilcoxon matched-pairs signed rank test where * = $p < 0.05$, ** = $p < 0.01$, *** = $p < 0.001$, **** = $p < 0.0001$, ns = not significant.

Intriguingly, the most striking reduction of MR1 surface levels was achieved in the absence of ligand (Figure 6.6a). Therefore, the effect of lumiflavin on MR1 surface levels at steady state was further examined in two different cell lines. Remarkably, MR1 surface expression was reduced by more than 50% after incubation with lumiflavin in both cell lines (Figure 6.7). Over the course of the project different

time points and concentrations of lumiflavin were tested and data from four experiments including a sample treated with 100 µM of LF for 5 h were pooled in Figure 6.7c. Although this did not reach statistical significance, all four experiments showed the same trend. These results are consistent with the idea that the analogue might prevent the uptake of riboflavin ubiquitously present in cell culture medium at baseline.

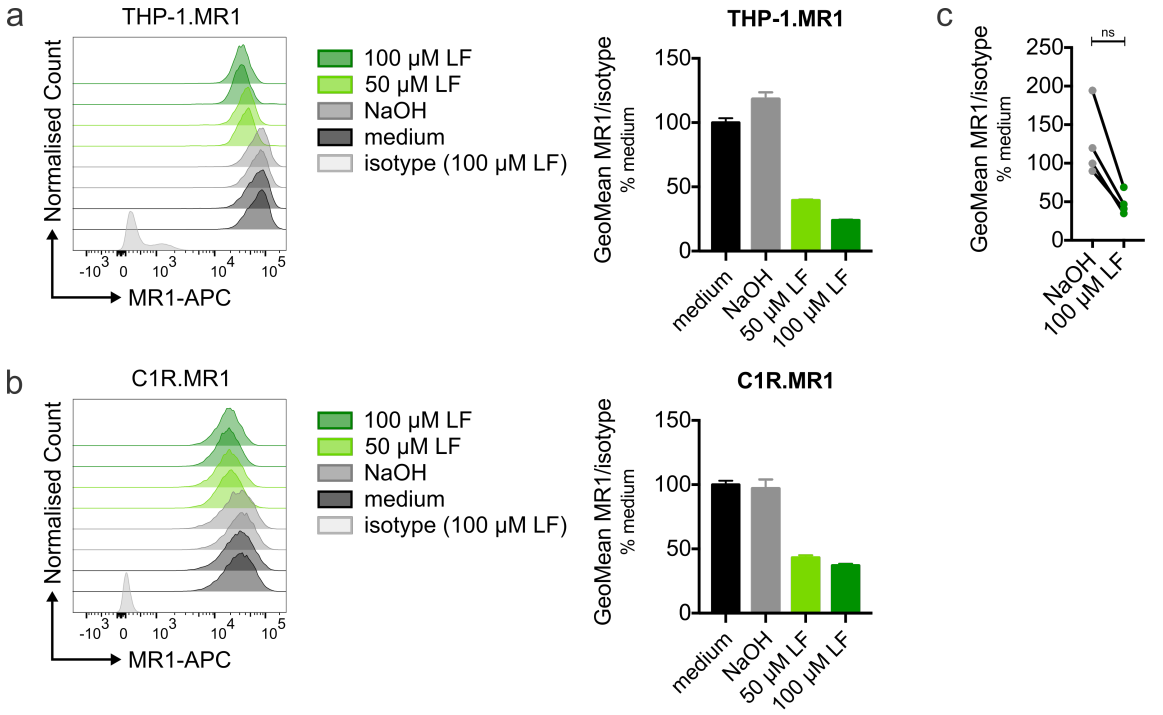


Figure 6.7: Lumiflavin reduces surface levels of MR1 at baseline. THP-1.MR1 (a) and C1R.MR1 (b) cells were pre-pulsed with 50 or 100 µM of lumiflavin (increasing shades of green, LF) o/n in duplicates and MR1 levels were measured by flow cytometry. The geometric mean (GeoMean) relative to the medium control is shown to the right of the histograms as median of the duplicates with range. Cells stained with APC-conjugated isotype control after incubation with 100 µM LF are shown as controls in histograms (isotype, light grey). Data in (c) are pooled from multiple experiments in which cells were treated with 100 µM of LF for 5 h and each symbol represents the median of technical duplicates of one experiment. Statistical significance was calculated using the Wilcoxon matched-pairs signed rank test where * = $p < 0.05$, ** = $p < 0.01$, *** = $p < 0.001$, **** = $p < 0.0001$, ns = not significant.

To test this hypothesis THP-1.MR1 cells were cultured in medium deficient of either riboflavin (RF) or folate and the effect of lumiflavin on MR1 surface levels under these conditions was examined. If indeed lumiflavin prevented the import of

riboflavin from the cell culture medium its effect should be abrogated in culture medium not containing this vitamin. In such a case, MR1 surface levels would be lower in RF-deficient medium than in full medium but not be further reduced in the presence of the analogue. In folate-deficient medium containing riboflavin, however, the decrease of MR1 surface levels upon treatment with lumiflavin should still be detectable. Intriguingly, incubation with lumiflavin in both RF- or folate-deficient medium still reduced the MR1 protein levels at the cell surface (Figure 6.8). As expected, MR1 surface levels were lower in cells cultured in the absence of riboflavin or folate compared to those grown in full medium. Yet, incubation with lumiflavin over night further diminished MR1 cell surface levels in all three types of medium in two independent experiments. (Figure 6.8). This effect also held true upon shorter incubation with LF for 5 h only in a preliminary test (data not shown). Due to the small sample size, statistical analysis of these data was not possible and these findings should, thus, be considered with caution until further results are generated. Of note, the absence of folate had a more profound effect on MR1 surface levels at baseline compared to the absence of riboflavin. This suggests that folates derived from the medium constitute a more important source of MR1 ligands than riboflavin in the medium, possibly due to their higher stability compared to the riboflavin-related compounds.

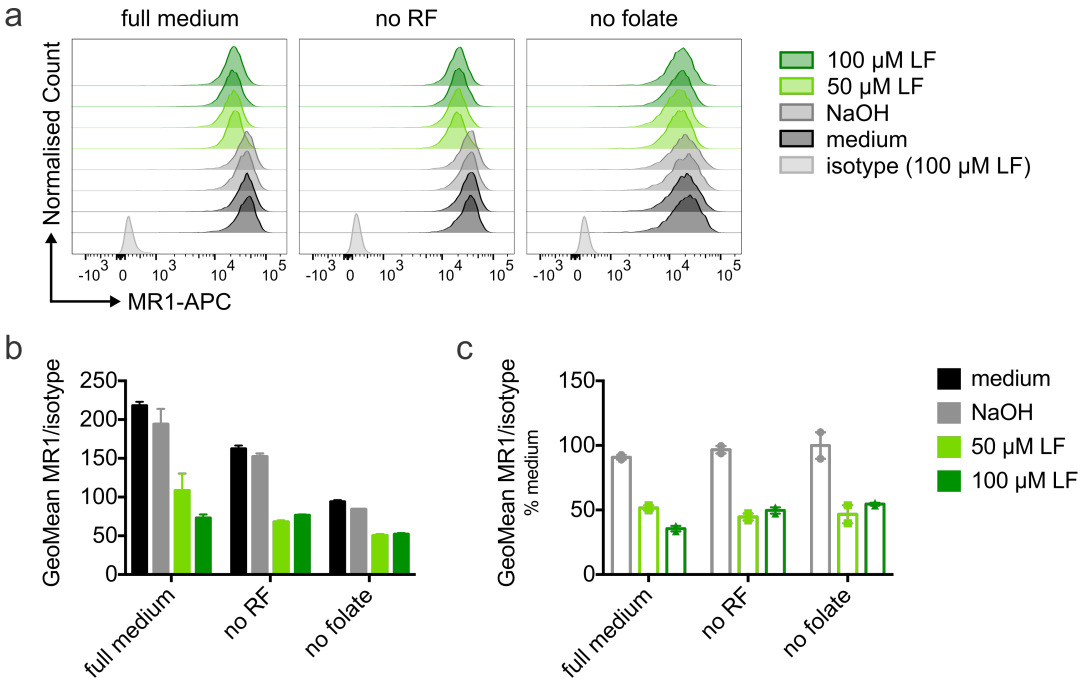


Figure 6.8: The effect of lumiflavin on MR1 surface levels persists in folate- and riboflavin-deficient media. THP-1.MR1 cells were cultured in riboflavin (RF)**-** or folate-deficient medium for at least four days before incubation in lumiflavin (LF) o/n in duplicates and MR1 levels were measured by flow cytometry. The geometric mean (GeoMean) is shown in (b) as median of the duplicates with range. Cells stained with APC-conjugated isotype control after incubation with 100 µM LF are shown as controls in histograms (isotype, light grey). Two o/n experiments are pooled in (c) and each symbol represents the median of technical duplicates of one experiment. Median and range are shown. Data are further supported by one experiment with a 5 h LF incubation yielding similar results.

Next, the ability of lumiflavin to inhibit the surface translocation of MR1 in response to the folate-derived MR1 ligand Acetyl-6-formylpterin (Ac6FP) was tested. Ac6FP is a synthetic derivative of 6-formylpterin, a naturally occurring photo-degradation product of folic acid which was among the first identified MR1 ligands[94,95,292,490]. Importantly, folate has been shown to not inhibit riboflavin uptake via transporters of the SLC52 family[473,475], indicating that it is not a substrate for these transporters. Like for 5-A-RU, however, pre-treatment with lumiflavin reduced the increase of MR1 surface levels in response to low levels of the MR1 stabilising ligand Ac6FP (Figure 6.9a and c). This effect could be titrated out with higher doses of Ac6FP and was also dependent on the concentration of lumiflavin. Lumiflavin did not have an effect on MR1 surface translocation in response to

higher concentrations of Ac6FP (data not shown) and as the data available for the lower Ac6FP concentrations was limited to two experiments, statistical significance could not be calculated. As observed before, MHC class I surface levels also seemed to be affected by lumiflavin incubation (Figure 6.9b and c).

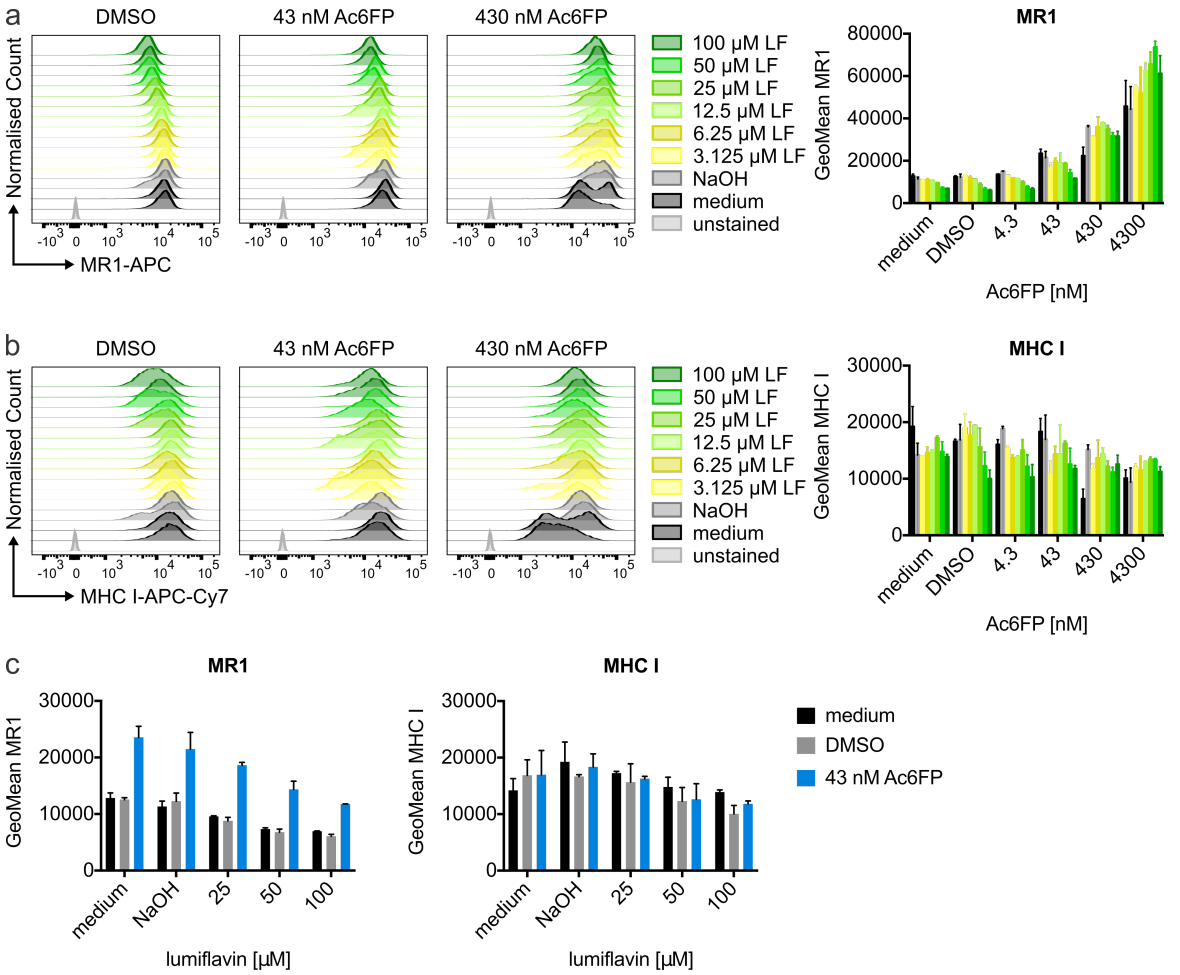


Figure 6.9: Lumiflavin reduces surface translocation of MR1 in response to low doses of folate-derived MR1 ligand. THP-1.MR1 cells were pre-pulsed with 3.125 - 100 µM lumiflavin (increasing shades of green, LF) for 30 min before incubation with increasing concentrations of Ac6FP in the presence of LF for 5h in duplicates. MR1 (a) and MHC class I (b) surface levels were measured by flow cytometry. The median geometric means (GeoMean) of the duplicates are shown to the right of the histograms with range. Cells stained with live/dead stain only are shown as controls in histograms (unstained, light grey). Quantification of surface levels in samples incubated with 43 nM Ac6FP is highlighted in (c). Data are supported by another experiment with similar results.

Together, these results suggest that the effect of lumiflavin on MR1 – and to an extent MHC class I – surface expression is independent of its reported inhibitory effect on cellular riboflavin transporters. Of note, depletion of intracellular riboflavin was not tested in the experimental setup used here and the observed effect on MR1 may be due to inhibition of cellular riboflavin transport or another property of lumiflavin. Thus, the effect of lumiflavin on total MR1 and MHC class I protein levels was assessed. Intracellular staining showed that incubation with lumiflavin for 5 h reduced total MR1 protein levels, though not to the same extent as surface levels (Figure 6.10a, compare to Figure 6.6). While it was not possible to calculate statistical significance for these results, the same trend was observed in two independent experiments. MR1 protein levels determined by Western Blot were also reduced by about 20% in cells treated with lumiflavin compared to untreated cells but only 10% lower than in cells treated with the solvent control NaOH (Figure 6.10b and c) in an initial test. MHC class I protein levels were unaffected in the same lysates (Figure 6.10b and c). Since these results represent one experiment with one technical replicate only they are very preliminary and more experiments are needed to accurately assess the effect of LF on total MR1 and MHC class I protein levels. Similarly preliminary data suggested that MR1 transcript levels were not reduced after incubation with the riboflavin analogue. (Figure 6.10d).

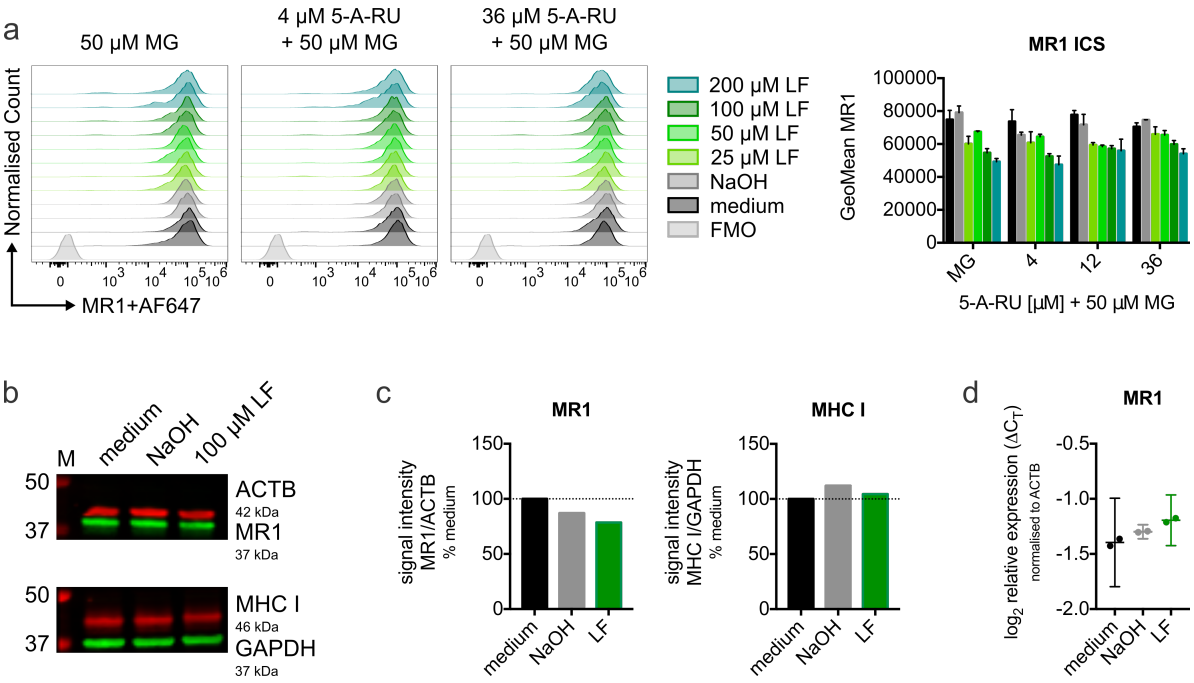


Figure 6.10: Lumiflavin marginally reduces MR1 but not MHC class I protein expression. THP-1.MR1 cells were pre-pulsed with 25 – 200 µM of lumiflavin (increasing shades of green, LF) for 30 min before incubation with increasing concentrations of 5-A-RU in the presence of LF for 5h (a) or incubated with 100 µM LF only for 5 h (b-d). (a) MR1 total protein levels were measured by flow cytometry using a pan-conformation polyclonal antibody + AlexaFluor647-coupled secondary antibody. The median geometric mean (GeoMean) of the duplicates is shown to the right of the histograms with range. Fluorescence minus one control is shown in histograms (FMO, light grey). (b) MR1 and MHC class I total protein levels were determined by Western Blot and quantified with the Odyssey® Near-Infrared imaging system. Quantification relative to the respective loading control is shown in (c). Lysates were run in duplicates and the membrane cut prior to primary antibody incubation. M denotes molecular weight marker and molecular weights of visible marker bands are indicated in kDa to the left of the blots. (d) MR1 transcript levels were measured by qRT-PCR and are shown normalised to ACTB. Each symbol represents the mean of technical duplicates with the 95% confidence interval (d). Dashed lines in (c) indicate 100% for clarity. Flow cytometry data are representative of two experiments with similar results.

6.5 Targeting SLC52A2 with shRNAs does not affect MR1 function

To more directly probe a potential role for the solute carrier family 52 transporters in MR1 ligand import an shRNA-mediated knock-down approach was employed. As expected based on the published expression patterns[471–475], SLC52A2 appeared to be the only family member expressed in the monocytic cell line THP-1 and the B lymphoblast cell line C1R based on an initial qRT-PCR (Figure 6.11a).

Thus, cells were transduced with shRNAs targeting this gene and statistically significant knock-down was achieved at the transcript level (Figure 6.11b) with varying efficiencies for all shRNAs used. Even though the overall ANOVA of the cell lines did not detect statistically significant differences comparing all groups, post-hoc testing with Dunnett's multiple comparisons test revealed highly significant reductions of SLC52A2 transcript levels in cells transduced with all five shRNAs compared to the respective scramble controls. Statistical significance could not be calculated for C1R.MR1 cell lines because the scramble control cell only yielded two reliable C_T values rather than three. However, this reduction at the transcript level did not translate into reduced protein expression as measured in a preliminary Western Blot (Figure 6.11c).

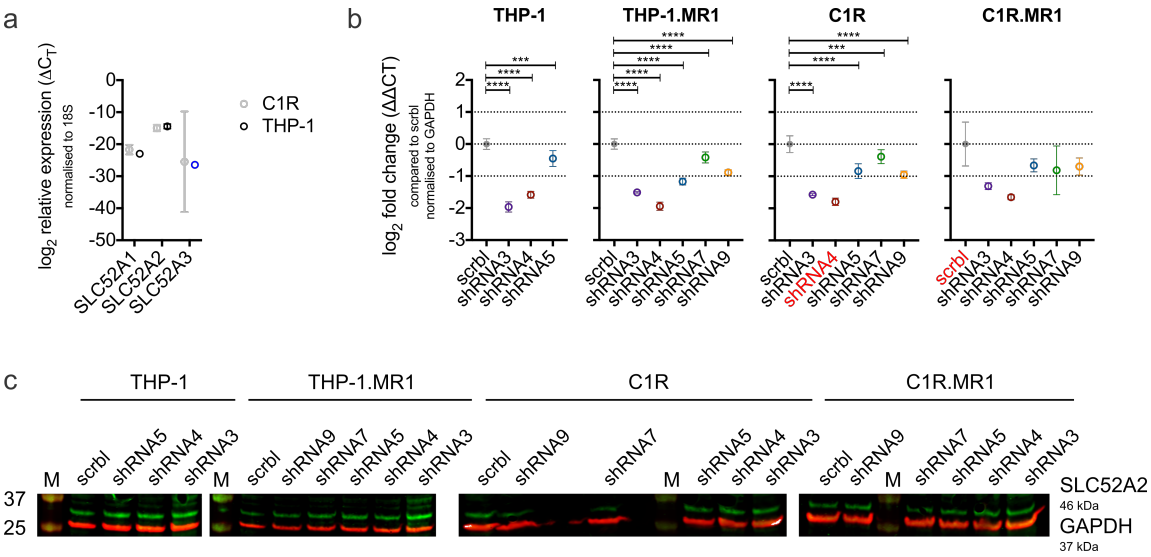


Figure 6.11: Transduction with shRNAs reduces SLC52A2 transcript levels but not protein expression. mRNA expression of the three SLC52A genes was quantified in C1R cells over-expressing CD1d and MR1 (C1R) and THP-1 cells over-expressing MR1 (THP-1) and is represented as mean of technical duplicates with 95% confidence interval (a). Data point in blue is a single measurement only. Data courtesy of Claudia Gonzales-Lopez. After transduction with different shRNAs targeting SLC52A2 transcript (b) and protein (c) levels of this gene were quantified in the indicated cell lines. Each symbol in (b) represents technical triplicates with mean and 95% confidence interval. Statistical significance was calculated using ANOVA with Dunnett's multiple comparisons test where * = $p < 0.05$, ** = $p < 0.01$, *** = $p < 0.001$, **** = $p < 0.0001$, ns = not significant. Dashed lines indicate $\Delta\Delta C_T$ corresponding to 0, 0.5-fold, and 2-fold difference compared to the respective scramble control cell line. Samples highlighted in red were measured in duplicates only and excluded from statistical analysis. Loading control GAPDH is shown in red in (c). M denotes molecular weight marker and molecular weights of visible marker bands are indicated in kDa to the left of the blot.

Nevertheless, MR1 surface levels were determined by flow cytometry in cells transduced with shRNAs 3 and 4 as these resulted in the lowest transcript levels of SLC52A2. An initial test suggested that MR1 surface expression in these cells was slightly lower than in the parent cell line only in THP-1 cells but this was also true for the same cell line transduced with a scramble control shRNA (Figure 6.12). Similarly, MR1-mediated antigen presentation to MAIT cells was not consistently reduced in cells transduced with SLC52A2 shRNA4 although a small reduction was evident in response to cells transduced with shRNA3 at some ligand concentrations but not others in a preliminary experiment (Figure 6.13). Statistical analysis of these results was not possible due small sample size and more

experiments are needed to draw substantiated conclusions on the effect of SLC52A2 KD on MR1-mediated antigen presentation. The preliminary data presented here, however, does not suggest a crucial role of the transporter in this process. Since SLC52A2 protein expression was normal in these cells as measured by Western Blot (Figure 6.11c) it cannot be known with certainty whether this lack of a phenotype is a true negative result or attributable to the lack of knock-down at the protein level.

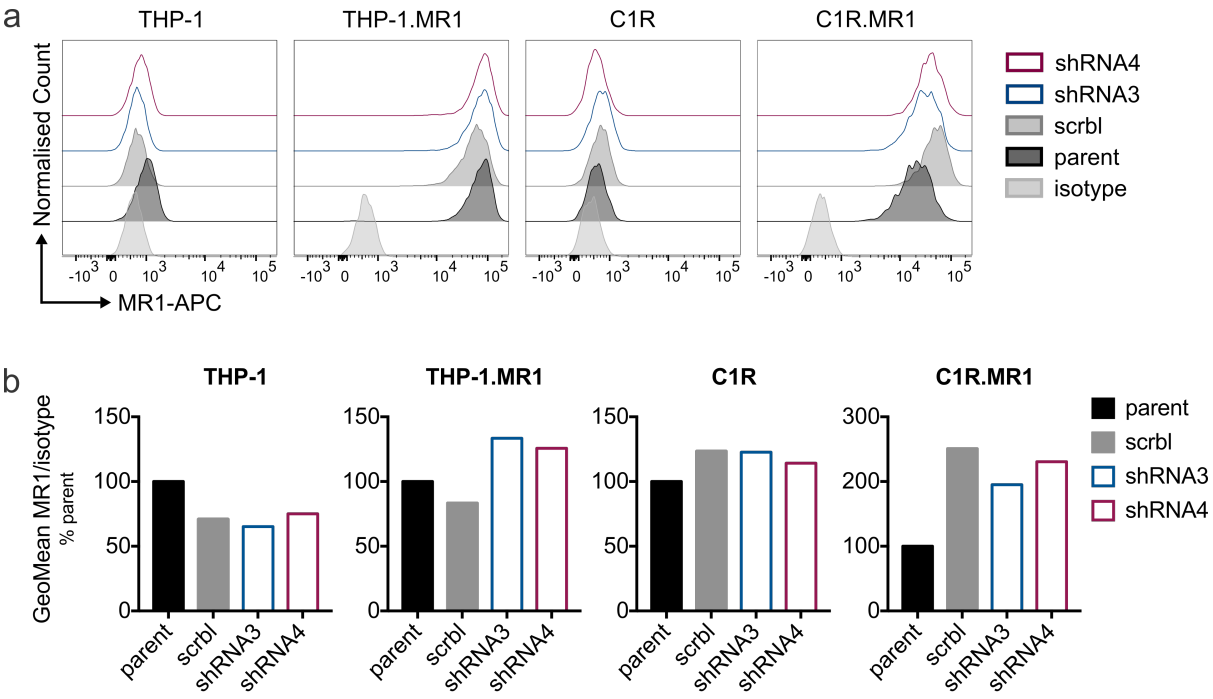


Figure 6.12: Transduction with SLC52A2 shRNAs does not result in reduced MR1 surface levels. The indicated cell lines were stably transduced with two different shRNAs targeting SLC52A2 (shRNA3 and shRNA4, blue and red) or a scramble control shRNA (scrbl, grey) and MR1 surface levels were measured by flow cytometry at steady state. Geometric Means of histograms in (a) are shown in (b) normalised to isotype control and relative to the parent cell line. The respective parent cell lines stained with APC-conjugated isotype control antibody are shown as controls in histograms (isotype, light grey).

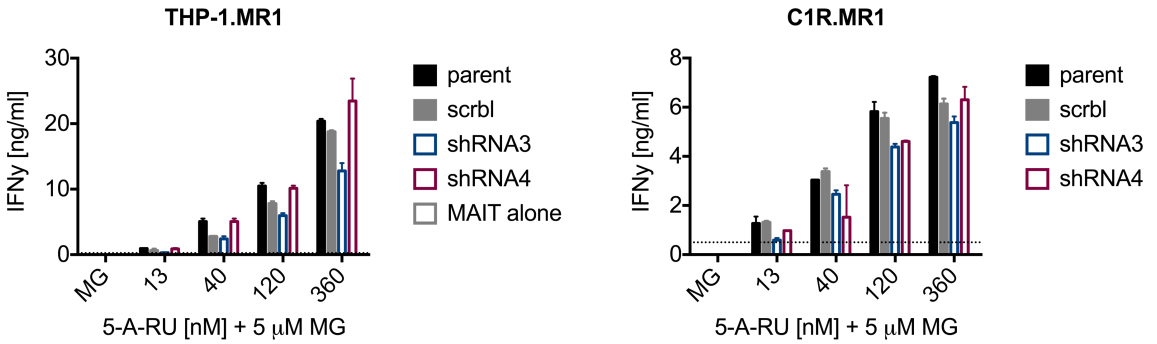


Figure 6.13: Transduction with SLC52A2 shRNAs does not result in reduced MR1 antigen presentation. The indicated cell lines were stably transduced with two different shRNAs targeting SLC52A2 (shRNA3 and shRNA4, blue and red) or a scramble control shRNA (scrbl, grey) and pulsed with increasing concentrations of 5-A-RU in the presence of 5 µM MG o/n before co-culture with sorted human MAIT cells for 36 h. IFNγ concentrations in the supernatant were measured by ELISA and are displayed as median of technical duplicates with range.

To better investigate the role of SLC52A2 a clean knock out clone deficient for this gene would be a useful tool. Therefore, the MR1 over-expressing, near-haploid HAP1 clone D9 was co-transfected with three plasmids encoding for the Cas9 nuclease and three distinct single guide RNAs (sgRNAs) targeting SLC52A2. Transfected cells were single cell sorted based on GFP expression and clones were tested for expression of the transporter by Western Blot. Of the 11 clones tested none were KO for SLC52A2 (Figure 6.14) and the bulk sorted GFP^+ population did not have reduced SLC52A2 protein levels either (data not shown). This result was confirmed with a different antibody as well (data not shown).

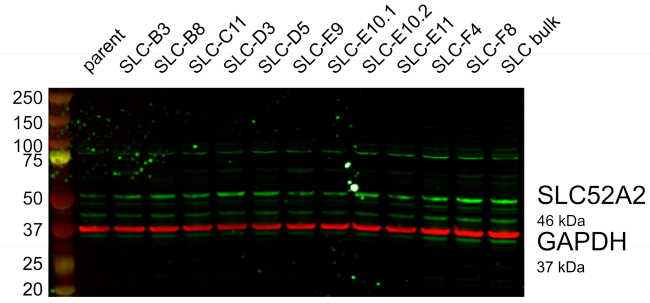


Figure 6.14: Co-transfection of three different sgRNAs targeting SLC52A2 does not yield any knock-out clones. Gene-edited HAP1.MR1 D9 clones were analysed by Western Blot. Names of the individual clones are shown above the respective lane, parent denotes parent clone D9. M denotes molecular weight marker and molecular weights are given in kDa to the left of the blot. Membranes were incubated with antibodies against GAPDH and SLC52A2 together and developed with the LI-COR® two-colour system.

6.6 Discussion

The data presented in this chapter establish an inhibitory effect of the riboflavin analogue lumiflavin on MR1-mediated presentation of the antigenic, soluble, extracellular ligand 5-OP-RU to sorted human MAIT cells *in vitro*. Preliminary data suggested that this effect was specific to the presentation of purified exogenous MR1 ligand and did not extend to MHC class I-mediated peptide presentation or the presentation of MR1 ligand associated with intact bacteria. However, more experiments are needed to substantiate this conclusion. Interestingly, bacterial supernatant which contains soluble MR1 ligands capable of activating MAIT cells[95,96,276] was presented equally well in the presence or absence of high concentrations of lumiflavin in an initial test. This is most likely attributable to the presence of TLR ligands in the bacterial supernatant which have previously been shown to potentiate the MAIT stimulatory capacity of THP-1.MR1 cells by transiently upregulating MR1 surface expression[258,276]. In addition, TLR stimulation would have activated the monocytic antigen presenting cell leading to the expression of co-stimulatory molecules and cytokines capable of triggering MR1-independent stimulation of the MAIT cells[67,276,491,492]. Cytokine-mediated MAIT cell activation is particularly relevant in longer co-culture experiments such as the ones presented here[276] and would likely not have been triggered in the experiments with purified MR1-ligand. Thus, the effect of lumiflavin may be masked by the cytokine-mediated MAIT cell activation in the presentation assays using bacterial stimuli. This hypothesis could be tested by measuring the concentrations of IL-12 and IL-18 in the co-culture supernatants and by including α-IL-12 and α-IL-18 blocking antibodies in the antigen presentation assay. Alternatively, the mechanism of uptake for soluble, exogenous ligand may differ from that of bacterially-derived

ligand as has been postulated before[258,262,276] and the effect of lumiflavin may be specific to the presentation pathway of sterile, soluble, exogenous ligand.

Probing the mechanism by which lumiflavin specifically reduced the MAIT cell IFNγ response to 5-OP-RU indicated that MR1 surface expression, and to an extent also total protein expression, was reduced upon treatment with the riboflavin analogue. Intriguingly, MHC class I surface levels were also lower after treatment with lumiflavin, yet peptide presentation was not affected in an initial test. This suggests that peptide presentation may not be as limited by the number of MHC class I molecules available at the cell surface as MR1-mediated presentation of soluble ligand. In fact, it has recently been shown that MR1 surface levels are a limiting factor for the presentation of exogenous ligand but not bacterially derived ligands to MAIT cells[276]. Alternatively, MHC I:peptide complexes may be more stable at the cell surface and hence a smaller number of molecules suffices to induce a full response. In general, the surface phenotype induced by lumiflavin was less specific to the MR1-5-OP-RU axis than the presentation phenotype. Apart from affecting both MR1 and MHC class I expression levels at baseline, lumiflavin also inhibited the upregulation of surface MR1 levels in response to low levels of Ac6FP, a folate-derivative that would not be hypothesised to be a substrate of the cellular riboflavin transporters. Furthermore, preliminary data suggested that the reducing effect of lumiflavin on MR1 surface levels persisted not only in the absence of 5-OP-RU but also in the absence of riboflavin in the cell culture medium. This is consistent with a model in which the reduced MR1-mediated antigen presentation capacity in the presence of

lumiflavin is independent of the specific inhibition of ligand import via the cellular riboflavin transporters.

Further support for this model is provided by a publically available doctoral thesis characterising the cellular response to lumiflavin-induced riboflavin deficiency[493]. In that study global tyrosine phosphorylation was found to be reduced in an intestinal cell line after 3 – 6 h of incubation with 40 µM LF, conditions comparable to those used here. Importantly, this alteration in the cellular phosphorylation state occurred prior to detectable biochemical changes in intracellular riboflavin concentration indicating that it, too, is independent of the inhibition of cellular riboflavin transporters. Profiling of the phosphoproteome after lumiflavin treatment revealed a small number of proteins differentially phosphorylated after 6 h of incubation with lumiflavin and a larger set of proteins with altered phosphorylation status after 24 h of incubation with the analogue. Interestingly, while the overall number of phosphorylated proteins was reduced upon treatment with lumiflavin, the proteins that were differentially phosphorylated tended to be hyperphosphorylated. Of note, the larger subset of differentially phosphorylated proteins at the later time point included proteins related to protein folding and antigen presentation such as calreticulin, protein disulfide isomerases, Heat shock protein HSP 90α, and a subunit of the proteasome[493]. While calreticulin is required for MHC class I assembly and loading[133,374,494] it is dispensable for MR1 antigen presentation[281]. Similarly, proteasomal degradation of cellular proteins is needed for the generation of antigens for MHC class I[117,495] but not for MR1[264,267,281]. Therefore, neither of these are likely to account for the MR1 presentation phenotype. Two of the proteins identified in the larger set were also hits in the

gene trap screen described in Chapter 3: NONO and EIF4B. NONO is a multi-functional nuclear protein[496] and EIFB4 is part of a protein complex that mediates the delivery of mRNA to the ribosome for translation[497]. Thus, neither of these is likely to specifically affect the surface expression of antigen presenting molecules either.

Instead, the proteins hyperphosphorylated after 6 h mostly comprised modulators of mRNA processing and the splice factors SRSF1 and SRSF9 were further validated by Western Blot[493]. This shorter time point is more relevant to the experimental system described in this chapter and altered stability of transcripts may account for the reduced intracellular protein levels of both MR1 and MHC class I (Figure 6.10). However, such a model is not consistent with the observation that high concentrations of MR1 ligands could titrate out the effect of lumiflavin (Figure 6.6 and Figure 6.9.) which suggests that the maximum MR1 surface expression level of MR1 is unaltered upon treatment with the riboflavin analogue. Consistent with this, MR1 transcript levels were not altered after incubation with lumiflavin. However, total intracellular MR1 protein levels appeared to be slightly lower after 5 h of lumiflavin treatment when measured by flow cytometry or Western Blot. Thus, lumiflavin may have a post-translational effect on MR1 protein stability or folding. This could be mediated by direct or indirect mechanisms including the modulation of the phosphorylation state of proteins needed for MR1 egress from the ER. To further delineate this effect the intracellular distribution of MR1 in the presence of lumiflavin could be investigated by confocal microscopy and biochemical means such as endoglycosidase H (EndoH) digestion.

Alternatively, it would be conceivable that lumiflavin could bind to MR1 directly, given its structural similarity to the pterin MR1 ligands. If this was the case, however, binding of this ligand would have to induce MR1 folding in a conformation that is not 26.5-reactive as staining with this antibody clone was reduced after incubation with lumiflavin. It would also be hypothesised to be unable to activate MAIT cells as it lacks the ribityl moiety that interact with the MAIT cell TCR[294]. To formally test this hypothesis an MR1 plate-bound assay or re-folding of recombinant MR1 in the presence of lumiflavin could be performed. If binding of lumiflavin allowed MR1 to associate with β_2m that could explain the slight reduction of MHC class I surface expression in the presence of the riboflavin analogue. Of note, riboflavin itself is unable to induce MR1 surface translocation or MAIT cell activation and hence unlikely to be an MR1 ligand[95].

Lack of RF has recently been shown to have down-stream effects on mitochondrial health which are thought to mediate the neuropathological effects of mutations in the RF transporters[485]. This is consistent with a reduction of intracellular ATP and increased production of reactive oxygen species in response to lumiflavin treatment reported in the doctoral thesis cited above[493,498]. Thus, it would be informative to investigate mitochondrial function in the LF-treated cells to investigate whether the MR1 phenotype may be due to abnormal mitochondrial activity and metabolic function.

Since the effect of lumiflavin appears to be uncoupled from its inhibition of the cellular riboflavin transporters and interfering with SLC52A2 expression did not generate cell lines deficient of this protein with the methods used here it is still

unclear whether the transporters of the SLC52 family play a role in MR1 ligand import. While the unspecific effect of lumiflavin does not rule out such a role it does not support it either. In order to formally address this question establishing a KO cell line for SLC52A2 is essential. shRNA-mediated knock-down with different shRNAs or CRISPR-mediated knock-out with sgRNAs targeting different regions should enable the generation of such a cell line. To ensure that all transcript variants are targeted multiple guides complementary to different loci within the coding region should be co-transfected. Alternatively, guides could be designed to cut upstream and downstream of the coding region to excise the entire open reading frame and cloned into vectors encoding different fluorescent proteins. In this way, double positive transfectants could be sorted to enrich for cells in which both sgRNAs are expressed and excision of the coding sequence is more likely.

On an organismal level, it would be interesting to determine the frequency and phenotype of MAIT cells in patients with neuropathies caused by SLC52A2 or SLC52A3 mutations to establish whether there is a correlation between the function of these transporters and the availability of MAIT cell ligand. However, it seems unlikely that loss of these genes would globally affect MAIT cell frequency and function since the most potent antigenic metabolites that constitute MR1 ligands are structurally different from riboflavin[94]. They share the ribityl moiety with the vitamin but they are unstable pyrimidine compounds and spontaneously cyclize to form weakly MAIT cell-activating ribityl-lumazines[96,499]. Riboflavin, on the other hand, adopts a tricyclic isoalloxazine ring structure. Of note, passive diffusion of riboflavin across intestinal cell monolayers has been described at high concentrations of the vitamin despite it featuring a hydrophilic ribityl group[500,501].

Therefore, further investigations to clarify the potential diffusion of soluble MR1 ligands are warranted as local concentrations of these antigenic metabolites may be very high in bacteria-containing endosomal compartments. In addition, it might be informative to investigate the role of cellular pyrimidine transporters in MR1 ligand import based on the structural similarity. One candidate could be the Pyrimidinergic Receptor P2Y6 which was differentially downregulated in the JAWSII Sec22b KD cells and a shared hit with the RNASeq analysis performed by Wu *et al*.[203].

On a different note, the physiological relevance of MR1-mediated presentation of extracellular soluble ligand remains to be formally established. While MAIT cells became activated and expanded in response to intranasal co-administration of soluble ligand and TLR agonists in the absence of intact bacteria in a mouse model[320], it is not clear whether this is the predominant source of MR1 ligand in the context of infection. A recent report by Harriff *et al*. showed that the trafficking molecules required for presentation of soluble, exogenous antigen by MR1 differ from those required for the presentation of MR1 ligands derived from the intracellular pathogen *Mycobacterium tuberculosis*[262]. This is in agreement with other studies showing that inhibition of phagocytosis or endosomal acidification differentially affected the presentation of intact bacteria and soluble ligand[258,276]. Furthermore, Harriff *et al.* found that a GFP-tagged MR1 fusion protein co-localised with markers of late endosome. In line with this, knock-down of two endosomal trafficking molecules in the antigen presenting cells significantly reduced the MAIT cell response to *M. tuberculosis*[262]. Based on these results, the authors of that report put forward a model in which MR1 encounters antigenic

metabolites in an endosomal compartment harbouring the microbe, obviating the need for the ligand to cross any membranes[262]. While this model does not account for the observation that soluble, extracellular ligands can encounter MR1 in an unfolded, ligand-receptive state in the ER *in vitro*[260] it may well represent a more physiologically relevant scenario in the context of bacterial infection. As of now, the relative contributions of soluble *versus* bacterially derived ligands to MAIT cell activation *in vivo* remain a subject of investigation.

7 Concluding Remarks

The data presented in this thesis contribute to the growing body of knowledge concerning the intracellular trafficking of the MHC class I-related protein 1 (MR1). In particular, the following results offer new insights into the biology of MR1-mediated antigen presentation and open up exciting new avenues of research:

1. Gene-trap technology enables the discovery of regulators of MR1 surface expression.

128 putative regulators of MR1 surface expression in the presence of the MR1-stabilising ligand Ac6FP were identified using a gene-trap screen in the near-haploid human cell line HAP. The hits comprised proteins involved in a wide variety of cellular processes including intracellular transport, metabolism, and post-translational processing. While one of these hits was followed up in the work presented here, much scope remains for the characterisation of the remaining candidate proteins. Furthermore, these results demonstrate that the gene-trap method in HAP1 cells can be adapted to the investigation of surface proteins including those involved in antigen presentation and opens up further opportunities for research. In particular, it would be extremely informative to repeat the screen in the presence of bacteria, or indeed in the absence of any ligand, to further delineate the specific pathways involved in the presentation of microbe-associated compared to soluble MR1 ligands.

2. The ER transporter ATP13A1 affects MR1-mediated antigen presentation by modulating the size of the intracellular pool of MR1.

CRISPR/Cas9-mediated knock-out of ATP13A1 in a HAP1 clone over-expressing MR1 lead to a dramatic reduction of total MR1 protein levels and a simultaneous decrease in MR1 surface levels and antigen presentation capacity. Preliminary findings suggest that the mechanism underlying this effect may be partially dependent on the intracellular concentrations of the metal cofactor manganese and does not appear to involve differential glycosylation, protein stability, or general ER stress. Further investigations into the transcriptional and translational effects of ATP13A1 deficiency as well as the extent to which these effects can be generalised to other cell lines are needed to confirm these initial data and determine the molecular mechanism responsible for the MR1 phenotype.

3. A shRNA targeting the SNARE Sec22b also targets a modulator of MR1 surface expression.

Surface expression of folded MR1 was reduced in a murine dendritic cell line expressing an shRNA that targets the SNARE Sec22b but this phenotype could not be rescued by restoration of Sec22b expression. Subsequent RNASeq analysis identified more than 500 genes differentially expressed in cells transduced with the shRNA, yielding a list of potential regulators of MR1 surface expression in murine cells. Despite technical limitations, this data set has the potential to form the basis for further investigations focussing on the most prominent hits and their potential role in MR1-mediated antigen presentation.

4. The riboflavin analogue lumiflavin affects MR1-mediated antigen presentation by a mechanism unrelated to the inhibition of cellular riboflavin transporters.

Pre-treatment with lumiflavin reduced the presentation of riboflavin-related MR1 ligands to MAIT cells. Preliminary data suggest that treatment with the riboflavin analogue also decreases MR1 surface levels in the presence or absence of MR1-stabilising ligands and that this persists even when riboflavin is absent from the culture medium. This is consistent with a model in which the effect of lumiflavin on MR1 is independent from its inhibitory effect on cellular riboflavin transport. MR1 protein levels appeared to be reduced upon lumiflavin treatment but transcript levels were unaffected in initial experiments, suggesting that lumiflavin exerts an effect on MR1 protein stability, possibly by limiting the pool of endogenous ligands. Further experiments are needed to confirm these observations and to determine whether this effect is direct or indirect. In particular, it would be interesting to establish whether lumiflavin can bind to MR1 itself.

In conclusion, this work provides a foundation for further research into the molecular and cellular mechanisms underlying the presentation of small molecule metabolites in the context of MR1. It adds to the current understanding of this non-classical antigen presentation pathway and complements on-going research efforts exploring the therapeutic potential of this unique branch of the immune system.

8
Bibliography

1. Murphy, K. & Weaver, C. *Janeway's Immunobiology*. (Garland Science, 2016).
2. Janeway, C. A. Approaching the asymptote? Evolution and revolution in immunology. *Cold Spring Harb. Symp. Quant. Biol.* **54 Pt 1**, 1–13 (1989).
3. Patel, S. Danger-Associated Molecular Patterns (DAMPs): the Derivatives and Triggers of Inflammation. *Curr. Allergy Asthma Rep.* **18**, 63 (2018).
4. Takeuchi, O. & Akira, S. Pattern recognition receptors and inflammation. *Cell* **140**, 805–820 (2010).
5. Arango Duque, G. & Descoteaux, A. Macrophage Cytokines: Involvement in Immunity and Infectious Diseases. *Front. Immunol.* **5**, (2014).
6. Sherwood, E. R. & Toliver-Kinsky, T. Mechanisms of the inflammatory response. *Best Pract. Res. Clin. Anaesthesiol.* **18**, 385–405 (2004).
7. Flannagan, R. S., Heit, B. & Heinrichs, D. E. Antimicrobial Mechanisms of Macrophages and the Immune Evasion Strategies of Staphylococcus aureus. *Pathogens* **4**, 826–868 (2015).
8. Nikolich-Zugich, J., Slifka, M. K. & Messaoudi, I. The many important facets of T-cell repertoire diversity. *Nat. Rev. Immunol.* **4**, 123–132 (2004).
9. Neuberger, M. S. Antibody diversification by somatic mutation: from Burnet onwards. *Immunol. Cell Biol.* **86**, 124–132 (2008).
10. Burnet, F. M. A modification of Jerne's theory of antibody production using the concept of clonal selection. *CA. Cancer J. Clin.* **26**, 119–121 (1976).
11. Hozumi, N. & Tonegawa, S. Evidence for somatic rearrangement of immunoglobulin genes coding for variable and constant regions. *Proc. Natl. Acad. Sci. U. S. A.* **73**, 3628–3632 (1976).
12. Singh, N. K. *et al.* Emerging Concepts in TCR Specificity: Rationalizing and (Maybe) Predicting Outcomes. *J. Immunol. Baltim. Md 1950* **199**, 2203–2213 (2017).
13. Lau, C. M. & Sun, J. C. The widening spectrum of immunological memory. *Curr. Opin. Immunol.* **54**, 42–49 (2018).
14. Iwasaki, A. & Medzhitov, R. Control of adaptive immunity by the innate immune system. *Nat. Immunol.* **16**, 343–353 (2015).
15. Richmond, J. M. & Harris, J. E. Immunology and Skin in Health and Disease. *Cold Spring Harb. Perspect. Med.* **4**, a015339 (2014).
16. Bischoff, S. C. *et al.* Intestinal permeability--a new target for disease prevention and therapy. *BMC Gastroenterol.* **14**, 189 (2014).
17. Hertz, C. J. *et al.* Activation of Toll-like receptor 2 on human tracheobronchial epithelial cells induces the antimicrobial peptide human beta defensin-2. *J. Immunol. Baltim. Md 1950* **171**, 6820–6826 (2003).
18. Selsted, M. E. & Ouellette, A. J. Mammalian defensins in the antimicrobial immune response. *Nat. Immunol.* **6**, 551–557 (2005).
19. Knowles, M. R. & Boucher, R. C. Mucus clearance as a primary innate defense mechanism for mammalian airways. *J. Clin. Invest.* **109**, 571–577 (2002).
20. McGuckin, M. A., Lindén, S. K., Sutton, P. & Florin, T. H. Mucin dynamics and enteric pathogens. *Nat. Rev. Microbiol.* **9**, 265–278 (2011).
21. Dunkelberger, J. R. & Song, W.-C. Complement and its role in innate and adaptive immune responses. *Cell Res.* **20**, 34–50 (2010).
22. Dustin, M. L. Complement Receptors in Myeloid Cell Adhesion and Phagocytosis. *Microbiol. Spectr.* **4**, (2016).
23. Fearon, D. T. Identification of the membrane glycoprotein that is the C3b receptor of the human erythrocyte, polymorphonuclear leukocyte, B lymphocyte, and monocyte. *J. Exp. Med.* **152**, 20–30 (1980).
24. Fällman, M., Andersson, R. & Andersson, T. Signaling properties of CR3 (CD11b/CD18) and CR1 (CD35) in relation to phagocytosis of complement-opsonized particles. *J. Immunol. Baltim. Md 1950* **151**, 330–338 (1993).

25. Morgan, B. P., Boyd, C. & Bubeck, D. Molecular cell biology of complement membrane attack. *Semin. Cell Dev. Biol.* **72**, 124–132 (2017).
26. Mosser, D. M. & Edwards, J. P. Exploring the full spectrum of macrophage activation. *Nat. Rev. Immunol.* **8**, 958–969 (2008).
27. Wynn, T. A., Chawla, A. & Pollard, J. W. Macrophage biology in development, homeostasis and disease. *Nature* **496**, 445–455 (2013).
28. Sun, L., Wu, J., Du, F., Chen, X. & Chen, Z. J. Cyclic GMP-AMP Synthase Is a Cytosolic DNA Sensor That Activates the Type I Interferon Pathway. *Science* **339**, 786–791 (2013).
29. Liu, P. T. *et al.* Toll-Like Receptor Triggering of a Vitamin D-Mediated Human Antimicrobial Response. *Science* **311**, 1770–1773 (2006).
30. Geering, B., Stoeckle, C., Conus, S. & Simon, H.-U. Living and dying for inflammation: neutrophils, eosinophils, basophils. *Trends Immunol.* **34**, 398–409 (2013).
31. Segal, A. W. How neutrophils kill microbes. *Annu. Rev. Immunol.* **23**, 197–223 (2004).
32. Thomas, C. J. & Schroder, K. Pattern recognition receptor function in neutrophils. *Trends Immunol.* **34**, 317–328 (2013).
33. Borregaard, N., Sørensen, O. E. & Theilgaard-Mönch, K. Neutrophil granules: a library of innate immunity proteins. *Trends Immunol.* **28**, 340–345 (2007).
34. Mukai, K., Tsai, M., Starkl, P., Marichal, T. & Galli, S. J. IgE and mast cells in host defense against parasites and venoms. *Semin. Immunopathol.* **38**, 581–603 (2016).
35. Mjösberg, J. & Spits, H. Human innate lymphoid cells. *J. Allergy Clin. Immunol.* **138**, 1265–1276 (2016).
36. Guermonprez, P., Valladeau, J., Zitvogel, L., Théry, C. & Amigorena, S. Antigen presentation and T cell stimulation by dendritic cells. *Annu. Rev. Immunol.* **20**, 621–667 (2002).
37. Johnson, L. A. & Jackson, D. G. Control of dendritic cell trafficking in lymphatics by chemokines. *Angiogenesis* **17**, 335–345 (2014).
38. Sallusto, F. *et al.* Rapid and coordinated switch in chemokine receptor expression during dendritic cell maturation. *Eur. J. Immunol.* **28**, 2760–2769 (1998).
39. Cooper, M. D., Peterson, R. D. A. & Good, R. A. Delineation of the Thymic and Bursal Lymphoid Systems in the Chicken. *Nature* **205**, 143–146 (1965).
40. Boehm, T. Design principles of adaptive immune systems. *Nat. Rev. Immunol.* **11**, 307–317 (2011).
41. Schatz, D. G., Oettinger, M. A. & Baltimore, D. The V(D)J recombination activating gene, RAG-1. *Cell* **59**, 1035–1048 (1989).
42. Rossjohn, J. *et al.* T Cell Antigen Receptor Recognition of Antigen-Presenting Molecules. *Annu. Rev. Immunol.* **33**, 169–200 (2015).
43. Lämmermann, T. & Sixt, M. The microanatomy of T-cell responses. *Immunol. Rev.* **221**, 26–43 (2008).
44. von Andrian, U. H. & Mempel, T. R. Homing and cellular traffic in lymph nodes. *Nat. Rev. Immunol.* **3**, 867–878 (2003).
45. Kuka, M. & Iannacone, M. Viral subversion of B cell responses within secondary lymphoid organs. *Nat. Rev. Immunol.* **18**, 255–265 (2018).
46. Wilmore, J. R. & Allman, D. Here, There, and Anywhere? Arguments for and against the Physical Plasma Cell Survival Niche. *J. Immunol.* **199**, 839–845 (2017).
47. Kurosaki, T., Kometani, K. & Ise, W. Memory B cells. *Nat. Rev. Immunol.* **15**, 149–159 (2015).
48. Cui, W. & Kaech, S. M. Generation of effector CD8+ T cells and their conversion to memory T cells. *Immunol. Rev.* **236**, 151–166 (2010).
49. Mueller, S. N., Gebhardt, T., Carbone, F. R. & Heath, W. R. Memory T cell subsets, migration patterns, and tissue residence. *Annu. Rev. Immunol.* **31**, 137–161 (2013).
50. Chess, L. The Birth of Functionally Distinct T Cell Subsets. *J. Immunol.* **176**, 3859–3860 (2006).
51. Meuer, S. C., Schlossman, S. F. & Reinherz, E. L. Clonal analysis of human cytotoxic T lymphocytes: T4+ and T8+ effector T cells recognize products of different major histocompatibility complex regions. *Proc. Natl. Acad. Sci.* **79**, 4395–4399 (1982).
52. Cantor, H. & Boyse, E. A. Functional subclasses of T-lymphocytes bearing different Ly antigens. I. The generation of functionally distinct T-cell subclasses is a differentiative process independent of antigen. *J. Exp. Med.* **141**, 1376–1389 (1975).
53. Neefjes, J., Jongsma, M. L. M., Paul, P. & Bakke, O. Towards a systems understanding of MHC class I and MHC class II antigen presentation. *Nat. Rev. Immunol.* **11**, 823–836 (2011).
54. Harty, J. T., Tvinnereim, A. R. & White, D. W. CD8+ T cell effector mechanisms in resistance to infection. *Annu. Rev. Immunol.* **18**, 275–308 (2000).

55. Raphael, I., Nalawade, S., Eagar, T. N. & Forsthuber, T. G. T cell subsets and their signature cytokines in autoimmune and inflammatory diseases. *Cytokine* **74**, 5–17 (2015).
56. Schuurhuis, D. H. *et al.* Immature dendritic cells acquire CD8(+) cytotoxic T lymphocyte priming capacity upon activation by T helper cell-independent or -dependent stimuli. *J. Exp. Med.* **192**, 145–150 (2000).
57. Matloubian, M., Concepcion, R. J. & Ahmed, R. CD4+ T cells are required to sustain CD8+ cytotoxic T-cell responses during chronic viral infection. *J. Virol.* **68**, 8056–8063 (1994).
58. Ostroumov, D., Fekete-Drimusz, N., Saborowski, M., Kühnel, F. & Woller, N. CD4 and CD8 T lymphocyte interplay in controlling tumor growth. *Cell. Mol. Life Sci. CMLS* **75**, 689–713 (2018).
59. Shankaran, V. *et al.* IFNgamma and lymphocytes prevent primary tumour development and shape tumour immunogenicity. *Nature* **410**, 1107–1111 (2001).
60. Schaerli, P. *et al.* CXC chemokine receptor 5 expression defines follicular homing T cells with B cell helper function. *J. Exp. Med.* **192**, 1553–1562 (2000).
61. Victora, G. D. *et al.* Germinal center dynamics revealed by multiphoton microscopy with a photoactivatable fluorescent reporter. *Cell* **143**, 592–605 (2010).
62. Quast, I., Peschke, B. & Lünemann, J. D. Regulation of antibody effector functions through IgG Fc N-glycosylation. *Cell. Mol. Life Sci. CMLS* **74**, 837–847 (2017).
63. Lanier, L. L. Shades of grey--the blurring view of innate and adaptive immunity. *Nat. Rev. Immunol.* **13**, 73–74 (2013).
64. Vermijlen, D. & Prinz, I. Ontogeny of Innate T Lymphocytes - Some Innate Lymphocytes are More Innate than Others. *Front. Immunol.* **5**, 486 (2014).
65. Godfrey, D. I., Uldrich, A. P., McCluskey, J., Rossjohn, J. & Moody, D. B. The burgeoning family of unconventional T cells. *Nat. Immunol.* **16**, 1114–1123 (2015).
66. Tyznik, A. J. *et al.* Cutting edge: the mechanism of invariant NKT cell responses to viral danger signals. *J. Immunol. Baltim. Md 1950* **181**, 4452–4456 (2008).
67. Ussher, J. E. *et al.* CD161++ CD8+ T cells, including the MAIT cell subset, are specifically activated by IL-12+IL-18 in a TCR-independent manner. *Eur. J. Immunol.* **44**, 195–203 (2014).
68. Finlay, B. B. & McFadden, G. Anti-immunology: evasion of the host immune system by bacterial and viral pathogens. *Cell* **124**, 767–782 (2006).
69. Blom, A. M. Strategies developed by bacteria and virus for protection from the human complement system. *Scand. J. Clin. Lab. Invest.* **64**, 479–496 (2004).
70. Spiller, O. B., Morgan, B. P., Tufaro, F. & Devine, D. V. Altered expression of host-encoded complement regulators on human cytomegalovirus-infected cells. *Eur. J. Immunol.* **26**, 1532–1538 (1996).
71. Spear, G. T. *et al.* Host cell-derived complement control proteins CD55 and CD59 are incorporated into the virions of two unrelated enveloped viruses. Human T cell leukemia/lymphoma virus type I (HTLV-I) and human cytomegalovirus (HCMV). *J. Immunol. Baltim. Md 1950* **155**, 4376–4381 (1995).
72. Gancz, D. & Fishelson, Z. Cancer resistance to complement-dependent cytotoxicity (CDC): Problem-oriented research and development. *Mol. Immunol.* **46**, 2794–2800 (2009).
73. Wilen, C. B., Tilton, J. C. & Doms, R. W. HIV: cell binding and entry. *Cold Spring Harb. Perspect. Med.* **2**, (2012).
74. McDougal, J. S. *et al.* Binding of HTLV-III/LAV to T4+ T cells by a complex of the 110K viral protein and the T4 molecule. *Science* **231**, 382–385 (1986).
75. Maddon, P. J. *et al.* The T4 gene encodes the AIDS virus receptor and is expressed in the immune system and the brain. *Cell* **47**, 333–348 (1986).
76. Okoye, A. A. & Picker, L. J. CD4(+) T-cell depletion in HIV infection: mechanisms of immunological failure. *Immunol. Rev.* **254**, 54–64 (2013).
77. Sha, S. *et al.* Mycobacterium tuberculosis Rv1987 induces Th2 immune responses and enhances Mycobacterium smegmatis survival in mice. *Microbiol. Res.* **197**, 74–80 (2017).
78. Dwivedi, V. P. *et al.* Mycobacterium tuberculosis Directs T Helper 2 Cell Differentiation by Inducing Interleukin-1β Production in Dendritic Cells. *J. Biol. Chem.* **287**, 33656–33663 (2012).
79. Yaseen, M. M., Abuharfeil, N. M., Alqudah, M. A. & Yaseen, M. M. Mechanisms and Factors That Drive Extensive Human Immunodeficiency Virus Type-1 Hypervariability: An Overview. *Viral Immunol.* **30**, 708–726 (2017).
80. Grant, M. & Larijani, M. Evasion of adaptive immunity by HIV through the action of host APOBEC3G/F enzymes. *AIDS Res. Ther.* **14**, 44 (2017).
81. Lehner, P. J., Hoer, S., Dodd, R. & Duncan, L. M. Downregulation of cell surface receptors by the K3 family of viral and cellular ubiquitin E3 ligases. *Immunol. Rev.* **207**, 112–125 (2005).

82. Reeves, E. & James, E. Antigen processing and immune regulation in the response to tumours. *Immunology* **150**, 16–24 (2017).
83. Hmama, Z., Peña-Díaz, S., Joseph, S. & Av-Gay, Y. Immunoevasion and immunosuppression of the macrophage by Mycobacterium tuberculosis. *Immunol. Rev.* **264**, 220–232 (2015).
84. Armstrong, J. A. & Hart, P. D. Response of Cultured Macrophages to Mycobacterium Tuberculosis, with Observations on Fusion of Lysosomes with Phagosomes. *J. Exp. Med.* **134**, 713–740 (1971).
85. Blum, J. S., Wearsch, P. A. & Cresswell, P. Pathways of antigen processing. *Annu. Rev. Immunol.* **31**, 443–473 (2013).
86. Rock, K. L., Reits, E. & Neefjes, J. Present Yourself! By MHC Class I and MHC Class II Molecules. *Trends Immunol.* **37**, 724–737 (2016).
87. Adams, E. J. Lipid presentation by human CD1 molecules and the diverse T cell populations that respond to them. *Curr. Opin. Immunol.* **26**, 1–6 (2014).
88. Porcelli, S., Morita, C. T. & Brenner, M. B. CD1b restricts the response of human CD4-8- T lymphocytes to a microbial antigen. *Nature* **360**, 593–597 (1992).
89. Beckman, E. M. *et al.* Recognition of a lipid antigen by CD1-restricted αβ+ T cells. *Nature* **372**, 691–694 (1994).
90. Sieling, P. A. *et al.* CD1-restricted T cell recognition of microbial lipoglycan antigens. *Science* **269**, 227–230 (1995).
91. Spada, F. M., Koezuka, Y. & Porcelli, S. A. CD1d-restricted Recognition of Synthetic Glycolipid Antigens by Human Natural Killer T Cells. *J. Exp. Med.* **188**, 1529–1534 (1998).
92. Rosat, J.-P. *et al.* CD1-restricted microbial lipid antigen-specific recognition found in the CD8+ αβ T cell pool. *J. Immunol.* **162**, 366–371 (1999).
93. Moody, D. B. *et al.* CD1c-mediated T-cell recognition of isoprenoid glycolipids in Mycobacterium tuberculosis infection. *Nature* **404**, 884–888 (2000).
94. McWilliam, H. E. G. & Villadangos, J. A. How MR1 Presents a Pathogen Metabolic Signature to Mucosal-Associated Invariant T (MAIT) Cells. *Trends Immunol.* **38**, 679–689 (2017).
95. Kjer-Nielsen, L. *et al.* MR1 presents microbial vitamin B metabolites to MAIT cells. *Nature* **491**, 717–723 (2012).
96. Corbett, A. J. *et al.* T-cell activation by transitory neo-antigens derived from distinct microbial pathways. *Nature* **509**, 361–365 (2014).
97. Beetz, S. *et al.* Innate immune functions of human gammadelta T cells. *Immunobiology* **213**, 173–182 (2008).
98. De Libero, G., Lau, S.-Y. & Mori, L. Phosphoantigen Presentation to TCR γδ Cells, a Conundrum Getting Less Gray Zones. *Front. Immunol.* **5**, (2015).
99. Harly, C. *et al.* Key implication of CD277/butyrophilin-3 (BTN3A) in cellular stress sensing by a major human γδ T-cell subset. *Blood* **120**, 2269–2279 (2012).
100. Vavassori, S. *et al.* Butyrophilin 3A1 binds phosphorylated antigens and stimulates human γδ T cells. *Nat. Immunol.* **14**, 908–916 (2013).
101. Schuette, V. & Burgdorf, S. The ins-and-outs of endosomal antigens for cross-presentation. *Curr. Opin. Immunol.* **26**, 63–68 (2014).
102. Crotzer, V. L. & Blum, J. S. Autophagy and adaptive immunity. *Immunology* **131**, 9–17 (2010).
103. Nimmerjahn, F. *et al.* Major histocompatibility complex class II-restricted presentation of a cytosolic antigen by autophagy. *Eur. J. Immunol.* **33**, 1250–1259 (2003).
104. Schmid, D., Pypaert, M. & Münz, C. Antigen-loading compartments for major histocompatibility complex class II molecules continuously receive input from autophagosomes. *Immunity* **26**, 79–92 (2007).
105. Adams, E. J. & Luoma, A. M. The adaptable major histocompatibility complex (MHC) fold: structure and function of nonclassical and MHC class I-like molecules. *Annu. Rev. Immunol.* **31**, 529–561 (2013).
106. Springer, T. A., Kaufman, J. F., Terhorst, C. & Strominger, J. L. Purification and structural characterisation of human HLA-linked B-cell antigens. *Nature* **268**, 213–218 (1977).
107. Bjorkman, P. J. *et al.* Structure of the human class I histocompatibility antigen, HLA-A2. *Nature* **329**, 506–512 (1987).
108. Nikolich-Žugich, J., Fremont, D. H., Miley, M. J. & Messaoudi, I. The role of mhc polymorphism in anti-microbial resistance. *Microbes Infect.* **6**, 501–512 (2004).
109. Yeager, M. & Hughes, A. L. Evolution of the mammalian MHC: natural selection, recombination, and convergent evolution. *Immunol. Rev.* **167**, 45–58 (1999).

110. Falk, K., Rötzschke, O., Stevanović, S., Jung, G. & Rammensee, H.-G. Allele-specific motifs revealed by sequencing of self-peptides eluted from MHC molecules. *Nature* **351**, 290–296 (1991).
111. Falk, K. *et al.* Allele-specific peptide ligand motifs of HLA-C molecules. *Proc. Natl. Acad. Sci. U. S. A.* **90**, 12005–12009 (1993).
112. Falk, K., Rötzschke, O., Stevanovíc, S., Jung, G. & Rammensee, H.-G. Pool sequencing of natural HLA-DR, DQ, and DP ligands reveals detailed peptide motifs, constraints of processing, and general rules. *Immunogenetics* **39**, 230–242 (1994).
113. Rammensee, H. G., Falk, K. & Rötzschke, O. MHC molecules as peptide receptors. *Curr. Opin. Immunol.* **5**, 35–44 (1993).
114. Hunt, D. F. *et al.* Characterization of peptides bound to the class I MHC molecule HLA-A2.1 by mass spectrometry. *Science* **255**, 1261–1263 (1992).
115. Hunt, D. F. *et al.* Peptides presented to the immune system by the murine class II major histocompatibility complex molecule I-Ad. *Science* **256**, 1817–1820 (1992).
116. Michalek, M. T., Grant, E. P., Gramm, C., Goldberg, A. L. & Rock, K. L. A role for the ubiquitin-dependent proteolytic pathway in MHC class I-restricted antigen presentation. *Nature* **363**, 552–554 (1993).
117. Rock, K. L. *et al.* Inhibitors of the proteasome block the degradation of most cell proteins and the generation of peptides presented on MHC class I molecules. *Cell* **78**, 761–771 (1994).
118. Reits, E. *et al.* Peptide Diffusion, Protection, and Degradation in Nuclear and Cytoplasmic Compartments before Antigen Presentation by MHC Class I. *Immunity* **18**, 97–108 (2003).
119. Silva, C. L., Portaro, F. C., Bonato, V. L., de Camargo, A. C. & Ferro, E. S. Thimet oligopeptidase (EC 3.4.24.15), a novel protein on the route of MHC class I antigen presentation. *Biochem. Biophys. Res. Commun.* **255**, 591–595 (1999).
120. Lévy, F. *et al.* The final N-terminal trimming of a subaminoterminal proline-containing HLA class I-restricted antigenic peptide in the cytosol is mediated by two peptidases. *J. Immunol. Baltim. Md 1950* **169**, 4161–4171 (2002).
121. Cerundolo, V. *et al.* Presentation of viral antigen controlled by a gene in the major histocompatibility complex. *Nature* **345**, 449–452 (1990).
122. Arnold, D. *et al.* Proteasome subunits encoded in the MHC are not generally required for the processing of peptides bound by MHC class I molecules. *Nature* **360**, 171–174 (1992).
123. Momburg, F. *et al.* Proteasome subunits encoded by the major histocompatibility complex are not essential for antigen presentation. *Nature* **360**, 174–177 (1992).
124. Townsend, A. & Trowsdale, J. The transporters associated with antigen presentation. *Semin. Cell Biol.* **4**, 53–61 (1993).
125. Neefjes, J. J., Momburg, F. & Hämmerling, G. J. Selective and ATP-dependent translocation of peptides by the MHC-encoded transporter. *Science* **261**, 769–771 (1993).
126. Saric, T. *et al.* An IFN-gamma-induced aminopeptidase in the ER, ERAP1, trims precursors to MHC class I-presented peptides. *Nat. Immunol.* **3**, 1169–1176 (2002).
127. York, I. A. *et al.* The ER aminopeptidase ERAP1 enhances or limits antigen presentation by trimming epitopes to 8-9 residues. *Nat. Immunol.* **3**, 1177–1184 (2002).
128. Saveanu, L. *et al.* Concerted peptide trimming by human ERAP1 and ERAP2 aminopeptidase complexes in the endoplasmic reticulum. *Nat. Immunol.* **6**, 689–697 (2005).
129. Chang, S.-C., Momburg, F., Bhutani, N. & Goldberg, A. L. The ER aminopeptidase, ERAP1, trims precursors to lengths of MHC class I peptides by a 'molecular ruler' mechanism. *Proc. Natl. Acad. Sci. U. S. A.* **102**, 17107–17112 (2005).
130. Kanaseki, T., Blanchard, N., Hammer, G. E., Gonzalez, F. & Shastri, N. ERAAP synergizes with MHC class I molecules to make the final cut in the antigenic peptide precursors in the endoplasmic reticulum. *Immunity* **25**, 795–806 (2006).
131. Reeves, E., Edwards, C. J., Elliott, T. & James, E. Naturally occurring ERAP1 haplotypes encode functionally distinct alleles with fine substrate specificity. *J. Immunol. Baltim. Md 1950* **191**, 35–43 (2013).
132. Papakyriakou, A. *et al.* The partial dissociation of MHC class I-bound peptides exposes their N terminus to trimming by endoplasmic reticulum aminopeptidase 1. *J. Biol. Chem.* **293**, 7538–7548 (2018).
133. Sadasivan, B., Lehner, P. J., Ortmann, B., Spies, T. & Cresswell, P. Roles for calreticulin and a novel glycoprotein, tapasin, in the interaction of MHC class I molecules with TAP. *Immunity* **5**, 103–114 (1996).
134. Purcell, A. W. *et al.* Quantitative and qualitative influences of tapasin on the class I peptide repertoire. *J. Immunol. Baltim. Md 1950* **166**, 1016–1027 (2001).

135. Williams, A. P., Peh, C. A., Purcell, A. W., McCluskey, J. & Elliott, T. Optimization of the MHC class I peptide cargo is dependent on tapasin. *Immunity* **16**, 509–520 (2002).
136. Tan, P. *et al.* Recruitment of MHC class I molecules by tapasin into the transporter associated with antigen processing-associated complex is essential for optimal peptide loading. *J. Immunol. Baltim. Md 1950* **168**, 1950–1960 (2002).
137. Zarling, A. L. *et al.* Tapasin is a facilitator, not an editor, of class I MHC peptide binding. *J. Immunol. Baltim. Md 1950* **171**, 5287–5295 (2003).
138. Wearsch, P. A. & Cresswell, P. Selective loading of high-affinity peptides onto major histocompatibility complex class I molecules by the tapasin-ERp57 heterodimer. *Nat. Immunol.* **8**, 873–881 (2007).
139. Hermann, C. *et al.* TAPBPR alters MHC class I peptide presentation by functioning as a peptide exchange catalyst. *eLife* **4**, (2015).
140. Morozov, G. I. *et al.* Interaction of TAPBPR, a tapasin homolog, with MHC-I molecules promotes peptide editing. *Proc. Natl. Acad. Sci. U. S. A.* **113**, E1006-1015 (2016).
141. Thomas, C. & Tampé, R. Structure of the TAPBPR-MHC I complex defines the mechanism of peptide loading and editing. *Science* **358**, 1060–1064 (2017).
142. Garstka, M. A. *et al.* The first step of peptide selection in antigen presentation by MHC class I molecules. *Proc. Natl. Acad. Sci.* **112**, 1505–1510 (2015).
143. Gruhler, A. & Früh, K. Control of MHC class I traffic from the endoplasmic reticulum by cellular chaperones and viral anti-chaperones. *Traffic Cph. Den.* **1**, 306–311 (2000).
144. Elliott, T., Cerundolo, V., Elvin, J. & Townsend, A. Peptide-induced conformational change of the class I heavy chain. *Nature* **351**, 402–406 (1991).
145. Schumacher, T. N. M. *et al.* Direct binding of peptide to empty MHC class I molecules on intact cells and in vitro. *Cell* **62**, 563–567 (1990).
146. Hein, Z. *et al.* Peptide-independent stabilization of MHC class I molecules breaches cellular quality control. *J. Cell Sci.* **127**, 2885–2897 (2014).
147. Wearsch, P. A., Peaper, D. R. & Cresswell, P. Essential glycan-dependent interactions optimize MHC class I peptide loading. *Proc. Natl. Acad. Sci. U. S. A.* **108**, 4950–4955 (2011).
148. Zhang, W., Wearsch, P. A., Zhu, Y., Leonhardt, R. M. & Cresswell, P. A role for UDP-glucose glycoprotein glucosyltransferase in expression and quality control of MHC class I molecules. *Proc. Natl. Acad. Sci. U. S. A.* **108**, 4956–4961 (2011).
149. Mahmutefendić, H., Blagojević, G., Tomaš, M. I., Kučić, N. & Lučin, P. Segregation of open Major Histocompatibility Class I conformers at the plasma membrane and during endosomal trafficking reveals conformation-based sorting in the endosomal system. *Int. J. Biochem. Cell Biol.* **43**, 504–515 (2011).
150. Parker, K. C., DiBrino, M., Hull, L. & Coligan, J. E. The beta 2-microglobulin dissociation rate is an accurate measure of the stability of MHC class I heterotrimers and depends on which peptide is bound. *J. Immunol. Baltim. Md 1950* **149**, 1896–1904 (1992).
151. Gakamsky, D. M. *et al.* An allosteric mechanism controls antigen presentation by the H-2K(b) complex. *Biochemistry* **38**, 12165–12173 (1999).
152. Montealegre, S. *et al.* Dissociation of β2-microglobulin determines the surface quality control of major histocompatibility complex class I molecules. *FASEB J. Off. Publ. Fed. Am. Soc. Exp. Biol.* **29**, 2780–2788 (2015).
153. Ishido, S., Goto, E., Matsuki, Y. & Ohmura-Hoshino, M. E3 ubiquitin ligases for MHC molecules. *Curr. Opin. Immunol.* **21**, 78–83 (2009).
154. Bartee, E., Mansouri, M., Hovey Nerenberg, B. T., Gouveia, K. & Früh, K. Downregulation of major histocompatibility complex class I by human ubiquitin ligases related to viral immune evasion proteins. *J. Virol.* **78**, 1109–1120 (2004).
155. Duncan, L. M., Nathan, J. A. & Lehner, P. J. Stabilization of an E3 ligase-E2-ubiquitin complex increases cell surface MHC class I expression. *J. Immunol. Baltim. Md 1950* **184**, 6978–6985 (2010).
156. Grommé, M. *et al.* Recycling MHC class I molecules and endosomal peptide loading. *Proc. Natl. Acad. Sci. U. S. A.* **96**, 10326–10331 (1999).
157. Landsverk, O. J. B., Bakke, O. & Gregers, T. F. MHC II and the endocytic pathway: regulation by invariant chain. *Scand. J. Immunol.* **70**, 184–193 (2009).
158. Roche, P. A. & Cresswell, P. Invariant chain association with HLA-DR molecules inhibits immunogenic peptide binding. *Nature* **345**, 615–618 (1990).
159. Anderson, M. S. & Miller, J. Invariant chain can function as a chaperone protein for class II major histocompatibility complex molecules. *Proc. Natl. Acad. Sci. U. S. A.* **89**, 2282–2286 (1992).

160. Bikoff, E. K. *et al.* Defective major histocompatibility complex class II assembly, transport, peptide acquisition, and CD4+ T cell selection in mice lacking invariant chain expression. *J. Exp. Med.* **177**, 1699–1712 (1993).
161. Ghosh, P., Amaya, M., Mellins, E. & Wiley, D. C. The structure of an intermediate in class II MHC maturation: CLIP bound to HLA-DR3. *Nature* **378**, 457–462 (1995).
162. Bakke, O. & Dobberstein, B. MHC class II-associated invariant chain contains a sorting signal for endosomal compartments. *Cell* **63**, 707–716 (1990).
163. Bremnes, B., Madsen, T., Gedde-Dahl, M. & Bakke, O. An LI and ML motif in the cytoplasmic tail of the MHC-associated invariant chain mediate rapid internalization. *J. Cell Sci.* **107 (Pt 7)**, 2021–2032 (1994).
164. Elliott, E. A. *et al.* The invariant chain is required for intracellular transport and function of major histocompatibility complex class II molecules. *J. Exp. Med.* **179**, 681–694 (1994).
165. Neefjes, J. CIIV, MIIC and other compartments for MHC class II loading. *Eur. J. Immunol.* **29**, 1421–1425 (1999).
166. Peters, P. J., Neefjes, J. J., Oorschot, V., Ploegh, H. L. & Geuze, H. J. Segregation of MHC class II molecules from MHC class I molecules in the Golgi complex for transport to lysosomal compartments. *Nature* **349**, 669–676 (1991).
167. Hsing, L. C. & Rudensky, A. Y. The lysosomal cysteine proteases in MHC class II antigen presentation. *Immunol. Rev.* **207**, 229–241 (2005).
168. Blum, J. S. & Cresswell, P. Role for intracellular proteases in the processing and transport of class II HLA antigens. *Proc. Natl. Acad. Sci.* **85**, 3975–3979 (1988).
169. Hsieh, C.-S., deRoos, P., Honey, K., Beers, C. & Rudensky, A. Y. A role for cathepsin L and cathepsin S in peptide generation for MHC class II presentation. *J. Immunol. Baltim. Md 1950* **168**, 2618–2625 (2002).
170. Denzin, L. K. & Cresswell, P. HLA-DM induces CLIP dissociation from MHC class II alpha beta dimers and facilitates peptide loading. *Cell* **82**, 155–165 (1995).
171. Sloan, V. S. *et al.* Mediation by HLA-DM of dissociation of peptides from HLA-DR. *Nature* **375**, 802–806 (1995).
172. Sherman, M. A., Weber, D. A. & Jensen, P. E. DM enhances peptide binding to class II MHC by release of invariant chain-derived peptide. *Immunity* **3**, 197–205 (1995).
173. Denzin, L. K., Fallas, J. L., Prendes, M. & Yi, W. Right place, right time, right peptide: DO keeps DM focused. *Immunol. Rev.* **207**, 279–292 (2005).
174. Kropshofer, H. *et al.* Editing of the HLA-DR-peptide repertoire by HLA-DM. *EMBO J.* **15**, 6144–6154 (1996).
175. Trombetta, E. S., Ebersold, M., Garrett, W., Pypaert, M. & Mellman, I. Activation of lysosomal function during dendritic cell maturation. *Science* **299**, 1400–1403 (2003).
176. Delamarre, L., Pack, M., Chang, H., Mellman, I. & Trombetta, E. S. Differential lysosomal proteolysis in antigen-presenting cells determines antigen fate. *Science* **307**, 1630–1634 (2005).
177. Wubbolts, R. *et al.* Direct vesicular transport of MHC class II molecules from lysosomal structures to the cell surface. *J. Cell Biol.* **135**, 611–622 (1996).
178. Kleijmeer, M. *et al.* Reorganization of multivesicular bodies regulates MHC class II antigen presentation by dendritic cells. *J. Cell Biol.* **155**, 53–63 (2001).
179. Vascotto, F. *et al.* The actin-based motor protein myosin II regulates MHC class II trafficking and BCR-driven antigen presentation. *J. Cell Biol.* **176**, 1007–1019 (2007).
180. Rocha, N. *et al.* Cholesterol sensor ORP1L contacts the ER protein VAP to control Rab7-RILP-p150 Glued and late endosome positioning. *J. Cell Biol.* **185**, 1209–1225 (2009).
181. van Niel, G. *et al.* Dendritic cells regulate exposure of MHC class II at their plasma membrane by oligoubiquitination. *Immunity* **25**, 885–894 (2006).
182. Shin, J.-S. *et al.* Surface expression of MHC class II in dendritic cells is controlled by regulated ubiquitination. *Nature* **444**, 115–118 (2006).
183. De Gassart, A. *et al.* MHC class II stabilization at the surface of human dendritic cells is the result of maturation-dependent MARCH I down-regulation. *Proc. Natl. Acad. Sci. U. S. A.* **105**, 3491–3496 (2008).
184. Thibodeau, J. *et al.* Interleukin-10-induced MARCH1 mediates intracellular sequestration of MHC class II in monocytes. *Eur. J. Immunol.* **38**, 1225–1230 (2008).
185. Walseng, E. *et al.* Ubiquitination regulates MHC class II-peptide complex retention and degradation in dendritic cells. *Proc. Natl. Acad. Sci. U. S. A.* **107**, 20465–20470 (2010).

186. Muno, D., Kominami, E. & Mizuochi, T. Generation of both MHC class I- and class II-restricted antigenic peptides from exogenously added ovalbumin in murine phagosomes. *FEBS Lett.* **478**, 178–182 (2000).
187. Bertholet, S. *et al.* Leishmania antigens are presented to CD8+ T cells by a transporter associated with antigen processing-independent pathway in vitro and in vivo. *J. Immunol. Baltim. Md 1950* **177**, 3525–3533 (2006).
188. Saveanu, L. *et al.* IRAP identifies an endosomal compartment required for MHC class I cross-presentation. *Science* **325**, 213–217 (2009).
189. Weimershaus, M. *et al.* Conventional dendritic cells require IRAP-Rab14 endosomes for efficient cross-presentation. *J. Immunol. Baltim. Md 1950* **188**, 1840–1846 (2012).
190. Lizée, G. *et al.* Control of dendritic cell cross-presentation by the major histocompatibility complex class I cytoplasmic domain. *Nat. Immunol.* **4**, 1065–1073 (2003).
191. Kovacsovics-Bankowski, M. & Rock, K. L. A phagosome-to-cytosol pathway for exogenous antigens presented on MHC class I molecules. *Science* **267**, 243–246 (1995).
192. Ackerman, A. L., Kyritsis, C., Tampé, R. & Cresswell, P. Early phagosomes in dendritic cells form a cellular compartment sufficient for cross presentation of exogenous antigens. *Proc. Natl. Acad. Sci. U. S. A.* **100**, 12889–12894 (2003).
193. Guermonprez, P. *et al.* ER-phagosome fusion defines an MHC class I cross-presentation compartment in dendritic cells. *Nature* **425**, 397–402 (2003).
194. Ackerman, A. L., Kyritsis, C., Tampé, R. & Cresswell, P. Access of soluble antigens to the endoplasmic reticulum can explain cross-presentation by dendritic cells. *Nat. Immunol.* **6**, 107–113 (2005).
195. Burgdorf, S., Schölz, C., Kautz, A., Tampé, R. & Kurts, C. Spatial and mechanistic separation of cross-presentation and endogenous antigen presentation. *Nat. Immunol.* **9**, 558–566 (2008).
196. Grotzke, J. E. & Cresswell, P. Are ERAD components involved in cross-presentation? *Mol. Immunol.* **68**, 112–115 (2015).
197. Imai, J., Hasegawa, H., Maruya, M., Koyasu, S. & Yahara, I. Exogenous antigens are processed through the endoplasmic reticulum-associated degradation (ERAD) in cross-presentation by dendritic cells. *Int. Immunol.* **17**, 45–53 (2005).
198. Ackerman, A. L., Giodini, A. & Cresswell, P. A role for the endoplasmic reticulum protein retrotranslocation machinery during crosspresentation by dendritic cells. *Immunity* **25**, 607–617 (2006).
199. Zehner, M. *et al.* Mannose receptor polyubiquitination regulates endosomal recruitment of p97 and cytosolic antigen translocation for cross-presentation. *Proc. Natl. Acad. Sci. U. S. A.* **108**, 9933–9938 (2011).
200. Cebrian, I. *et al.* Sec22b regulates phagosomal maturation and antigen crosspresentation by dendritic cells. *Cell* **147**, 1355–1368 (2011).
201. Nair-Gupta, P. *et al.* TLR Signals Induce Phagosomal MHC-I Delivery from the Endosomal Recycling Compartment to Allow Cross-Presentation. *Cell* **158**, 506–521 (2014).
202. Alloatti, A. *et al.* Critical role for Sec22b-dependent antigen cross-presentation in antitumor immunity. *J. Exp. Med.* **214**, 2231–2241 (2017).
203. Wu, S. J. *et al.* A Critical Analysis of the Role of SNARE Protein SEC22B in Antigen Cross-Presentation. *Cell Rep.* **19**, 2645–2656 (2017).
204. Montealegre, S. & van Endert, P. MHC Class I Cross-Presentation: Stage Lights on Sec22b. *Trends Immunol.* **38**, 618–621 (2017).
205. Van Rhijn, I., Godfrey, D. I., Rossjohn, J. & Moody, D. B. Lipid and small-molecule display by CD1 and MR1. *Nat. Rev. Immunol.* **15**, 643–654 (2015).
206. Felício, L. P. *et al.* Worldwide HLA-E nucleotide and haplotype variability reveals a conserved gene for coding and 3′ untranslated regions. *Tissue Antigens* **83**, 82–93 (2014).
207. Manvailer, L. F. S. *et al.* HLA-F polymorphisms in a Euro-Brazilian population from Southern Brazil. *Tissue Antigens* **84**, 554–559 (2014).
208. Donadi, E. A. *et al.* Implications of the polymorphism of HLA-G on its function, regulation, evolution and disease association. *Cell. Mol. Life Sci.* **68**, 369–395 (2011).
209. Braud, V., Jones, E. Y. & McMichael, A. The human major histocompatibility complex class Ib molecule HLA-E binds signal sequence-derived peptides with primary anchor residues at positions 2 and 9. *Eur. J. Immunol.* **27**, 1164–1169 (1997).
210. Ishitani, A. *et al.* Protein expression and peptide binding suggest unique and interacting functional roles for HLA-E, F, and G in maternal-placental immune recognition. *J. Immunol. Baltim. Md 1950* **171**, 1376–1384 (2003).

211. Posch, P. E., Borrego, F., Brooks, A. G. & Coligan, J. E. HLA-E is the ligand for the natural killer cell CD94/NKG2 receptors. *J. Biomed. Sci.* **5**, 321–331 (1998).
212. Braud, V. M. *et al.* HLA-E binds to natural killer cell receptors CD94/NKG2A, B and C. *Nature* **391**, 795–799 (1998).
213. Garcia-Beltran, W. F. *et al.* Open conformers of HLA-F are high-affinity ligands of the activating NK-cell receptor KIR3DS1. *Nat. Immunol.* **17**, 1067–1074 (2016).
214. Carosella, E. D., Rouas-Freiss, N., Tronik-Le Roux, D., Moreau, P. & LeMaoult, J. HLA-G: An Immune Checkpoint Molecule. *Adv. Immunol.* **127**, 33–144 (2015).
215. Kraemer, T., Blasczyk, R. & Bade-Doeding, C. HLA-E: a novel player for histocompatibility. *J. Immunol. Res.* **2014**, 352160 (2014).
216. Reinink, P. & Van Rhijn, I. Mammalian CD1 and MR1 genes. *Immunogenetics* **68**, 515–523 (2016).
217. Calabi, F. & Milstein, C. A novel family of human major histocompatibility complex-related genes not mapping to chromosome 6. *Nature* **323**, 540–543 (1986).
218. Shamshiev, A. *et al.* Presentation of the same glycolipid by different CD1 molecules. *J. Exp. Med.* **195**, 1013–1021 (2002).
219. Huang, S. *et al.* Discovery of deoxyceramides and diacylglycerols as CD1b scaffold lipids among diverse groove-blocking lipids of the human CD1 system. *Proc. Natl. Acad. Sci.* **108**, 19335–19340 (2011).
220. Gadola, S. D. *et al.* Structure of human CD1b with bound ligands at 2.3 A, a maze for alkyl chains. *Nat. Immunol.* **3**, 721–726 (2002).
221. Zajonc, D. M., Elsliger, M. A., Teyton, L. & Wilson, I. A. Crystal structure of CD1a in complex with a sulfatide self antigen at a resolution of 2.15 A. *Nat. Immunol.* **4**, 808–815 (2003).
222. Koch, M. *et al.* The crystal structure of human CD1d with and without alpha-galactosylceramide. *Nat. Immunol.* **6**, 819–826 (2005).
223. Scharf, L. *et al.* The 2.5 Å structure of CD1c in complex with a mycobacterial lipid reveals an open groove ideally suited for diverse antigen presentation. *Immunity* **33**, 853–862 (2010).
224. Garcia-Alles, L. F. *et al.* Endogenous phosphatidylcholine and a long spacer ligand stabilize the lipid-binding groove of CD1b. *EMBO J.* **25**, 3684–3692 (2006).
225. Brozovic, S. *et al.* CD1d function is regulated by microsomal triglyceride transfer protein. *Nat. Med.* **10**, 535–539 (2004).
226. Kaser, A. *et al.* Microsomal triglyceride transfer protein regulates endogenous and exogenous antigen presentation by group 1 CD1 molecules. *Eur. J. Immunol.* **38**, 2351–2359 (2008).
227. Garcia-Alles, L. F. *et al.* Structural reorganization of the antigen-binding groove of human CD1b for presentation of mycobacterial sulfoglycolipids. *Proc. Natl. Acad. Sci.* **108**, 17755–17760 (2011).
228. Mansour, S. *et al.* Cholesteryl esters stabilize human CD1c conformations for recognition by self-reactive T cells. *Proc. Natl. Acad. Sci. U. S. A.* **113**, E1266-1275 (2016).
229. McCarthy, C. *et al.* The length of lipids bound to human CD1d molecules modulates the affinity of NKT cell TCR and the threshold of NKT cell activation. *J. Exp. Med.* **204**, 1131–1144 (2007).
230. de Jong, A. *et al.* CD1a-autoreactive T cells recognize natural skin oils that function as headless antigens. *Nat. Immunol.* **15**, 177–185 (2014).
231. Barral, D. C. & Brenner, M. B. CD1 antigen presentation: how it works. *Nat. Rev. Immunol.* **7**, 929–941 (2007).
232. Jackman, R. M., Moody, D. B. & Porcelli, S. A. Mechanisms of lipid antigen presentation by CD1. *Crit. Rev. Immunol.* **19**, 49–63 (1999).
233. Briken, V., Moody, D. B. & Porcelli, S. A. Diversification of CD1 proteins: sampling the lipid content of different cellular compartments. *Semin. Immunol.* **12**, 517–525 (2000).
234. Briken, V., Jackman, R. M., Watts, G. F., Rogers, R. A. & Porcelli, S. A. Human CD1b and CD1c isoforms survey different intracellular compartments for the presentation of microbial lipid antigens. *J. Exp. Med.* **192**, 281–288 (2000).
235. Sugita, M. *et al.* Separate pathways for antigen presentation by CD1 molecules. *Immunity* **11**, 743–752 (1999).
236. Cernadas, M. *et al.* Early recycling compartment trafficking of CD1a is essential for its intersection and presentation of lipid antigens. *J. Immunol. Baltim. Md 1950* **184**, 1235–1241 (2010).

237. Chiu, Y. H. *et al.* Distinct subsets of CD1d-restricted T cells recognize self-antigens loaded in different cellular compartments. *J. Exp. Med.* **189**, 103–110 (1999).
238. Sugita, M., van Der Wel, N., Rogers, R. A., Peters, P. J. & Brenner, M. B. CD1c molecules broadly survey the endocytic system. *Proc. Natl. Acad. Sci. U. S. A.* **97**, 8445–8450 (2000).
239. Sugita, M. *et al.* Cytoplasmic tail-dependent localization of CD1b antigen-presenting molecules to MIICs. *Science* **273**, 349–352 (1996).
240. Briken, V., Jackman, R. M., Dasgupta, S., Hoening, S. & Porcelli, S. A. Intracellular trafficking pathway of newly synthesized CD1b molecules. *EMBO J.* **21**, 825–834 (2002).
241. Elewaut, D. *et al.* The adaptor protein AP-3 is required for CD1d-mediated antigen presentation of glycosphingolipids and development of Valpha14i NKT cells. *J. Exp. Med.* **198**, 1133–1146 (2003).
242. Schaible, U. E., Hagens, K., Fischer, K., Collins, H. L. & Kaufmann, S. H. Intersection of group I CD1 molecules and mycobacteria in different intracellular compartments of dendritic cells. *J. Immunol. Baltim. Md 1950* **164**, 4843–4852 (2000).
243. Beatty, W. L. *et al.* Trafficking and release of mycobacterial lipids from infected macrophages. *Traffic Cph. Den.* **1**, 235–247 (2000).
244. Prigozy, T. I. *et al.* The mannose receptor delivers lipoglycan antigens to endosomes for presentation to T cells by CD1b molecules. *Immunity* **6**, 187–197 (1997).
245. van den Elzen, P. *et al.* Apolipoprotein-mediated pathways of lipid antigen presentation. *Nature* **437**, 906–910 (2005).
246. Mukherjee, S., Soe, T. T. & Maxfield, F. R. Endocytic sorting of lipid analogues differing solely in the chemistry of their hydrophobic tails. *J. Cell Biol.* **144**, 1271–1284 (1999).
247. Moody, D. B. *et al.* Lipid length controls antigen entry into endosomal and nonendosomal pathways for CD1b presentation. *Nat. Immunol.* **3**, 435–442 (2002).
248. Zhou, D. *et al.* Editing of CD1d-bound lipid antigens by endosomal lipid transfer proteins. *Science* **303**, 523–527 (2004).
249. León, L. *et al.* Saposins utilize two strategies for lipid transfer and CD1 antigen presentation. *Proc. Natl. Acad. Sci. U. S. A.* **109**, 4357–4364 (2012).
250. Salio, M. *et al.* Saposins modulate human invariant Natural Killer T cells self-reactivity and facilitate lipid exchange with CD1d molecules during antigen presentation. *Proc. Natl. Acad. Sci. U. S. A.* **110**, E4753-4761 (2013).
251. de la Salle, H. *et al.* Assistance of microbial glycolipid antigen processing by CD1e. *Science* **310**, 1321–1324 (2005).
252. Garcia-Alles, L. F. *et al.* Crystal structure of human CD1e reveals a groove suited for lipid-exchange processes. *Proc. Natl. Acad. Sci. U. S. A.* **108**, 13230–13235 (2011).
253. Facciotti, F. *et al.* Fine tuning by human CD1e of lipid-specific immune responses. *Proc. Natl. Acad. Sci. U. S. A.* **108**, 14228–14233 (2011).
254. Dascher, C. C. & Brenner, M. B. Evolutionary constraints on CD1 structure: insights from comparative genomic analysis. *Trends Immunol.* **24**, 412–418 (2003).
255. Kasmar, A. G. *et al.* Cutting Edge: CD1a tetramers and dextramers identify human lipopeptide-specific T cells ex vivo. *J. Immunol. Baltim. Md 1950* **191**, 4499–4503 (2013).
256. Kasmar, A. G. *et al.* CD1b tetramers bind αβ T cell receptors to identify a mycobacterial glycolipid-reactive T cell repertoire in humans. *J. Exp. Med.* **208**, 1741–1747 (2011).
257. Ly, D. *et al.* CD1c tetramers detect ex vivo T cell responses to processed phosphomycoketide antigens. *J. Exp. Med.* **210**, 729–741 (2013).
258. Lamichhane, R. & Ussher, J. E. Expression and trafficking of MR1. *Immunology* **151**, 270–279 (2017).
259. Yamaguchi, H. & Hashimoto, K. Association of MR1 Protein, an MHC Class I-Related Molecule, with β2-Microglobulin. *Biochem. Biophys. Res. Commun.* **290**, 722–729 (2002).
260. McWilliam, H. E. G. *et al.* The intracellular pathway for the presentation of vitamin B-related antigens by the antigen-presenting molecule MR1. *Nat. Immunol.* **17**, 531–537 (2016).
261. Aldemir, H. Novel MHC class I-related molecule MR1 affects MHC class I expression in 293T cells. *Biochem. Biophys. Res. Commun.* **366**, 328–334 (2008).
262. Harriff, M. J. *et al.* Endosomal MR1 Trafficking Plays a Key Role in Presentation of Mycobacterium tuberculosis Ligands to MAIT Cells. *PLoS Pathog.* **12**, e1005524 (2016).
263. Chua, W.-J. *et al.* Endogenous MHC-related protein 1 is transiently expressed on the plasma membrane in a conformation that activates mucosal-associated invariant T cells. *J. Immunol. Baltim. Md 1950* **186**, 4744–4750 (2011).
264. Le Bourhis, L. *et al.* Antimicrobial activity of mucosal-associated invariant T cells. *Nat. Immunol.* **11**, 701–708 (2010).

265. Huang, S. *et al.* Evidence for MR1 Antigen Presentation to Mucosal-associated Invariant T Cells. *J. Biol. Chem.* **280**, 21183–21193 (2005).
266. Ljunggren, H. G. *et al.* Empty MHC class I molecules come out in the cold. *Nature* **346**, 476–480 (1990).
267. Abós, B. *et al.* Human MR1 expression on the cell surface is acid sensitive, proteasome independent and increases after culturing at 26°C. *Biochem. Biophys. Res. Commun.* **411**, 632–636 (2011).
268. Hashimoto, K., Hirai, M. & Kurosawa, Y. A gene outside the human MHC related to classical HLA class I genes. *Science* **269**, 693–695 (1995).
269. Keller, A. N., Corbett, A. J., Wubben, J. M., McCluskey, J. & Rossjohn, J. MAIT cells and MR1-antigen recognition. *Curr. Opin. Immunol.* **46**, 66–74 (2017).
270. Harriff, M. J. *et al.* MR1 displays the microbial metabolome driving selective MR1-restricted T cell receptor usage. *Sci. Immunol.* **3**, (2018).
271. Keller, A. N. *et al.* Drugs and drug-like molecules can modulate the function of mucosal-associated invariant T cells. *Nat. Immunol.* **18**, 402–411 (2017).
272. McWilliam, H. E. & Villadangos, J. A. MR1 antigen presentation to MAIT cells: new ligands, diverse pathways? *Curr. Opin. Immunol.* **52**, 108–113 (2018).
273. Meermeier, E. W. *et al.* Human TRAV1-2-negative MR1-restricted T cells detect S. pyogenes and alternatives to MAIT riboflavin-based antigens. *Nat. Commun.* **7**, 12506 (2016).
274. Gozalbo-López, B. *et al.* The MHC-related protein 1 (MR1) is expressed by a subpopulation of CD38+, IgA+ cells in the human intestinal mucosa. *Histol. Histopathol.* **24**, 1439–1449 (2009).
275. Riegert, P., Wanner, V. & Bahram, S. Genomics, isoforms, expression, and phylogeny of the MHC class I-related MR1 gene. *J. Immunol. Baltim. Md 1950* **161**, 4066–4077 (1998).
276. Ussher, J. E. *et al.* TLR signaling in human antigen-presenting cells regulates MR1-dependent activation of MAIT cells. *Eur. J. Immunol.* **46**, 1600–1614 (2016).
277. Harriff, M. J. *et al.* Human lung epithelial cells contain Mycobacterium tuberculosis in a late endosomal vacuole and are efficiently recognized by $CD8^+$ T cells. *PloS One* **9**, e97515 (2014).
278. Gold, M. C. *et al.* Human mucosal associated invariant T cells detect bacterially infected cells. *PLoS Biol.* **8**, e1000407 (2010).
279. Salerno-Goncalves, R., Rezwan, T. & Sztein, M. B. B cells modulate mucosal associated invariant T cell immune responses. *Front. Immunol.* **4**, 511 (2014).
280. Miley, M. J. *et al.* Biochemical features of the MHC-related protein 1 consistent with an immunological function. *J. Immunol. Baltim. Md 1950* **170**, 6090–6098 (2003).
281. Huang, S. *et al.* MR1 uses an endocytic pathway to activate mucosal-associated invariant T cells. *J. Exp. Med.* **205**, 1201–1211 (2008).
282. Tilloy, F. *et al.* An invariant T cell receptor alpha chain defines a novel TAP-independent major histocompatibility complex class Ib-restricted alpha/beta T cell subpopulation in mammals. *J. Exp. Med.* **189**, 1907–1921 (1999).
283. Lepore, M. *et al.* Functionally diverse human T cells recognize non-microbial antigens presented by MR1. *eLife* **6**, (2017).
284. Ling, L. *et al.* Circulating and tumor-infiltrating mucosal associated invariant T (MAIT) cells in colorectal cancer patients. *Sci. Rep.* **6**, 20358 (2016).
285. Leeansyah, E., Loh, L., Nixon, D. F. & Sandberg, J. K. Acquisition of innate-like microbial reactivity in mucosal tissues during human fetal MAIT-cell development. *Nat. Commun.* **5**, 3143 (2014).
286. Hermanson, G. T. *Bioconjugate Techniques*. (Academic Press, 2010).
287. Porcelli, S., Yockey, C. E., Brenner, M. B. & Balk, S. P. Analysis of T cell antigen receptor (TCR) expression by human peripheral blood CD4-8- alpha/beta T cells demonstrates preferential use of several V beta genes and an invariant TCR alpha chain. *J. Exp. Med.* **178**, 1–16 (1993).
288. Treiner, E. *et al.* Selection of evolutionarily conserved mucosal-associated invariant T cells by MR1. *Nature* **422**, 164–169 (2003).
289. Martin, E. *et al.* Stepwise Development of MAIT Cells in Mouse and Human. *PLoS Biol.* **7**, (2009).
290. Dusseaux, M. *et al.* Human MAIT cells are xenobiotic-resistant, tissue-targeted, CD161hi IL-17-secreting T cells. *Blood* **117**, 1250–1259 (2011).
291. Reantragoon, R. *et al.* Antigen-loaded MR1 tetramers define T cell receptor heterogeneity in mucosal-associated invariant T cells. *J. Exp. Med.* **210**, 2305–2320 (2013).

292. Eckle, S. B. G. *et al.* A molecular basis underpinning the T cell receptor heterogeneity of mucosal-associated invariant T cells. *J. Exp. Med.* **211**, 1585–1600 (2014).
293. Lepore, M. *et al.* Parallel T-cell cloning and deep sequencing of human MAIT cells reveal stable oligoclonal TCRβ repertoire. *Nat. Commun.* **5**, 3866 (2014).
294. Gherardin, N. A. *et al.* Diversity of T Cells Restricted by the MHC Class I-Related Molecule MR1 Facilitates Differential Antigen Recognition. *Immunity* **44**, 32–45 (2016).
295. Howson, L. J., Salio, M. & Cerundolo, V. MR1-Restricted Mucosal-Associated Invariant T Cells and Their Activation during Infectious Diseases. *Front. Immunol.* **6**, 303 (2015).
296. Ussher, J. E., Klenerman, P. & Willberg, C. B. Mucosal-associated invariant T-cells: new players in anti-bacterial immunity. *Microb. Immunol.* **5**, 450 (2014).
297. Tang, X.-Z. *et al.* IL-7 licenses activation of human liver intrasinusoidal mucosal-associated invariant T cells. *J. Immunol. Baltim. Md 1950* **190**, 3142–3152 (2013).
298. Schmaler, M. *et al.* Modulation of bacterial metabolism by the microenvironment controls MAIT cell stimulation. *Mucosal Immunol.* **11**, 1060–1070 (2018).
299. Gold, M. C. *et al.* MR1-restricted MAIT cells display ligand discrimination and pathogen selectivity through distinct T cell receptor usage. *J. Exp. Med.* **211**, 1601–1610 (2014).
300. Leung, D. T. *et al.* Circulating mucosal associated invariant T cells are activated in Vibrio cholerae O1 infection and associated with lipopolysaccharide antibody responses. *PLoS Negl. Trop. Dis.* **8**, e3076 (2014).
301. Le Bourhis, L. *et al.* MAIT cells detect and efficiently lyse bacterially-infected epithelial cells. *PLoS Pathog.* **9**, e1003681 (2013).
302. Salerno-Goncalves, R. *et al.* Challenge of Humans with Wild-type Salmonella enterica Serovar Typhi Elicits Changes in the Activation and Homing Characteristics of Mucosal-Associated Invariant T Cells. *Front. Immunol.* **8**, 398 (2017).
303. Howson, L. J. *et al.* MAIT cell clonal expansion and TCR repertoire shaping in human volunteers challenged with Salmonella Paratyphi A. *Nat. Commun.* **9**, 253 (2018).
304. Greene, J. M. *et al.* MR1-restricted mucosal-associated invariant T (MAIT) cells respond to mycobacterial vaccination and infection in nonhuman primates. *Mucosal Immunol.* **10**, 802–813 (2017).
305. Dias, J., Leeansyah, E. & Sandberg, J. K. Multiple layers of heterogeneity and subset diversity in human MAIT cell responses to distinct microorganisms and to innate cytokines. *Proc. Natl. Acad. Sci. U. S. A.* **114**, E5434–E5443 (2017).
306. Kurioka, A. *et al.* MAIT cells are licensed through granzyme exchange to kill bacterially sensitized targets. *Mucosal Immunol.* **8**, 429–440 (2015).
307. Salio, M. *et al.* Activation of Human Mucosal-Associated Invariant T Cells Induces CD40L-Dependent Maturation of Monocyte-Derived and Primary Dendritic Cells. *J. Immunol. Baltim. Md 1950* **199**, 2631–2638 (2017).
308. Hartmann, N. *et al.* Riboflavin Metabolism Variation among Clinical Isolates of Streptococcus pneumoniae Results in Differential Activation of Mucosal-associated Invariant T Cells. *Am. J. Respir. Cell Mol. Biol.* **58**, 767–776 (2018).
309. Kurioka, A. *et al.* Diverse Streptococcus pneumoniae Strains Drive a Mucosal-Associated Invariant T-Cell Response Through Major Histocompatibility Complex class I-Related Molecule-Dependent and Cytokine-Driven Pathways. *J. Infect. Dis.* **217**, 988–999 (2018).
310. Smith, D. J., Hill, G. R., Bell, S. C. & Reid, D. W. Reduced mucosal associated invariant T-cells are associated with increased disease severity and Pseudomonas aeruginosa infection in cystic fibrosis. *PloS One* **9**, e109891 (2014).
311. Booth, J. S. *et al.* Mucosal-Associated Invariant T Cells in the Human Gastric Mucosa and Blood: Role in Helicobacter pylori Infection. *Front. Immunol.* **6**, 466 (2015).
312. Grimaldi, D. *et al.* Specific MAIT cell behaviour among innate-like T lymphocytes in critically ill patients with severe infections. *Intensive Care Med.* **40**, 192–201 (2014).
313. Spaan, M. *et al.* Frequencies of Circulating MAIT Cells Are Diminished in Chronic HCV, HIV and HCV/HIV Co-Infection and Do Not Recover during Therapy. *PloS One* **11**, e0159243 (2016).
314. Cosgrove, C. *et al.* Early and nonreversible decrease of CD161++ /MAIT cells in HIV infection. *Blood* **121**, 951–961 (2013).
315. van Wilgenburg, B. *et al.* MAIT cells are activated during human viral infections. *Nat. Commun.* **7**, 11653 (2016).
316. Liuzzi, A. R. *et al.* Unconventional Human T Cells Accumulate at the Site of Infection in Response to Microbial Ligands and Induce Local Tissue Remodeling. *J. Immunol. Baltim. Md 1950* **197**, 2195–2207 (2016).

317. Jiang, J. *et al.* Mucosal-associated invariant T-cell function is modulated by programmed death-1 signaling in patients with active tuberculosis. *Am. J. Respir. Crit. Care Med.* **190**, 329–339 (2014).
318. Georgel, P., Radosavljevic, M., Macquin, C. & Bahram, S. The non-conventional MHC class I MR1 molecule controls infection by Klebsiella pneumoniae in mice. *Mol. Immunol.* **48**, 769–775 (2011).
319. Meierovics, A., Yankelevich, W.-J. C. & Cowley, S. C. MAIT cells are critical for optimal mucosal immune responses during in vivo pulmonary bacterial infection. *Proc. Natl. Acad. Sci. U. S. A.* **110**, E3119-3128 (2013).
320. Chen, Z. *et al.* Mucosal-associated invariant T-cell activation and accumulation after in vivo infection depends on microbial riboflavin synthesis and co-stimulatory signals. *Mucosal Immunol.* **10**, 58–68 (2017).
321. Wang, H. *et al.* MAIT cells protect against pulmonary Legionella longbeachae infection. *Nat. Commun.* **9**, 3350 (2018).
322. Meierovics, A. I. & Cowley, S. C. MAIT cells promote inflammatory monocyte differentiation into dendritic cells during pulmonary intracellular infection. *J. Exp. Med.* **213**, 2793–2809 (2016).
323. D'Souza, C. *et al.* Mucosal-Associated Invariant T Cells Augment Immunopathology and Gastritis in Chronic Helicobacter pylori Infection. *J. Immunol. Baltim. Md 1950* **200**, 1901–1916 (2018).
324. Lek, M. *et al.* Analysis of protein-coding genetic variation in 60,706 humans. *Nature* **536**, 285–291 (2016).
325. Seshadri, C. *et al.* A polymorphism in human MR1 is associated with mRNA expression and susceptibility to tuberculosis. *Genes Immun.* **18**, 8–14 (2017).
326. Koay, H.-F. *et al.* A three-stage intrathymic development pathway for the mucosal-associated invariant T cell lineage. *Nat. Immunol.* **17**, 1300–1311 (2016).
327. Pincikova, T. *et al.* Severely Impaired Control of Bacterial Infections in a Patient With Cystic Fibrosis Defective in Mucosal-Associated Invariant T Cells. *Chest* **153**, e93–e96 (2018).
328. Haeryfar, S. M. M., Shaler, C. R. & Rudak, P. T. Mucosa-associated invariant T cells in malignancies: a faithful friend or formidable foe? *Cancer Immunol. Immunother. CII* (2018). doi:10.1007/s00262-018-2132-1
329. Rudak, P. T., Choi, J. & Haeryfar, S. M. M. MAIT cell-mediated cytotoxicity: Roles in host defense and therapeutic potentials in infectious diseases and cancer. *J. Leukoc. Biol.* **104**, 473–486 (2018).
330. Peterfalvi, A. *et al.* Invariant Valpha7.2-Jalpha33 TCR is expressed in human kidney and brain tumors indicating infiltration by mucosal-associated invariant T (MAIT) cells. *Int. Immunol.* **20**, 1517–1525 (2008).
331. Won, E. J. *et al.* Clinical relevance of circulating mucosal-associated invariant T cell levels and their anti-cancer activity in patients with mucosal-associated cancer. *Oncotarget* **7**, 76274–76290 (2016).
332. Willing, A. *et al.* $CD8^+$ MAIT cells infiltrate into the CNS and alterations in their blood frequencies correlate with IL-18 serum levels in multiple sclerosis. *Eur. J. Immunol.* **44**, 3119–3128 (2014).
333. Salou, M. *et al.* Neuropathologic, phenotypic and functional analyses of Mucosal Associated Invariant T cells in Multiple Sclerosis. *Clin. Immunol. Orlando Fla* **166**–**167**, 1–11 (2016).
334. Treiner, E. & Liblau, R. S. Mucosal-Associated Invariant T Cells in Multiple Sclerosis: The Jury is Still Out. *Front. Immunol.* **6**, 503 (2015).
335. Chiba, A., Murayama, G. & Miyake, S. Mucosal-Associated Invariant T Cells in Autoimmune Diseases. *Front. Immunol.* **9**, 1333 (2018).
336. Chiba, A. *et al.* Activation status of mucosal-associated invariant T cells reflects disease activity and pathology of systemic lupus erythematosus. *Arthritis Res. Ther.* **19**, 58 (2017).
337. Rouxel, O. *et al.* Cytotoxic and regulatory roles of mucosal-associated invariant T cells in type 1 diabetes. *Nat. Immunol.* **18**, 1321–1331 (2017).
338. Ussher, J. E., Willberg, C. B. & Klenerman, P. MAIT cells and viruses. *Immunol. Cell Biol.* **96**, 630–641 (2018).
339. Loh, L. *et al.* Human mucosal-associated invariant T cells contribute to antiviral influenza immunity via IL-18-dependent activation. *Proc. Natl. Acad. Sci. U. S. A.* **113**, 10133–10138 (2016).

340. Traunecker, A., Oliveri, F. & Karjalainen, K. Myeloma based expression system for production of large mammalian proteins. *Trends Biotechnol.* **9**, 109–113 (1991).
341. Palmowski, M. J. *et al.* Intravenous injection of a lentiviral vector encoding NY-ESO-1 induces an effective CTL response. *J. Immunol. Baltim. Md 1950* **172**, 1582–1587 (2004).
342. Demaison, C. *et al.* High-level transduction and gene expression in hematopoietic repopulating cells using a human immunodeficiency [correction of imunodeficiency] virus type 1-based lentiviral vector containing an internal spleen focus forming virus promoter. *Hum. Gene Ther.* **13**, 803–813 (2002).
343. Blomen, V. A. *et al.* Gene essentiality and synthetic lethality in haploid human cells. *Science* **350**, 1092–1096 (2015).
344. Brockmann, M. *et al.* Genetic wiring maps of single-cell protein states reveal an off-switch for GPCR signalling. *Nature* **546**, 307–311 (2017).
345. Loregger, A. *et al.* Haploid Mammalian Genetic Screen Identifies UBXD8 as a Key Determinant of HMGCR Degradation and Cholesterol Biosynthesis. *Arterioscler. Thromb. Vasc. Biol.* **37**, 2064–2074 (2017).
346. Carette, J. E. *et al.* Haploid genetic screens in human cells identify host factors used by pathogens. *Science* **326**, 1231–1235 (2009).
347. Langmead, B., Trapnell, C., Pop, M. & Salzberg, S. L. Ultrafast and memory-efficient alignment of short DNA sequences to the human genome. *Genome Biol.* **10**, R25 (2009).
348. Quinlan, A. R. & Hall, I. M. BEDTools: a flexible suite of utilities for comparing genomic features. *Bioinforma. Oxf. Engl.* **26**, 841–842 (2010).
349. Stelzer, G. *et al.* The GeneCards Suite: From Gene Data Mining to Disease Genome Sequence Analyses. *Curr. Protoc. Bioinforma.* **54**, 1.30.1-1.30.33 (2016).
350. Bateman, A. *et al.* UniProt: the universal protein knowledgebase. *Nucleic Acids Res.* **45**, D158–D169 (2017).
351. OMIM. Online Mendelian Inheritance in Man, OMIM®. McKusick-Nathans Institute of Genetic Medicine, Johns Hopkins University (Baltimore, MD). Accessed throughout April 2017. URL: https://omim.org/.
352. Ashburner, M. *et al.* Gene ontology: tool for the unification of biology. The Gene Ontology Consortium. *Nat. Genet.* **25**, 25–29 (2000).
353. The Gene Ontology Consortium. The Gene Ontology Resource: 20 years and still GOing strong. *Nucleic Acids Res.* **47**, D330–D338 (2019).
354. Uhlén, M. *et al.* A human protein atlas for normal and cancer tissues based on antibody proteomics. *Mol. Cell. Proteomics MCP* **4**, 1920–1932 (2005).
355. Szklarczyk, D. *et al.* STRING v10: protein-protein interaction networks, integrated over the tree of life. *Nucleic Acids Res.* **43**, D447-452 (2015).
356. Wang, T. *et al.* Identification and characterization of essential genes in the human genome. *Science* **350**, 1096–1101 (2015).
357. Ezkurdia, I. *et al.* Multiple evidence strands suggest that there may be as few as 19 000 human protein-coding genes. *Hum. Mol. Genet.* **23**, 5866–5878 (2014).
358. Han, K. *et al.* Regulated RalBP1 Binding to RalA and PSD-95 Controls AMPA Receptor Endocytosis and LTD. *PLoS Biol.* **7**, e1000187 (2009).
359. Zheng, M. *et al.* Agonist-induced changes in RalA activities allows the prediction of the endocytosis of G protein-coupled receptors. *Biochim. Biophys. Acta* **1863**, 77–90 (2016).
360. Corrotte, M. *et al.* Ral Isoforms Are Implicated in FcγR-Mediated Phagocytosis: Activation of Phospholipase D by RalA. *J. Immunol.* **185**, 2942–2950 (2010).
361. Martin, T. D. *et al.* Ral and Rheb GTPase activating proteins integrate mTOR and GTPase signaling in aging, autophagy, and tumor cell invasion. *Mol. Cell* **53**, 209–220 (2014).
362. Paul, P. *et al.* A Genome-wide Multidimensional RNAi Screen Reveals Pathways Controlling MHC Class II Antigen Presentation. *Cell* **145**, 268–283 (2011).
363. Cohen, Y. *et al.* The yeast p5 type ATPase, spf1, regulates manganese transport into the endoplasmic reticulum. *PloS One* **8**, e85519 (2013).
364. Parra-Cuadrado, J. F., Gómez del Moral, M., García-Pavía, P., Setién, F. & Martínez-Naves, E. Characterization of the MHC class I-related MR1 locus in nonhuman primates. *Immunogenetics* **53**, 643–648 (2001).
365. Moffat, J. M., Mintern, J. D. & Villadangos, J. A. Control of MHC II antigen presentation by ubiquitination. *Curr. Opin. Immunol.* **25**, 109–114 (2013).
366. Cho, K.-J., Walseng, E., Ishido, S. & Roche, P. A. Ubiquitination by March-I prevents MHC class II recycling and promotes MHC class II turnover in antigen-presenting cells. *Proc. Natl. Acad. Sci. U. S. A.* **112**, 10449–10454 (2015).

367. Cadwell, K. & Coscoy, L. Ubiquitination on nonlysine residues by a viral E3 ubiquitin ligase. *Science* **309**, 127–130 (2005).
368. Helenius, A. & Aebi, M. Roles of N-linked glycans in the endoplasmic reticulum. *Annu. Rev. Biochem.* **73**, 1019–1049 (2004).
369. Ellgaard, L., McCaul, N., Chatsisvili, A. & Braakman, I. Co- and Post-Translational Protein Folding in the ER. *Traffic* **17**, 615–638 (2016).
370. Paduraru, C. *et al.* An N-linked glycan modulates the interaction between the CD1d heavy chain and beta 2-microglobulin. *J. Biol. Chem.* **281**, 40369–40378 (2006).
371. Grinna, L. S. & Robbins, P. W. Glycoprotein biosynthesis. Rat liver microsomal glucosidases which process oligosaccharides. *J. Biol. Chem.* **254**, 8814–8818 (1979).
372. Grinna, L. S. & Robbins, P. W. Substrate specificities of rat liver microsomal glucosidases which process glycoproteins. *J. Biol. Chem.* **255**, 2255–2258 (1980).
373. Totani, K., Ihara, Y., Matsuo, I. & Ito, Y. Substrate specificity analysis of endoplasmic reticulum glucosidase II using synthetic high mannose-type glycans. *J. Biol. Chem.* **281**, 31502–31508 (2006).
374. Cresswell, P., Bangia, N., Dick, T. & Diedrich, G. The nature of the MHC class I peptide loading complex. *Immunol. Rev.* **172**, 21–28 (1999).
375. Mentrup, T., Fluhrer, R. & Schröder, B. Latest emerging functions of SPP/SPPL intramembrane proteases. *Eur. J. Cell Biol.* **96**, 372–382 (2017).
376. Chen, Y. *et al.* Rab10 and myosin-Va mediate insulin-stimulated GLUT4 storage vesicle translocation in adipocytes. *J Cell Biol* **198**, 545–560 (2012).
377. Babbey, C. M. *et al.* Rab10 Regulates Membrane Transport through Early Endosomes of Polarized Madin-Darby Canine Kidney Cells. *Mol. Biol. Cell* **17**, 3156–3175 (2006).
378. Chen, C. C.-H. *et al.* RAB-10 Is Required for Endocytic Recycling in the Caenorhabditis elegans Intestine. *Mol. Biol. Cell* **17**, 1286–1297 (2006).
379. Schuck, S. *et al.* Rab10 is Involved in Basolateral Transport in Polarized Madin–Darby Canine Kidney Cells. *Traffic* **8**, 47–60 (2007).
380. Burd, C. & Cullen, P. J. Retromer: A Master Conductor of Endosome Sorting. *Cold Spring Harb. Perspect. Biol.* **6**, a016774 (2014).
381. Gomez, T. S. & Billadeau, D. D. A FAM21-Containing WASH Complex Regulates Retromer-Dependent Sorting. *Dev. Cell* **17**, 699–711 (2009).
382. Linardopoulou, E. V. *et al.* Human Subtelomeric WASH Genes Encode a New Subclass of the WASP Family. *PLoS Genet.* **3**, (2007).
383. McNally, K. E. *et al.* Retriever is a multiprotein complex for retromer-independent endosomal cargo recycling. *Nat. Cell Biol.* **19**, 1214–1225 (2017).
384. Heo, I. *et al.* TUT4 in Concert with Lin28 Suppresses MicroRNA Biogenesis through Pre-MicroRNA Uridylation. *Cell* **138**, 696–708 (2009).
385. Pedram, P., Zhai, G., Gulliver, W., Zhang, H. & Sun, G. Two novel candidate genes identified in adults from the Newfoundland population with addictive tendencies towards food. *Appetite* **115**, 71–79 (2017).
386. Wang, K.-S., Liu, X., Zhang, Q. & Zeng, M. ANAPC1 and SLCO3A1 are associated with nicotine dependence: meta-analysis of genome-wide association studies. *Drug Alcohol Depend.* **124**, 325–332 (2012).
387. Tydell, C. C. *et al.* Molecular Dissection of Prethymic Progenitor Entry into the T Lymphocyte Developmental Pathway. *J. Immunol.* **179**, 421–438 (2007).
388. Silva, A. F. A. da *et al.* Trisomy 21 Alters DNA Methylation in Parent-of-Origin-Dependent and -Independent Manners. *PLOS ONE* **11**, e0154108 (2016).
389. Sbrissa, D. *et al.* A mammalian ortholog of Saccharomyces cerevisiae Vac14 that associates with and up-regulates PIKfyve phosphoinositide 5-kinase activity. *Mol. Cell. Biol.* **24**, 10437–10447 (2004).
390. Ikonomov, O. C., Sbrissa, D., Foti, M., Carpentier, J.-L. & Shisheva, A. PIKfyve Controls Fluid Phase Endocytosis but Not Recycling/Degradation of Endocytosed Receptors or Sorting of Procathepsin D by Regulating Multivesicular Body Morphogenesis. *Mol. Biol. Cell* **14**, 4581–4591 (2003).
391. Schultheis, P. J. *et al.* Characterization of the P5 subfamily of P-type transport ATPases in mice. *Biochem. Biophys. Res. Commun.* **323**, 731–738 (2004).
392. Cronin, S. R., Rao, R. & Hampton, R. Y. Cod1p/Spf1p is a P-type ATPase involved in ER function and Ca2+ homeostasis. *J. Cell Biol.* **157**, 1017–1028 (2002).
393. Grey, H. M. *et al.* The small subunit of HL-A antigens is beta 2-microglobulin. *J. Exp. Med.* **138**, 1608–1612 (1973).

394. Seong, R. H., Clayberger, C. A., Krensky, A. M. & Parnes, J. R. Rescue of Daudi cell HLA expression by transfection of the mouse beta 2-microglobulin gene. *J. Exp. Med.* **167**, 288–299 (1988).
395. Kwasnicka-Crawford, D. A. *et al.* Characterization of a novel cation transporter ATPase gene (ATP13A4) interrupted by 3q25–q29 inversion in an individual with language delay. *Genomics* **86**, 182–194 (2005).
396. Kühlbrandt, W. Biology, structure and mechanism of P-type ATPases. *Nat. Rev. Mol. Cell Biol.* **5**, 282–295 (2004).
397. Suzuki, C. Immunochemical and mutational analyses of P-type ATPase Spf1p involved in the yeast secretory pathway. *Biosci. Biotechnol. Biochem.* **65**, 2405–2411 (2001).
398. Suzuki, C. & Shimma, Y. I. P-type ATPase spf1 mutants show a novel resistance mechanism for the killer toxin SMKT. *Mol. Microbiol.* **32**, 813–823 (1999).
399. Park, J.-S., Blair, N. F. & Sue, C. M. The role of ATP13A2 in Parkinson's disease: Clinical phenotypes and molecular mechanisms. *Mov. Disord. Off. J. Mov. Disord. Soc.* **30**, 770–779 (2015).
400. Madan, M. *et al.* ATP13A3 and caveolin-1 as potential biomarkers for difluoromethylornithine-based therapies in pancreatic cancers. *Am. J. Cancer Res.* **6**, 1231–1252 (2016).
401. van Beek, N. *et al.* A family with atypical Hailey Hailey disease--is there more to the underlying genetics than ATP2C1? *PloS One* **10**, e0121253 (2015).
402. Vallipuram, J., Grenville, J. & Crawford, D. A. The E646D-ATP13A4 mutation associated with autism reveals a defect in calcium regulation. *Cell. Mol. Neurobiol.* **30**, 233–246 (2010).
403. Kleijmeer, M. J. *et al.* Location of MHC-encoded transporters in the endoplasmic reticulum and cis-Golgi. *Nature* **357**, 342–344 (1992).
404. Kelly, A. *et al.* Assembly and function of the two ABC transporter proteins encoded in the human major histocompatibility complex. *Nature* **355**, 641–644 (1992).
405. Spies, T. *et al.* Presentation of viral antigen by MHC class I molecules is dependent on a putative peptide transporter heterodimer. *Nature* **355**, 644–646 (1992).
406. Attaya, M. *et al.* Ham-2 corrects the class I antigen-processing defect in RMA-S cells. *Nature* **355**, 647–649 (1992).
407. Cronin, S. R., Khoury, A., Ferry, D. K. & Hampton, R. Y. Regulation of Hmg-Coa Reductase Degradation Requires the P-Type Atpase Cod1p/Spf1p. *J. Cell Biol.* **148**, 915–924 (2000).
408. Vashist, S., Frank, C. G., Jakob, C. A. & Ng, D. T. W. Two distinctly localized p-type ATPases collaborate to maintain organelle homeostasis required for glycoprotein processing and quality control. *Mol. Biol. Cell* **13**, 3955–3966 (2002).
409. Jonikas, M. C. *et al.* Comprehensive characterization of genes required for protein folding in the endoplasmic reticulum. *Science* **323**, 1693–1697 (2009).
410. Wang, C. *et al.* Manganese Increases the Sensitivity of the cGAS-STING Pathway for Double-Stranded DNA and Is Required for the Host Defense against DNA Viruses. *Immunity* **48**, 675-687.e7 (2018).
411. Tsuchiya, S. *et al.* Establishment and characterization of a human acute monocytic leukemia cell line (THP-1). *Int. J. Cancer* **26**, 171–176 (1980).
412. Laugel, B. *et al.* Engineering of Isogenic Cells Deficient for MR1 with a CRISPR/Cas9 Lentiviral System: Tools To Study Microbial Antigen Processing and Presentation to Human MR1-Restricted T Cells. *J. Immunol. Baltim. Md 1950* **197**, 971–982 (2016).
413. Mak, J. Y. W. *et al.* Stabilizing short-lived Schiff base derivatives of 5-aminouracils that activate mucosal-associated invariant T cells. *Nat. Commun.* **8**, 14599 (2017).
414. Pinello, L. *et al.* Analyzing CRISPR genome-editing experiments with CRISPResso. *Nature Biotechnology* (2016). doi:10.1038/nbt.3583
415. Maley, F., Trimble, R. B., Tarentino, A. L. & Plummer, T. H. Characterization of glycoproteins and their associated oligosaccharides through the use of endoglycosidases. *Anal. Biochem.* **180**, 195–204 (1989).
416. Freeze, H. H. & Kranz, C. Endoglycosidase and Glycoamidase Release of N-Linked Glycans. *Curr. Protoc. Mol. Biol. Ed. Frederick M Ausubel Al* **0 17**, (2010).
417. Gauster, M., Blaschitz, A. & Dohr, G. Monoclonal antibody HC10 does not bind HLA-G. *Rheumatology* **46**, 892–893 (2007).
418. Kokame, K., Agarwala, K. L., Kato, H. & Miyata, T. Herp, a New Ubiquitin-like Membrane Protein Induced by Endoplasmic Reticulum Stress. *J. Biol. Chem.* **275**, 32846–32853 (2000).

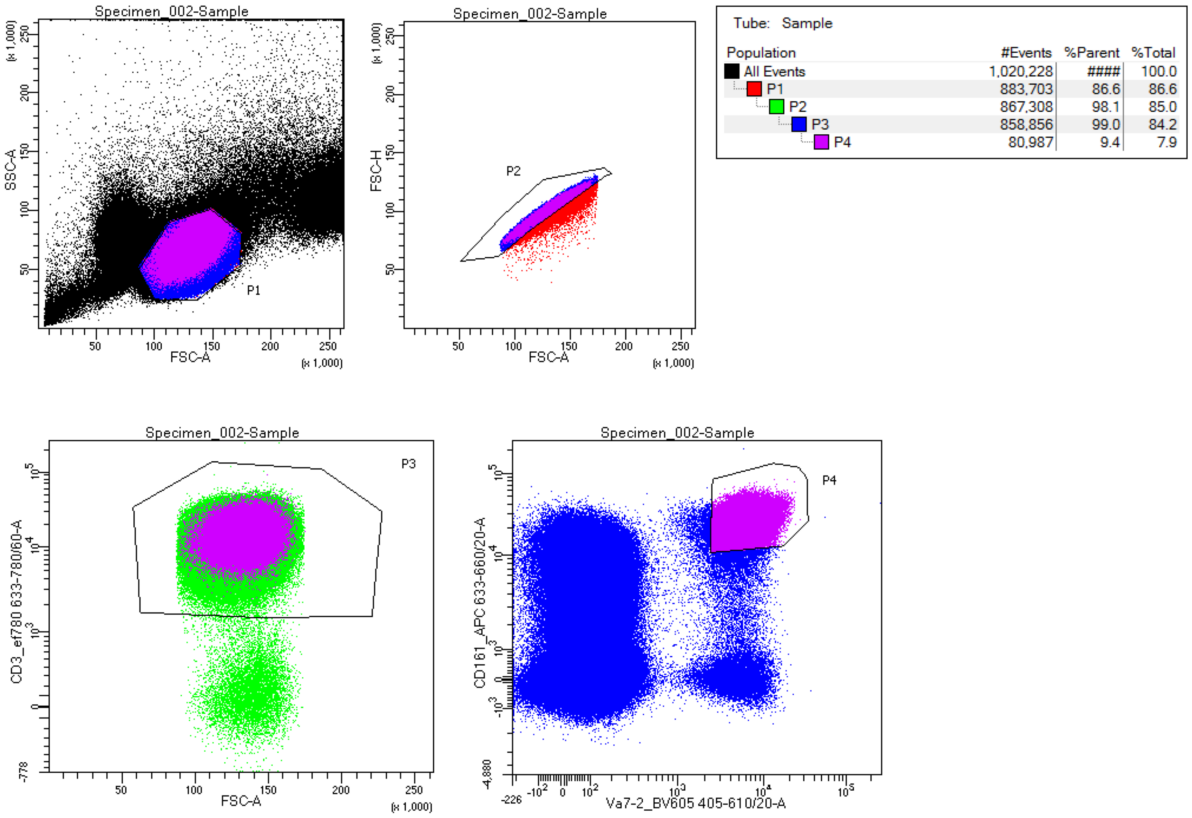
419. Huang, C.-H., Chu, Y.-R., Ye, Y. & Chen, X. Role of HERP and a HERP-related Protein in HRD1-dependent Protein Degradation at the Endoplasmic Reticulum. *J. Biol. Chem.* **289**, 4444–4454 (2014).
420. Okuda-Shimizu, Y. & Hendershot, L. M. Characterization of an ERAD Pathway for Nonglycosylated BiP Substrates, which Require Herp. *Mol. Cell* **28**, 544–554 (2007).
421. Yoshida, H., Matsui, T., Yamamoto, A., Okada, T. & Mori, K. XBP1 mRNA is induced by ATF6 and spliced by IRE1 in response to ER stress to produce a highly active transcription factor. *Cell* **107**, 881–891 (2001).
422. Calfon, M. *et al.* IRE1 couples endoplasmic reticulum load to secretory capacity by processing the XBP-1 mRNA. *Nature* **415**, 92–96 (2002).
423. Sehgal, P. *et al.* Inhibition of the sarco/endoplasmic reticulum (ER) Ca2+-ATPase by thapsigargin analogs induces cell death via ER Ca2+ depletion and the unfolded protein response. *J. Biol. Chem.* **292**, 19656–19673 (2017).
424. Lee, D. H. & Goldberg, A. L. Proteasome inhibitors: valuable new tools for cell biologists. *Trends Cell Biol.* **8**, 397–403 (1998).
425. Goldberg, A. L. Development of proteasome inhibitors as research tools and cancer drugs. *J Cell Biol* **199**, 583–588 (2012).
426. Magnaghi, P. *et al.* Covalent and allosteric inhibitors of the ATPase VCP/p97 induce cancer cell death. *Nat. Chem. Biol.* **9**, 548–556 (2013).
427. Raasi, S. & Wolf, D. H. Ubiquitin receptors and ERAD: a network of pathways to the proteasome. *Semin. Cell Dev. Biol.* **18**, 780–791 (2007).
428. Odero, M. D., Zeleznik-Le, N. J., Chinwalla, V. & Rowley, J. D. Cytogenetic and molecular analysis of the acute monocytic leukemia cell line THP-1 with an MLL-AF9 translocation. *Genes. Chromosomes Cancer* **29**, 333–338 (2000).
429. García-Rodríguez, N. *et al.* Manganese redistribution by calcium-stimulated vesicle trafficking bypasses the need for P-type ATPase function. *J. Biol. Chem.* **290**, 9335–9347 (2015).
430. Corradi, G. R., de Tezanos Pinto, F., Mazzitelli, L. R. & Adamo, H. P. Shadows of an absent partner: ATP hydrolysis and phosphoenzyme turnover of the Spf1 (sensitivity to Pichia farinosa killer toxin) P5-ATPase. *J. Biol. Chem.* **287**, 30477–30484 (2012).
431. Ho, C. *et al.* Electrospray Ionisation Mass Spectrometry: Principles and Clinical Applications. *Clin. Biochem. Rev.* **24**, 3–12 (2003).
432. Hofer, A. M. & Machen, T. E. Technique for in situ measurement of calcium in intracellular inositol 1,4,5-trisphosphate-sensitive stores using the fluorescent indicator mag-fura-2. *Proc. Natl. Acad. Sci. U. S. A.* **90**, 2598–2602 (1993).
433. Combettes, L., Cheek, T. R. & Taylor, C. W. Regulation of inositol trisphosphate receptors by luminal Ca2+ contributes to quantal Ca2+ mobilization. *EMBO J.* **15**, 2086–2093 (1996).
434. Tanimura, A. & Turner, R. J. Inositol 1,4,5-trisphosphate-dependent oscillations of luminal [Ca2+] in permeabilized HSY cells. *J. Biol. Chem.* **271**, 30904–30908 (1996).
435. Ng, D. T., Spear, E. D. & Walter, P. The unfolded protein response regulates multiple aspects of secretory and membrane protein biogenesis and endoplasmic reticulum quality control. *J. Cell Biol.* **150**, 77–88 (2000).
436. Hampton, R. Y. Genetic analysis of hydroxymethylglutaryl-coenzyme A reductase regulated degradation. *Curr. Opin. Lipidol.* **9**, 93–97 (1998).
437. Ravid, T., Doolman, R., Avner, R., Harats, D. & Roitelman, J. The ubiquitin-proteasome pathway mediates the regulated degradation of mammalian 3-hydroxy-3-methylglutaryl-coenzyme A reductase. *J. Biol. Chem.* **275**, 35840–35847 (2000).
438. Ingolia, N. T., Ghaemmaghami, S., Newman, J. R. S. & Weissman, J. S. Genome-Wide Analysis in Vivo of Translation with Nucleotide Resolution Using Ribosome Profiling. *Science* **324**, 218–223 (2009).
439. Krumpe, K. *et al.* Ergosterol content specifies targeting of tail-anchored proteins to mitochondrial outer membranes. *Mol. Biol. Cell* **23**, 3927–3935 (2012).
440. García-Rodríguez, N. *et al.* Impaired manganese metabolism causes mitotic misregulation. *J. Biol. Chem.* **287**, 18717–18729 (2012).
441. Söllner, T. *et al.* SNAP receptors implicated in vesicle targeting and fusion. *Nature* **362**, 318–324 (1993).
442. Söllner, T., Bennett, M. K., Whiteheart, S. W., Scheller, R. H. & Rothman, J. E. A protein assembly-disassembly pathway in vitro that may correspond to sequential steps of synaptic vesicle docking, activation, and fusion. *Cell* **75**, 409–418 (1993).

443. Gerst, J. E. SNAREs and SNARE regulators in membrane fusion and exocytosis. *Cell. Mol. Life Sci. CMLS* **55**, 707–734 (1999).
444. McNew, J. A. *et al.* Compartmental specificity of cellular membrane fusion encoded in SNARE proteins. *Nature* **407**, 153–159 (2000).
445. Sutton, R. B., Fasshauer, D., Jahn, R. & Brunger, A. T. Crystal structure of a SNARE complex involved in synaptic exocytosis at 2.4 A resolution. *Nature* **395**, 347–353 (1998).
446. Risselada, H. J. & Grubmüller, H. How SNARE molecules mediate membrane fusion: Recent insights from molecular simulations. *Curr. Opin. Struct. Biol.* **22**, 187–196 (2012).
447. Zhang, T., Wong, S. H., Tang, B. L., Xu, Y. & Hong, W. Morphological and functional association of Sec22b/ERS-24 with the pre-Golgi intermediate compartment. *Mol. Biol. Cell* **10**, 435–453 (1999).
448. Becker, T., Volchuk, A. & Rothman, J. E. Differential use of endoplasmic reticulum membrane for phagocytosis in J774 macrophages. *Proc. Natl. Acad. Sci. U. S. A.* **102**, 4022–4026 (2005).
449. Kagan, J. C., Stein, M.-P., Pypaert, M. & Roy, C. R. Legionella subvert the functions of Rab1 and Sec22b to create a replicative organelle. *J. Exp. Med.* **199**, 1201–1211 (2004).
450. Arasaki, K. & Roy, C. R. Legionella pneumophila promotes functional interactions between plasma membrane syntaxins and Sec22b. *Traffic Cph. Den.* **11**, 587–600 (2010).
451. Ewels, P., Magnusson, M., Lundin, S. & Käller, M. MultiQC: summarize analysis results for multiple tools and samples in a single report. *Bioinforma. Oxf. Engl.* **32**, 3047–3048 (2016).
452. Dobin, A. *et al.* STAR: ultrafast universal RNA-seq aligner. *Bioinformatics* **29**, 15–21 (2013).
453. Li, H. *et al.* The Sequence Alignment/Map format and SAMtools. *Bioinforma. Oxf. Engl.* **25**, 2078–2079 (2009).
454. Liao, Y., Smyth, G. K. & Shi, W. featureCounts: an efficient general purpose program for assigning sequence reads to genomic features. *Bioinforma. Oxf. Engl.* **30**, 923–930 (2014).
455. Robinson, M. D., McCarthy, D. J. & Smyth, G. K. edgeR: a Bioconductor package for differential expression analysis of digital gene expression data. *Bioinforma. Oxf. Engl.* **26**, 139–140 (2010).
456. Huang, S. *et al.* MR1 antigen presentation to mucosal-associated invariant T cells was highly conserved in evolution. *Proc. Natl. Acad. Sci. U. S. A.* **106**, 8290–8295 (2009).
457. Hipp, M. M. *et al.* Processing of Human Toll-like Receptor 7 by Furin-like Proprotein Convertases Is Required for Its Accumulation and Activity in Endosomes. *Immunity* **39**, 711–721 (2013).
458. Reimand, J. *et al.* g:Profiler-a web server for functional interpretation of gene lists (2016 update). *Nucleic Acids Res.* **44**, W83-89 (2016).
459. Kurata, M. *et al.* Expression, purification, and inhibitory activities of mouse cytotoxic T-lymphocyte antigen-2alpha. *Protein Expr. Purif.* **32**, 119–125 (2003).
460. Silva-Vilches, C. *et al.* Low doses of cholera toxin and its mediator cAMP induce CTLA-2 secretion by dendritic cells to enhance regulatory T cell conversion. *PLOS ONE* **12**, e0178114 (2017).
461. Sugita, S. *et al.* Acquisition of T Regulatory Function in Cathepsin L-Inhibited T Cells by Eye-Derived CTLA-2α during Inflammatory Conditions. *J. Immunol.* **183**, 5013–5022 (2009).
462. Yoshie, O. & Matsushima, K. CCR4 and its ligands: from bench to bedside. *Int. Immunol.* **27**, 11–20 (2015).
463. Needleman, P. *et al.* Identification of an enzyme in platelet microsomes which generates thromboxane A2 from prostaglandin endoperoxides. *Nature* **261**, 558–560 (1976).
464. Tanabe, T. & Ullrich, V. Prostacyclin and thromboxane synthases. *J. Lipid Mediat. Cell Signal.* **12**, 243–255 (1995).
465. von Kügelgen, I. & Hoffmann, K. Pharmacology and structure of P2Y receptors. *Neuropharmacology* **104**, 50–61 (2016).
466. Hatsuzawa, K. *et al.* Sec22b is a negative regulator of phagocytosis in macrophages. *Mol. Biol. Cell* **20**, 4435–4443 (2009).
467. Zemmour, J., Little, A. M., Schendel, D. J. & Parham, P. The HLA-A,B 'negative' mutant cell line C1R expresses a novel HLA-B35 allele, which also has a point mutation in the translation initiation codon. *J. Immunol. Baltim. Md 1950* **148**, 1941–1948 (1992).
468. Foraker, A. B., Khantwal, C. M. & Swaan, P. W. Current perspectives on the cellular uptake and trafficking of riboflavin. *Adv. Drug Deliv. Rev.* **55**, 1467–1483 (2003).
469. Said, H. M. Intestinal absorption of water-soluble vitamins in health and disease. *Biochem. J.* **437**, 357–372 (2011).

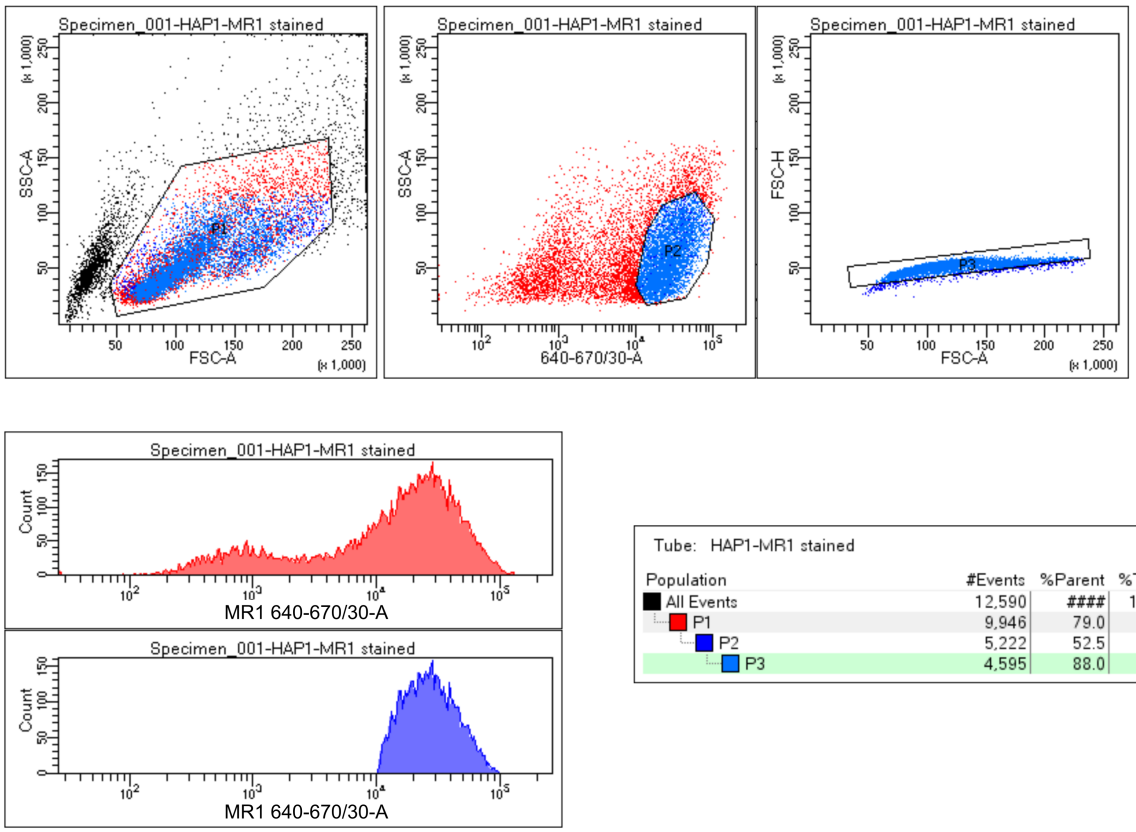
470. Barile, M., Giancaspero, T. A., Leone, P., Galluccio, M. & Indiveri, C. Riboflavin transport and metabolism in humans. *J. Inherit. Metab. Dis.* **39**, 545–557 (2016).
471. Fujimura, M. *et al.* Functional characteristics of the human ortholog of riboflavin transporter 2 and riboflavin-responsive expression of its rat ortholog in the small intestine indicate its involvement in riboflavin absorption. *J. Nutr.* **140**, 1722–1727 (2010).
472. Yonezawa, A., Masuda, S., Katsura, T. & Inui, K. Identification and functional characterization of a novel human and rat riboflavin transporter, RFT1. *Am. J. Physiol. Cell Physiol.* **295**, C632-641 (2008).
473. Yamamoto, S. *et al.* Identification and functional characterization of rat riboflavin transporter 2. *J. Biochem. (Tokyo)* **145**, 437–443 (2009).
474. Yonezawa, A. & Inui, K. Novel riboflavin transporter family RFVT/SLC52: identification, nomenclature, functional characterization and genetic diseases of RFVT/SLC52. *Mol. Aspects Med.* **34**, 693–701 (2013).
475. Yao, Y. *et al.* Identification and comparative functional characterization of a new human riboflavin transporter hRFT3 expressed in the brain. *J. Nutr.* **140**, 1220–1226 (2010).
476. Johnson, J. O. *et al.* Exome sequencing reveals riboflavin transporter mutations as a cause of motor neuron disease. *Brain J. Neurol.* **135**, 2875–2882 (2012).
477. Haack, T. B. *et al.* Impaired riboflavin transport due to missense mutations in SLC52A2 causes Brown-Vialetto-Van Laere syndrome. *J. Inherit. Metab. Dis.* **35**, 943–948 (2012).
478. Srour, M. *et al.* Mutations in riboflavin transporter present with severe sensory loss and deafness in childhood. *Muscle Nerve* **50**, 775–779 (2014).
479. Foley, A. R. *et al.* Treatable childhood neuronopathy caused by mutations in riboflavin transporter RFVT2. *Brain J. Neurol.* **137**, 44–56 (2014).
480. Guissart, C. *et al.* Genes for spinocerebellar ataxia with blindness and deafness (SCABD/SCAR3, MIM# 271250 and SCABD2). *Eur. J. Hum. Genet.* **24**, 1154–1159 (2016).
481. Babanejad, M. *et al.* SLC52A2 mutations cause SCABD2 phenotype: A second report. *Int. J. Pediatr. Otorhinolaryngol.* **104**, 195–199 (2018).
482. Menezes, M. P. *et al.* Auditory neuropathy in Brown-Vialetto-Van Laere syndrome due to riboflavin transporter RFVT2 deficiency. *Dev. Med. Child Neurol.* **58**, 848–854 (2016).
483. Menezes, M. P. *et al.* Pathophysiology of motor dysfunction in a childhood motor neuron disease caused by mutations in the riboflavin transporter. *Clin. Neurophysiol.* **127**, 911–918 (2016).
484. Jaeger, B. & Bosch, A. M. Clinical presentation and outcome of riboflavin transporter deficiency: mini review after five years of experience. *J. Inherit. Metab. Dis.* **39**, 559–564 (2016).
485. Manole, A. *et al.* Clinical, pathological and functional characterization of riboflavin-responsive neuropathy. *Brain J. Neurol.* **140**, 2820–2837 (2017).
486. Subramanian, V. S., Ghosal, A., Kapadia, R., Nabokina, S. M. & Said, H. M. Molecular Mechanisms Mediating the Adaptive Regulation of Intestinal Riboflavin Uptake Process. *PloS One* **10**, e0131698 (2015).
487. Chen, J. L. *et al.* Identification of NY-ESO-1 peptide analogues capable of improved stimulation of tumor-reactive CTL. *J. Immunol. Baltim. Md 1950* **165**, 948–955 (2000).
488. Qiu, P. *et al.* Mutation detection using Surveyor nuclease. *BioTechniques* **36**, 702–707 (2004).
489. Turtle, C. J. *et al.* Innate signals overcome acquired TCR signaling pathway regulation and govern the fate of human CD161hi CD8α+ semi-invariant T cells. *Blood* **118**, 2752–2762 (2011).
490. Patel, O. *et al.* Recognition of vitamin B metabolites by mucosal-associated invariant T cells. *Nat. Commun.* **4**, 2142 (2013).
491. Pasare, C. & Medzhitov, R. Toll-like receptors: linking innate and adaptive immunity. *Adv. Exp. Med. Biol.* **560**, 11–18 (2005).
492. Jo, J. *et al.* Toll-like receptor 8 agonist and bacteria trigger potent activation of innate immune cells in human liver. *PLoS Pathog.* **10**, e1004210 (2014).
493. Lee, E.-S. Biochemical and cellular consequences of lumiflavin-induced riboflavin depletion in human intestinal epithelial cells. (2015). Accessed Sept 14 2017. http://etheses.whiterose.ac.uk/8901/1/ Eun-Sook%20Lee_PhD%20thesis_Final%20version.pdf
494. Harris, M. R., Yu, Y. Y., Kindle, C. S., Hansen, T. H. & Solheim, J. C. Calreticulin and calnexin interact with different protein and glycan determinants during the assembly of MHC class I. *J. Immunol. Baltim. Md 1950* **160**, 5404–5409 (1998).

495. Sijts, E. J. A. M. & Kloetzel, P.-M. The role of the proteasome in the generation of MHC class I ligands and immune responses. *Cell. Mol. Life Sci.* **68**, 1491–1502 (2011).
496. Shav-Tal, Y. & Zipori, D. PSF and p54(nrb)/NonO--multi-functional nuclear proteins. *FEBS Lett.* **531**, 109–114 (2002).
497. Gingras, A. C., Raught, B. & Sonenberg, N. eIF4 initiation factors: Effectors of mRNA recruitment to ribosomes and regulators of translation. *Annu. Rev. Biochem.* **68**, 913–963 (1999).
498. Lee, E.-S., Corfe, B. M. & Powers, H. J. Riboflavin depletion of intestinal cells in vitro leads to impaired energy generation and enhanced oxidative stress. *Eur. J. Nutr.* **52**, 1513–1521 (2013).
499. McWilliam, H. E. G., Birkinshaw, R. W., Villadangos, J. A., McCluskey, J. & Rossjohn, J. MR1 presentation of vitamin B-based metabolite ligands. *Curr. Opin. Immunol.* **34**, 28–34 (2015).
500. Huang, S. N. & Swaan, P. W. Involvement of a receptor-mediated component in cellular translocation of riboflavin. *J. Pharmacol. Exp. Ther.* **294**, 117–125 (2000).
501. Zielińska-Dawidziak, M., Grajek, K., Olejnik, A., Czaczyk, K. & Grajek, W. Transport of high concentration of thiamin, riboflavin and pyridoxine across intestinal epithelial cells Caco-2. *J. Nutr. Sci. Vitaminol. (Tokyo)* **54**, 423–429 (2008).

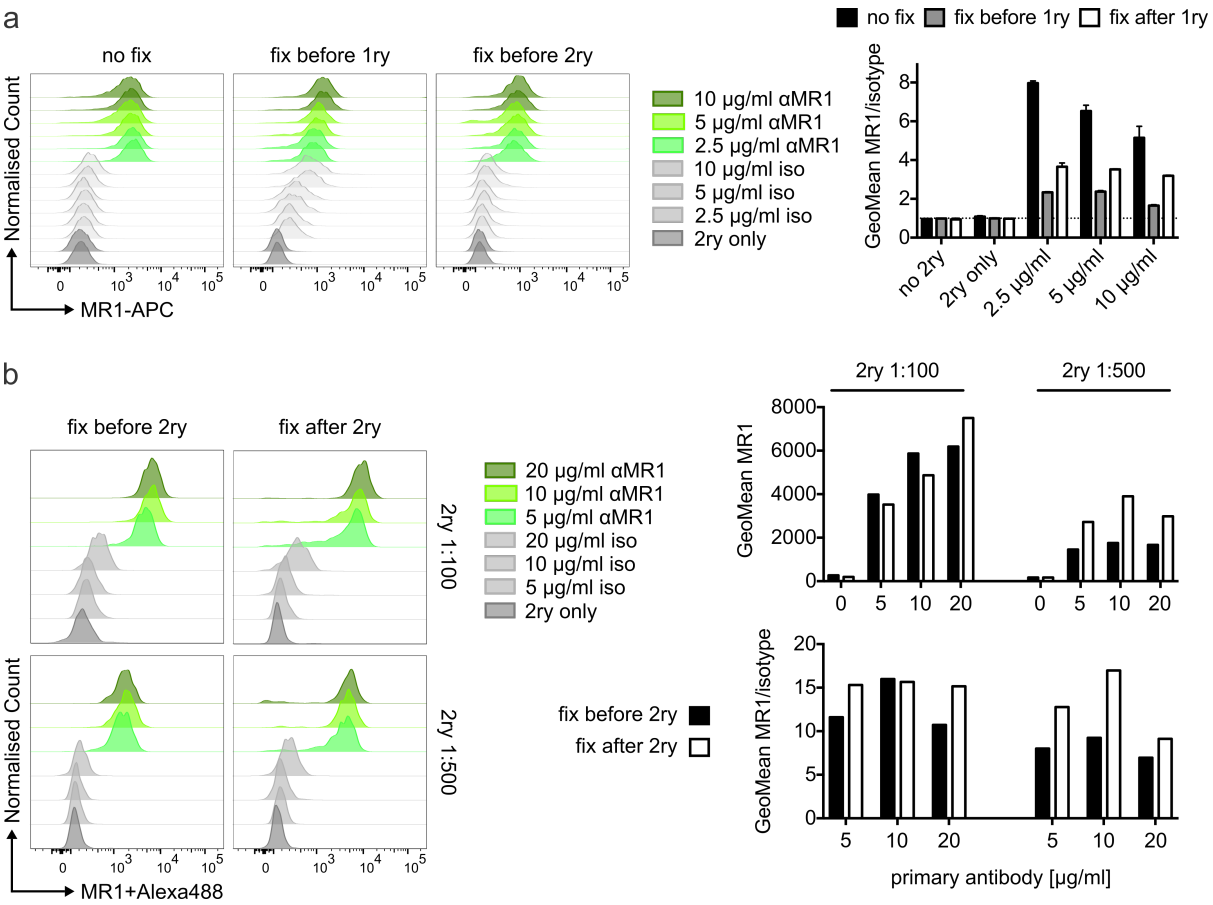
9
Supplementary Material



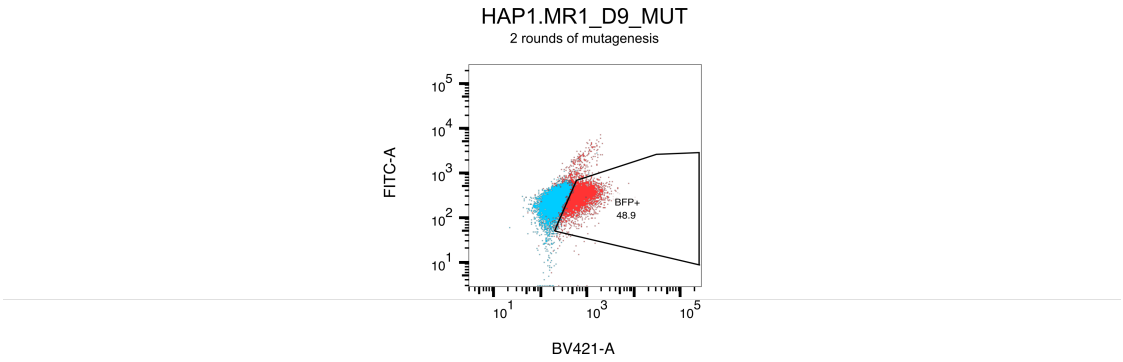
Supplementary Figure 1: Representative gating strategy for MAIT cell sorting. PBMCs were isolated from healthy blood donors, enriched for $CD2^+$ cells by MACS separation, and stained for CD3, CD161 and the Vα7.2 TCR α chain. MAIT cells were defined as CD3+ CD161high Vα7.2+ and sorted in bulk. Sorted population: P4. In all MAIT cell sorts purity was between 92 and 98%.



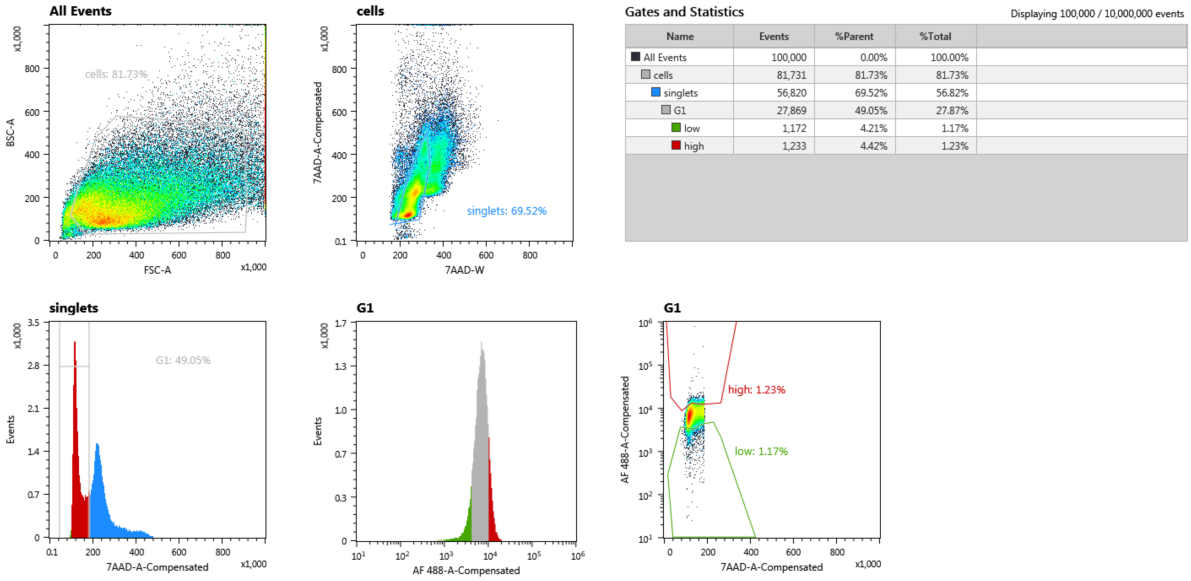
Supplementary Figure 2: Sorting strategy for HAP1 clones over-expressing MR1. HAP1 WT cells were transduced with lentiviral particles encoding the human MR1 cDNA sequence, stained for surface expression of MR1, and single cell sorted to generate HAP1.MR1 clones. Sorted population: P3.



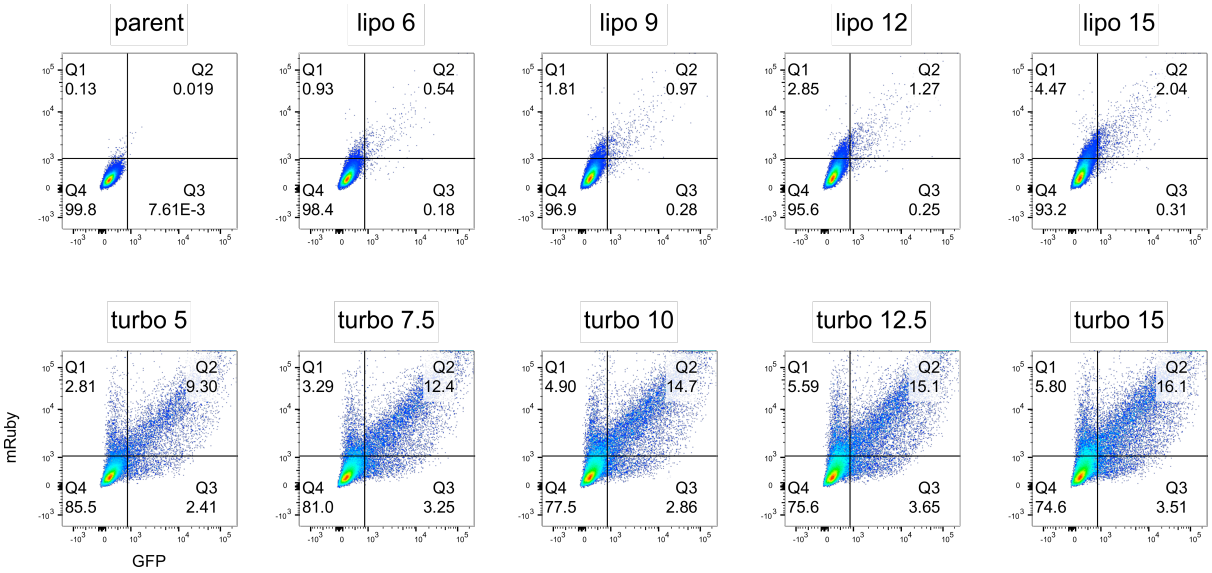
Supplementary Figure 3: Optimisation of surface staining protocol for the gene-trap screen. Mutagenised HAP1.MR1 had to be stained for surface expression of MR1 but also be fixed and permeabilised to stain for ploidy with Propidium Iodide. To determine the best staining protocol fixation at the indicated staining steps was tested in two different experiments (a,b). Different concentrations of αMR1 or isotype control primary antibodies (αMR1, iso) and secondary (2ry) antibody were also tested. Secondary antibody was used 1:500 in (a). Data in (a) are shown as median of technical duplicates with range.



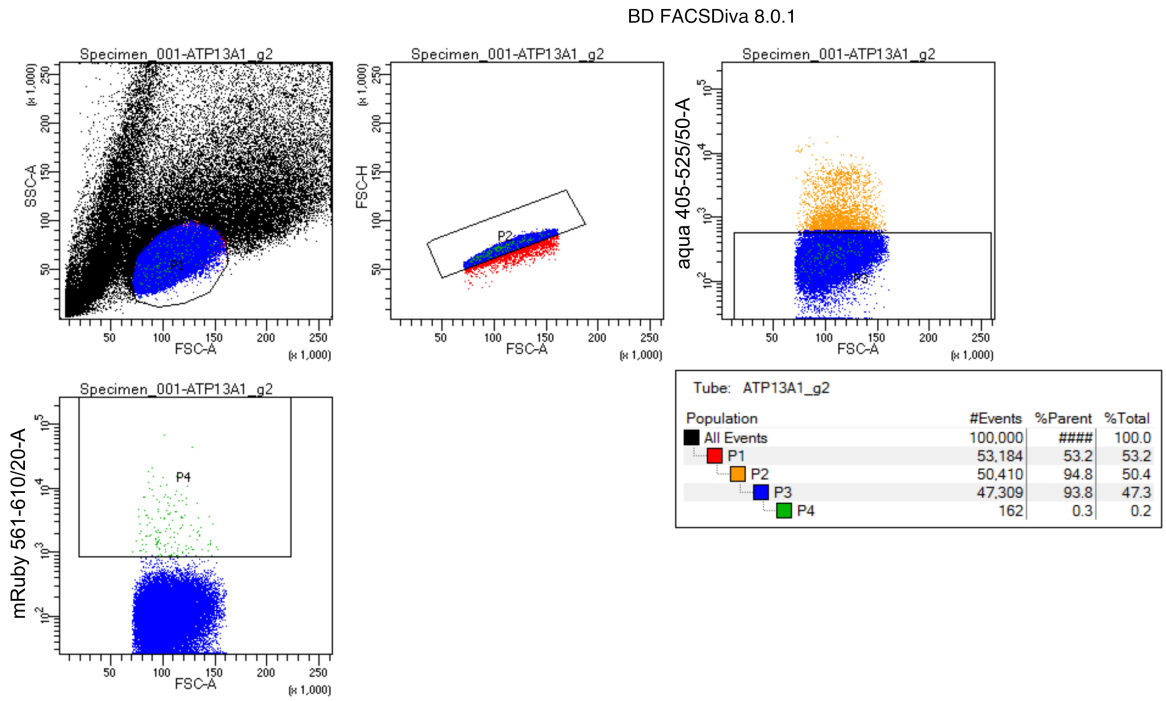
Supplementary Figure 4: Transduction efficiency of gene-trap screen. The HAP1.MR1 clone D9 was transduced with the gene-trap virus which also encodes a BFP cassette and transduction efficiency was estimated by flow cytometry after two consecutive rounds of mutagenesis. Untransduced HAP1 wild type cells are shown in blue. Figure courtesy of Erica De Zan.



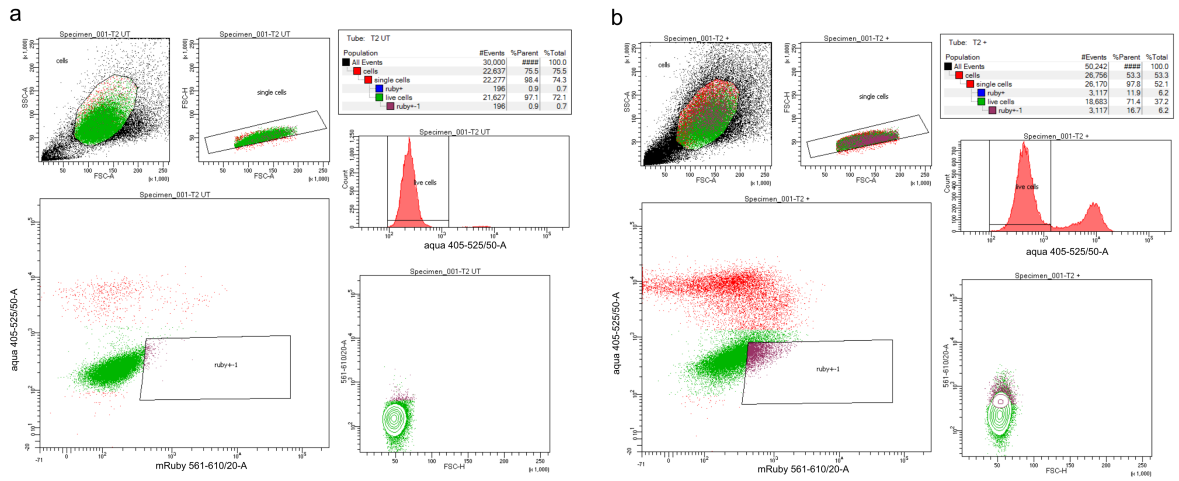
Supplementary Figure 5: Sorting strategy for gene-trap screen sort. The mutagenised HAP1.MR1 clone D9 was stained as described in Chapter 3 and sorted as shown. Gates were set on the G1 population to include only cells haploid at the time of sorting. Figure courtesy of Erica De Zan.



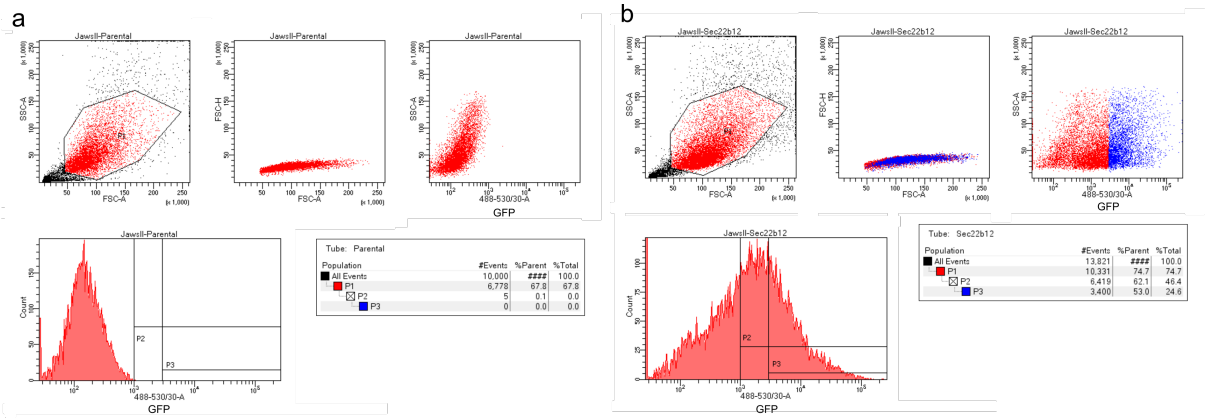
Supplementary Figure 6: Optimisation of transfection protocol for CRISPR/Cas9 plasmids. A polyclonal population of HAP1 cells over-expressing MR1 was co-transfected with 1.25 µg each of two plasmids encoding mRuby and GFP, respectively. The indicated volumes of lipofectamine (lipo) or turbofectin (turbo) were used according to the manufacturer's instructions and expression of the fluorescent proteins was assessed by flow cytometry after 48 h.



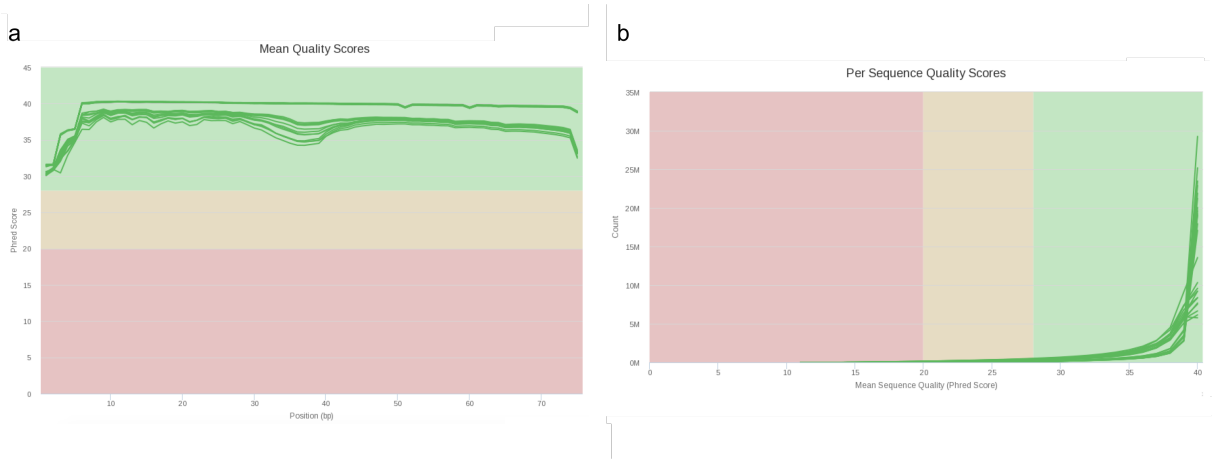
Supplementary Figure 7: Example of sorting strategy for sorting of HAP1.MR1 CRISPR/Cas9 clones. HAP1.MR1 clone D9 was transiently transfected with CRISPR/Cas9 plasmids as described in Chapter 3 and live transfected cells were single cell sorted based on mRuby expression. The gating strategy for the transfection with the single ATP13A1-targeting plasmid 1 is shown as an example. Sorted population: P4.



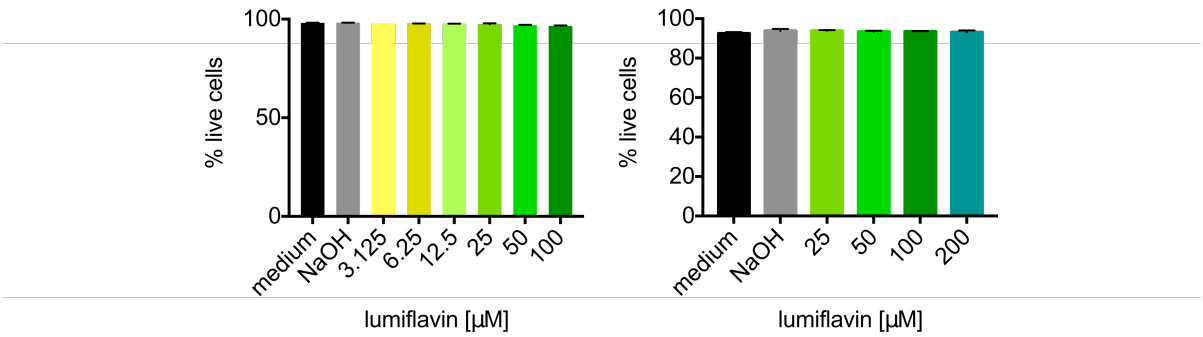
Supplementary Figure 8: Example of sorting strategy for sorting of THP-1 ATP13A1 KO clones. THP-1 and THP-1.MR1 clones were transiently co-transfected with three CRISPR/Cas9 plasmids targeting ATP13A1 as described in Chapter 4 and live transfected cells were single cell sorted based on mRuby expression. The gating strategy for the clone T2 is shown as an example in (b) with the untransfected parent clone shown in (a) for comparison. Sorted population: mRuby+ from live cells.



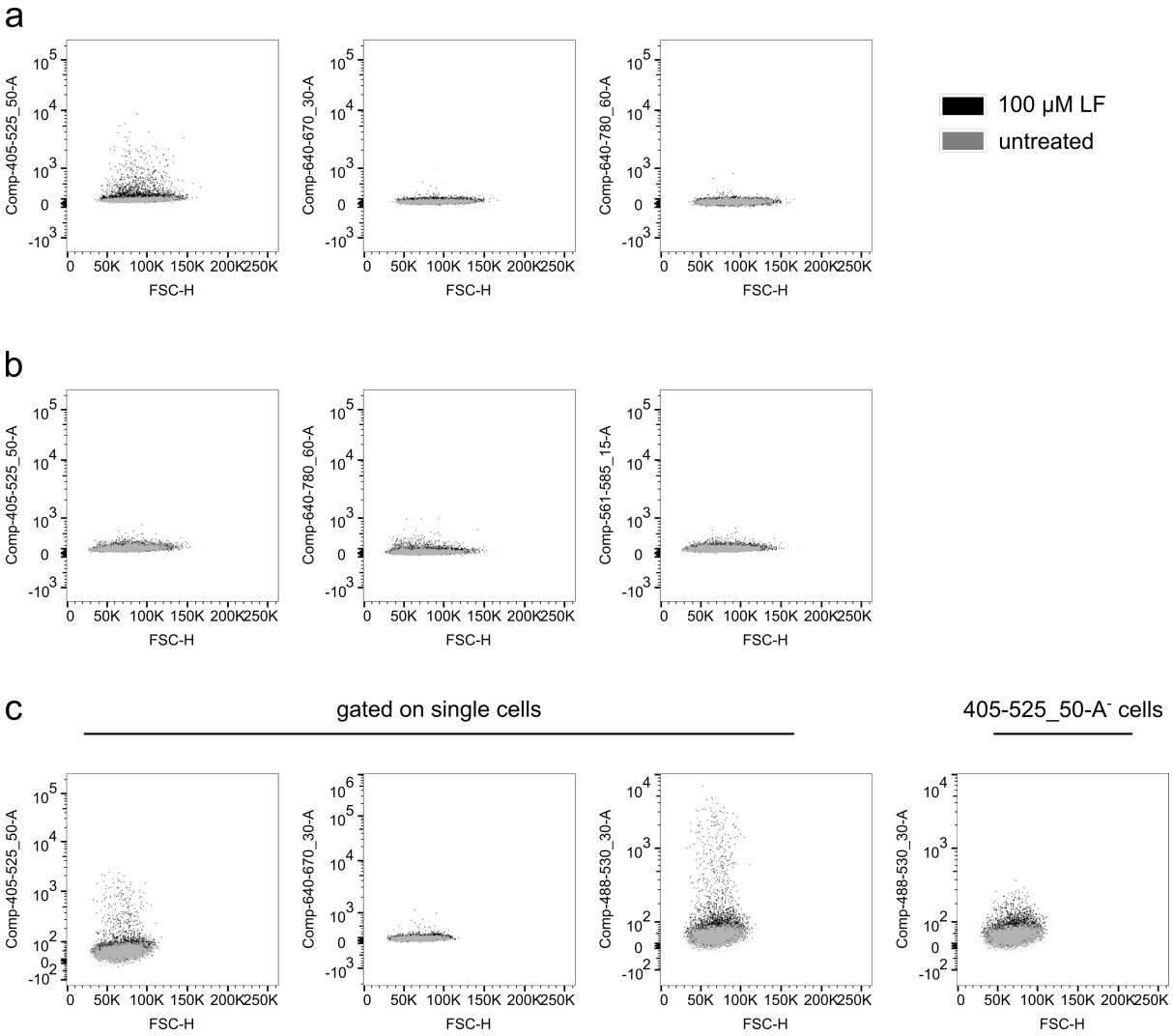
Supplementary Figure 9: Sorting strategy for JAWSII rescued cell line R-1000. JAWSII Sec22b KD cells were transduced with lentiviral particles encoding the murine Sec22b cDNA sequence and the GFP variant Emerald as described in Chapter 5 and live transduced cells were bulk sorted based on Emerald expression as shown in (b). Sorted population: P3. The untransfected parent clone shown in (a) for comparison.



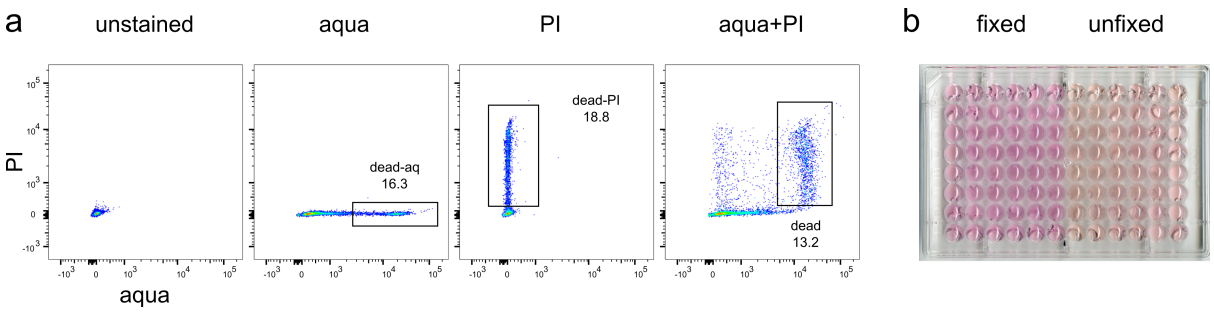
Supplementary Figure 10: Quality scores for RNASeq data. Collated mean quality scores (a) and per sequence quality scores (b) for the 12 samples submitted for RNA sequencing. Phred Scores are a measure of base calling accuracy and related to the error probability of assigning an inaccurate base. Figure was generated with MultiQC[451].



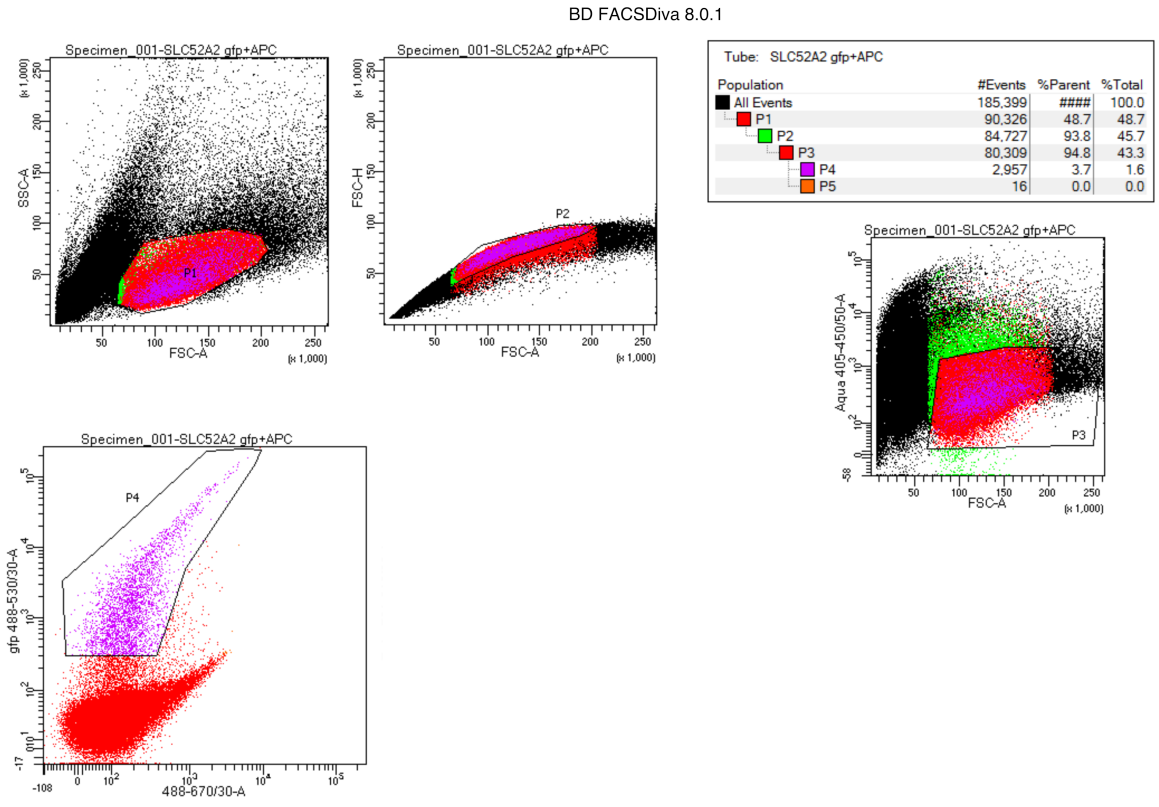
Supplementary Figure 11: Cellular toxicity of lumiflavin. THP-1.MR1 cells were treated with the indicated concentrations of lumiflavin for 5 h and viability was assessed by flow cytometry. Data are from two representative experiments (see **Figure 6.9** and **Figure 6.6**) and displayed as median of technical duplicates with range.



Supplementary Figure 12: Autofluorescence of lumiflavin. THP-1.MR1 cells were treated with 100 µM lumiflavin (LF, black) or not (grey), washed, and fluorescence in relevant flow cytometry channels was tested without staining the cells (see **Figure 6.6**c, **Figure 6.7**c, and **Figure 6.9**) . (a), (b), and (c) represent three different experiments and cells shown are gated on single cells except for the right-hand panel in (c) which was gated on cells negative for the indicated channel.



Supplementary Figure 13: Viability of THP-1.MR1 cells upon glutaraldehyde fixation. THP-1.MR1 cells were fixed as described in Chapter 6. Their viability was assessed by flow cytometry immediately after fixation (a) and visually based on changes in the coloration of the cell culture medium after 36 h. Data are from two different experiments.



Supplementary Figure 14: Sorting strategy for sorting of HAP1.MR1 SLC52A2 CRISPR/Cas9 clones. HAP1.MR1 clone D9 was transiently transfected with CRISPR/Cas9 plasmids as described in Chapter 6 and live transfected cells were single cell sorted based on GFP expression. Sorted population: P4.

Supplementary Table 1: Oligonucleotide sequences. Adapter sequences for deep sequencing belong to Illumina, Inc. Oligonucleotide sequences © 2018 Illumina, Inc. All rights reserved. Derivative works created by Illumina customers are authorized for use with Illumina instruments and products only. All other uses are strictly prohibited.

Linker for Emerald removal

CK001_XhoI5_BamHI_NotI3	TCGAGtgctagaaggcctacGGATCCGC
CK002_NotI5_BamHI_XhoI3	GGCCGCGGATCCgtaggccttctagcaC

Primers for the recovery of insertion sites

LTR sequencing primer	/doublebiotin/ggtctccaaatctcggtggaac
ssDNA linker for deep sequencing	/phospho/atcgtatgccgtcttctgcttgactcagtagttgtgcgatggattgatg/dideoxycytidine/
P5-containing adapter	AATGATACGGCGACCACCGAGATCTGATGGTTCTCTAGCTTGCC
P7-containing adapter	CAAGCAGAAGACGGCATACGA
sequencing primer	CTAGCTTGCCAAACCTAC AGGTGGGGTCTTTCA

Primers for Sec22b cloning

CK003_BamHI_Sec22b_fw	ccgGGATCCccaccatggtgctgctgacgatgatcg
CK004_XhoI_Sec22b_rev	ccgCTCGAGtcacagccaccaaaaccgcac

Primers for XBP1 splicing assay

Peter Walter XBP1 splicing fw primer	ttacgggagaaaactcacggc
Peter Walter XBP1 splicing rev primer	gggtccaacttgtccagaatgc

Plasmid sequencing

sffv1_promoterSeq_fw	TGCTTCTCGCTTCTGTTCG

CRISPR clone sequencing

CK012_ZCCHC11_fw1	ccattttcagtcaagaggaatgttgc
CK13_ZCCHC11_rev1	aagagtcctgtccgtggtcagc
CK14_ZCCHC11_fw2	taggtcatcagcagatagcagaag
CK15_ZCCHC11_rev2	ctgtaactctcagtgacatgg
CK16_ZCCHC11_fw3	ctcctcagcctcagccatttcca
CK17_ZCCHC11_rev3	ctgaattccccactgcaccactgt
CK18_ZCCHC14_fw1	aaggagcacctgccgacagt
CK19_ZCCHC14_rev1	tcagagctctccaagtgaatctcca
CK20_ZCCHC14_fw2	ttgtggaagccacagtctct
CK21_ZCCHC14_rev2	cttctccatggagagctgctt
CK22_ZCCHC14_fw3	ggtctaggatttcccagctt
CK23_ZCCHC14_rev3	gcatggctaaggactggat
CK24_ATP13A1_fw1	acttcaggaccagtggctctgaa
CK25_ATP13A1_rev1	ttcacaatgggcgtactctcgt
CK26_ATP13A1_fw2	tcccagctttaagtgtggcacca
CK27_ATP13A1_rev2	aaggacagcacctcaagcccgtcttc
CK28_ATP13A1_fw3	gtggacttgtacaaggagtttgagccaa
CK29_ATP13A1_rev3	acctgggcaatgaccagcttgaa
CK30_ATP13A1_fw4	aaggagtttgagccaagcctggtca
CK31_ATP13A1_rev4	aggagcaggacctgggcaatga
CK32_b2m_fw1	cgagactctaagaaaaggaaactg

CK33_b2m_fw2	aatataagtggaggcgtcgcg
CK34_b2m_rev1	caccaaggagaacttggagaa
CK35_b2m_fw3	ctccaaagattcaggtttactcacg
CK36_b2m_rev3	atatcagatgggatgggactc
CK37_GANAB_fw1	cgggatgtgcataacatctatggcct
CK38_GANAB_rev1	tcaaagcgcatagctgagagga
CK39_GANAB_fw2	tggtctaggaaagcctcactga
CK40_GANAB_rev2	ctgtgagactagcatattgccggaa
CK41_GANAB_fw3	ccacactgcctatttctcttaacagg
CK42_GANAB_rev3	ccaacccctgtactcacgaga
CK43_REPS1_fw1	gtgcctcttgtttctgtatcca
CK44_REPS1_rev1	ctgattgtgcttcaccaaagg
CK45_REPS1_fw2	tcctttgctgcttagccaagtg
CK46_REPS1_rev2	acaggcatgagcaaccacact
CK052_VAC14_fw1	tcatggaaacggctaggacact
CK053_VAC14_rev1	gacaaaaggggtgggatgctga
CK054_VAC14_fw2	acaaaggcctgagcaccttc
CK055_VAC14_rev2	cttgctcagcccgtcaaag
CK056_VPS29_fw1	ctgggattcgggatctcttatgagac
CK057_VPS29_rev1	acctcatcgaagtctcctctcaca
CK058_VPS29_fw2	ccagaacagaaagttgtgactgttgg
CK059_VPS29_rev2	ctcacgtttccaaggcattatatgc
CK060_GRIK2_fw1	tgcctttactttaacggcagca
CK061_GRIK2_rev1	ggataaggaatctgtgatgttcgctg
CK062_GRIK1_fw2	atgtgggcctttatgagtagcag
CK063_GRIK2_rev2	tgacatataacctacccatgggagtg
CK064_GRIK2_fw3	gacctttatctcctcttcagcctgtg
CK065_GRIK2_rev3	cagtgctgtcatcatacacaaccgtg

ATP13A1 cDNA sequencing

CK068_ATP13A1_fw8	cgtgtggctcccaagcagaa
CK069_ATP13A1_fw9	ggcagcagttgggtgcagat
CK070_ATP13A1_rev7	cctggaagcctctgttgctctgat
CK071_24illumina_fw1	ACACTCTTTCCCTACACGACGCTCTTCCGATCTacttcaggaccagtggctctgaa
CK072_25illumina_rev1	GTGACTGGAGTTCAGACGTGTGCTCTTCCGATCTttcacaatgggcgtactctcgt
CK073_26illumina_fw2	ACACTCTTTCCCTACACGACGCTCTTCCGATCTtcccagctttaagtgtggcacca
CK074_27illumina_rev2	GTGACTGGAGTTCAGACGTGTGCTCTTCCGATCTaaggacagcacctcaagcccgtcttc
CK075_28illumina_fw1	ACACTCTTTCCCTACACGACGCTCTTCCGATCTgtggacttgtacaaggagtttgagccaa
CK076_29illumina_rev3	GTGACTGGAGTTCAGACGTGTGCTCTTCCGATCTacctgggcaatgaccagcttgaa
CK077_68illumina_fw4	ACACTCTTTCCCTACACGACGCTCTTCCGATCTcgtgtggctcccaagcagaa
CK078_69illumina_fw5	ACACTCTTTCCCTACACGACGCTCTTCCGATCTggcagcagttgggtgcagat

Index D501	AGGCTATA
Index D502	GCCTCTAT
Index D503	AGGATAGG
Index D504	TCAGAGCC
Index D701	ATTACTCG
Index D702	TCCGGAGA
Index D703	CGCTCATT

SLC52A2 CRISPR sequencing

EC005_SLC52A2_fw	cccaggaaggtgggctttggcac
EC005_SLC52A2_rev	gcaggtggctcaagaagggcagg

Oligonucleotides for CRISPR/Cas9 sgRNA cloning including BbsI adapters

ATP13	guide1_sense	CACCGGGTTGTCGAGCGGCGACGG
ATP13	guide1_antisense	AAATCCGTCGCCGCTCGACAACCC
ATP13	guide2_sense	CACCGGTTGGCACCACCTTCACAA
ATP13	guide2_antisense	AAATTTGTGAAGGTGGTGCCAACC
ATP13	guide3_sense	CACCgGCAGGCTCTCCATGAAGGGC
ATP13	guide3_antisense	AAATGCCCTTCATGGAGAGCCTGCc
ZCCHC14	guide1_sense	CACCGGAGGAGCTGGAGTACTCCG
ZCCHC14	guide1_antisense	AAATCGGAGTACTCCAGCTCCTCC
ZCCHC14	guide2_sense	CACCgGCATGGGAGCAGTGAGGCAA
ZCCHC14	guide2_antisense	AAATTTGCCTCACTGCTCCCATGCc
ZCCHC14	guide3_sense	CACCgGAAGAAGCTCAAGACCCAGC
ZCCHC14	guide3_antisense	AAATGCTGGGTCTTGAGCTTCTTCc
GANAB	guide1_sense	CACCGGAGCCAGCGAAGAAGGCCC
GANAB	guide1_antisense	AAATGGGCCTTCTTCGCTGGCTCC
GANAB	guide2_sense	CACCgGAAGATGATGGACTACCTGC
GANAB	guide2_antisense	AAATGCAGGTAGTCCATCATCTTCc
GANAB	guide3_sense	CACCgGAACAGTGTGGAGTTAACCA
GANAB	guide3_antisense	AAATTGGTTAACTCCACACTGTTCc
IRF2	guide1_sense	CACCgGCATGCGGCTAGACATGGGT
IRF2	guide1_antisense	AAATACCCATGTCTAGCCGCATGCc
IRF2	guide2_sense	CACCgGACTTCTTCAATATCAGGCA
IRF2	guide2_antisense	AAATTGCCTGATATTGAAGAAGTCc
IRF2	guide3_sense	CACCgGAAGTCAGGACCGCATACTC
IRF2	guide3_antisense	AAATGAGTATGCGGTCCTGACTTCc
REPS1	guide1_sense	CACCGGCAAACTGTTGCACCGGTG
REPS1	guide1_antisense	AAATCACCGGTGCAACAGTTTGCC
REPS1	guide2_sense	CACCGGACATCAAGTTATTCCATG
REPS1	guide2_antisense	AAATCATGGAATAACTTGATGTCC
REPS1	guide3_sense	CACCgGAGATCTGCACATCCCACAC
REPS1	guide3_antisense	AAATGTGTGGGATGTGCAGATCTCc
VPS29	guide1_sense	CACCGGCAAACTGTTGCACCGGTG
VPS29	guide1_antisense	AAATCACCGGTGCAACAGTTTGCC
VPS29	guide2_sense	CACCGGACATCAAGTTATTCCATG
VPS29	guide2_antisense	AAATCATGGAATAACTTGATGTCC
VPS29	guide3_sense	CACCgGAGATCTGCACATCCCACAC
VPS29	guide3_antisense	AAATGTGTGGGATGTGCAGATCTCc
RAB10	guide1_sense	CACCGGATATCTTCAGCTAACGTG
RAB10	guide1_antisense	AAATCACGTTAGCTGAAGATATCC
RAB10	guide2_sense	CACCgGTTTATTTCAGGGATACAGC
RAB10	guide2_antisense	AAATGCTGTATCCCTGAAATAAACc
RAB10	guide3_sense	CACCgGATGGTGTGAAATCGCTCC
RAB10	guide3_antisense	AAATGGAGCGATTTCACACCATCc
B2M	guide1_sense	CACCGGCCGAGATGTCTCGCTCCG

B2M	guide1_antisense	AAATCGGAGCGAGACATCTCGGCC
B2M	guide2_sense	CACCgGAGTAGCGCGAGCACAGCTA
B2M	guide2_antisense	AAATTAGCTGTGCTCGCGCTACTCc
B2M	guide3_sense	CACCGGGCTGTGACAAAGTCACA
B2M	guide3_antisense	AAATTGTGACTTTGTCACAGCCC
RALGAPB	guide1_sense	CACCGGAGGGGCAACAAAGAAAGC
RALGAPB	guide1_antisense	AAATGCTTTCTTTGTTGCCCCTCC
RALGAPB	guide2_sense	CACCGGTATTAGTTCAGCAAGTGG
RALGAPB	guide2_antisense	AAATCCACTTGCTGAACTAATACC
RALGAPB	guide3_sense	CACCgGAAAACAGCCAAGGAGATGG
RALGAPB	guide3_antisense	AAATCCATCTCCTTGGCTGTTTTCc
VAC14	guide1_sense	CACCGGAGCATGAGCAGGCCGTAG
VAC14	guide1_antisense	AAATCTACGGCCTGCTCATGCTCC
VAC14	guide2_sense	CACCGGTCTGCAGCAGCTCAGGGT
VAC14	guide2_antisense	AAATACCCTGAGCTGCTGCAGACC
VAC14	guide3_sense	CACCGGACTCAGGGCTCTACCTGA
VAC14	guide3_antisense	AAATTCAGGTAGAGCCCTGAGTCC
GRIK2	guide1_sense	CACCGGAACGTGGGATCCAGCCAG
GRIK2	guide1_antisense	AAATCTGGCTGGATCCCACGTTCC
GRIK2	guide2_sense	CACCGGAAAGCATAATCAGAGGTG
GRIK2	guide2_antisense	AAATCACCTCTGATTATGCTTTCC
GRIK2	guide3_sense	CACCgGCAGTCCATCTGCAATGCTC
GRIK2	guide3_antisense	AAATGAGCATTGCAGATGGACTGCc
CUL3	guide1_sense	CACCGGAAGAACCAATTGTAAAGG
CUL3	guide1_antisense	AAATCCTTTACAATTGGTTCTTCC
CUL3	guide2_sense	CACCgGAGCATCTCAAACACAACGA
CUL3	guide2_antisense	AAATTCGTTGTGTTTGAGATGCTCc
CUL3	guide3_sense	CACCgGTCGAATCTGAGCAAAGGCA
CUL3	guide3_antisense	AAATTGCCTTTGCTCAGATTCGACc
TMEM131	guide1_sense	CACCGGGACTCTGGCCCCAAGGAA
TMEM131	guide1_antisense	AAATTTCCTTGGGGCCAGAGTCCC
TMEM131	guide2_sense	CACCGGAGACGGGGAAGCAGGTGT
TMEM131	guide2_antisense	AAATACACCTGCTTCCCCGTCTCC
TMEM131	guide3_sense	CACCGGCAGGGATGGGGAAGCGGG
TMEM131	guide3_antisense	AAATCCCGCTTCCCCATCCCTGCC
ZCCHC11	guide1_sense	CACCGGGTGGAAATAAGTCTACAG
ZCCHC11	guide1_antisense	AAATCTGTAGACTTATTTCCACCC
ZCCHC11	guide2_sense	CACCGGAAGGCCATGAAAATGCAG
ZCCHC11	guide2_antisense	AAATCTGCATTTTCATGGCCTTCC
ZCCHC11	guide3_sense	CACCgGCCATGGATGGGCCAGGACG
ZCCHC11	guide3_antisense	AAATCGTCCTGGCCCATCCATGGCc
SPPL3	guide1_sense	CACCGGCCAGTGAGAACCCAGATG
SPPL3	guide1_antisense	AAATCATCTGGGTTCTCACTGGCC
SPPL3	guide2_sense	CACCgGAGGCTCGGCAGGCGGACAA
SPPL3	guide2_antisense	AAATTTGTCCGCCTGCCGAGCCTCc
SPPL3	guide3_sense	CACCgGCTTCCGGGATAGAACGTCA
SPPL3	guide3_antisense	AAATTGACGTTCTATCCCGGAAGCc

SLC52A2	guide7_sense	CACCGgcacctgcaccacccggat
SLC52A2	guide7_antisense	AAACatccgggtggtgcaggtgcC
SLC52A2	guide8_sense	CACCGgtctctgtgcttgtggctct
SLC52A2	guide8_antisense	AAACagagccacaagcacagagacC
SLC52A2	guide9_sense	CACCGgacctgctcgtcctttcctg
SLC52A2	guide9_antisense	AAACcaggaaaggacgagcaggtcC

Sec22b shRNAs
Sigma-Aldrich #SHCLNV-NM_004892

shRNA	clone	target sequence
2	TRCN0000163868	CCTACCAGATGTACCTTGGAA
6	TRCN0000159152	GCCATCAATGAGATTTAACTT
7	TRCN0000159288	GCCACAATTTGCTAACATTTA
9	TRCN0000240494	TAGAACCCAGTAGGTGTATAT
11	TRCN0000240495	TGGATTCAAAGGCTAACAATT
JAWSII Sec22b KD[200]		CCACTGTGTCTAGGCCCTATT or CCCTATTCCTTCATCGAGTTT[200]

SLC52A2 shRNAs
Sigma-Aldrich #SHCLNV-NM_024531

shRNA	clone	target sequence
3	TRCN0000008274	CTGTGCCTCGAATGTCACTTT
4	TRCN0000008272	CCTAAGGCCTATCAGCTTCTA
5	TRCN0000011421	ACCTCGCTTCTTACGGTCATT
7	TRCN0000369172	CTACCTGTGGTGGTCAAAGAG
9	TRCN0000356989	TGGCGTGTTCTCCTACGTGAA

Supplementary Table 2: Gene-trap screen hits. All statistically significant (fcpv < 0.1) hits of the gene-trap screen described in Chapter 3. fcpv = false discovery rate-corrected p-value, ins = number of insertions, mi = mutational index (see Chapter 3). Hits shown in grey were excluded based on function (see comment), taking into consideration the transgenic expression of MR1. Hits chosen for follow up are highlighted in yellow. MR1 is highlighted in green.

gene	fcpv	ins	mi	alternative names	comment
SPEN	5.06E-218	1111	0.060603	MINT, SHARP, RBM 15C, HIAA0929	transcription -> not relevant
ZCCHC14	3.20E-65	305	0.03975	BDG-29, KIAA0579	
DYRK1A	5.87E-62	676	0.217746	MNB; DYRK; HP86; MNBH; MRD7; DYRK1	shows up in every screen!
SETD1B	1.53E-58	351	0.088533	KMT2G; Set1B	transcription -> not relevant
CUL3	2.92E-41	458	4.34688	PHA2E	
B2M	1.50E-34	160	0.034276	IMD43	positive control
PPP2R4	1.11E-32	406	3.9555	PP2A; PR53; PPP2R4	PP2A proteins are unspecific
ZNF292	3.89E-28	790	0.415213	ZN-16; Zn-15; ZFP292; Nbla00365; bA393I2.3	transcription -> not relevant
TIPRL	4.26E-28	177	9.38911	TIP; TIP41; TIPRL1	PP2A proteins are unspecific
PARN	1.86E-27	494	0.322375	DAN; DKCB6; PFBMFT4	
KMT2A	2.26E-27	133	0.041508	HRX; MLL; MLL1; TRX1; ALL-1; CXXC7; HTRX1; MLL1A; WDSTS	transcription -> not relevant
TMEM131	4.76E-25	435	3.10286	RW1; CC28; YR-23; PRO1048	
RALGAPB	4.01E-24	256	4.60609	KIAA1219; RalGAPbeta	
ACACA	1.33E-23	1154	0.521543	ACC; ACAC; ACC1; ACCA; ACACAD	also in Erica's screen
GANAB	7.54E-23	125	0.063036	G2AN; GIIA; PKD3; GLUII	
DOT1L	3.24E-22	195	0.163473	DOT1; KMT4	transcription -> not relevant
HDAC9	3.81E-21	7985	1.25588	HD7; HD9; HD7b; HDAC; HDRP; MITR; HDAC7; HDAC7B; HDAC9B; HDAC9FL	transcription -> not relevant
PPP4R2	6.60E-20	213	4.59708	-	DNA replication -> not relevant
WAC	1.84E-18	220	0.228952	Wwp4; DESSH; BM-016; PRO1741	DNA replication -> not relevant
VPS29	7.06E-18	169	0.175878	DC7; DC15; PEP11	
MLLT10	4.44E-16	688	0.492799	AF10	transcription -> not relevant
SND1	7.42E-15	205	0.257599	p100; TDRD11; Tudor-SN	transcription -> not relevant
REPS1	4.91E-14	222	0.285382	RALBP1	
HTT	6.56E-13	261	0.338095	HD; IT15	
ZCCHC11	7.87E-13	420	2.24398	TUT4; PAPD3	

gene	fcpv	ins	mi	alternative names	comment
CREBBP	1.96E-12	339	0.401701	CBP; RSTS; KAT3A; RSTS1	transcription -> not relevant
EP300	2.17E-12	192	0.279634	p300; KAT3B; RSTS2	transcription -> not relevant
LIN28B	6.51E-12	517	2.00714	CSDD2	
ATF7IP	6.56E-12	815	1.73167	AM; MCAF; p621; MCAF1; ATF-IP	transcription -> not relevant
ANKRD17	9.70E-12	502	2.02144	GTAR; MASK2; NY-BR-16	
PICALM	9.78E-11	447	2.04249	LAP; CALM; CLTH	
DBF4	9.78E-11	127	4.33638	ASK; CHIF; DBF4A; ZDBF1	DNA replication -> not relevant
ZBTB20	1.30E-10	9522	1.16226	HOF; DPZF; PRIMS; ODA-8S; ZNF288	transcription -> not relevant
IRF2	2.47E-10	100	0.17299	-	
NCOA2	7.02E-10	1259	1.49599	SRC2; TIF2; GRIP1; KAT13C; NCoA-2; bHLHe75	transcription -> not relevant
PPP6R3	8.24E-10	370	2.13445	SAPL; PP6R3; SAPLa; SAPS3; SAP190; C11orf23	
ERC1	9.74E-10	964	0.63046	ELKS; Cast2; ERC-1; RAB6IP2	
CARM1	1.29E-09	483	0.516564	PRMT4	transcription -> not relevant
ROBO1	1.40E-09	7801	1.1715	SAX3; DUTT1	
ATP13A1	2.34E-09	55	0.061309	ATP13A; CGI-152	
ADSS	2.52E-09	111	0.219461	ADEH; ADSS 2	
RQCD1	2.55E-09	109	4.45374	RCD1; CAF40; CT129; RCD-1; RQCD1	transcription -> not relevant
TFDP1	3.90E-09	99	4.78269	DP1; DILC; Dp-1; DRTF1	transcription -> not relevant
CDC25A	5.48E-09	318	2.18709	CDC25A2	DNA replication -> not relevant
MNT	6.02E-09	374	0.483744	ROX; MAD6; MXD6; bHLHd3	transcription -> not relevant
MGA	6.44E-09	399	0.49613	MAD5; MXD5	transcription -> not relevant
UBE2H	1.26E-08	1436	0.701329	GID3; UBC8; UBCH; UBCH2; E2-20K	
YWHAE	1.37E-08	197	0.361438	MDS; HEL2; MDCR; KCIP-1; 14-3-3E	
EIF4B	1.46E-08	333	0.469197	EIF-4B; PRO1843	
BAZ1B	3.70E-08	478	1.82386	WSTF; WBSCR9; WBSCR10	transcription -> not relevant
KDM3B	4.03E-08	372	0.499795	5qNCA; NET22; C5orf7; JMJD1B	transcription -> not relevant
ACTR3	4.41E-08	199	0.375896	-	
USP14	5.35E-08	1839	0.73996	TGT	

gene	fcpv	ins	mi	alternative names	comment
GPBP1	5.45E-08	215	0.392563	GPBP; SSH6; VASCULIN	transcription -> not relevant
MR1	7.41E-08	277	0.446842	HLALS	
DPH5	8.43E-08	97	0.225816	AD-018; CGI-30; NPD015; HSPC143	
CSNK2A1	2.15E-07	104	0.253015	CKII; CK2A1; OCNDS; CSNK2A3	cell cycle control -> not relevant
DACH1	2.47E-07	5107	1.18803	DACH	transcription -> not relevant
NAA30	2.72E-07	76	5.15051	MAK3; Mak3p; NAT12; NAT12P; C14orf35	
BIRC6	4.39E-07	545	0.587288	BRUCE; APOLLON	
SSR3	4.42E-07	57	0.125022	TRAPG	
FANCL	4.71E-07	80	4.60548	POG; PHF9; FAAP43	DNA replication -> not relevant
AHCY	4.89E-07	123	0.298873	SAHH; adoHcyase	
XPO6	5.23E-07	608	0.606784	EXP6; RANBP20	
RFXAP	6.59E-07	73	0.18854	-	
DCAF7	7.22E-07	56	0.127522	AN11; HAN11; WDR68; SWAN-1	
CDK6	7.46E-07	564	1.66201	MCPH12; PLSTIRE	cell cycle control -> not relevant
KMT2E	8.82E-07	697	1.57359	MLL5; NKp44L; HDCMC04P	cell cycle control -> not relevant
PUM1	1.35E-06	194	0.409876	PUMH; HSPUM; PUMH1; PUML1	
ARPC2	1.90E-06	90	0.247472	ARC34; PRO2446; p34-Arc; PNAS-139	
RAB10	1.90E-06	136	0.340463	-	
VHL	2.10E-06	42	0.081746	RCA1; VHL1; pVHL; HRCA1	
TLK2	2.20E-06	415	0.558645	HsHPK; PKU-ALPHA	cell cycle control -> not relevant
ARHGEF38	3.31E-06	299	1.96376	KIAA0651, LFP40	
BPTF	3.47E-06	118	0.315296	FAC1; FALZ; NURF301	transcription -> not relevant
RFWD2	3.48E-06	577	0.617166	COP1; RNF200	
IMMT	3.83E-06	66	0.189765	HMP; P87; P89; PIG4; Mic60; PIG52; MINOS2; P87/89	
DCPS	3.83E-06	66	0.189765	ARS; DCS1; HSL1; HINT5; HINT-5; HSPC015	
KIAA1033	4.53E-06	312	0.516129	SWIP; MRT43; WASHC4	
CUX1	5.13E-06	360	0.5447	CDP; CUX; p75; CASP; CDP1; COY1; Clox; p100; p110; p200; CUTL1; GOLIM6; CDP/Cut; Cux/CDP; Nbla10317	

gene	fcpv	ins	mi	alternative names	comment
ASCC3	6.07E-06	147	0.370468	RNAH; HELIC1; ASC1p200	DNA replication -> not relevant
ADNP	6.25E-06	252	2.05154	ADNP1; HVDAS; MRD28	transcription -> not relevant
VAC14	7.38E-06	75	4.25119	TRX; SNDC; TAX1BP2; ArPIKfyve	
TAPBP	9.12E-06	138	2.69792	TAP binding protein	
PMVK	1.08E-05	83	0.253774	PMK; PMKA; PMKASE; POROK1; HUMPMKI	
NHLRC2	1.11E-05	80	0.245234	-	
HSD17B12	1.33E-05	109	0.316271	KAR; SDR12C1	
NFYC	2.20E-05	133	2.65703	HSM; CBFC; HAP5; CBF-C; NF-YC; H1TF2A	transcription -> not relevant
KDM2A	2.70E-05	434	0.596283	FBL7; CXXC8; FBL11; FBXL11; JHDM1A; LILINA	transcription -> not relevant
TIMM50	3.24E-05	37	0.093768	TIM50; TIM50L	
MOGS	3.24E-05	37	0.093768	DER7; GCS1; CDG2B; CWH41	
ALG8	3.30E-05	217	0.474648	CDG1H	
FBXO42	3.81E-05	109	0.332886	JFK; Fbx42	
RBM15	4.33E-05	67	0.231859	OTT; OTT1; SPEN	transcription -> not relevant
TSC1	5.95E-05	147	2.40905	LAM; TSC	
ZNF236	6.18E-05	121	0.366031	ZNF236A; ZNF236B	transcription -> not relevant
SRD5A3	6.57E-05	189	0.458874	CDG1P; CDG1Q; KRIZI; SRD5A2L; SRD5A2L1	
PBRM1	6.74E-05	1158	1.35057	PB1; BAF180	transcription -> not relevant
CCDC6	7.63E-05	123	0.373687	H4; PTC; TPC; TST1; D10S170	
RAD51B	7.66E-05	316	1.78342	REC2; R51H2; RAD51L1	DNA replication -> not relevant
PPAT	8.58E-05	152	0.419216	GPAT; PRAT; ATASE	
VPS41	9.55E-05	592	1.51592	HVPS41; HVSP41; hVps41p	
NLGN1	9.82E-05	3258	1.19182	NL1	
KDM6A	1.01E-04	219	1.9998	UTX; KABUK2; bA386N14.2	transcription -> not relevant
SLTM	1.06E-04	311	0.557361	Met	transcription -> not relevant
NDUFAF6	1.37E-04	206	2.02086	C8orf38	
RPTOR	1.37E-04	153	0.428966	KOG1; Mip1	cell cycle control -> not relevant
LAMTOR2	1.39E-04	39	7.22688	p14; ENDAP; ROBLD3; HSPC003; MAPBPIP; MAPKSP1AP; Ragulator2	

gene	fcpv	ins	mi	alternative names	comment
MTF2	1.55E-04	221	0.502988	M96; PCL2; TDRD19A; dJ976O13.2	transcription -> not relevant
YTHDF2	1.60E-04	104	0.354226	CAHL; HGRG8; NY-REN-2	
LAMTOR5	1.64E-04	97	2.90225	XIP; HBXIP	
TTI1	1.67E-04	30	0.075908	smg-10; KIAA0406	DNA replication -> not relevant
ZFX	1.83E-04	396	0.607213	ZNF926	transcription -> not relevant
NPM1	2.18E-04	37	0.128813	B23; NPM	
UBE2G2	3.29E-04	71	0.28465	UBC7	
CNOT2	3.29E-04	176	0.470359	NOT2; CDC36; NOT2H; HSPC131	
TAP1	3.57E-04	79	3.13523	APT1; PSF1; ABC17; ABCB2; PSF-1; RING4; TAP1N; D6S114E; TAP1*0102N	
GART	3.58E-04	225	0.520771	AIRS; GARS; PAIS; PGFT; PRGS; GARTF	
NFIC	3.62E-04	339	0.58981	CTF; NFI; CTF5; NF-I	transcription -> not relevant
TRPM3	3.63E-04	3368	1.17609	GON-2; MLSN2; LTRPC3	
CTNNA1	3.69E-04	857	0.722966	MDPT2; CAP102	
VPS53	4.56E-04	39	0.15628	HCCS1; PCH2E; hVps53L; pp13624	
BRIP1	4.99E-04	288	1.74539	OF; BACH1; FANCJ	DNA replication -> not relevant
EIF3L	5.92E-04	52	0.222425	EIF3EIP; EIF3S11; HSPC021; HSPC025; MSTP005; EIF3S6IP	
RHEB	6.09E-04	35	0.137124	RHEB2	cell cycle control -> not relevant
UBE2L3	6.11E-04	199	1.95862	E2-F1; L-UBC; UBCH7; UbcM4	
KAT7	6.72E-04	73	0.298299	HBO1; HBOA; MYST2; ZC2HC7	transcription -> not relevant
SLIT2	8.29E-04	3361	1.16863	SLIL3; Slit-2	
LAMTOR4	8.34E-04	90	2.76326	C7orf59	
SEC63	9.25E-04	51	0.227722	ERdj2; PCLD2; SEC63L; DNAJC23; PRO2507	
BMPR2	9.33E-04	233	0.545129	BMR2; PPH1; BMPR3; BRK-3; POVD1; T-ALK; BMPR-II	
MAGI2	1.03E-03	3795	1.15605	AIP1; AIP-1; ARIP1; SSCAM; MAGI-2; ACVRIP1	
FIG4	1.04E-03	58	3.67885	YVS; BTOP; SAC3; ALS11; CMT4J; KIAA0274; dJ249I4.1	
RANBP1	1.07E-03	156	0.472298	HTF9A	cell cycle control -> not relevant
C16orf62	1.12E-03	125	0.429848	-	
POU6F2	1.19E-03	3261	1.16771	WT5; WTSL; RPF-1	transcription -> not relevant

gene	fcpv	ins	mi	alternative names	comment
PDS5A	1.29E-03	98	0.383748	PIG54; SCC112; SCC-112	cell cycle control -> not relevant
TAF11	1.32E-03	41	0.182178	TAF2I; PRO2134; TAFII28; MGC:15243	transcription -> not relevant
SGF29	1.32E-03	41	0.182178	STAF36; TDRD29; CCDC101	transcription -> not relevant
NUP188	1.37E-03	53	0.24714	hNup188; KIAA0169	
GPC3	1.39E-03	3118	1.17049	SGB; DGSX; MXR7; SDYS; SGBS; OCI-5; SGBS1; GTR2-2	
GTF3C2	1.40E-03	70	0.314873	TFIIIC110; TFIIIC-BETA	transcription -> not relevant
DPH6	1.40E-03	708	0.715934	ATPBD4	
TAP2	1.40E-03	60	3.49199	APT2; PSF2; ABC18; ABCB3; PSF-2; RING11; D6S217E	
DLG2	1.43E-03	7947	1.10329	PSD93; PSD-93; PPP1R58; chapsyn-110	
ADK	1.48E-03	2178	0.828117	AK	
NONO	1.51E-03	100	0.393048	P54; NMT55; NRB54; MRXS34; P54NRB; PPP1R114	
UBE2G1	1.53E-03	716	0.719182	UBC7; E217K; UBE2G	
GNG7	1.83E-03	543	0.685871	-	
TRIM28	1.88E-03	18	0.062513	KAP1; TF1B; RNF96; TIF1B; PPP1R157	transcription -> not relevant
TFAP4	1.95E-03	240	0.561787	AP-4; bHLHc41	transcription -> not relevant
FCHO2	1.99E-03	162	2.01174	-	
EIF2A	2.25E-03	251	0.573704	CDA02; EIF-2A; MST089; MSTP004; MSTP089	
UBR5	2.41E-03	96	0.394713		
ZFR	2.56E-03	88	0.376029	ZFR1; SPG71	
MTHFD1	2.76E-03	93	0.390695	MTHFC; MTHFD	
FLCN	2.91E-03	47	3.93226	BHD; FLCL	
WHSC1	2.99E-03	283	0.598843	NSD2, WHS; TRX5; KMT3F; KMT3G; MMSET; WHSC1; REIIBP	cell cycle control -> not relevant
DNAJC7	3.03E-03	170	0.508235	DJ11; DJC7; TPR2; TTC2	
VPS50	3.08E-03	124	0.451945	VPS54L; CCDC132	
VPS13D	3.61E-03	87	0.381905	-	
EXOC4	3.85E-03	1111	0.779109	SEC8; Sec8p; SEC8L1	
PSIP1	3.85E-03	70	0.340865	p52; p75; PAIP; DFS70; LEDGF; PSIP2	transcription -> not relevant
GGNBP2	3.86E-03	268	0.59311	DIF3; LZK1; DIF-3; LCRG1; ZFP403; ZNF403	

gene	fcpv	ins	mi	alternative names	comment
EZH2	4.18E-03	118	0.44812	WVS; ENX1; EZH1; KMT6; WVS2; ENX-1; EZH2b; KMT6A	transcription -> not relevant
STT3B	4.26E-03	190	0.539769	SIMP; CDG1X; STT3-B	
CSMD3	4.26E-03	2282	1.18722	-	
TASP1	4.47E-03	398	1.51649	C20orf13; dJ585I14.2	
IMMP2L	4.50E-03	1289	1.25536	IMP2; IMP2-LIKE; IMMP2L-IT1	
BMP2K	4.72E-03	99	0.419089	BIKE; HRIHFB2017	transcription -> not relevant
SPPL3	4.80E-03	73	0.347792	IMP2; PSH1; PSL4; PRO4332; MDHV1887	
CHMP3	4.80E-03	47	0.251693	NEDF; VPS24; CGI-149	
HLA-A	4.80E-03	18	18.0669	HLAA	
PDAP1	5.02E-03	37	0.205686	PAP; PAP1; HASPP28	
RANBP3	5.49E-03	183	1.84008	-	
ANKRD11	5.86E-03	227	0.578321	T13; LZ16; ANCO1; ANCO-1	transcription -> not relevant
PHF12	6.05E-03	159	0.516442	PF1	transcription -> not relevant
SYNRG	6.32E-03	222	0.575611	SYNG; AP1GBP1	
SRF	6.45E-03	52	0.285116	MCM1	transcription -> not relevant
LSM14A	6.67E-03	149	0.505036	RAP55; FAM61A; RAP55A; C19orf13	
CADM2	6.68E-03	4625	1.12407	NECL3; IGSF4D; Necl-3; synCAM2; SynCAM 2	
PDCD10	6.70E-03	71	2.71009	CCM3; TFAR15	
CDYL	6.73E-03	195	0.556242	CDYL1	transcription -> not relevant
NFE2L1	6.84E-03	316	0.633298	NRF1; TCF11; LCR-F1	
TAF1B	7.26E-03	33	0.18977	SL1; RAF1B; RAFI63; TAFI63; MGC:9349	transcription -> not relevant
SMURF1	7.26E-03	337	0.64265	-	
CYLD	7.29E-03	105	2.21935	EAC; MFT; SBS; TEM; BRSS; CDMT; MFT1; CYLD1; CYLDI; USPL2	
COMMD7	7.29E-03	100	0.434057	C20orf92; dJ1085F17.3	
SHMT2	7.29E-03	106	0.439245	GLYA; SHMT; HEL-S-51e	
SRRD	7.34E-03	19	0.05904	SRR1L; HC/HCC	
RALGAPA2	7.34E-03	539	1.40644	p220; AS250; C20orf74; dJ1049G11; bA287B20.1; dJ1049G11.4	
XPOT	7.34E-03	133	0.49047	XPO3	

gene	fcpv	ins	mi	alternative names	comment
EIF3K	7.49E-03	36	0.212542	M9; ARG134; PLAC24; PTD001; EIF3S12; HSPC029; MSTP001; PLAC-24; PRO1474; EIF3-p28	
SPATA5	7.50E-03	40	0.225423	AFG2; SPAF; EHLMRS	
FAM198B	7.90E-03	995	1.28207	ENED; AD021; AD036; C4orf18	
GRIK2	8.08E-03	1585	1.21683	EAA4; GLR6; MRT6; GLUK6; GLUR6; GluK2	
ASXL2	8.08E-03	209	0.570404	ASXH2; SHAPNS	transcription -> not relevant
APAF1	8.13E-03	148	0.510087	CED4; APAF-1	
TBCK	8.35E-03	1192	1.25333	TBCKL; IHPRF3; HSPC302	
PRSS12	8.96E-03	754	1.32938	MRT1; BSSP3; BSSP-3	

Supplementary Table 3: Collated information about putative positive regulators of MR1 surface expression. Collated information from the indicated sources for the genes listed. Umbrella terms were assigned manually. All websites were accessed throughout April 2017. Copyrightable data from UniProtKB[350] are under the Creative Commons Attribution (CC BY 4.0) License. OMIM = Online Mendelian Inheritance in Man[351]. Copyrightable data from The Human Protein Atlas (www.proteinatlas.org)[354] are under the Creative Commons Attribution-ShareAlike 3.0 International License. Data from the ExAC Browser[324] are under the ODC Open Database License (ODbL) license. Gene ontology (GO) term[352,353] data are licensed under the Creative Commons Attribution 4.0 Unported License and were accessed through the other databases such as GeneCards[349]. Constraint metrics are shown in orange if the gene was considered intolerant based on thresholds reported in the ExAC Browser. Functions related to MR1 trafficking are printed in bold.

gene	name	alternative names (PubMed)	function (PubMed, Genecards, UniProt)	disease association (OMIM and UniProt)	subcellular localisation (UniProt and GO)	subcellular localisation (protein atlas)	RNA tissue expression (protein atlas)	Missense Constraint (ExAC)	pLI (ExAC)	other (UniProt)
endocytosis, vesicular transport and Golgi										
VPS29	retromer complex component	DC7; DC15; PEP11	**retrograde transport of proteins from endosomes to the trans-Golgi network**	-	cytoplasm, endosome, retromer complex	vesicles, cytosol	all	1.39	0.93	
REPS1	RALBP1 associated Eps domain containing 1	RALBP1	signaling adaptor protein, participates in signaling, **endocytosis and cytoskeletal changes**	-	membrane, clathrin-coated pit	vesicles, PM, cytosol	all	0.66	1.00	Binding to RALBP1 does not affect its Ral-binding activity
HTT	huntingtin	HD; IT15	May play a role in **microtubule-mediated transport or vesicle function**.	Huntington Disease	nucleus, axon, centriole, cytoplasm, ER, Golgi, endosome	nucleoplasm, cytosol	all	2.49	1.00	highest expression in the brain
ERC1	ELKS/RAB6-interacting/CAST family member 1	ELKS; Cast2; ERC-1; RAB6IP2	regulate neurotransmitter release -> **vesicle transport? Rab6 binding**	papillary thyroid carcinomas	cytoplasm, Golgi, presynaptic membrane	vesicles, PM, cytosol	all	1.53	0.00	needed for activation of NFkB, isoforms expressed differentially
RAB10	member RAS oncogene family	-	**regulate intracellular vesicle trafficking**	-	Golgi, endosome, ER, recycling endosome	n/a	all	3.01	0.94	regulates TLR4 trafficking to the membrane
KIAA1033	WASH complex subunit 4	SWIP; MRT43; WASHC4	**intracellular transport of endosomes**	Autosomal recessive non-syndromic intellectual disability	early endosome, WASH complex	nucleoplasm	all	0.11	0.16	inhibits recruitement of Arp2/3 by NPF
CUX1	cut like homeobox 1	CDP; CUX; p75; CASP; CDP1; COY1; Clox; p100; p110; p200; CUTL1; GOLIM6; CDP/Cut; Cux/CDP; Nbla10317	may regulate gene expression, morphogenesis, and differentiation; **May be involved in intra-Golgi retrograde transport (two isoforms)**	-	nucleus, cytosol, Golgi (two isoforms)	nucleoplasm, Golgi	all	5.05	1.00	repressor of developmentally regulated gene expression, Represses T-cell receptor (TCR) beta enhancer function by binding to MARbeta, an ATC-rich DNA sequence located upstream of the TCR beta enhancer
VPS53	GARP complex subunit	HCCS1; PCH2E; hVps53L; pp13624	**retrograde transport from early and late endosomes to the trans-Golgi network (TGN)**	Pontocerebellar hypoplasia 2E	Golgi, recycling endosome	cytosol, Golgi	all	1.33	0.00	Localises to the trans-Golgi network as part of the GARP complex, while it localises to recycling endosomes as part of the EARP complex

gene	name	alternative names (PubMed)	function (PubMed, Genecards, UniProt)	disease association (OMIM and UniProt)	subcellular localisation (UniProt and GO)	subcellular localisation (protein atlas)	RNA tissue expression (protein atlas)	Missense Constraint (ExAC)	pLI (ExAC)	other (UniProt)
C16orf62	C16orf62	-	**Copper-dependent ATP7A trafficking between the trans-Golgi network and vesicles in the cell periphery**	-	early endosome	mitochondria	all	0.72	0.00	cooperation with the WASH complex on early endosomes
VPS50	EARP/GARPII complex subunit	VPS54L; CCDC132, syndetin	**endocytic recycling**	-	EARP complex, recycling endosome	PM, cytosol	all	no ExAC entry	no ExAC entry	Not involved in retrograde transport from early and late endosomes to the TGN
VPS13D	vacuolar protein sorting 13 homolog D	-	**trafficking of membrane proteins** between the trans-Golgi network and the prevacuolar compartment	-	extracellular exosome	vesicles, nucleoplasm, cytosol	all	1.85	1.00	-
EXOC4	exocyst complex component 4	SEC8; Sec8p; SEC8L1	**targeting exocytic vesicles to specific docking sites on the plasma membrane**	-	cytoplasm, exocyst, PM, synapse	nucleoli, nucleus	all	-0.27	0.00	-
CHMP3	charged multivesicular body protein 3	NEDF; VPS24; CGI-149	**sorts transmembrane proteins into lysosomes/ vacuoles via the multivesicular body (MVB) pathway**	involved in viral budding (HIV)	cytosol, late endosome, ESCRT III complex	n/a	all	0.13	0.04	-
SYNRG	synergin gamma	SYNG; AP1GBP1	interacts with the gamma subunit of AP1 **clathrin-adaptor** complex at the Golgi	-	Golgi, cytoplasm, AP-1 complex	cytosol	all	0.25	0.97	-
phosphatidylinositol										
ZCCHC14	zinc finger CCHC-type containing 14	BDG-29, KIAA0579	nucleic acid binding and **phosphatidylinositol binding**	-	n/a	nuclear membrane (?)	all	0.89	0.95	-
glyscosylation in the ER										
GANAB	glucosidase II alpha subunit	G2AN; GIIA; PKD3; GLUII	**modification of immature glycoproteins in the ER**	Polycystic kidney disease 3	ER, Golgi, melanosome	ER, nuclear membrane, cytosol	all	2.38	1.00	-
MOGS	mannosyl-oligosaccharide glucosidase	DER7; GCS1; CDG2B; CWH41	**modification of immature glycoproteins in the ER**	Congenital disorder of glycosylation, type IIb	ER	ER	all	0.66	0.00	-
ALG8	alpha-1,3-glucosyltransferase	CDG1H	**modification of immature glycoproteins in the ER**	Congenital disorder of glycosylation, type Ih	ER	nucleoplasm	all	-0.11	0.00	-
SRD5A3	steroid 5 alpha-reductase 3	CDG1P; CDG1Q; KRIZI; SRD5A2L; SRD5A2L1	required for the synthesis of dolichol-linked monosaccharides and the oligosaccharide precursor used for **N-linked glycosylation** of proteins	Congenital disorder of glycosylation, type Iq and Kahrizi syndrome	ER	PM, cytosol	all	0.42	0.04	-

gene	name	alternative names (PubMed)	function (PubMed, Genecards, UniProt)	disease association (OMIM and UniProt)	subcellular localisation (UniProt and GO)	subcellular localisation (protein atlas)	RNA tissue expression (protein atlas)	Missense Constraint (ExAC)	pLI (ExAC)	other (UniProt)
STT3B	catalytic subunit of the oligosaccharyltransferase complex	SIMP; CDG1X; STT3-B	**modification of immature glycoproteins in the ER**	Congenital disorder of glycosylation, type Ix	ER	ER	all	3.83	0.98	-
ER transport										
ATP13A1	ATPase 13A1	ATP13A; CGI-152	Mediates manganese **transport into the ER**	-	ER	vesicles	all	3.15	0.99	Depletion of ATP13A1 with siRNAs leads to induction of the unfolded protein response (UPR) and increased activity of glucosylceramide synthase (GlcCer)
SSR3	signal sequence receptor subunit 3	TRAPG	**protein translocation across the ER membrane**	-	ER	cytosol	all	0.52	0.30	TRAP proteins are part of a complex whose function is to bind calcium to the ER membrane and thereby regulate the retention of ER resident proteins.
SEC63	SEC63 homolog, protein translocation regulator	ERdj2; PCLD2; SEC63L; DNAJC23; PRO2507	**protein translocation apparatus of the endoplasmic reticulum**	Polycystic liver disease 2	ER	ER	all	1.57	0.00	-
cytoskeleton										
ACTR3	ARP3 actin related protein 3 homolog	-	**actin branching**	-	cytoskeleton, cell projection, cell-cell junction	n/a	all	3.64	1.00	-
ARPC2	actin related protein 2/3 complex subunit 2	ARC34; PRO2446; p34-Arc; PNAS-139	**actin branching**	-	cytoskeleton, cell projection, focal adhesion	cytosol, Golgi	all	2.95	0.99	-
CCDC6	coiled-coil domain containing 6	H4; PTC; TPC; TST1; D10S170	tumor suppressor, structural constituent of cytoskeleton	Papillary or follicular thyroid carcinoma	cytosol, cytoskeleton	cytosol	all	3.44	0.97	-
CTNNA1	catenin alpha 1	MDPT2; CAP102	**links** cadherins **to actin**	Macular dystrophy, patterned, 2 and hereditary diffuse gastric cancer	cytoskeleton, cell junction	PM, cell junctions	all	3.48	0.97	
immune system										
B2M	beta2 microglobulin	IMD43	HLA class I light chain, stabilises MR1 and MHC-I structure	Immunodeficiency 43 and Amyloidosis, familial visceral	secreted, cell surface, ER, early endosome, Golgi, class I protein complex	Golgi, PM, cytosol	all	1.37	0.86	-

gene	name	alternative names (PubMed)	function (PubMed, Genecards, UniProt)	disease association (OMIM and UniProt)	subcellular localisation (UniProt and GO)	subcellular localisation (protein atlas)	RNA tissue expression (protein atlas)	Missense Constraint (ExAC)	pLI (ExAC)	other (UniProt)
IRF2	interferon regulatory factor 2	-	represses type I IFN and IFN-inducible MHC class I genes, activates IL-7 production	-	nucleus, cytosol, focal adhesion	nucleoplasm, cytosol	all	2.86	0.38	Expressed throughout the epithelium of the colon; Also expressed in lamina propria.
MR1	major histocompatibility complex, class I-related	HLALS	antigen presentation of small molecule metabolites	-	PM, ER, secreted (isoform 4)	PM (polyclonal Ab)	mixed	-1.25	0.00	Associated with the PLC, TAPBP, CALR and PDIA3
RFXAP	regulatory factor X associated protein	-	controls the **cell type specificity and inducibility of MHC class II gene expression**	Bare lymphocyte syndrome, type II, complementation group D	nucleus	nuclear speckles	mixed	2.39	0.44	-
SPPL3	signal peptide peptidase like 3	IMP2; PSH1; PSL4; PRO4332; MDHV1887	Intramembrane-cleaving aspartic protease, regulation of cellular **glycosylation** processes, **required for TCR signalling**	-	ER, Golgi, PM	PM, vesicles	all	3.27	0.91	-
nucleotide metabolism										
PPAT	phosphoribosyl pyrophosphate amidotransferase	GPAT; PRAT; ATASE	nucleotide synthesis	-	cytosol	Midbody ring (?)	all	3.48	0.99	step 1 in IMP pathway
GART	phosphoribosylglycinamide formyltransferase, phosphoribosylglycinamide synthetase, phosphoribosylaminoimidazole synthetase	AIRS; GARS; PAIS; PGFT; PRGS; GARTF	nucleotide synthesis	-	cytosol, extracellular exosome	nucleoplasm, mitochondria, cytosol	all	-0.69	0.06	step 2 in IMP pathway
ADK	adenosine kinase	AK	nucleotide homeostasis	Hypermethioninemia due to adenosine kinase deficiency	nucleus, cytoplasm	nucleoplasm, cytosol	all	0.55	0.32	-
MTHFD1	methylenetetrahydrofolate dehydrogenase, cyclohydrolase and formyltetrahydrofolate synthetase 1	MTHFC; MTHFD	nucleotide synthesis	{Abruptio placentae, susceptibility to} and {Spina bifida, folate-sensitive, susceptibility to} and colorectal cancer	cytoplasm, mitochondria	cytosol	all	1.69	0.61	-
YWHAE	tyrosine 3-monooxygenase/ tryptophan 5-monooxygenase activation protein epsilon	MDS; HEL2; MDCR; KCIP-1; 14-3-3E	signal transduction	Miller-Dieker syndrome	nucleus, cytoplasm, melanosome, axon, focal adhesion, mitochondrion	cytosol	all	3.25	0.96	-
GNG7	G protein subunit gamma 7	-	GPCR signalling	-	PM, heterotrimeric G-protein complex	n/a	all	0.24	0.48	Down-regulated in pancreatic and esophageal cancer

gene	name	alternative names (PubMed)	function (PubMed, Genecards, UniProt)	disease association (OMIM and UniProt)	subcellular localisation (UniProt and GO)	subcellular localisation (protein atlas)	RNA tissue expression (protein atlas)	Missense Constraint (ExAC)	pLI (ExAC)	other (UniProt)
COMMD7	COMM domain containing 7	C20orf92; dJ1085F17.3	NFkB signaling, may modulate cullin-RING E3 ub ligase	-	cytoplasmic vesicles	vesicles	all	0.06	0.00	highest expression in lungs
nuclear transport										
XPO6	exportin 6	EXP6; RANBP20	transport of cargo across the nuclear envelope	-	Shuttles between the nucleus and the cytoplasm	nucleus, nucleoli, PM, cytosol	all	3.77	1.00	Mediates the nuclear export of actin and profilin-actin complexes in somatic cells
NUP188	nucleoporin 188	hNup188; KIAA0169	nuclear import	Copy number variations of NUP188 gene may be a cause of heterotaxy, a congenital heart disease resulting from abnormalities in left-right (LR) body patterning	nuclear envelope, NPC	nucleus	all	0.27	0.99	-
ZFR	zinc finger RNA binding protein	ZFR1; SPG71	nucleocytoplasmic shuttling	Autosomal recessive spastic paraplegia type 71	chromosome, cytoplasm, nucleus	nucleoplasm	all	4.18	1.00	Associated with chromosome foci in meiotic cells. Localises in somatodendritic compartment of primary hippocampal neurons. Co-localises with STAU2 in several cytosolic RNA granules (By similarity)
XPOT	exportin for tRNA	XPO3	export of tRNA from the nucleus to the cytoplasm	-	Shuttles between the nucleus and the cytoplasm.	nucleoplasm, cytosol	all	1.55	1.00	-
mitochondrial										
IMMT	inner membrane mitochondrial protein	HMP; P87; P89; PIG4; Mic60; PIG52; MINOS2; P87/89	mitochondrial cristae morphology	-	mitochondrial inner membrane, MICOS complex	mitochondria	all	-0.47	0.00	
TIMM50	translocase of inner mitochondrial membrane 50	TIM50; TIM50L	mitochondrial import	-	Mitochondrion inner membrane, Nucleus	nucleoplasm, mitochondria	all	1.17	0.44	
SHMT2	serine hydroxymethyl-transferase 2	GLYA; SHMT; HEL-S-51e	glycine synthesis in mitochondria	-	mitochondrial inner membrane, BRISC complex, cytoplasm, nucleus, mito matrix	microtubules, mitochondria	all	2.06	0.01	In eukaryotes there are two forms of the enzymes: a cytosolic one and a mitochondrial one.

gene	name	alternative names (PubMed)	function (PubMed, Genecards, UniProt)	disease association (OMIM and UniProt)	subcellular localisation (UniProt and GO)	subcellular localisation (protein atlas)	RNA tissue expression (protein atlas)	Missense Constraint (ExAC)	pLI (ExAC)	other (UniProt)
SPATA5	spermatogenesis associated 5	AFG2; SPAF; EHLMRS	**membrane fusion**, DNA replication, microtubule severing, and protein degradation, potential mito targeting sequence	Epilepsy, hearing loss, and mental retardation syndrome	cytoplasm, mitochondria	cytosol	mixed	-0.18	0.00	May be involved in morphological and functional mitochondrial transformations during spermatogenesis
ubiquitination and protein turnover										
UBE2H	ubiquitin conjugating enzyme E2 H	GID3; UBC8; UBCH; UBCH2; E2-20K	protein turnover, among its related pathways are Immune System and Class I MHC mediated **antigen processing and presentation**	-	cytoplasm	mitochondria	all	3.41	0.97	-
USP14	ubiquitin specific peptidase 14	TGT	deubiquitinating enzyme	-	PM, cytosol, proteasome	cytosol	all	2.23	0.93	-
BIRC6	baculoviral IAP repeat containing 6	BRUCE; APOLLON	ubiquitination/protein turnover; anti-apoptotic	-	Golgi, Midbody, Endosome, MTOC	Golgi, vesicles	mixed	1.40	1.00	Concentrates in a pericentriolar compartment in interphase, moves partially to spindle poles in metaphase, and finally localises to the spindle midzone and the midbody in telophase and during cytokinesis
DCAF7	DDB1 and CUL4 associated factor 7	AN11; HAN11; WDR68; SWAN-1	scaffold protein for protein complexes involved in kinase signaling	-	cytoplasm, nucleus, Cul4-RING E3 ub ligase complex	nucleoplasm, cytosol	all	3.16	0.88	Over-expression of DIAHP1 or active RHOA causes translocation from the nucleus to cytoplasm
VHL	von Hippel-Lindau tumor suppressor	RCA1; VHL1; pVHL; HRCA1	ubiquitination and degradation of HIF and Pol II	Erythrocytosis, familial, 2 and Hemangioblastoma, cerebellar, somatic and Pheochromocytoma and Renal cell carcinoma, somatic and von Hippel-Lindau syndrome	cytoplasm, nucleus, ER (two isoforms)	nucleoplasm, cytosol	all	0.76	0.03	-
RFWD2	ring finger and WD repeat domain 2	COP1; RNF200	ubiquitination and proteasomal degradation, promotion of cell survival	-	cytoplasm, Golgi, nuclear speckle	n/a	all	3.51	1.00	-
FBXO42	F-box protein 42	JFK; Fbx42	recognizes p53/TP53, promoting its ubiquitination and degradation	-	n/a	nucleoplasm	all	1.89	0.98	-
UBE2G2	ubiquitin conjugating enzyme E2 G2	UBC7	among its related pathways are Immune System and Class I MHC mediated **antigen processing and presentation**	-	cytosol, ER	n/a	all	2.06	0.25	involved in ERAD

gene	name	alternative names (PubMed)	function (PubMed, Genecards, UniProt)	disease association (OMIM and UniProt)	subcellular localisation (UniProt and GO)	subcellular localisation (protein atlas)	RNA tissue expression (protein atlas)	Missense Constraint (ExAC)	pLI (ExAC)	other (UniProt)
UBE2G1	ubiquitin conjugating enzyme E2 G1	UBC7; E217K; UBE2G	degradation of muscle-specific proteins?, among its related pathways are **Immune System and Class I MHC mediated antigen processing** and presentation	-	cytoplasm, cytosol, exosome	nucleoplasm, cytosol	all	2.44	0.75	mainly expressed in skeletal muscle
UBR5	ubiquitin protein ligase E3 component n-recognin 5	DD5; EDD; HYD; EDD1	N-end rule pathway, DNA damage repair	-	nucleus	nucleoplasm, cytosol	all	6.53	1.00	-
SMURF1	SMAD specific E3 ubiquitin protein ligase 1	-	ubiquitin ligase that is specific for receptor-regulated SMAD proteins in the bone morphogenetic protein (BMP) pathway	-	cytoplasm, PM, axon, nucleoplasm	n/a	all	3.11	1.00	Promotes ubiquitination and subsequent proteasomal degradation of TRAF family members and RHOA
mRNA processing and translation										
PARN	poly(A)-specific ribonuclease	DAN; DKCB6; PFBMFT4	nonsense-mediated mRNA decay	Dyskeratosis congenita, autosomal recessive 6 and Pulmonary fibrosis and/or bone marrow failure, telomere-related, 4	cytoplasm, nucleus, nucleoli	nucleoli, nuclear speckles	all	-0.22	0.39	-
EIF4B	eukaryotic translation initiation factor 4B	EIF-4B; PRO1843	Required for the binding of mRNA to ribosomes	-	cytosol, EIF4F-complex, polysome	cytosol	all	3.15	1.00	-
DPH5	diphthamide biosynthesis 5	AD-018; CGI-30; NPD015; HSPC143	Diphthamide is a post-translationally modified histidine residue found only on translation elongation factor 2	-	cytosol	Golgi	all	-0.36	0.00	-
PUM1	pumilio RNA binding family member 1	PUMH; HSPUM; PUMH1; PUML1	translational regulator of specific mRNAs	-	cytoplasm, p-body, nucleus	nucleus, cytosol	all	4.59	1.00	Recruited to cytoplasmic stress granules upon viral infection
DCPS	decapping enzyme, scavenger	ARS; DCS1; HSL1; HINT5; HINT-5; HSPC015	cleavage of a residual cap structure following the degradation of mRNAs	Al-Raqad syndrome	cytoplasm, nucleus, mitochondrion, p-body	nucleoplasm, cytosol	all	-0.36	0.00	Predominantly localised in the nucleus. Nucleocytoplasmic shuttling protein that can transiently enter the cytoplasm in mammalian cells in a XPO1/CRM1-dependent manner
YTHDF2	YTH N6-methyladenosine RNA binding protein 2	CAHL; HGRG8; NY-REN-2	mRNA stability	-	cytosol, nucleus, p-body	cytosol	all	2.47	0.99	Localises to the cytosol and relocates to the nucleus following heat shock stress

gene	name	alternative names (PubMed)	function (PubMed, Genecards, UniProt)	disease association (OMIM and UniProt)	subcellular localisation (UniProt and GO)	subcellular localisation (protein atlas)	RNA tissue expression (protein atlas)	Missense Constraint (ExAC)	pLI (ExAC)	other (UniProt)
NPM1	nucleophosmin	B23; NPM	Associated with nucleolar ribonucleoprotein structures and bind single-stranded nucleic acids	Leukemia, acute myeloid, somatic and non-Hodgkin lymphoma and myelodysplastic syndrome	nucleolus, nucleoplasm, MTOC, cytosol	nucleus, nucleoli	all	1.89	0.96	found in the cytoplasm in patients with primary acute myelogenous leukemia (AML), but not with secondary AML
CNOT2	CCR4-NOT transcription complex subunit 2	NOT2; CDC36; NOT2H; HSPC131	mRNA synthesis and degradation	-	CCR4-NOT complex, cytoplasm, nucleus, p-body, PM	nucleus, cytosol	all	3.66	1.00	-
EIF3L	eukaryotic translation initiation factor 3 subunit L	EIF3EIP; EIF3S11; HSPC021; HSPC025; MSTP005	protein synthesis	-	cytosol, EIF3-complex, nucleoplasm	nucleus, nucleoli	all	2.88	0.94	-
DPH6	diphthamine biosynthesis 6	ATPBD4	Diphthamide is a post-translationally modified histidine residue found only on translation elongation factor 2	-	cytosol, nucleoli	nucleus, nucleoli	all	0.05	0.00	-
NONO	non-POU domain containing, octamer-binding	P54; NMT55; NRB54; MRXS34 P54NRB; PPP1R114	RNA-binding protein which plays various roles in the nucleus	Mental retardation, X-linked, syndromic 34 and papillary renal cell carcinoma	nuclear speckles, nucleoli, RNAPolII-complex	nucleoplasm	all	3.71	0.99	-
EIF2A	eukaryotic translation initiation factor 2A	CDA02; EIF-2A; MST089; MSTP004; MSTP089	translation	-	blood microparticles, cytoplasm, eIF2-complex	mitochondria, cytosol	all	-0.37	0.00	-
LSM14A	mRNA processing body assembly factor	RAP55; FAM61A; RAP55A; C19orf13	pre-mRNA splicing	-	cytoplasm, p-body	cytosol, cytoplasmic bodies	mixed	1.82	0.38	Essential for formation of P-bodies, cytoplasmic structures that provide storage sites for non-translating mRNAs
EIF3K	eukaryotic translation initiation factor 3 subunit K	M9; ARG134; PLAC24; PTD001; EIF3S12; HSPC029; MSTP001; PLAC-24; PRO1474; EIF3-p28	translation	-	cytosol, EIF3-complex, nucleoplasm	cytosol	all	0.87	0.00	-
miscellaneous										
ACACA	acetyl-CoA carboxylase alpha	ACC; ACAC; ACC1; ACCA; ACACAD	fatty acid synthesis	Acetyl-CoA carboxylase deficiency	cytoplasm, actin, fibrillar center, mitochondria	nucleoli fibrillar center, actin filaments, cytosol	mixed	7.52	1.00	not detected in the liver

gene	name	alternative names (PubMed)	function (PubMed, Genecards, UniProt)	disease association (OMIM and UniProt)	subcellular localisation (UniProt and GO)	subcellular localisation (protein atlas)	RNA tissue expression (protein atlas)	Missense Constraint (ExAC)	pLI (ExAC)	other (UniProt)
AHCY	adenosylhomocysteinase	SAHH; adoHcyase	regulates the intracellular S-adenosylhomocysteine (SAH) concentration thought to be important for transmethylation reactions	Hypermethioninemia with deficiency of S-adenosylhomocysteine hydrolase	cytoplasm, melanosome	cytosol	all	1.84	0.94	part of Amino-acid biosynthesis
PMVK	phosphomevalonate kinase	PMK; PMKA; PMKASE; POROK1; HUMPMKI	isoprenoid biosynthesis in peroxisomes	Porokeratosis 1, multiple types	peroxisome, cytosol	n/a	all	1.07	0.00	-
NHLRC2	NHL repeat containing 2	-	response to elevated platelet cytosolic Ca2+ ??	-	extracellular region, platelet alpha granule lumen	nucleoplasm	all	-0.25	0.00	cell redox homeostasis
HSD17B12	hydroxysteroid 17-beta dehydrogenase 12	KAR; SDR12C1	fatty acid synthesis	-	ER membrane	n/a	all	0.54	0.01	-
BMPR2	bone morphogenetic protein receptor type 2	BMR2; PPH1; BMPR3; BRK-3; POVD1; T-ALK; BMPR-II	BMP signalling	Pulmonary hypertension, familial primary, 1, with or without HHT and Pulmonary hypertension, primary, fenfluramine or dexfenfluramine-associated and Pulmonary venoocclusive disease 1	cell mebrane	nucleoplasm, PM	all	1.45	1.00	-
DNAJC7	DnaJ heat shock protein family (Hsp40) member C7	DJ11; DJC7; TPR2; TTC2	co-chaperone regulating the molecular chaperones HSP70 and HSP90 in folding of steroid receptors,	-	cytoplasm, nucleus, microtubules	nucleoplasm, cytosol	all	2.29	1.00	-
GGNBP2	gametogenetin binding protein 2	DIF3; LZK1; DIF-3; LCRG1; ZFP403; ZNF403	spermatogenesis	-	cytoplasmic vesicles	ER	all	2.71	1.00	-
PDAP1	PDGFA associated protein 1	PAP; PAP1; HASPP28	Enhances PDGFA-stimulated cell growth in fibroblasts, but inhibits the mitogenic effect of PDGFB, Among its related pathways are Immune System	-	extracellular region, ficolin1-rich granule lumen	PM, cytosol	all	1.63	0.01	-
NFE2L1	nuclear factor, erythroid 2 like 1	NRF1; TCF11; LCR-F1	globin gene expression in erythrocytes	-	ER, nucleus	nucleus, cytosol	all	1.82	1.00	-
SRRD	SRR1 domain containing	SRR1L; HC/HCC	circadian rhythm?	-	n/a	cytosol	all	-1.25	0.00	-
APAF1	apoptotic peptidase activating factor 1	CED4; APAF-1	initiates apoptosis	-	extracellular region, ficolin1-rich granule lumen, cytoplasm, apoptosome	nucleoplasm, Golgi, cytosol	mixed	0.86	0.00	-

Supplementary Table 4: Collated information about putative negative regulators of MR1 surface expression. Collated information from the indicated sources for the genes listed. Umbrella terms were assigned manually. All websites were accessed throughout April 2017. Copyrightable data from UniProtKB[350] are under the Creative Commons Attribution (CC BY 4.0) License. OMIM = Online Mendelian Inheritance in Man[351]. Copyrightable data from The Human Protein Atlas (www.proteinatlas.org)[354] are under the Creative Commons Attribution-ShareAlike 3.0 International License. Data from the ExAC Browser[324] are under the ODC Open Database License (ODbL) license. Gene ontology (GO) term[352,353] data are licensed under the Creative Commons Attribution 4.0 Unported License and were accessed through the other databases such as GeneCards[349]. Constraint metrics are shown in orange if the gene was considered intolerant based on thresholds reported in the ExAC Browser. Functions related to MR1 trafficking are printed in bold.

gene	name	alternative names (PubMed)	function (PubMed, Genecards, UniProt)	disease association? (OMIM and UniProt)	subcellular localisation (UniProt and GO)	subcellular localisation (protein atlas)	RNA tissue expression (protein atlas)	Missense Constraint (ExAC)	pLI (ExAC)	other (UniProt)
endocytosis, vesicular transport and Golgi										
RALGAPB	Ral GTPase activating protein non-catalytic beta subunit	KIAA1219; RalGAPbeta	Among its related pathways are **Vesicle-mediated transport and Translocation of GLUT4 to the plasma membrane**.	n/a	cytosol	nuclear speckles	all	2.59	1.00	
PICALM	phosphatidylinositol binding clathrin assembly protein	LAP; CALM; CLTH	regulator of AP2-dependent **clathrin-mediated endocytosis**	Leukemia, acute myeloid, somatic and diffuse histiocytic lymphomas	clathrin-coated pit and vesicles, Golgi, nucleus	vesicles	all	0.15	0.97	Co-localised with clathrin in the Golgi area
PPP6R3	protein phosphatase 6 regulatory subunit 3	SAPL; PP6R3; SAPLa; SAPS3; SAP190; C11orf23	regulatory subunit for the protein phosphatase-6 catalytic subunit,**Transport to the Golgi and subsequent modification and Vesicle-mediated transport**, cell cycle progression in response to IL2	-	cytoplasm, nucleus, Golgi, PM	nucleoplasm, PM, cytosol	all	1.08	1.00	May have an important role in maintaining immune self-tolerance
NAA30	N(alpha)-acetyltransferase 30, NatC catalytic subunit	MAK3; Mak3p; NAT12; NAT12P; C14orf35	Necessary for the **lysosomal localisation** and function of ARL8B	-	cytoplasm, nucleus, NatC complex	cytoplasm	all	2.72	0.97	-
VPS41	HOPS complex subunit	HVPS41; HVSP41; hVps41p	**formation and fusion of transport vesicles from the Golgi**	-	late endosome, lysosome, Golgi, clathrin-coated vesicles, AP-3 complex, HOPS complex, microtubules	n/a	all	1.01	0.00	Involved in the direct trans-Golgi network to late endosomes transport of lysosomal membrane proteins independently of HOPS

gene	name	alternative names (PubMed)	function (PubMed, Genecards, UniProt)	disease association? (OMIM and UniProt)	subcellular localisation (UniProt and GO)	subcellular localisation (protein atlas)	RNA tissue expression (protein atlas)	Missense Constraint (ExAC)	pLI (ExAC)	other (UniProt)
FCHO2	FCH domain only 2	-	early step of **clathrin-mediated endocytosis**	-	clathrin-coated pit and vesicles, cytosol, PM	vesicles, centrosomes, cytosol	all	0.53	1.00	Associated with forming but not mature clathrin-coated vesicles
RALGAPA2	Ral GTPase activating protein catalytic alpha subunit 2	p220; AS250; C20orf74; dJ1049G11; bA287B20.1; dJ1049G11.4	among its related pathways are **Vesicle-mediated transport** and **Translocation of GLUT4 to the plasma membrane**	-	PM, cytosol	PM, cytosol	all	-1.36	0.00	-
phosphatidylinositol										
VAC14	PIKFYVE complex component	TRX; SNDC; TAX1BP2; ArPIKfyve	**PI homeostasis in endosomal vesicles**	Striatonigral degeneration, childhood-onset	endosome, ER, Golgi, PAS complex	vesicles, cytosol	all	2.48	0.63	
FIG4	FIG4 phosphoinositide 5-phosphatase	YVS; BTOP; SAC3; ALS11; CMT4J; KIAA0274; dJ249I4.1	regulation of various phosphoinositides -> **vesicle trafficking**	Polymicrogyria, bilateral temporooccipital and Amyotrophic lateral sclerosis 11 and Charcot-Marie-Tooth disease, type 4J and Yunis-Varon syndrome	endosome, ER, Golgi, lipid particle	vesicles, lipid droplets	all	1.22	0.00	Localisation requires VAC14 and PIKFYVE
GPC3	glypican 3	SGB; DGSX; MXR7; SDYS; SGBS; OCI-5; SGBS1; GTR2-2	PI cleavage, metabolism of fat-soluble **vitamins**	Simpson-Golabi-Behmel syndrome, type 1 and Wilms tumor, somatic	PM	PM	lung, kidney, female -> **mucosal?**	0.98	0.99	Cell surface proteoglycan that bears heparan sulfate
immune system										
TMEM131	transmembrane Protein 131	RW1; CC28; YR-23; PRO1048	May play a role in the **immune response to viral infection**	-	membrane	vesicles, intermediate filaments	all	0.39	1.00	-
ANKRD17	ankyrin repeat domain 17	GTAR; MASK2; NY-BR-16	both DNA replication and in both anti-viral and anti-bacterial **innate immune pathways**	-	Localised on chromatin in a cell cycle-dependent manner	nucleus, nuclear membrane	all	5.24	1.00	-
TAPBP	TPN; TAPA; TPSN; NGS17	TAP binding protein	mediates interaction between class I and TAP	Bare lymphocyte syndrome, type I	ER	n/a	all	1.23	0.00	Up to 4 MHC class I/tapasin complexes bind to 1 TAP
TAP1	transporter 1, ATP binding cassette subfamily B member	APT1; PSF1; ABC17; ABCB2; PSF-1; RING4; TAP1N; D6S114E; TAP1*0102N	pumping of degraded cytosolic peptides across the endoplasmic reticulum into the membrane-bound compartment where class I molecules assemble	Bare lymphocyte syndrome, type I	ER	ER, MTOC	mixed	2.75	0.29	-

gene	name	alternative names (PubMed)	function (PubMed, Genecards, UniProt)	disease association? (OMIM and UniProt)	subcellular localisation (UniProt and GO)	subcellular localisation (protein atlas)	RNA tissue expression (protein atlas)	Missense Constraint (ExAC)	pLI (ExAC)	other (UniProt)
TAP2	transporter 2, ATP binding cassette subfamily B member	APT2; PSF2; ABC18; ABCB3; PSF-2; RING11; D6S217E	pumping of degraded cytosolic peptides across the endoplasmic reticulum into the membrane-bound compartment where class I molecules assemble	Bare lymphocyte syndrome, type I, due to TAP2 deficiency and Wegener-like granulomatosis	ER	ER, nuclear speckles	mixed	n/a	n/a	-
HLA-A	major histocompatibility complex, class I, A	HLAA	HLA class I heavy chain	{Hypersensitivity syndrome, carbamazepine-induced, susceptibility to}	PM, early endosome, ER, Golgi	Golgi, PM	mixed	0.62	0.13	-
synapse formation										
NLGN1	neuroligin 1	NL1	formation and remodeling of central nervous system synapses	-	PM, synapse	nuclear bodies, PM	brain, male	1.43	0.76	Colocalised with DLG4/PSD-95 and GRIN1/NMDAR1 (By similarity)
MAGI2	membrane associated guanylate kinase, WW and PDZ domain containing 2	AIP1; AIP-1; ARIP1; SSCAM; MAGI-2; ACVRIP1	scaffold molecule at synaptic junctions by assembling neurotransmitter receptors and cell adhesion proteins	-	cytoplasm, late endosome, synaptosome, PM, cell-cell junctions	n/a	brain, endocrine	3.19	0.88	Localised diffusely in the cytoplasm before nerve growth factor (NGF) stimulation. Recruted to late endosomes after NGF stimulation. Membrane-associated in synaptosomes (By similarity)
DLG2	discs large MAGUK scaffold protein 2	PSD93; PSD-93; PPP1R58; chapsyn-110	multimeric scaffold for the clustering of receptors, ion channels, and associated signaling proteins	-	PM, synapse, axon	vesicles, PM	brain, endocrine, skin	1.64	0.67	-
CADM2	cell adhesion molecule 2	NECL3; IGSF4D; Necl-3; synCAM2; SynCAM 2	cell aggregation, synapse organization	-	PM, synapse, axon	n/a	brain	1.31	0.98	-
GRIK2	glutamate ionotropic receptor kainate type subunit 2	EAA4; GLR6; MRT6; GLUK6; GLUR6; GluK2	transmission of excitatory stimuli across the synapse	Mental retardation, autosomal recessive, 6	postsynaptic cell membrane	n/a	brain	2.83	0.99	
PRSS12	protease, serine 12	MRT1; BSSP3; BSSP-3	structural reorganizations associated with learning and memory operations	Mental retardation, autosomal recessive 1	secreted, synaptic cleft, PM	nucleus, actin filaments	mixed	1.05	0.00	Neurotrypsin
signaling										
ARHGEF38	Rho guanine nucleotide exchange factor 38	KIAA0651, LFP40	GPCR signalling, involved in **innate immune signaling** transduction pathway	-	cytoplasm	nucleoplasm, centrosome	lung, liver, GI, male, female -> **mucosal?**	-0.79	0.01	-

gene	name	alternative names (PubMed)	function (PubMed, Genecards, UniProt)	disease association? (OMIM and UniProt)	subcellular localisation (UniProt and GO)	subcellular localisation (protein atlas)	RNA tissue expression (protein atlas)	Missense Constraint (ExAC)	pLI (ExAC)	other (UniProt)
nuclear transport										
RANBP3	RAN binding protein 3	-	nucleocytoplasmic shuttling	-	cytoplasm, nucleus	nucleoplasm	all	2.12	1.00	Acts as a cofactor for XPO1/CRM1-mediated nuclear export
mitochondrial										
NDUFAF6	NADH:ubiquinone oxidoreductase complex assembly factor 6	C8orf38	mitochondrial respiratory chain	Leigh syndrome due to mitochondrial complex I deficiency	mito inner membrane, nucleus (2 isoforms)	n/a	mixed	0.01	0.00	-
IMMP2L	inner mitochondrial membrane peptidase subunit 2	IMP2; IMP2-LIKE; IMMP2L-IT1	processing the signal peptide sequences used to direct mitochondrial proteins to the mitochondria	Tourette syndrome	mito inner membrane	mitochondria	all	-0.09	0.04	
mTOR and metabolism										
TSC1	tuberous sclerosis 1	LAM; TSC	Involved in microtubule-mediated protein transport, but this seems to be due to unregulated mTOR signaling.	Lymphangioleiomyomatosis and Tuberous sclerosis-1 and Isolated focal cortical dysplasia type lib	cytoplasm, cytoskeleton, PM, TSC1-TSC2 complex	cytosol	all	2.87	1.00	At steady state found in association with membranes
LAMTOR2	late endosomal/lysosomal adaptor, MAPK and MTOR activator 2	p14; ENDAP; ROBLD3; HSPC003; MAPBPIP; MAPKSP1AP; Ragulator2	associated with a **primary immunodeficiency** syndrome, role in **endosomal biogenesis**, part of the Ragulator complex it is involved in amino acid sensing and activation of mTORC1	Immunodeficiency due to defect in MAPBP-interacting protein	late endosome, lysosome, Ragulator complex	nucleoplasm, vesicles	all	2.16	0.48	-
LAMTOR5	late endosomal/lysosomal adaptor, MAPK and MTOR activator 5	XIP; HBXIP	part of the Ragulator complex -> involved in amino acid sensing and activation of mTORC1	-	cytosol, lysosome, Ragulator complex	cytosol	all	0.36	0.01	-
LAMTOR4	late endosomal/lysosomal adaptor, MAPK and MTOR activator 4	C7orf59	part of the Ragulator complex -> involved in amino acid sensing and activation of mTORC1	-	lysosome, Ragulator complex	vesicles	all	0.31	0.03	-

gene	name	alternative names (PubMed)	function (PubMed, Genecards, UniProt)	disease association? (OMIM and UniProt)	subcellular localisation (UniProt and GO)	subcellular localisation (protein atlas)	RNA tissue expression (protein atlas)	Missense Constraint (ExAC)	pLI (ExAC)	other (UniProt)
FLCN	folliculin	BHD; FLCL	energy and/or nutrient sensing through the AMPK and mTOR signaling pathways	Birt-Hogg-Dube syndrome and Colorectal cancer, somatic and Pneumothorax, primary spontaneous and Renal carcinoma, chromophobe, somatic and Renal cell carcinoma	cytoplasm, nucleus, cytosol, lysosome, PM	PM, cytosol	all	1.53	0.96	Mainly localised in the nucleus
TBCK	TBC1 domain containing kinase	TBCKL; IHPRF3; HSPC302	actin organization, cell growth and cell proliferation by regulating the mammalian target of the rapamycin (mTOR) signaling pathway	Disease - Hypotonia, infantile, with psychomotor retardation and characteristic facies 3	cytoplasm, mitotic spindle, midbody	nucleoplasm, nucleoli fibrillar center	mixed	-1.02	0.00	Mainly localised in the cytoplasm during interphase. During metaphase, TBCK accumulates at the mitotic spindle. At the end of mitosis, it is detected at the midbody
ubiquitination and protein turnover										
CUL3	cullin 3	PHA2E	core component and scaffold protein of an **E3 ubiquitin ligase** complex, among its related pathways are **Immune System**	Pseudohypoaldosteronism, type IIE	nucleus, Golgi, Cul3-RING ub ligase complex	n/a	all	4.95	0.97	-
UBE2L3	ubiquitin conjugating enzyme E2 L3	E2-F1; L-UBC; UBCH7; UbcM4	ubiquitination of p53, c-Fos, and the NF-kB precursor p105 in vitro	Systemic lupus erythematosus	nucleus, cytoplasm, ub ligase complex	nucleus, cytosol	all	3.11	0.78	-
CYLD	CYLD lysine 63 deubiquitinase	EAC; MFT; SBS; TEM; BRSS; CDMT; MFT1; CYLD1; CYLDI; USPL2	cleaves Lys-63-linked polyubiquitin chains, Immune System, NFkB signaling, microtubule dynamics	Brooke-Spiegler syndrome and Cylindromatosis, familial and Trichoepithelioma, multiple familial, 1	cytoplasm, cytoskeleton, PM, MTOC, cilia basal body	nucleoplasm, MTOC	all	3.45	0.99	Detected at the microtubule cytoskeleton during interphase. Detected at the midbody during telophase. During metaphase, it remains localised to the centrosome but is also present along the spindle
mRNA processing and translation										
ZCCHC11	zinc finger CCHC-type containing 11	TUT4; PAPD3	degradation of mRNA	-	nucleus, cytoplasm	nucleoli, cytosol	all	1.88	1.00	Translocates into the cytoplasm following treatment of the cell with LPS
LIN28B	lin-28 homolog B	CSDD2	Suppressor of microRNA (miRNA) biogenesis	Neuroblastoma	cytosol, nucleus, nucleoli	nucleus, nucleoli, cytosol	female	1.59	0.72	-

gene	name	alternative names (PubMed)	function (PubMed, Genecards, UniProt)	disease association? (OMIM and UniProt)	subcellular localisation (UniProt and GO)	subcellular localisation (protein atlas)	RNA tissue expression (protein atlas)	Missense Constraint (ExAC)	pLI (ExAC)	other (UniProt)
miscellaneous										
ROBO1	roundabout guidance receptor 1	SAX3; DUTT1	member of the immunoglobulin gene superfamily, axon guidance and neuronal precursor cell migration	Maps within a region of overlapping homozygous deletions characterized in both small cell lung cancer cell lines (SCLC) and in a breast cancer cell line. The promoter region of ROBO1 shows complete hypermethylation of CpG sites in the BT-20 breast tumor cell lines, some primary invasive breast carcinomasa and some primary clear cell renal cell carcinomas (CC-RCC)	PM, axon, cytoplasm	PM	mixed	-0.27	0.00	Receptor for SLIT1 and SLIT2
TRPM3	transient receptor potential cation channel subfamily M member 3	GON-2; MLSN2; LTRPC3	constitutive calcium import	-	PM	n/a	kidney, male, female, brain	2.81	0.00	-
SLIT2	slit guidance ligand 2	SLIL3; Slit-2	axon guidance and neuronal migration	-	secreted, PM	n/a	mixed	1.71	1.00	The C-terminal cleavage protein is more diffusible than the larger N-terminal protein that is more tightly cell associated
CSMD3	CUB and Sushi multiple domains 3	-	epilepsy?	-	PM	n/a	brain, male	-0.12	1.00	-
TASP1	taspase 1	C20orf13; dJ585I14.2	endopeptidase required to cleave MLL, a protein required for the maintenance of HOX gene expression, and TFIIA, a basal transcription factor	-	n/a	PM	mixed	1.69	0.96	-
PDCD10	programmed cell death 10	CCM3; TFAR15	apoptosis, vascular development, **Golgi structural integrity**	Cerebral cavernous malformations 3	cytoplasm, Golgi, PM	n/a	all	1.62	0.99	Partially co-localises with endogenous PXN at the leading edges of migrating cells.
FAM198B	family with sequence similarity 198 member B	ENED; AD021; AD036; C4orf18	???	-	Golgi	nucleoplasm, nucleoli fibrillar center, Golgi	all	-0.09	0.00	-

Supplementary Table 5: Summary statistics for samples submitted for RNA sequencing. RIN = RNA integrity number, conc = concentration, nd = not determined.

sample	cell line	RIN	conc [ng/ul]	volume [ul]	260/280	260/230	extraction method	DNase digestion	% mapped	lines before MAPQ filtering	lines after MAPQ filtering	% loss	lines after removing duplexes	% loss
scr01	scramble	8.6	200	30	2.01	1.68	QIAGEN	on-column	85.34%	61,758,204	47,222,414	23.54	35,585,042	24.64
scr02	scramble	8.2	188	30	2.01	1.05	QIAGEN	on-column	86.35%	59,590,168	45,677,128	23.35	34,093,253	25.36
scr03	scramble	8.5	200	18	1.99	0.46	Ambion	in solution	88.28%	69,933,700	55,414,976	20.76	43,731,666	21.08
scr04	scramble	8.6	74	30	1.93	0.46	Ambion	in solution	88.35%	78,810,076	63,088,356	19.95	50,097,432	20.59
KD01	Sec22b KD	8.3	150	30	1.99	1.65	QIAGEN	on-column	85.17%	54,131,596	41,318,996	23.67	30,661,209	25.79
KD02	Sec22b KD	8.3	60	18	nd	nd	Ambion	in solution	88.77%	67,428,924	54,344,816	19.40	44,131,892	18.79
KD03	Sec22b KD	8.4	176	30	1.96	0.64	Ambion	in solution	89.12%	72,763,174	58,087,332	20.17	46,656,969	19.68
KD04	Sec22b KD	9.1	126	30	2.01	0.89	QIAGEN	on-column	88.64%	63,517,544	50,790,184	20.04	40,973,618	19.33
R01	rescue	8.9	164	30	2.01	1.15	QIAGEN	on-column	89.05%	59,501,478	48,033,936	19.27	37,163,479	22.63
R02	rescue	10	72	30	1.99	1.68	QIAGEN	in solution	87.98%	66,533,534	52,612,002	20.92	41,752,830	20.64
R03	rescue	9	162	30	nd	nd	Ambion	in solution	88.95%	90,134,028	71,279,188	20.92	55,242,267	22.50
R04	rescue	9.1	164	30	2.02	0.91	QIAGEN	on-column	88.13%	56,459,414	44,755,180	20.73	36,261,235	18.98

Supplementary Table 6: Genes differentially expressed in JAWSII scramble control cells vs Sec22b KD cells. Cut-off: FDR < 0.01 and logFC > |1.5|, FC = fold change, CPM = counts per million, FDR = false discovery rate. Sorted by FDR.

genes	logFC	logCPM	F	PValue	FDR
Impact	-4.455461396	5.789748197	844.9703248	1.51E-12	1.74E-08
Perp	-4.599028137	5.173862714	719.810785	4.06E-12	2.34E-08
2510009E07Rik	-9.860692622	4.28998399	608.3724183	1.28E-11	4.92E-08
Palm	-3.119615795	5.599292772	416.0240817	1.03E-10	2.76E-07
Clu	5.285562772	4.890147879	415.0954556	1.20E-10	2.76E-07
Necab1	-3.928937184	3.982627586	369.1436561	2.13E-10	4.09E-07
Hmgcll1	-7.603998186	2.937480831	358.5691105	2.80E-10	4.37E-07
Mst1	-3.873021842	3.927071612	347.0336481	3.03E-10	4.37E-07
Arhgef10l	7.797732608	2.45650831	310.2939057	6.47E-10	8.29E-07
Cd180	6.900168393	3.017626305	297.5152993	8.24E-10	9.51E-07
Tceal8	5.954106587	1.507184141	283.938583	9.36E-10	9.82E-07
Shisa9	-3.139487577	4.253584406	279.9474472	1.06E-09	1.02E-06
Spsb1	-4.031990878	2.404859507	271.4552783	1.22E-09	1.08E-06
Cntn3	3.120051809	3.70860925	268.4787128	1.31E-09	1.08E-06
Ptger3	-2.590447188	3.723817607	262.1691006	1.49E-09	1.14E-06
Grik2	4.535890679	1.661946554	254.603198	1.76E-09	1.27E-06
Prkar1b	3.96718761	2.265945856	245.6339836	2.17E-09	1.47E-06
Dab2ip	7.848675183	1.429523931	243.5991666	2.50E-09	1.60E-06
Myo16	6.848792357	1.837407023	237.0201846	3.04E-09	1.67E-06
Gfod1	-4.084750144	2.506376394	230.489267	3.13E-09	1.67E-06
Adrbk2	4.660261569	4.128486498	234.967601	3.19E-09	1.67E-06
Fam49a	5.894001657	2.389117235	233.3273411	3.32E-09	1.67E-06
Il18rap	7.500332239	0.433755471	228.0055603	3.33E-09	1.67E-06
Pde2a	3.996799114	3.772568188	215.9050575	5.17E-09	2.48E-06
Lama4	-4.403301416	1.646817927	208.9186136	5.50E-09	2.54E-06
Arap3	2.33857851	6.196602488	208.5699336	6.29E-09	2.79E-06
Plin4	-4.550000865	6.447374173	202.9422558	7.34E-09	3.14E-06
Odf3l1	3.6951707	2.856022547	199.346537	7.96E-09	3.28E-06
Olfm1	3.563044645	0.771107135	194.1666399	8.36E-09	3.33E-06
Ush1g	2.644181865	2.724825262	191.7678706	8.98E-09	3.45E-06
Kcnk5	-5.598275853	0.821903176	186.094197	1.07E-08	3.96E-06
Wbscr27	3.822167132	2.179480813	184.4209929	1.16E-08	4.15E-06
Tgfbi	3.475409222	3.824443242	186.3729394	1.19E-08	4.15E-06
Prkcb	4.222163504	4.900817271	180.3327863	1.43E-08	4.86E-06
Sec22b	1.92006735	7.632921729	178.3194767	1.52E-08	5.00E-06
Msr1	1.693419551	6.842176696	172.7869906	1.63E-08	5.22E-06
Ripk3	-3.572018504	3.870044713	164.4414109	2.40E-08	7.16E-06
Sept5	-2.516661452	5.040486516	164.2281931	2.42E-08	7.16E-06
Cd74	1.61272827	10.59444021	160.5122354	2.56E-08	7.21E-06
Zfp105	-7.219891833	0.761284208	160.7581099	2.56E-08	7.21E-06
Scrn1	4.497320085	0.470294074	156.7276386	2.82E-08	7.74E-06
Ccdc120	-6.190706938	0.624865033	153.8633627	3.15E-08	8.45E-06

genes	logFC	logCPM	F	PValue	FDR
Psma8	-5.647194557	0.73351189	152.8813495	3.24E-08	8.50E-06
Ptpn18	2.511560349	3.527139685	151.6854499	3.54E-08	9.07E-06
Fcgr1	3.439678972	5.288096077	150.977812	3.87E-08	9.71E-06
Cd86	2.930992172	3.814012568	147.5213386	4.40E-08	1.08E-05
Slmo1	-4.873802209	0.810377549	143.5272089	4.62E-08	1.08E-05
Phf11b	4.450287045	2.904490264	145.8817369	4.69E-08	1.08E-05
Cfh	7.281608303	1.730750902	145.8782201	4.69E-08	1.08E-05
Pax3	2.252223608	2.307298649	136.9271248	6.01E-08	1.36E-05
Apbb2	5.545384421	0.593781172	135.8735022	6.74E-08	1.47E-05
Ptgis	-4.198697218	0.959192205	132.1100406	7.48E-08	1.60E-05
Serpinb8	-2.663803121	4.410736438	133.2138952	7.75E-08	1.60E-05
AW551984	4.102439497	1.172790787	132.3228616	7.79E-08	1.60E-05
Chpf	-2.314766583	5.690241196	131.6637673	8.27E-08	1.67E-05
Cyp2d22	-2.911513392	2.830653197	130.7650203	8.46E-08	1.67E-05
Ifi44	7.226634529	2.345757993	130.8188382	8.57E-08	1.67E-05
Ctla2b	4.155117853	2.697213871	125.6339177	1.07E-07	2.06E-05
Casp4	1.609450378	4.307964584	121.2694911	1.18E-07	2.23E-05
Plxdc2	-2.551134361	2.970287847	120.8016218	1.26E-07	2.34E-05
Nfatc2	2.990329755	2.181853316	116.6040799	1.53E-07	2.75E-05
Thrb	2.85295252	2.00167973	115.7992651	1.55E-07	2.75E-05
Tgfb2	-4.163034836	3.571613186	116.220227	1.64E-07	2.79E-05
Gm13544	-3.837266516	1.574667206	114.7367822	1.67E-07	2.79E-05
Fam160a1	-1.927074978	2.151669688	111.8522249	1.84E-07	3.00E-05
Pcyt1b	-2.941056039	3.039357249	113.6806993	1.85E-07	3.00E-05
Slc9a3r2	-2.82117194	1.65146588	111.5010958	1.88E-07	3.00E-05
Gja5	4.013236147	0.87081664	110.8266384	1.98E-07	3.09E-05
Eid1	2.122531072	3.94127438	111.4561656	2.06E-07	3.17E-05
Lamc2	-3.572438665	4.202343287	110.7885177	2.13E-07	3.19E-05
Cd48	-1.567064803	4.322973714	108.2497278	2.21E-07	3.26E-05
Hapln4	3.223448919	1.90941807	109.1987807	2.29E-07	3.31E-05
Uchl1	4.800444972	1.221299677	109.2587273	2.29E-07	3.31E-05
Zmat4	3.270928116	0.069582247	104.7677456	2.64E-07	3.75E-05
Barx2	5.2071127	0.649234226	106.152142	2.68E-07	3.77E-05
Rhoj	3.961582953	-0.022260358	103.5957412	2.80E-07	3.85E-05
Rasd2	6.437100832	1.662985447	105.0260556	2.84E-07	3.86E-05
Clcf1	-2.596960302	2.750222995	103.3506388	3.03E-07	4.05E-05
Tagap	1.794198304	3.343661216	101.9553705	3.06E-07	4.05E-05
Dync1i1	3.314480962	0.879152164	101.6494939	3.17E-07	4.15E-05
Cst7	2.677151634	0.895045647	100.9310875	3.23E-07	4.19E-05
Apol9a	4.857655755	2.846423574	102.2507819	3.28E-07	4.21E-05
Rfng	-1.705599674	5.784970928	100.777376	3.55E-07	4.45E-05
Tmem202	2.018521467	2.493950701	97.75005263	3.84E-07	4.64E-05
Prnp	2.390532475	1.390425536	97.65615978	3.86E-07	4.64E-05
Itga7	-3.229622108	2.787286066	99.03086604	3.90E-07	4.64E-05
Ear1	-1.936220683	6.517440838	98.47310158	4.02E-07	4.73E-05

genes	logFC	logCPM	F	PValue	FDR
Fam189b	2.390070837	1.949936903	95.34845391	4.40E-07	5.07E-05
Atp9a	2.520484222	1.027517458	95.06503815	4.47E-07	5.08E-05
Cd14	1.890235684	7.099268239	96.46011248	4.49E-07	5.08E-05
Aldh1b1	1.990465938	4.729696326	94.59679771	4.99E-07	5.53E-05
Sv2a	2.563494656	2.237909608	93.47026323	5.08E-07	5.53E-05
Nxf7	2.181597481	3.730451015	93.34352412	5.36E-07	5.73E-05
Rhox2h	-2.632384867	3.535653048	93.16281805	5.42E-07	5.73E-05
Slc9a2	2.143137091	3.060252055	92.31790386	5.47E-07	5.73E-05
Slc2a3	3.305500444	0.875778894	91.77059467	5.54E-07	5.76E-05
Col4a4	5.301975327	-0.394535416	91.59573542	5.66E-07	5.83E-05
Etl4	3.896326482	1.55880033	91.48933038	5.97E-07	6.09E-05
Fhod3	-4.546713292	2.333888476	90.27650447	6.41E-07	6.48E-05
Plin5	-4.680511616	1.091446522	88.93200477	6.94E-07	6.78E-05
5430416O09Rik	-4.192511677	0.480233847	87.31240264	7.32E-07	7.09E-05
Rbms3	-2.60907926	3.781703982	87.84056897	7.41E-07	7.10E-05
Ptpn22	2.060210134	2.780417104	86.68594743	7.45E-07	7.10E-05
Lrrc27	1.656979848	5.396047127	86.65101941	7.96E-07	7.35E-05
H2-Ob	3.190411254	5.987401904	86.41456094	8.08E-07	7.36E-05
Gpr56	2.387895906	1.270791543	85.09936612	8.10E-07	7.36E-05
Krt79	-3.294104403	5.510228266	86.24522517	8.16E-07	7.36E-05
Cpq	4.711759086	-0.167440474	85.07606084	8.51E-07	7.61E-05
Cystm1	3.295368041	2.148509467	85.13915209	8.74E-07	7.76E-05
Oasl2	5.044888485	5.811068077	84.03635526	9.37E-07	8.08E-05
Csn1s1	3.563461487	6.703806951	84.00573556	9.38E-07	8.08E-05
Ccdc166	-4.043985976	0.53941168	83.73104411	9.53E-07	8.08E-05
Ttc12	4.657371281	0.143906062	83.12670646	9.92E-07	8.24E-05
A330021E22Rik	-3.441828828	1.644062137	82.9632266	1.00E-06	8.24E-05
Ctla2a	6.470918105	1.641091937	66.84895413	1.01E-06	8.24E-05
Rasgrp3	3.115128457	2.277511882	82.01282271	1.07E-06	8.59E-05
Zbtb32	-1.951711375	6.137427041	81.7751933	1.08E-06	8.64E-05
4930523C07Rik	-2.815126564	2.07162713	81.45080715	1.09E-06	8.64E-05
Gimap9	1.581905162	3.632091545	80.32460835	1.10E-06	8.71E-05
Daglb	-4.845089307	-0.066998741	80.88172162	1.15E-06	8.99E-05
Tap1	1.538314894	6.934195498	79.35873939	1.27E-06	9.80E-05
Wfdc12	-2.908502289	3.884965471	79.16928306	1.28E-06	9.86E-05
H2-Q5	3.048778888	2.981019291	79.05279701	1.29E-06	9.87E-05
Cygb	-4.663072085	-0.054125817	78.67622216	1.31E-06	9.97E-05
H2-Q4	2.096409791	6.616774563	77.04290319	1.48E-06	0.00011006
Apol9b	4.141009042	1.746178695	76.80644343	1.50E-06	0.000111126
A230050P20Rik	2.86714045	1.416260609	76.6404834	1.52E-06	0.000111674
Phf11a	4.386346486	1.384120292	76.54489941	1.53E-06	0.000111694
Fndc1	6.421557362	0.65169323	76.37710634	1.55E-06	0.000112271
Cx3cl1	2.48545837	2.309097934	76.05323864	1.58E-06	0.000113873
Grb10	3.913455686	1.847304724	75.97298214	1.59E-06	0.000113873
Fxyd7	3.158601956	1.057407687	75.89804517	1.60E-06	0.000113873

genes	logFC	logCPM	F	PValue	FDR
AA467197	6.146585671	4.722338362	75.67082449	1.62E-06	0.00011496
Chl1	-3.18675202	2.11364003	75.5217569	1.64E-06	0.00011544
4930550L24Rik	2.961840211	2.895050205	75.01026369	1.70E-06	0.000118164
Ptrf	-2.766074229	5.240720176	74.37220778	1.78E-06	0.00012244
Gbp4	2.680666106	0.199432572	73.31626342	1.78E-06	0.00012244
2010002M12Rik	5.257427036	0.039591738	74.0677873	1.82E-06	0.000123963
Pianp	2.823512186	1.219343722	73.81211747	1.83E-06	0.000123963
2410004P03Rik	-1.545302875	2.657173085	72.81258944	1.85E-06	0.000124536
Cmklr1	2.744034448	2.576081355	73.75283801	1.86E-06	0.000124536
Tm7sf3	-1.518432099	5.088572634	73.41962149	1.90E-06	0.000126037
Il1r1	-3.369363295	0.085795946	71.55263452	2.03E-06	0.000132763
Glrp1	2.701908621	1.572648186	72.23949691	2.06E-06	0.000133621
Nrbp2	-3.972577105	1.454871802	72.12961141	2.08E-06	0.000134329
Cryab	5.773935783	2.361827825	71.96274469	2.11E-06	0.000134795
Htra3	-2.895017659	5.212339945	71.82304379	2.13E-06	0.000135065
Rhox2d	-5.760301725	2.422930922	71.73082935	2.15E-06	0.000135224
Pram1	2.213687479	3.083572972	71.28545301	2.22E-06	0.0001389
Steap1	-4.488594589	1.789907668	70.59249383	2.33E-06	0.000144531
Tal1	2.391860449	2.269889443	70.47785674	2.35E-06	0.000144702
Proca1	-2.471612764	0.754113842	69.49669158	2.36E-06	0.000144702
Pnpla5	-2.999592184	0.105173504	69.2543392	2.40E-06	0.000145668
Gas7	4.918075068	-0.14720444	70.12477651	2.41E-06	0.000145668
Scml4	1.983479962	2.095734317	69.05157891	2.44E-06	0.000146505
Hepacam2	2.665756885	1.032545231	68.50303281	2.56E-06	0.000152594
Etv1	2.556861132	1.530588747	69.18256227	2.57E-06	0.000152594
Slc39a10	1.652205841	2.696861274	68.22882863	2.60E-06	0.000153523
Mfap3l	4.121989788	-0.25721907	68.9307949	2.63E-06	0.000154861
P2ry1	2.505664344	0.311427741	67.53060802	2.74E-06	0.000159727
Unc5b	2.901523806	2.454622587	68.33943244	2.76E-06	0.000159727
Cd52	2.782851605	6.523183167	68.25657866	2.77E-06	0.000159727
Apoc1	-4.370686599	2.088381292	68.19433438	2.79E-06	0.000159727
Ly6e	1.569320608	9.777318489	68.13923469	2.80E-06	0.000159727
Nynrin	-2.894994697	0.828166313	67.09209314	2.83E-06	0.000160901
Mrap	-2.861926192	1.030481749	66.69873527	2.97E-06	0.000167203
Rgma	4.019045321	0.05774283	67.14933005	3.02E-06	0.000168866
Oas1g	2.625483389	3.864276424	65.59036252	3.40E-06	0.000189564
Fcrls	9.862695913	1.18216913	51.27547883	3.57E-06	0.000196208
Hspb8	-1.786893816	2.816307596	64.40445206	3.57E-06	0.000196208
Ly6a	2.516411837	3.615975449	64.24816031	3.78E-06	0.000203672
Gfra1	1.99951833	3.079443375	64.19777437	3.80E-06	0.000203672
Nap1l3	-3.646641056	-0.301984406	63.37331707	3.89E-06	0.000205752
Tinagl1	2.970907352	0.493673307	63.53744032	3.92E-06	0.000205752
Gpr97	4.422393403	-0.382106747	63.7725324	3.93E-06	0.000205752
Cbr2	-1.833489162	4.062330951	63.72526874	3.94E-06	0.000205752
Adam28	-3.545233296	2.03597348	63.66748063	3.96E-06	0.000205775

genes	logFC	logCPM	F	PValue	FDR
Klra17	-4.218951756	0.62858327	63.38970163	4.05E-06	0.000209034
Sash1	1.532818937	3.899491612	63.2440859	4.06E-06	0.000209034
Col24a1	4.045123223	4.941862809	63.11695821	4.14E-06	0.000212216
1500015A07Rik	1.645477671	2.8697035	61.6093073	4.43E-06	0.000223205
Oas1a	2.053509663	5.983099529	61.93427377	4.56E-06	0.000228561
Kcnk13	1.75188802	2.031390725	61.04183474	4.61E-06	0.000228821
A530032D15Rik	2.096616458	2.301961074	61.71579436	4.61E-06	0.000228821
Spats2	-6.222261392	2.248622651	61.7625263	4.62E-06	0.000228821
Zbtb7c	3.770911885	1.35311914	61.26814151	4.81E-06	0.000234318
Ebf1	-4.442339903	1.194926405	59.90522089	5.40E-06	0.000256434
Nr1i2	-2.282434999	0.557519253	58.62302351	5.66E-06	0.000265308
Rbfox1	1.683019724	1.942618466	58.48378885	5.73E-06	0.000267444
Gfpt2	-2.966684533	2.233275022	59.08800256	5.78E-06	0.000268936
Cysltr1	3.282826664	2.316743242	58.94591209	5.85E-06	0.000271126
Fgf1	3.565197441	1.240865417	58.38114476	6.14E-06	0.000282326
Cxx1c	1.925335405	1.494644422	57.41785294	6.29E-06	0.000286615
4933412E12Rik	1.832308864	1.852608037	57.29219068	6.36E-06	0.000288669
Cyp2u1	2.627664622	0.092888312	57.01261746	6.52E-06	0.000294739
Cited1	3.508222468	0.184266034	57.39222125	6.69E-06	0.000300452
Bmp8a	-4.155899897	4.324463916	56.88943242	7.00E-06	0.00031279
1700001O22Rik	-2.244046178	0.24242966	56.09066524	7.08E-06	0.000314655
Napsa	2.045614041	7.019619056	56.73447874	7.09E-06	0.000314655
Pbx1	-3.384100673	1.983851805	56.5005848	7.24E-06	0.000319096
Gm7609	3.601103568	-0.485531663	56.22314614	7.25E-06	0.000319096
P2rx5	-3.648974063	0.525724002	56.08670932	7.51E-06	0.000329465
Aoah	1.699953663	5.393108547	55.738861	7.75E-06	0.000338582
Adamdec1	-2.959235845	5.874354123	55.656453	7.81E-06	0.000339806
Rap1gap2	-3.247871262	0.761283021	55.23645638	8.11E-06	0.000349201
Map2k6	2.680525733	-0.259537462	54.58414408	8.11E-06	0.000349201
Slc2a4	-2.213140241	1.062781708	53.88670321	8.65E-06	0.000369295
Treml4	-2.398486511	5.8320707	54.48973911	8.68E-06	0.000369295
Cp	2.082493617	1.765898657	53.9287864	8.93E-06	0.000377427
Trim40	3.537762886	1.573781466	53.97651619	9.09E-06	0.00038253
Akr1c13	1.786398831	3.714753418	53.73447843	9.30E-06	0.000385859
B4galt6	-5.511102775	1.426644281	53.69360342	9.34E-06	0.000385931
Tmem14a	2.259130018	0.756176357	52.89855554	9.53E-06	0.000391176
Sp100	1.969522132	5.098388037	53.470738	9.53E-06	0.000391176
Grid1	-2.938563105	1.951982675	53.23874044	9.74E-06	0.00039548
Ltb4r1	-3.204568594	3.935583303	52.85362323	1.01E-05	0.000407096
Amotl2	-2.444405889	3.676512241	52.46863632	1.05E-05	0.000420428
Arhgap8	2.021696737	2.735867342	52.42481466	1.05E-05	0.000420428
Wwtr1	2.637906493	0.604200334	52.18551412	1.07E-05	0.000425051
Olfr1259	-3.104207736	-0.25530746	51.42340979	1.09E-05	0.000430251
Pknox2	1.682141906	4.650419074	51.94792486	1.10E-05	0.000431347
Nlrc5	2.167863571	4.095211044	51.86598263	1.11E-05	0.000433247

genes	logFC	logCPM	F	PValue	FDR
Phf11d	2.66125151	3.045668052	51.64551195	1.13E-05	0.000439408
Trim30a	2.390829542	5.65711431	51.61177758	1.14E-05	0.000439408
Mmp27	-3.102919309	1.755961493	51.23626973	1.18E-05	0.000452788
Ccl22	3.201269274	3.660709313	51.19437754	1.18E-05	0.000452788
Kcnip4	-2.004751756	1.964849146	50.73375636	1.21E-05	0.000463425
Shisa4	-2.530261598	3.518680535	50.54430695	1.26E-05	0.000478061
Zmpste24	-1.570145667	4.971920874	50.53016691	1.26E-05	0.000478061
Hgfac	3.20255881	1.655871018	50.48196418	1.27E-05	0.000478409
Etv4	-3.299879924	2.581647994	50.45528142	1.27E-05	0.000478409
D630033O11Rik	1.62509814	1.683590811	49.65678299	1.30E-05	0.000486711
Zeb1	1.561533906	1.612226238	49.64781123	1.30E-05	0.000486711
St6gal1	1.702233313	6.25084548	50.17300407	1.30E-05	0.000486711
Cd83	-2.316164292	0.655039321	49.42155128	1.34E-05	0.000493736
Tnc	-4.024470411	1.210099456	49.9015011	1.34E-05	0.000493736
Ear5	-3.841777032	4.334848304	49.6698642	1.37E-05	0.000503513
Klra10	-2.484687098	2.728564338	49.53324639	1.39E-05	0.000504284
Pdgfa	1.767468445	2.95275925	49.52614859	1.39E-05	0.000504284
Fam132b	-2.213301613	0.407586141	48.77692062	1.42E-05	0.000510919
Rps6ka2	1.907437399	4.041761918	49.30161565	1.42E-05	0.000510919
BC049352	3.427136576	-0.01444208	49.21005859	1.43E-05	0.000512277
Acaa1b	-4.284003179	1.100149164	49.12523411	1.45E-05	0.000515021
Kcnh4	-2.629133113	1.31645034	48.9908994	1.47E-05	0.000520354
Fam46c	4.591501831	-0.017811231	48.48356871	1.54E-05	0.00054247
Sdsl	-3.407712455	0.727482754	48.22385031	1.58E-05	0.000553486
Lamb2	-3.236741924	3.713071945	47.93693345	1.63E-05	0.000568083
Pdia5	2.489507404	2.012904001	47.85638304	1.64E-05	0.000569311
Slc4a5	-2.057187959	-0.315314638	47.19105592	1.67E-05	0.00057646
I830012O16Rik	3.765462652	1.5874779	47.61195921	1.69E-05	0.000580181
Enpp1	3.306388335	0.949746869	47.3727581	1.73E-05	0.000591024
Serpina3g	2.356109475	2.659800794	47.14514622	1.77E-05	0.000599666
Fyb	3.619030322	0.472906306	46.40232912	1.91E-05	0.000643649
Grm8	10.68381122	1.964019349	73.82094475	1.91E-05	0.000643649
Elovl7	1.554049915	4.804386097	46.26414017	1.94E-05	0.000646137
Nckap5l	1.626493383	7.384983562	46.25678134	1.94E-05	0.000646137
Gpr141	3.256899484	3.796414689	45.95229623	2.00E-05	0.000661353
Sesn3	-1.984970225	1.212959253	45.37137761	2.03E-05	0.000665435
Sdr42e1	-1.824738062	2.235802081	45.52115113	2.04E-05	0.000665435
Trim2	2.105115493	2.052708084	45.78552063	2.04E-05	0.000665435
Fam213b	2.983437865	1.002603325	45.58212827	2.08E-05	0.000671509
Fam198b	1.595348709	3.81968174	45.51985282	2.09E-05	0.000671509
Trim30d	3.003401571	3.901530272	45.20626597	2.17E-05	0.000688048
Krt222	-2.268541423	0.671906509	44.91568072	2.17E-05	0.000688048
Cadps	7.204576649	0.21413462	33.33140805	2.18E-05	0.000689258
Mum1l1	-1.978801921	2.943922885	44.96930663	2.22E-05	0.000694944
Scgb1a1	-5.399946078	0.057049559	44.94749836	2.23E-05	0.000694944

genes	logFC	logCPM	F	PValue	FDR
Rhox2g	-4.420897818	2.765363663	44.87600225	2.24E-05	0.000697386
Fmn2	2.33492598	-0.32304373	44.20267174	2.29E-05	0.000711387
Sparcl1	-3.790606685	6.124402283	44.58642268	2.31E-05	0.000715558
Folr2	2.628963543	-0.327998422	44.16678417	2.32E-05	0.000716573
Spry1	2.153484437	1.43139826	44.46608316	2.34E-05	0.000721034
Chdh	-3.15523182	0.285629265	44.2755411	2.39E-05	0.000730197
Gm5431	3.015918577	2.108795573	44.17528326	2.42E-05	0.000734847
Gsta3	3.197376652	3.935705208	43.98744278	2.47E-05	0.000745508
Abcg4	-1.671743827	4.200916692	43.86179226	2.50E-05	0.000753813
Erv3	-3.038693784	1.590260621	43.72755138	2.54E-05	0.000762957
Dlg3	3.644312651	1.098580554	43.58873131	2.58E-05	0.000772632
Afap1	2.173409303	1.797533442	43.36719445	2.64E-05	0.000785514
Fxyd2	2.995369753	0.199786029	43.3528185	2.65E-05	0.000785514
Zbp1	1.653095707	5.326584849	43.33185525	2.65E-05	0.000785514
BC024139	-3.545659894	0.043776455	43.28864635	2.66E-05	0.000785514
Gm14446	3.558212554	-0.270178229	42.85301857	2.78E-05	0.000813135
Pdzk1ip1	2.813489876	2.537981207	42.67590476	2.85E-05	0.000829843
Ifi202b	1.587123296	5.169797774	42.66530538	2.86E-05	0.000829843
Hpgd	3.672160829	4.614148163	42.46882825	2.92E-05	0.000841904
Fam131a	-2.286254243	1.131277949	42.33863914	2.96E-05	0.000852151
Otop1	-5.494284313	1.306681685	42.11917161	3.04E-05	0.000869112
F11r	-2.996203151	2.854577319	41.72647517	3.17E-05	0.000897854
Erc2	-2.589536222	3.16110895	41.68496642	3.19E-05	0.000899494
Map2	-5.031887062	1.146627219	41.5867341	3.23E-05	0.000907382
Zfp30	-3.565243518	-0.597783009	41.22455498	3.36E-05	0.000936578
Lamb1	-2.991834606	2.03947535	40.959695	3.47E-05	0.000960887
Iigp1	2.675718261	1.395621713	40.67082052	3.58E-05	0.000991122
Stk32c	3.148589518	-0.121803189	40.59951447	3.61E-05	0.000994581
Irf7	2.408468248	5.251845873	40.26064337	3.76E-05	0.001032143
Rgs3	2.273549068	0.586878428	39.97068944	3.82E-05	0.001043479
Tspan12	4.660724294	0.595533276	29.03685487	3.85E-05	0.00104524
Tm4sf19	-2.547784465	1.540935064	40.05181602	3.85E-05	0.00104524
Cmpk2	2.751111632	3.39205635	39.86767474	3.94E-05	0.001065358
Rpph1	2.803324151	1.348474199	39.84966957	3.94E-05	0.001065358
Ddx60	2.347066711	5.000156442	39.72957681	4.00E-05	0.001078026
Glt28d2	-2.710455741	-0.113851088	39.39093935	4.03E-05	0.001079156
Drd1a	-2.0262327	1.150429194	39.40683289	4.05E-05	0.001082305
Myzap	1.724201803	3.625010036	39.32749822	4.20E-05	0.001107357
Ces2c	-2.2871221	4.373883752	39.13787061	4.29E-05	0.001124954
Greb1	3.428634719	-0.062743805	39.09008785	4.32E-05	0.001128831
Csn2	1.580665982	9.269580735	38.95654468	4.39E-05	0.00114443
Wfdc10	2.870324073	0.474967748	38.87303295	4.43E-05	0.001149513
Prl2c5	-3.508490898	0.401793173	38.7720286	4.48E-05	0.001154405
Ap1s3	2.27646137	-0.435718056	38.17197782	4.61E-05	0.001184707
Amy1	1.584013659	0.359860572	38.00612246	4.71E-05	0.001203956

genes	logFC	logCPM	F	PValue	FDR
Il27	1.924840802	2.726900133	38.3152132	4.74E-05	0.001209156
Mmrn1	4.964451834	0.853560858	27.54043117	4.78E-05	0.001217382
Fkbp10	1.766427075	0.634421952	37.81284597	4.82E-05	0.001219299
Spon2	-3.485605621	2.425916244	38.03924503	4.90E-05	0.00123621
Nmnat2	-2.448426984	0.935939526	38.00747307	4.92E-05	0.00123621
Klra9	-2.142262226	3.93779886	37.83550814	5.02E-05	0.001257038
Myom3	-1.84220447	4.486599257	37.33471325	5.34E-05	0.001319923
Klk1b27	2.323235064	0.580861085	37.0637847	5.53E-05	0.001356414
H2-T23	1.608816546	6.951137971	37.04178973	5.54E-05	0.001357251
Pecam1	-1.556345645	2.411255251	36.89935603	5.56E-05	0.001359509
Mx1	4.429071227	-0.270522954	36.96798903	5.59E-05	0.001361884
Tnfrsf11a	2.030622107	0.679459817	36.75374853	5.61E-05	0.001361884
Mogat2	-1.978812221	5.493048036	36.86409821	5.67E-05	0.001370263
Slfn4	1.67293481	6.107779807	36.8364209	5.69E-05	0.001372143
Oas3	3.737174021	6.647703072	36.72312165	5.77E-05	0.00138887
Plxnb3	-1.782655243	2.524331778	36.66079282	5.81E-05	0.001395391
Mamdc2	-3.410709159	1.275861733	36.46976594	5.95E-05	0.001418746
Dok7	2.436543346	3.369993126	36.23224115	6.14E-05	0.001453355
Sil1	-1.81132611	3.016620322	36.06479311	6.27E-05	0.001478542
Apbb1	2.25791802	2.64389303	35.77446027	6.51E-05	0.001526151
F3	2.137850603	2.108068978	35.76875585	6.51E-05	0.001526151
Xaf1	2.496426857	4.950405611	35.32069189	6.90E-05	0.001600514
Adcy6	-2.158260033	1.062475082	35.0635903	7.10E-05	0.001637621
Abhd6	4.888994132	-0.205763872	24.34518044	7.52E-05	0.001720712
Lmo2	1.705188925	4.298623392	34.41509133	7.76E-05	0.001769525
Rhbdf1	-2.319918236	0.713720263	34.29054425	7.89E-05	0.00178829
Abcc9	-3.606086264	0.149661132	34.20248277	7.98E-05	0.001798673
Samd14	-1.668148552	3.669749852	34.15224525	8.04E-05	0.001802039
Igf2r	-2.748147908	3.73650984	34.14108084	8.05E-05	0.001802039
Btc	-1.687761227	0.174946119	33.82769035	8.06E-05	0.001802039
Sorl1	2.615526801	4.548224779	34.04076796	8.16E-05	0.001816445
Fam109b	-1.627032406	2.088206489	33.9869418	8.18E-05	0.001818145
Eya4	1.88206687	2.148470862	33.97548327	8.23E-05	0.00182526
Afap1l1	1.893939201	0.711019551	33.72084664	8.32E-05	0.001842394
Dppa2	-2.57719761	-0.169987769	33.75795878	8.36E-05	0.001844541
Il17rc	-2.717007121	2.745891941	33.73042882	8.50E-05	0.001864515
Pitpnm2	1.606607441	1.154682845	33.44906032	8.53E-05	0.001866581
Pcdh10	2.283608727	-0.118762512	33.32580964	8.78E-05	0.001911027
Gm5483	2.89438147	0.563447731	33.44841114	8.83E-05	0.001918333
S1pr4	1.682819793	1.216417479	33.09972245	8.99E-05	0.001949087
Tiam2	1.961174142	3.81572835	32.97422624	9.42E-05	0.001998955
Ms4a7	1.613649754	3.906233605	32.96547851	9.43E-05	0.001998955
Cnn2	-2.192761032	2.063407064	32.95407302	9.44E-05	0.001998955
Klk1b1	2.981361054	3.926434706	32.61333797	9.90E-05	0.00208649
Zfp951	-2.838589063	0.060088252	32.48323928	0.00010074	0.002116465

genes	logFC	logCPM	F	PValue	FDR
Plekhh1	-3.061915729	0.440980887	32.40102473	0.00010189	0.002136728
Thbs1	6.734152488	1.714435591	22.80019913	0.000102609	0.002147898
Yipf7	3.661365514	0.254606765	32.15465207	0.000105428	0.002183145
Trpc4	-2.616475198	2.281027912	32.09980603	0.000106236	0.002193756
Inpp4b	6.258081311	-0.655447399	22.38208066	0.000106321	0.002193756
Zfp11	-1.716975935	1.001531734	31.7195764	0.000108607	0.002224992
Slc1a3	-2.648521348	0.906658394	31.71236028	0.000112147	0.002285221
Sgsm1	-3.14772931	1.108318976	31.45590596	0.000116272	0.002328271
Gbp9	2.397715097	3.485834574	31.41034504	0.000117023	0.002338227
Arhgap29	2.950390104	-0.693038789	31.40120389	0.000117175	0.002338227
Lrrc34	-1.795036044	1.86156451	31.374154	0.000117624	0.00234314
Clec4a1	-1.846798086	2.233304254	31.19068275	0.000120726	0.002400779
Pde1a	-2.128707302	2.294410869	31.06467408	0.000122911	0.002440036
Apoc2	-1.821279542	1.445088554	30.91683898	0.000125535	0.002487833
Gm6634	6.071703608	-0.808896229	21.27657569	0.00012863	0.002536109
Cidec	-1.528589912	3.033392219	30.69831089	0.000129534	0.002540884
Tmem45a	-3.227951223	-0.731150417	30.59729972	0.000131432	0.002573748
Klra3	-1.984394759	6.045485362	30.51267153	0.000133048	0.002600971
Fbxo2	-1.665860481	1.636101361	30.43394698	0.000133737	0.002610022
Slc13a4	-1.843144112	0.769355122	30.25954871	0.000135128	0.002629539
Treml1	2.42196525	2.33916804	30.25728569	0.000138066	0.002676392
Angptl6	2.015119476	2.207553256	30.17690241	0.000139691	0.002690481
Efnb1	-1.540411143	1.745647118	30.02802976	0.000139726	0.002690481
Pappa	-3.204279371	1.590020914	30.13425926	0.000140562	0.002702074
Pdgfb	2.93838336	4.671821771	29.9731467	0.000143911	0.002757266
Fam124a	-2.457490523	2.973148082	29.92902184	0.000144845	0.00276139
Mx2	2.806793338	1.062963868	29.79737293	0.000147672	0.002810647
Syne1	2.092739766	4.234712704	29.68671454	0.000150099	0.002846588
Oasl1	2.709928069	1.582080603	29.67758738	0.000150301	0.002846588
Ifit2	2.103053895	5.310079872	29.65653645	0.000150769	0.002846658
Als2cr12	-2.603918254	0.001558757	29.44850883	0.000152406	0.002872302
Vill	-2.800621423	5.83066227	29.52085057	0.000153824	0.002894297
Amph	-2.265881519	0.517469417	29.49152618	0.000154494	0.002895555
Sectm1a	-2.375446176	2.087461335	28.99789393	0.000166296	0.003044537
Gpr33	-2.33308924	-0.104222098	28.95108337	0.000167469	0.003061152
S1pr1	2.445825805	0.058091173	28.80777867	0.00017112	0.003110178
Ifit3	3.356537301	4.005733854	28.52279675	0.000178662	0.00322992
Rhpn2	-1.752341759	3.590895101	28.3238645	0.000184157	0.003298656
Ces5a	2.549932114	1.026776846	28.32304712	0.00018418	0.003298656
Zfp109	-3.379423428	0.043149632	28.26052031	0.000185948	0.003320011
Zkscan7	-1.883008832	1.160652102	27.70582762	0.000202534	0.003564949
Apold1	1.967378531	1.030481859	27.69869868	0.000202758	0.003564949
1110046J04Rik	1.572056175	2.176270862	27.63669348	0.000204719	0.003588502
Rtn2	-2.97445884	1.158611452	27.59408473	0.00020608	0.003606878
Ifi27l2a	1.739536108	6.74545958	27.52243039	0.000208393	0.003641829

genes	logFC	logCPM	F	PValue	FDR
Gprc5b	3.152115926	1.841384003	27.21974849	0.000218503	0.003795508
Gcat	-2.23246714	3.530974753	27.09110446	0.000222973	0.003867327
Mapk8ip1	-2.341702927	2.367312143	27.00856903	0.000225897	0.003906295
Capn5	1.548299835	3.491006075	26.82297403	0.000232638	0.004010829
Dmkn	-1.719102086	1.281881494	26.73332634	0.000235978	0.004056286
Pltp	-2.503732192	2.381626363	26.61774531	0.000240367	0.004115848
Ctf1	-1.928484257	0.451674119	26.52038778	0.000243267	0.004138416
Itln1	2.971775304	0.353506988	26.36026071	0.000250493	0.004223953
Bst2	1.746622603	8.036516207	26.30100979	0.000252893	0.004251993
Rnase6	-1.877516232	1.877837114	26.26818173	0.000254234	0.004262121
Plcd1	-2.588046298	0.58726907	26.2319088	0.000255726	0.004280908
2210404O09Rik	-1.571409022	0.961743985	25.9171771	0.000263364	0.004377007
Nfatc4	-1.581480903	2.504331046	25.93352637	0.000268394	0.004433805
Pamr1	1.937743864	1.627949896	25.78230471	0.000275094	0.004519848
Gm266	1.761854346	-0.062731681	25.53982632	0.00027742	0.004551577
4931408D14Rik	-2.326226858	0.529022989	25.53157656	0.000286638	0.00465784
Tusc5	-2.145195661	-0.426739835	25.34122298	0.000286723	0.00465784
Atp1b2	-2.58100343	1.317436447	25.51814363	0.000287272	0.004660195
Oas2	2.877368853	5.436288774	25.29960869	0.000297826	0.004811092
Mical2	-3.116295518	1.201440633	25.23345745	0.000301109	0.00485733
Grin1	2.411373886	0.54413121	25.00553794	0.00031275	0.00499621
Gm826	2.016921947	0.489330742	24.92590724	0.000316941	0.005056156
Pdzrn3	1.77474538	4.353288615	24.89199056	0.000318746	0.005070921
Glra3	2.103465337	0.403290087	24.84098698	0.000320404	0.005090271
Cd163	2.387609675	1.395040014	24.75300245	0.000326269	0.005169213
Cyp2j9	-2.513340481	-0.147893568	24.72574875	0.000327768	0.005185845
Jup	-1.672208321	1.394261951	24.70348498	0.000328999	0.005198011
Pth1r	-1.799268079	0.404797945	24.49833391	0.000336557	0.005295839
Ccl2	3.342058696	1.517077748	24.45951644	0.000342847	0.005356561
Kcnk3	-3.604726693	-0.206813624	24.15669558	0.000360995	0.005596391
Rhox5	1.510410522	4.329386436	24.10073157	0.00036447	0.005639642
Arg1	2.743882376	0.739378783	24.07627033	0.000366002	0.005651226
Gbp11	1.541006007	2.308932031	24.03880316	0.000368362	0.005680066
Fstl1	-1.723065715	1.214126759	23.05045297	0.00043756	0.006545807
Usp18	3.077914506	4.755222938	23.03362121	0.000438864	0.00655681
Ttll11	2.607472898	-0.140110064	22.96677844	0.000444087	0.006609166
Des	1.639517125	-0.283786643	22.75487287	0.000448371	0.006630143
Cxcl3	-3.008040208	0.81831385	22.71677784	0.000464279	0.006812967
Ptpn5	3.04636536	0.849655363	22.15124237	0.000514052	0.00740209
Cyp4f18	-2.324061523	6.334932742	22.06783593	0.000521909	0.007477889
Angptl2	-2.939280619	5.501443265	22.05853833	0.000522794	0.007481269
Lama5	2.261972067	2.430558477	21.9335816	0.000534854	0.007570645
Lrrc73	-2.371258956	0.14209193	21.86530553	0.000541581	0.007643202
Tlr11	1.567656317	0.250146341	21.7021769	0.000543302	0.007643202
Entpd3	-3.115993316	3.59582945	21.84714021	0.000543387	0.007643202

genes	logFC	logCPM	F	PValue	FDR
AI427809	-2.698670956	-0.285838732	21.82207258	0.000545891	0.007669075
Adamts9	1.959792208	-0.048380097	21.60196681	0.00056847	0.007909212
Grin3a	-3.565211658	0.959493689	21.43552537	0.000586272	0.008127471
Sarm1	-2.88852714	0.882645367	21.319583	0.000599058	0.008274887
Pgf	1.600255122	3.818616588	21.1394621	0.000619574	0.008477069
Apln	1.545400912	0.389890625	20.80830604	0.000650052	0.00880012
Hpse	3.910342683	2.300490533	20.85986077	0.000653074	0.008830664
Fndc9	-1.747112049	1.37101165	20.79230639	0.000661483	0.00891302
Abcg3	2.344035905	1.644351325	20.21801979	0.000738325	0.009732388

Supplementary Table 7: Genes differentially expressed in JAWSII scramble control cells vs R-1000 Sec22b rescued cells. Cut-off: FDR < 0.01 and logFC > |1.5|, FC = fold change, CPM = counts per million, FDR = false discovery rate. Sorted by FDR.

gene	logFC	logCPM	F	PValue	FDR
Impact	-4.41738054	5.789748197	832.9209602	1.64E-12	1.90E-08
Perp	-4.603183162	5.173862714	721.0411848	4.01E-12	2.32E-08
Palm	-3.762319103	5.599292772	579.668201	1.47E-11	5.63E-08
2510009E07Rik	-9.501140263	4.28998399	559.7343245	2.09E-11	6.02E-08
Mst1	-4.290773738	3.927071612	418.1733824	1.02E-10	2.35E-07
Grik2	7.196511642	1.661946554	386.2690647	1.55E-10	2.98E-07
Adrbk2	6.690856883	4.128486498	358.5674367	2.80E-10	4.62E-07
Tgfbi	5.447626612	3.824443242	350.0588333	3.22E-10	4.64E-07
Hmgcll1	-7.396662001	2.937480831	337.8383729	3.96E-10	5.07E-07
Arhgef10l	8.951379672	2.45650831	331.2664878	4.43E-10	5.11E-07
Clu	4.370923489	4.890147879	320.35188	5.38E-10	5.40E-07
Prnp	5.776466018	1.390425536	310.0009603	5.62E-10	5.40E-07
Shisa9	-3.174485892	4.253584406	286.3128723	9.33E-10	8.28E-07
Cd180	6.35494995	3.017626305	277.6784416	1.23E-09	9.92E-07
Ptpn18	3.548201977	3.527139685	269.486583	1.34E-09	9.92E-07
Pde2a	4.699935537	3.772568188	272.1343508	1.38E-09	9.92E-07
Ush1g	3.192284181	2.724825262	261.2224156	1.52E-09	1.01E-06
Fam49a	6.872668187	2.389117235	265.7141465	1.58E-09	1.01E-06
Necab1	-3.220531723	3.982627586	254.9984249	1.82E-09	1.01E-06
Dab2ip	8.638506586	1.429523931	256.2575833	1.87E-09	1.01E-06
Arap3	2.637701902	6.196602488	257.4021466	1.89E-09	1.01E-06
Tceal8	5.165768485	1.507184141	250.47997	1.94E-09	1.01E-06
Serpinb8	-3.66662391	4.410736438	240.8425355	2.77E-09	1.38E-06
Sept5	-3.07911914	5.040486516	239.4424912	2.87E-09	1.38E-06
Ctla2b	8.051067211	2.697213871	236.1824401	3.10E-09	1.43E-06
Wbscr27	4.396794292	2.179480813	225.1957354	3.73E-09	1.65E-06
Etv1	6.866659751	1.530588747	225.6563411	3.96E-09	1.69E-06
Pax3	2.99137493	2.307298649	219.4024952	4.15E-09	1.71E-06
Sec22b	-2.114640722	7.632921729	218.8585114	4.76E-09	1.89E-06
Peli2	2.18958013	4.130916591	210.5220387	5.26E-09	2.02E-06

gene	logFC	logCPM	F	PValue	FDR
Cxx1c	4.501411922	1.494644422	208.1091752	5.62E-09	2.03E-06
Gfod1	-3.877165286	2.506376394	208.0645697	5.63E-09	2.03E-06
Ptger3	-2.277301767	3.723817607	205.5222254	6.04E-09	2.11E-06
Prkar1b	3.412997823	2.265945856	199.0839368	7.25E-09	2.46E-06
Oaf	1.815466217	5.34175245	197.44003	7.60E-09	2.50E-06
Dync1i1	5.986445857	0.879152164	193.6084986	8.73E-09	2.80E-06
Rhox2h	-3.854527448	3.535653048	190.9311932	1.04E-08	3.14E-06
Thrb	3.908752379	2.00167973	186.2763133	1.08E-08	3.14E-06
Myo16	5.224014121	1.837407023	189.2532133	1.09E-08	3.14E-06
Nynrin	-4.513565711	0.828166313	184.6315657	1.11E-08	3.14E-06
Fcgr1	3.918579984	5.288096077	188.5060791	1.11E-08	3.14E-06
Cd14	2.705770032	7.099268239	185.4817777	1.22E-08	3.35E-06
Plin4	-4.30863371	6.447374173	183.7849507	1.29E-08	3.39E-06
Olfm1	3.34990181	0.771107135	179.8658818	1.29E-08	3.39E-06
AW551984	5.284052706	1.172790787	175.0031586	1.63E-08	4.18E-06
Gimap9	2.358042404	3.632091545	167.0962111	1.96E-08	4.92E-06
Pitpnm2	4.59038692	1.154682845	165.8179092	2.08E-08	5.11E-06
Eid1	2.6639874	3.94127438	166.756277	2.22E-08	5.15E-06
Lamc2	-4.456247289	4.202343287	166.6115273	2.23E-08	5.15E-06
Gpr56	3.645303572	1.270791543	163.2676427	2.24E-08	5.15E-06
Il18rap	4.602973958	0.433755471	162.7385701	2.28E-08	5.15E-06
Cd86	3.11420682	3.814012568	163.7594382	2.46E-08	5.26E-06
Atp9a	3.600105018	1.027517458	160.5257953	2.46E-08	5.26E-06
Pcyt1b	-3.544612531	3.039357249	162.4564319	2.57E-08	5.39E-06
Slmo1	-5.0502962	0.810377549	156.6378475	2.83E-08	5.82E-06
Rhoj	6.187669651	-0.022260358	152.6759192	3.27E-08	6.50E-06
Zmat4	4.475073399	0.069582247	150.5847489	3.53E-08	6.90E-06
Apbb2	6.179328393	0.593781172	151.0085108	3.75E-08	7.20E-06
4930523C07Rik	-3.824903299	2.07162713	149.8814586	3.94E-08	7.44E-06
Uchl1	6.730981334	1.221299677	147.788997	4.36E-08	8.11E-06
Ripk3	-3.349261931	3.870044713	145.7184113	4.72E-08	8.50E-06
Afap1	4.877645221	1.797533442	144.9430485	4.86E-08	8.62E-06
Cst7	3.327568449	0.895045647	140.4102421	5.23E-08	9.13E-06
Itga7	-3.821527358	2.787286066	139.7419503	5.95E-08	1.02E-05
Gm13544	-4.162882821	1.574667206	135.8590378	6.57E-08	1.11E-05
Psma8	-5.367477817	0.73351189	134.4471139	6.66E-08	1.11E-05
Nrbp2	-5.267544322	1.454871802	136.4112566	6.80E-08	1.12E-05
Smtn	3.12228097	1.175336058	132.3161892	7.28E-08	1.18E-05
Kcnk5	-4.86833954	0.821903176	131.6179086	7.50E-08	1.20E-05
Rhox2g	-7.173957295	2.765363663	130.9170906	8.53E-08	1.33E-05
Nipsnap1	2.286300068	3.29695624	128.6931373	8.65E-08	1.33E-05
Spsb1	-2.745424835	2.404859507	127.3066883	9.02E-08	1.37E-05
Trim2	4.025956368	2.052708084	126.2050575	1.04E-07	1.54E-05
Spry1	4.290709943	1.43139826	124.5709665	1.12E-07	1.64E-05
Col24a1	6.709834281	4.941862809	124.079426	1.15E-07	1.65E-05

gene	logFC	logCPM	F	PValue	FDR
Lama4	-3.391220322	1.646817927	120.8530665	1.20E-07	1.71E-05
Barx2	6.154219236	0.649234226	121.4947759	1.29E-07	1.81E-05
Cmklr1	3.738356903	2.576081355	120.8911279	1.32E-07	1.82E-05
Scrn1	3.522319375	0.470294074	118.796176	1.32E-07	1.82E-05
Tnks1bp1	-2.087311296	5.152404221	119.2312691	1.43E-07	1.88E-05
Adam28	-4.79988128	2.03597348	119.0989851	1.43E-07	1.88E-05
Ccdc120	-5.585046503	0.624865033	116.8187877	1.46E-07	1.89E-05
Chchd10	2.039845364	3.557033117	115.754806	1.55E-07	1.99E-05
Clcf1	-2.762908674	2.750222995	116.2883022	1.60E-07	2.02E-05
Sv2a	2.877239975	2.237909608	113.5089852	1.77E-07	2.22E-05
Angptl2	-7.051361677	5.501443265	114.2618023	1.80E-07	2.22E-05
Pcdh7	2.145015478	2.969135985	112.0285104	1.83E-07	2.22E-05
Klra10	-3.797307365	2.728564338	113.8215736	1.84E-07	2.22E-05
Akr1c13	2.701650776	3.714753418	113.6848289	1.85E-07	2.22E-05
Cfh	5.290580862	1.730750902	113.5189618	1.86E-07	2.22E-05
Limd1	-1.724632749	6.285067037	113.0558722	1.91E-07	2.24E-05
4933412E12Rik	2.685403745	1.852608037	110.7127554	1.95E-07	2.27E-05
Plxdc2	-2.433973595	2.970287847	110.8046675	2.02E-07	2.30E-05
Clec4d	1.561168421	6.876889352	110.6009275	2.15E-07	2.43E-05
Tm7sf3	-1.876254209	5.088572634	110.2877779	2.18E-07	2.44E-05
Fam189b	2.559964824	1.949936903	107.4742851	2.29E-07	2.54E-05
Map2	-7.214539691	1.146627219	108.6704134	2.36E-07	2.57E-05
Scml4	2.545017939	2.095734317	106.2731595	2.44E-07	2.63E-05
Zfp105	-6.244621159	0.761284208	106.2288427	2.54E-07	2.67E-05
Ttc12	6.419663717	0.143906062	105.8329463	2.73E-07	2.78E-05
Cp	3.103647813	1.765898657	104.9341976	2.76E-07	2.79E-05
Tnip3	1.53560373	4.186904536	103.7040288	2.79E-07	2.80E-05
Odf3l1	2.438732427	2.856022547	104.4220218	2.89E-07	2.87E-05
Klhl41	-6.281184191	0.572153801	103.7291347	3.04E-07	3.00E-05
Lmo2	3.150007196	4.298623392	102.7474775	3.20E-07	3.10E-05
Slc2a4	-2.981282937	1.062781708	100.8740133	3.24E-07	3.12E-05
Cpne2	1.742773297	3.820407903	100.5740449	3.30E-07	3.15E-05
Adamdec1	-4.170055851	5.874354123	101.7570197	3.37E-07	3.19E-05
Ms4a7	2.978613483	3.906233605	101.3502914	3.45E-07	3.21E-05
Il27ra	1.566848015	3.379891068	99.69153275	3.46E-07	3.21E-05
Ap1s3	5.080187698	-0.435718056	99.18411393	3.55E-07	3.28E-05
Hapln4	3.039241594	1.90941807	100.3926865	3.61E-07	3.31E-05
Myzap	2.940331343	3.625010036	99.86828376	3.73E-07	3.36E-05
Rgma	6.273185615	0.05774283	99.38499657	3.83E-07	3.39E-05
Rhox5	3.356466372	4.329386436	99.3001162	3.85E-07	3.39E-05
Fam160a1	-1.79827284	2.151669688	97.50700103	3.90E-07	3.40E-05
Ctla2a	10.1990339	1.641091937	82.79706385	3.95E-07	3.43E-05
Rasd2	5.864017355	1.662985447	98.30714584	4.06E-07	3.49E-05
Nxf7	2.240474073	3.730451015	97.56742144	4.23E-07	3.61E-05
Tagap	1.729995493	3.343661216	95.82980429	4.28E-07	3.61E-05

gene	logFC	logCPM	F	PValue	FDR
Cfb	1.669760818	10.19760023	96.80182106	4.41E-07	3.69E-05
Fkbp10	3.14110614	0.634421952	94.11895385	4.72E-07	3.89E-05
Lbh	1.555142995	3.982009425	93.73934712	4.82E-07	3.91E-05
Nfatc2	2.590078409	2.181853316	94.25703669	4.85E-07	3.91E-05
Sdr42e1	-2.616330643	2.235802081	93.85047962	4.98E-07	3.99E-05
Rasgrp3	3.443478007	2.277511882	94.35300552	5.06E-07	4.00E-05
BC026585	2.593729188	3.592653676	93.49847738	5.31E-07	4.17E-05
Slc39a10	1.947808967	2.696861274	91.19785841	5.59E-07	4.36E-05
Map2k6	3.981588199	-0.259537462	90.40362229	5.86E-07	4.54E-05
Siglece	2.423453405	2.308496523	89.67318587	6.28E-07	4.80E-05
A230050P20Rik	3.175857798	1.416260609	89.85905921	6.57E-07	4.95E-05
Olfr1259	-3.860292685	-0.25530746	88.5050358	6.57E-07	4.95E-05
Fxyd7	3.56010581	1.057407687	89.34053455	6.77E-07	5.04E-05
Cysltr1	4.370732875	2.316743242	89.07132989	6.88E-07	5.06E-05
Col4a4	4.969272945	-0.394535416	88.21706486	6.92E-07	5.06E-05
Cryab	7.372737859	2.361827825	88.05797101	7.31E-07	5.30E-05
Rfng	-1.58484799	5.784970928	87.3464024	7.63E-07	5.50E-05
Cd24a	3.085770376	7.570207929	86.66977728	7.96E-07	5.70E-05
Tm4sf19	-3.687179171	1.540935064	86.43814908	8.07E-07	5.72E-05
Pianp	3.115892619	1.219343722	86.10536268	8.13E-07	5.72E-05
Fam213b	4.878140541	1.002603325	86.31389826	8.13E-07	5.72E-05
Rnd1	1.535405581	2.905994493	84.94941492	8.18E-07	5.72E-05
Tmem202	1.862656897	2.493950701	84.84679766	8.23E-07	5.72E-05
2610203C22Rik	2.166032002	0.971955229	84.3608007	8.49E-07	5.86E-05
Wwtr1	3.719212964	0.604200334	85.31078378	8.62E-07	5.88E-05
Cyp2d22	-2.331452587	2.830653197	84.87576304	8.79E-07	5.92E-05
Mrap	-3.183276117	1.030481749	84.06630236	8.83E-07	5.92E-05
2010109I03Rik	1.846263059	2.978994423	83.68724397	8.86E-07	5.92E-05
Gpr97	6.545652591	-0.382106747	84.87181568	8.89E-07	5.92E-05
Grid1	-3.695292377	1.951982675	84.70266453	8.98E-07	5.92E-05
1500015A07Rik	1.936382983	2.8697035	83.54185008	9.04E-07	5.92E-05
Slpi	2.68497314	5.256944687	84.20939494	9.27E-07	6.01E-05
Steap1	-4.846213401	1.789907668	84.18603179	9.28E-07	6.01E-05
Zhx2	3.613911333	0.036105619	82.77069536	9.40E-07	6.05E-05
Cntn3	1.597935637	3.70860925	82.38822719	9.68E-07	6.15E-05
Adamts9	5.990431337	-0.048380097	83.47878053	9.70E-07	6.15E-05
Phf11b	2.992920059	2.904490264	83.32628893	9.80E-07	6.17E-05
Gas7	6.094592884	-0.14720444	82.81806979	1.01E-06	6.31E-05
AF251705	2.095604389	5.032214809	82.5895899	1.03E-06	6.36E-05
Fgf1	4.655959107	1.240865417	82.05682054	1.06E-06	6.48E-05
Serpina3g	3.266546276	2.659800794	81.55659564	1.10E-06	6.66E-05
Ebf1	-5.089229543	1.194926405	81.34155282	1.11E-06	6.72E-05
Chpf	-1.788802595	5.690241196	81.09803561	1.13E-06	6.79E-05
Il1rn	1.66272502	7.000569252	80.88313472	1.15E-06	6.85E-05
Gdf15	-2.193793356	6.692840229	80.75078528	1.16E-06	6.87E-05

gene	logFC	logCPM	F	PValue	FDR
Col18a1	3.95607003	1.925588068	79.76757448	1.23E-06	7.29E-05
Ifi44	4.19931821	2.345757993	78.53682274	1.34E-06	7.87E-05
Sparcl1	-5.287224137	6.124402283	78.24564639	1.36E-06	7.99E-05
Gja5	2.98988439	0.87081664	77.1491539	1.39E-06	8.08E-05
Sorl1	4.434875634	4.548224779	77.85537996	1.40E-06	8.11E-05
Cx3cl1	2.524545223	2.309097934	77.52390975	1.43E-06	8.26E-05
Apol9a	3.873906932	2.846423574	77.08756424	1.47E-06	8.42E-05
Scgb1a1	-6.438463914	0.057049559	76.14986099	1.57E-06	8.89E-05
Ltb4r1	-3.917201583	3.935583303	75.97514302	1.59E-06	8.95E-05
F3	3.298129322	2.108068978	75.90888592	1.60E-06	8.95E-05
Gstm2	-1.805146435	5.498623656	75.76905659	1.61E-06	8.97E-05
Mfap3l	4.524532451	-0.25721907	75.70251825	1.62E-06	8.97E-05
C1s	3.393630828	3.637704753	75.53264447	1.64E-06	9.05E-05
Zfp532	1.747812047	4.445850312	75.22640319	1.68E-06	9.20E-05
Sil1	-2.633533885	3.016620322	74.9073886	1.71E-06	9.36E-05
Gstm5	2.307332972	4.317692823	74.45980189	1.77E-06	9.61E-05
Cyp2u1	3.106727425	0.092888312	73.04327454	1.82E-06	9.80E-05
Hgfac	4.211468401	1.655871018	73.98314162	1.83E-06	9.80E-05
Myom3	-2.612529798	4.486599257	72.93304755	1.97E-06	0.000104615
Ptpn22	1.845098393	2.780417104	71.76983825	2.02E-06	0.000106882
Flt3l	2.051772058	1.456796265	71.37805254	2.05E-06	0.000107617
Vsig10	1.927457004	1.840623183	71.37274092	2.05E-06	0.000107617
Ramp1	1.791582729	6.320019083	72.26907643	2.06E-06	0.000107716
Angpt2	-1.851119988	2.288274726	71.23185081	2.07E-06	0.000107754
Apol9b	3.835067225	1.746178695	72.12808564	2.08E-06	0.000107837
A530013C23Rik	1.865862086	1.974207927	71.07527602	2.10E-06	0.000108026
Tgfb2	-3.203676151	3.571613186	71.58376066	2.17E-06	0.000110667
Shisa4	-3.029070523	3.518680535	71.36897455	2.20E-06	0.000111008
Erc2	-3.464376719	3.16110895	71.34906913	2.21E-06	0.000111008
A330021E22Rik	-3.183451962	1.644062137	71.29449738	2.21E-06	0.000111008
Bmp8a	-4.679940847	4.324463916	70.44928568	2.36E-06	0.000116096
Gfra1	2.104656548	3.079443375	69.87355284	2.46E-06	0.000119592
Zbtb32	-1.803683873	6.137427041	69.71600521	2.49E-06	0.000120486
Grb10	3.712537145	1.847304724	69.33901106	2.56E-06	0.000122529
Lama5	4.834152858	2.430558477	69.32083899	2.56E-06	0.000122529
Ptrf	-2.683582932	5.240720176	69.2305774	2.58E-06	0.000122845
Nkx6-3	-3.44969074	3.623004087	68.72460888	2.68E-06	0.000127055
5430416O09Rik	-3.760526836	0.480233847	67.65144803	2.79E-06	0.000130502
Gpr141	4.243541406	3.796414689	67.99217904	2.83E-06	0.000131555
Syne1	3.395155087	4.234712704	67.45504892	2.95E-06	0.000136482
Klra17	-4.307790673	0.62858327	66.87531372	3.08E-06	0.000141532
Klra3	-3.0270048	6.045485362	66.35687854	3.21E-06	0.000146134
Tal1	2.258994149	2.269889443	64.3988933	3.74E-06	0.000166679
Ablim3	3.20886154	1.285276569	64.3772584	3.74E-06	0.000166679
Slc10a6	1.547889453	3.588050811	63.44830627	3.89E-06	0.000171775

gene	logFC	logCPM	F	PValue	FDR
Ggt7	2.786289661	1.740506372	63.3890422	4.05E-06	0.000177619
Greb1	5.5869491	-0.062743805	63.19919913	4.11E-06	0.000178993
Rap1gap2	-3.453906537	0.761283021	63.08788202	4.15E-06	0.000179928
Acpp	4.433754997	2.955322545	62.89885117	4.21E-06	0.000181334
Fcrls	8.297393413	1.18216913	49.23980802	4.24E-06	0.000181763
Aoah	1.80479796	5.393108547	62.66727892	4.29E-06	0.0001834
Zeb1	1.747667909	1.612226238	61.51262144	4.43E-06	0.000187078
Cd38	2.015427495	3.490854031	62.1337682	4.48E-06	0.000188749
Sash1	1.513432934	3.899491612	61.78688776	4.57E-06	0.00019172
Cd163	4.518617429	1.395040014	61.58141042	4.69E-06	0.000196071
Csn1s1	2.930764399	6.703806951	61.40663916	4.76E-06	0.0001982
Als2cr12	-3.529858112	0.001558757	60.09488755	5.13E-06	0.000211958
Mgam	-4.669827715	5.033650367	60.23150804	5.25E-06	0.00021546
Prelid2	1.722769738	5.189781815	59.3448052	5.66E-06	0.000230197
Plin5	-3.900696995	1.091446522	59.32272164	5.67E-06	0.000230197
Glrp1	2.374664522	1.572648186	58.39245954	6.12E-06	0.00024265
Gm7609	3.651495754	-0.485531663	58.05510228	6.17E-06	0.000243655
Tcf7	-3.818789308	2.561616759	58.17681311	6.25E-06	0.000245323
Klk1b27	3.121535936	0.580861085	58.05301507	6.32E-06	0.000247124
Ccdc80	-2.641840336	3.97709502	57.8898748	6.41E-06	0.000249797
Phf11a	3.451089708	1.384120292	57.79486541	6.46E-06	0.000250177
Awat2	-3.32350045	4.008527385	57.62799344	6.56E-06	0.000252616
Apoc1	-4.027742408	2.088381292	57.57576042	6.59E-06	0.000252616
Cdh6	2.604511964	2.902926646	57.56839137	6.59E-06	0.000252616
Abcg4	-1.918376908	4.200916692	57.42355617	6.68E-06	0.000254984
Tubb4a	2.882607152	2.45276875	57.30096829	6.75E-06	0.000255881
Tspan12	9.283154655	0.595533276	44.10678082	6.76E-06	0.000255881
Wfdc10	3.794677185	0.474967748	57.2704194	6.77E-06	0.000255881
Gm5483	4.309984905	0.563447731	57.06392085	6.89E-06	0.000258862
Fyb	4.224660389	0.472906306	56.89293891	6.99E-06	0.000261084
Klk1b1	4.386126126	3.926434706	56.79523645	7.06E-06	0.000262493
Colec12	1.821436591	6.467671753	56.0981189	7.50E-06	0.000275673
Cd52	2.483899096	6.523183167	56.04849264	7.54E-06	0.000276016
Adcy6	-2.67451972	1.062475082	55.91250342	7.58E-06	0.000276073
Cited1	3.364449264	0.184266034	55.67377661	7.80E-06	0.000282732
Mtmr11	1.572461337	2.475196845	54.90387144	7.88E-06	0.000284893
Oasl2	3.786740039	5.811068077	55.08430333	8.22E-06	0.00029445
Acot2	1.911479131	2.268441234	54.7342133	8.26E-06	0.000295
D630033O11Rik	1.701524635	1.683590811	54.26566524	8.36E-06	0.000297451
Cystm1	2.496031733	2.148509467	54.70511396	8.51E-06	0.000301231
Oas1a	1.909197078	5.983099529	54.69746761	8.51E-06	0.000301231
Folr2	3.035260445	-0.327998422	53.94752549	8.69E-06	0.000306125
BC024139	-3.89713914	0.043776455	54.40756469	8.71E-06	0.000306125
Prkcb	2.069666386	4.900817271	54.34501929	8.79E-06	0.000308243
Oas1g	2.3349182	3.864276424	54.30907923	8.82E-06	0.000308322

gene	logFC	logCPM	F	PValue	FDR
Chl1	-2.692871057	2.11364003	54.19421499	8.91E-06	0.000310644
Pamr1	2.978327405	1.627949896	54.09485601	9.00E-06	0.000311608
Utp14b	-1.596038169	4.28175494	53.9759771	9.10E-06	0.000313153
Fam65c	4.196363884	1.895655045	53.08932604	9.87E-06	0.000332046
Mmrn1	9.498600435	0.853560858	40.25742901	9.92E-06	0.000332719
Cyp11a1	-2.828405453	4.593366656	52.93461302	1.00E-05	0.00033396
4930550L24Rik	2.400911583	2.895050205	52.55826515	1.04E-05	0.000343976
Msln	1.948078121	2.30550069	52.15208575	1.08E-05	0.000356399
Ccl22	3.202731439	3.660709313	51.61787549	1.13E-05	0.000371782
St6gal1	1.729106755	6.25084548	51.43820836	1.15E-05	0.000377156
Entpd3	-4.938154278	3.59582945	51.36879259	1.16E-05	0.000377535
Rhpn2	-2.350938206	3.590895101	50.94763527	1.21E-05	0.000388708
Gbp4	2.092715647	0.199432572	50.29516461	1.22E-05	0.000388708
Fam46c	4.820690664	-0.017811231	50.84500991	1.22E-05	0.000388708
Zmpste24	-1.574606426	4.971920874	50.83389597	1.22E-05	0.000388708
Clec1a	1.79732078	4.190089112	50.42961452	1.27E-05	0.000401879
Amy1	1.842467838	0.359860572	49.67321599	1.30E-05	0.000406666
Tinagl1	2.521898707	0.493673307	49.69657598	1.34E-05	0.00041872
Ptgis	-2.684342924	0.959192205	49.32967488	1.36E-05	0.000421643
Sdc2	-4.127101802	1.505435186	49.63877776	1.37E-05	0.000426069
Abcg3	4.323809273	1.644351325	49.6173889	1.38E-05	0.000426069
Cxcl2	3.391426981	4.491657595	49.32301358	1.42E-05	0.00043516
Dock6	2.564912836	1.093195651	49.11074296	1.45E-05	0.000440917
Dcn	3.821284369	4.590015325	49.08424036	1.45E-05	0.000440919
Krt1	-1.55578101	6.87304857	48.90987757	1.48E-05	0.000447475
Tmem51	1.873379813	2.294552811	48.73215885	1.49E-05	0.00044946
Zfyve9	-2.656315164	1.013456046	48.7871352	1.50E-05	0.00044946
Cadps	8.79249489	0.21413462	36.41167523	1.51E-05	0.000451222
Afap1l1	2.335335352	0.711019551	48.36846805	1.51E-05	0.000451222
Trim30d	3.162832508	3.901530272	48.60708011	1.52E-05	0.000451763
Pkdcc	1.857198166	5.77172617	48.17123865	1.59E-05	0.000467237
Rps6ka2	1.871622821	4.041761918	48.11292941	1.60E-05	0.000468655
Prl3a1	4.655498678	-0.271822794	47.82346014	1.65E-05	0.000477086
Plcd1	-3.395696612	0.58726907	47.8161838	1.65E-05	0.000477086
Igf2r	-3.281550135	3.73650984	47.63896955	1.68E-05	0.000481945
Pecam1	-1.763410063	2.411255251	47.45191169	1.68E-05	0.000481945
Chdh	-3.265208519	0.285629265	47.47016341	1.71E-05	0.000484682
Atp1a3	2.893201775	1.041354788	47.42556424	1.72E-05	0.000484682
Hp	4.540055162	6.238497672	46.98589073	1.80E-05	0.00050184
Klra9	-2.401683714	3.93779886	46.76915371	1.84E-05	0.00050893
Emp1	-1.610535267	7.932743742	46.72899904	1.85E-05	0.000509188
Grm8	10.67981432	1.964019349	74.42626162	1.87E-05	0.000510576
Fzd1	4.67973333	-0.247654368	46.55855049	1.88E-05	0.000512152
Gfpt2	-2.61566502	2.233275022	46.34392942	1.92E-05	0.000518824
Eya4	2.275513736	2.148470862	46.30967561	1.93E-05	0.000519069

gene	logFC	logCPM	F	PValue	FDR
Slc2a3	2.094623344	0.875778894	45.54563999	2.02E-05	0.000536769
Trim30a	2.245900186	5.65711431	45.64968798	2.07E-05	0.000546767
2010002M12Rik	3.216616227	0.039591738	45.59873742	2.08E-05	0.000547272
Sesn3	-1.973149456	1.212959253	45.13058866	2.08E-05	0.000547272
Abhd6	8.354329765	-0.205763872	33.19562941	2.10E-05	0.000550259
Aqp1	-2.525251086	1.466348088	45.49916978	2.10E-05	0.000550259
Trpc4	-3.112020581	2.281027912	45.2318287	2.16E-05	0.000564819
Mdfi	2.137064968	0.175925837	44.69741224	2.17E-05	0.000567345
Tex14	2.833238301	0.277138061	44.99296711	2.22E-05	0.000574185
Chst15	2.159053136	4.777501652	44.72909959	2.28E-05	0.000589326
Treml4	-2.139892443	5.8320707	44.66326346	2.30E-05	0.000592182
Etv4	-3.09156056	2.581647994	44.56947617	2.32E-05	0.000595525
Grcc10	1.55967851	5.457821807	44.22691776	2.41E-05	0.000612427
Fam124a	-2.929997996	2.973148082	44.21640067	2.41E-05	0.000612427
Csn2	1.67687484	9.269580735	43.83044986	2.51E-05	0.000632532
Fndc9	-2.510830228	1.37101165	43.56982971	2.58E-05	0.000649413
4930481A15Rik	1.536847767	1.672505325	42.98584878	2.62E-05	0.000656684
Pcnx	2.307548538	4.168585789	43.30152558	2.66E-05	0.00066308
Il17rc	-3.125423906	2.745891941	43.08634557	2.73E-05	0.00067407
Stab1	2.856514341	0.23228044	42.99335362	2.75E-05	0.00067873
Gcat	-2.866490216	3.530974753	42.92326057	2.78E-05	0.00068257
Kif19a	2.023451313	2.134114582	42.6668861	2.86E-05	0.00069754
Eno2	2.232420492	3.667968675	42.63310019	2.87E-05	0.00069754
Rlbp1	-2.280188193	0.25355915	42.13121802	2.91E-05	0.000704422
Pram1	1.647114921	3.083572972	42.02388102	3.07E-05	0.000736044
Cpq	2.59247553	-0.167440474	41.78546482	3.09E-05	0.00074044
Efcab6	1.507502504	1.871154403	41.29303969	3.18E-05	0.00075806
Fxyd2	2.84038427	0.199786029	41.38034296	3.30E-05	0.000783724
Akr1c12	1.91233157	2.0015172	41.29200247	3.34E-05	0.000790059
Rpph1	2.877398546	1.348474199	41.14106368	3.39E-05	0.000800564
Pnpla5	-2.373410313	0.105173504	40.70360933	3.41E-05	0.000801794
Shroom3	2.805127095	1.256301985	41.06365744	3.42E-05	0.000802791
Ablim1	-2.890803815	1.302435118	40.92060094	3.48E-05	0.000811181
Fhod3	-3.060384566	2.333888476	40.74743306	3.55E-05	0.000825902
Panx1	4.499003207	2.423036034	40.6915943	3.57E-05	0.000829586
Vsig8	1.844149247	0.919966145	40.11640349	3.65E-05	0.000845216
Prl2c5	-3.560637486	0.401793173	40.26357148	3.76E-05	0.00086844
Oas1b	1.81918977	2.76294221	40.03770714	3.86E-05	0.000886788
Rbms3	-1.74398894	3.781703982	40.02642495	3.86E-05	0.000886788
Ccdc62	1.620030804	1.636114799	39.45201321	3.95E-05	0.000903773
Gbp2	1.662161575	4.076119706	39.36706923	4.18E-05	0.000949985
Fstl3	-2.811390658	0.141366933	38.91081065	4.41E-05	0.000991316
Gm4890	1.727344774	0.419990246	38.46098973	4.45E-05	0.000996981
P2ry1	1.766861904	0.311427741	38.44051727	4.46E-05	0.000997538
Fam19a5	1.932363888	3.421162081	38.44749026	4.66E-05	0.001030344

gene	logFC	logCPM	F	PValue	FDR
Gm11110	2.323907684	2.677952803	38.3572205	4.71E-05	0.001038259
Hao1	2.28547862	-0.140326717	37.93443214	4.76E-05	0.001042299
Rapgef5	2.197555819	-0.204406353	37.87178168	4.79E-05	0.001045388
Thbs1	10.42791852	1.714435591	27.3826806	4.89E-05	0.001065181
Ccdc166	-2.862397535	0.53941168	38.00990166	4.91E-05	0.001066163
Arg1	3.747843272	0.739378783	37.99530889	4.93E-05	0.001066163
Csn1s2a	-2.811750339	1.640415675	37.62819117	5.15E-05	0.001104929
Nfatc4	-1.890496937	2.504331046	37.2792958	5.38E-05	0.001138816
Col23a1	-2.253872594	1.340658049	36.92435762	5.62E-05	0.001183772
Bmper	2.306255544	1.824793302	36.76533208	5.74E-05	0.001201006
Serpina3m	-3.727233861	0.484659879	36.73181793	5.76E-05	0.0012027
Il1r1	-2.483935491	0.085795946	36.35849266	5.79E-05	0.001203537
Dhdh	2.514232355	4.759780172	36.6805869	5.80E-05	0.001203537
Htra3	-2.024167085	5.212339945	36.67661207	5.80E-05	0.001203537
Tuba1a	-1.972215665	6.622385672	36.62636953	5.84E-05	0.001204664
Mum1l1	-1.783680524	2.943922885	36.46138734	5.96E-05	0.001225587
Ear5	-3.25669351	4.334848304	36.363175	6.04E-05	0.001238685
Apln	2.12346199	0.389890625	36.11553867	6.08E-05	0.001244109
P2rx5	-2.994650192	0.525724002	36.26621075	6.11E-05	0.00124733
Gm16845	1.521364182	1.908419631	35.86767821	6.21E-05	0.001263291
Fstl1	-2.133490187	1.214126759	35.97361085	6.34E-05	0.001281137
Iigp1	2.521075003	1.395621713	35.96249757	6.35E-05	0.001281137
Ccdc38	-3.617147663	1.760702067	35.95020869	6.36E-05	0.001281137
Pdgfra	1.75216624	5.932555121	35.86148685	6.43E-05	0.001290447
Olfr1033	1.599838313	0.614554917	35.40367483	6.54E-05	0.001303878
Inpp4b	7.859827945	-0.655447399	25.23366715	6.55E-05	0.001303878
Nov	-1.584635921	7.589705282	35.53023494	6.71E-05	0.001326119
Vill	-3.054415251	5.83066227	35.5279807	6.71E-05	0.001326119
Spats2	-4.801205239	2.248622651	35.33311334	6.89E-05	0.00135757
A530032D15Rik	1.528136123	2.301961074	34.9336833	7.22E-05	0.001408101
Tenc1	-1.606278168	4.862087262	34.84550353	7.34E-05	0.00142113
Mamdc2	-3.334752841	1.275861733	34.60536939	7.57E-05	0.001460235
Gimap6	3.807550949	0.838352944	34.53007832	7.65E-05	0.001467406
Ear11	-3.999378793	5.131214687	34.37755009	7.80E-05	0.00148732
Gm6634	7.652716638	-0.808896229	24.02262306	7.88E-05	0.001490842
Col5a1	2.295662054	6.115339578	34.11158319	8.08E-05	0.001525531
Fam132b	-1.860493299	0.407586141	33.63631874	8.27E-05	0.00155406
Chi3l4	-1.60690985	0.499818041	33.51716718	8.41E-05	0.001569131
Cxcl16	2.617571416	1.535322799	33.6837774	8.56E-05	0.001591757
Slfn4	1.613043989	6.107779807	33.65583814	8.59E-05	0.001592943
Mogat2	-1.882762303	5.493048036	33.64226428	8.60E-05	0.001592943
Cyp4f18	-2.984168833	6.334932742	33.60189348	8.65E-05	0.001599039
Sema3b	-2.251977805	0.450588868	33.50358956	8.77E-05	0.001615154
Vps37b	1.54795291	3.604045867	33.48829167	8.78E-05	0.001615905
Plekhh1	-3.093859458	0.440980887	33.43018674	8.85E-05	0.001626023

gene	logFC	logCPM	F	PValue	FDR
Ltbp4	-1.75213546	2.239676971	33.35404513	8.94E-05	0.001640217
Ces2c	-2.120286871	4.373883752	33.2791321	9.04E-05	0.001651672
Kcnip4	-1.622878548	1.964849146	33.14552185	9.08E-05	0.001657851
Crabp2	-4.086494291	2.0910678	33.12102631	9.23E-05	0.00167421
Efnb1	-1.611560405	1.745647118	32.83172275	9.38E-05	0.001698921
Slc28a2	2.68066853	0.254641167	32.85167848	9.58E-05	0.001728665
Atp1b2	-2.916502819	1.317436447	32.62370724	9.88E-05	0.001769696
Ednra	2.516850442	1.490013892	32.43129578	0.000101465	0.001806014
Ccdc7	-2.092397371	-0.202047814	31.838348	0.000106053	0.001870351
Cdk18	2.066712365	4.783287668	32.03382558	0.000107216	0.001883109
Nos2	3.607379996	4.042029558	31.94923811	0.000108489	0.001898799
Gbp9	2.522826396	3.485834574	31.8736707	0.000109641	0.001913152
4933431E20Rik	2.07998348	3.750332223	31.84241793	0.000110121	0.001915741
Tnfrsf11a	1.849402337	0.679459817	31.54581599	0.000112394	0.001949409
Cdh5	2.504139725	3.122281194	31.43804388	0.000116566	0.002015702
Rhox2d	-3.895017048	2.422930922	31.16807392	0.000121115	0.00208247
Lphn2	2.829112441	1.240060624	31.15573403	0.000121327	0.00208247
Arhgap29	2.890304304	-0.693038789	30.8424765	0.000126879	0.002161631
Cd300ld	2.521889864	5.935154522	30.78102036	0.000128003	0.002173822
Ly6a	1.648984536	3.615975449	30.69908146	0.000129519	0.002190432
Oasl1	2.710686333	1.582080603	30.59336015	0.000131507	0.002211894
Agt	-2.359382579	6.640072677	30.59305815	0.000131513	0.002211894
Chn1	-1.532124096	1.352978703	30.33754231	0.00013187	0.002213958
Gm826	2.263648653	0.489330742	30.54160587	0.000132493	0.002216198
Amhr2	-1.678909089	1.64818766	30.45879289	0.000133547	0.002225907
Drd1a	-1.783357837	1.150429194	30.24570233	0.000135564	0.002253023
Mx1	3.557202676	-0.270522954	29.67778481	0.000150297	0.002445024
Hepacam2	1.581224569	1.032545231	29.42478861	0.0001511	0.002451185
H2-Ob	1.753729608	5.987401904	29.62202468	0.000151539	0.002454846
Proca1	-1.642428164	0.754113842	29.28133185	0.000153836	0.002485075
Slc7a3	1.57504408	0.08767813	29.20397929	0.000155634	0.002508693
Tmem158	-1.772286054	2.701541943	29.43765138	0.000155733	0.002508693
A430078G23Rik	1.561814874	0.312348827	29.06348019	0.000158963	0.002550038
Capn6	-1.530482933	4.387449455	29.28710002	0.000159258	0.002551133
Notch1	2.756280465	3.337659631	29.27804353	0.000159473	0.002551133
Ccl5	2.212139589	3.692027219	29.26641823	0.00015975	0.002552017
Lpcat4	-1.751018618	2.96757417	29.19461374	0.00016147	0.002570065
Tmem25	1.930144909	2.395088982	29.19139108	0.000161548	0.002570065
AI427809	-3.043555079	-0.285838732	29.15791893	0.000162358	0.002575843
Dok7	2.09525055	3.369993126	29.05100048	0.000164977	0.002606635
Sema4d	2.478931773	5.169267146	28.94854733	0.000167533	0.002630304
Slc39a4	1.663875162	2.152665361	28.93622736	0.000167843	0.002630304
Fhl1	-2.779817268	2.46102294	28.89694868	0.000168838	0.002642296
Gphn	3.876612082	2.668645907	28.72920594	0.000173162	0.002702639
Cmpk2	2.225351139	3.39205635	28.470739	0.000180081	0.002780533

gene	logFC	logCPM	F	PValue	FDR
Spon2	-3.011843525	2.425916244	28.45608419	0.000180483	0.002783014
Rnls	-1.566136689	0.243852364	28.05888535	0.000185345	0.00284656
Il27	1.616554347	2.726900133	28.19794223	0.000187738	0.002868035
Pou2af1	-2.509425774	1.06536077	28.15670862	0.000188928	0.002882398
Awat1	-1.982742162	6.178551643	27.91749575	0.000196008	0.002966877
Mfap5	1.950714367	0.550094086	27.90139455	0.000196496	0.00297036
Ildr1	2.593381173	-0.012621056	27.87816181	0.000197202	0.002975892
Kcnh4	-2.005529288	1.31645034	27.80997907	0.000199292	0.002994203
Naip1	1.525004466	4.506077243	27.73720083	0.000201551	0.003022996
Gm13546	-2.28147616	1.487223561	27.66193622	0.000203918	0.003047537
Gprc5b	3.176361194	1.841384003	27.66000267	0.000203979	0.003047537
Ccdc19	2.534295425	-0.120826092	27.57232501	0.00020678	0.003069493
Slc22a17	-2.061736561	-0.061771134	27.205551	0.000214343	0.003165466
Cd72	1.712100843	1.929100871	27.21536094	0.000218654	0.003204518
Itgb4	-1.510848112	1.639803793	26.98063575	0.000222746	0.003243877
Tmem14a	1.511131078	0.756176357	26.66477612	0.000231405	0.003347555
Des	1.80003478	-0.283786643	26.64088201	0.000231803	0.003347555
Tal2	1.595774373	0.69522667	26.64129531	0.000232479	0.003351759
Amotl2	-1.756101943	3.676512241	26.71055305	0.000236835	0.003401814
Stap2	1.799325455	0.816261821	26.64177619	0.000239447	0.003435046
Chst1	1.856562974	0.937826974	26.62590341	0.000240054	0.003436327
Anxa8	-2.838541848	4.828959188	26.55022064	0.000242975	0.003472712
Rhd	-2.536144582	0.853572015	26.53349109	0.000243627	0.003477712
Irf7	1.89486272	5.251845873	26.35908809	0.00025054	0.003559502
Il1rl2	2.333702946	1.486735043	26.35782581	0.000250591	0.003559502
Ly6i	1.981229537	3.80216207	25.87350557	0.00027103	0.003807629
AI506816	-1.665446804	1.65179668	25.82235629	0.000273301	0.003821967
Ces5a	2.377145382	1.026776846	25.8067266	0.000273999	0.003826032
Celf4	2.543564273	-0.126438049	25.68511322	0.000279503	0.003893465
Ltbp3	3.083717797	2.104906502	25.62400246	0.000282318	0.003918476
Col28a1	2.321039178	0.118523243	25.43923605	0.000290033	0.004001478
Fbxo2	-1.516199431	1.636101361	25.34590399	0.000293999	0.004036891
Zfp109	-3.235313786	0.043149632	25.32767211	0.000296445	0.004065636
Cd300lb	3.485249253	4.989520017	25.29941867	0.000297835	0.004075004
Adam33	1.622713724	1.707668232	25.15512586	0.000305052	0.004154036
Sbk1	1.627462548	2.795115824	25.12591503	0.000306538	0.004169346
Prss16	2.341351674	0.437636519	25.02647443	0.000311659	0.004224065
Pdzk1ip1	2.061870273	2.537981207	25.01493068	0.00031226	0.004227244
Gm19689	1.633783682	1.18812909	24.89283371	0.000318701	0.004294274
Trim40	2.126957956	1.573781466	24.76714313	0.000325494	0.004365408
Grin1	2.362800443	0.54413121	24.72403137	0.000327863	0.004376822
Tmtc1	-1.891008577	1.432945252	24.69681706	0.000329369	0.004386329
Foxc1	1.546782666	1.106781888	24.60171337	0.000331671	0.004402172
Pou2f2	2.219277201	0.986908182	24.54798974	0.000337748	0.004464676
Cygb	-2.932067496	-0.054125817	24.52553503	0.000337909	0.004464676

gene	logFC	logCPM	F	PValue	FDR
Cgref1	-2.093942109	0.694750699	24.54084794	0.000338156	0.004464676
Cyp2s1	-1.778683261	1.781917694	24.38044582	0.000347481	0.004556761
Gm4847	-3.778257233	2.604352474	24.36751263	0.000348246	0.004556761
Tnfsf9	1.728407078	2.458772211	24.25498745	0.000354984	0.004615992
Oas2	2.919747409	5.436288774	24.20601365	0.000357964	0.004649503
4933430I17Rik	1.758554548	-0.077851302	23.88558244	0.000369065	0.004752909
Xaf1	2.020955244	4.950405611	24.01191961	0.000370067	0.004753509
Ksr1	3.090341698	2.365835547	24.01150813	0.000370093	0.004753509
Ckb	1.866703298	2.445534116	24.00104761	0.000370759	0.004756764
Wfdc12	-1.564874919	3.884965471	23.81738025	0.00038268	0.004882557
Ddx60	1.784614041	5.000156442	23.7398136	0.000387849	0.004937766
Krt79	-1.666637592	5.510228266	23.69503152	0.00039087	0.004965085
Airn	-3.343836217	1.113259609	23.6288143	0.000395388	0.005016952
Ttll11	2.634455689	-0.140110064	23.5308079	0.000402188	0.005075315
Myo7b	1.851720547	0.340951983	23.50982049	0.000403662	0.005088347
Slc40a1	1.518066234	2.767882965	23.49759244	0.000404524	0.005093641
Fam20c	1.617012	7.646689814	23.33518348	0.000416174	0.005200274
Nlrp1a	1.82603781	0.022039569	23.19655421	0.000416599	0.005200274
Il12rb2	2.672672236	2.9315932	23.2677471	0.000421127	0.005245435
Sla2	-2.416646026	0.988155326	23.0579273	0.000436982	0.005389165
Elovl3	-2.363118237	1.121555465	23.00487317	0.000441102	0.00542974
Klrb1c	1.898979184	0.940505462	22.93234637	0.000446806	0.00548241
Aqp3	-2.731021188	3.810387757	22.92429934	0.000447445	0.005484407
Aspa	-1.884289294	0.534451306	22.90360561	0.000449091	0.005498742
Pcdh10	1.807615461	-0.118762512	22.77301458	0.000452469	0.005522512
Kcnk3	-3.516344854	-0.206813624	22.75978321	0.00046073	0.00559375
Rtn2	-2.730538248	1.158611452	22.6493308	0.000469909	0.005687229
Tnfaip6	-1.725971176	1.712969239	22.55312968	0.000478078	0.005755899
Gm11992	2.207785973	1.059624131	22.40611852	0.000490885	0.005897776
Yipf7	2.76719723	0.254606765	22.36550338	0.000494493	0.00592007
Glt28d2	-2.094109159	-0.113851088	22.24824227	0.000495433	0.005921585
Esr1	3.2271598	1.586068377	22.32764961	0.000497885	0.005938574
Gipr	2.084608429	1.416188043	22.3002717	0.000500354	0.00595776
Pdzrn3	1.686464768	4.353288615	22.25779198	0.000504215	0.005995477
AA467197	2.729830356	4.722338362	22.11796635	0.00051717	0.00613687
Itm2a	3.545769509	-0.036221476	21.99620309	0.00052877	0.006242405
I830012O16Rik	2.154931763	1.5874779	21.76478205	0.000551666	0.006433683
Dpy19l3	3.378660665	0.886140488	21.55855076	0.000573052	0.006642796
Pdia5	1.577799133	2.012904001	21.47483958	0.000582009	0.006719608
Pdgfb	2.391645448	4.671821771	21.40154039	0.000589986	0.006784545
Col4a2	-1.65129077	0.693174161	21.31197168	0.000597207	0.006847107
Lyve1	-2.371144227	0.219300916	21.15422105	0.000617863	0.007041923
Arhgap22	1.853993365	4.497972675	21.14892828	0.000618476	0.007041954
Gpr34	2.000081022	0.724454268	21.05030491	0.000630033	0.007145333
Itln1	2.554148659	0.353506988	21.0106323	0.000634754	0.007184737

gene	logFC	logCPM	F	PValue	FDR
Tusc5	-1.955799764	-0.426739835	20.75462042	0.000649367	0.007328805
Cd83	-1.538244134	0.655039321	20.76781479	0.000649388	0.007328805
Rab44	1.948646945	5.752196316	20.78554531	0.000662332	0.007431257
2610034B18Rik	2.424438199	-0.00462992	20.47024299	0.000703356	0.007823058
Jup	-1.530109345	1.394261951	20.40380217	0.000712376	0.007900525
Gm20748	-2.046653012	2.683650027	20.36579123	0.000717597	0.007943154
Gsta3	2.034721564	3.935705208	20.29059819	0.000728058	0.00802962
Dmkn	-1.501057676	1.281881494	20.28963423	0.000728193	0.00802962
Arap2	1.672251206	0.099958819	20.14823165	0.000737997	0.008122189
Lhx1	1.510688678	0.76120854	20.17155041	0.000739437	0.008130283
Folh1	1.518921601	2.21540963	19.9968862	0.000770667	0.008393644
Cd28	2.777724951	1.227153225	19.98536737	0.000772396	0.008404546
Gm10872	-2.511384565	-0.075827749	19.94912213	0.000777868	0.008448149
B4galt6	-3.555870569	1.426644281	19.81846099	0.000797975	0.008634
Zkscan7	-1.600169068	1.160652102	19.64961175	0.000824866	0.008825609
Stk32c	1.902753925	-0.121803189	19.51802555	0.00084656	0.008993971
Oas3	2.661043705	6.647703072	19.35988162	0.000873521	0.009209503
Cyp26b1	-1.976141491	5.551206393	19.11186319	0.000917857	0.009563293
Mllt4	1.524471853	3.937577705	18.94984591	0.000948243	0.009800209
Nmnat2	-1.754446615	0.935939526	18.85930606	0.000965736	0.00990996

Supplementary Table 8: Genes differentially expressed in JAWSII Sec22b KD cells vs R-1000 Sec22b rescued cells. Cut-off: FDR < 0.01 and logFC > |1.5|, FC = fold change, CPM = counts per million, FDR = false discovery rate. Sorted by FDR.

genes	logFC	logCPM	F	PValue	FDR
Sec22b	-4.034708072	7.632921729	669.8211954	7.22E-12	8.33E-08
Prnp	3.385933543	1.390425536	90.70781451	5.76E-07	0.00331987
Unc5b	-3.213113706	2.454622587	84.17336209	9.29E-07	0.003570304
Etv1	4.309798619	1.530588747	72.18073629	2.06E-06	0.004382966
Erv3	4.339256848	1.590260621	69.87443259	2.46E-06	0.004382966
Cntn3	-1.522116172	3.70860925	67.51009693	2.75E-06	0.004382966
Awat2	-3.672779393	4.008527385	65.30814614	3.48E-06	0.004382966
Pitpnm2	2.98377948	1.154682845	64.35259006	3.54E-06	0.004382966
Cxx1c	2.576076517	1.494644422	63.44145443	3.78E-06	0.004382966
Klhl41	-3.741510849	0.572153801	64.05044345	3.84E-06	0.004382966
Cyp11a1	-3.106700874	4.593366656	62.81630632	4.24E-06	0.004382966
Fam213a	1.813830255	3.806256775	61.92808987	4.56E-06	0.004382966
Etl4	-3.167557854	1.55880033	59.20092063	5.73E-06	0.005081323
Angptl2	-4.112081058	5.501443265	57.33064607	6.73E-06	0.005545238
Slpi	2.100829314	5.256944687	53.17977703	9.79E-06	0.006628154
Prkcb	-2.152497118	4.900817271	52.56162371	1.04E-05	0.006628154
Tiam2	-2.474045386	3.81572835	52.16496372	1.08E-05	0.006628154

genes	logFC	logCPM	F	PValue	FDR
Daglb	3.154238384	-0.066998741	51.19397755	1.18E-05	0.006628154
Klrb1c	2.732697545	0.940505462	51.12731897	1.19E-05	0.006628154
Fndc1	-5.50855912	0.65169323	50.49562942	1.26E-05	0.006628154
BC026585	1.871569381	3.592653676	49.91027058	1.34E-05	0.006713315
2610028E06Rik	1.593037037	1.819895998	48.84447225	1.41E-05	0.006774907
Tgfbi	1.972217389	3.824443242	48.27846355	1.57E-05	0.007265829
Tnc	3.805086101	1.210099456	47.44989083	1.71E-05	0.007600292
Sdc2	-3.90668034	1.505435186	44.35107052	2.37E-05	0.009387257

Supplementary Table 9: Intersection of genes differentially expressed in JAWSII scramble control cells vs R-1000 Sec22b rescued cells and JAWSII scramble control cells vs Sec22b KD cells but not between R-1000 and Sec22b KD cells. Cut-off: FDR < 0.01 and logFC > |1.5|, FC = fold change, CPM = counts per million, FDR = false discovery rate. Sorted by logFC. Sec22b was added to the set for comparison even though it is differentially expressed in all three comparisons.

	scramble vs rescue			scramble vs KD		
genes	logFC	logCPM	FDR	logFC	logCPM	FDR
Grm8	10.67981432	1.964019349	0.000510576	10.68381122	1.964019349	0.000643649
Thbs1	10.42791852	1.714435591	0.001065181	6.734152488	1.714435591	0.002147898
Ctla2a	10.1990339	1.641091937	3.43E-05	6.470918105	1.641091937	8.24E-05
Mmrn1	9.498600435	0.853560858	0.000332719	4.964451834	0.853560858	0.001217382
Tspan12	9.283154655	0.595533276	0.000255881	4.660724294	0.595533276	0.00104524
Arhgef10l	8.951379672	2.45650831	5.11E-07	7.797732608	2.45650831	8.29E-07
Cadps	8.79249489	0.21413462	0.000451222	7.204576649	0.21413462	0.000689258
Dab2ip	8.638506586	1.429523931	1.01E-06	7.848675183	1.429523931	1.60E-06
Abhd6	8.354329765	-0.205763872	0.000550259	4.888994132	-0.205763872	0.001720712
Fcrls	8.297393413	1.18216913	0.000181763	9.862695913	1.18216913	0.000196208
Ctla2b	8.051067211	2.697213871	1.43E-06	4.155117853	2.697213871	2.06E-05
Inpp4b	7.859827945	-0.655447399	0.001303878	6.258081311	-0.655447399	0.002193756
Gm6634	7.652716638	-0.808896229	0.001490842	6.071703608	-0.808896229	0.002536109
Cryab	7.372737859	2.361827825	5.30E-05	5.773935783	2.361827825	0.000134795
Grik2	7.196511642	1.661946554	2.98E-07	4.535890679	1.661946554	1.27E-06
Fam49a	6.872668187	2.389117235	1.01E-06	5.894001657	2.389117235	1.67E-06
Uchl1	6.730981334	1.221299677	8.11E-06	4.800444972	1.221299677	3.31E-05
Col24a1	6.709834281	4.941862809	1.65E-05	4.045123223	4.941862809	0.000212216
Adrbk2	6.690856883	4.128486498	4.62E-07	4.660261569	4.128486498	1.67E-06
Gpr97	6.545652591	-0.382106747	5.92E-05	4.422393403	-0.382106747	0.000205752
Ttc12	6.419663717	0.143906062	2.78E-05	4.657371281	0.143906062	8.24E-05
Cd180	6.35494995	3.017626305	9.92E-07	6.900168393	3.017626305	9.51E-07
Rgma	6.273185615	0.05774283	3.39E-05	4.019045321	0.05774283	0.000168866
Rhoj	6.187669651	-0.022260358	6.50E-06	3.961582953	-0.022260358	3.85E-05
Apbb2	6.179328393	0.593781172	7.20E-06	5.545384421	0.593781172	1.47E-05
Barx2	6.154219236	0.649234226	1.81E-05	5.2071127	0.649234226	3.77E-05

	scramble vs rescue			scramble vs KD		
genes	logFC	logCPM	FDR	logFC	logCPM	FDR
Gas7	6.094592884	-0.14720444	6.31E-05	4.918075068	-0.14720444	0.000145668
Adamts9	5.990431337	-0.048380097	6.15E-05	1.959792208	-0.048380097	0.007909212
Dync1i1	5.986445857	0.879152164	2.80E-06	3.314480962	0.879152164	4.15E-05
Rasd2	5.864017355	1.662985447	3.49E-05	6.437100832	1.662985447	3.86E-05
Greb1	5.5869491	-0.062743805	0.000178993	3.428634719	-0.062743805	0.001128831
Cfh	5.290580862	1.730750902	2.22E-05	7.281608303	1.730750902	1.08E-05
AW551984	5.284052706	1.172790787	4.18E-06	4.102439497	1.172790787	1.60E-05
Myo16	5.224014121	1.837407023	3.14E-06	6.848792357	1.837407023	1.67E-06
Tceal8	5.165768485	1.507184141	1.01E-06	5.954106587	1.507184141	9.82E-07
Ap1s3	5.080187698	-0.435718056	3.28E-05	2.27646137	-0.435718056	0.001184707
Col4a4	4.969272945	-0.394535416	5.06E-05	5.301975327	-0.394535416	5.83E-05
Fam213b	4.878140541	1.002603325	5.72E-05	2.983437865	1.002603325	0.000671509
Afap1	4.877645221	1.797533442	8.62E-06	2.173409303	1.797533442	0.000785514
Lama5	4.834152858	2.430558477	0.000122529	2.261972067	2.430558477	0.007570645
Fam46c	4.820690664	-0.017811231	0.000388708	4.591501831	-0.017811231	0.00054247
Pde2a	4.699935537	3.772568188	9.92E-07	3.996799114	3.772568188	2.48E-06
Fgf1	4.655959107	1.240865417	6.48E-05	3.565197441	1.240865417	0.000282326
Il18rap	4.602973958	0.433755471	5.15E-06	7.500332239	0.433755471	1.67E-06
Mfap3l	4.524532451	-0.25721907	8.97E-05	4.121989788	-0.25721907	0.000154861
Cd163	4.518617429	1.395040014	0.000196071	2.387609675	1.395040014	0.005169213
Zmat4	4.475073399	0.069582247	6.90E-06	3.270928116	0.069582247	3.75E-05
Sorl1	4.434875634	4.548224779	8.11E-05	2.615526801	4.548224779	0.001816445
Wbscr27	4.396794292	2.179480813	1.65E-06	3.822167132	2.179480813	4.15E-06
Klk1b1	4.386126126	3.926434706	0.000262493	2.981361054	3.926434706	0.00208649
Clu	4.370923489	4.890147879	5.40E-07	5.285562772	4.890147879	2.76E-07
Cysltr1	4.370732875	2.316743242	5.06E-05	3.282826664	2.316743242	0.000271126
Abcg3	4.323809273	1.644351325	0.000426069	2.344035905	1.644351325	0.009732388
Gm5483	4.309984905	0.563447731	0.000258862	2.89438147	0.563447731	0.001918333
Spry1	4.290709943	1.43139826	1.64E-05	2.153484437	1.43139826	0.000721034
Gpr141	4.243541406	3.796414689	0.000131555	3.256899484	3.796414689	0.000661353
Fyb	4.224660389	0.472906306	0.000261084	3.619030322	0.472906306	0.000643649
Hgfac	4.211468401	1.655871018	9.80E-05	3.20255881	1.655871018	0.000478409
Ifi44	4.19931821	2.345757993	7.87E-05	7.226634529	2.345757993	1.67E-05
Trim2	4.025956368	2.052708084	1.54E-05	2.105115493	2.052708084	0.000665435
Map2k6	3.981588199	-0.259537462	4.54E-05	2.680525733	-0.259537462	0.000349201
Fcgr1	3.918579984	5.288096077	3.14E-06	3.439678972	5.288096077	9.71E-06
Thrb	3.908752379	2.00167973	3.14E-06	2.85295252	2.00167973	2.75E-05
Apol9a	3.873906932	2.846423574	8.42E-05	4.857655755	2.846423574	4.21E-05
Apol9b	3.835067225	1.746178695	0.000107837	4.141009042	1.746178695	0.000111126
Wfdc10	3.794677185	0.474967748	0.000255881	2.870324073	0.474967748	0.001149513
Oasl2	3.786740039	5.811068077	0.00029445	5.044888485	5.811068077	8.08E-05
Arg1	3.747843272	0.739378783	0.001066163	2.743882376	0.739378783	0.005651226
Cmklr1	3.738356903	2.576081355	1.82E-05	2.744034448	2.576081355	0.000124536
Wwtr1	3.719212964	0.604200334	5.88E-05	2.637906493	0.604200334	0.000425051

	scramble vs rescue			scramble vs KD		
genes	logFC	logCPM	FDR	logFC	logCPM	FDR
Grb10	3.712537145	1.847304724	0.000122529	3.913455686	1.847304724	0.000113873
Gm7609	3.651495754	-0.485531663	0.000243655	3.601103568	-0.485531663	0.000319096
Gpr56	3.645303572	1.270791543	5.15E-06	2.387895906	1.270791543	7.36E-05
Atp9a	3.600105018	1.027517458	5.26E-06	2.520484222	1.027517458	5.08E-05
Fxyd7	3.56010581	1.057407687	5.04E-05	3.158601956	1.057407687	0.000113873
Mx1	3.557202676	-0.270522954	0.002445024	4.429071227	-0.270522954	0.001361884
Ptpn18	3.548201977	3.527139685	9.92E-07	2.511560349	3.527139685	9.07E-06
Scrn1	3.522319375	0.470294074	1.82E-05	4.497320085	0.470294074	7.74E-06
Phf11a	3.451089708	1.384120292	0.000250177	4.386346486	1.384120292	0.000111694
Rasgrp3	3.443478007	2.277511882	4.00E-05	3.115128457	2.277511882	8.59E-05
Prkar1b	3.412997823	2.265945856	2.46E-06	3.96718761	2.265945856	1.47E-06
Syne1	3.395155087	4.234712704	0.000136482	2.092739766	4.234712704	0.002846588
Cited1	3.364449264	0.184266034	0.000282732	3.508222468	0.184266034	0.000300452
Rhox5	3.356466372	4.329386436	3.39E-05	1.510410522	4.329386436	0.005639642
Olfm1	3.34990181	0.771107135	3.39E-06	3.563044645	0.771107135	3.33E-06
Cst7	3.327568449	0.895045647	9.13E-06	2.677151634	0.895045647	4.19E-05
F3	3.298129322	2.108068978	8.95E-05	2.137850603	2.108068978	0.001526151
Serpina3g	3.266546276	2.659800794	6.66E-05	2.356109475	2.659800794	0.000599666
2010002M12Rik	3.216616227	0.039591738	0.000547272	5.257427036	0.039591738	0.000123963
Ccl22	3.202731439	3.660709313	0.000371782	3.201269274	3.660709313	0.000452788
Ush1g	3.192284181	2.724825262	1.01E-06	2.644181865	2.724825262	3.45E-06
Gprc5b	3.176361194	1.841384003	0.003047537	3.152115926	1.841384003	0.003795508
A230050P20Rik	3.175857798	1.416260609	4.95E-05	2.86714045	1.416260609	0.000111674
Trim30d	3.162832508	3.901530272	0.000451763	3.003401571	3.901530272	0.000688048
Lmo2	3.150007196	4.298623392	3.10E-05	1.705188925	4.298623392	0.001769525
Fkbp10	3.14110614	0.634421952	3.89E-05	1.766427075	0.634421952	0.001219299
Klk1b27	3.121535936	0.580861085	0.000247124	2.323235064	0.580861085	0.001356414
Pianp	3.115892619	1.219343722	5.72E-05	2.823512186	1.219343722	0.000123963
Cd86	3.11420682	3.814012568	5.26E-06	2.930992172	3.814012568	1.08E-05
Cyp2u1	3.106727425	0.092888312	9.80E-05	2.627664622	0.092888312	0.000294739
Cp	3.103647813	1.765898657	2.79E-05	2.082493617	1.765898657	0.000377427
Hapln4	3.039241594	1.90941807	3.31E-05	3.223448919	1.90941807	3.31E-05
Folr2	3.035260445	-0.327998422	0.000306125	2.628963543	-0.327998422	0.000716573
Phf11b	2.992920059	2.904490264	6.17E-05	4.450287045	2.904490264	1.08E-05
Pax3	2.99137493	2.307298649	1.71E-06	2.252223608	2.307298649	1.36E-05
Gja5	2.98988439	0.87081664	8.08E-05	4.013236147	0.87081664	3.09E-05
Ms4a7	2.978613483	3.906233605	3.21E-05	1.613649754	3.906233605	0.001998955
Pamr1	2.978327405	1.627949896	0.000311608	1.937743864	1.627949896	0.004519848
Myzap	2.940331343	3.625010036	3.36E-05	1.724201803	3.625010036	0.001107357
Csn1s1	2.930764399	6.703806951	0.0001982	3.563461487	6.703806951	8.08E-05
Oas2	2.919747409	5.436288774	0.004649503	2.877368853	5.436288774	0.004811092
Arhgap29	2.890304304	-0.693038789	0.002161631	2.950390104	-0.693038789	0.002338227
Rpph1	2.877398546	1.348474199	0.000800564	2.803324151	1.348474199	0.001065358
Sv2a	2.877239975	2.237909608	2.22E-05	2.563494656	2.237909608	5.53E-05

	scramble vs rescue			scramble vs KD		
genes	logFC	logCPM	FDR	logFC	logCPM	FDR
Fxyd2	2.84038427	0.199786029	0.000783724	2.995369753	0.199786029	0.000785514
Yipf7	2.76719723	0.254606765	0.00592007	3.661365514	0.254606765	0.002183145
AA467197	2.729830356	4.722338362	0.00613687	6.146585671	4.722338362	0.00011496
Oasl1	2.710686333	1.582080603	0.002211894	2.709928069	1.582080603	0.002846588
Cd14	2.705770032	7.099268239	3.35E-06	1.890235684	7.099268239	5.08E-05
Akr1c13	2.701650776	3.714753418	2.22E-05	1.786398831	3.714753418	0.000385859
4933412E12Rik	2.685403745	1.852608037	2.27E-05	1.832308864	1.852608037	0.000288669
Eid1	2.6639874	3.94127438	5.15E-06	2.122531072	3.94127438	3.17E-05
Oas3	2.661043705	6.647703072	0.009209503	3.737174021	6.647703072	0.00138887
Arap3	2.637701902	6.196602488	1.01E-06	2.33857851	6.196602488	2.79E-06
Ttll11	2.634455689	-0.140110064	0.005075315	2.607472898	-0.140110064	0.006609166
Cpq	2.59247553	-0.167440474	0.00074044	4.711759086	-0.167440474	7.61E-05
Nfatc2	2.590078409	2.181853316	3.91E-05	2.990329755	2.181853316	2.75E-05
Fam189b	2.559964824	1.949936903	2.54E-05	2.390070837	1.949936903	5.07E-05
Itln1	2.554148659	0.353506988	0.007184737	2.971775304	0.353506988	0.004223953
Scml4	2.545017939	2.095734317	2.63E-05	1.983479962	2.095734317	0.000146505
Cx3cl1	2.524545223	2.309097934	8.26E-05	2.48545837	2.309097934	0.000113873
Gbp9	2.522826396	3.485834574	0.001913152	2.397715097	3.485834574	0.002338227
Tinagl1	2.521898707	0.493673307	0.00041872	2.970907352	0.493673307	0.000205752
Iigp1	2.521075003	1.395621713	0.001281137	2.675718261	1.395621713	0.000991122
Cystm1	2.496031733	2.148509467	0.000301231	3.295368041	2.148509467	7.76E-05
Cd52	2.483899096	6.523183167	0.000276016	2.782851605	6.523183167	0.000159727
Odf3l1	2.438732427	2.856022547	2.87E-05	3.6951707	2.856022547	3.28E-06
4930550L24Rik	2.400911583	2.895050205	0.000343976	2.961840211	2.895050205	0.000118164
Pdgfb	2.391645448	4.671821771	0.006784545	2.93838336	4.671821771	0.002757266
Ces5a	2.377145382	1.026776846	0.003826032	2.549932114	1.026776846	0.003298656
Glrp1	2.374664522	1.572648186	0.00024265	2.701908621	1.572648186	0.000133621
Grin1	2.362800443	0.54413121	0.004376822	2.411373886	0.54413121	0.00499621
Gimap9	2.358042404	3.632091545	4.92E-06	1.581905162	3.632091545	8.71E-05
Afap1l1	2.335335352	0.711019551	0.000451222	1.893939201	0.711019551	0.001842394
Oas1g	2.3349182	3.864276424	0.000308322	2.625483389	3.864276424	0.000189564
Eya4	2.275513736	2.148470862	0.000519069	1.88206687	2.148470862	0.00182526
Gm826	2.263648653	0.489330742	0.002216198	2.016921947	0.489330742	0.005056156
Tal1	2.258994149	2.269889443	0.000166679	2.391860449	2.269889443	0.000144702
Trim30a	2.245900186	5.65711431	0.000546767	2.390829542	5.65711431	0.000439408
Nxf7	2.240474073	3.730451015	3.61E-05	2.181597481	3.730451015	5.73E-05
Cmpk2	2.225351139	3.39205635	0.002780533	2.751111632	3.39205635	0.001065358
I830012O16Rik	2.154931763	1.5874779	0.006433683	3.765462652	1.5874779	0.000580181
Trim40	2.126957956	1.573781466	0.004365408	3.537762886	1.573781466	0.00038253
Apln	2.12346199	0.389890625	0.001244109	1.545400912	0.389890625	0.00880012
Gfra1	2.104656548	3.079443375	0.000119592	1.99951833	3.079443375	0.000203672
Dok7	2.09525055	3.369993126	0.002606635	2.436543346	3.369993126	0.001453355
Slc2a3	2.094623344	0.875778894	0.000536769	3.305500444	0.875778894	5.76E-05
Gbp4	2.092715647	0.199432572	0.000388708	2.680666106	0.199432572	0.00012244

	scramble vs rescue			scramble vs KD		
genes	logFC	logCPM	FDR	logFC	logCPM	FDR
Pdzk1ip1	2.061870273	2.537981207	0.004227244	2.813489876	2.537981207	0.000829843
Gsta3	2.034721564	3.935705208	0.00802962	3.197376652	3.935705208	0.000745508
Xaf1	2.020955244	4.950405611	0.004753509	2.496426857	4.950405611	0.001600514
Slc39a10	1.947808967	2.696861274	4.36E-05	1.652205841	2.696861274	0.000153523
1500015A07Rik	1.936382983	2.8697035	5.92E-05	1.645477671	2.8697035	0.000223205
Oas1a	1.909197078	5.983099529	0.000301231	2.053509663	5.983099529	0.000228561
Stk32c	1.902753925	-0.121803189	0.008993971	3.148589518	-0.121803189	0.000994581
Irf7	1.89486272	5.251845873	0.003559502	2.408468248	5.251845873	0.001032143
Rps6ka2	1.871622821	4.041761918	0.000468655	1.907437399	4.041761918	0.000510919
Tmem202	1.862656897	2.493950701	5.72E-05	2.018521467	2.493950701	4.64E-05
Tnfrsf11a	1.849402337	0.679459817	0.001949409	2.030622107	0.679459817	0.001361884
Ptpn22	1.845098393	2.780417104	0.000106882	2.060210134	2.780417104	7.10E-05
Amy1	1.842467838	0.359860572	0.000406666	1.584013659	0.359860572	0.001203956
Pcdh10	1.807615461	-0.118762512	0.005522512	2.283608727	-0.118762512	0.001911027
Aoah	1.80479796	5.393108547	0.0001834	1.699953663	5.393108547	0.000338582
Des	1.80003478	-0.283786643	0.003347555	1.639517125	-0.283786643	0.006630143
Ddx60	1.784614041	5.000156442	0.004937766	2.347066711	5.000156442	0.001078026
P2ry1	1.766861904	0.311427741	0.000997538	2.505664344	0.311427741	0.000159727
H2-Ob	1.753729608	5.987401904	0.002454846	3.190411254	5.987401904	7.36E-05
Zeb1	1.747667909	1.612226238	0.000187078	1.561533906	1.612226238	0.000486711
Tagap	1.729995493	3.343661216	3.61E-05	1.794198304	3.343661216	4.05E-05
St6gal1	1.729106755	6.25084548	0.000377156	1.702233313	6.25084548	0.000486711
D630033O11Rik	1.701524635	1.683590811	0.000297451	1.62509814	1.683590811	0.000486711
Pdzrn3	1.686464768	4.353288615	0.005995477	1.77474538	4.353288615	0.005070921
Csn2	1.67687484	9.269580735	0.000632532	1.580665982	9.269580735	0.00114443
Ly6a	1.648984536	3.615975449	0.002190432	2.516411837	3.615975449	0.000203672
Pram1	1.647114921	3.083572972	0.000736044	2.213687479	3.083572972	0.0001389
Il27	1.616554347	2.726900133	0.002868035	1.924840802	2.726900133	0.001209156
Slfn4	1.613043989	6.107779807	0.001592943	1.67293481	6.107779807	0.001372143
Hepacam2	1.581224569	1.032545231	0.002451185	2.665756885	1.032545231	0.000152594
Pdia5	1.577799133	2.012904001	0.006719608	2.489507404	2.012904001	0.000569311
A530032D15Rik	1.528136123	2.301961074	0.001408101	2.096616458	2.301961074	0.000228821
Sash1	1.513432934	3.899491612	0.00019172	1.532818937	3.899491612	0.000209034
Tmem14a	1.511131078	0.756176357	0.003347555	2.259130018	0.756176357	0.000391176
Dmkn	-1.501057676	1.281881494	0.00802962	-1.719102086	1.281881494	0.004056286
Fbxo2	-1.516199431	1.636101361	0.004036891	-1.665860481	1.636101361	0.002610022
Jup	-1.530109345	1.394261951	0.007900525	-1.672208321	1.394261951	0.005198011
Cd83	-1.538244134	0.655039321	0.007328805	-2.316164292	0.655039321	0.000493736
Wfdc12	-1.564874919	3.884965471	0.004882557	-2.908502289	3.884965471	9.86E-05
Zmpste24	-1.574606426	4.971920874	0.000388708	-1.570145667	4.971920874	0.000478061
Rfng	-1.58484799	5.784970928	5.50E-05	-1.705599674	5.784970928	4.45E-05
Zkscan7	-1.600169068	1.160652102	0.008825609	-1.883008832	1.160652102	0.003564949
Efnb1	-1.611560405	1.745647118	0.001698921	-1.540411143	1.745647118	0.002690481
Kcnip4	-1.622878548	1.964849146	0.001657851	-2.004751756	1.964849146	0.000463425

	scramble vs rescue			scramble vs KD		
genes	logFC	logCPM	FDR	logFC	logCPM	FDR
Proca1	-1.642428164	0.754113842	0.002485075	-2.471612764	0.754113842	0.000144702
Krt79	-1.666637592	5.510228266	0.004965085	-3.294104403	5.510228266	7.36E-05
Rbms3	-1.74398894	3.781703982	0.000886788	-2.60907926	3.781703982	7.10E-05
Nmnat2	-1.754446615	0.935939526	0.00990996	-2.448426984	0.935939526	0.00123621
Amotl2	-1.756101943	3.676512241	0.003401814	-2.444405889	3.676512241	0.000420428
Pecam1	-1.763410063	2.411255251	0.000481945	-1.556345645	2.411255251	0.001359509
Drd1a	-1.783357837	1.150429194	0.002253023	-2.0262327	1.150429194	0.001082305
Mum1l1	-1.783680524	2.943922885	0.001225587	-1.978801921	2.943922885	0.000694944
Chpf	-1.788802595	5.690241196	6.79E-05	-2.314766583	5.690241196	1.67E-05
Fam160a1	-1.79827284	2.151669688	3.40E-05	-1.927074978	2.151669688	3.00E-05
Zbtb32	-1.803683873	6.137427041	0.000120486	-1.951711375	6.137427041	8.64E-05
Fam132b	-1.860493299	0.407586141	0.00155406	-2.213301613	0.407586141	0.000510919
Tm7sf3	-1.876254209	5.088572634	2.44E-05	-1.518432099	5.088572634	0.000126037
Mogat2	-1.882762303	5.493048036	0.001592943	-1.978812221	5.493048036	0.001370263
Nfatc4	-1.890496937	2.504331046	0.001138816	-1.581480903	2.504331046	0.004433805
Abcg4	-1.918376908	4.200916692	0.000254984	-1.671743827	4.200916692	0.000753813
Tusc5	-1.955799764	-0.426739835	0.007328805	-2.145195661	-0.426739835	0.00465784
Sesn3	-1.973149456	1.212959253	0.000547272	-1.984970225	1.212959253	0.000665435
Kcnh4	-2.005529288	1.31645034	0.002994203	-2.629133113	1.31645034	0.000520354
Htra3	-2.024167085	5.212339945	0.001203537	-2.895017659	5.212339945	0.000135065
Glt28d2	-2.094109159	-0.113851088	0.005921585	-2.710455741	-0.113851088	0.001079156
Sec22b	-2.114640722	7.632921729	1.89E-06	1.92006735	7.632921729	5.00E-06
Ces2c	-2.120286871	4.373883752	0.001651672	-2.2871221	4.373883752	0.001124954
Fstl1	-2.133490187	1.214126759	0.001281137	-1.723065715	1.214126759	0.006545807
Treml4	-2.139892443	5.8320707	0.000592182	-2.398486511	5.8320707	0.000369295
Ptger3	-2.277301767	3.723817607	2.11E-06	-2.590447188	3.723817607	1.14E-06
Cyp2d22	-2.331452587	2.830653197	5.92E-05	-2.911513392	2.830653197	1.67E-05
Rhpn2	-2.350938206	3.590895101	0.000388708	-1.752341759	3.590895101	0.003298656
Pnpla5	-2.373410313	0.105173504	0.000801794	-2.999592184	0.105173504	0.000145668
Klra9	-2.401683714	3.93779886	0.00050893	-2.142262226	3.93779886	0.001257038
Plxdc2	-2.433973595	2.970287847	2.30E-05	-2.551134361	2.970287847	2.34E-05
Il1r1	-2.483935491	0.085795946	0.001203537	-3.369363295	0.085795946	0.000132763
Fndc9	-2.510830228	1.37101165	0.000649413	-1.747112049	1.37101165	0.00891302
Myom3	-2.612529798	4.486599257	0.000104615	-1.84220447	4.486599257	0.001319923
Gfpt2	-2.61566502	2.233275022	0.000518824	-2.966684533	2.233275022	0.000268936
Sdr42e1	-2.616330643	2.235802081	3.99E-05	-1.824738062	2.235802081	0.000665435
Sil1	-2.633533885	3.016620322	9.36E-05	-1.81132611	3.016620322	0.001478542
Adcy6	-2.67451972	1.062475082	0.000276073	-2.158260033	1.062475082	0.001637621
Ptrf	-2.683582932	5.240720176	0.000122845	-2.766074229	5.240720176	0.00012244
Ptgis	-2.684342924	0.959192205	0.000421643	-4.198697218	0.959192205	1.60E-05
Chl1	-2.692871057	2.11364003	0.000310644	-3.18675202	2.11364003	0.00011544
Rtn2	-2.730538248	1.158611452	0.005687229	-2.97445884	1.158611452	0.003606878
Spsb1	-2.745424835	2.404859507	1.37E-05	-4.031990878	2.404859507	1.08E-06
Clcf1	-2.762908674	2.750222995	2.02E-05	-2.596960302	2.750222995	4.05E-05

	scramble vs rescue			scramble vs KD		
genes	logFC	logCPM	FDR	logFC	logCPM	FDR
Ccdc166	-2.862397535	0.53941168	0.001066163	-4.043985976	0.53941168	8.08E-05
Gcat	-2.866490216	3.530974753	0.00068257	-2.23246714	3.530974753	0.003867327
Atp1b2	-2.916502819	1.317436447	0.001769696	-2.58100343	1.317436447	0.004660195
Fam124a	-2.929997996	2.973148082	0.000612427	-2.457490523	2.973148082	0.00276139
Cygb	-2.932067496	-0.054125817	0.004464676	-4.663072085	-0.054125817	9.97E-05
Slc2a4	-2.981282937	1.062781708	3.12E-05	-2.213140241	1.062781708	0.000369295
Cyp4f18	-2.984168833	6.334932742	0.001599039	-2.324061523	6.334932742	0.007477889
P2rx5	-2.994650192	0.525724002	0.00124733	-3.648974063	0.525724002	0.000329465
Spon2	-3.011843525	2.425916244	0.002783014	-3.485605621	2.425916244	0.00123621
Klra3	-3.0270048	6.045485362	0.000146134	-1.984394759	6.045485362	0.002600971
Shisa4	-3.029070523	3.518680535	0.000111008	-2.530261598	3.518680535	0.000478061
AI427809	-3.043555079	-0.285838732	0.002575843	-2.698670956	-0.285838732	0.007669075
Vill	-3.054415251	5.83066227	0.001326119	-2.800621423	5.83066227	0.002894297
Fhod3	-3.060384566	2.333888476	0.000825902	-4.546713292	2.333888476	6.48E-05
Sept5	-3.07911914	5.040486516	1.38E-06	-2.516661452	5.040486516	7.16E-06
Etv4	-3.09156056	2.581647994	0.000595525	-3.299879924	2.581647994	0.000478409
Plekhh1	-3.093859458	0.440980887	0.001626023	-3.061915729	0.440980887	0.002136728
Trpc4	-3.112020581	2.281027912	0.000564819	-2.616475198	2.281027912	0.002193756
Il17rc	-3.125423906	2.745891941	0.00067407	-2.717007121	2.745891941	0.001864515
Shisa9	-3.174485892	4.253584406	8.28E-07	-3.139487577	4.253584406	1.02E-06
Mrap	-3.183276117	1.030481749	5.92E-05	-2.861926192	1.030481749	0.000167203
A330021E22Rik	-3.183451962	1.644062137	0.000111008	-3.441828828	1.644062137	8.24E-05
Tgfb2	-3.203676151	3.571613186	0.000110667	-4.163034836	3.571613186	2.79E-05
Necab1	-3.220531723	3.982627586	1.01E-06	-3.928937184	3.982627586	4.09E-07
Zfp109	-3.235313786	0.043149632	0.004065636	-3.379423428	0.043149632	0.003320011
Ear5	-3.25669351	4.334848304	0.001238685	-3.841777032	4.334848304	0.000503513
Chdh	-3.265208519	0.285629265	0.000484682	-3.15523182	0.285629265	0.000730197
Igf2r	-3.281550135	3.73650984	0.000481945	-2.748147908	3.73650984	0.001802039
Mamdc2	-3.334752841	1.275861733	0.001460235	-3.410709159	1.275861733	0.001418746
Ripk3	-3.349261931	3.870044713	8.50E-06	-3.572018504	3.870044713	7.16E-06
Lama4	-3.391220322	1.646817927	1.71E-05	-4.403301416	1.646817927	2.54E-06
Plcd1	-3.395696612	0.58726907	0.000477086	-2.588046298	0.58726907	0.004280908
Rap1gap2	-3.453906537	0.761283021	0.000179928	-3.247871262	0.761283021	0.000349201
Erc2	-3.464376719	3.16110895	0.000111008	-2.589536222	3.16110895	0.000899494
Kcnk3	-3.516344854	-0.206813624	0.00559375	-3.604726693	-0.206813624	0.005596391
Als2cr12	-3.529858112	0.001558757	0.000211958	-2.603918254	0.001558757	0.002872302
Pcyt1b	-3.544612531	3.039357249	5.39E-06	-2.941056039	3.039357249	3.00E-05
B4galt6	-3.555870569	1.426644281	0.008634	-5.511102775	1.426644281	0.000385931
Prl2c5	-3.560637486	0.401793173	0.00086844	-3.508490898	0.401793173	0.001154405
Serpinb8	-3.66662391	4.410736438	1.38E-06	-2.663803121	4.410736438	1.60E-05
Tm4sf19	-3.687179171	1.540935064	5.72E-05	-2.547784465	1.540935064	0.00104524
Grid1	-3.695292377	1.951982675	5.92E-05	-2.938563105	1.951982675	0.00039548
5430416O09Rik	-3.760526836	0.480233847	0.000130502	-4.192511677	0.480233847	7.09E-05
Palm	-3.762319103	5.599292772	5.63E-08	-3.119615795	5.599292772	2.76E-07

	scramble vs rescue			scramble vs KD		
genes	logFC	logCPM	FDR	logFC	logCPM	FDR
Klra10	-3.797307365	2.728564338	2.22E-05	-2.484687098	2.728564338	0.000504284
Itga7	-3.821527358	2.787286066	1.02E-05	-3.229622108	2.787286066	4.64E-05
4930523C07Rik	-3.824903299	2.07162713	7.44E-06	-2.815126564	2.07162713	8.64E-05
Rhox2h	-3.854527448	3.535653048	3.14E-06	-2.632384867	3.535653048	5.73E-05
Olfr1259	-3.860292685	-0.25530746	4.95E-05	-3.104207736	-0.25530746	0.000430251
Gfod1	-3.877165286	2.506376394	2.03E-06	-4.084750144	2.506376394	1.67E-06
Rhox2d	-3.895017048	2.422930922	0.00208247	-5.760301725	2.422930922	0.000135224
BC024139	-3.89713914	0.043776455	0.000306125	-3.545659894	0.043776455	0.000785514
Plin5	-3.900696995	1.091446522	0.000230197	-4.680511616	1.091446522	6.78E-05
Ltb4r1	-3.917201583	3.935583303	8.95E-05	-3.204568594	3.935583303	0.000407096
Apoc1	-4.027742408	2.088381292	0.000252616	-4.370686599	2.088381292	0.000159727
Gm13544	-4.162882821	1.574667206	1.11E-05	-3.837266516	1.574667206	2.79E-05
Adamdec1	-4.170055851	5.874354123	3.19E-05	-2.959235845	5.874354123	0.000339806
Mst1	-4.290773738	3.927071612	2.35E-07	-3.873021842	3.927071612	4.37E-07
Klra17	-4.307790673	0.62858327	0.000141532	-4.218951756	0.62858327	0.000209034
Plin4	-4.30863371	6.447374173	3.39E-06	-4.550000865	6.447374173	3.14E-06
Impact	-4.41738054	5.789748197	1.90E-08	-4.455461396	5.789748197	1.74E-08
Lamc2	-4.456247289	4.202343287	5.15E-06	-3.572438665	4.202343287	3.19E-05
Nynrin	-4.513565711	0.828166313	3.14E-06	-2.894994697	0.828166313	0.000160901
Perp	-4.603183162	5.173862714	2.32E-08	-4.599028137	5.173862714	2.34E-08
Bmp8a	-4.679940847	4.324463916	0.000116096	-4.155899897	4.324463916	0.00031279
Adam28	-4.79988128	2.03597348	1.88E-05	-3.545233296	2.03597348	0.000205775
Spats2	-4.801205239	2.248622651	0.00135757	-6.222261392	2.248622651	0.000228821
Steap1	-4.846213401	1.789907668	6.01E-05	-4.488594589	1.789907668	0.000144531
Kcnk5	-4.86833954	0.821903176	1.20E-05	-5.598275853	0.821903176	3.96E-06
Entpd3	-4.938154278	3.59582945	0.000377535	-3.115993316	3.59582945	0.007643202
Slmo1	-5.0502962	0.810377549	5.82E-06	-4.873802209	0.810377549	1.08E-05
Ebf1	-5.089229543	1.194926405	6.72E-05	-4.442339903	1.194926405	0.000256434
Nrbp2	-5.267544322	1.454871802	1.12E-05	-3.972577105	1.454871802	0.000134329
Sparcl1	-5.287224137	6.124402283	7.99E-05	-3.790606685	6.124402283	0.000715558
Psma8	-5.367477817	0.73351189	1.11E-05	-5.647194557	0.73351189	8.50E-06
Ccdc120	-5.585046503	0.624865033	1.89E-05	-6.190706938	0.624865033	8.45E-06
Zfp105	-6.244621159	0.761284208	2.67E-05	-7.219891833	0.761284208	7.21E-06
Scgb1a1	-6.438463914	0.057049559	8.89E-05	-5.399946078	0.057049559	0.000694944
Rhox2g	-7.173957295	2.765363663	1.33E-05	-4.420897818	2.765363663	0.000697386
Map2	-7.214539691	1.146627219	2.57E-05	-5.031887062	1.146627219	0.000907382
Hmgcll1	-7.396662001	2.937480831	5.07E-07	-7.603998186	2.937480831	4.37E-07
2510009E07Rik	-9.501140263	4.28998399	6.02E-08	-9.860692622	4.28998399	4.92E-08